https://doi.org/10.35662/unine-thesis-3088

Faculty of Science

Laboratory of Technologies for Heritage Materials

Development and evaluation of sustainable hydrogel formulations for the microbial cleaning of historical metal artefacts

A dissertation submitted to the University of Neuchâtel

for the degree of *Docteur ès Sciences*

Presented by

Luana Cuvillier

Jury members:

Prof. Edith Joseph, thesis director, University of Neuchâtel, Haute Ecole Arc, Switzerland

Prof. Stephan von Reuss, thesis co-director, Université de Neuchâtel, Switzerland

Dr. Elodie Guilminot, thesis co-supervisor, Laboratoire Arc'Antique, France

Dr. Elena Bernardi, Università di Bologna, Italy

Prof. Dominique Hourdet, Sorbonne Université, France

Thesis defended on November 28th 2023

unine
Université de Neuchâtel
Faculté des sciences

Rue Emile-Argand 11
CH-2000 Neuchâtel
doctorat.sciences@unine.ch

IMPRIMATUR POUR THESE DE DOCTORAT

La Faculté des sciences de l'Université de Neuchâtel autorise l'impression de la présente thèse soutenue par

Madame Luana CUVILLIER

Titre :

"Development and evaluation of sustainable hydrogels formulations for the microbial cleaning of historical metal artefacts"

sur le rapport des membres du jury composé comme suit:

- Prof. Edith Joseph, directrice de thèse, Université de Neuchâtel et Haute Ecole ARC Neuchâtel Berne Jura, Suisse
- Prof. Stefan von Reuss, Université de Neuchâtel, Suisse
- Dr Elodie Guilminot, Laboratoire Arc'Antique, France
- Prof. Dominique Hourdet, Sorbonne Université, Paris, France
- Dre Elena Bernardi, Université de Bologne, Italie

Neuchâtel, le 15 janvier 2024

Le Doyen, Prof. R. Bshary

« Aussi vite que possible, mais aussi lentement que nécessaire »

Alain Berset

Abstract

Iron, copper and silver-based objects are a significant part of our cultural heritage. Unfortunately, these metals suffer inevitable degradation through the spontaneous process of corrosion towards which they naturally tend. On indoor-exposed historical metal surfaces, this phenomenon gives way to the formation of mainly oxide and/or sulfide compounds. For aesthetical or functional purposes, treatment of these surfaces is often carried out to remove the undesired corrosion phases.

Various methods are currently available to professionals for the cleaning of this type of metallic substrate. However, none of them is entirely satisfactory, dealing with hazardous compounds, devices with limited availability or specific necessary skills, not completely efficient or difficult to control, sometimes resulting in the damage of the considered surface. In addition, there is the will to go towards more sustainable practices, taking into account the safety of the object, the operator as well as the environment.

For this reason, research has been looking at other possibilities, including the use of gels, in particular hydrogels, as carriers for aqueous treating solutions. They allow the confinement of the active solution along with more selective, less invasive application. Parallelly, new tendencies are opting for less toxic and more naturally-based solutions. For instance, heritage preservation treatments based on the potential of a variety of microbiological organisms.

To this purpose, the present thesis aims at developing and investigating a corrosion removal treatment combining both approaches, thus achieving a fully bio-derived reliable solution.

The first step was to select adequate biogenic compounds, exploiting fungi and bacteria as microscale chemical factories for the uptake of iron, copper or silver ions. To this end, microbial interaction with soluble and insoluble metals were assessed. In particular, it showed *Aspergillus niger*'s and *Beauveria bassiana*'s significant performances to achieve cleaning on iron and copper substrates respectively through the biogenic formation of oxalates. No microorganism could be distinguished for the remediation of silver. In addition, the action of secondary metabolites, mainly siderophores and organic acids, on the dissolution of powdered corrosion products was investigated over time using ICP-OES. In particular, although acids perform outstandingly at low pH, siderophores were confirmed to be remarkable candidates for the chelation of iron at any pH. For copper, the aminopolycarboxylic acid EDDS showed performances competing with EDTA, a common chelator with sustainability concerns. The same compound also achieved reduction of soluble silver into nanoparticles.

As second step, to deliver the metabolites solution, investigation of several polysaccharides was performed. In particular, formulation of a rigid chitosan-based gel was attempted and compared to agar characteristics. In addition, investigation of interactions between the gels and subsequent selected

cleaning solutions was carried out. Microscale morphology and mechanical properties showed no evidence for interactions between the polymer network and the carried solutes. The silver uptaking properties of the developed formulation were also evaluated using spectroscopic techniques. These properties could be further exploited to use some hydrogels as "uptaking devices", allowing to break-free from the use of an additional chelating solution, following the principle of less is more and achieve more simple formulations.

Rheological and oximetric measurements also showed the "residues potential" of non-rigid gels along with their potential deleterious effects, respectively. Attempts at finding methods to detect these residues using imaging techniques achieved qualitative and semi-quantitative results showing that agar was leaving rather bulky, punctual residues whereas xanthan gum's were spread out on the surface.

Evaluation of the combined selected active agents and polysaccharides was performed on artificially and naturally corroded samples using a multi-analytical approach, including spectroscopy, spectrocolorimetry along with elemental analysis and micro and macro-observations. Successful applications were tested on real artefacts obtained from heritage institutions.

Finally, environmental and health hazards of the developed formulations were evaluated using the Life Cycle Assessment approach, showing bio-derived compounds might not be, currently, the most performing, according to the initial hypothesis and the considered criteria.

Overall, this thesis allowed to develop alternative biologically derived formulations for the removal of corrosion on iron and copper artefacts, with a real step towards effective practical use by professionals. Future work could be foreseen for the use of microbes or metabolites on silver-based surfaces along with further enhancing global sustainability performances.

Keywords: Historical metals, heritage conservation, iron oxyhydroxides, silver sulfides, copper tarnish, biotechnology, siderophores, hydrogels; agar-agar, chitosan, sustainability.

Résumé

Les objets en fer, cuivre et argent font partie intégrante du patrimoine culturel commun. Malheureusement, ces métaux seront inévitablement dégradés via le processus spontané de corrosion auquel ils sont sujets. Sur les surfaces des métaux historiques conservés en intérieur, ce phénomène donne lieu à la formation d'oxydes et/ou de sulfures dans la plupart des cas. Pour des raisons esthétiques ou fonctionnelles, ces objets sont souvent traités afin de retirer la corrosion.

Plusieurs méthodes sont actuellement à la disposition des professionnels pour le nettoyage de ce type de substrat métallique. Néanmoins, aucun n'est entièrement satisfaisant, du fait de la présence de composés nocifs, du besoin d'équipement ou de compétences spécifiques ou encore la difficulté de contrôle pour ne pas endommager la surface à traiter. De plus, il y a une volonté croissante de se tourner vers des pratiques plus durables, qui prennent en considération à la fois la sécurité de l'objet, de l'opérateur mais également de l'environnement.

Pour cette raison, d'autres possibilités ont été étudiées par différents groupes de recherches, comprenant l'utilisation de gels, en particulier d'hydrogels, pour véhiculer les solutions aqueuses de traitement. Ils permettent le confinement des solutions de traitement mais aussi des applications plus sélectives et moins invasives. En parallèle, de nouvelles tendances se tournent vers des solutions moins toxiques et plus proches de la nature. Par exemple, les traitements de conservation du patrimoine recourant au potentiel de divers microorganismes biologiques.

Dans ce but, cette thèse cherche à développer et étudier un traitement de retrait de la corrosion combinant les deux approches, atteignant une solution fiable et entièrement biosourcée.

La première étape consiste à sélectionner les composés biogéniques appropriés, en exploitant champignons et bactéries comme des usines chimiques à l'échelle microscopique pour l'absorption du fer, du cuivre ou de l'argent. A cette fin, l'interaction microbienne avec des métaux sous forme soluble ou insoluble a été évaluée. En particulier, cela a montré les performances notables d'*Aspergillus niger* et *Beauveria bassiana* pour le nettoyage de surfaces en base fer ou base cuivre respectivement, via la formation d'oxalates biogéniques. Aucun microorganisme ne s'est distingué pour la remédiation de l'argent. En outre, l'effet de métabolites secondaires, principalement des sidérophores et acides organiques, sur la dissolution de produits de corrosion a été étudiée grâce à l'ICP-OES. En particulier, bien que les acides se soient montrés exceptionnellement efficaces pour des pH bas, les sidérophores ont confirmé être des candidats remarquables pour la chélation du fer sur toute la gamme de pH étudiée. En ce qui concerne le cuivre, l'acide aminopolycarboxylique EDDS a montré des performances équivalentes à l'EDTA, un complexant communément utilisé mais dont la durabilité est interrogée. L'EDDS a aussi montré des capacités de réduction de l'argent soluble en nanoparticules.

En seconde étape, pour véhiculer les solutions de métabolites, plusieurs polysaccharides ont été étudiés. En particulier la formulation d'un gel rigide à base de chitosan a été tentée et comparée aux caractéristiques de l'agar, pionnier dans le domaine. En outre, l'interaction entre les gels et les solutions de traitement sélectionnées en amont a été étudiée. La morphologie à l'échelle microscopique ainsi que les propriétés mécaniques n'ont pas montré l'interaction entre les réseaux polymériques et le soluté implémenté. Les propriétés de complexation de l'argent de la formulation développée ont été analysées grâce à des techniques spectroscopiques. Ces propriétés pourraient être exploitées de manière plus approfondies afin d'utiliser les hydrogels comme des systèmes de complexation, permettant de s'affranchir de l'utilisation d'une solution additionnelle, en suivant le principe du « moins c'est mieux » et ainsi tendre vers plus de sobriété.

Des mesures rhéologiques et oximétriques ont aussi montré la propension de certains gels non rigides à laisser des résidus, avec la preuve de leur effet nocif sur les surfaces métalliques. Des tentatives pour trouver des méthodes de détection de ces résidus en utilisant des techniques d'imagerie ont permis des approches qualitatives, et potentiellement semi-quantitatives avec du travail supplémentaire, montrant que l'agar laisse des résidus ponctuels alors que la gomme xanthane laisse des résidus très étalés sur la surface.

L'évaluation des agents actifs et polysaccharides combinés a été effectuée sur des échantillons corrodés artificiellement et naturellement, en recourant à une approche multi-analytique comprenant de la spectroscopie, de la spectrocolorimétrie ainsi que des analyses élémentaires et des observations micro- et macroscopiques. Les formulations fructueuses ont été testées sur des objets obtenus auprès d'institutions du patrimoine.

Enfin, les risques environnementaux et pour la santé des formulations développées ont été évalués grâce à l'approche de l'Analyse du cycle de vie, montrant qu'à ce stade, les composés biosourcés ne sont pas nécessairement l'alternative la plus performante selon les hypothèses initiales et les critères évalués.

Globalement, cette thèse a permis de développer des formulations, à partir de dérivés biologiques, pour le retrait de la corrosion sur les objets patrimoniaux ferreux et cuivreux, avec une vraie avancée vers l'utilisation effective de cette alternative par les professionnels du domaine. Des travaux ultérieurs pourraient être envisagés pour l'utilisation de microbes ou métabolites sur les surfaces en argent, mais également pour améliorer les performances globales en termes de durabilité.

Mots-clés : Métaux historiques, conservation du patrimoine, oxyhydroxides de fer, sulfures d'argent, ternissement du cuivre, biotechnologie, siderophores, hydrogels, agar-agar, chitosan, durabilité.

Abbreviations

AAB Artificially Aged Brass
AAC Artificially Aged Copper
AAS Atomic Absorption Spectrometry
AgNCs Silver nanoclusters
AgNPs Silver nanoparticles
AS Artificially aged Steel
ATR Attenuated Total Reflectance
BET Bruauner-Emmett-Teller method
CAS Chrome Azurol Sulfonate
CMC Carboxymethyl cellulose
CS-ItA-LCys Chitosan-based formulation with addition of itaconic anhydride and L-cysteine
DFO Deferoxamine Mesylate
DMM Decision Making Model
EDS Energy-dispersive X-ray Spectroscopy
EDDS Ethylenediamine disuccinic acid
EDTA/Na_2EDTA Ethylenediaminetetraacetic acid disodium salt
EoL End of Life
EPS Extracellular Polymeric Substances
FTIR Fourier Transform Infrared Spectroscopy
IA Itaconic Acid
IAn Itaconic Anhydrid
ICP-OES Inductively Coupled Plasma-Optical Emission Spectroscopy
L-Cys L-Cysteine
LAA L-aspartic acid
LCA Life Cycle Assessment
LC-UV Liquid Chromatography coupled to Ultra Violet detection
LMWOA Low Molecular Weight Organic Acid
MHL Musée Historique de Lausanne
MIC Microbially Induced Corrosion
NAC Naturally Aged Copper
NB Nutrient Broth
NS Naturally aged Steel
POP Persistant Organic Pollutants
PVA Poly Vinyl Alcohol
PVD Pyoverdine
RH Relative Humidity
RM Raw materials
RT Room Temperature
SEM Scanning Electron Microscopy
SOB Sulfate-oxidizing Bacteria
SPE Solid Phase Extraction

SRB Sulfate-reducing Bacteria
SVHC Substances of Very High Concern
TOF-MS Time of Flight- Mass Spectrometry
UHPLC Ultra High Performance Liquid Chromatography
UV-Vis Ultraviolet-Visible spectroscopy
XRF X-Ray Fluorescence spectroscopy

Acknowledgments

This thesis is my work, but it would not have come out the same without the help of several people. Once again proof, if needed, that no (great) work can be achieved alone. I would like to address a special thank you to each of the following:

To my supervisors for giving me the opportunity to complete a PhD thesis. Edith for putting this interesting research project up, giving me freedom on the directions while teaching me to pay attention to details. Elodie pour la pertinence, la bienveillance et la constructivité de tes conseils et remarques. Stephan, for availability and council with an external eye on the research topic.

I would like to thank anyone who I benefitted help from for research or administrative purposes: Laura Brambilla for global support, Matthieu Bueche for laser diffraction, Cédric Caillet for consumables support, Cesar Escobar for oximetry, Gaétan Glauser for MS, Nathalie Guichard for AAS, Gilles Hoffmann for his patience with our expense reports, Dominique Hourdet for insight on the interpretation of gels microstructure, Tony Journot for gel characterization (and chess games), Jean-Yves-Mevellec for the access to Raman equipment, Antonio Mucciolo for great Cryo-SEM imaging, Charlène Pelé-Mezziani for advice and support, Isabelle Rérat for her professionalism, Armelle Vallat for ICP, Armand Vinçotte for siderophores provision in France, along with Erwan, Marie and Thomas, interns that crossed the path of this project.

To conservators (Virginie Dupuy, Claire De Lalande, Claude-Alain Künzi) for allowing us to work on objects from their collections and to restorers (Michaela Florescu, Romain Jeanneret, Aymeric Raimon) for numerous advice and making sure we did not destroy case studies.

À Lidia, tout ce que je pourrais écrire ne suffira jamais à exprimer ma gratitude pour tout ce que tu as fait. Ton expertise de travail en laboratoire, ta précision, ta motivation sans faille, et j'en passe. Je te remercie pour ces petites discussions, et pour m'avoir tant de fois amenée et ramenée de l'hôpital. Je te souhaite sincèrement le meilleur. L'amitié n'a pas d'âge !

To other PhD students from the Chemistry Institute: Sarah, Désirée, Chrysanthi, Mareike, Antoine and Santi, for shared barbecues, hockey games, raclettes, movie or game nights. It was helpful to feel part of something to clean up my head at times. I would also like to mention researchers from the Institute of Physics allowing to breathe up from the Chemistry environment.

To the Service Sports of the University of Neuchâtel along with the Piscine du Nid-du-Crô and everyone related to swimming, in particular Caroline, Antoine, Camille, Jade and Camilo. More than a sport it was a moving meditation. I would also like to thank the SSVNN for the moments shared during the "writing" process of this manuscript, which were a breath of fresh air.

To the Orthopedic department of the hospital of Neuchâtel, who made me keep both feet down to earth, especially to Dr.méd. N. Makarem who made hospital visits more pleasant.

To Arianna, I could not have imagined a better fit for colleague. You are a unique amazing woman. I enjoyed the fact that getting on well together resided in our differences and what we could learn from each other as complementary, in lab but also outside. I am happy to say I gained a friend.

To Mathilde, who from a colleague turned into a flatmate and then into a friend. I enjoyed our talks about light topics but also more important conversations. I would also point out the tremendous help you provided while I was stuck at home. Wish you the best and hope to keep seeing you now and then.

To Milena, I am grateful to have had you as a flatmate. As much as it is important to have a great working environment, having somewhere that feels like home is also essential.

To Diego, whose presence was unexpected but made me grow as a person, further than I could have imagined.

To the friends that I kept in mind during these years and were part of it in a way: Adrien, Emilie, Gustave, Gwenaëlle, Lisa and Océane.

To the close friends that were always here to cheer-up, have fun but also share doubts and concerns, about work and about other aspects of life especially Clotilde, Inès, Fanny, Hugo, Marsanne, Nicolas and Thomas.

To Marin, whose joyfulness was big enough to counteract the lack of sun in the city of Neuchâtel in winter and who made me go out of my comfort zone.

To my parents for supporting me, and my brother for showing me that success and bravery can also reside in what society sees as ”failing”.

Table of contents

Figures index

Tables index

1. General introduction

© L. Preud'homme/Arc'Antique

This chapter is partly based on the following reviews:

Cuvillier, L.; Ganesan, S.; James, S.; Monachon, M.; Passaretti, A.; Albelda-Berenguer, M.; Mathys, L.; Joseph, E. Green corrosion mitigation and conservation strategies for metal heritage in *EFC series (Greenbook), Bridging the gap: corrosion science for heritage context*, D. Neff, Eds. Academic Press, **2023**, pp. ISBN 9780443186905 *Under publication*

Passaretti, A.; Cuvillier, L.; Sciutto, G.; Guilminot, E.; Joseph, E. Biologically Derived Gels for the Cleaning of Historical and Artistic Metal Heritage. *Appl. Sci*. **2021**, *11*, 3405

In 2017, following the "Gels in the Conservation of Art"[1] conference that took place in London, a project named "Gels Métaux" was put in place. A conservation scientist and two conservators, facing the observation that gels, an increasing heritage conservation tool, was lacking assessments on metals, took the initiative to allow stakeholders to emulate the applied research. The project tackles various delicate topics: gel preparation protocols, compatibility between formulations and active agents (i.e., chelators), and introducing gels into new branches of metal conservation like archaeological findings [1–4]. Initiated in France, it is expanding to a larger scale, calling forth an international appeal. In that context, the HELIX project was set-up.

The HELIX project is financed by the Swiss National Science Foundation (SNSF) and developed at the Haute Ecole Arc Conservation Restauration, in collaboration with the University of Neuchâtel, the University of Bologna, and Arc' Antique conservation and research laboratory. It aims to exploit chemical uptake processes occurring in microorganisms to remediate to the presence of degradation products on copper, iron, and silver historical and decorative alloys, mostly present in indoor environment, by developing innovative green and eco-friendly cleaning methods. The goal is to propose a sustainable, reliable method that is conscious of the challenges in the conservation field while limiting the risks for the artwork itself, the operator, and the environment. The project is organized in four different work packages (WP), each focusing on one aspect of the research topic (Figure 1.1). This project gives birth to two PhD theses, focused respectively on the use of hydrogels and organogels from renewable sources. This thesis concentrates on the removal of corrosion using hydrogels and will not address the removal of organic coatings. In that context, this chapter contextualises the research and gives an overview of the current state of the art, regarding the differents aspects of the thesis.

[1] https://academicprojects.co.uk/archive/gels-conference/

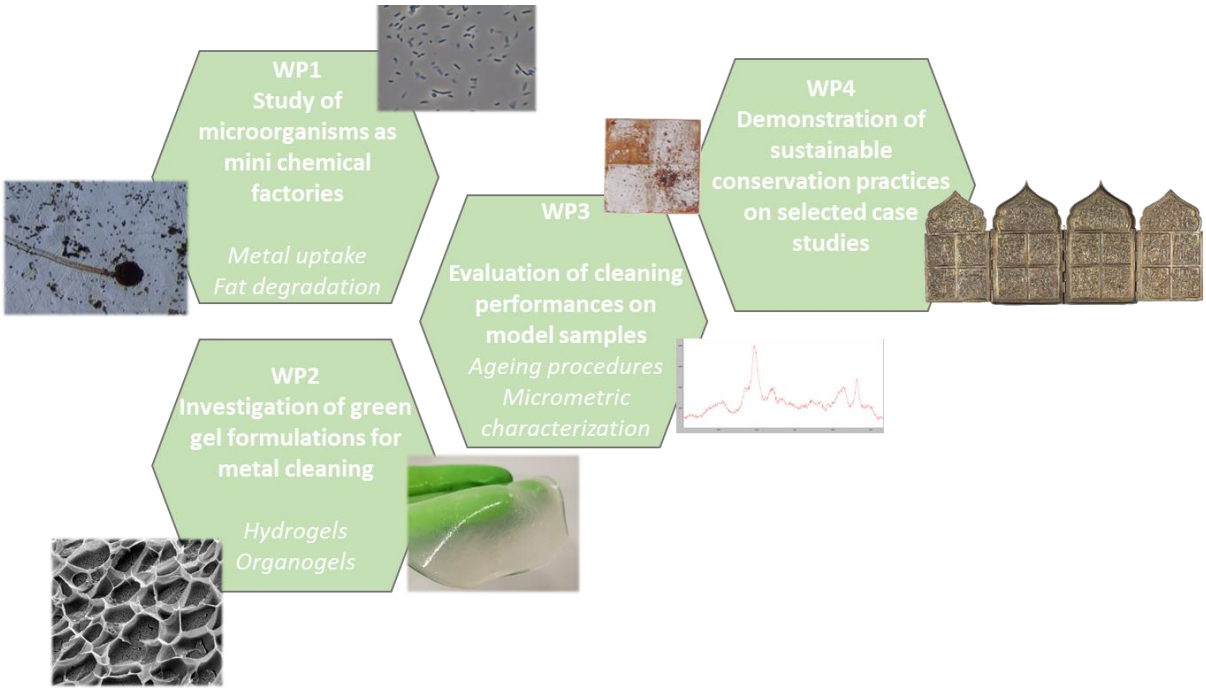

Figure 1.1 Repartition of the activites foreseen in the HELIX project into Work packages.

1.1 Corrosion of indoor historical metal heritage

Metals have had such a profound impact on the history of human societies that Bronze and Iron age are considered milestones in the history of humankind. The diversity of their use from the beginning of human history to contemporary era is remarkable and bears witness of the various inherent chemico-physical and aesthetic properties of metals. Indeed, they have been used to manufacture tools and weapons as much as construction materials. Metals have played a key role in modern architecture, transportations, and communications, including revolutions associated to informatics or internet. As a consequence of this large range of applications, it is extremely common to find metals in museum collections for their archaeological, historical, cultural or artistic focus [1]. Their spectrum of applications through the ages is broad: sculptures, musical instruments, jewelry, utensils, scientific instruments, decorative arts, weapons and so forth [2–7]. Historical metals are found in outdoor and indoor environments. In addition to functional purposes, they were sometimes combined with non-metallic items to improve aestheticism of the objects. Shiny metals are praised for jewels, ornaments, medals, and religious objects and, as such, are symbols of beauty, wealth, prestige, or affection. Their impact for the cultural heritage is such that there is a working group from the International Council of Museums (ICOM) dedicated to strengthening their study and care worldwide. The importance of metals in the manufacture of artistic or decorative works still strives in modern and contemporary era with the emergence of the so called "Modern metals" [8]. Out of the plethora of metals that can be found in reserves, iron-, copper- and silver- based ones have the most significant occurrence.

Few metals are used in their pure chemical state, they are usually mixed with one or more chemical elements, in variable amount, to produce tunable improved properties [9]. These mixtures are called alloys and can be of two major categories:

- The combination of several metals: brass is a mixture of copper and zinc, bronze is a mixture of copper and tin, and sterling silver is a mixture of silver and copper
- A metal combined with a non-metal: steel is composed of iron and carbon

The core problem for the preservation of metals is the spontaneous process of corrosion towards which they naturally tend [10]. The instability of metals is inherent to their nature. Indeed, it is a thermodynamically favored phenomenon. The cause of corrosion is the natural mechanism by which any metal reaches an equilibrium with the surrounding environment in a stable state. A stable state of a metal is, usually, one of its naturally occurring minerals rather than its metal form and that is the reason for corrosion to occur. Most metals naturally exist in the state of ores, which can only be converted to pure metals using an input of energy. Consequently, the need to release that energy to

fetch a more stable state will initiate the corrosion mechanism.

Corrosion can be described as the interaction of metal with its environment, resulting in the changes of its properties and characteristics [11]. Most common examples refer to oxidation of metal in air or aqueous environments. The presence of a liquid electrolyte, either as moisture or as a thin water film, the basic dual presence of water and oxygen along with the characteristics of the surrounding environment rule and meddle the phenomenon [12–15].

Corrosion is a major industrial concern, which alters metals' original features and represents a tremendous economic loss in whichever sector, as well as a conservation issue in the heritage field. Corrosion costs is estimated between 1% and 5% of yearly gross domestic product (GDP) for any country [16]. Indoor corrosion is usually overlooked compared to its outdoor counterpart. This is due to atmosphere control (i.e., filtration, dehumidification, temperature control, air flow design) combined to an attenuated concentration of contaminants or corrosive agents which results in a lower corrosion rate [17][18]. However, depending on the level of control the environment remains aggressive to metal objects, especially in some reserves where the relative humidity of the atmosphere plays a great role, in terms of presence of liquid electrolytes. Therefore, indoor corrosion shall not be ignored. The two main corrosive agents are chloride ions and sulfur compounds but other compounds, mainly pollutants, are also involved (i.e., organic compounds, CO, SO_2, NO_2, O_3, particulate matter). Indoors, inorganic ionic substances as well as organic molecules accumulation is primarily due to adsorbed sulphate aerosol particles [19].

The alteration of a metal depends on its nature and on the environment pH, along with oxidizing or reducing power [16,20]. A metal can display three different behaviors:

- Inert – the metal does not react with the environment. The corrosion mechanism does not take place.
- Active – the metal reacts with the environment, corrosion mechanism occurs, and the resulting corrosion products are reactive, i.e., non-stable.
- Passive – Corrosion mechanism forms a thin, compact and inert layer of corrosion products that are not reactive, and which hence forms a protective film, slowing down further corrosion.

In this work, the focus will be put on the corrosion of indoor metals and specifically copper and silver tarnishing and iron oxidation. The phenomenon called tarnishing, can be described as a thin layer of corrosion that forms mainly over silver, copper, brass but also other metals including aluminum. It can be considered a passivation of the metal, as it is self-limiting, and the formed layer will protect the underlying ones from reacting. On silver and copper, the layer is usually comprised of sulfides. In contrast, iron oxidation forms a tough porous coating of iron oxyhydroxides that adheres more loosely, allowing further corrosion. Details of these phenomenon are provided in the following section.

1.1.1 Iron and steel

The Iron Age began around 2000 B.C., when iron became dominant for tool production. Pure iron is a grey-whitish metal, relatively soft. It rusts very easily, and this is why it is often combined with other elements, in particular carbon (C), to obtain steel (0.2-2%$_{wC/w}$), cast iron (2-4%$_{wC/w}$) or other special alloys to make it harder and more resistant. Iron is broadly used because of its abundance. Iron-based alloys have been used for a variety of purposes including chains, nails, horseshoes, helmets, armors, construction structures and more recently, railroads, kitchen tools, weapons such as Damascus knives but also pigments such as ochres, which contain iron oxyhydroxides and oxides [21].

Formation of rust can be caused by impurities, mainly dust or acidic compounds in the indoor environment. Indeed, all these impurities are susceptible to attract and retain humidity against the surface of the metal and therefore encourage localized corrosion. Globally, it is accepted that rust is composed of ferrihydrite $5Fe_2O_3{\cdot}9H_2O$ and α-, β- and γ-FeOOH, respectively goethite, akageneite and lepidocrocite [22–24]. In rare cases, chloride ions present in sweat can lead to the formation of active rust, as akageneite β-FeOOH [25]. The formation reaction is resulting from a redox reaction (1.1, 1.2, 1.3), and involving the following processes (1.4):

$$Fe_{(s)} \longrightarrow Fe^{2+} + 2\ e^- \quad (1.1)$$

$$O_2 + H_2O + 4\ e^- \longrightarrow 4\ OH^- \quad (1.2)$$

$$2\ Fe + O_2 + 2H_2O \rightarrow 2\ Fe(OH)_2 \quad (1.3)$$

$$4\ Fe(OH)_2 + O_2 \rightarrow 4\ FeOOH + 2\ H_2O \quad (1.4)$$

Fe^{2+} ions produced in the initial reaction are then oxidized by atmospheric oxygen following reaction (1.5), to then produce insoluble hydrated oxide containing Fe^{3+}, e.g. ferrihydrite.

$$4\ Fe^{2+} + O^2 \rightarrow 4\ Fe^{3+} + 2\ O^{2-} \quad (1.5)$$

$$Fe^{3+} + H_2O \rightarrow 2\ Fe_2O_3{\cdot}xH_2O + H^+ \quad (1.6)$$

In a controlled atmosphere, iron-based alloys, which are corroded, often display a layer of orange reddish oxides, also known as goethite, α-FeOOH. As long as the relative humidity (RH) rate stays below 65%, this form of rust is stable and assumed to be a non-reactive phase with an important protective ability [26]. In the presence of moisture and at pH between 5 and 7.5 [27], goethite turns into lepidocrocite, γ-FeOOH, which is of an orange vivid color and is believed to play an active role in the corrosion mechanisms. Indeed, lepidocrocite is the non-compact crystalline polymorph of goethite and is less stable. Some authors have studied the consequences of the goethite-to-lepidocrocite content ratio

in the rust layers, also reported as the "protective ability index α/γ » [28]. In the case of a ratio greater than 2, the rust layer is quite stable – assuming it is dense enough [29].

The red-orange aspect of rust is the reason for the removal of the iron oxyhydroxides layer, as a grey appearance is often preferred for historical indoor objects.

A fundamental tool for interpreting electrochemical phenomena is a potential-pH diagram. Also called Pourbaix diagram, it allows to determine the regions of thermodynamic stability of a metal and its corrosion products in a given environment, usually water with pollutants. It is presented at fixed temperature, with axes of pH and E (oxidation or reduction potential of the system). The area between the dotted lines is the region of thermostability in water. They allow to foresee if corrosion can occur and to estimate the composition of the formed corrosion products. The Pourbaix diagram of iron is shown in Figure 1.2.

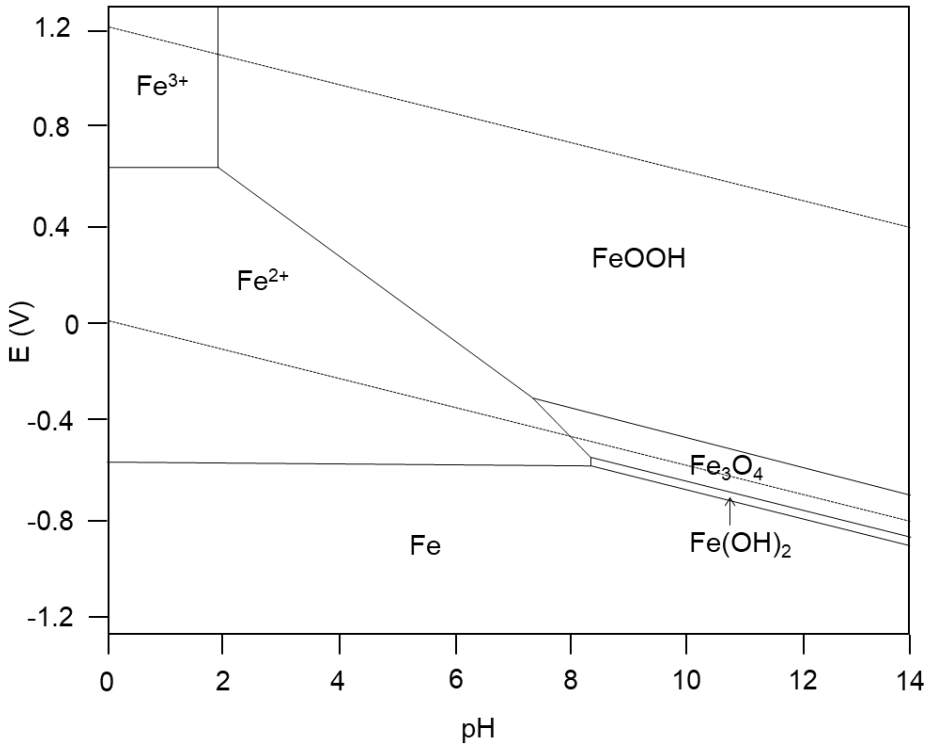

Figure 1.2 Simplified Pourbaix diagram for an iron-water system at 1 atm and 25 °C, extracted from [30].

1.1.2 Copper and its alloys

Copper is one of the first metals used by mankind, its first used is reported to 8500 B.C. It has been exploited by native populations on all continents [31]. Pale red or pinkish in its pure state, copper has interesting mechanical properties thus presenting a good machinability. It is non-magnetic but is an excellent thermal and electrical conductor [1]. Because it is soft, it is often alloyed with other metals to strengthen it, in particular zinc (Zn) to obtain brass, and tin (Sn) to obtain bronze but also a combination with nickel and zinc to obtain nickel silver, used as a dupe for silver [32].

A non-exhaustive list of its use throughout history includes water pipes, roofs, tools, mirrors, and artistic purposes uses such as painting substrates or green/blue pigments (e.g., malachite, azurite). Brass is and has been widely used for weapons, lamps, jewels, musical instruments whereas bronze is more common for historical monuments, bells or coins [1,11,31].

In whichever environment, the very first corrosion product formed on copper alloys is a passive layer of dark-red to orange-red cuprous oxide (cuprite, Cu_2O) [11,33–35] formed following the reaction (2.1). However, some serious corrosion studies [36], raised a scientific controversy, stating that copper may be corroded by pure oxygen-free water, with respect to reaction (2.2).

$$2\ Cu_{(s)} + ½\ O_2 \rightarrow Cu_2O_{(s)} + 2\ H^+ + 2\ e^- \quad (2.1)$$

$$2\ Cu(s) + H_2O \leftrightarrow Cu_2O + H_2 \quad (2.2)$$

This layer is formed instantly after exposure to the environment, but the rate of formation decreases overtime, resulting in a rather thin layer not exceeding 50 Å most of the time [37].

Cuprous oxide protects copper in a dry atmosphere. In the presence of water as an adsorbed film, the metal reacts with sulfur in its reduced form (e.g. hydrogen sulfur H_2S) arising from materials used in display cabinets, storage rooms (e.g. vulcanized rubber) and objects (wood) [38,39]. The metal reacts with sulfur, giving way to dark copper sulfur compounds like covellite but mainly chalcocite [1,40], following this reaction:

$$2\ Cu_{(s)} + H_2S \rightarrow Cu_2S_{(s)} + 2\ e^- + 2\ H^+ \text{ [41]} \quad (2.2)$$

In addition, sometimes, sweat, volatile organic acids, dust, contact with other objects during long-time storage or other residues at the surface of copper-based objects can cause fingerprints or punctual green corrosion, mainly hydroxide sulfates (brochantite $Cu_4SO_4(OH)_6$, antlerite $Cu_3(OH)_4SO_4$, posnjakite $Cu_4(SO_4)(OH)_6{\cdot}H_2O$). As example for brochantite, the most identified copper sulfate, an overall formation reaction is proposed here:

$$2\ Cu_2O + SO_2 + 3\ H_2O + 3/2\ O_2 \rightarrow Cu_4SO_4(OH)_6 \text{ [42]} \quad (2.3)$$

The copper water-sulfur system Pourbaix diagram can be consulted in Figure 1.3.

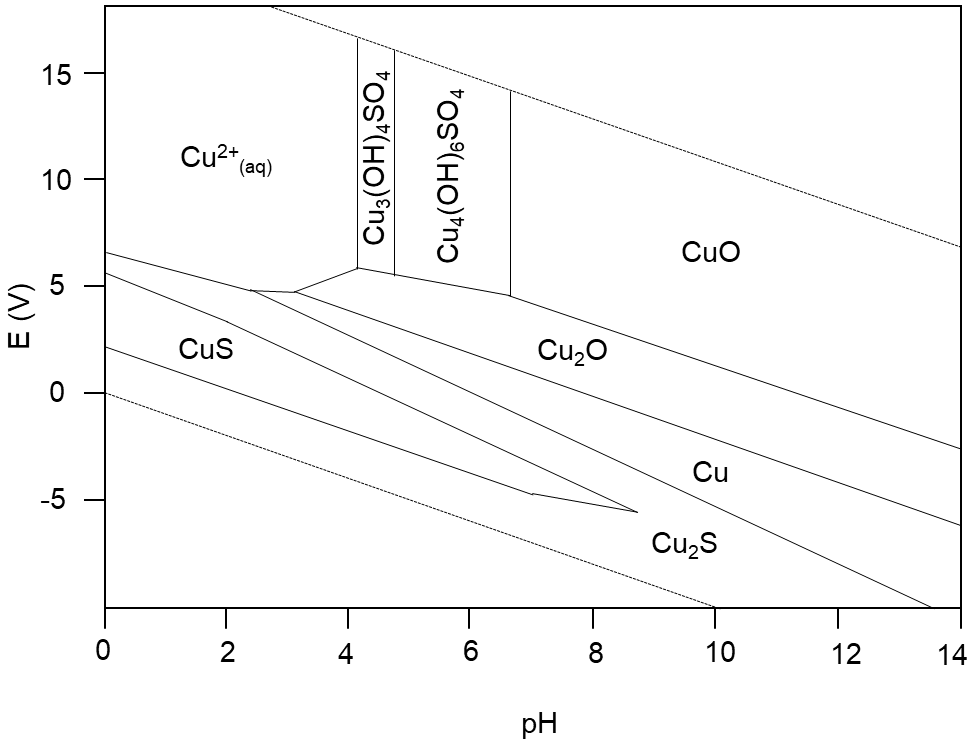

Figure 1.3 Pourbaix diagram for a copper-water-sulfur system at 1 atm and 25 °C, reproduced from [43].

On copper-alloys in indoor environment, encountered corrosion products are mainly similar to the ones found on pure copper although minor presence of tin corrosion products have be identified for bronze alloys [32]. The most commonly identified corrosion product on bronze is cuprite [42]. Regarding brass, a well-known phenomenon must be mentioned: dezincification. For some high zinc- content Cu-Zn alloy, zinc will be preferentially removed during the corrosion process [15]. *Dezincification is more common in high chloride ion-containing environments and is therefore disregarded in this work as indoor environments are not considered leading to high concentrations in chloride ions [44].*

1.1.3 Silver and its alloys

Pure silver is a white ductile metal. It is often associated to copper to harden it and improve its properties. It has been exploited by indigenous civilization in America and Asia as well as Europeans during the Roman period for jewelry and coins. Europeans used it in higher proportion when they brought it back from their 18th century expeditions for silverware, ornament art but also for photography process. Silver is a noble metal and has been highly appreciated from ancient times to the present day. It is traditionally used decoratively and functionally in fine cutlery and tableware and is valued for its high luster and long life. It has also been widely used in electrical contact applications because of its high conductivity in addition to application in photographic processes [5]. Although silver is a noble metal, it is prone to corrosion due to the presence of pollutants in the environment.

Indoor, there are two main factors influencing the rate of atmospheric corrosion: relative humidity and gaseous pollutants [46]. The principal constituent of the tarnish layers on silver is acanthite, Ag_2S, with an overall reaction proceeding as in equation (3). The Pourbaix diagram of silver can be consulted on Figure 1.4.

$$4\ Ag_{(s)} + O_2 + 2\ H_2S \rightarrow 2\ Ag_2S_{(s)} + 2\ H_2O \quad (3)$$

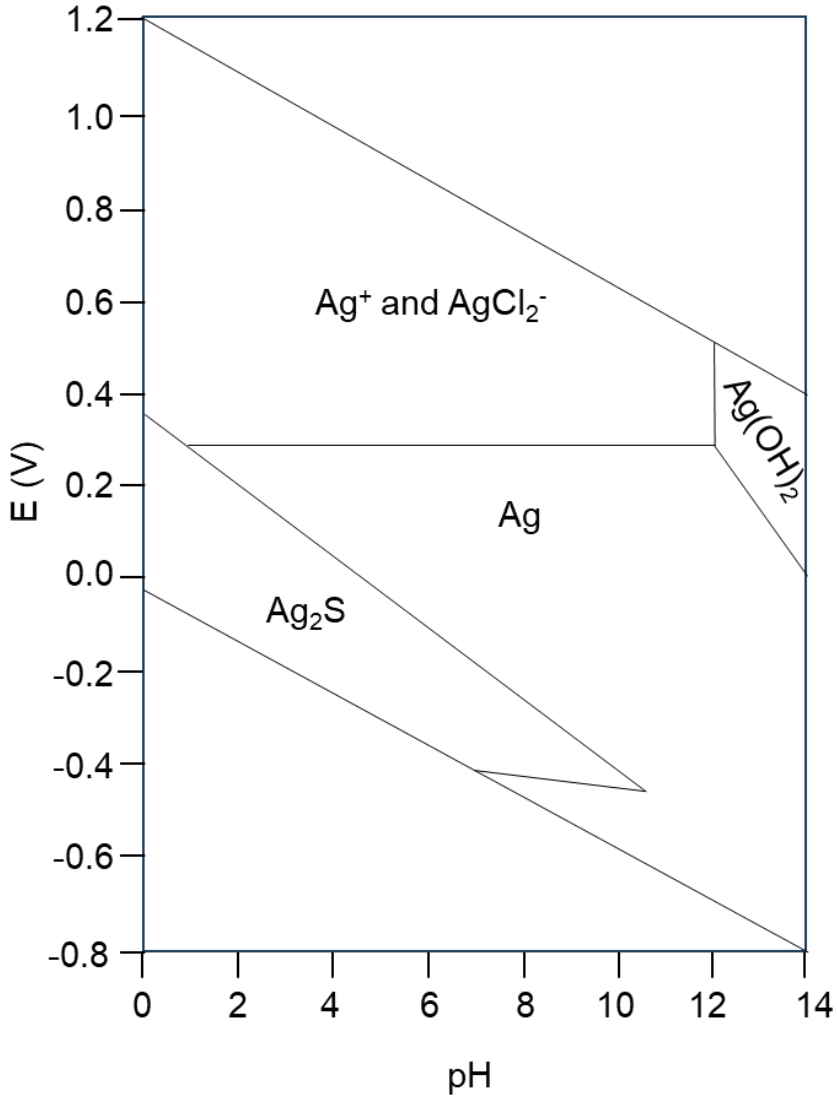

Figure 1.4 Pourbaix diagram for a silver-water-sulfur system at 1 atm and 25 °C, reproduced from [47].

Similarly to copper, associated pollutants are reduced forms of sulfur (H_2S, organic sulfur compounds) [48,49]. As stated by Vassiliou *et al.* [50], silver will start tarnishing at concentration of sulfur as low as 0.2 ppb, which is way below the concentration produced by museum visitors for instance, between 150 and 600 ppb in a 24 hours residence time and sufficient to initiate the tarnishing process [45,46,50,51]. As the tarnish film thickens, the color and reflection of the surface changes from light iridescent hues to a denser black layer [46]. This dulls the surface and detracts from appearance. Although rarely

dangerous for the object, tarnish is aesthetically displeasing and disturbs the legibility of many objects. Tarnishing starts to be visible at a thickness above 10-20 nm which corresponds to a slight yellowing and is considered unacceptable by conservators and curators [46,50].

Notably, most silvered objects are however not pure silver but alloys. The higher the amount of copper in the alloy, the faster the tarnishing rate, as copper corrodes faster than silver in the presence of sulfur compounds [52]. On top of that, the addition of copper not only has an effect on the corrosion rate but also on the type of corrosion products, leading to the formation of dark-blueish corrosion products, characterized as covellite (CuS) or chalcocite (Cu_2S), completely undesired on silver-based objects [46,53].

1.1.4 Chemico-physical properties of corrosion compounds under study

Based on literature data, seven corrosion products, representative for indoor corrosion or tarnishing were selected for this work (Table 1.1). These compounds present different properties including solubility product constant or oxidation state of the metal atom. According to the International Union of Pure and Applied Chemistry (IUPAC), the oxidation state of an atom is the charge of this atom after ionic approximation of its heteronuclear bonds, which is therefore closely related to its surroundings ligands [54].

The solubility product expresses the extent to which a solid will dissolve in a solvent (water in this case). In other words, the ratio between the solid and the concentration of its ions in a saturated solution. At a given temperature, the dissolution of a solid M_xA_y into an aqueous solution can be described as:

$$M_xA_{y(s)} \rightleftharpoons xM^{y-}_{(aq)} + yA^{x-}_{(aq)} \tag{4.1}$$

Using the law of mass-action, the following equilibrium constant K_{sp} is obtained:

$$K_{sp} = \frac{a(M^{y-}_{(aq)})^x \cdot a\left(A^{x-}_{(aq)}\right)^y}{a(H_2O) \cdot a(M_xA_{y(s)})} \tag{4.2}$$

With the activity a of H_2O and the solid M_xA_y equal to 1 in water and the activity of ions in an aqueous environment being the concentration of the ion it gives:

$$K_{sp} = [M^{y+}]^x \cdot [A^{x-}]^y \tag{4.3}$$

K_{sp} is called the solubility product constant. Its value relates to the degree to which the compound can dissociate in water. Hence the lower the pK_{sp} ($-\log(K_{sp})$) is, the more soluble a compound is.

Table 1.1 Summary table of targeted indoor corrosion products along with physico-chemical characteristics.

	Formula	**Name**	**Metal atom oxidation state**	**pK_{sp} at 25°C in water** [43,55–60]
Iron	α-FeOOH	Goethite	+III	42
	γ-FeOOH	Lepidocrocite	+III	42
Copper	Cu_2O	Cuprite	+I	15
	Cu_2S	Chalcocite	+I	49
	CuS	Covellite	+II	37
	$Cu_4SO_4(OH)_6$	Brochantite	+II	69
Silver	Ag_2S	Acanthite	+I	51

1.2 Cleaning metal artefacts [62,63]

In heritage conservation, corrosion is a dreaded reality as it implies the decay of ancient and/or valuable artefacts, therefore implying the potential loss of information and hindering the passing down to future generations. Preventive conservation and especially monitoring of the environmental conditions in relation to corrosion threshold values for the metals in question is a first step into avoiding intervention on an object. Unfortunately, sometimes, the latter is inevitable. In some cases, corrosion products, often tarnishing, can be desired, as they are visually pleasant or have historical and artistic values (traces of manufacture technique employed or ancient use, aesthetic and/or protective patinas). This can be acceptable if and only if the corrosion products are stable and not detrimental. In addition to the potential loss of the objects, decrease in the readability and aesthetics (shininess) of the object can occur. One of the first steps to artefact care is to determine whether the alteration is desirable, undesirable, or even detrimental. The context and the hazardous nature of the corrosion will determine whether it is conserved or removed during the intervention phase and influence the choice of treatment and its application.

Although there is often a first attempt to minimize the corrosion phenomena by the use of protective coatings, or the stabilization of corrosion layers, removal of the corrosion products can be foreseen to improve the aesthetics or readability of the objects (e.g., carvings blurred by the presence of corrosion products). Indeed, it is often sought for to go back to the original state of the object, especially for historical objects such as jewels, technical objects, musical instruments and religious objects but to also keep traces of the life of the objects as they are witnesses testifying of the past. This emphasizes the need for a controlled cleaning of these objects.

Cleaning is a critical step in conservation-restoration interventions as it removes unwanted layers from an artefact. It must be performed according to the nature of the corrosion compounds to be removed in addition to adaptively to the zone to be treated, avoiding any action on the original surface. To standardize the practice, the European Confederation of Conservator Restorer's Organization (ECCO) established a code of ethics [61]. Briefly, the guidelines suggest limiting interventions to the minimum necessary and focusing on the causes of the deterioration. Hence, cleaning treatments should focus on the controlled elimination of compounds interacting with the objects from the surface, recovering an acceptable visual aspect of the artwork.

Cleaning of metals contrasts from other materials in the very nature of what is discarded. In other fields, cleaning usually involves the removal of "dirt" which can be simplified as exogeneous and/or oily material deposited on the original surface, or altered varnish layers. Usually if dirt appeared through the use of the object, it can be claimed that it represents part of the object's history and should not be

discarded in the same way than dust accumulated during inadequate storage. In the case of metals, the situation is even more delicate as corrosion does not represent extrinsic matter accumulated on top of the original surface. Corrosion is the original material transformed into another form. Corrosion removal is actually a removal of part of the original substrate itself. Previous conservation practices would not always respect the integrity of an artefact when treating [62], resulting in the loss of the original surface (OS). Because corrosion is part of the original material constituting the object, the definition of the original surface of metal is complex. A definition has been theorized by Bertholon [63]. For archeological objects it is the surface of an object when it was abandoned, whereas for historical objects the definition is more ambiguous as it depends on the artefact's nature (e.g., last used for a tool, original patina for a sculpture).

Although improving nowadays, little attention is paid to the possible loss of information that could occur during the conservation treatment. Confidence in conservation practices suffered serious damage from overcleaning of artefacts, the use of improper chemical treatments and various other practices that were not sufficiently controlled which posed safety and re-treatability issues [62]. The concept of reversibility and re-treatability has been theorized several times in conservation literature [64,65]. Although reversibility is believed to be unattainable, especially for cleaning which is an irreversible process as any interventions will remove portions from the object, some recommendations must be kept in mind to choose the best treatment: possibility for objects to return to their conservation conditions prior to treatment, avoid of the use of materials whose future removal will endanger the object. Many cleaning protocols are based on chemical or physical procedures with potential negative effects for conservators' health and/or for the materials constituting the artworks. The choice of treatments is generally a compromise for conservators to ensure that assets outweigh the drawbacks and effort should be on associating the least interventive methods.

1.2.1 Current cleaning methods

An optimal cleaning treatment for metals should remove the corrosion and/or tarnish substances without affecting the underlying surface. To simplify, the techniques employed to eliminate corrosion products are classified in three principal groups: mechanical, chemical and electrochemical techniques [57]. Novel techniques are also being explored by scientists, for instance laser, which is expensive and hard to access, or plasma cleaning, still in need of finetuning before a implementation by stakeholders [66–68]. It is particularly important to keep in mind that any cleaning procedure carried out by a conservation professional depends on the type of object, the expected outcome, the conservator's skills, and available equipment.

1.2.1.1 Mechanical cleaning (abrasion)

Mechanically cleaning a metal surface consists in removing the undesired corrosion product resorting to an external force, whether by picking it off with a tool (scalpel, cotton) or rubbing with another material (abrasive paste, sandblasting, brushing). It is currently the most used option for metal cleaning in heritage conservation. It has been reported for iron [69], copper and silver substrates [70,71]. Although extensively spread techniques, dexterity and know-how are necessary to use scalpels or rotary tools. The efficacy of the cleaning depends upon the hardness of the material in contact with the surface, the force applied, and the duration of intervention. Abrasive systems can be performed wet or dry, using different types of abrasive (e.g., SiO_2, Al_2O_3, calcium carbonate, walnut shells, glass beads), and if needed a fluid to suspend the abrasive (e.g., water, alcohol, paste). Sometimes, a substrate to carry the mixture is necessary, and can even be used alone as the rubbing action can be sufficient in some cases (e.g., cloth, cotton swab…). These abrasives may produce surface scratching, which can be avoided preferring the use of soft and small-sized particles for long polishing time [46].

Mechanical methods exhibit several assets including the ease of use and the applicability to small or large objects. In addition, and especially for silver, the color and gloss of the metal are back to the original aspect, which is frequently sought for when cleaning historical artefacts [72]. The level of control when cleaning the material is the most valued aspect for these methods, in the sense that the intensity of exerted forces can be adapted, and the overall intervention stopped rapidly if necessary. However, many studies report important mass losses with rotary tools and hard abrasives, such as multi-purpose metal polishes [72]. This unrestrained mass-loss deterioration, in addition to impairing the microstructure of the object, can have macro consequences, as successive polishing and scratches can ruin motifs on objects, a good example being on coins or medals. Their use is also discouraged on fragile objects due to the risk of breaking [46,58].

For silver polishing, a significant part of the mechanical treatments relies on commercial products, being more practical as they do not require any preparation steps. Then again, their precise composition is usually unknown, leaving uncertainty regarding any possible change to the formulation and therefore as regards the effectiveness and aggressiveness depending on the compounds present. In addition, commercial products are not always adapted to the intended use and can cause damage such as scratches or mass loss greater than expected [72]. Abrasive remains are thought to be easy to remove, as they can be seen to the naked eye. However, this is misrepresenting as for instance, invisible compounds from commercial products formulations (i.e., perfume, additives, surfactants) might remain on the surface and potentially induce further corrosion or tarnishing. In the case of silver, faster re-tarnishing was observed after mechanical cleaning as a bright new and reactive surface was exposed to the environment [70,72]. Finally, there is close to no selectivity when resorting to mechanical cleaning. Of

course, meticulousness allows to perform a precise work, but it is sometimes difficult to differentiate between compounds to be kept or removed, as some of them can sometimes be desired as part of the objects' history.

1.2.1.2 Electrochemical cleaning [71–74]

Electrochemical cleaning is rather uncommon for historical ironwork as the main consequence is the diffusion of chloride ions out of the object. To treat corroded ferrous objects, those are immersed in an alkaline electrolyte (i.e., NaOH). In the case of akageneite (β-FeOOH) presence in the iron oxides layer, which is deleterious to iron stability, the imposed current will free the chloride ions and lead to the formation of $Fe(OH)_2$ [75]. Moreover, there is no long-term assessment of post-treatment stability of iron objects after electrolysis, which makes it a rather rare cleaning technique used on iron objects.

About electrolysis of copper alloys, it is deemed aggressive and difficult to control, with a high risk of redepositing reduced copper. Consequently, electrolytic cleaning of sterling silver or any other silver-copper alloy is not favored as reduction of both silver and copper sulfide happens ($E°Ag = 0.7996$ V, $E°Cu = 0.521$ V [21]). This results in deposition of metallic copper on the silver object surface, altering the original visual aspect of the object. To overcome this downside, one must verify the composition of the silver-based artefacts to avoid any unexpected poor outcomes. In case of silver-copper alloys, the cleaning is performed in two steps: initial chemical removal of copper corrosion products and subsequent electrolytic cleaning of silver.

Silver is probably the historical metal substrate for which electrochemical methods are the most performed, resorting to galvanic or electrolytic reduction. In the first case, a lesser noble metal (e.g., aluminum or zinc) becomes the anode and corrodes while the most noble metal, silver, remains uncorroded. It gives way to a secondary hydrogen-forming reaction, which allows to reduce silver sulfide to silver and form H_2S gas. In the second case, electrolytic reduction, an external source of energy (i.e., battery, potentiostat) is used to reduce the corrosion products to elemental silver. The most common electrolytes employed by professionals are sodium sesquicarbonate, NaOH, $NaNO_3$ or KNO_3 [70,76]. Therefore, the final aspect after electrochemical cleaning is dependent on the type of silver, which can turn unacceptable in regard to conservation practices and ethics, unless it is combined with other methods, in particular chelating agents.

One advantage of electrolytic methods is their degree of control, as the imposed potential can be matched to specific reduction processes. They are also useful for large objects, as electrolytic treatments can be run for long periods of time with little input from the conservator thereby saving labor. Oppositely to mechanical and chemical methods, electrochemical cleaning does not result in original metal loss, or almost negligible after successive cleanings. This is because the process simply implies to

reverse the chemical reaction of oxidation that damaged the object surface in the first place. However, this silver sulfide to silver reduction preserves the silver sulfide morphology, thus resulting in a rough surface, making the metal more reactive than after a mechanical cleaning. In addition, this method is not frequently used as is requires advanced equipment and skills [72]. However, when assembling is done, cleaning of small objects is quick. The recent development of electrolytic portable tools (PLECO pencil) allows better handling by conservators that do not have extensive electrochemical backgrounds and also in-situ measurements and therefore could help spreading the technique [77].

1.2.1.3 Chemical cleaning [71,74]

Chemical cleaning of metals refers to the use of a chemical reagent, often in aqueous solution, to solubilize otherwise insoluble metal salts [24]. Chemical cleaning is often combined with mechanical cleaning, for instance with the rubbing of cotton swabs dampened with chemical reagent solutions. The above-mentioned polishing pastes sometimes contain chemical reagents (i.e. ammonia) in order to enhance the cleaning performance [70].

The first approach to the chemical cleaning of corroded metals involves complexing agents that represent strong ligands for metal ions. Chelators are polydentate complexing agents; organic or inorganic compounds capable of surrounding di or tri-valent ions such as those of copper and iron. The ligand contained in the sequestering agent binds the ion to form complex ring-like structures called 'chelates', either with covalent or co-ordinate bonds. In the case of complexation for cleaning purposes, the formed compounds are soluble [24].

These agents, such as the sodium salts of ethylenediaminetetraacetic acid (EDTA) and Tri ammonium citrate (TAC), have been used extensively in conservation in attempts to mitigate corrosion products without causing harm to the base metal. It has been used to clean iron and copper alloys [24,46,71]. In addition, these chemicals, in particular EDTA, are scrutinized for their environmental toxicity [78]. Indeed, there are some concerns about its poor biodegradation in conventional wastewater treatment plants and natural environments, and its effect in mobilizing heavy metals from solid phases to pose a risk to groundwater [79].

As much as there are studies assessing the action of chelating agents, literature is rare when it comes to having an exhaustive comparative overlook assessing different methods on different alloys. It is therefore up to conservators to appraise studies or perform test patches on the object they plan to treat. Concerning iron oxides, a variety of chelating agents is being employed for their dissolution, including forth-mentioned EDTA but also citrate ions or salts of other carboxylic acids, such as oxalic, ascorbic and tartaric acid, used for their low pH which will exclude iron oxides from their stability region and solubilize them (cf. Pourbaix diagram, Figure 1.2) [24].

Regarding cuprous chemical corrosion removal, it can be achieved thanks to several approaches using chelating agents such as Na_2EDTA, tetraethylenepentamine (TEPA), diethylenetriaminepentaacetic acid (DTPA), tri ammonium citrate (TAC), or reducing agents [80,81]. On copper-based alloys, similarly to iron, carboxylic acids including citric acid are reported as being efficient [82]. Although complexing agents exhibit low aggressivity towards metallic copper [71], damage is observed on the metal surface after immersion in *stripping* agents like formic acid [83]. The chelator EDTA is currently extensively resorted to as it is effective on most of copper corrosion compounds. Still, a study examining reaction of Na_2EDTA on copper revealed that chelation rate varied according to corrosion products present [84]. This would result in selective removal of corrosion products which is an asset as it implies being able to control which compounds to keep, in case some of the present degradation compounds need to be preserved on the surface. However, this selectivity implies more parameters to be taken into account than solely the ligand, in particular the pH, which influences the stability region of the corrosion product as well as the ligand's complexing abilities, the solubility product constant K_{sp}, and the so-called formation constant (K_f), which will be developed further in the manuscript.

For silver, chemical methods are less common. Because Ag_2S is close to insoluble in water [72], stripping it with organic acids or complexing agents is ineffective, apart from the use of nitric of sulfuric acid, which are hazardous. Other chemicals such as thiourea acid solutions have been employed due to their fast-cleaning effects and ease of use. Conservators have reported the need of skilled manipulation in order to avoid damaging objects [72]. Therefore, thiourea acid solutions, popular in the past, are now only barely used due to their side effects. Furthermore, this chemical substance has been suspected to cause skin disease of the operators [85].

Overall, traditional acid stripping solutions can be aggressive to metal and corrosion products alike as their action cannot be tuned, and are only relevant where it is ethical to remove all corrosion products [86]. Chelating agents, on the other hand, can be slow to act and may be more selective in their action on corrosion products. Careful study is essential to obtain suitable pH values for optimizing complexation. As mentioned, nowadays conservators commonly resort to EDTA and DTPA which are synthetized compounds and known to be persistent when released in water and in the environment and that can have deleterious effects [78].

It is not possible to control the rate and to stop a chemical cleaning process as promptly as mechanical cleaning to avoid potential damage of the object. Furthermore, all stripping methods require post-treatment clearances to remove residual chemicals that would continue to corrode metals due their acidic nature for instance. In addition, the penetration of chemical solution in the corrosion layers desired to be kept is a concern for long-term fragilization of the objects.

In addition, all chemicals require to be handled with care, as most of them are irritant for the end-user's skin. Cleaning methods which employ water or other liquids are more difficult to control than dry cleaning techniques and their application to metal is contradictory with the inherent sensitivity of metal to moisture.

1.2.2 Drawbacks of current cleaning methods

Forth-mentioned solutions to mitigate corrosion definitely all display drawbacks that cannot be overlooked, either in terms of environmental impact, risks for the artworks and/or health issues for conservation professionals (table 1.2). In addition, these well-established techniques are sometimes unsuitable when the metal is near sensitive materials (e.g., silver threads in textile, metal inlays on wooden statues) because they result in the inevitable chemical damage or mechanical scrape of the very sensitive organic materials. The lack of a problem-free method to remove corrosion is the reason that at present some objects' cleaning is problematic [77]. As both chemical and mechanical techniques can damage the underlying metal, there is a great deal of interest in developing new cleaning technologies which are less aggressive to the metal surface underneath the corrosion layer.

Table 1.2 Recapitulative assets and drawbacks of common cleaning methods for iron, copper and silver objects along with main target metal.

	Mechanical (Fe, Cu, Ag)	**Chemical (Fe, Cu)**	**Electrochemical (Ag)**
Assets	- Ease of use - High level of control (pressure, end of treatment, fine-tuning of abrasive)	- Selective cleaning sometimes possible	- Degree of control - No metal loss - Applicable to large and small objects - Adapted to tarnished silver
Drawbacks	- High dexterity required - Surface scratching - Mass-loss - Inadequate for fragile objects - Lack of selectivity - Commercial products can be inadequate and contain undesired additives	- Acids can damage metal substrate - Not applicable to silver - Action can be slow or too fast (low control rate) - Persistence of some chemicals in the environment - May be hazardous to human - Eventual residual substances are deleterious	- Long-term efficacy questionable - No applicable to copper-containing alloys - Not applicable to copper or iron - Rough surface obtained after treatment / increased silver surface reactivity - Requires advanced skills - Requires advanced equipment

To solve a difficult problem, nature can be used as a source of inspiration. In recent years, the development of environmentally friendly methods has become a significant alternative towards more sustainable practices [81,87]. Confronted with the transmission of heritage to the next generations, stakeholders in the field have also a major role to assume towards a global societal change. With the aim of developing more sustainable alternatives without conceding on the treatment performances or the safety of the artworks, different solutions carried out by conservation scientists emerged [88].

Research on innovative cleaning methods is now moving towards biotechnology by searching for new chemicals, exploiting the specific metabolic capabilities of microorganisms and enhancing the properties of enzymes, for the bioremediation of polluted artworks. Many successful biotechnologies using microorganisms have been developed to restore or clean a variety of objects [61,89].

1.3 Microbes in cultural heritage conservation

1.3.1 Microbially Induced Corrosion

In popular belief, microorganisms are often associated with deleterious consequences for the preservation of cultural heritage. It is a fact that microorganisms are a major cause of deterioration on cultural artefacts of any type of substrates [90]. Microbial processes, including bioweathering (rocks and ores), biodeterioration (organic substrates) or biocorrosion (metals), thus contribute to irreversible changes or even worse, loss of valuable heritage [91,92].

On metals more specifically, microbially induced corrosion is a great concern, and not only regarding cultural heritage. Microorganisms have long been known to influence or even initiate corrosion, causing corrosion of pipe tubes 10 to 1000 times faster than normal [93]. This phenomenon is called Microbially Induced Corrosion (MIC). It is not a form of corrosion in itself but can accelerate most forms of corrosion (i.e., crevice, pits, galvanic etc.). MIC can be attributed to multiple microorganisms including algae, fungi, and bacteria. Recent papers have studied the influence of bacterial communities composition on bronze outdoor decay [94]. The availability of oxygen has also been found to be a major factor in corrosion of metals in saltwater environments, typically on archeological findings [92,95]. Microorganisms' reproduction, resulting in a biofilm on a material's surface, will create in a microenvironment. Consequent changes in pH, dissolved oxygen, or metabolic reaction such as hydrogen, sulfide, ammonia, organic acid or even inorganic compound production can lead to reactions which increase corrosion rates [96]. MIC has been mainly attributed to several groups of microorganisms, such as Sulfate reducing bacteria (SRB), Sulfide oxidizing bacteria (SOB) and acid producing fungi [93]. Most damaging corrosion takes place in the presence of a multispecies biofilm [96]. SRB are anaerobic microorganisms that can survive in an aerobic environment for a period until finding a compatible environment. They chemically reduce sulfates to sulfides, producing compounds such as hydrogen sulfide (H_2S), or iron sulfide (Fe_2S) in the case of ferrous metals. SOB are aerobic species which oxidize sulfide or elemental sulfur into sulfates. Some species oxidize sulfur into sulfuric acid (H_2SO_4) leading to a highly acidic ($pH \leq 1$) microenvironment. SRB are often found in conjunction with SOB [93].

1.3.2 Microbially induced remediation of metal artefacts

Microorganisms drive the elemental cycling on Earth. As much as some microorganisms have been the cause of a problem, it is usually the case that other microorganisms are involved in opposite pathways and therefore can be beneficial for conservation process [97]. As the saying goes, one man's trash is another man's treasure. Some metabolic reactions considered harmful for some artefacts could well be

beneficial for other problematics. As an example, *Streptomyces sp.* is considered responsible for the deterioration of mural paintings through biomineralization and biopigment production [98]. However, it also has the ability to produce siderophores, which is an iron-uptaking compound that has also been used in cultural heritage conservation for contaminated wood [99].

Likewise to what mankind has achieved throughout history, for fermented food or waste water treatment, it appears that biological metabolism can be profited from to safeguard heritage and substitute current treatments [100]. This gives way to new perspectives for the development of methods and resources for the conservation of cultural relics, with potential improvement in terms of sustainability, effectiveness and toxicity. Microbial mechanisms are exploited aiming to consolidate, clean, stabilize or even protect surfaces of cultural items. Successful examples of application of bioconservation methods have been well documented in previous literature for various substrates like stones [101,102], paper [103], textiles [104], wood [105], paintings and other polychrome works [106,107]. For many years now, biomineralization, i.e., the formation of biogenic minerals, has also been studied for the benefits in preservation of heritage materials. Stone monuments, mural paintings, frescoes, mainly those compose of carbonate minerals such as limestone and marble, have profited of carbonatogenesis, a process where calcium carbonate compounds precipitate due to microbial metabolism. Interestingly, bioconservation is less common for metal artefacts.

1.3.2.1 Biomineralization of metal objects

Metal substrates, in particular iron and copper, have also profited from biomineralization treatments. In the last decade, it has been studied at the University of Neuchâtel, Switzerland. Specifically, copper-based artefacts have been treated with fungal strains reported to form biogenic oxalates, an ability that allows the transformation of metal compounds into metal oxalates. The capacity of fungi to transform copper compounds into copper oxalates (CuOx) has been exploited in the field of soil remediation and applied to copper-based artefacts in order to obtain biopassivation of the treated surfaces [108–110]. Metal oxalates, and in particular copper oxalates, create attractive compact patinas that are not associated with cyclical corrosion, providing a good protection of the surface [109,110]. The entomopathogenic fungi *Beauveria bassiana* converts reactive copper phases and reaches up to almost 100% conversion of copper corrosion compounds such as copper hydroxy sulfates and hydroxy chlorides into chemically stable copper oxalates [109,111]. The occurring processes behind this bio-based treatment have been investigated. The metabolic pathway seems to first transform CuCl into copper hydroxy chlorides, which are then turned into CuOx under the action of the oxalic acid secreted by the fungi [112]. The solubility of the metal compounds appeared to be determinant in the preference of fungal uptake: oxides are more likely to be taken up compared to elemental metal, allowing a

controlled action of the bio-based treatment [108]. Furthermore, biogenic CuOx can be considered as a protective system. The minerals formed blend into the natural corrosion patina, creating a compatible passivation layer that is more effective than current coatings. Indeed, results showed a better weathering resistance than usual protective systems or corrosion inhibitors, such as microcrystalline waxes or BTA respectively, thus ensuring the bio-based treatment provides a more efficient corrosion mitigation over time [113].

Similarly, for the biomineralization, hence stabilization, of archeological iron artefacts in the presence of chlorinated compounds, alternative methods using bacteria were investigated. Several species were able to reach the reduction of iron compounds, in particular akageneite β-FeOOH, into stable biogenic minerals simultaneously to the diffusion of chlorides out from the treated object [114]. Promising results showed the removal of the harmful corrosion layer without altering the metal substrate underneath [115–117]. Fungal strains have also been assessed, including *Beauveria bassiana* [114]. However, it turns out that they are not the best candidates to stabilize corroded iron but showed potential for dechlorination [118]. An overview table of the studied mechanisms is provided in Table 1.3.

Table 1.3 Overview of studied mechanisms for the stabilization of archeological iron artefacts.

Tested strains	Type	Obtained minerals	Remarks
Desulfitobacterium hafniense TCE1 [117]	Bacteria	Homogenous layer of mixed stable iron minerals, vivianite $Fe_3(PO_4)_2 \cdot 8H_2O$ and magnetite Fe_3O_4 layer	Medium influence the obtained mineral phases, influencing the color of the formed layer Abiotic reduction of iron may be because of Na_2S in the medium
Shewanella îoihica [115]	Bacteria	Iron phosphates and iron carbonates (siderite, $FeCO_3$).	Need of chloride ions supply
Aeromonas CA23 and CU5 [115]	Bacteria	Vivianite and siderite	Partial reoxidation, fish pathogenicity of *Aeromonas* strains
Beauveria bassiana S6 [118]	Fungi	Iron oxalates	Obtainement and identification is not always replicable

1.3.2.2 Biocleaning of metal objects

In recent decades, biological cleaning has greatly improved as a result of research into biotechnologies and today plays an important role in the preservation and restoration of cultural assets. Nowadays, biocleaning by viable bacterial cells or hydrolytic enzymes represents a resource with great potential, decreasing risks for artworks and for human health. Again, it has been applied to different problematics including the removal of organic substances, black crusts, and mineral salts from different materials such as stone, wall paintings, etc. Moreover, different metabolisms have been exploited to different treatments all-leading to the recovery of the surface original appearance [88,119].

When it comes to metal substrates, as discussed in section 3.2.1, research has focused on stabilization and passivation of iron and copper alloys with remarkable results. Although few attempts have been made to develop a bio-based method for the removal of corrosion products from metals [58,120], exploitation of microbial properties for biocleaning is lacking.

Microorganisms can work as micro-chemical factories to bioaccumulate some metals. To exploit these abilities to remove corrosion, it is interesting to wonder why and how some species can achieve such actions.

Metals are essential for life. In particular iron and copper are important metals for biological processes, but as with many things, the dose makes the poison, hence those metals can also be toxic or biocidal. Especially, copper and silver are known to be strong biocides [121].

Uptake of metals and metalloids can be achieved by microbes in a plethora of ways. Organisms like microbes come up without various approaches as a way of fetching these nutrients in their environment or scavenging them to prevent them from entering the organism's cell walls [118]. Solutions for removing corrosion through biological compounds or pathways exist, involving either living microorganisms or their secondary metabolites.

Secondary metabolites are some of the most complex and important metabolites of industrial interest. They usually form at the end of the growth phase, in the stationary phase of microbial growth. Secondary metabolites usually share the following characteristics [122]:

- Not essential for growth and reproduction
- Their formation is highly dependent on growth conditions, especially on the composition of the growth medium
- They are often produced as a group of closely related compounds
- Usually overproduced, by contrast to primary metabolites that are linked to energy and growth and therefore cannot be significantly overproduced

Well-known secondary metabolites include enzymes or antibiotics such as penicillin[122]. For metal remediation, the focus will be put on the latter and especially on the following sub-categories: siderophores, Extracellular Polymeric Substances (EPS) and organic acids.

1.3.2.2.1 Low molecular weight organic acids

Low Molecular Weight Organic Acids (LMWOA), including citric, itaconic, phosphoric, succinic or oxalic acid possess chelating properties and are therefore reliable alternatives as complexing agents [123]. They are commonly available in nature as microbial metabolites deriving from soil matter decomposition, food fermentation, or allowing microorganisms to induce mineral dissolution. Most of them are well documented as safe and water-soluble products that are hence more ecologically friendly [124]. For example, citric acid broadly used in industry is obtained from fungal species, in particular *Aspergillus Niger* [125]. A wide selection of microbes have the ability to produce LMWOA [126,127]. For a long-time overlooked for heritage purposes, these biodegradable chelators have gained attention, in particular citric acid and Ethylenediamine-*N,N'*-disuccinic acid (EDDS) [128]. EDDS has recently been praised for having a chemical structure close to EDTA and similar properties without environmental

drawbacks. Not only is the [S,S]-EDDS stereoisomer biodegradable but can be produced by bacterial fermentation [129,130].

The fungi *Beauveria bassiana* mentioned above regarding biomineralization was revealed to have versatile application thanks to its production of oxalic acid and can be used as a chelator for metal ions, in particular copper [37]. The fungi, detecting metals, in particular copper, as toxic for itself, produces the acid in order to chelate the metal ions as extracellular metal oxalates [131], making them less harmful for its growth. The use of oxalic acid is mostly employed as cleaning method on coins [74], but its use from synthetic provenance is not recommended [132].

Citric acid is produced microbiologically by the mold *Aspergillus niger*. Citric acid fermentation is carried out aerobically in large fermenters and a key requirement for high yields is that the medium is iron deficient. This is because *A. niger*'s excretion of large amounts of citric acid can be obtained because the organism uses citrate to scavenge iron for uptake into its cell [122].

1.3.2.2.2 Extracellular Polymeric Substances

Extracellular Polymeric substances (EPS) are high molecular weight natural polymers secreted by microorganisms. They are the main component of biofilms matrix [133]. They are starting to gain more visibility in multiple fields of applications [134]. For instance, EPS from *Aureobasidium pullulans* can be used as thickener for the production of biodegradable plastics [135]. EPS are also employed in wastewater treatment thanks to the ability of the biosorbent matrixes to chelate toxic metals [136]. Furthermore, their production is also reported to decrease the corrosion rate of iron by the formation of an iron-EPS complex [137].

When studying the production of iron oxalates by *B. bassiana*, Comensoli *et al.* noticed that the fungal preferentially produces EPS [114], able to chelate iron [93], which is mentioned as a biocleaning potential.

1.3.2.2.3 Siderophores

One of the most promising bio-based materials for the removal of corrosion are siderophores. Siderophores are secondary metabolites produced by bacteria or fungi in conditions of iron-deficiency, iron being an essential element for some species. They are natural iron-specific complexing agents which could be a reliable alternative to chemical complexing agent. They are secondary metabolites used to fetch iron in iron-lacking environments to ensure the right development of the microorganism [138]. Their production has been detected in a large palette of microbes [138]. Siderophores can be categorized according to their functional groups [139]. There are three main types: catecholates, hydroxamates, and carboxylates. In addition, some of them display more than one of the moieties stated before; these are considered as mixed types [140].

They display a high affinity for ferric iron by forming complexes that can be then taken up by the secreting organism, turning Fe^{3+} into soluble Fe^{2+} in the cell membrane. Briefly, these metabolites can take up iron forming a ferri-siderophore complex that is recognized and translocated inside the cell. It is believed that the iron will be released from the complex following a reduction from Fe^{3+} to Fe^{2+} inside the cell, as the affinity of siderophores for ferrous iron is lower than for ferric iron. Fe^{3+} is a stronger Lewis acid than Fe^{2+}, therefore electron-pair donor groups present in siderophore molecules bind ferric rather than ferrous iron [141].

Notably, siderophores exhibit remarkably high iron binding affinities, making them serious competitors for synthetic chelators [141]. The affinity can be evaluated thanks to the formation, binding or stability constant K_f (or β) of each siderophore with metal ions, which is defined using the ratio between formed complexes and free ions. The higher the log β, the more stable the complex. In opposition to other complexing agents such as EDTA, siderophores show a specific affinity for iron, albeit they can bind other ions but to a lower extent [139].

Indeed, siderophores not only have the capability to scavenge iron but also to chelate a variety of other metals ions frequently encountered in metal artefacts, including Ag^{+}, Al^{3+}, Cr^{2+}, Cu^{2+}, Ni^{2+}, Pb^{2+}, Sn^{2+} or Zn^{2+} depending on the type of siderophores [142]. However, most of the time there is a lower binding affinity than for iron ions [143]. Indeed, their global "metallophore" properties can be accounted for by siderophores scavenging other ions to protect the bacteria from other metals toxicity if needed. The metal-siderophore complex binding constant thus must be lower than the one for the ferri-siderophore complex in order to prevent the siderophore receptor from the uptake of the toxic metal, acting as a Troyan horse and consequently having detrimental effects [144]. Table 1.4 shows different formation constants of general siderophores with common elements in metal cultural heritage [139,141,145,146].

Table 1.4 Characteristics of siderophores produced by bacterial strains *Streptomyces pilosus*, *Pseudomonas fluorescens*, *Escherichia coli* in comparison to Na_2EDTA.

Strain	***Streptomyces pilosus***	***Pseudomonas fluorescens***	***Escherichia coli***	**EDTA**
Main siderophore produced	Deferoxamine	Pyoverdine	Enterobactine	n/a
Siderophore type	Hydroxamate	Mixed	Catecholate	n/a
Log β Fe^{3+}	30.6	30.8	49	25.1
Log β Fe^{2+}	10.2	9.78	23.9	14.3
Log β Cu^{2+}	14.1	14.9	n/a	18.8
Log β Zn^{2+}	10.1	11.8	n/a	16.5

The variety of siderophores and siderophore types in nature shows an interesting potential ability to fine-tune the treatment according to the need and targeted product. For instance, a siderophore having rather high affinities with other ions might not be suitable for the cleaning of painted metals, as it could impair the paint layer by chelating pigments. This relative selectivity makes them polyvalent and extremely interesting for the treatment of alloys composed of different elements and presenting a mixture of corrosion products. In addition, some of them demonstrated biodegradable features, which is an important step towards complete sustainability and avoid environmental persistence as opposed to EDTA [147].

Siderophores have already been used for conservation purposes but not directly on metal objects. Their chelating action was compared to EDTA and DTPA in an attempt to remove iron stains from paper and wooden substrates [148]. EDS and colorimetric analyses proved the efficacy of the green chelators in terms of iron removal [148]. They have also showed their efficiency towards the preservation of waterlogged archaeological wood by removing iron sulfides. Siderophores were used to target Fe in iron sulfides [99,149].

1.3.2.2.4 Cell-wall uptake

In a comparable way than EPS, fungal biomass is of interest for the biosorption of metals, in particular into their cell walls. Recent studies investigated the fungal strain *Alternaria* sp. for the biocleaning of iron objects thanks to its ability to take up iron in its melanized cell walls, melanin acting as a chelating agent [150]. After a 4-week immersion in an alkaline medium, coupons showed a less reddish appearance and a decrease of the corrosion layer thickness compared to abiotic controls [114]. Indeed, under stress conditions, some fungal strains produce melanin pigments, which are recognized as metal-

binding compounds [151]. Other strains have received great attention regarding their ability to take up copper, usually toxic, in the biomass, such as *Aureobasidium pullulans* also using melanin [152,153]. Another reason fungal cell walls can be accounted for the uptake of metals is that they are composed of polymers, such as chitin and chitosan, which are known to chelate metals, in particular copper, but also iron [154,155].

1.3.2.2.5 Sulfur oxidizing bacteria

Another alternative for corrosion removal would be to rely on oxidation processes by specific microorganisms. Sulfur Oxidizing Bacteria (SOB) are promising candidates for the remediation of metal tarnish thanks to oxidation processes occurring in an aerobic environment. Extensively used in biohydrometallurgy for the recovery of metal, SOB can oxidize reduced sulfur forms (i.e. sulfides, elemental sulfur, thiosulfates, and sulfites) by either direct or indirect mechanisms [156]. The "direct" mechanism occurs when the bacterial membranes are in direct contact to the mineral surface, through enzymatic interactions [156]. On the other hand, the "indirect" mechanism does not require physical contact between the mineral surface and bacteria, the reduced sulfur forms are oxidized indirectly through ferrous iron oxidation using the growth medium. Briefly, the bacteria biologically oxidizes Fe^{2+} into Fe^{3+}. The metal is then chemically oxidized by this obtained Fe^{3+} which is reduced again to Fe^{2+} in the process. The microorganism then re-oxidizes this Fe^{2+}, completing the cycle and allowing further bioleaching. In the meantime, sulfuric acid produced by the biological oxidation of reduced sulfur compounds also promotes further metal solubilization [157].

Scott used the fascinating property of *Acidithiobacillus ferrooxidans*, a well-documented SOB, on copper outdoor weathered patinas [120]. The bioactive media was used to treat weathered surfaces of copper and bronze. It allowed to reveal the subjacent reddish-brown layer of copper oxides, mainly cuprite, with minimal or no loss of form and without exposing the original bare metal. This is possible because it occurs in an aerobic acidic medium [58], in which this bacteria can oxidize copper hydroxy sulfates, and due to the fact that the short application time does not allow the acidic solution to erode copper oxides and reach metal. An attempt with *Acidithiobacillus ferrooxidans* was also performed for the cleaning of the silver centerpiece by Wenzel Jamnister (1549, Rijksmuseum, Amsterdam) at the Utrecht University, to biologically remove Ag_2S [58]. The study explored both direct and indirect mechanisms to achieve the foreseen goals. Given the biocidal character of silver [158], the direct mechanism with SOB applied on the tarnished surface directly, resulted in the quasi-instant death of bacteria, hence annihilating any sufficient action to observe silver sulfide removal. On the contrary, the indirect metabolic pathway using ferric iron produced during the bacterial growth led to tarnish removal, although uneven. Unfortunately, SEM showed that the aspect of original metal surface was modified, as confirmed by an excessively high mass loss compared to the coupons' weight prior tarnishing [58].

Nevertheless, it has been achieved an extraction of elemental silver from spent silver-zinc button batteries in the absence of living bacteria, using only the cell-free filtrate that would be of interest for an easy use in conservation departments [159]. It is interesting to note that *A. ferrooxidans*, if it has cleaning potential, is a known MIC for iron and steel [93], highlighting the duality of microorganisms when it comes to heritage purposes, showing either noxious or helpful features depending on the context.

As underlined by the failure of the direct mechanism, silver is a strong antimicrobial [160]. Nevertheless, it might be possible to foresee breeding of higher bacterial silver resistance via gradual increase of $AgNO_3$ concentration in the culture medium to adapt Ag resistant strains, and then use UV mutation to further improve Ag resistance [161].

1.3.2.2.6 Nanoparticles

The fungi *Beauveria bassiana* has also been assessed for the protection of archaeological silver and iron artefacts with moderately successful results. *B. bassiana* has been found to biosynthesize silver nanoparticles (AgNPs) [109]. However, this only occurs when it is in contact with a solution of silver nitrate. Indeed, the microbiological process behind involves a nitrate reductase enzyme [162]. This makes difficult the implementation of the technology to silver conservation since most silver objects mainly display silver sulfides or silver chlorides as tarnishing compounds. It would require a preliminary step using HNO_3, a hazardous acid, to form $AgNO_3$, but which would also dissolve metallic silver. In addition, the esthetic aspect would not be acceptable as AgNPs are yellow to brown[163]. On top of that, on silver-copper alloys, a precipitation of green copper oxalates occurs, which is not esthetically acceptable for silver objects [109].

Similarly, bioproduction of iron and copper nanoparticles is potentially scientifically possible [164,165]. However, bioproduced iron nanoparticles are reported to be black, which does not comply with the desired aesthetics properties of the treated object. Similarly, for copper, different visual outcomes of the nanoparticles ranging from reddish-brown to violet are reported. It would require extensive control of the reaction to achieve nanoparticles of which size and shape would influence the optical properties and result in a color matching the original metal appearance [164,166,167].

1.4 Gels as carriers for heritage conservation purposes

The application of biological remediation to artefacts can be performed in solution, but conservators have always been using techniques trying to confine the intervention as much as possible (e.g., cotton swabs, compresses). To allow bio-derived components to be used in an even more controlled way, various methodologies are at the disposition of conservators to obviate the use of unrestrained cleaning solutions and allow for example chelating agents to be used in a controlled manner [168–171]; however, the most reliable, tailorable, and performing are certainly gels [172]. Historically, immobilized microbes in gels were first developed for in-situ production of enzymes because using free cells in liquid cultures has some disadvantages, including easy washout of microbes for instance [173].

At the beginning of the nineties, gels were introduced to the community of art conservation [174]. The focus was first on the cleaning of paintings as water- and solvent-sensitive targets [175]; thus, gel formulations seemed optimal for higher-controlled and less invasive interventions. Considering the promising evidences, this technique became rapidly captivating in several specializations, including wall paintings and stone care, followed by paper or wooden substrates [176–180]. Nowadays gel-based cleaning protocols are recognized as safe and are successfully applied , thanks to the high retention and interesting rheological properties of gels that allow a precise and selective intervention confined to the outermost layer [181,182]. In addition, such systems can adsorb the undesired substances to be removed (i.e., corrosion products and degraded protective materials) on the polymeric matrix. Finally, they drastically limit solvent evaporation thereby creating a less hazardous work environment for operators, allowing the use of lower amounts of reagents and giving the conservator a longer time to work and therefore better control over the treatment [183].

Although there is no clear definition, gels are accepted as being systems made of at least two components: a polymer and a fluid phase. The polymer, acting as a thickening agent, forms a three-dimensional network in the liquid medium [184]. This cross-linked system can trap the liquid, limiting simultaneously evaporation and release. The liquid circulates freely in this network but interactions with the polymer chains limit the evaporation. According to the chemical nature of polymers, the interactions between chains can be reversible thanks to weak bonds—i.e., hydrogen bonds, van der Waals—or irreversible in presence of covalent bonding. The different bonding leads to the formation of physical or chemical gels, respectively, displaying distinct features [172]. In particular, the inherent forces within chemical gels are stronger than the adhesive forces between gel and substrate to be cleaned. This implies an easier removal of such formulation, thereby lessening extra mechanical steps to get rid of potential residues [185]. In addition, the potential presence of residues is being studied as long-term effects of gel remains could be deleterious [186]. Gels can be loaded with different solvents

that are slowly released at the gel-object interface in a controlled manner. In the context of this work, the solvent resorted to is water, which makes the studied systems classified as hydrogels [172].

The use of gels is still arising on metal artworks, even though there is the need for selective interventions, considering how heterogenous metals can be: composite artefacts, gilded artworks, painted metals, etc. In a comparative study on gel and swab cleaning on brass, Atomic Force Microscopy (AFM) images showed the existence of scratches after cotton swabbing due to the subsequent motion of free particles originally present on the metal. On the contrary, the gel performances, although slightly less efficient, was smooth and non-invasive, leaving no physical changes on the brass surface [187]. Successful applications on a composite copper-wooden gun from an Islamic art collection, retrieving the original shine of the object or also on coin collections were performed [188].

Notably, some studies regarding the use of synthetic gels have been published for metal conservation [189]. Water-based formulations made of the synthetic polymer poly(vinyl alcohol) (PVA) and borax were designed by Baglioni *et al.* and assessed on copper alloys [80,190]. Despite the captivating potentialities, high attention must be addressed to their waste management and the correlated ecological impact. For instance, PVA is readily water-soluble; however, inadequate disposal can cause pollution of groundwater [191]. Its biodegradation is performed by very peculiar bacteria, barely represented in nature [192,193]. Recent works report the use of polysaccharides (i.e. rice starch) to try to achieve more sustainable PVA-based formulations [194]. Another critical point is the sustainability of thickening agents' production. Although bio-derived from cellulose, often the synthesis of cellulose-based polymers cannot be considered green, since it may require reagents hazardous for the aquatic environment (e.g. chloroacetic acid used for the synthesis of carboxymethyl cellulose) [195].

1.4.1 Biobased hydrogels for metal preservation

A wide variety of hydrogels based on natural polymers have been exploited, especially in the biomedical field, including polysaccharides (e.g. carrageenan, alginate, starch) and proteins (e.g. collagen and gelatin) [196]. However, in art conservation, mainly polysaccharides have been employed (Figure 1.5). The resulting formulations all belong to the class of physical gels. Indeed, the water is retained within the gel network, held together by hydrogen bonding between the polar groups of the bio-polymers [197]. Although the literature mentioning their application on metals is rare [188], bio-based systems appear as relevant candidates for metal preservation.

Rigid hydrogels are reliable delivery systems due to their capability to retain solvents that allow to focus the cleaning on the outermost layer, thereby limiting negative actions on eventual sensitive underlying materials. Moreover, their compact consistency makes them appreciated for their easy removal or even peelability [107]. However, their main advantage is also their main weakness. Being rigid, it is difficult

to achieve good performances on rough substrates where the contact gel-surface is difficult to maintain. In art conservation, the leading thickening agent in this category is uncontestably agar.

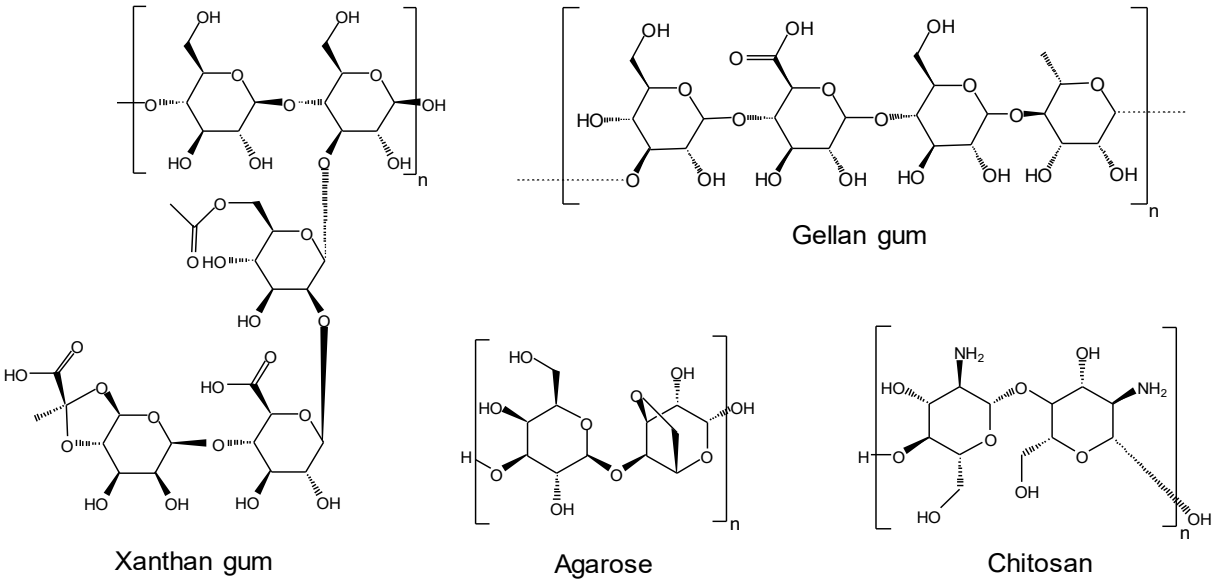

Figure 1.5 Biopolymers used for hydrogel formulations in cultural heritage conservation: structural formula of xanthan gum, gellan gum, agarose and chitosan.

1.4.1.1 Agar

Agar is a gelling agent, extracted from red seaweed membranes, in particular *Gelidium* sp., *Pterocladia* sp. and *Gracilaria* sp. [198], which forms a rigid hydrogel after being heated above 90 °C and cooled down [107]. Agar is broadly available, with various purity and composition according to different assigned purposes in the food industry, microbiology, biomedicine, or art conservation [199,200]. The gelling compound is agarose, which is more often used with agaropectin, being less expensive [107]. Agarose and agaropectin are both polymers composed of D-galactose linked with 3,6 anhydro L-galactose but the agaropectin form is sulfated. Upon heating, hydrogen bonds between the structural units of agarose (Figure 1.6a) break and the latter are dispersed into the water as random coils forming a clear solution (Figure 1.6b). With consecutive cooling, agarose chains intertwin through hydrogen bonding, forming a double helix structure (Figure 1.6c). These double helixes will arrange in aggregate to form the gel network, with pores which can hold water (Figure 1.6d) [201].

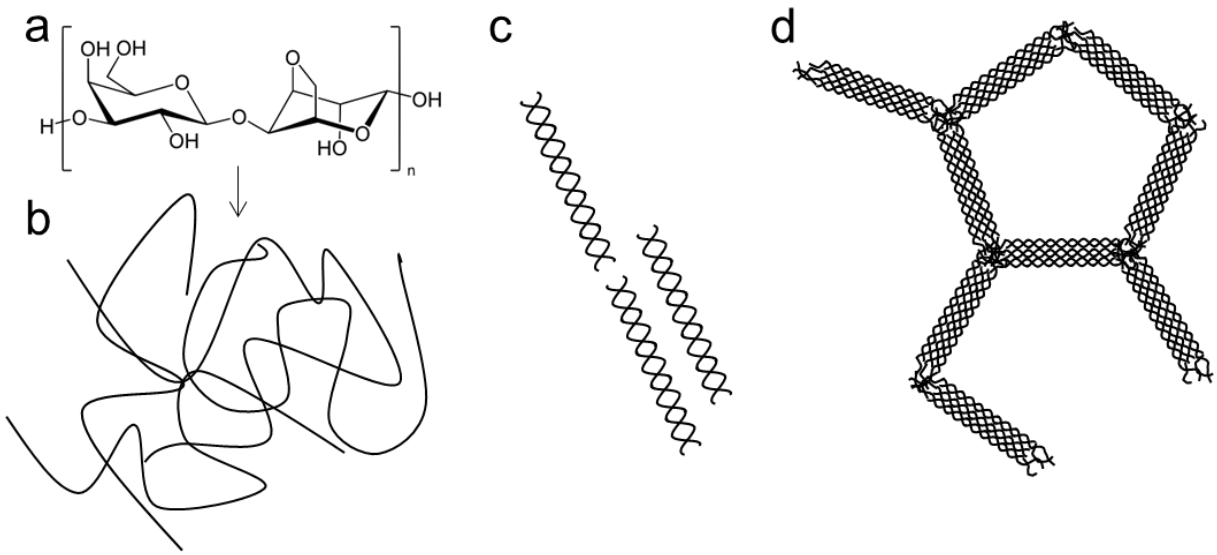

Figure 1.6 Agar gelation structure from [201], (a) agarose polymer unit, (b) random coils, (c) double helixes, (d) aggregated double helix network.

Agar is usually prepared at concentration from 2 to 5% w/v. The concentration of agar used influences the properties of the gel, in particular pore size. Overall water content and water mobility are directly dependent on that parameter [199].

When it comes to its preparation, the heating process can be a downside for conservators, especially when they are required to work out of their lab, with no heating devices. Although an agar gel cannot be formed directly with acidic or alkaline solutions, the gels can be loaded by absorption of the solutions once the gel is created. Indeed, hydrolysis of agar reduces its molecular weight and consequently lowers its gelling power. Acidic agar hydrolysis appears as a result of low pH (below 5.5) and long dissolution time at a high temperature. Alkaline hydrolysis is relevant at pH over 8 [202]. Nevertheless, recent studied have shown the gelation of agar at a wide pH range between 2 and 11 [203].

A gel called Nevek® has been recently developed and is mentioned as particularly suitable for the cleaning of metal surfaces [204]. It is a ready-to-use 5% double-heated agar with the addition of 5% ethanol to avoid microbial growth during storage. This option therefore cannot be foreseen for immobilizing microbes. In previous literature, several protocols based on agar were tested on metals [205–207]. However, they were not performing well on 3D objects due to their rigidity and thus their tendency to break easily [208]. To overcome these inconveniences, several application solutions have been proposed in the literature such as direct application of agar onto the surface or using a spray when still hot (gelation occur instantaneously when entering in contact with the surface), helping to obtain better contact and an agar layer uniformly deposited following surface morphology [204,209].

1.4.1.2 Gellan gum

Gellan gum is a polysaccharide produced by the bacterium *Sphingomonas elodea* [183]. Similar to agar, it forms a thermoreversible double-helical rigid gel upon cooling, compatible with soaking of acidic and alkaline solutions once prepared and best-performing if applied warm [204,210]. Though some references mention the incompatibility of gellan gum with complexing agents [206]. In addition to the transparency considered an asset as it allowed to observe and monitor the changes during intervention, its gelling properties are displayed even with low concentrations (0.5 to 5 g/L) and are stable in a wide pH range (2.5-11) [211,212].

One of the great assets of gellan gum is that it can be prepared at room temperature to form a viscous solution. This is of interest in case of impossibility to heat the incorporated reagents. As an example, gellan gum was selected for the treatment of copper artefacts, thanks to its adherence on vertical surfaces, ease of removal, and compatibility with the chosen active agents (i.e. fungal strains) [211].

1.4.1.3 Xanthan gum

Xanthan gum is a thickening agent biosynthesized by the bacterium *Xanthomonas campestris* through the fermentation of sucrose or glucose [196]. Xanthan gum can be in an ordered (helix) or disordered conformation (random coil) [213]. This excludes the possibility of obtaining a rigid peelable gel. Xanthan gum gels can sustain a wide pH range (2-12) while maintaining gelling properties [188,214], although appears to be less effective in alkaline solutions [204]. The inherent high viscosity of xanthan gum makes its removal from metal substrates complicated [204,206], requiring the use of water or solvent afterward for a complete elimination, which would devaluate the primary goal of the use of gels.

1.4.1.4 Chitosan

Chitosan is the N-deacetylated form of chitin. which is, in turn, the most abundant animal polysaccharide present in the exoskeleton of crustaceans and the cell wall of fungi [196]. It has gained more attention in the past decades especially in the medical field or for heavy metal remediation [196,215,216]. Chitosan is more and more used in heritage conservation, for instance for its protective assets as coating or anti-microbial activity as nanoparticles [217,218]. In addition, chitosan is a known compound for the complexation of copper ions [219,220]. The abundant amino and hydroxyl groups present are responsible for this ability [221,222]. Regarding its properties as a thickening agent, it can be prepared per se, achieving a viscous texture, or in a peelable form thanks to alkaline solutions loading [216]. This allows reducing the risk of residues when removing the gel after cleaning, which is, as mentioned, of concern for the field professionals.

Hydrogels mentioned above are the primary ones used by conservators, combined with the most adapted ones for the development of a completely bio-based cleaning gel formulation.

1.5 Thesis outline

As presented in this chapter, the phenomenon of surface alteration on historical metal artworks is a concern in terms of visual aspect or object preservation, among others, and can be related to corrosion processes. Also, the presence of aged organic coatings (i.e., wax, varnish) applied during past conservation interventions can fail achieving originally intended protection and need to be replaced. As discussed, cleaning of artworks is however a complex issue and hence a critical part of the conservation intervention. Indeed, the principal cleaning methods frequently reported are not risk-free. Therefore, there is a need expressed by stakeholders to develop alternative cleaning methods that remove corrosion compounds and non-original organic substances, improving the visual aspect of the metal artworks without impacting their surface texture.

The HELIX project aims at taking advantage of the capabilities of naturally occurring microorganisms, adopting strategies to remove the degradation products present on different alloys commonly found in historical objects. In parallel, to comply with the guidelines when cleaning water-sensitive metal substrates, bio-based gel systems that present no toxicity are identified or specifically designed to develop biocleaning methods. Hence, different combinations of bio-based gels amended with microbial extracts are then tested on model metal coupons presenting different types of corrosion and/or organic coatings encountered on contemporary or decorative artworks. The proposed cleaning formulations are also applied and assessed on real artefacts with emblematic alteration features related to corrosion or the presence of degraded protective coatings. Ideally, this method should comply with retrieving the visual appearance and readability of the object, avoiding residues of the cleaning products, avoiding harmful chemicals for both conservator and the environment. There is also the will to be involved in transfer into praxis of the proposed cleaning methods. Indeed, this investigation requires not only the perspectives from a single discipline but a trans-disciplinary and collaborative research to be instigated. As part of the HELIX project, this thesis will partially address all the WP (Figure 1.1), focusing on hydrogels and removal of metal corrosion products, the removal of organic coatings being addressed in another thesis carried out within the project. Specifically, WP1 (Study of microorganisms as mini chemical factories) will be addressed in the second chapter with two main foci, the screening and evaluation of microorganisms to act as micro-chemical factories and the study of the efficacy of biological metal remediating agents vs. chemical ones to take up indoor corrosion products. Chapter 3 will investigate hydrogel formulations (WP2 – Investigation of green gels formulations for metal cleaning), focusing on the use of common natural polymers in cultural heritage conservation and the

development of emerging natural polymers with interesting properties for metal cleaning, in addition to addressing the residues question. Chapter 4 will present results of the evaluation of different formulations on naturally aged coupons and compare with the results on artificially aged ones (WP3 – Evaluation of cleaning performances on model samples) and on case-studies (WP4 – Demonstration of sustainable conservation practices on selected case studies)). Finally, Chapter 5 will propose a critical reflection on the developed technology, tackling real praxis implementation and sustainability.

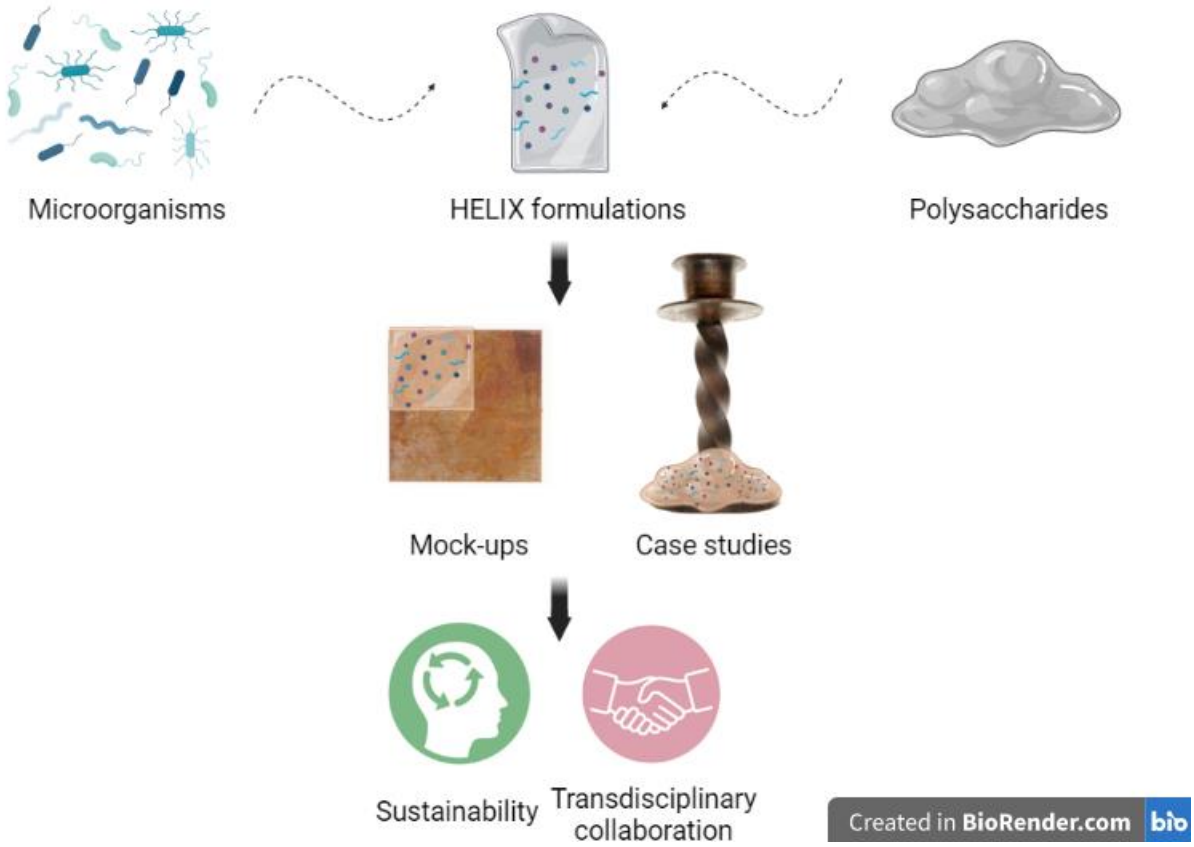

Figure 1.7 Thesis graphical abstract.

1.6 Bibliography

1. Selwyn, L. *Metals and Corrosion: A Handbook for the Conservation Professional*; Canadian Conservation Institute, 2004; ISBN 9780662379843.
2. Bertolotti, G.; Bersani, D.; Lottici, P.P.; Alesiani, M.; Malcherek, T.; Schlüter, J. Micro-Raman Study of Copper Hydroxychlorides and Other Corrosion Products of Bronze Samples Mimicking Archaeological Coins. *Anal. Bioanal. Chem.* **2012**, *402*, 1451–1457, doi:10.1007/s00216-011-5268-9.
3. Chiavari, C.; Martini, C.; Prandstraller, D.; Niklasson, A.; Johansson, L.-G.; Svensson, J.-E.; Åslund, A.; Bergsten, C.J. Atmospheric Corrosion of Historical Organ Pipes: The Influence of Environment and Materials. *Corros. Sci.* **2008**, *50*, 2444–2455, doi:10.1016/j.corsci.2008.06.045.
4. Lehmann, E.H.; Hartmann, S.; Speidel, M.O. Investigation of the Content of Ancient Tibetan Metallic Buddha Statues by Means of Neutron Imaging Methods. *Archaeometry* **2009**, *52*, 416–428, doi:10.1111/j.1475-4754.2009.00488.x.
5. Giumlia-Mair, A.; Lucchini, E. Surface Analyses on Modern and Ancient Copper Based Fakes. *Surf. Eng.* **2005**, *21*, 406–410, doi:10.1179/174329305X64402.
6. Felix, V.S.; Pereira, M.O.; Freitas, R.P.; Aranha, P.J.M.; Heringer, P.C.S.; Anjos, M.J.; Lopes, R.T. Analysis of Silver Coins from Colonial Brazil by Hand Held XRF and Micro-XRF. *Appl. Radiat. Isot.* **2020**, *166*, 109409, doi:10.1016/j.apradiso.2020.109409.
7. Gharib, A.; Mohamed, H.; Abdel Ghany, N. Nondestructive Techniques in the Study of a Gilded Metallic Sword from the Islamic Art Museum. *Egypt. J. Archaeol. Restor. Stud.* **2018**, *8*, 15–21.
8. Costa, V. *Modern Metals in Cultural Heritage: Understanding and Characterization*; Getty Publications, 2019; ISBN 978-1-60606-605-8.
9. Baker, I. Grand Challenges in Metals and Alloys. *Front. Met. Alloy.* **2022**, *1*, doi:10.3389/ftmal.2022.894403.
10. Chilton, J.P. The Corrosion of Metals. *J. R. Soc. Arts* **1971**, *119*, 614–629.
11. Albini, M. Fungal Biogenic Patina : Optimization of an Innovative Conservation Treatment for Copper-Based Artefacts, University of Neuchâtel, 2017.
12. Beech, I.B.; Sunner, J. Biocorrosion: Towards Understanding Interactions between Biofilms and Metals. *Curr. Opin. Biotechnol.* **2004**, *15*, 181–186, doi:10.1016/j.copbio.2004.05.001.
13. Neff, D.; Reguer, S.; Bellot-Gurlet, L.; Dillmann, P.; Bertholon, R. Structural Characterization of Corrosion Products on Archaeological Iron: An Integrated Analytical Approach to Establish Corrosion Forms. *J. Raman Spectrosc.* **2004**, *35*, 739–745, doi:10.1002/jrs.1130.
14. Baglioni, P.; Chelazzi, D.; Giorgi, R.; Poggi, G. Colloid and Materials Science for the Conservation of Cultural Heritage: Cleaning, Consolidation, and Deacidification. *Langmuir* **2013**, *29*, 5110–5122, doi:10.1021/la304456n.
15. *Corrosion*; Shreir, L.L., Jarman, R.A., Burstein, G.T., Eds.; Elsevier, 1994; ISBN 9780080523514.
16. Harsimran, S.; Santosh, K.; Rakesh, K. Overview of Corrosion and Its Control: A Critical Review. *Proc. Eng. Sci.* **2021**, *3*, 13–24, doi:10.24874/PES03.01.002.
17. Rice, D.W.; Cappell, R.J.; Kinsolving, W.; Laskowski, J.J. Indoor Corrosion of Metals. *J. Electrochem. Soc.* **1980**, *127*, 891–901, doi:10.1149/1.2129780.
18. Couture-Rigert, D.E.; Sirois, P.J.; Moffatt, E.A. An Investigation into the Cause of Corrosion on Indoor Bronze Sculpture. *Stud. Conserv.* **2012**, *57*, 142–163, doi:10.1179/2047058412Y.0000000004.
19. Mendoza, A.R.; Corvo, F. Outdoor and Indoor Atmospheric Corrosion of Non-Ferrous Metals. *Corros. Sci.* **2000**, *42*, 1123–1147, doi:10.1016/S0010-938X(99)00135-3.
20. Part I: General Aspects of Corrosion, Corrosion Control, and Corrosion Prevention. In *Corrosion Atlas Case Studies*; Khoshnaw, F., Gubner, R., Eds.; Elsevier, 2021; pp. 25–42.
21. Scott, D.A.; Eggert, G. Corrosion, Colorants, Conservation. In *Iron and Steel in Art*; Archetype Publications, 2009; p. 196 ISBN 978-1-904982-05-0.
22. Dillmann, P.; Mazaudier, F.; Hœrlé, S. Advances in Understanding Atmospheric Corrosion of Iron. I. Rust Characterisation of Ancient Ferrous Artefacts Exposed to Indoor Atmospheric

Corrosion. *Corros. Sci.* **2004**, *46*, 1401–1429, doi:10.1016/j.corsci.2003.09.027.
23. Cudennec, Y.; Lecerf, A. The Transformation of Ferrihydrite into Goethite or Hematite, Revisited. *J. Solid State Chem.* **2006**, *179*, 716–722, doi:10.1016/j.jssc.2005.11.030.
24. Macchia, A.; Ruffolo, S.A.; Rivaroli, L.; La Russa, M.F. The Treatment of Iron-Stained Marble: Toward a "Green" Solution. *Int. J. Conserv. Sci.* **2016**, *7*, 323–332.
25. Frini, A.; Maaoui, M. El Kinetics of the Formation of Goethite in the Presence of Sulfates and Chlorides of Monovalent Cations. *J. Colloid Interface Sci.* **1997**, *190*, 269–277, doi:10.1006/jcis.1997.4845.
26. Monnier, J.; Bellot-Gurlet, L.; Baron, D.; Neff, D.; Guillot, I.; Dillmann, P. A Methodology for Raman Structural Quantification Imaging and Its Application to Iron Indoor Atmospheric Corrosion Products. *J. Raman Spectrosc.* **2011**, *42*, 773–781, doi:10.1002/jrs.2765.
27. Cudennec, Y.; Lecerf, A. Étude Des Mécanismes de Formation Des Oxy-Hydroxydes de Fer ; Hypothèses de Transformations Topotactiques. *Comptes Rendus Chim.* **2003**, *6*, 437–444, doi:10.1016/S1631-0748(03)00069-9.
28. Monnier, J.; Guillot, I.; Legrand, L.; Dillmann, P. Reactivity Studies of Atmospheric Corrosion of Heritage Iron Artefacts. *Corros. Conserv. Cult. Herit. Met. Artefacts* **2013**, 285–310, doi:10.1533/9781782421573.3.285.
29. Yamashita, M.; Miyuki, H.; Matsuda, Y.; Nagano, H.; Misawa, T. The Long Term Growth of the Protective Rust Layer Formed on Weathering Steel by Atmospheric Corrosion during a Quarter of a Century. *Corros. Sci.* **1994**, *36*, 283–299, doi:10.1016/0010-938X(94)90158-9.
30. Fioravante, I.; Nunes, R.; Acciari, H.; Codaro, E. Films Formed on Carbon Steel in Sweet Environments - A Review. *J. Braz. Chem. Soc.* **2019**, doi:10.21577/0103-5053.20190055.
31. Cartwright, M. Copper in Antiquity Available online: https://www.worldhistory.org/copper/.
32. Knotkova, D.; Kreislova, K. Atmospheric Corrosion and Conservation of Copper and Bronze. In *Environmental Deterioration of Materials*; WIT Press, 2007; pp. 107–142.
33. Otero, E.; Bastidas, J.M.; López, W.; Fierro, J.L.G. Characterization of Corrosion Products on Chalcographic Copper Plates after 200 Years' Exposure to Indoor Atmospheres. *Mater. Corros.* **1994**, *45*, 387–391, doi:10.1002/maco.19940450704.
34. Krätschmer, A.; Odnevall Wallinder, I.; Leygraf, C. The Evolution of Outdoor Copper Patina. *Corros. Sci.* **2002**, *44*, 425–450, doi:10.1016/S0010-938X(01)00081-6.
35. Valdez Salas, B.; Schorr Wiener, M.; Zlatev Koytchev, R.; López Badilla, G.; Ramos Irigoyen, R.; Carrillo Beltrán, M.; Radnev Nedev, N.; Curiel Alvarez, M.; Rosas Gonzalez, N.; Bastidas Rull, J.M. Copper Corrosion by Atmospheric Pollutants in the Electronics Industry. *ISRN Corros.* **2013**, *2013*, 1–7, doi:10.1155/2013/846405.
36. Bråkenhielm, C.R. *Mechanisms of Copper Corrosion in Aqueous Environments*; Stockholm, Sweden, 2009;
37. de la Fuente, D.; Simancas, J.; Morcillo, M. Morphological Study of 16-Year Patinas Formed on Copper in a Wide Range of Atmospheric Exposures. *Corros. Sci.* **2008**, *50*, 268–285, doi:10.1016/j.corsci.2007.05.030.
38. v. d. Leest, R.E. On the Atmospheric Corrosion of Thin Copper Films. *Werkstoffe und Korrosion* **1986**, *37*, 629–632, doi:10.1002/maco.19860371204.
39. Kosaric, N.; Duvnjak, Z.; Farkas, A.; Sahm, H.; Bringer-Meyer, S.; Goebel, O.; Mayer, D. Ethanol. In *Ullmann's Encyclopedia of Industrial Chemistry*; Wiley-VCH Verlag GmbH & Co. KGaA: Weinheim, Germany, 2011; Vol. 44, pp. 1–72.
40. Cano, E.; Polo, J.L.; La Iglesia, A.; Bastidas, J.M. Rate Control for Copper Tarnishing. *Corros. Sci.* **2005**, *47*, 977–987, doi:10.1016/j.corsci.2004.06.026.
41. Caporuscio, F.A.; Palaich, S.E.M.; Cheshire, M.C.; Jové Colón, C.F. Corrosion of Copper and Authigenic Sulfide Mineral Growth in Hydrothermal Bentonite Experiments. *J. Nucl. Mater.* **2017**, *485*, 137–146, doi:10.1016/j.jnucmat.2016.12.036.
42. Muller, J. Etude Électrochimique et Caractérisation Des Produits de Corrosion Formés à La

Surface Des Bronzes Cu-Sn En Milieu Sulfate, PhD thesis- Université Paris Est – Créteil, 2010. https://theses.hal.science/tel-00492692
43. Zittlau, A.H.; Shi, Q.; Boerio-Goates, J.; Woodfield, B.F.; Majzlan, J. Thermodynamics of the Basic Copper Sulfates Antlerite, Posnjakite, and Brochantite. *Geochemistry* **2013**, *73*, 39–50, doi:10.1016/j.chemer.2012.12.002.
44. Scott, D.. *Copper and Bronze in Art: Corrosion, Colorants, Conservation*; Scott, D.A., Ed.; Getty Institute of Conservation: Los Angeles, 2002; ISBN 978-0-89236-638-5.
45. Lyon, S.B. Corrosion of Noble Metals. *Shreir's Corros.* **2010**, *1*, 2205–2223, doi:10.1016/B978-044452787-5.00109-8.
46. Costa, V. The Deterioration of Silver Alloys and Some Aspects of Their Conservation. *Stud. Conserv.* **2001**, *46*, 18–34, doi:10.1179/sic.2001.46.supplement-1.18.
47. Huisman, H.; Ackermann, R.; Claes, L.; van Eijck, L.; de Groot, T.; Joosten, I.; Kemmers, F.; Kerkhoven, N.; de Kort, J.-W.; Lo Russo, S.; et al. Change Lost: Corrosion of Roman Copper Alloy Coins in Changing and Variable Burial Environments. *J. Archaeol. Sci. Reports* **2023**, *47*, 103799, doi:10.1016/j.jasrep.2022.103799.
48. Sinclair, J.D. Tarnishing of Silver by Organic Sulfur Vapors: Rates and Film Characteristics. *J. Electrochem. Soc.* **1982**, *129*, 33–40, doi:10.1149/1.2123787.
49. Franey, J.P.; Kammlott, G.W.; Graedel, T.E. The Corrosion of Silver by Atmospheric Sulfurous Gases. *Corros. Sci.* **1985**, *25*, 133–143, doi:10.1016/0010-938X(85)90104-0.
50. Vassiliou, P. Ancient Silver Artefacts: Corrosion Processes and Preservation Strategies. **2013**, 213–235, doi:10.1533/9781782421573.3.213.
51. Ankersmit, H.A.; Tennent, N.H.; Watts, S.F. Hydrogen Sulfide and Carbonyl Sulfide in the Museum Environment — Part 1. **2005**, *39*, 695–707, doi:10.1016/j.atmosenv.2004.10.013.
52. Ortíz-Corona, J.; Rodríguez-Gómez, F.J. Role of Copper in Tarnishing Process of Silver Alloys in Sulphide Media. *Trans. Nonferrous Met. Soc. China* **2019**, *29*, 2646–2657, doi:10.1016/S1003-6326(19)65171-X.
53. Ingo, G.M.; Angelini, E.; Riccucci, C.; de Caro, T.; Mezzi, A.; Faraldi, F.; Caschera, D.; Giuliani, C.; Di Carlo, G. Indoor Environmental Corrosion of Ag-Based Alloys in the Egyptian Museum (Cairo, Egypt). *Appl. Surf. Sci.* **2015**, *326*, 222–235, doi:10.1016/j.apsusc.2014.11.135.
54. *The IUPAC Compendium of Chemical Terminology*; Gold, V., Ed.; International Union of Pure and Applied Chemistry (IUPAC): Research Triangle Park, NC, 2019;
55. Ion Exchange and Ion Exchangers: An Introduction. In *Ion Exchange in Environmental Processes*; John Wiley & Sons, Inc.: Hoboken, New Jersey, 2017; pp. 1–49.
56. Vlek, P.L.G.; Blom, T.J.M.; Beek, J.; Lindsay, W.L. Determination of the Solubility Product of Various Iron Hydroxides and Jarosite by the Chelation Method. *Soil Sci. Soc. Am. J.* **1974**, *38*, 429–432, doi:10.2136/sssaj1974.03615995003800030018x.
57. Cornell, R.M.; Schwertmann, U. *The Iron Oxides*; Wiley, 2003; ISBN 9783527302741.
58. Scheepers, G.; Koster, M.; Bennekom, J. Van Exploring the Use of Acidithiobacillus Ferrooxidans for the Removal of Sulphides from Tarnished Silver. *Estud. Conserv. e Restauro* **2019**, *2*, 19–30.
59. Horton, D.J.; Ha, H.; Foster, L.L.; Bindig, H.J.; Scully, J.R. Tarnishing and Cu Ion Release in Selected Copper-Base Alloys: Implications towards Antimicrobial Functionality. *Electrochim. Acta* **2015**, *169*, 351–366, doi:10.1016/j.electacta.2015.04.001.
60. Rizo, J.; Díaz, D.; Reyes-Trejo, B.; Arellano-Jiménez, M.J. Cu 2 O Nanoparticles for the Degradation of Methyl Parathion. *Beilstein J. Nanotechnol.* **2020**, *11*, 1546–1555, doi:10.3762/bjnano.11.137.
61. Balloi, A.; Palla, F. Biocleaning. In *Biotechnology and Conservation of Cultural Heritage*; Springer International Publishing: Cham, 2017; pp. 67–84.
62. Degrigny, C. Examination and Conservation of Historical and Archaeological Metal Artefacts: A European Overview. *Corros. Met. Herit. Artefacts Investig. Conserv. Predict. Long Term Behav.* **2007**, 1–17, doi:10.1533/9781845693015.1.

63. Bertholon, R. La Limite de La Surface d ' Origine Des Objets Métalliques Archéologiques . Caractérisation , Localisation et Approche To Cite This Version : HAL Id : Tel-00331190. **2008**.
64. Smith, R.D. Reversibility: A Questionable Philosophy. *Restaurator* **1988**, *9*, doi:10.1515/rest.1988.9.4.199.
65. Appelbaum, B. Criteria for Treatment: Reversibility. *J. Am. Inst. Conserv.* **1987**, *26*, 65–73, doi:10.1179/019713687806027852.
66. Bertasa, M.; Botteon, A.; Brambilla, L.; Riedo, C.; Chiantore, O.; Poli, T.; Sansonetti, A.; Scalarone, D. Cleaning Materials: A Compositional Multi-Analytical Characterization of Commercial Agar Powders. *J. Anal. Appl. Pyrolysis* **2017**, *125*, 310–317, doi:10.1016/j.jaap.2017.03.011.
67. Siano, S.; Agresti, J.; Cacciari, I.; Ciofini, D.; Mascalchi, M.; Osticioli, I.; Mencaglia, A.A. Laser Cleaning in Conservation of Stone, Metal, and Painted Artifacts: State of the Art and New Insights on the Use of the Nd:YAG Lasers. *Appl. Phys. A* **2012**, *106*, 419–446, doi:10.1007/s00339-011-6690-8.
68. Schalm, O.; Storme, P.; Gambirasi, A.; Favaro, M.; Patelli, A. How Effective Are Reducing Plasma Afterglows at Atmospheric Pressure in Removing Sulphide Layers: Application on Tarnished Silver, Sterling Silver and Copper. *Surf. Interface Anal.* **2018**, *50*, 32–42, doi:10.1002/sia.6329.
69. Koh, Y.S.; Powell, J.; Kaplan, A.F.H. Removal of Layers of Corrosion from Steel Surfaces: A Qualitative Comparison of Laser Methods and Mechanical Techniques. *J. Laser Appl.* **2007**, *19*, 99–106, doi:10.2351/1.2567378.
70. Palomar, T.; Ramírez Barat, B.; García, E.; Cano, E. A Comparative Study of Cleaning Methods for Tarnished Silver. *J. Cult. Herit.* **2016**, *17*, 20–26, doi:10.1016/j.culher.2015.07.012.
71. Watkinson, D. Preservation of Metallic Cultural Heritage. In *Shreir's Corrosion*; Elsevier, 2010; pp. 3307–3340.
72. Palomar, T.; Ramírez Barat, B.; Cano, E. Evaluation of Cleaning Treatments for Tarnished Silver: The Conservator's Perspective. *Int. J. Conserv. Sci.* **2018**, *9*, 81–90, doi:10.13039/501100006111.
73. Degrigny, C. Use of Electrochemical Techniques for the Conservation of Metal Artefacts: A Review. *J. Solid State Electrochem.* **2010**, *14*, 353–361, doi:10.1007/s10008-009-0896-0.
74. Turner-Walker, G. *A Practical Guide to the Care and Conservation of Metals*; Headquarters Administration of Cultural Heritage, Council for Cultural Affairs: Taichung City, Taiwan, 2008; ISBN 978-986-01-7298-0.
75. Kergourlay, F.; Rémazeilles, C.; Neff, D.; Foy, E.; Conforto, E.; Guilminot, E.; Reguer, S.; Dillmann, P.; Nicot, F.; Mielcarek, F.; et al. Mechanisms of the Dechlorination of Iron Archaeological Artefacts Extracted from Seawater. *Corros. Sci.* **2011**, *53*, 2474–2483, doi:10.1016/j.corsci.2011.04.003.
76. Novakovic, J.; Vassiliou, P.; Georgiza, E. Electrochemical Cleaning of Artificially Tarnished Silver. *Int. J. Electrochem. Sci.* **2013**, *8*, 7223–7232.
77. Degrigny, C.; Jeanneret, R.; Witschard, D.; Baudin, C.; Bussy, G.; Carrel, H. A New Electrolytic Pencil for the Local Cleaning of Silver Tarnish. *Stud. Conserv.* **2016**, *61*, 162–173, doi:10.1179/2047058415Y.0000000015.
78. Oviedo, C.; Rodríguez, J. EDTA: The Chelating Agent under Environmental Scrutiny. *Quim. Nova* **2003**, *26*, 901–905, doi:10.1590/S0100-40422003000600020.
79. Xie, C.Z. Environmental Impacts of Effluent Containg EDTA from Dairy Processing Plants, The University of Waikato, 2009.
80. Guaragnone, T.; Casini, A.; Chelazzi, D.; Giorgi, R. PVA-Based Peelable Films Loaded with Tetraethylenepentamine for the Removal of Corrosion Products from Bronze. *Appl. Mater. Today* **2020**, *19*, 100549, doi:10.1016/j.apmt.2019.100549.
81. Passaretti, A.; Cuvillier, L.; Sciutto, G.; Guilminot, E.; Joseph, E. Biologically Derived Gels for the Cleaning of Historical and Artistic Metal Heritage. *Appl. Sci.* **2021**, *11*, 3405, doi:10.3390/app11083405.
82. Giraud, T.; Gomez, A.; Lemoine, S.; Pelé-Meziani, C.; Raimon, A.; Guilminot, E. Use of Gels for

the Cleaning of Archaeological Metals. Case Study of Silver-Plated Copper Alloy Coins. *J. Cult. Herit.* **2021**, *52*, 73–83, doi:10.1016/j.culher.2021.08.014.
83. Eggert, G.; Fischer, A. The Formation of Formates: A Review of Metal Formates on Heritage Objects. *Herit. Sci.* **2021**, *9*, 26, doi:10.1186/s40494-021-00499-z.
84. Huda, K. A Note on the Efficacy of Ethylenediaminetetra-Acetic Acid Disodium Salt as a Stripping Agent for Corrosion Products of Copper. *Stud. Conserv.* **2002**, *47*, 211–216, doi:10.1179/sic.2002.47.3.211.
85. Dooms-Goossens, A.; Debusschère, K.; Morren, M.; Roelandts, R.; Coopman, S. Silver Polish: Another Source of Contact Dermatitis Reactions to Thiourea. *Contact Dermatitis* **1988**, *19*, 133–135, doi:10.1111/j.1600-0536.1988.tb05511.x.
86. Palomar, T.; Oujja, M.; Llorente, I.; Ramírez Barat, B.; Cañamares, M. V.; Cano, E.; Castillejo, M. Evaluation of Laser Cleaning for the Restoration of Tarnished Silver Artifacts. *Appl. Surf. Sci.* **2016**, *387*, 118–127, doi:10.1016/j.apsusc.2016.06.017.
87. *Biotechnology and Conservation of Cultural Heritage*; Palla, F., Barresi, G., Eds.; Springer, 2017; ISBN 978-3-319-46168-7.
88. Elhagrassy, A.F.; Hakeem, A.; Alhagrassy, A.F. Comparative Study of Biological Cleaning and Laser Techniques for Conservation of Weathered Stone in Failaka Island, Kuwait. *Sci. Cult.* **2018**, *4*, 43–50, doi:10.5281/zenodo.1214561.
89. Joseph, E. *Microorganisms in the Deterioration and Preservation of Cultural Heritage*; Joseph, E., Ed.; Springer International Publishing: Cham, 2021; ISBN 978-3-030-69410-4.
90. Branysova, T.; Demnerova, K.; Durovic, M.; Stiborova, H. Microbial Biodeterioration of Cultural Heritage and Identification of the Active Agents over the Last Two Decades. *J. Cult. Herit.* **2022**, *55*, 245–260, doi:10.1016/j.culher.2022.03.013.
91. Cappitelli, F.; Villa, F.; Sanmartín, P. Interactions of Microorganisms and Synthetic Polymers in Cultural Heritage Conservation. *Int. Biodeterior. Biodegrad.* **2021**, *163*, 105282, doi:10.1016/j.ibiod.2021.105282.
92. del Junco, A.S.; Moreno, D.A.; Ranninger, C.; Ortega-Calvo, J.J.; Sáiz-Jiménez, C. Microbial Induced Corrosion of Metallic Antiquities and Works of Art: A Critical Review. *Int. Biodeterior. Biodegrad.* **1992**, *29*, 367–375, doi:10.1016/0964-8305(92)90053-Q.
93. Lane, R.A. Under the Microscope: Understanding, Detecting, and Preventing Microbiologically Influenced Corrosion. *J. Fail. Anal. Prev.* **2005**, *5*, 10–12, doi:10.1361/154770205X65891.
94. Timoncini, A.; Costantini, F.; Bernardi, E.; Martini, C.; Mugnai, F.; Mancuso, F.P.; Sassoni, E.; Ospitali, F.; Chiavari, C. Insight on Bacteria Communities in Outdoor Bronze and Marble Artefacts in a Changing Environment. *Sci. Total Environ.* **2022**, *850*, 157804, doi:10.1016/j.scitotenv.2022.157804.
95. Rémazeilles, C.; Neff, D.; Kergourlay, F.; Foy, E.; Conforto, E.; Guilminot, E.; Reguer, S.; Refait, P.; Dillmann, P. Mechanisms of Long-Term Anaerobic Corrosion of Iron Archaeological Artefacts in Seawater. *Corros. Sci.* **2009**, *51*, 2932–2941, doi:10.1016/j.corsci.2009.08.022.
96. Kip, N.; van Veen, J.A. The Dual Role of Microbes in Corrosion. *ISME J.* **2015**, *9*, 542–551, doi:10.1038/ismej.2014.169.
97. Junier, P.; Joseph, E. Microbial Biotechnology Approaches to Mitigating the Deterioration of Construction and Heritage Materials. *Microb. Biotechnol.* **2017**, *10*, 1145–1148, doi:10.1111/1751-7915.12795.
98. Sakr, A.A.; Ghaly, M.F.; Edwards, H.G.M.; Ali, M.F.; Abdel-Haliem, M.E.F. Involvement of Streptomyces in the Deterioration of Cultural Heritage Materials Through Biomineralization and Bio-Pigment Production Pathways: A Review. *Geomicrobiol. J.* **2020**, *37*, 653–662, doi:10.1080/01490451.2020.1754533.
99. Monachon, M.; Albelda-berenguer, M.; Lombardo, T.; Cornet, E.; Moll-dau, F.; Schramm, J.; Schmidt-ott, K.; Joseph, E. Evaluation of Bio-based Extraction Methods by Spectroscopic Methods. *Minerals* **2020**, *10*, 1–17, doi:10.3390/min10020203.

100. Albelda-Berenguer, M. Biological Strategies for the Preservation of Waterlogged Archaeological Wood, Universit of Neuchâtel, 2020.
101. Ortega-Morales, B.O.; Gaylarde, C.C. Bioconservation of Historic Stone Buildings—An Updated Review. *Appl. Sci.* **2021**, *11*, 5695, doi:10.3390/app11125695.
102. Romano, I.; Abbate, M.; Poli, A.; D'Orazio, L. Bio-Cleaning of Nitrate Salt Efflorescence on Stone Samples Using Extremophilic Bacteria. *Sci. Rep.* **2019**, *9*, 1–11, doi:10.1038/s41598-018-38187-x.
103. Barbabietola, N.; Tasso, F.; Alisi, C.; Marconi, P.; Perito, B.; Pasquariello, G.; Sprocati, A.R. A Safe Microbe-Based Procedure for a Gentle Removal of Aged Animal Glues from Ancient Paper. *Int. Biodeterior. Biodegrad.* **2016**, *109*, 53–60, doi:10.1016/j.ibiod.2015.12.019.
104. Gherardi, F.; Turyanska, L.; Ferrari, E.; Weston, N.; Fay, M.W.; Colston, B.J. Immobilized Enzymes on Gold Nanoparticles: From Enhanced Stability to Cleaning of Heritage Textiles. *ACS Appl. Bio Mater.* **2019**, *2*, 5136–5143, doi:10.1021/acsabm.9b00802.
105. Palla, F.; Bruno, M.; Mercurio, F.; Tantillo, A.; Rotolo, V. Essential Oils as Natural Biocides in Conservation of Cultural Heritage. *Molecules* **2020**, *25*, 730, doi:10.3390/molecules25030730.
106. Prati, S.; Sciutto, G.; Volpi, F.; Rehorn, C.; Vurro, R.; Blümich, B.; Mazzocchetti, L.; Giorgini, L.; Samorì, C.; Galletti, P.; et al. Cleaning Oil Paintings: NMR Relaxometry and SPME to Evaluate the Effects of Green Solvents and Innovative Green Gels. *New J. Chem.* **2019**, *43*, 8229–8238, doi:10.1039/c9nj00186g.
107. Cremonesi, P. Rigid Gels and Enzyme Cleaning. *Smithson. Contrib. to Museum Conserv.* **2012**, *3*, 179–183.
108. Albini, M.; Chiavari, C.; Bernardi, E.; Martini, C.; Mathys, L.; Joseph, E. Evaluation of the Performances of a Biological Treatment on Tin-Enriched Bronze. *Environ. Sci. Pollut. Res.* **2017**, *24*, 2150–2159, doi:10.1007/s11356-016-7361-2.
109. Joseph, E.; Cario, S.; Simon, A.; Wörle, M.; Mazzeo, R.; Junier, P.; Job, D. Protection of Metal Artifacts with the Formation of Metal-Oxalates Complexes by Beauveria Bassiana. *Front. Microbiol.* **2012**, *2*, doi:10.3389/fmicb.2011.00270.
110. Dutton, M. V.; Evans, C.S. Oxalate Production by Fungi: Its Role in Pathogenicity and Ecology in the Soil Environment. *Can. J. Microbiol.* **1996**, *42*, 881–895, doi:10.1139/m96-114.
111. Joseph, E.; Simon, A.; Mazzeo, R.; Job, D.; Wörle, M. Spectroscopic Characterization of an Innovative Biological Treatment for Corroded Metal Artefacts. *J. Raman Spectrosc.* **2012**, *43*, 1612–1616, doi:10.1002/jrs.4164.
112. Gutknecht, N.; Joseph, E. Stabilisation of Archaeological Copper-Alloy Objects from Chloride-Induced Active Corrosion with Beauveria Bassiana. In *Metal 2019 Proceedings of the Interim Meeting of the ICOM-CC Metals Working Group*; Chemello, C., Brambilla, L., Joseph, E., Eds.; Neuchâtel, Switzerland, 2019; pp. 12–15 ISBN 978-92-9012-458-0.
113. Albini, M.; Letardi, P.; Mathys, L.; Brambilla, L.; Schröter, J.; Junier, P.; Joseph, E. Comparison of a Bio-Based Corrosion Inhibitor versus Benzotriazole on Corroded Copper Surfaces. *Corros. Sci.* **2018**, *143*, 84–92, doi:10.1016/j.corsci.2018.08.020.
114. Comensoli, L.; Kooli, W.; Monachon, M.; Albini, M.; Junier, P.; Joseph, E. The Potential of Microorganisms for the Conservation-Restoration of Iron Artworks. In Proceedings of the Metal 2019, 9th interim meeting of the ICOM-CC metals working group; Neuchâtel, Switzerland, 2019; pp. 242–249.
115. Kooli, W.M.; Junier, T.; Shakya, M.; Monachon, M.; Davenport, K.W.; Vaideeswaran, K.; Vernudachi, A.; Marozau, I.; Monrouzeau, T.; Gleasner, C.D.; et al. Remedial Treatment of Corroded Iron Objects by Environmental Aeromonas Isolates. *Appl. Environ. Microbiol.* **2019**, *85*, 1–18, doi:10.1128/AEM.02042-18.
116. Kooli, W.M.; Comensoli, L.; Maillard, J.; Albini, M.; Gelb, A.; Junier, P.; Joseph, E. Bacterial Iron Reduction and Biogenic Mineral Formation for the Stabilisation of Corroded Iron Objects. *Sci. Rep.* **2018**, *8*, 1–11, doi:10.1038/s41598-017-19020-3.
117. Comensoli, L.; Maillard, J.; Albini, M.; Sandoz, F.; Junier, P.; Joseph, E. Use of Bacteria To

Stabilize Archaeological Iron. *Appl. Environ. Microbiol.* **2017**, *83*, 1–14, doi:10.1128/AEM.03478-16.
118. Comensoli, L. Interaction between Microbes, Iron and Chlorine for the Development of Biotechnological Approaches to Stabilize Corroded Iron, University of Neuchâtel, 2017.
119. Bosch-Roig, P.; Ranalli, G. The Safety of Biocleaning Technologies for Cultural Heritage. *Front. Microbiol.* **2014**, *5*, doi:10.3389/fmicb.2014.00155.
120. Scott, J. A New Method for Conserving Weathered Surfaces of Copper and Bronze. In Proceedings of the Bronze Conservation Colloquium; Eggert, G., Schmutzler, B., Eds.; Stuttgart, 2012; pp. 64–67.
121. Coombs, K.; Rodriguez-quijada, C.; Clevenger, J.O.; Sauer-budge, A.F. Current Understanding of Potential Linkages between Biocide Tolerance and Antibiotic Cross-Resistance. **2023**.
122. Madigan; Martinko; Dunlap; Clark *Brock Biology of Microogranisms, 12th International Edition*; Pearson Education, 2009; ISBN 978-0321536150.
123. Do Nascimento, C.W.A.; Amarasiriwardena, D.; Xing, B. Comparison of Natural Organic Acids and Synthetic Chelates at Enhancing Phytoextraction of Metals from a Multi-Metal Contaminated Soil. *Environ. Pollut.* **2006**, *140*, 114–123, doi:10.1016/j.envpol.2005.06.017.
124. Chen, H.; Dou, J.; Xu, H. The Effect of Low-Molecular-Weight Organic-Acids (LMWOAs) on Treatment of Chromium-Contaminated Soils by Compost-Phytoremediation: Kinetics of the Chromium Release and Fractionation. *J. Environ. Sci. (China)* **2018**, *70*, 45–53, doi:10.1016/j.jes.2017.11.007.
125. Upton, D.J.; McQueen-Mason, S.J.; Wood, A.J. An Accurate Description of Aspergillus Niger Organic Acid Batch Fermentation through Dynamic Metabolic Modelling. *Biotechnol. Biofuels* **2017**, *10*, 258, doi:10.1186/s13068-017-0950-6.
126. Liaud, N.; Giniés, C.; Navarro, D.; Fabre, N.; Crapart, S.; Gimbert, I.H.-; Levasseur, A.; Raouche, S.; Sigoillot, J.-C. Exploring Fungal Biodiversity: Organic Acid Production by 66 Strains of Filamentous Fungi. *Fungal Biol. Biotechnol.* **2014**, *1*, 1–10, doi:10.1186/s40694-014-0001-z.
127. Sauer, M.; Porro, D.; Mattanovich, D.; Branduardi, P. Microbial Production of Organic Acids: Expanding the Markets. *Trends Biotechnol.* **2008**, *26*, 100–108, doi:10.1016/j.tibtech.2007.11.006.
128. Chen, L.; Wang, D.; Long, C.; Cui, Z. Effect of Biodegradable Chelators on Induced Phytoextraction of Uranium- and Cadmium- Contaminated Soil by Zebrina Pendula Schnizl. *Sci. Rep.* **2019**, *9*, 19817, doi:10.1038/s41598-019-56262-9.
129. Takahashi, R.; Yamayoshi, K.; Fujimoto, N.; Suzuki, M. Production of (s, s)-Ethylenediamine-n, N′-Disuccinic Acid from Ethylenediamine and Fumaric Acid by Bacteria. *Biosci. Biotechnol. Biochem.* **1999**, *63*, 1269–1273, doi:10.1271/bbb.63.1269.
130. Zwicker, N.; Theobald, U.; Zähner, H.; Fiedler, H.P. Optimization of Fermentation Conditions for the Production of Ethylene-Diamine-Disuccinic Acid by Amycolatopsis Orientalis. *J. Ind. Microbiol. Biotechnol.* **1997**, *19*, 280–285, doi:10.1038/sj.jim.2900458.
131. Fomina, M.; Hillier, S.; Charnock, J.M.; Melville, K.; Alexander, I.J.; Gadd, G.M. Role of Oxalic Acid Overexcretion in Transformations of Toxic Metal Minerals by Beauveria Caledonica. *Appl. Environ. Microbiol.* **2005**, *71*, 371–381, doi:10.1128/AEM.71.1.371-381.2005.
132. Joseph, E.; James, S.; Albelda-Berenguer, M.; Albini, M.; Comensoli, L.; Cornet, E.; Domon Beuret, E.; Kooli, W.; Brambilla, L.; Mathys, L.; et al. Ground-Breaking Approaches for a Green and Sustainable Metal Conservation. In Proceedings of the Proceedings of 19th ICOM-CC Triennial Conference Transcending Boundaries: Integrated Approaches to Conservation; ICOM-CC: Beijing, 2021.
133. Staudt, C.; Horn, H.; Hempel, D.C.; Neu, T.R. Volumetric Measurements of Bacterial Cells and Extracellular Polymeric Substance Glycoconjugates in Biofilms. *Biotechnol. Bioeng.* **2004**, *88*, 585–592, doi:10.1002/bit.20241.
134. Mahapatra, S.; Banerjee, D. Fungal Exopolysaccharide: Production, Composition and Applications. *Microbiol. Insights* **2013**, *6*, MBI.S10957, doi:10.4137/MBI.S10957.
135. Paul, F.; Morin, A.; Monsan, P. Microbial Polysaccharides with Actual Potential Industrial

Applications. *Biotechnol. Adv.* **1986**, *4*, 245–259, doi:10.1016/0734-9750(86)90311-3.
136. Moon, S.-H.; Park, C.-S.; Kim, Y.-J.; Park, Y.-I. Biosorption Isotherms of Pb (II) and Zn (II) on Pestan, an Extracellular Polysaccharide, of Pestalotiopsis Sp. KCTC 8637P. *Process Biochem.* **2006**, *41*, 312–316, doi:10.1016/j.procbio.2005.07.013.
137. Chongdar, S.; Gunasekaran, G.; Kumar, P. Corrosion Inhibition of Mild Steel by Aerobic Biofilm. *Electrochim. Acta* **2005**, *50*, 4655–4665, doi:10.1016/j.electacta.2005.02.017.
138. Albelda-Berenguer, M.; Monachon, M.; Joseph, E. Siderophores: From Natural Roles to Potential Applications. In *Advances in Applied Microbiology*; 2019; pp. 193–225.
139. Rapti, S.; Boyatzis, S.C.; Rivers, S.; Pournou, A. Siderophores and Their Applications in Wood, Textile, and Paper Conservation. In *Microorganisms in the Deterioration and Preservation of Cultural Heritage*; Springer International Publishing: Cham, 2021; pp. 301–339 ISBN 9783030694111.
140. Pérez-Miranda, S.; Zamudio-Rivera, L.S.; Cisneros-Dévora, R.; George-Téllez, R.; Fernández, F.J. Theoretical Insight and Experimental Elucidation of Desferrioxamine B from Bacillus Sp. AS7 as a Green Corrosion Inhibitor. *Corros. Eng. Sci. Technol.* **2021**, *56*, 93–101, doi:10.1080/1478422X.2020.1824441.
141. Albelda-Berenguer, M.; Monachon, M.; Joseph, E. *Siderophores: From Natural Roles to Potential Applications*; 1st ed.; Elsevier Inc., 2019; Vol. 106; ISBN 9780128169759.
142. Braud, A.; Hoegy, F.; Jezequel, K.; Lebeau, T.; Schalk, I.J. New Insights into the Metal Specificity of the Pseudomonas Aeruginosa Pyoverdine-Iron Uptake Pathway. *Environ. Microbiol.* **2009**, *11*, 1079–1091, doi:10.1111/j.1462-2920.2008.01838.x.
143. Schalk, I.J.; Hannauer, M.; Braud, A. New Roles for Bacterial Siderophores in Metal Transport and Tolerance. *Environ. Microbiol.* **2011**, *13*, 2844–2854, doi:10.1111/j.1462-2920.2011.02556.x.
144. Chaturvedi, K.S.; Hung, C.S.; Crowley, J.R.; Stapleton, A.E.; Henderson, J.P. The Siderophore Yersiniabactin Binds Copper to Protect Pathogens during Infection. *Nat. Chem. Biol.* **2012**, *8*, 731–736, doi:10.1038/nchembio.1020.
145. Niinae, M.; Nishigaki, K.; Aoki, K. Removal of Lead from Contaminated Soils with Chelating Agents. *Mater. Trans.* **2008**, *49*, 2377–2382, doi:10.2320/matertrans.M-MRA2008825.
146. Brandel, J.; Humbert, N.; Elhabiri, M.; Schalk, I.J.; Mislin, G.L.A.; Albrecht-Gary, A.M. Pyochelin, a Siderophore of Pseudomonas Aeruginosa: Physicochemical Characterization of the Iron(Iii), Copper(Ii) and Zinc(Ii) Complexes. *Dalt. Trans.* **2012**, *41*, 2820–2834, doi:10.1039/c1dt11804h.
147. Fazary, A.E.; Al-Shihri, A.S.; Alfaifi, M.Y.; Saleh, K.A.; Alshehri, M.A.; Elbehairi, S.E.I.; Ju, Y.-H. Microbial Production of Four Biodegradable Siderophores under Submerged Fermentation. *Int. J. Biol. Macromol.* **2016**, *88*, 527–541, doi:10.1016/j.ijbiomac.2016.03.011.
148. Rapti, S.; Boyatis, S.; Rivers, S.; Velios, A.; Pournou, A. Removing Iron Stains from Wood and Textile Objects: Assessing Gelled Siderophores as Novel Green Chelators. In Proceedings of the Gels in the Conservation of Artconservation; Angelova, L., Ormsby, Bronwyn Townsend, Joyce Wolbers, R., Eds.; Archetype Publications: London, 2017; pp. 343–348.
149. Albelda Berenguer, M.; Monachon, M.; Jacquet, C.; Junier, P.; Rémazeilles, C.; Schofield, E.J.; Joseph, E. Biological Oxidation of Sulfur Compounds in Artificially Degraded Wood. *Int. Biodeterior. Biodegrad.* **2019**, *141*, 62–70, doi:10.1016/j.ibiod.2018.06.009.
150. Hong, L.; Simon, J.D. Current Understanding of the Binding Sites, Capacity, Affinity, and Biological Significance of Metals in Melanin. *J. Phys. Chem. B* **2007**, *111*, 7938–7947, doi:10.1021/jp071439h.
151. Oh, J.-J.; Kim, J.Y.; Kim, Y.J.; Kim, S.; Kim, G.-H. Utilization of Extracellular Fungal Melanin as an Eco-Friendly Biosorbent for Treatment of Metal-Contaminated Effluents. *Chemosphere* **2021**, *272*, 129884, doi:10.1016/j.chemosphere.2021.129884.
152. Gadd, G.M.; de Rome, L. Biosorption of Copper by Fungal Melanin. *Appl. Microbiol. Biotechnol.* **1988**, *29*, 610–617, doi:10.1007/BF00260993.
153. Gadd, G.M.; Griffiths, A.J. Effect of Copper on Morphology of Aureobasidium Pullulans. *Trans. Br. Mycol. Soc.* **1980**, *74*, 387–392, doi:10.1016/s0007-1536(80)80168-9.

154. Probst, C.; Garcia-Santamarina, S.; Brooks, J.T.; Van Der Kloet, I.; Baars, O.; Ralle, M.; Thiele, D.J.; Alspaugh, J.A. Interactions between Copper Homeostasis and the Fungal Cell Wall Affect Copper Stress Resistance. *PLOS Pathog.* **2022**, *18*, e1010195, doi:10.1371/journal.ppat.1010195.
155. Franco, L. de O.; Maia, R. de C.C.; Porto, A.L.F.; Messias, A.S.; Fukushima, K.; Campos-Takaki, G.M. de Heavy Metal Biosorption by Chitin and Chitosan Isolated from Cunninghamella Elegans (IFM 46109). *Brazilian J. Microbiol.* **2004**, *35*, 243–247, doi:10.1590/S1517-83822004000200013.
156. Monachon, M.; Albelda-Berenguer, M.; Joseph, E. Biological Oxidation of Iron Sulfides. In *Advances in Applied Microbiology Volume 107*; Gadd, G.M., Sariaslani, S., Eds.; Elsevier, 2019; pp. 1–27 ISBN 978-0-12-817618-4.
157. Valdés, J.; Pedroso, I.; Quatrini, R.; Dodson, R.J.; Tettelin, H.; Blake, R.; Eisen, J.A.; Holmes, D.S. Acidithiobacillus Ferrooxidans Metabolism: From Genome Sequence to Industrial Applications. *BMC Genomics* **2008**, *9*, 597, doi:10.1186/1471-2164-9-597.
158. Chernousova, S.; Epple, M. Silver as Antibacterial Agent: Ion, Nanoparticle, and Metal. *Angew. Chemie - Int. Ed.* **2013**, *52*, 1636–1653, doi:10.1002/anie.201205923.
159. Jadhav, U.; Hocheng, H. Extraction of Silver from Spent Silver Oxide-Zinc Button Cells by Using Acidithiobacillus Ferrooxidans Culture Supernatant. *J. Clean. Prod.* **2013**, *44*, 39–44, doi:10.1016/j.jclepro.2012.11.035.
160. Gupta, A.; Silver, S. Molecular Genetics: Silver as a Biocide: Will Resistance Become a Problem? *Nat. Biotechnol.* **1998**, *16*, 888–888, doi:10.1038/nbt1098-888.
161. WU, X. ling; QIU, G. zhou; GAO, J.; DING, J. nan; KANG, J.; LIU, X. xing Mutagenic Breeding of Silver-Resistant Acidithiobacillus Ferrooxidans and Exploration of Resistant Mechanism. *Trans. Nonferrous Met. Soc. China (English Ed.* **2007**, *17*, 412–417, doi:10.1016/S1003-6326(07)60107-1.
162. Guilger-Casagrande, M.; Lima, R. de Synthesis of Silver Nanoparticles Mediated by Fungi: A Review. *Front. Bioeng. Biotechnol.* **2019**, *7*, 1–16, doi:10.3389/fbioe.2019.00287.
163. González, A.L.; Noguez, C.; Beránek, J.; Barnard, A.S. Size, Shape, Stability, and Color of Plasmonic Silver Nanoparticles. *J. Phys. Chem. C* **2014**, *118*, 9128–9136, doi:10.1021/jp5018168.
164. Chauhan, P.S.; Shrivastava, V.; Tomar, R.S. Bio Fabrication of Copper Nanoparticles: A Next Generation Antibacterial Agent against Wound Associated Pathogens. *Turkish J. Pharm. Sci.* **2018**, doi:10.4274/tjps.52724.
165. Batool, F.; Iqbal, M.S.; Khan, S.-U.-D.; Khan, J.; Ahmed, B.; Qadir, M.I. Biologically Synthesized Iron Nanoparticles (FeNPs) from Phoenix Dactylifera Have Anti-Bacterial Activities. *Sci. Rep.* **2021**, *11*, 22132, doi:10.1038/s41598-021-01374-4.
166. Mott, D.; Galkowski, J.; Wang, L.; Luo, J.; Zhong, C.-J. Synthesis of Size-Controlled and Shaped Copper Nanoparticles. *Langmuir* **2007**, *23*, 5740–5745, doi:10.1021/la0635092.
167. Dang, T.M.D.; Le, T.T.T.; Fribourg-Blanc, E.; Dang, M.C. Synthesis and Optical Properties of Copper Nanoparticles Prepared by a Chemical Reduction Method. *Adv. Nat. Sci. Nanosci. Nanotechnol.* **2011**, *2*, 015009, doi:10.1088/2043-6262/2/1/015009.
168. Brajer, I.; Fossé-Le Rouzic, M.; Shashoua, Y.; Taube, M.; Chelazzi, D.; Baglioni, M.; Baglioni, P. The Removal of Aged Acrylic Coatings from Wall Paintings Using Microemulsions. In *ICOM-CC 17th Triennial Conference Preprints*; Bridgland, J., Ed.; Paris: International Council of Museums: Melbourne, Australia, 2014; p. 8 ISBN 9789290124108.
169. Chelazzi, D.; Giorgi, R.; Baglioni, P. Microemulsions, Micelles, and Functional Gels: How Colloids and Soft Matter Preserve Works of Art. *Angew. Chemie Int. Ed.* **2018**, *57*, 7296–7303, doi:10.1002/anie.201710711.
170. Baglioni, P.; Berti, D.; Bonini, M.; Carretti, E.; Dei, L.; Fratini, E.; Giorgi, R. Micelle, Microemulsions, and Gels for the Conservation of Cultural Heritage. *Adv. Colloid Interface Sci.* **2014**, *205*, 361–371, doi:10.1016/j.cis.2013.09.008.
171. Mazzoni, M.; Alisi, C.; Tasso, F.; Cecchini, A.; Marconi, P.; Sprocati, A.R. Laponite Micro-Packs

for the Selective Cleaning of Multiple Coherent Deposits on Wall Paintings: The Case Study of Casina Farnese on the Palatine Hill (Rome-Italy). *Int. Biodeterior. Biodegrad.* **2014**, *94*, 1–11, doi:10.1016/j.ibiod.2014.06.004.

172. Fratini, E.; Carretti, E. Chapter 10. Cleaning IV: Gels and Polymeric Dispersions. In *Nanoscience for the Conservation of Works of Art*; 2013; pp. 252–279 ISBN ISBN 978-1-84973-566-7.
173. Mehrotra, T.; Dev, S.; Banerjee, A.; Chatterjee, A.; Singh, R.; Aggarwal, S. Use of Immobilized Bacteria for Environmental Bioremediation: A Review. *J. Environ. Chem. Eng.* **2021**, *9*, 105920, doi:10.1016/j.jece.2021.105920.
174. Wolbers, R. Restoration'92: Conservation, Training, Materials and Techniques: Latest Developments. In *Preprints to the Conference Held at the RAI International Exhibition and Congress Centre*; Amsterdam, The Netherlands, 1992; pp. 74–75 ISBN 9781871656183.
175. Wolbers, R. Cleaning Painted Surfaces: Aqueous Methods. In; Archetype Publications, 2000; p. 198.
176. Van Loon, A.; Hartman, L.E.; van den Burg, J.; Haswell, R.; Pottasch, C. The Development of an Aqueous Gel Testing Procedure for the Removal of Lead-Rich Salt Crusts on the Surface of Paintings by Giovanni Antonio Pellegrini (1675–1741) in the "Golden Room" of the Mauritshuis. In; Springer: Berlin/Heidelberg, Germany, 2019; pp. 283–296.
177. Toreno, G.; Isola, D.; Meloni, P.; Carcangiu, G.; Selbmann, L.; Onofri, S.; Caneva, G.; Zucconi, L. Biological Colonization on Stone Monuments: A New Low Impact Cleaning Method. *J. Cult. Herit.* **2018**, *30*, 100–109, doi:10.1016/j.culher.2017.09.004.
178. Cushman, M.; Wolbers, R. A New Approach to Cleaning Iron Stained Marble Surfaces. *WAAC Newsl.* **2007**, *29*, 23–28.
179. Mazzuca, C.; Micheli, L.; Carbone, M.; Basoli, F.; Cervelli, E.; Iannuccelli, S.; Sotgiu, S.; Palleschi, A. Gellan Hydrogel as a Powerful Tool in Paper Cleaning Process: A Detailed Study. *J. Colloid Interface Sci.* **2014**, *416*, 205–211, doi:10.1016/j.jcis.2013.10.062.
180. Delattre, C.; Bouvet, S.; Le Bourg, E. Gellan Gum and Agar Compared to Aqueous Immersion for Cleaning Paper. In *Gels in the Conservation of Art*; Angelova, L. V., Ormsby, B., Townsend, J.H., Wolbers, R., Eds.; Archetype Publications: London, 2017; pp. 57–61 ISBN 9781909492509.
181. Guilminot, E.; Leroux, M.; Raimon, A.; Chalvidal, C. Projet Collaboratif Sur l'utilisation Des Gels Pour Le Traitement Des Métaux : Démarche et Fonctionnement. In *Journées des Restaurateurs en Archéologie. Journée d'Étude, de Recherche et d'Innovation*; Lyon, France, 2018; p. 14.
182. Baij, L.; Hermans, J.; Ormsby, B.; Noble, P.; Iedema, P.; Keune, K. A Review of Solvent Action on Oil Paint. *Herit. Sci.* **2020**, *8*, 43, doi:10.1186/s40494-020-00388-x.
183. Wolbers, R. Terminology and Properties of Selected Gels. In *Gels in the Conservation of Art*; Angelova, L. V., Ormsby, B., Townsend, J.H., Wolbers, R., Eds.; Archetype Publications: London, 2017; pp. 381–394 ISBN 9781909492509.
184. Rogovina, L.Z.; Vasil'ev, V.G.; Braudo, E.E. Definition of the Concept of Polymer Gel. *Polym. Sci. - Ser. C* **2008**, *50*, 85–92, doi:10.1134/S1811238208010050.
185. Baglioni, P.; Baglioni, M.; Bonelli, N.; Chelazzi, D.; Giorgi, R. Smart Soft Nanomaterials for Cleaning. In *Nanotechnologies and Nanomaterials for Diagnostic, Conservation and Restoration of Cultural Heritage*; Elsevier, 2019; pp. 171–204.
186. Stulik, D.; Miller, D.; Khanjian, H.; Khandekar, N.; Wolbers, R.; Carlson, J.; Petersen, C. Solvent Gels for the Cleaning of Works of Art: The Residue Question. In *Solvent Gels for the Cleaning of Works of Art: The Residue Question*; Wolbers, R., Ed.; Getty Institute of Conservation, 2004; Vol. 1, p. 180 ISBN 0-89236-759-8.
187. Duncan, T.T.; Berrie, B.H.; Weiss, R.G. A Comparison between Gel and Swab Cleaning: Physical Changes to Delicate Surfaces. In *Gels in the Conservation of Art*; Angelova, L. V., Ormsby, B., Townsend, J.H., Wolbers, R., Eds.; Archetype Publications: London, 2017; pp. 250–256 ISBN 9781909492509.
188. Guilminot, E. The Use of Hydrogels in the Treatment of Metal Cultural Heritage Objects. *Gels*

2023, *9*, 191, doi:10.3390/gels9030191.
189. Smith, S.S. Layer by Layer: The Removal of Complex Soiling on a Collection of Modern Art Bronzes Using Buffered PH-Adjusted Aquous Gels. In *Gels in the Conservation of Art*; Angelova, L. V., Ormsby, B., Townsend, J.H., Wolbers, R., Eds.; Archetype Publications: London, 2017; pp. 349–355 ISBN 9781909492509.
190. Parisi, E.I.; Bonelli, N.; Carretti, E.; Giorgi, R.; Ingo, G.M.; Baglioni, P. Film Forming PVA-Based Cleaning Systems for the Removal of Corrosion Products from Historical Bronzes. *Pure Appl. Chem.* **2018**, *90*, 507–522, doi:10.1515/pac-2017-0204.
191. Rolsky, C.; Kelkar, V. Degradation of Polyvinyl Alcohol in US Wastewater Treatment Plants and Subsequent Nationwide Emission Estimate. *Int. J. Environ. Res. Public Health* **2021**, *18*, 6027, doi:10.3390/ijerph18116027.
192. Chiellini, E.; Corti, A.; D'Antone, S.; Solaro, R. Biodegradation of Poly (Vinyl Alcohol) Based Materials. *Prog. Polym. Sci.* **2003**, *28*, 963–1014, doi:10.1016/S0079-6700(02)00149-1.
193. Feldman, D. Poly(Vinyl Alcohol) Recent Contributions to Engineering and Medicine. *J. Compos. Sci.* **2020**, *4*, 175, doi:10.3390/jcs4040175.
194. Rosciardi, V.; Chelazzi, D.; Baglioni, P. "Green" Biocomposite Poly (Vinyl Alcohol)/Starch Cryogels as New Advanced Tools for the Cleaning of Artifacts. *J. Colloid Interface Sci.* **2022**, *613*, 697–708, doi:10.1016/j.jcis.2021.12.145.
195. Duplat, V.; Rouchon, V.; Desloges, I.; Papillon, M.C. Steel versus Paper : The Conservation of a Piece of Modern Art Consisting of a Rust Print on Paper. *J. Pap. Conserv.* **2009**, *10*, 26–34.
196. Varghese, S.A.; Rangappa, S.M.; Siengchin, S.; Parameswaranpillai, J. Natural Polymers and the Hydrogels Prepared from Them. In *Hydrogels Based on Natural Polymers*; Elsevier, 2020; pp. 17–47.
197. Dalvi-Isfahan, M.; Hamdami, N.; Le-Bail, A. Effect of Freezing under Electrostatic Field on Selected Properties of an Agar Gel. *Innov. Food Sci. Emerg. Technol.* **2017**, *42*, 151–156, doi:10.1016/j.ifset.2017.06.013.
198. Tamura, M.; Takagi, K. Towards the Sustainable Use of Agar / Agarose in Conservation: A Case Study of the Izu Peninsula, Japan. In *Gels in the Conservation of Art*; Angelova, L. V., Ormsby, B., Townsend, J.H., Wolbers, R., Eds.; Archetype Publications: London, UK, 2017; pp. 152–154 ISBN 9781909492509.
199. Bertasa, M.; Chiantore, O.; Poli, T.; Riedo, C.; Di Tullio, V.; Canevali, C.; Sansonetti, A.; Scalarone, D. A Study of Commercial Agar Gels as Cleaning Materials. In Proceedings of the Gels in the Conservation of Art; Angelova, L. V., Ormsby, B., Townsend, J.H., Wolbers, R., Eds.; Archetype Publications: London, 2017; pp. 11–18.
200. Wolbers, R. Terminology and Properties of Selected Gels. In Proceedings of the Gels in the Conservation of Art; Angelova, L. V., Ormsby, B., Townsend, J.H., Wolbers, R., Eds.; Archetype Publications: London, 2017; pp. 381–394.
201. Jiang, F.; Xu, X.-W.; Chen, F.-Q.; Weng, H.-F.; Chen, J.; Ru, Y.; Xiao, Q.; Xiao, A.-F. Extraction, Modification and Biomedical Application of Agarose Hydrogels: A Review. *Mar. Drugs* **2023**, *21*, 299, doi:10.3390/md21050299.
202. Armisén, R.; Gaiatas, F. Agar. In *Handbook of Hydrocolloids*; Elsevier, 2009; pp. 82–107.
203. Yu, Z.; Zhan, J.; Wang, H.; Zheng, H.; Xie, J.; Wang, X. Analysis of Influencing Factors on Viscosity of Agar Solution for Capsules. *J. Phys. Conf. Ser.* **2020**, *1653*, 012059, doi:10.1088/1742-6596/1653/1/012059.
204. Guilminot, E.; Gomez, A.; Raimon, A.; Leroux, M. Use of Gels for the Treatment of Metals. In Proceedings of the Metal 2019 Proceedings of the Interim Meeting of the ICOM-CC Metals Working Group; Chemello, C., Brambilla, L., Joseph, E., Eds.; International Councils of Museums - Committee for Conservation, 2019; p. 473.
205. Marchand, G.; Chevallier, R.; Guilminot, E.; Rossetti, L.; Lemoine, S. Study of the Conservation Treatment Applied to the Archaeological Horn Silver Artifacts. In Proceedings of the Interim

Meeting for the International Council of Museums Committee for Conservation Metal Working Group, Metal 2013; International Councils of Museums - Committee for Conseravtion and Historic Scotland: Edinburgh, Scotland, 2013; pp. 245–250.
206. Fays, M. « d'or, d'argent et de Pate Noire : Incrustations Révélées » Étude et Conservation-Restauration de Cinq Objets Islamiques En Alliage Cuivreux Incrustés., Institut National du Patrimoine, 2018.
207. Wolbers, R.; Rivers, S.; Yamashita, Y. Corroded Applied Lead-Based Decoration (Hyomon) on Japanese Lacquer: Principles and Case Studies. *Stud. Conserv.* **2014**, *59*, S191–S194, doi:10.1179/204705814X13975704319316.
208. São João, J.; Branco, L.C.; Leite Fragoso, S. Trials Fo Agar Gels and Task-Specific Salts for the Electrochemical Reduction of Silver Sulphide on Silver Leaf. In Proceedings of the Gels in the Conservation of Art; Angelova, L. V., Ormsby, B., Townsend, J.H., Wolbers, R., Eds.; Archetype Publications: London, 2017; pp. 287–291.
209. Giordano, A.; Caruso, M.R.; Lazzara, G. New Tool for Sustainable Treatments: Agar Spray—Research and Practice. *Herit. Sci.* **2022**, *10*, 123, doi:10.1186/s40494-022-00756-9.
210. Hongu, T.; Phillips, G.O.; Takigami, M. Polymer Fibers for Health and Nutrition. In *New Millennium Fibers*; Elsevier, 2005; pp. 218–246.
211. Domon Beuret, E.; Mathys, L.; Brambilla, L.; Albini, M.; Cevey, C.; Bertholon, R.; Junier, P.; Joseph, E. Biopatines: Des Champignons Au Service Des Alliages Cuivreux. In *Cahier n°22 - XXVIIIe Journées des restaurateurs en archéologie. Arles, October 2014. ARAAFU*; Paris, France, 2015; pp. 45–48.
212. Tako, M.; Sakae, A.; Nakamura, S. Rheological Properties of Gellan Gum in Aqueous Media. *Agric. Biol. Chem.* **1989**, *53*, 771–776, doi:10.1080/00021369.1989.10869354.
213. García-Ochoa, F.; Santos, V..; Casas, J..; Gómez, E. Xanthan Gum: Production, Recovery, and Properties. *Biotechnol. Adv.* **2000**, *18*, 549–579, doi:10.1016/S0734-9750(00)00050-1.
214. Kuppuswami, G.M. Fermentation (Industrial) and Production of Xanthan Gum. In *Encyclopedia of Food Microbiology*; Elsevier, 2014; pp. 816–821.
215. Chan, K.; Morikawa, K.; Shibata, N.; Zinchenko, A. Adsorptive Removal of Heavy Metal Ions, Organic Dyes, and Pharmaceuticals by Dna–Chitosan Hydrogels. *Gels* **2021**, *7*, 1–10, doi:10.3390/gels7030112.
216. Fiamingo, A.; Montembault, A.; Boitard, S.E.; Naemetalla, H.; Agbulut, O.; Delair, T.; Campana-Filho, S.P.; Menasché, P.; David, L. Chitosan Hydrogels for the Regeneration of Infarcted Myocardium: Preparation, Physicochemical Characterization, and Biological Evaluation. *Biomacromolecules* **2016**, *17*, 1662–1672, doi:10.1021/acs.biomac.6b00075.
217. Giuliani, C.; Pascucci, M.; Riccucci, C.; Messina, E.; Salzano de Luna, M.; Lavorgna, M.; Ingo, G.M.; Di Carlo, G. Chitosan-Based Coatings for Corrosion Protection of Copper-Based Alloys: A Promising More Sustainable Approach for Cultural Heritage Applications. *Prog. Org. Coatings* **2018**, *122*, 138–146, doi:10.1016/j.porgcoat.2018.05.002.
218. Wang, X.; Hu, Y.; Zhang, Z.; Zhang, B. The Application of Thymol-Loaded Chitosan Nanoparticles to Control the Biodeterioration of Cultural Heritage Sites. *J. Cult. Herit.* **2022**, *53*, 206–211, doi:10.1016/j.culher.2021.12.002.
219. Mekahlia, S.; Bouzid, B. Chitosan-Copper (II) Complex as Antibacterial Agent: Synthesis, Characterization and Coordinating Bond- Activity Correlation Study. *Phys. Procedia* **2009**, *2*, 1045–1053, doi:10.1016/j.phpro.2009.11.061.
220. Trimukhe, K.; Varma, A. A Morphological Study of Heavy Metal Complexes of Chitosan and Crosslinked Chitosans by SEM and WAXRD. *Carbohydr. Polym.* **2008**, *71*, 698–702.

2. Microbes and metabolites for the uptake of corrosion products

P. fluorescens © Thermo fisher Scientific

The initial step into the development of bio-based methods for cleaning heritage metal objects is the study of microorganisms as micro-chemical factories. First by exploring living microorganisms' abilities to bioaccumulate some metals and then by using extracted compounds to avoid the handling of microorganisms in case the metabolic pathway allows.

Several fungal or bacterial strains have demonstrated promising results in terms of metal chelation and different metabolic processes can be exploited to remove corrosion products according to the chemical species present in the corrosion layer.

In the first part of this chapter, an insight is taken into the use of living microorganisms displaying interesting properties for the uptake of iron, copper, or silver. Specific assays are performed for the selection of different microorganisms, such as growth in presence of soluble and/or insoluble metal species, trying to investigate the reactions involved in metallic ions uptake. Afterwards, for promising strains allowing for the use of microbial extracts, filtered liquid cultures without living cells but containing metabolites as active agents are produced, purified as far as possible and quantified. When possible, the use of extracts will indeed allow an easier application by conservators and transfer to real praxis. Finally, the uptake by selected metabolites is evaluated, considering different physico-chemical parameters, including corrosion powder particle size and surface area as well as pH of the chelating agents' solution.

2.1 Insight into the use of living microorganisms

The inherent characteristics of selected living microorganisms are studied as a first step into their use for heritage metal remediation (Table 2.1). All selected strains are of risk class 1, except *Aspergillus niger* which is a class 2 microorganism according to the Swiss federal classification of microorganisms. This ranges organisms from 1 to 4, 1 being the lower risk class [1]. Risk group 1 organisms do not cause disease in healthy adult humans and risk group 2 may cause disease in adults, but which are treatable or preventable.

For iron and copper, reported fungal abilities of secondary metabolites production (i.e., siderophores, extracellular polymeric substances (EPS), and low molecular weight organic acids (LMWOA), or cell-wall uptake are of interest. Fungal species are less studied than bacterial species for the production of siderophores. Nevertheless, the fungal strain *Cunninghamella elegans* has been reported to have a particularly enhanced siderophores production [2], in the form of rhizoferrin, which is the only fungal carboxylate siderophore [3]. Moreover, it was also reported to perform cell-wall uptake thanks to the presence of chitin [4]. Works on the biopassivation of corroded copper objects through the production of copper oxalates are using the ability of *Beauveria bassiana* to produce oxalic acid, uptaking copper ions priorly to transforming them into oxalates [5]. *Alternaria alternata* and *Aureobasidium melanogenum* were reported for cell-wall uptake of iron or copper respectively [6–8], mainly thanks to the melanization of their cell wall. Indeed, melanin is able to chelate toxicmetals like copper, avoiding the penetration inside the fungal cell [9]. Finally, *Aspergillus niger* is a well-known producer of LMWOA, in particular citric acid [10], which is widely employed in conservation practices.

After evaluation of their ability to grow in presence of targeted corrosion products, interactions (e.g., absorption, conversion) were deeply studied through various spectroscopic techniques such as Ultraviolet-Visible spectroscopy (UV-Vis), Fourier Transformed InfraRed spectroscopy (FTIR), and inductively coupled plasma optical emission spectroscopy (ICP-OES), but also visual assessments (optical microscopy, colorimetry). Investigation of the metabolic pathways can be useful to understand whether studied fungi take up iron as a nutrient, as iron takes part in many metabolic processes [11] such as iron reduction activities [12].

For silver, a preliminary step was necessary to assess the resistance of selected microorganisms due to known silver antimicrobial properties. The study was restrained to two relevant bacterial strains. First, *Acidithiobacillus ferroxidans*, a extremophilic strain often encountered in coal mines and known to oxidize sulfides [13]. The accumulation of silver sulfides has also been observed on *A. ferrooxidans* cells, showing its potential silver resistance [14]. Thus, these observations make it a good candidate for silver sulfide removal in the context of tarnished silver cleaning.

Then, the ability of pyoverdine, a mixed type (i.e., displaying several binding moieties) of siderophore produced by *Pseudomonas yamanorum* [15,16], to take up silver ions is of interest and therefore the silver resistance of *P. yamanorum* was evaluated [17].

Literature also reports other bacterial strains able to resist silver, such as *Pseudomonas stutzeri AG259* originally isolated from the soil of a silver mine [18]. This strain was evaluated to be able to resist silver at concentrations up to 0.5 mM thanks to immobilization of silver by sulfide [21]. However, this strain was not studied further in this work because some of its metabolic pathways are the opposite of what is desired as tarnished silver cleaning action. Indeed, *P. stutzeri* produces H_2S which would likely retarnish the surface and is therefore not advisable for silver cleaning purposes.

Fungal strains are often reported in literature for silver nanoparticle (AgNPs) production, which is not so appealing for Ag_2S removal due to the need for silver to be in soluble phase, if not under its nitrate form ($AgNO_3$), added to the brown to black appearance of AgNPs [19,20].

Table 2.1 Microorganisms tested in the span of this study along with associated metabolic pathways reported for metal uptake.

Targeted metal	Name	Siderophore production	EPS	Cell-wall uptake	LMWOA	Remarks	Risk class
Iron	*Cunninghamella elegans*	×		×			1
	Alternaria alternata			×			1
	Aspergillus niger				×		2
	Beauveria bassiana		×		×		1
Copper	*Aureobasidium melanogenum*			×			1
	Beauveria bassiana				×		1
Silver	*Acidithiobacillus ferrooxidans*					Extremophile SOB	1
	Pseudomonas yamanorum	×					1

2.1.1 Materials and methods

2.1.1.1 Iron and copper

2.1.1.1.1 Strains and media

Fungal strains (Table 2.2) were screened for their abilities to take up iron and/or copper, through various uptake mechanisms (i.e., absorption, complexation).

Table 2.2 Fungal strains and culture media used for the screening intended for iron or copper remediation.

Targeted metal	Name	Provider	Strain identifier	Culture medium
Iron	*Cunninghamella elegans*	MUCL[1]	16087	Malt Yeast Extract
	Alternaria alternata	Université de Neuchâtel		Malt 1.2%$_w$
	Aspergillus niger	Université de Neuchâtel	NEUM8 [21]	Malt 1.2%$_w$
	Beauveria bassiana	Université de Neuchâtel	S6	Malt 1.2%$_w$
Copper	*Aureobasidium melanogenum*	MUCL[1]	IHEM 05468	Potato dextrose 4%$_w$
	Beauveria bassiana	Université de Neuchâtel	S6	Malt 1.2%$_w$

2.1.1.1.2 Growth capacities in presence of metal corrosion

Strains were inoculated on agar plates of their respective culture medium with and without addition of 2.5 $g \cdot L^{-1}$ α-FeOOH (goethite, from Alfa-Aesar) or Cu_2O (cuprite, from Sigma-Aldrich) according to the targeted metal. Pictures were taken each day and fungal growth rate was evaluated, measuring the average colony diameter with a ruler each day until the mycelium was covering the entire the Petri dish surface. Measured values were normalized with respect to the inoculate (value at 0 days). Fungal biomass was then observed under a Leica 2700DM stereomicroscope in bright field mode. Three independent replicas were performed.

2.1.1.1.3 Uptake evaluation in liquid cultures

The following protocol was adapted from Comensoli *et al* [22]. Strains were inoculated in 25 mL of their respective medium and cultured at 28 °C, 160 rpm. After 3 days of growth in plain medium to allow for a minimal growth, either soluble metal (10 mM iron citrate or $CuSO_4 \cdot 5H_2O$) or 1.5 cm^2 naturally lightly

corroded iron or copper plates were added aseptically to the medium. Iron citrate not being soluble, 61 mg were added directly into the 25 mL liquid cultures. For copper, 300 µL of 0.83 M copper sulfate stock solution (2.07 g of $CuSO_4 \cdot 5H_2O$ in 10 mL milli Q water) were added in 25 mL liquid cultures. Each test was performed in triplicates. Controls with no supplementation of metal source were prepared as well as abiotic controls. All different cultures were sampled (300 µL) each day for 7 days and then every three days for 3 weeks. Because of consequent manipulation of the flasks, contamination of the samples was tested on petri dish plates and contaminated samples were discarded from the study. At the end of experiment, the filtered biomasses were thoroughly rinsed before analysis. Although the presence of atmospheric oxygen influences results through redox reaction, experiments were carried out in uncontrolled aerobic conditions because application for practical treatment is undeniably performed under aerobic conditions, with these redox reactions influencing the overall process.

2.1.1.1.4 Characterization techniques

For iron, culture samples were analyzed using ferrozine assay. Ferrozine® assay measures iron concentration [Fe^{2+}] in solution [23]. Briefly, 30 µL of 5 M HCl was added to 300 µL of sample. 100 µL were then taken and mixed with 900 µL of Ferrozine reagent 0.1% w/v prepared in 100 mM HEPES pH 7. To measure total iron, 150 µL of hydroxylamine-HCl, a reducing agent, were added. The absorbance was measured at 562 nm using a 96-well Victor Nivo microplate reader (Perkin Elmer) after 2 minutes to allow reaction. Total iron and Fe^{2+} in solution were calculated using standard calibration curves with known concentrations of iron (Figure S2.1). [Fe^{3+}] concentration was calculated subtracting [Fe^{2+}] concentration from total iron concentration.

For copper, culture samples were freed from mycelium using toothbrushes, filtered using 0.45 µm PTFE filters, diluted and analyzed thanks to ICP-OES (Optima 2100 DV, Perkin Elmer®, details in Table S2.1). Copper and iron plates were characterized using a Minolta CM-508D spectrophotometer, performing three measurements on each side (front and back), before and after immersion in respective culture solutions. SCE data were used for iron and SCI data were used for copper to account for gloss observed with copper-based substrate [24].

Raman spectroscopy was used to identify compounds present on metal plates before and after immersion using a Renishaw Virsa system with the following parameters: 785 nm laser, 50× objective, 1s acquisition time, and 50 accumulations in the range 50-1250 cm^{-1}.

Biomass samples from liquid cultures were observed using a Leica 2700DM stereomicroscope and further analyzed with a ThermoFischer is5 FTIR spectrometer, in ATR (attenuated Total Reflectance) mode, spectral range 650-4000 cm^{-1} with 4 cm^{-1} spectral resolution and 16 scans. Post-processing using OMNIC software included baseline correction and atmospheric correction (H_2O, CO_2).

Statistical significance of the result was verified using one way or two-way ANOVA tests, in particular Tuckey post-hoc test using RStudio.

2.1.1.2 Silver

2.1.1.2.1 Strains and medium

Bacterial strains studied for the removal of silver tarnish were *Pseudomonas yamanorum* DSM2005 (University of Neuchâtel), and *Acidithiobacillus ferrooxidans* DSM14882 (DSMZ).

A. ferroxidans was cultivated in DSMZ 882[2] medium whereas *P. yamanorum* was cultivated in Nutrient broth (NB) or Succinate medium (SM), poor in iron, to enhance the production of reported silver-complexing siderophores. Details concerning specific media employed can be found in Table S2.2.

2.1.1.2.2 Silver resistance tests

Strains were cultivated in 25 mL of their respective medium with addition of soluble silver ($AgNO_3$) in various concentrations of: 0 mM, 0.001 mM, 0.002 mM, 0.005 mM, 0.01 mM, 0.2 mM, 0.5 mM and 1 mM. To do so, 0, 25, 50, 125 and 250 µL of 1 mM stock solution (0.17 g/L) were added into 25 mL DSMZ 882 or SM medium. Cultures were left for 14 days at 25 °C without agitation for *A. ferroxidans* and for 5 days at 28 °C with 130 rpm agitation for *P. yamanorum*, regardless of the medium (NB or SM) used. Abiotic controls were prepared, and tests were performed in triplicate.

2.1.1.2.3 Characterization techniques

Samples were collected aseptically at the end of experiment and observed using a Leica DM2700M microscope in bright field mode.

Fluorescence of the culture solution was also verified using a Victor-Nivo multimode microplate reader from Perkin Elmer, in fluorescence mode to account for pyoverdine production with λ_{ex}= 450 ± 10 nm and λ_{em} = 405 ± 10 nm [17].

2.1.2 Results and discussion

2.1.2.1 Iron

To assess the impact of metal presence on the growth of fungi, the growth rates of studied strains on plain or iron-supplemented agar plates are plotted on figure 2.1.

Cunninghamella elegans growth in presence of iron was slowed down to 0.48 cm/day in average versus 0.53 cm/day on malt yeast extract medium, corresponding to a 9.4% difference in average after 12 days. Taking a closer look, the rate actually slowed down for *C. elegans* on iron after 7 days, dropping from 0.56 cm/day to 0.35 cm/day which is not the case for *C. elegans* culture on plain medium, showing the fungi was affected by the presence of iron source on the long term, with a diminution of the growth rate

[2] https://www.dsmz.de/microorganisms/medium/pdf/DSMZ_Medium882.pdf

by 37.5% after 7 days, and which becomes significant after 10 days. For *Beauveria bassiana*, no statistically significant split was observed, with a growth rate of 0.31 cm/day on malt agar and 0.27 cm/day on malt agar medium amended with goethite, which corresponds to a 12.9% difference. For *Alternaria* sp., growth was similar with or without the adjunction of iron in the malt agar medium with a growth of 0.49 cm/day. In all cases, difference between plain or iron-enriched medium were not statistically significant and therefore, it can be stated that fungi were also able to grow when iron was present, although a decrease is observed for *C. elegans.*

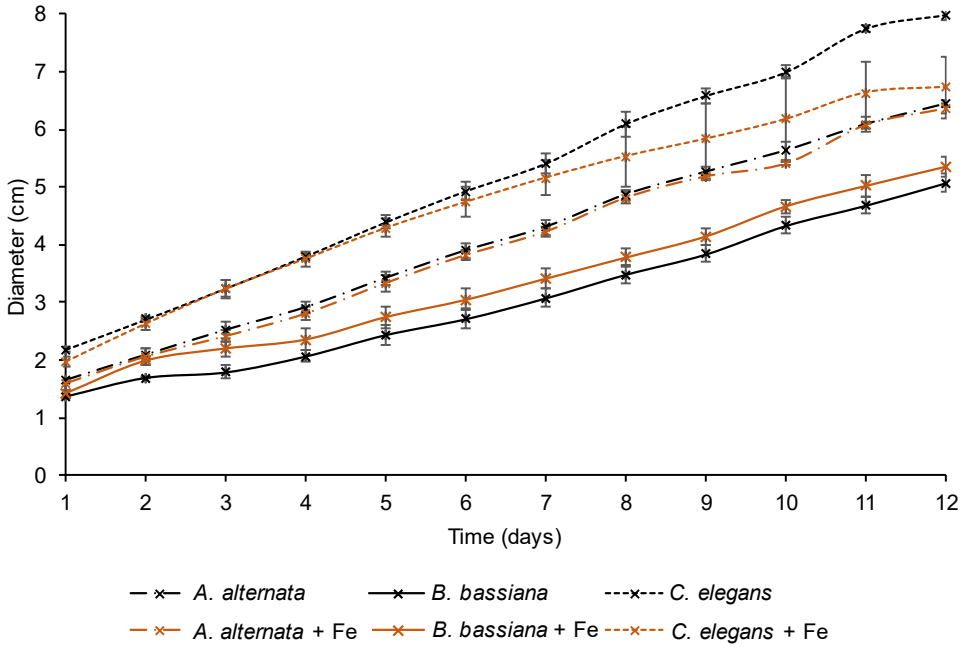

Figure 2.1 Growth rate of *A. alternata, C. elegans* and *B. bassiana* on plain (black) or iron-enriched (orange) culture medium. Diameter at 0 days corresponds to the inoculate. Error bars refer to standard deviation of independent replicas.

Strong sporulation of *Aspergillus niger* on both plain and Fe-enriched agar plates resulted in the presence of multiple colonies and the impossibility to measure the growth rate. Still, it is possible to comment that the presence of iron did not inhibit the growth of the fungi (Figure 2.2b). Visual aspects of *A. niger* fungal mycelium on plain or iron-enriched medium were similar.

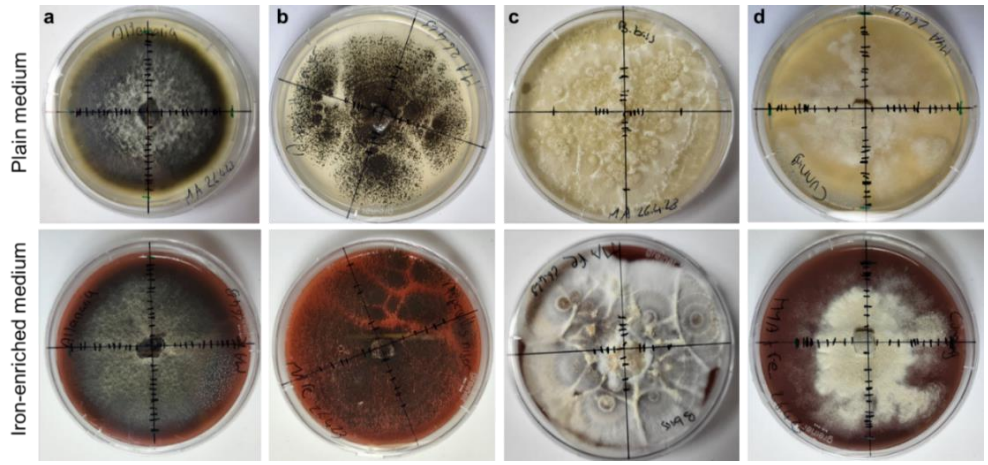

Figure 2.2 Agar plates of plain or iron-supplemented medium with fungi: *A. alternata* (a), *A. niger* (b), *B. bassiana* (c), *C. elegans* (d), after 15 days.

In liquid cultures of studied fungal strains (figure 2.3), the presence of soluble iron affected the appearance of the biomass, turning to dark color in particular for *Alternaria* and *Cunninghamella* culture solutions. The aspect of the medium after 1 month of incubation with the corroded steel plate resulted in different aspects. In particular, the appearance of *Alternaria* and *Aspergillus* culture solutions was quite different from the abiotic control. Especially, for *Aspergillus*, it is barely noticeable that there could be iron in the medium as the solution turns clear and uncolored. For *Alternaria*, the culture solution becomes cloudy and slightly orange-shade-tinted with time. These observations suggest that some interactions occur between the metal and the fungi, which will be further interpreted thanks to Figure 2.4.

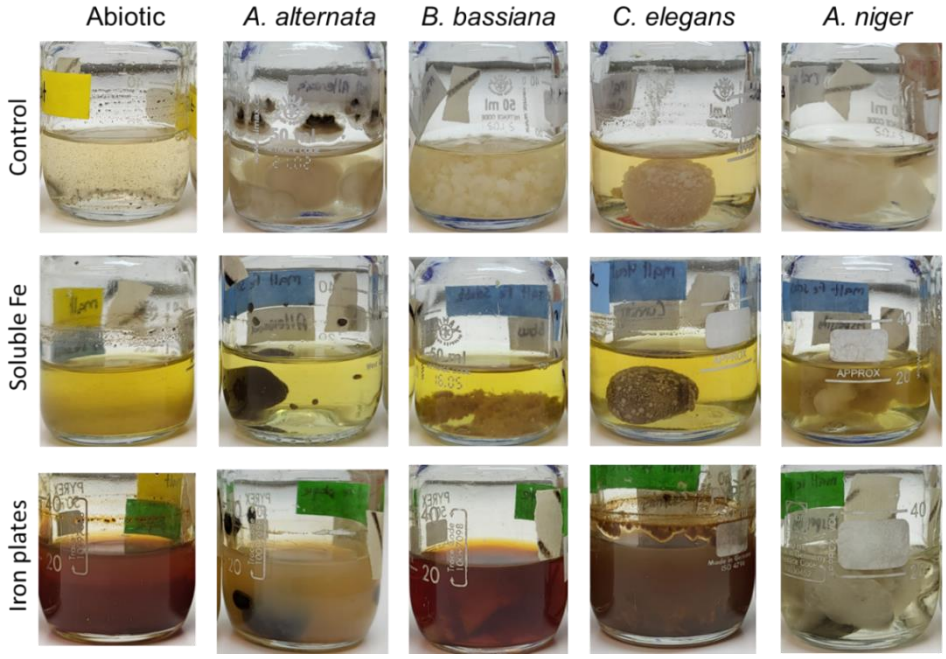

Figure 2.3 Liquid cultures of fungal strains incubated for 1 month in plain medium, soluble iron-supplemented medium or medium with corroded iron plate

To verify any iron uptake or reduction, quantification via ferrozine assay was performed. Ferrozine assay of the culture solutions overtime with different fungi is displayed in figure 2.4.

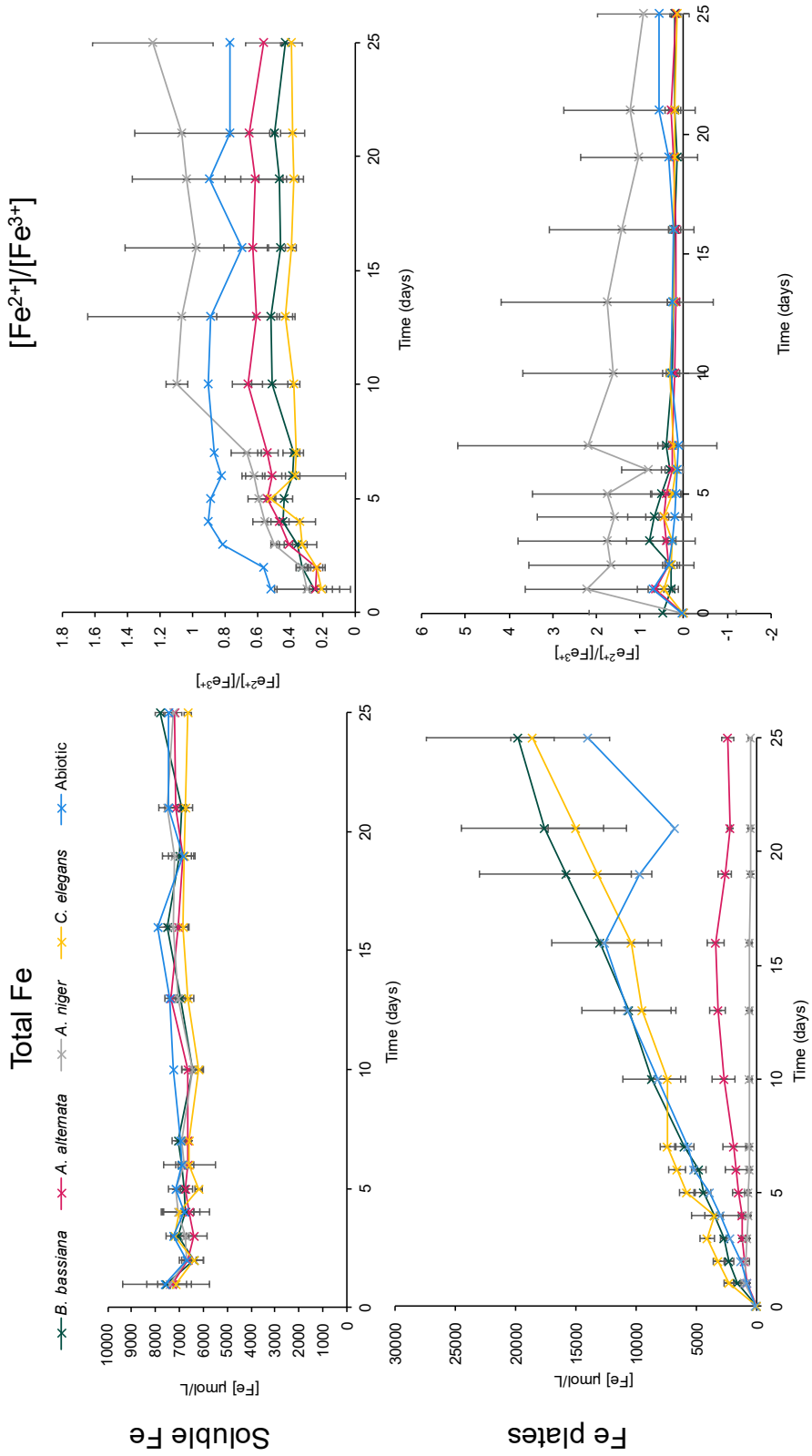

Figure 2.4 Ferrozine assay displayed as total iron detected and Fe^{2+}/Fe^{3+} ratio for cultures amended with soluble Fe or Fe plate. Soluble iron values start at day 1 to allow for the full solubilization of the added iron citrate. Error bars refer to standard deviation of independent replicas.

Interaction with soluble iron

For cultures containing soluble iron, there are no statistically significant changes in respect to the abiotic control (blue curve) whether for total amount of iron, standing for iron uptake, or $\frac{Fe^{2+}}{Fe^{3+}}$ standing for iron conversion. Only *A. niger* shows an increase in the $\frac{Fe^{2+}}{Fe^{3+}}$ ratio that is statistically significant until 7 days of culture but becomes unreliable with respect to the abiotic control after this duration. It is important to also consider that experiments were not performed in strict anoxic conditions, thus side redox reactions could influence the Fe^{2+} to Fe^{3+} ratio, increasing the presence of the latter due to oxidation reactions. It is therefore believed that the amount of solubilized iron, theoretically 10 mM but experimentally closer to 7 mM (Figure 2.4), was too high for the fungi to strive in this environment and therefore annihilated their growth. In the previous section on Petri dishes, goethite was not entirely solubilized hence did not have the same effect.

Interaction with iron plates

Inversely, cultures with iron plates achieved valuable results. The total iron concentration rose constantly for *Cunninghamella elegans* and *Beauveria bassiana,* up until about 20 mM (figure 2.4), similarly to the abiotic control as the iron from the corroded plate was getting solubilized, indicating no uptake from either of these strains. For *Alternaria alternata* and even more *Aspergillus niger*, the total amount of iron measured in solution remains low, indicating a possible uptake. This is in accordance with the previous visual observations of the liquid cultures, as *Alternaria* and *Aspergillus* were the ones which appearance differed from the abiotic control. Furthermore, in the unique case of *Aspergillus niger*, the $\frac{Fe^{2+}}{Fe^{3+}}$ ratio higher than for the abiotic control, indicating an iron conversion, more specifically reduction. Nevertheless, the extremely high standard deviation values obtained prevent any data exploitation hence conclusion drawn out of these iron conversion results (i.e., results are not statistically confirmed). Iron is essential to life but can also be toxic to biological systems [25,26]. Possibly, the soluble form of iron, therefore ionic, inhibited the normal metabolism of studied fungi, resulting in the absence of interaction with the metal. Indeed, in the presence of higher concentrations of solid iron (2.5 g/L FeOOH, 28 mM in agar Petri dishes or 20 mM with iron plates after 1 month), fungal growth was still observed (Figure 2.2), contrary to lower concentrations of soluble iron (7 to 10 mM). For such, the toxicity rather comes from the form of the iron in contact rather than the concentration itself, as it can be found in literature [27]. On the opposite, iron oxides from plates solubilize in solution at constant rate, close to 800 µM/day, allowing microorganisms to adapt progressively to the increasing concentration of iron in solution [27].

The uptake from *Alternaria* could be due to cell wall adsorption or the excretion of siderophores by *A. alternata* [28,29]. For *Aspergillus*, the uptake was originally thought to be due to the production of organic

acids, expectedly citric acid [30]. However, further Raman analysis of the iron plates after immersion showed the conversion of iron phases present (lepidocrocite, γ-FeOOH) into ferrous oxalates ($FeC_2O_4 \cdot x\ H_2O$) (Figure 2.5). Indeed, Raman peaks at 218, 250, 303, 349, 378, 527 and 650 cm^{-1}, characteristic of lepidocrocite [31], were detected before the experiment. After immersion into *Aspergillus niger* culture, Raman peaks corresponding to the presence of iron oxalates were detected [32]. Main bands are found at 108, 202, 248, 519, 582 and 915 cm^{-1}, typical of ferrous oxalates. Other small peaks at 304 and 856 cm^{-1} are found in ferric oxalates Raman spectra but are not predominant here [33].

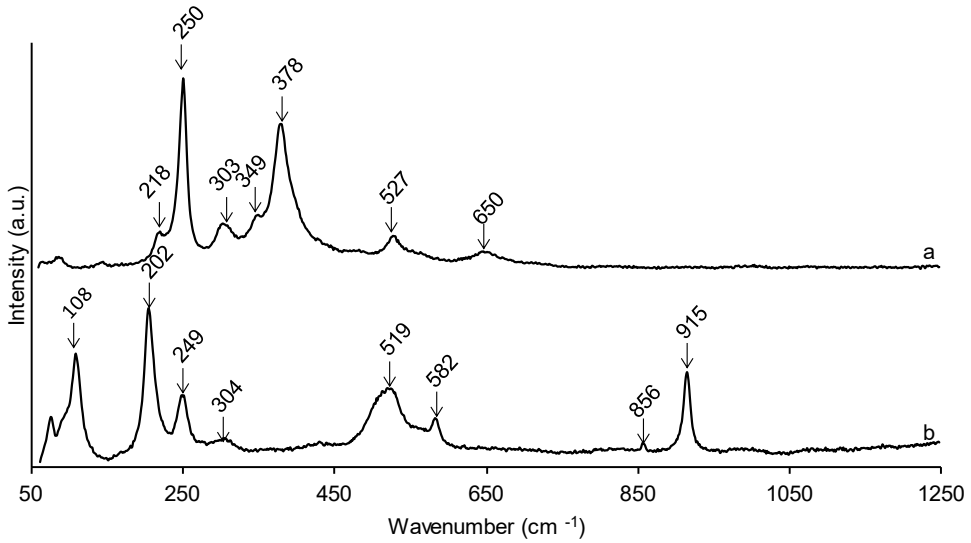

Figure 2.5 Raman spectra of immersed iron plates before (a) and after (b) 1-month growth in *A. niger* liquid culture.

It is believed that *A. niger* first takes up Fe^{3+} thanks to oxalic acid secreted by the fungi as secondary metabolites [34,35], explaining the low total iron amount detected in solution, then turns Fe^{3+} into Fe^{2+} thanks to microbiological pathways and finally excretes Fe^{2+} into the medium in the form of oxalates [36]. This passivation of iron through the formation of Fe-oxalates by definition limits further iron corrosion as passivation is the formation of a self-limiting corrosion layer that protects the underlying metal from further corrosion [37]. This could also explain the lower quantities of iron found in solution after 1 month. For such, the *A. niger* strain used in this work, secretes oxalic acid rather than citric acid as stated beforehand [21,38]. A deeper understanding of the underlying processes could be of use in heritage conservation, especially for iron passivation [28], as ferrous oxalates are poorly soluble in water contrary to ferric oxalates [34].

Visual observations of the corroded iron plates after immersion showed an obvious difference for the ones in the *Aspergillus niger* containing flasks (figure 2.6). Other plates showed equally or more corroded aspect. Interestingly, pH of malt agar medium was measured at 5.2 and dropped to 4.85 after 1 month of corroded iron plate immersion whereas it stayed constant without the addition of a corroded plate. At such unadjusted and unbuffered pH, the liquid culture environment tends to enhance further

corrosion as this pH range in aqueous environments corresponds to the ionic form of iron in the Pourbaix diagram (Figure I.2). if there is no action from the microorganism.

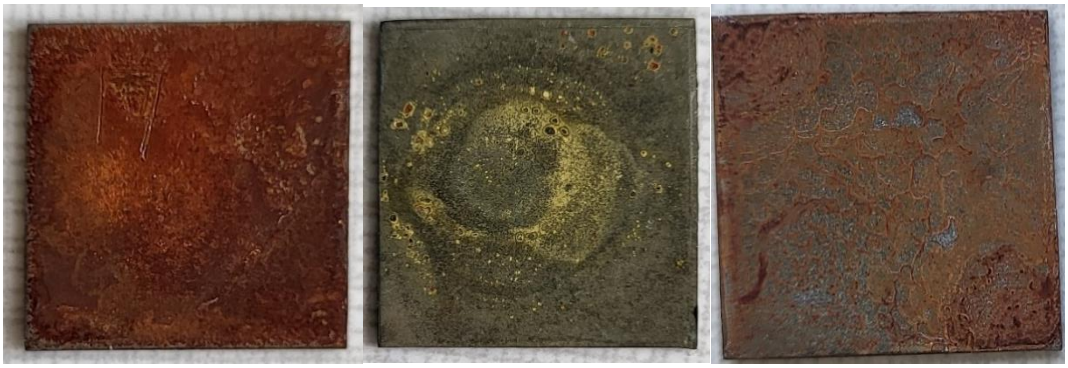

Figure 2.6 1.5 cm² iron plates before (left) and after immersion into *A. niger* (middle) and *C. elegans* (right) cultures.

This was confirmed by colorimetric data (figure 2.7), showing the plates immersed in *A. niger* shifting towards less reddish (lower a*) and lighter (higher L*) appearance, confirming the removal of iron oxyhydroxides and formation of yellow ferrous oxalates (Figure 2.6) [37]. *C. elegans* also shows a colorimetric shift towards less orange values. Raman analysis showed no change in the corrosion layer composition (data not shown). For such further studies would be interesting to explain this color shift for *C. elegans*, as no uptake was observed.

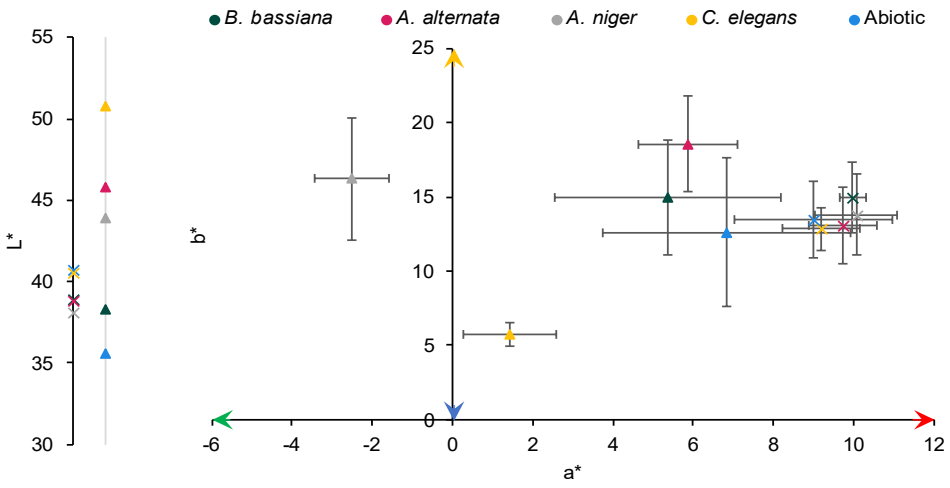

Figure 2.7 Colorimetric values of iron plates before (crosses) and after (triangles) immersion into fungal cultures. Error bars refer to standard deviation of independent replicas .

Most strains were not affected by the presence of corroded iron plates in agar medium but it was the case for liquid cultures with the presence of soluble iron at the tested concentration (7-10 mM). Furthermore, liquid cultures in non-pH adjusted medium tend to become more acidic while iron dissolves and therefore enhance iron corrosion as it is not in the stability range of iron oxyhydroxides as can be seen on iron Pourbaix diagram (Figure I.2). Although some action was detected in *Alternaria* cultures with iron plates, the only one with a clear action over iron metal samples was *Aspergillus niger*,

with the uptake of iron and conversion into ferrous oxalates. To verify iron uptake by *Alternaria* and *Aspergillus* in their respective biomass, it would be worthy to perform acidic digestion of the fungal mycelia, quantify the amount of iron in the biomass and compare it to the amount of iron in the culture solution. For such experiments, ICP measurements could be more reliable than Ferrozine assays, yielding values with lower standard deviation.

2.1.2.2 Copper

Similar experiments were carried out regarding copper with promising strains: *Beauveria bassiana* and *Aureobasidium melanogenum*. The average measured growth rate of *Aureobasidium melanogenum* (0.63 cm/day) is twice as fast than *Beauveria* (0.31 cm/day) (Figure 2.8). However, *Aureobasidium* growth was completely inhibited on the copper-enriched agar plates (Figure 2.9a). The concentration used (2.5 g/L Cu_2O ≈ 79 mM Cu) is much higher, hence more toxic, than the concentrations tested for copper uptake for *A. melanogenum* in literature (5 mM Cu) [7,39], but relevant as the use of those microorganisms for bioremediation purposes requires high copper tolerance. Regarding *Beauveria bassiana*, the presence of copper in the medium resulted in a slightly slower average growth of the fungi (0.27 cm/day), which was statistically significant after 12 days.

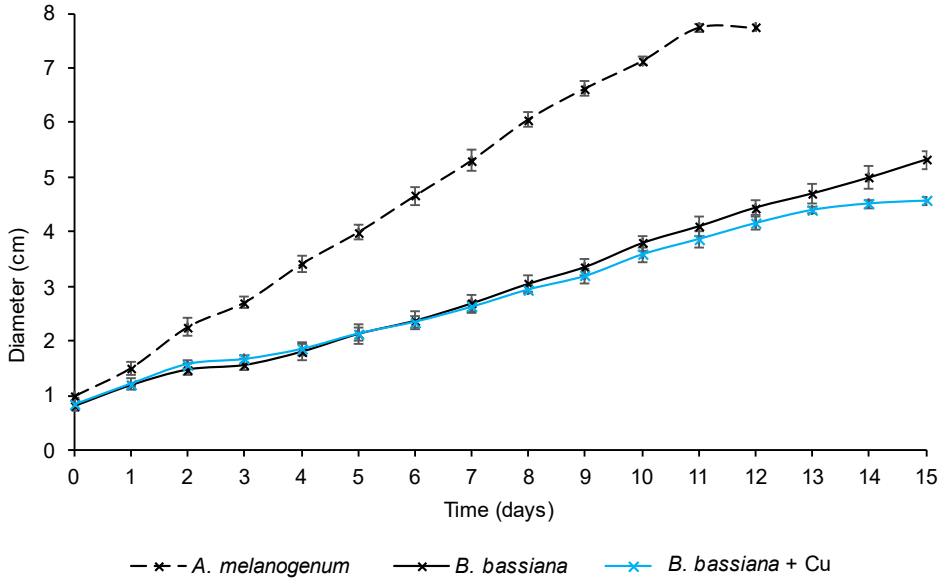

Figure 2.8 Growth rate of *A. melanogenum* and *B. bassiana* on plain (black) or copper-enriched (blue) medium. No growth observed for *A. melanogenum* on copper-enriched medium. Diameter at 0 days corresponds to the inoculate. Error bars refer to standard deviation of independent replicas.

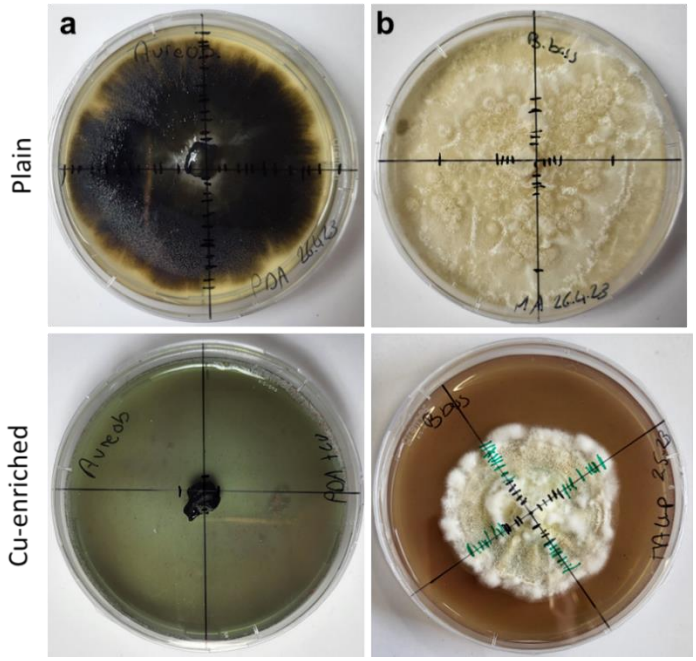

Figure 2.9 Agar plates of plain or copper-supplemented medium with fungi: of *A. melanogenum* (a) and *B. bassiana* (b).

After approximately 10 days of *B. bassiana*'s growth, greenish hues started to appear in the fungal biomass (Figure 2.10c). On the verso of the petri-dishes, some ring patterns were observed (Figure 2.10b). This is in accordance to previous observations [40]. These rings, corresponding to Liesegang pattern, appear with the combination of reaction, diffusion, and precipitation processes. The mechanism is believed to be based on depletion of supersaturation of copper in the medium when oxalates are formed, creating spaces between copper-oxalates concentric excretions [41]. Interestingly, when there is a strong sporulation, these rings cannot be differentiated but appear more as spots for each colony(Figure 2.10d). Microscope observation of these greenish area present aggregates (Figure 2.10e), that have previously been identified as copper oxalates and thoroughly studied [5]. The formation of these oxalates rings is strongly linked to the role of oxalic acid overexcretion by the fungi, which therefore could be of interest for copper uptake [42].

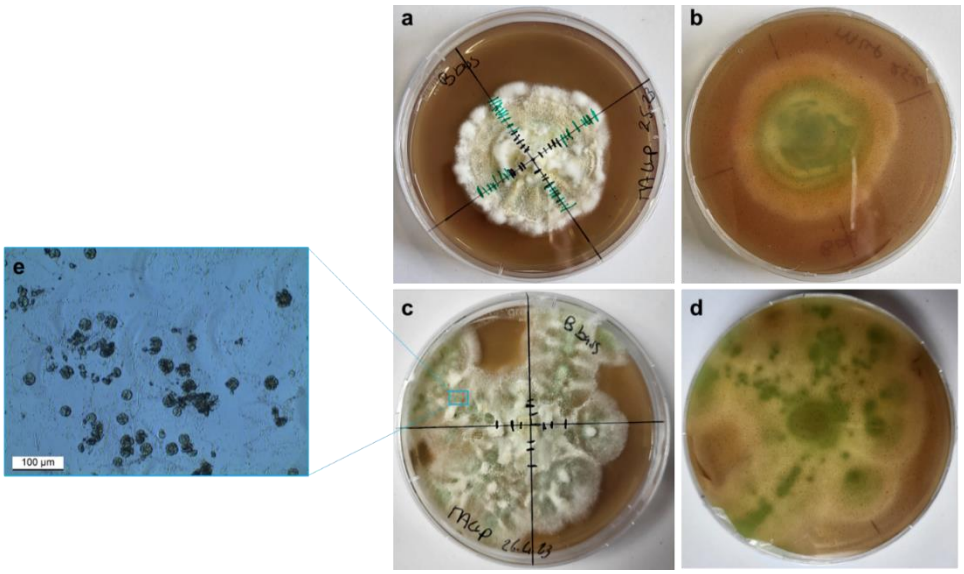

Figure 2.10 Copper-enriched agar plates after 13 days of incubation of *B. bassiana* without (a,b) or with (c,d) multiple colonies due to sporulation and optical microscope observation of the mycelium with green aggregates attributed to copper oxalates (e).

In liquid cultures, it is important to note that in one out of the triplicates, a very different aspect of fungal growth took place for the plain medium and the copper plate for *A. melanogenum* with a darkening of the medium (figure 2.11). So far, the phenomenon could not be explained. There does not seem to be any action from the fungi on soluble copper in addition to lack of further fungal growth. Similarly to iron, soluble copper is believed to be noxious for *A. melanogenum*.

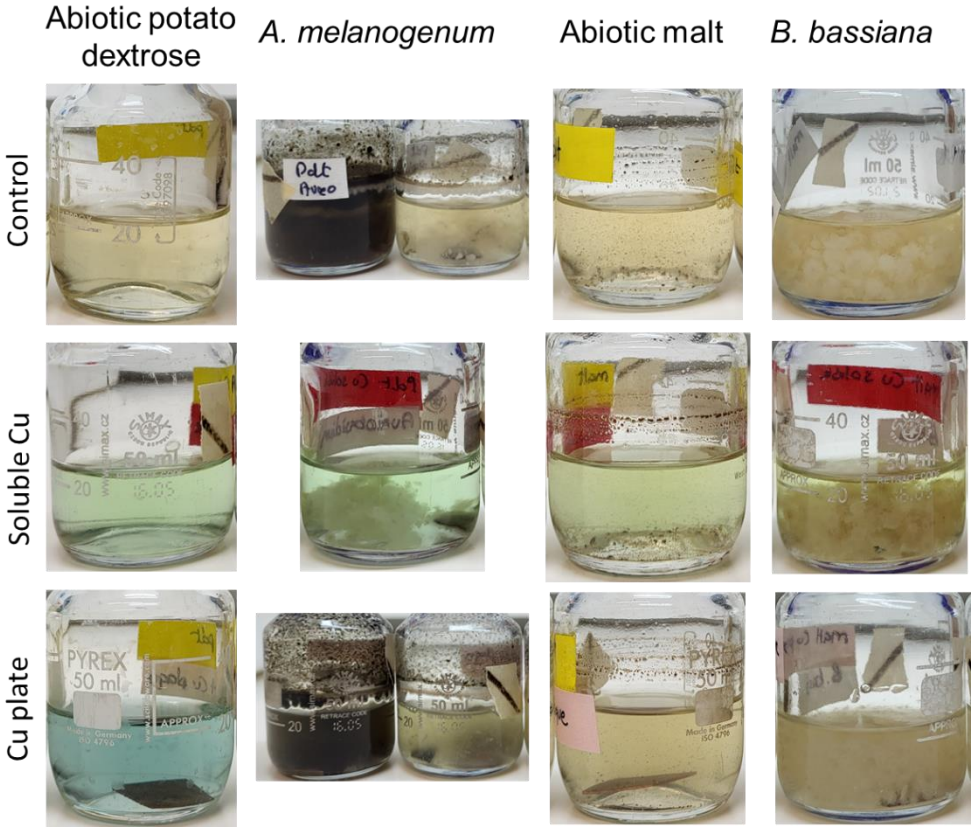

Figure 2.11 Liquid cultures of fungal strains in plain medium, soluble copper supplemented medium or medium with an added tarnished copper plate, after 1 month.

This is supported by the copper content detected with ICP-OES in *A. melanogenum* culture with soluble copper (Figure 2.12) which remained similar through the culturing period at a value of [Cu] = 9.6 ± 06 mM. The blueish hue of the abiotic potato dextrose medium with copper plates disappeared in the presence of *Aureobasidium*. In cultures with added copper plates, the behavior was visually different for *A. melanogenum* compared to the abiotic control, with a strong blue appearance, related to the presence of copper ions, as confirmed by ICP-OES quantification (Figure 2.12). These results suggest the dissolution of copper from the plate into the potato dextrose medium, with a potential action from the fungi as this increase to approximately 3 mM of copper did not occur in the culture containing *A. melanogenum*. Alternatively, the presence of the fungi could also modify the medium and its ability to solubilize copper from the plate.

Regarding *Beauveria bassiana* in soluble copper culture, ICP-OES results show a slight but significant decrease in copper concentration, going from 9.0 ± 1.9 to 6.6 ± 0.8 mM (Figure 2.12), that is not observed in the abiotic control. Indeed, there visually seem to be a greater fungal growth than for *Aureobasidium melanogenum* (Figure 2.11). In the culture with the corroded copper plates, quantification of copper showed that in presence of *B. bassiana*, copper dissolution was statistically significantly enhanced, reaching values almost doubled compared to the abiotic control. This is connected to the excretion of oxalic acid by the fungi, that helps the dissolution of copper [41].

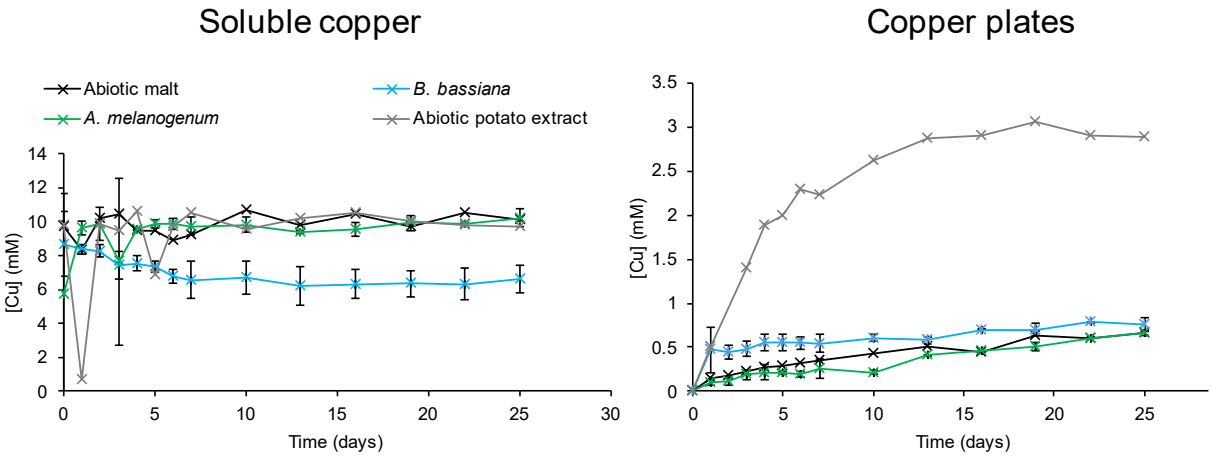

Figure 2.12 ICP-OES measurements of copper in liquid cultures overtime. Error bars refer to standard deviation of independent replicas.

FTIR analyses of the biomass of *B. bassiana* (figure 2.13) show the appearance of sharp bands at 822, 1320, 1363 and 1617 cm^{-1}, which are characteristics of copper oxalates [5,43], due to the solubilized copper transformation via the fungi [41].

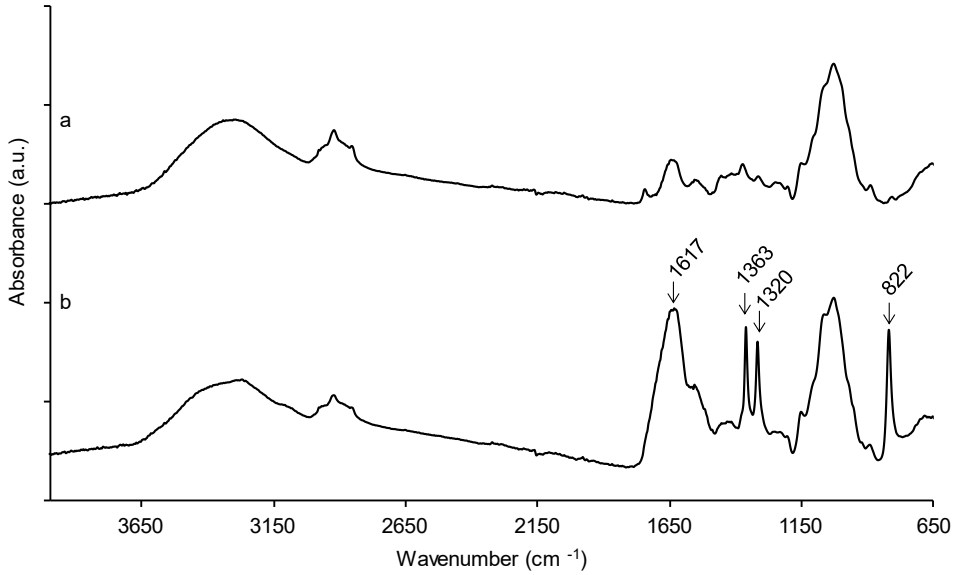

Figure 2.13 FTIR spectra of *B. bassiana* biomass in plain (a) or copper-implemented medium (b).

Visual observations of the plates after immersion showed a clear removal of the corrosion layer for *B. bassiana* samples, reaching a shiny metallic appearance, and were confirmed by colorimetric measurements (Figure 2.14) which showed a statistically significant shift (p-value = 0.02).

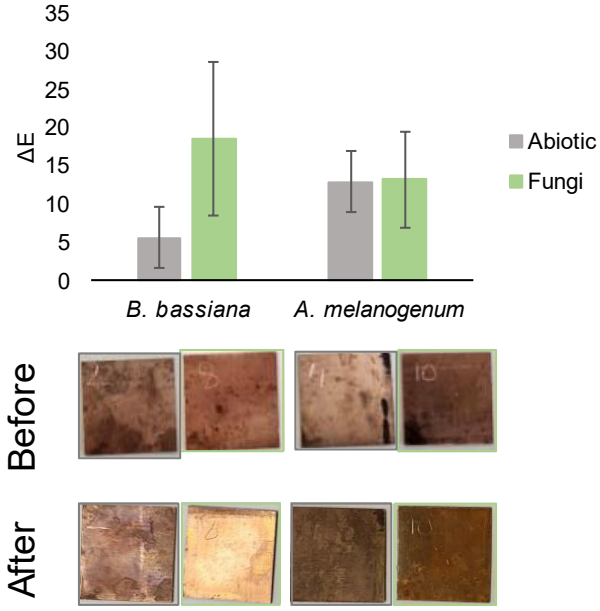

Figure 2.14 Pictures and color differences of copper plates before and after immersion in fungal culture.

In detailed colorimetric data, copper samples after immersion in the *B. bassiana* culture stood out, shifting to light and orangish values (Figure 2.15).

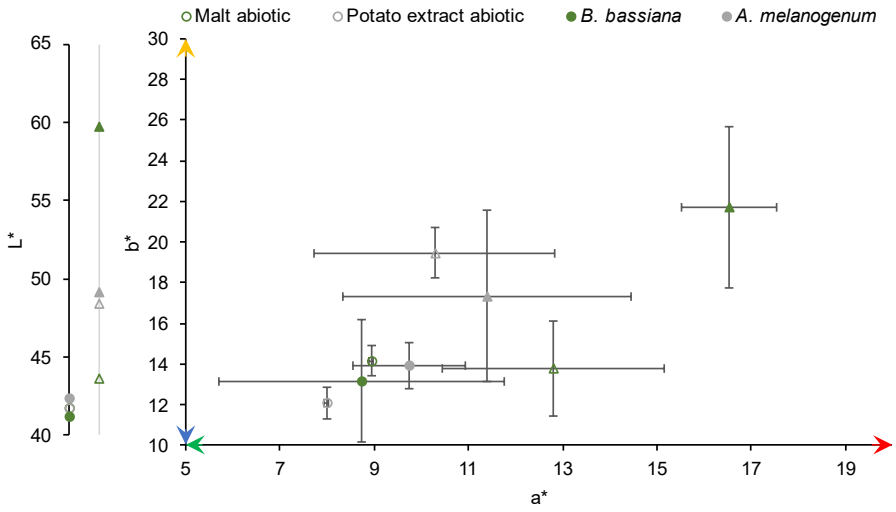

Figure 2.15 Colorimetric values of copper plates before (circles) and after (triangles) immersion into fungal cultures (filled marks) or abiotic (empty marks). Error bars refer to standard deviation of independent replicas.

Overall, on agar media repleted with cuprite (Cu_2O), only *B. bassiana* displayed interesting growth properties, as had been demonstrated previously [40]. In liquid culture, visible action of *Beauveria bassiana* was observable both with added soluble copper or copper plates. The action on corroded copper plates yielded extremely good results in the presence of *Beauveria bassiana*. Overall, *A. melanogenum* intolerance to high copper concentrations makes it a poor candidate for direct application on copper-based artifacts, contrarily to *B. bassiana,* whose tolerance and action on copper has long been assessed. As discussed, the action of *Beauveria bassiana* is most likely due to its production of LMOWA, in particular oxalic acid. It would therefore be interesting to make use of that metabolite to break free from living fungus. Nevertheless, it should be noted that when using oxalic acid from industrial origin, studies have shown the apparition of powdery blue copper corrosion products [44]. Hence, the need for a bioproduced oxalic acid may be mandatory, as its action could be slightly modified due to the presence of other secondary metabolites or compounds from the culture medium.

2.1.2.3 Silver

To assess *Acidithiobacillus ferrooxidans* growth in presence of different concentrations of silver nitrate added to medium, the coloration of the medium is a good indicator. Indeed, along with the exponential growth phase, the bacteria, a SOB, performs ferrous iron oxidation using iron present in the culture medium, therefore giving an orangish hue. As it can be observed in figure 2.16, an increasing concentration of silver is slowing down growth. After 4 days, only silver-free and minimal silver concentration (0.001 mM) cultures showed bacterial growth (data not shown for cultures not showing signs bacterial growth). After 8 days, silver-free cultures seemed to thrive while only a very light-yellow hue can be observed on other concentrations. After 14 days, all concentrations showed signs of bacterial growth although it seemed low at high Ag^+ concentrations (0.2, 0.5 and 1 mM of silver, data not shown).

Notably, there is a lack of homogeneity between the three culture replicates, which can also suggest poor reproducibility of the experiment. Still, discarding the odd culture, conclusions drawn previously based on visual observation of the culture medium are reliable.

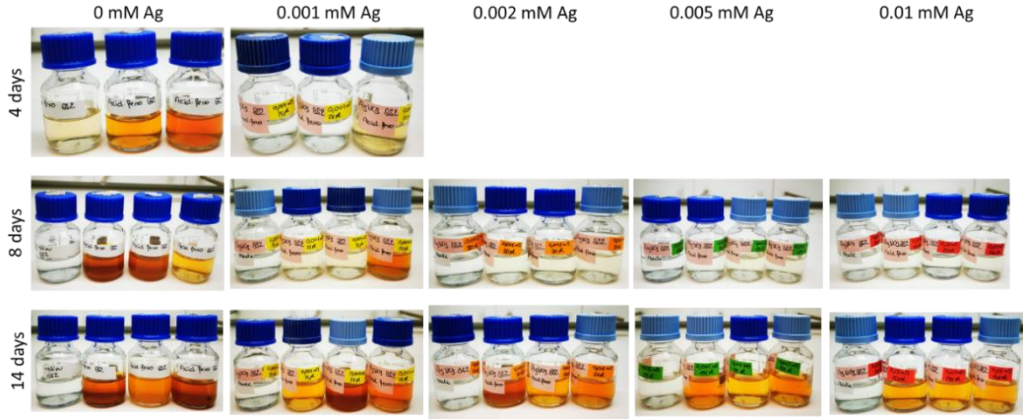

Figure 2.16 *Acidithiobacillus ferrooxidans* cultures replicates after 4-, 8- and 14-days showing signs of bacterial growth in presence of various concentrations of $AgNO_3$. Abiotic control shown on the left for 8 and 14 days of growth, not shown for 4 days.

Microscope observations of the culture media after 14 days confirm the presence of bacteria even at the highest concentration of silver ions (figure 2.17a), although the population density is low. Its relatively high resistance can be explained by the fact that *A. ferrooxidans* is an extremophilic bacteria, able to resist extreme environmental conditions, often found in mines and in particular silver mines. Nonetheless, so far, attempts of direct contact of the bacteria with metal silver resulted in its instant death [13]. Experimental evidence in other studies demonstrated the possibility of training this bacteria to resist higher concentrations of silver ions [45], but whether it will ever be enough to be in contact with pure metal remains to be investigated.

Although an asset to yield higher silver resistance, extremophilic growth conditions of *A. ferrooxidans* are not optimal for a hypothetical real-praxis implementation of silver cleaning as the extremely low pH of the culture (pH = 2) could be aggressive to potential surrounding fragile materials in the case of composite objects (e.g., wood, other metals).

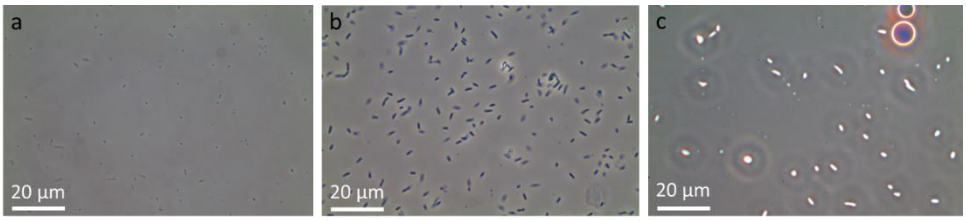

Figure 2.17 Microscope observation of cultures of (a) *A. ferrooxidans* with 1 mM silver after 14 days, (b) *P. yamanorum* with 0.1 mM silver after 5 days, (c) *P. yamanorum* with 0.001mM silver after 5 days.

Regarding *Pseudomonas yamanorum*, its growth was assessed thanks to the turbidity of medium (Figure 2.18) and through microscopical observations (Figure 2.17 b and c). In NB medium (Figure 2.18a), *P. yamanorum* was able to strive up until 0.1 mM of silver.

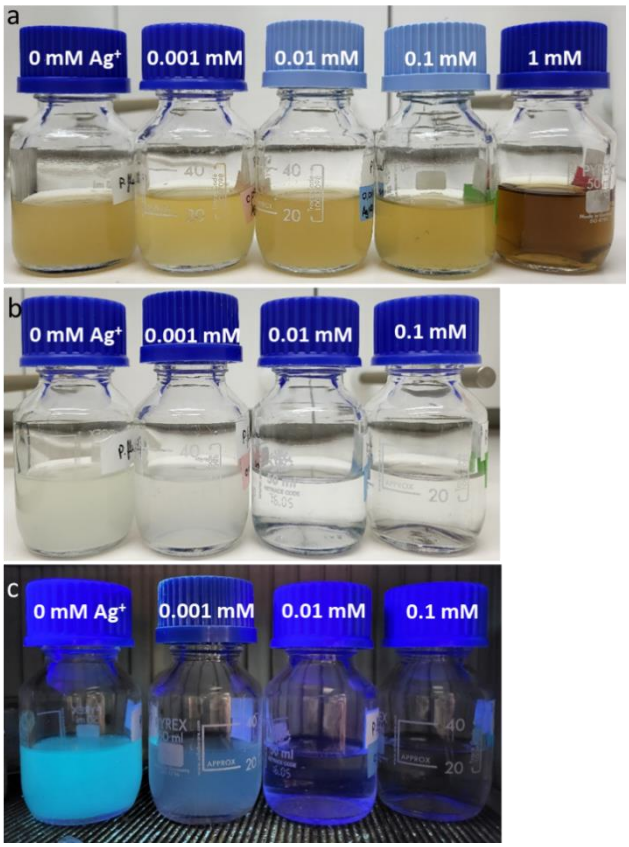

Figure 2.18 *Pseudomonas yamanorum* culture with various silver concentrations (a) in nutrient broth (a), (b) in succinate medium (c) in SM under UV-light illumination, after 5 days.

In order to boost the production of siderophores, the evaluation of growth was also performed in SM medium. The presence of siderophores after incubation in SM medium was confirmed using UV-Vis spectroscopy (Figure 2.19). In that medium, the bacteria were able to grow only at small concentration of soluble silver (0.001 mM) (Figure 2.18 b and c). This is explained by the fact that the SM medium, which is iron deficient, is already stressing the bacteria to overproduce siderophores to fetch nutrients. It is therefore more complicated for the bacteria to grow and pyoverdine having an affinity/interaction with silver, will uptake silver as a replacement or iron [46]. Unfortunately, the uptake of greater amounts of silver into the cell is deadly to the bacteria.

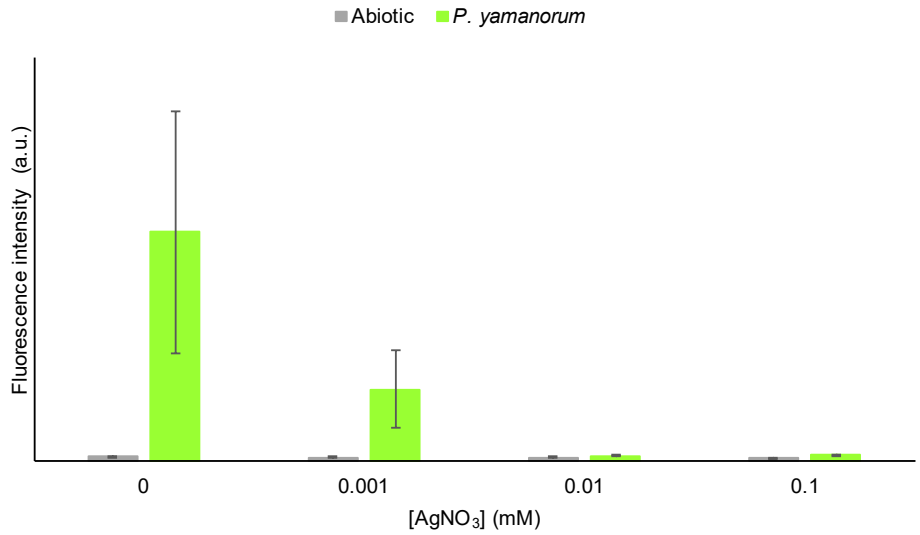

Figure 2.19 Fluorescence intensity of SM media after 5 days of *P. yamanorum* growth.

This preliminary experiment demonstrates the difficulty to identify silver-resistant bacteria. In addition, for heritage conservation applications, Ag^+ resistance is not enough, strains also must be useful and safe for tarnish removal (Ag_2S). Further research needs to be conducted to ascertain the viability of their direct application on metal objects. Some fungi have been reported to absorb silver ions in quantities up to 330 mg/L [47], however, this study was carried out on soluble silver and the result are not directly transferable to silver sulfides due to Ag_2S's low K_{sp} (Table I.1). Given the high toxicity of silver, other bio-based methods not implying the use of living organisms can also be foreseen for future research. Some research have also shown that it was possible to take up metals with dead fungal biomass, which could be a very interesting reflection to counteract the biocide parameter of silver [28,48,49]. Additionally, the use of plant-based materials, in particular soapnuts, was reported to be effective in removing silver tarnishing thanks to the presence of saponin, a surfactant [50]. For such, other surfactants from biological origin could be tested (i.e. rhamnolipids, sophorolipids) [51–53]. In addition, papers have demonstrated the efficiency of sodium glycinate, an amino acid that can be found in gelatin and silk fibroin, to react with silver to form silver glycinate, soluble in water and subsequently clean tarnish silver pieces [54].

2.2 Metabolites production

Although some results obtained with living organisms are promising, the use of isolated metabolites allows to break free from any constraints inherent to microbial growth and/or brought by culture media needed for living organisms, in particular pH control and carbon sources or other nutriments addition. It might therefore be interesting to take advantage of the metabolic pathways used by microorganisms. Attempts at production of metabolites showing high solubilization abilities is proposed in this section. More specifically in this work siderophore and organic acid production is proposed. Indeed, siderophores are known for their metal complexation, especially iron [55]. In addition, *A. niger* and *B. bassiana* S6 presented high potential for cleaning application during previous screening tests. Hence further tests for their production of acid, mainly citric and oxalic are of interest. As 99% of world's industrial production of citric acid occurs via microbial processes, in particular using *Aspergillus niger* [56], only production of LMWOA by *B. bassiana* was attempted here.

2.2.1 Materials and methods

2.2.1.1 CAS-agar plate assay

Strains producing different types of metabolites were chosen for the experimental procedure. Thus, the goal of this section is to select microorganisms with the best production rates of siderophores or iron-chelating metabolites that will be further investigated for their ability to remove undesired corrosion products from indoor historical iron artifacts. Three bacterial (*Escherichia coli*, *Streptomyces pilosus* and *Pseudomonas yamanorum*) and two fungal (*Beauveria bassiana* and *Aspergillus niger*) strains were inoculated on Chrome Azurol Sulfonate (CAS) agar plates in order to assess their iron-scavenging metabolites production. The procedure described by Louden *et al.* [57] was followed. Briefly, strains were precultured on agar plates of their respective medium (table 2.3) until visible biomass growth. Cells or mycelium were then inoculated on CAS-agar plates according to the method described in Figure 2.20. For each microorganism, three plates were inoculated to ensure reproducibility.

Table 2.3 Selected strains for CAS-assay.

Name	Provider	Temperature (°C)	Medium
Escherichia coli K12	LAMUN, University of Neuchâtel, Switzerland	40	Nutrient broth
Streptomyces pilosus DSM 40097	DSMZ GmbH, Germany	28	Glucose-Yeast-Malt
Pseudomonas yamanorum DSM2005	LAMUN, Université de Neuchâtel, Switzerland	28	Nutrient broth
Beauveria bassiana S6	LAMUN, Université de Neuchâtel, Switzerland	28	Malt
Aspergillus niger NEUM8	LAMUN, Université de Neuchâtel, Switzerland	28	Malt

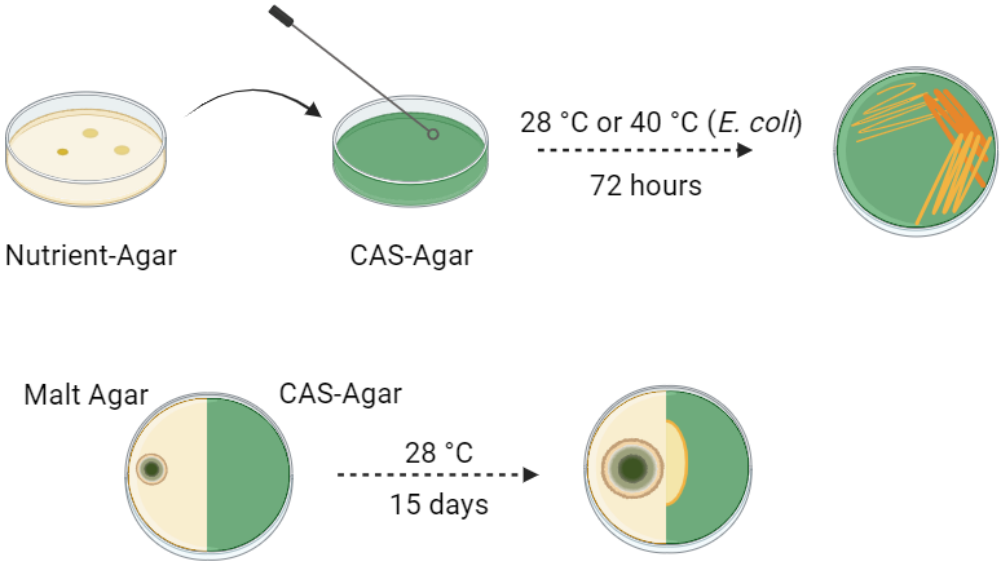

Figure 2.20 Siderophore production assessment by bacteria (top) and fungi (bottom).

2.2.1.2 Siderophore production and quantification

P. yamanorum DSM 2005 was selected for this preliminary test of production and purification due to the easy detection of highly fluorescent pyoverdine (PVD), the most common siderophore produced by *Pseudomonas* species [15]. To do so, a protocol from Duckworth *et al.* was adapted [58]. Prior to any labwork, all glassware was carefully washed with 5 M HCl and then rinsed with milli-Q water to ensure a completely iron-deprived environment. The *P. yamanorum* strain DSM 2005 was taken from a nutrient agar plate and inoculated in 3 flasks containing SM medium (Table S2.2) to have triplicates. Incubation was carried at 28 °C for 96 hours under agitation in 2 L Erlenmeyer flasks. The culture was then centrifuged (5000 rpm, 15 minutes) and the supernatant filtered using Whatman 42 filters on a filtration system followed by filtration through 0.45 μm cellulose acetate membrane filters (Millipore, United States). To purify this cell-free supernatant, solid phase extraction was run using Chromabond C18ec columns (70 mL/ 10 g) (Macherey-Nagel, Germany). The cell-free extract was applied to the C18ec column, which was conditioned with methanol and milli-Q water. For every 200 – 250 mL of cell-free supernatant extract a new column was used. The C18ec columns were eluted subsequently with water or methanol. Eluates were collected until yellow coloration was no longer visible and combined in two flasks according to the elution solvent. Eluates were then kept at 4 °C.

Absorbance of the eluates was obtained using a Victor Nivo multiplate reader (Perkin Elmer), over the 200-1000 nm range.

Liquid Chromatography UltraViolet (LC-UV) (UHPLC, Ultimate 3000, Dionex ®) was used to quantify pyoverdine in the eluates. Samples were injected onto a Waters ® column (2.1 × 50 mm, 1.7 μm BEH C18 Acquity) with the temperature kept at 25 °C and a flow rate of 0.4 mL/min. Solvents consisted of Milli-Q water + 0.05% formic acid along with acetonitrile + 0.05% formic acid. Oxalic acid was detected at 360 nm and quantified using a standard curve (50 to 1000 μg/mL) with known concentration of standard pyoverdine (Sigma-Aldrich).

Time of flight – Mass spectrometry (TOF-MS) (Acquity UPLC coupled to a Synapt G2 mass spectrometer from Waters) was applied to characterize the pyoverdines in the different eluates. Chromatographic separations were achieved using an Acquity HSS T3 column (Waters). Solvents consisted of Milli-Q water + 0.05% formic acid along with acetonitrile + 0.05% formic acid at a flow rate of 0.4 mL/min at 25 °C. Mass spectrometry was performed using electro spray ionization (ESI) in positive mode in the mass range from 50 to 1400 amu.

2.2.1.3 Biogenic oxalic acid production and quantification

Beauveria bassiana S6 spores were added in to 50 mL malt medium (1.2% w/v) in 100 mL flasks and left to incubate at room temperature, protected from light and under agitation at 140 rpm for 2 days. The culture solution was divided to have triplicates. After which, 1.5 × 3 cm copper plates naturally covered with copper patina identified as atacamite ($Cu_2Cl(OH)_3$) and brochantite $Cu_4SO_4(OH)_6$ using FTIR spectroscopy were aseptically added to 1/3 of the culture solution. Another 1/3 was implemented with corroded copper plates presenting cuprite as corrosion layer. The last third was left as control. Cultures were left under agitation for another 3 days. Plates were removed and the culture solutions filtrated successively with gauze, centrifuged in falcon tubes with 0.2 μm PVDF filters (25 minutes, 2000 rpm). The final filtrate was then diluted five times and analyzed for oxalic acid concentration via Ultra High-Performance Liquid Chromatography (UHPLC) with UV-detection. The UHPLC was coupled to a diode array detector (DAD) set at 210 ± 2 nm (Ultimate 3000 RS-Dionex, Thermo Fisher Scientific). A 10-μL sample was injected onto a Prevail™ organic acid column (5 μm particle size, 150 x 4.6 mm, Grace Davison Discovery Sciences) with temperature kept at 40 °C. The mobile phase consisted of 50 mM phosphate buffer adjusted to pH 2.5 with phosphoric acid, with a flow rate of 1 ml/min. Oxalic acid was identified by retention time comparison with a certified standard (Merck KGaA) and quantified by external calibration using a linear regression built from five calibration points (0.1 to 1 mg/mL).

2.2.2 Results and discussion

2.2.2.1 Siderophore production evaluation and assessment

Upon incubation using the CAS agar assay, the three bacterial strains showed encouraging results (Figure 2.21a-b-c), recognizable by the orangish color of the siderophore complexes [59]. After 15 days, results with fungal strains were low compared to bacterial strains (Figure 2.21d-e). Metabolites released by both *B. bassiana* and *A. niger* seem to complex iron in the CAS-agar plate, however, although the production of siderophores is reported for these strains [60,61], the coloration is not as vivid orange as for bacterial siderophores. This suggested an interference from other produced metabolites [62,63]. Indeed, they are most known for production of organic acids, like citric and oxalic which can also complex iron [41].

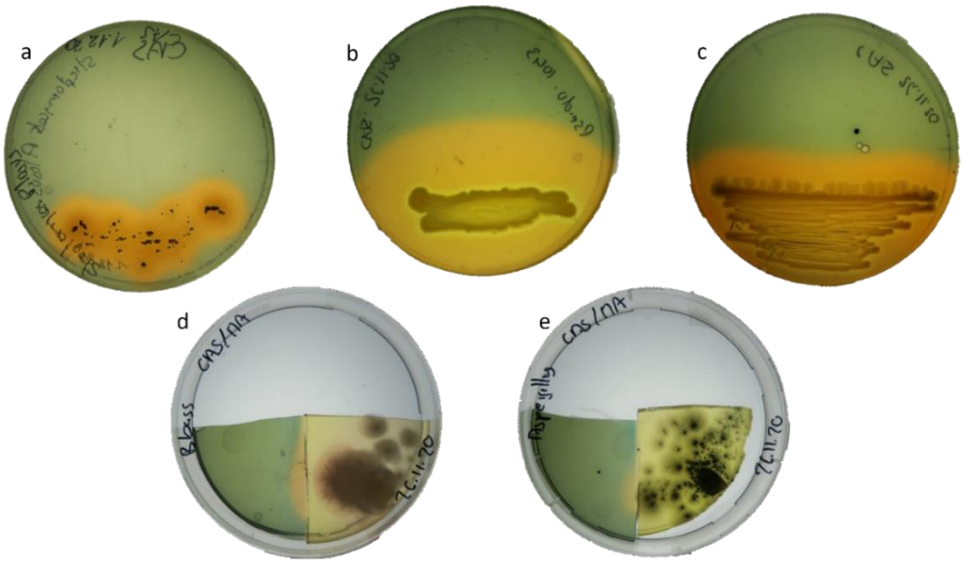

Figure 2.21 CAS-Agar plates after incubation of *Streptomyces pilosus* (a), *Pseudomonas yamanorum* (b), *Escherichia coli* (c), *Beauveria bassiana* (d), *Aspergillus niger* (e).

Only bacterial strains were therefore considered for the further production of siderophores. Even though enterobactin, the main siderophore detected in the K12 *E. coli* strain [11], is known to have the highest binding affinity, or stability constant (logβ = 49), deferoxamine, the main siderophore of *S. pilosus* (logβ = 30.6) is also well described in literature and has been used in heritage conservation studies for the removal of iron [64–66]. The stability constant is a measure of the interaction strength between the metal and the ligand forming a complex and is detailed further in the chapter (section 3). Deferoxamine is commercially available in pharmacies as a mesylate salt, under the name Desferal®, a drug for iron or aluminum overloads produced by Novartis. Its high iron-binding constant and rather simple availability make it one of the most documented in literature, along with enterobactine from *E. coli*. Because of its easy availability in large quantities, it was further decided to use the commercial form of deferoxamine. Although the direct application of living microorganisms for heritage conservation is a common praxis [40,67,68], the use of pure compounds is ideally favored. Certainly, the medium composition could have drawbacks on the preservation of the objects. The addition of any culture medium, with a carbon source and other nutrients, can favor the development of negative autochthonous organisms present on the objects. On the contrary, the use of purified metabolites could allow the use of constant and higher concentrations of the active molecules.

Production of pyoverdine, the main siderophore of *P. yamanorum*, was attempted as it is easily monitored throughout its production thanks to its bright yellow color along with strong fluorescence under UV light. Although is it commercially available, it is rather expensive (290 CHF/ 1 mg) considering the quantities that could be needed for corrosion removal.

2.2.2.2 Pyoverdine production

Pyoverdine, along with pyochelin, are the main siderophores produced by *Pseudomonas* species. It has been extensively studied, mainly for its fluorescent property. Actually, there are over 60 different types of pyoverdines differing from each other with respect to their structural parts [69]. Indeed, pyoverdines have three distinct structural parts including a chromophore core (figure 2.22), giving its yellow color and yellow-green fluorescence, a side chain and variable peptide chain of at least six amino-acids [70]. Pyoverdine is a mixed type siderophore, meaning its iron chelating properties are due to the presence of several moieties (i.e., catecholate and hydroxamate groups) in the structure.

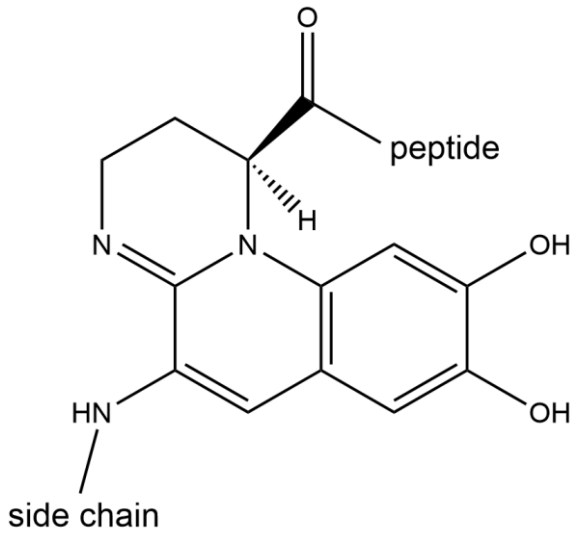

Figure 2.22 General structure of pyoverdines, presenting the chromophore core to which are attached the peptide and side chains, based on [70,71].

Production of pyoverdine (PVD) was achieved with *Pseudomonas yamanorum* DSM2005 considering its performance observed in previous experiment with CAS (Figure 2.21) along with the reported ability of the siderophore to complex silver [17], which is of interest for silver cleaning purpose. The culture medium was iron-free and contains succinic acid, both traits are reported to enhance the production of pyoverdine moieties [72]. Succinic acid enhances the synthesis of PVD over other carbon sources such as glucose [73]. To obtain an enriched and partially purified PVD solution, the culture supernatants were run through solid phase extraction (SPE), in order to remove undesired compounds from the bacterial extract (Figure 2.23).

Another advantage of working with *Pseudomonas* spp. is the easy detection of PVD whether in day light thanks to its yellow color or under UV-light thanks to its fluorescence (Figure S2.2). After solid-phase purification, several eluates in water or methanol were obtained. PVD was detected with LC-UV in water and methanol eluates (Table S2.3). During the process, it was preferred to elute as much pyoverdine as possible, although this would result in a lower liquid concentration, but it was assumed

to collect a higher total amount of substance to be used in further experiments. The water eluted batch showed higher amounts of pyoverdine extracted (Table S2.3).

Absorbance spectrum of the obtained enriched and partially purified solution (Figure 2.23) was similar to the ones in literature for pyoverdines from *P. yamanorum* strains, with peaks at around 230 and 400 nm and shoulders near 265 and 380 nm [74]. It was shown that absorbance of pyoverdines is pH dependent [75], with the peak near 400 nm shifting towards lower wavelength with decreasing pH. Here, the obtained solutions had a basic pH, close to 9, which is in accordance with a main absorbance peak at 403 nm along with a shoulder near 380 nm [75].

The results thus confirm the presence of a chromophore typical of pyoverdine in the structure of the produced molecules.

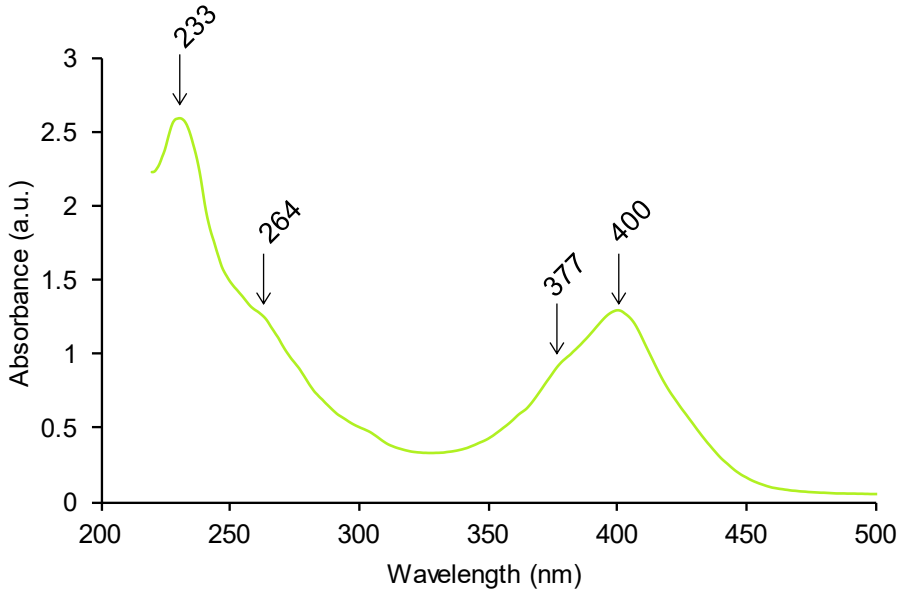

Figure 2.23 UV-vis absorbance spectra of filtered and partially purified *P. yamanorum* culture.

In further HPLC-TOF-MS characterization (Figure S2.4), the retention time from the enriched PVD solution is close to those obtained for the commercial pyoverdine standard (Sigma Aldrich) (5.40 to 6.00 minutes), meaning a similar polarity of the analyzed compounds. However, the obtained chromatograms, both from water and methanol eluate could not be overlayed on the standard curve, which suggests that the obtained metabolites were of different structure.

The presence of various molecular ion signals *m*/*z* at 358.505, 364.492, 352.487 and 358.505, 364.493, 369.165, 372.515, 393.177 peaks in the MS spectra of H_2O and MeOH respectively (Figure S2.4) shows that a mixture is obtained, as expected: as stated in Chapter 1, secondary metabolites are often produced in groups of closely related molecules.

Furthermore, the molecular ion signals are different in the MeOH and H_2O eluates, indicating the presence of a mixture in both cases but a different one as the masses of ionized compounds are not the

same. In addition, in the MS spectra of PVDs, mono-, doubly- and triply-charged ions can be observed, as it has been reported elsewhere [76,77].

Overall, the absorbance, backed-up with the retention time and the similar spectrum in MS suggest the production of a mixture of different pyoverdine molecules. However, although molar mass of the monoionized compound (Figures S2.3b and S2.4b) is close to what could be expected for a pyoverdine (between 1090 and 1400 g/mol) [78], no match could be found in renowned databases[3] nor in published literature. The used *P. yamanorum* DSM 2005 strain can possibly produce diverse types of pyoverdines. They are believed to be cleaved during the purification process [79]. Therefore, successful production of pyoverdines was achieved both using H_2O or MeOH as eluants but cannot be unambiguously established although it is quite likely. Further characterization should be performed to assess the exact structure of the obtained pyoverdines present in these eluates, following a comprehensive procedure by Rehm *et al.* for instance [70], or a siderotyping method [76].

2.2.2.3 Extraction of oxalic acid

Biogenic oxalic acid was produced via culturing of *Beauveria bassiana* S6 strain (figure S2.3). This fungus is studied in the metal conservation field for oxalate production with a mechanism that includes an initial uptake of the copper ions from the patination layer of outdoor copper artworks by oxalic acid mediated dissolution, followed by biomineralization as metal oxalates [80,81]. Thus, it is believed that if the pathway is stopped earlier, only the uptake occurs. In addition, as seen in section 1, when in contact with copper or iron solid phases, the production of oxalic acid by fungi resulted in the formation of copper oxalates or iron oxalates, by *B. bassiana* and *A. niger* respectively.

Previous studies had shown that the production of organic acid can be increased by the presence of copper compounds such as copper oxides [5], in particular the presence of cuprite resulted in the overexcretion of citric acid [41]. The presence of a harmful compound, such as metal elements for fungi, triggers their production of LMWOA. Organic acids allow to sequester harmful ions, making them no longer a threat.

Results obtained from HPLC quantification of studied culture media show the overexcretion of oxalic acid, in particular in the combined presence of copper hydroxysulfates (brochantite) and copper hydroxychlorides (atacamite) on patinated plate (Table S2.4).

Test applications of pure oxalic acid on corroded copper coupons resulted in the removal of too much of the original corrosion layer, which was not the case for treatment with oxalic acid-producing fungi [82], which shows that there seem to be “fungi effect”.

[3] https://dnp.chemnetbase.com/chemical/ChemicalSearch.xhtml?dswid=6439

The enhancement of oxalic acid production results in the presence of copper in the medium, that could be quantified using ICP-OES to 2.017 ± 0.008 mg/L. This presence of copper in the treating solution prior to application on artefacts is not desired as it saturates the medium for further copper uptake. Moreover, it could result in further corrosion on iron-based substrates (chalcopyrite $CuFeS_2$ for instance [83]). Additionally, the presence of malt medium requires rather time-consuming additional steps to get purified oxalic acid. So far, the biotechnological production of oxalic acid requires further global efforts to be produced industrially [84].

2.3 Interaction of complexing metabolites with corrosion products

The use of commercially available secondary metabolites allows for the use of higher concentrations of complexing agents. Regardless, because of the high-retailing price, self-produced pyoverdine is still tested for ion uptake.

Here, the aim is to study the dissolution of common corrosion products in the presence of various chelators from self- or industrial production from biological or chemical origin.

The obtained mixture of pyoverdine (section 2) was compared to commercial deferoxamine (DFO), retailed by Novartis under the name Desferal®[4] and to the typically used chemical chelator (disodium ethylenediaminetetraacetic acid) Na_2EDTA. In addition, ethylenediamine-*N,N'*-disuccinic acid (EDDS), a biodegradable alternative to EDTA was also studied [85,86]. Other well-known complexing solutions were also tested, namely citric and oxalic acid. Citric acid is industrially produced from the fungi *A. niger*, hence considered bio-originated [56]. Oxalic acid produced by *Beauveria bassiana* as explained in section 2 was also tested and compared to industrial oxalic acid, produced from total synthesis [84].

Given the low solubility product constants (K_{sp}) of selected corrosion products, there are several options to enhance their solubility. It is theoretically possible to increase the temperature to increase K_{sp}, however this option is not preferred for cultural heritage objects, especially in the case of composite objects. Other factors influencing the solubility of corrosion minerals are the pH of the solution, the presence of complexing agents (also known as ligands), or the presence of reducing conditions that enhance the solubility of Fe^{3+} oxides by promoting reductive dissolution [87]. Properties of the minerals also play a role in the solubilization of a compounds, in particular particle size and surface area, affecting the reaction kinetics [87]. In this chapter, the main option evaluated is the complexation reaction of corrosion products.

Complexation is the reaction by which free metal ion in a solution (M^+) and one or more ligands (L) are going to form a new compound, the complex (ML_n) (equation 3.1). The formation of this new product in solution will cause the free metal ion's concentration to decrease and therefore enhance the solubility of the mineral. Indeed, free metal ions and complexed metal ions do not have the same properties and are considered different species in solution. Basically, it moves the equilibrium of the reaction to the right.

$$M^{n+}{}_{(aq)} + xL^{a-}{}_{(aq)} \rightleftharpoons ML_x{}^{b+ \text{ or } -} \quad (3.1)$$

[4] https://www.novartis.com/us-en/sites/novartis_us/files/desferal.pdf

Using the law of mass-action, the formation constant K_f of the complex, which is also called the stability constant β, is obtained:

$$K_f = \beta = \frac{[ML_x^{b+}]}{[M^{n+}] \times [L]^x} \quad (3.2)$$

The more a complex is stable, the less it dissociates. The dissociation constant K_d relates to the dissociation of the complex and $K_d = \frac{1}{\beta}$. To simplify here, only the global K_f is considered, not the successive formation constants.

A chelator or chelating agent is a polydentate complexing agent, meaning containing two or more electron-donor groups so that more than one bond is formed between the metal ion and the ligand [88]. They usually have higher Kf than monodentate complexing agents [89].

Therefore, the global reaction constant of the combined solubilization and complexation is $K_{sp} \times K_f$, with the equilibrium displaced towards the dissolution of the mineral thanks to the presence of the complexing agent. The subsequent dissolution of a mineral is thus depending on a variety of parameters, including concentration of the chelators, mineral solubility product and metal-complex stability constant.

2.3.1 Materials and methods

All experiments were carried out at room temperature (approximately 25 °C).

2.3.1.1 Chelators

Different chelating agents were selected (Table 2.4). All solutions were prepared with Milli-Q® water to a concentration of $5 \cdot 10^{-4}$ M for experiments related to mineral dissolution over time. This concentration was selected as it was the highest one that could be obtained for self-produced pyoverdine (section 2) given the number of samples to be prepared.

500 mL of $5 \cdot 10^{-4}$ stock solution were prepared, adding 0.092 g (EDTA), 0.162 g (Desferal®), 0.022 g (oxalic acid), 0.047 g (citric acid), 0.255 mL (35% EDDS) for experiments related to mineral dissolution over time. The exclusion of pyoverdine and biogenic oxalic acid for further experiments allowed to study the influence of pH with solution concentration of 10^{-2} M.

500 mL of 10^{-2} stock solution were prepared, containing 1.86 g (EDTA), 3.29 g (Desferal®), 0.45 g (oxalic acid), 0.96 g (citric acid), 4.85 mL (35% EDDS) for experiments related to the influence of pH. pH of each solution was determined using a Metrohm electrode and adjusted using NaOH or HCl solutions (see section 3.1.4 *Influence of pH*). Results are displayed in Table 2.4.

Table 2.4 Studied chelators and associated physico-chemical features.

	Citric acid [79,90,91]	**Oxalic acid** [79,90,92]	***B. bassiana* extract**	**EDTA** [64]	**EDDS** [93]	**DFO** [64]	**PVD** [15,64]	**Milli-Q®**
Provider	Carl-Roth	Sigma-Aldrich	Self-produced	CTS®	Sigma-Aldrich	Novartis	Self-produced	Millipore
pH at $5 \cdot 10^{-4}$ M	4.1	3.4	6.3	5.9	8.5	6.4	9.4	5.5
pH at 10^{-2} *M*	2.5	1.9	n/a	4.6	9.6	5.4	n/a	5.5
$\log\beta$ Cu^{2+}	5.9	4.8	n/a	18.8	18.7	14.1	14.9	n/a
$\log\beta$ Fe^{3+}	17	7.5	n/a	25.1	20.6	30.6	30.8	n/a
$\log\beta$ Fe^{2+}	3.2	4.7	n/a	14.3	n/a	10.3	9.8	n/a

2.3.1.2 Corrosion products

According to the compounds identified in chapter 1 (Table I.1), seven powdered corrosion products were used: goethite, lepidocrocite, cuprite, covellite, chalcocite, brochantite and silver sulfide. Relevant corresponding data can be found in table 2.5. Specific surface areas were determined by a N_2 BET[5] adsorption method (3Flex, Micromeritics) and particle sizes were measured using laser diffraction (PSA1190, Anton Paar). The BET method is a common practice to measure the SSA and pore sizes of powdered samples under high-vacuum conditions. The SSA is determined from the volume of N_2 gas adsorbed on the surface [94]. Particle size was measured in solution under stirring to simulate colloidal suspension and the behavior of powder in solution. It was performed first without and then with ultrasonic agitation and repeated five times for each case.

Table 2.5 Studied corrosion products and their associated physico-chemical characteristics.

Formula		α-FeOOH	γ-FeOOH	Cu_2O	CuS	Cu_2S	$Cu_4SO_4(OH)_6$	Ag_2S
Mineral name		Goethite	Lepidocrocite	Cuprite	Covellite	Chalcocite	Brochantite	Acanthite
Provider/Synthesis		Alfa-Aesar	Alfa-Aesar	Sigma-Aldrich	Sigma-Aldrich	Sigma-Aldrich	Tanaka *et al*. protocol [95]	Sigma-Aldrich
Mean particle size (µm), volume weighted	*Without sonication*	16 ± 1.7	21.8 ± 0.31	61 ± 1.4	24 ± 1.7	55 ± 1.2	113 ± 3	n/a
	After sonication	6 ± 0.6	16.9 ± 0.2	24 ± 2.1	25 ± 2	39 ± 0.2	19.5 ± 0.4	n/a
BET surface area ($m^2 \cdot g^{-1}$)		12.3	56.8	0.377	0.496	0.414	20.9	n/a
pK_{sp}		42 [96]	42 [87]	15 [97]	37 [98]	49 [99]	69 [100]	51 [13]

2.3.1.3 Mineral dissolution evaluation over time

All dissolution experiments were performed in closed 2 mL Eppendorf tubes. Experiments were performed in triplicates. Corrosion products were weighted to obtain a large molar excess of corrosion products (over 10:1) in 1.5 mL of ligand solution. Solutions of $5 \cdot 10^{-4}$ M ligands were then added. Tubes were vortexed and left for 15 min, 30 min, 45 min, 1 h, 2 h, 4 h, 8 h, 16 h or 24 hours with periodic agitation in order to have insights into the kinetics of the reaction of the dissolution reaction. Blanks with no corrosion products were also prepared.

After each time interval, tubes were centrifuged at 12000 rpm for 2 minutes to separate insolubilized

[5] Bruauner-Emmett-Teller (BET)

corrosion powder. The supernatant was removed, centrifuged a second time and used for further analysis. The total iron in solution was measured using ICP-OES (10× dilution in Milli-Q® water).

2.3.1.4 Influence of pH

In 2 mL Eppendorf tubes, corrosion products were weighted in order to obtain a large molar ratio excess of corrosion products (over 10:1) in 1.5mL of ligand solution. Given results obtained with PVD from the previous section, it was discarded which allowed to increase the concentration of ligands to 10^{-2}M for this study. Experiments were carried out in triplicates by the same operator on the same day, limiting possible block effects.

Solutions, excluding biogenic oxalic acid and pyoverdine, were adjusted to pH 4, 7 or 10 using NaOH or HCl and then added to the Eppendorf tubes. pH adjusted solutions were not buffered or adjusted further during the reaction in order to simulate what happens during a corrosion removal intervention, as the modification of pH could affect the other parts of a metallic object if composite. Moreover, the presence of added buffer may also interact with ongoing reactions and result in undesired or simultaneous chemical processes [79]. Tubes were vortexed and left for 24 h with periodic agitation. After each time interval, tubes were centrifuged at 12000 rpm for 2 minutes to separate insolubilized corrosion powder. The supernatant was removed, centrifuged a second time and used for further analysis. The total iron in solution was measured using ICP-OES (100× dilution in Milli-Q® water).

2.3.1.5 ICP-OES metal detection

Inductively Coupled Plasma-Optical Emission Spectrometry (ICP-OES) was utilized to determine total element concentrations in the different experimental solutions. Samples were centrifuged and diluted as stated to be in the detection range (0-2 ppm). Total concentrations were determined using an Optima 2100 DV (Perkin-Elmer, United States) optical emission spectrometer. Details are in Table S2.1.

2.3.1.6 UV-Vis detection

Given the low solubility of Ag_2S, quantification of solubilized acanthite in the presence of different organics ligands via ICP-OES gave null results. Interactions with silver were therefore studied on its soluble form. Absorbance values of 10 mM $AgNO_3$ (Fluka) alone and mixed with chelators (DFO, PVD, EDDS and EDTA) at 10 mM concentration and pH 4, 7 or 9 were registered with a 96-well microplate reader UV-Vis spectrophotometer (Victor Nivo, Perkin Elmer) on the whole absorbance spectra (200-1000 nm).

2.3.1.7 Raman characterization

After UV-vis characterization, further analyses were performed to acertain conclusions drawn from that technique. Raman spectroscopy was performed on a solution of 10 mM $AgNO_3$ mixed with 35%w/v

EDDS and let to react overnight. Measurements were performed using a Renishaw Virsa™ Raman analyzer micro spectrometer equipped with 50× magnification objective was employed using a 532 nm laser. Spectra were recorded with a laser power of 10 mW in the spectral range of 50–1600 cm^{-1} with thirty accumulations of 1 s each.

2.3.2 Results and discussion

2.3.2.1 Iron

Although not associated with cyclic corrosion, the removal of iron oxyhydroxides, typically goethite (α-FeOOH) and lepidocrocite (γ-FeOOH), the main phases encountered on indoor historical iron-alloyed objects is often desired for aesthetic purpose [101]. Looking at bio-based solutions to remove these compounds, solubilization is one of the most promising paths. Thus, the solubilization of these compounds was studied in the presence of dissolution-enhancing compounds, i.e., complexing agents. In nature, living organisms struggle to access iron because of the poor solubility of iron sources, i.e. iron oxides [79]. For that reason, many organisms have evolved with a solution in response to the low solubility of iron oxides at neutral or basic pH to retrieve iron present in these minerals: siderophores [102].

Here, the performance of siderophores to enhance iron oxides' dissolution was compared to LMWOA or other well-known complexing agents. Figure 2.24a and 2.24b display the amount of iron ions dissolved over a period of 24 hours (1440 minutes) in presence of different dissolution-enhancing ligands for goethite and lepidocrocite respectively.

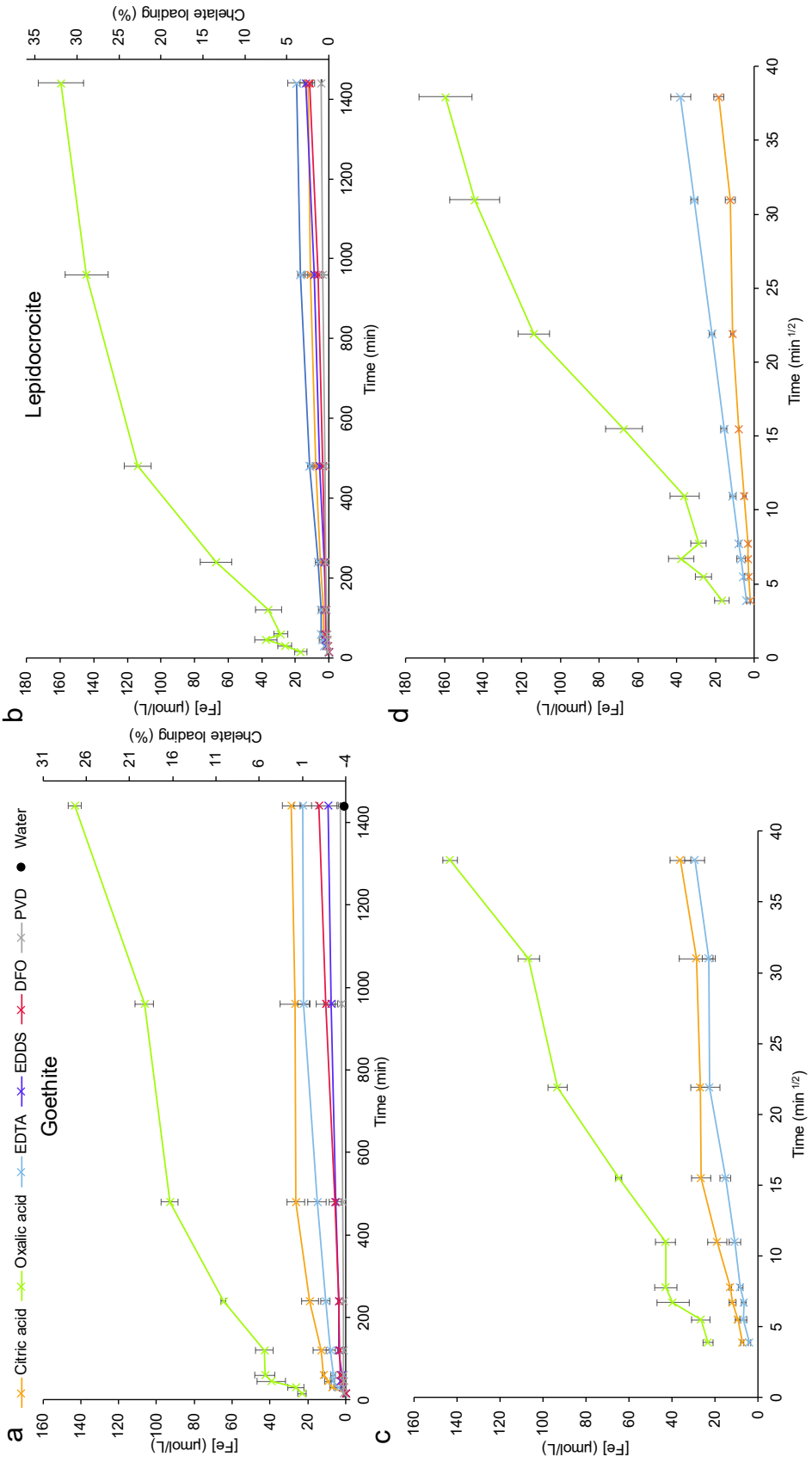

Figure 2.24 Iron detected by ICP-OES after iron oxides dissolution in presence of several $5 \cdot 10^{-4}$ M ligand solutions (oxalic acid (green), citric acid (orange), EDTA (blue), EDDS (purple), DFO (red), PVD (grey) and water (black)), plotted versus time (a and b) or square-root of time (c and d, with only EDTA, citric and oxalic acids reported).

Both in the case of goethite and lepidocrocite, oxalic acid is by far the most effective ligand with a p-value below 0.001 when compared to all the other ligands, with the highest Fe concentration detected. Oxalic acid is known to be one of, if not the, most performing organic acid to dissolve iron oxides [35,103]. Although at first glance its performance can appear interesting for iron cleaning purpose, this also implies a lack of gradualness, restraining the possibility of control over a treatment. Although citric acid theoretically forms stronger complexes ($\log K_f = 17$) with iron than oxalic acid ($\log K_f = 7.5$), citric acid yields results that are much less impressive than those seen with oxalic acid, which is similar to what has been observed previously, where oxalic acid was more effective than citric acid for the dissolution of hematite, a ferrous oxide (Fe_2O_3) [104]. This is probably due to oxalic acid pH being lower than citric acid's (Table 2.4).

For both iron oxyhydroxides, EDTA, EDDS, DFO and citric acid perform in the same range (Figure 2.24 a and b), although slight differences are observed between the various chelators. In the case of goethite, citric acid does not perform significantly better than EDTA but the difference of dissolved iron in solution is significant between citric acid and DFO or EDDS. Regarding these two chelators and EDTA, no significant difference was found. For lepidocrocite, statistical analysis shows no difference between chelators other than oxalic acid.

Beauveria bassiana's medium supernatant (containing oxalates) did not allow any solubilization hence is not shown on the graphs. This is accounted for by two things. First, the copper ions dissolved from the added plates in the culture to boost the production of the oxalic acid (section 2.2.3) are still present. The presence of copper could interfere with subsequent iron complex formation or dissolution. Additionally, the compounds from the malt medium, rendering the solution pH close to neutral (pH=6.28), far from what is expected from an acid (table 2.4) also annihilate the performance of oxalic acid. Similarly, pyoverdine (Figure 2.24 a and b, grey curve, PVD) yielded disappointing results, hardly reaching dissolved iron levels similar to water alone for both α-FeOOH and γ-FeOOH, meaning its capacity to improve dissolution is minimal. This was equally accounted for by pH of the solution, which was close to 9, in the stability range for iron oxides according to E-pH diagrams (Figure I.2), meaning FeOOH transformation is not thermodynamically favored in these conditions.

Noticeably, iron maximum detection is reached at 30 minutes for both corrosion products. This is believed to be accounted for by a systematic error, due to periodic stirring, which influences the phenomenon dominating the dissolution process (kinetics or diffusion).

Interestingly, regarding the dissolution rate for DFO and EDDS, the slope is more fitted to a linear regression function of time ($\mu mol.L^{-1}.min^{-1}$), with a coefficient of determination R^2 closer to 1 (Table 2.6), indicating a zero-order reaction. On the other hand, for oxalic and citric acids as well as for EDTA, the slope is rather a function of the square-root of time (figure 2.24 c, d) ($\mu mol.L^{-1}.min^{-1/2}$), with R^2 more fitted

than for a function of time (Table 2.6). Overall, the equilibrium state is never reached in the 24-hours timespan studied since the metal to ratio ligand never exceeds 4.7 and 3.2% for goethite or lepidocrocite, respectively. In order to reach this point, it would be advisable to pursue data collection for a longer period, until reaching a plateau.

Table 2.6 Coefficient of determination R^2 of dissolution rate (kinetics) as a function of time ($\mu mol.L^{-1}.min^{-1}$)or squareroot of time ($\mu mol.L^{-1}.min^{-1/2}$) of goethite and lepidocrocite in presence of different ligands.

		Citric acid	Oxalic acid	EDTA	EDDS	DFO
Goethite	R^2 for dissolution rate in $\mu mol.L^{-1}.min^{-1}$	0.7629	0.9354	0.8654	0.9511	0.9851
	R^2 for dissolution rate in $\mu mol.L^{-1}.min^{-1/2}$	0.8923	0.9807	0.9586	0.9040	0.9509
Lepidocrocite	R^2 for dissolution rate in $\mu mol.L^{-1}.min^{-1}$	0.9315	0.9054	0.9516	0.9887	0.9957
	R^2 for dissolution rate in $\mu mol.L^{-1}.min^{-1/2}$	0.9754	0.9729	1	0.9401	0.9734

It has been hypothesized that during a solid dissolution, the kinetic model is based of Fick's second law on the diffusion layer and expressed by the Noyes-Whitney-Nernst-Brunner (NWNB) equation (3.3) [105–108] . It states that the rate of dissolution of a solid is dependent upon its solubility (Cs), the concentration of solute in solution at a particular time (Ct), diffusion constant k, and the surface area of the solid (S).

$$dC/dT = kS(Cs-Ct) \quad (3.3)$$

Basically, it considers that dissolution is the reverse process of crystal growth and involves two steps: first, surface reaction and disintegration of the surface species and second mass transfer of these species into the bulk solution across the diffusion layer [109].

The NWNB equation is valid for a dissolution process corresponding to a first order reaction, meaning depending on the concentration of only one of the reactants [110]. Here, because the corrosion products were added in large excess, their concentration could be considered constant over time and the reaction as following a pseudo-first order, only dependent on the concentration of ligands, and therefore the mathematical model for diffusion could be applied. However, no single mathematical approach is widely accepted to determine dissolution processes [110].

Moreover, it is not so clear whether the mineral dissolution processes is diffusion-controlled or surface-reaction controlled [111]. According to peer-reviewed papers [112], the effect of siderophores and other organic ligands on iron oxides dissolution is a ligand-controlled dissolution mechanism, which is a surface-controlled process, meaning the dissolution rate is a function of the surface concentration of the ligand.

There are three main surface-controlled reactions leading iron oxides to release iron into aqueous

solution: protonation, complexation (ligand-process) and reduction [113]. Here, the last possibility is disregarded because of the absence of any reducing agent. Protonation and complexation give way to the production of iron ions or iron-complexes respectively. These reactions consist of several steps in which the first step involves the formation of a surface complex by adsorption of protons or ligands from the solute respectively, or even a combination of these [113,114]. This leads to a weakening of the Fe-O bond and then to the detachment of the iron cation. This step of breaking the bond between the components of the crystal lattice is the rate-determining step of iron release in the solution [104].

One of the main assumptions of this surface-controlled process model is that dissolution mechanisms (i.e. protonation and complexation) occur independently [112]. The independence of these reactions is not straightforward as pH modifications can affect the rates of both dissolution processes. For instance, pH changes can influence ligand-controlled dissolution by modifying the concentration and speciation of adsorbed ligands (figure 2.25), which therefore can result in an apparent shift in the dissolution rate. As a consequence, the pH influence on dissolution and adsorption has been reported to be a parallel, independent parameter [112], and elsewhere it was an accountable, non-independent parameter [115].

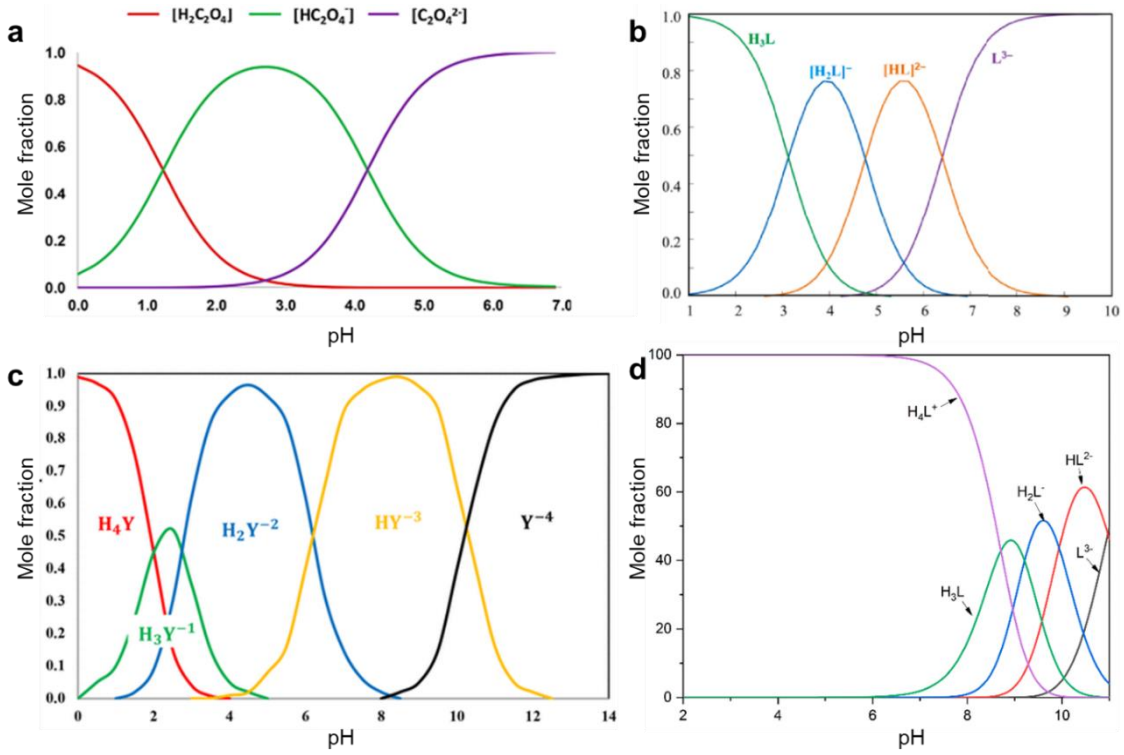

Figure 2.25 Speciation diagrams of (a) oxalic acid, (b) citric acid, (c) EDTA, (d) DFO ionic species at room temperature in water. Obtained from [114,116–118]. L and Y stand for the ligand formula.

For such, one can notice that the main difference between the curves being time-dependent or square root of time dependent in figure 2.24 is the pH of the associated ligand species (table 2.4). The ones following a square root of time linear regression are the ones with the lower pH (below 6). Therefore, it is possible that the protonation reaction affects the dissolution rate for oxalic acid, citric acid, and EDTA.

That is the reason why other studies state that these reaction pathways determine simultaneously and not independently the kinetics of mineral dissolution [119].

To have a better overview of this phenomenon, ligand solutions were adjusted at three different pH values: 4, 7 and 10 to simulate acidic, neutral and basic solutions respectively using NaOH and HCl, and added to goethite and lepidocrocite for 24 hours.

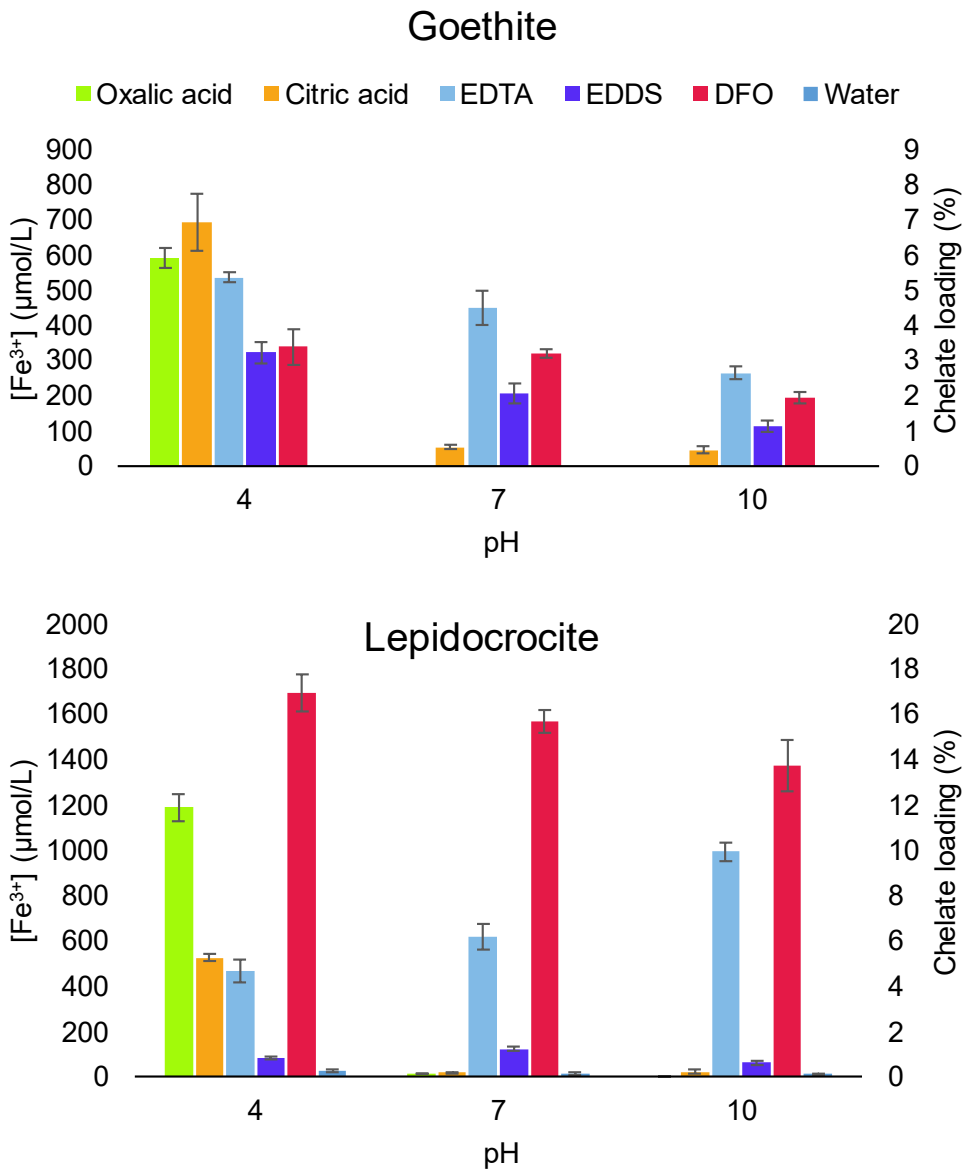

Figure 2.26 Dissolved iron detected via ICP-OES in 10^{-2} M ligand solutions at pH 4, 7 or 10 after 24 hours of corrosion products immersion.

For citric and oxalic acids, the formation of the complexes is clearly pH dependent (Figure 2.26). One can note a discrepancy between the performance of DFO in the kinetical study versus the pH-dependance study compared to other chelators, with clear better performance in the second part of the study (pH-adjusted solutions), which so far could not be explained. Indeed, here, iron to DFO ratio

reaches up to 7 and 17% for goethite and lepidocrocite respectively versus 4.8% and 3.2% in the kinetics study. Again, here, equilibrium state is never reached as the 1:1 molar ratio is never attained.

As a first insight, the main difference between the two series (pH-adjusted or not) is the ligand and solid concentration, changing from $5 \cdot 10^{-4}$ M to 10^{-2} M. Indeed, non-pH adjusted solution of DFO is already close to pH 7 so there is no consequent difference regarding that matter.

Papers have demonstrated that low Fe^{2+} concentrations catalyze the dissolution of various Fe^{3+} hydroxides in presence of diverse ligands, including DFO, over a broad pH range (4 to 8.5) [120]. Although goethite and lepidocrocite are ferric compounds, the presence of dissolved Fe^{2+} has been related to photo-reductive dissolution of Fe^{+3} hydroxides by visible light [121]. This photo-reductive dissolution, occurring both at acidic and basic pH [122], is enhanced by the presence of certain ligands [123–125], including DFO but also occurs on absence of any organic or inorganic ligands other than H_2O [125,126] As the experiments were carried out at visible light, this photoreduction of Fe^{3+} to Fe^{2+} is a conceivable option explaining why higher concentrations of ligands and/or corrosion products increase the concentration of Fe^{2+} and consequently the concentration of solubilized iron, resulting in a better performance from DFO.

Further experiments at more numerous pH values, different ligand concentrations and different timings should be foreseen to ascertain the phenomenon.

For both goethite and lepidocrocite (Figure 2.26), oxalic and citric acid resulted in little or no iron dissolution at neutral and basic pH while they were the best performing at an acidic pH (Table 2.7).

Table 2.7 Ranking ligands from best (1) to least (5) performing after 24 hours of corrosion products according to the metal to ligand uptake ratio.

	Goethite			**Lepidocrocite**		
pH values	4	7	10	4	7	10
1	Citric acid	EDTA	EDTA	DFO	DFO	DFO
2	Oxalic acid	DFO	DFO	Oxalic acid	EDTA	EDTA
3	EDTA	EDDS	EDDS	Citric acid	EDDS	EDDS
4	DFO	Citric acid	Citric acid	EDTA	Citric acid	Citric acid
5	EDDS	Oxalic acid	Oxalic acid	EDDS	Oxalic acid	Oxalic acid

Focusing on goethite (Figure 2.26), EDDS performs close to DFO at acidic pH and its solubilization power slightly decreases with increasing pH, similarly to EDTA. DFO exhibits overall lower iron dissolution than EDTA (Table 2.7) but its solubilizing power does not decrease between pH 4 and 7 (figure 2.26).

At pH 7, oxalic and citric acid are fully deprotonated (figure 2.25 b and c). Indeed, chelating agents are usually represented as H_nY, with n the number of protons that can be released. In aqueous solution, chelating agents can lose those protons until reaching the fully ionized form. This is what is called the speciation of a chelating agent (figure 2.25).

As described, the dissolution of a solid is caused by its reaction with the protons released and/or the ionized form of the chelating agent. In the case of citric and oxalic acids, proton's action in neutral to alkaline solution might be balanced by greater concentrations of OH^- ions. Hence, it can be stated that their surface-controlled process is mainly protonation-controlled, being annihilated when their protonation is counterbalanced by the presence of hydroxyl groups at higher pH values, or more simply, when they are neutralized. Some paper theorized that the effect of protons H^+ in the action of oxalic and citric acid on iron oxides is to control the uptake of speciated chelators onto the mineral surface, indirectly influencing the dissolution of iron oxyhydroxides [104].

For EDTA and EDDS, the presence of other binding sites/moieties than OH groups, typically amine sites (Figure 2.27), could enhance the complexing reaction even at high pH. In addition, both EDTA and DFO display their fully deprotonated form only above pH 10 (figure 2.25). Although there is a change of performance with the pH, the reaction is not completely annihilated. This shows that the dissolution processes are a combination of reactions with protons (protonation) and the ionized form of the chelating agent (ligand-controlled).

Citric and oxalic acid being only effective in the acidic range, there is a lack of versatility for heritage artefacts cleaning where working over a larger span of pH might be required depending on the nature of the substrate (i.e., to avoid further damaging of metal surfaces or organic materials).

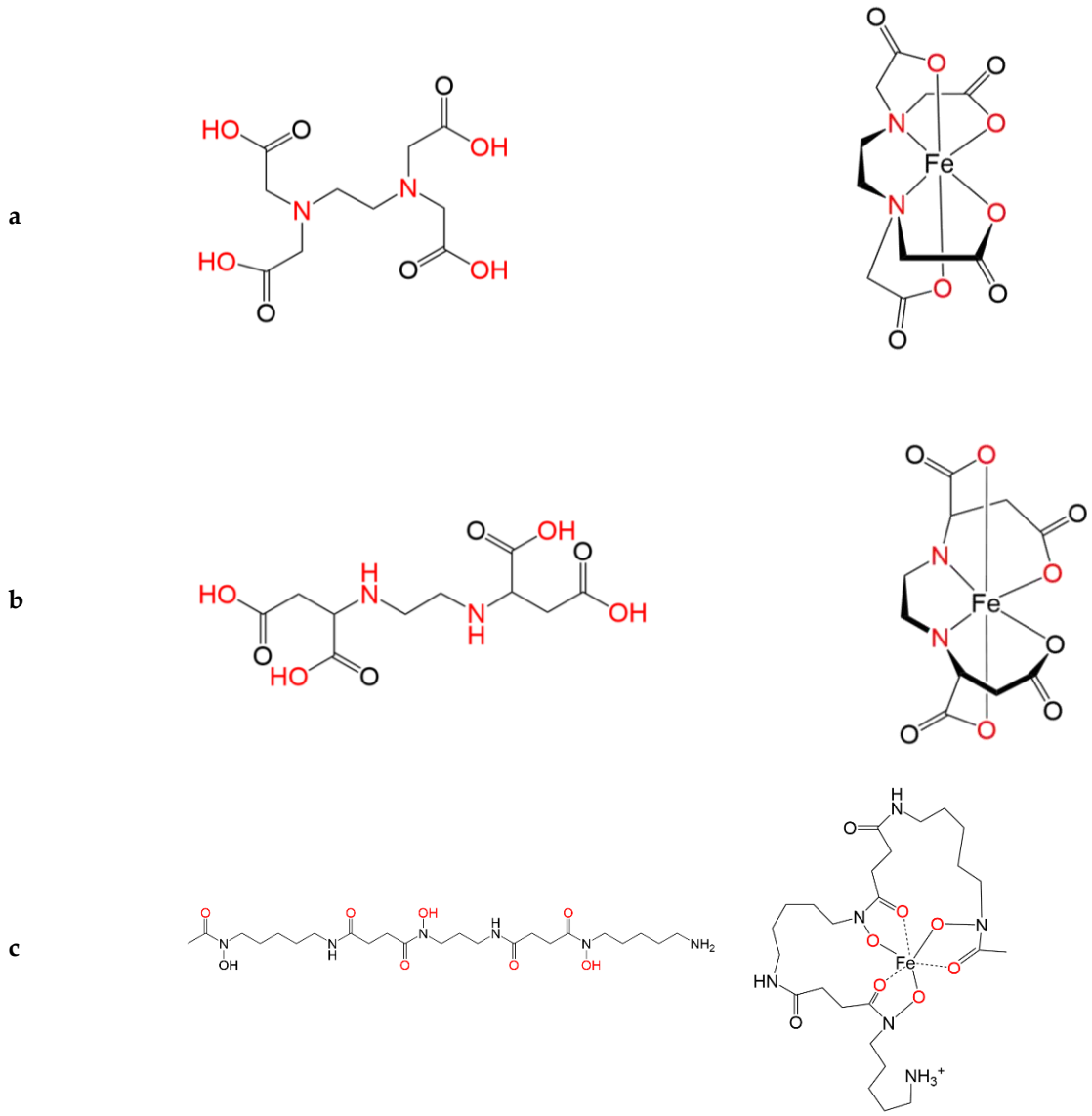

Figure 2.27 Molecular structure of EDTA (a), EDDS (b) and DFO (c) and their iron complexes [116]. Binding sites are indicated in red.

Fe-siderophore complexes are more stable at neutral to alkaline pH as otherwise there is a competition with protons H^+ [127]. Here, DFO solubilization seems to be maximum at acidic to neutral pH but still performing in the alkaline range. This is interesting for heritage metal cleaning purposes as it would allow a great versatility, adapting to various material types and cleaning interventions. For goethite, solubilization power of EDTA decreases with an increasing pH (Figure 2.26). This is identical to what has been published elsewhere where the influence of EDTA protonation on the dissolution rate of goethite was studied [128]. It was found that the Fe-EDTA complex is very stable in the acidic range whereas in the alkaline range no EDTA adsorption occurred. This observation seems odd when looking at the dominant pH range of fully ionized EDTA (Figure 2.25) but must be put in perspective with the competing phenomena: EDTA speciation versus enhanced dissolution of iron. Stability of iron minerals is highly related to pH. Looking at the Pourbaix diagram, (Figure 2.28), it is

clear that iron oxides are the most stable species at neutral to alkaline pH and on the contrary, their stability decreases at more acidic pH values [112], thermodynamically favored for the dissolution into ionic form.

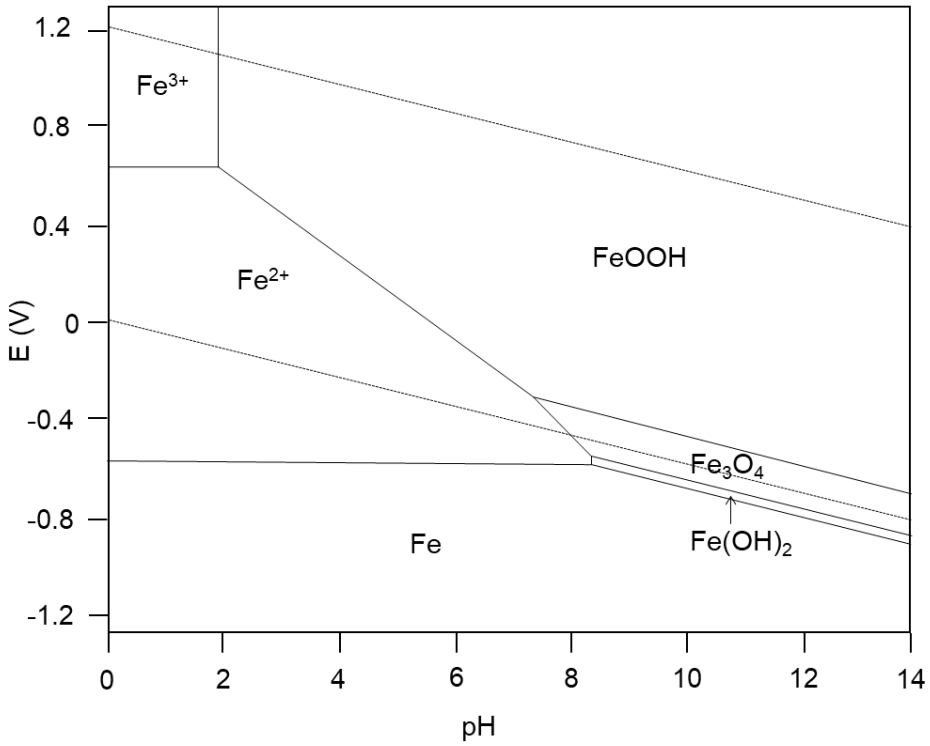

Figure 2.28 Simplified Pourbaix diagram for an iron-water system at 1 atm and 25 °C, extracted from [129].

The stability constant K_f for complexes usually encountered in tables is the one related to the fully ionized form [130,131]. Therefore complexation/solubilization should be higher at alkaline pH. Discrepancies are accounted of apparent complexation constant. Indeed, complexation equilibrium are based on the amount of iron ions available in solution. Although poorly soluble, iron oxides' solubility is still higher at acidic pH. The complexation reaction is therefore more driven by the presence of solubilized compounds in the solution rather than the strength of complexation. To simplify, if the chelator can complex a lot of ions but there are no ions around, it is useless. When reaching lower pH values, the speciation of ligands changes and the equilibrium of the solid is displaced to an area where the stable phase is mainly the soluble one (iron ions). This also explains why EDDS was less performing than EDTA in Figure 2.24, as its original pH is alkaline (8.5 at $5 \cdot 10^{-4}$ M and 9.6 at 10^{-2} M) (Table 2.4).

However, this does not explain why deferoxamine's chelating properties seem unaffected by pH changes. Scientific studies have shown that although the DFO molecules is fully protonated at acidic or neutral pH (figure 2.25 d) [132], the Fe^{3+}-DFO affinity is such that all ferric ions are complexed by the siderophore already at very low pH (figure 2.29).

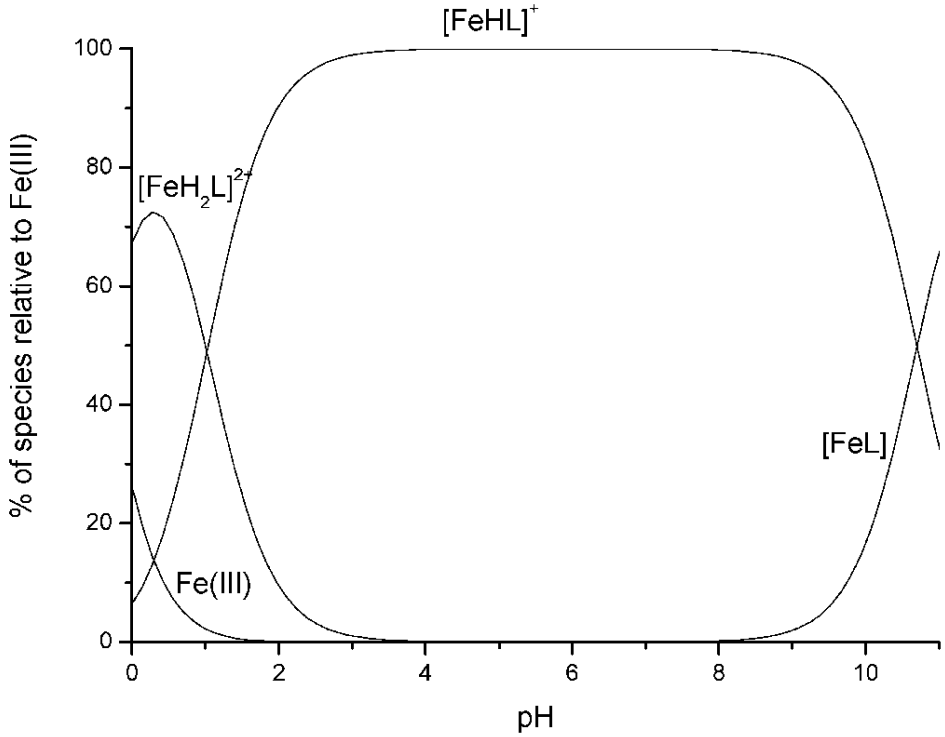

Figure 2.29 Distribution plot for Fe^{3+}-DFO complex-formation equilibria at 25 °C [133].

One can notice that the major complex species in the 1-10 pH range is a protonated specie. Indeed, the terminal amino group is protonated and not involved in complexation [116]. This is in agreement with the X-ray crystal structure of ferrioxamine, where the six oxygen atoms of the hydroxamate groups bind the iron in a distorted octahedral structure (figure 2.27 c),[134], the side chain containing the protonated terminal amine stretching away from the metal ion. This was explained as the terminal amino group oriented outside is available and serves as derivatizing DFO to act as a vector for other molecules while keeping its biological primary purpose, iron chelation [135].

The amino group would get protonated by HCl until reaching a 10^{-2} M $DFOH^+$ solution, therefore not influencing the iron binding and partly explaining the pH- independence of this reaction.

When focusing on lepidocrocite (figure 2.26), there is no clear influence of pH on the performance of EDDS (*p*-value>0.2 between pH 4 and 7, and *p*-value>0.5 between pH 7 and 10, showing no statistically significant differences), EDTA performs better with increasing pH and DFO performance decreases slightly with the pH increase. In addition, DFO performs better than any other ligand overall on this corrosion product (Table 2.8). Lepidocrocite is reported to be less thermodynamically stable [136,137]. Consequently, it is expected that lepidocrocite could be more easily solubilized and lead to higher concentration of iron ions in solution. Indeed, although the K_{sp} of goethite and lepidocrocite is similar (Table 2.4), it seems that lepidocrocite solubilizes slightly, even in the absence of ligands, as indicated by detected values of iron ions in HCl solution, Milli-Q water or NaOH solution (25 ± 4.5 μmol/L, 13 ±

4.1 μmol/L and 1.9 ± 0.9 μmol/L, respectively), which is not the case for goethite (null Fe detection) . In addition, the reported available surface area for lepidocrocite is well above the one of goethite, allowing for faster kinetics, which could also explain the greater amount of solubilized iron. As mentioned above, the limiting step for iron oxides' dissolution is the attack of a proton on the mineral surface (Fe-O bond), resulting in the release of an iron ion-complex. This releasing step is strongly dependent on iron oxide mineralogy and crystallinity, as iron oxides with poorer crystallinity like lepidocrocite readily dissolve whereas more energy is needed for more crystalline compounds like goethite, with input of energy potentially provided by an increase of temperature [138]. Nevertheless, the unexpectedly high values obtained for iron concentration after contact with DFO for lepidocrocite, although consistent in the replicates, seem odd and are contradicting those obtained in figure 2.24. Therefore, it might be connected to a systematic error and should be ascertained, as the lower thermodynamical stability and discrepancy with non-adjusted pH solutions are not sufficient to explain such differences. In addition, further studies should be performed, taking into account various parameters including controlled concentrations of ligand and metal to check for the influence of these metrics.

Furthermore, there is still a discrepancy with the results obtained for EDTA, as the amount of solubilized iron seems to increase with pH, contrary to what is theoretically expected. Indeed, the conditional stability constant, taking into account both stability range of lepidocrocite and formation constant of the complex due to the deprotonation of the ligand, should be decreasing with pH. The reported suitable range for Fe^{3+} chelation for EDDS and EDTA are 3-9 and 2-11 respectively [130].

Although it might not seem like it at first glance, mineral dissolution in ligand-aqueous solution is not a straightforward system to study. In addition to the combined complexation-protonation processes, other reactions coexist and are often not taken into account. For instance, here, the pH was not buffered and therefore the solutions varied in pH overtime during the reaction. Some studies have shown that unbuffered DFO solution shifted from 5-6 to neutrality 7 after immersion of iron minerals [79]. This was accounted for the dissolution of FeOOH species, releasing hydroxyl groups in the solution, according to the equation (3.4), hence increasing slightly the pH. These statements are surprising as according to DFO molecular structure (Figure 2.27), DFO complexation with Fe releases three protons, with the solution therefore getting acidic. Again, there are competing phenomena here. However, DFO chelation is not very sensitive to pH changes [116].

$$FeOOH + H_2O \rightarrow Fe^{3+} + 3\ OH^- \quad (3.4)\ [87]$$

As a result of all this, reaction mechanisms are very complex and not yet fully understood. For this reason, most mechanisms presented in the literature are based solely on simplified systems. For instance, only the initial dissolution rate is considered to ease the theoretical interpretation. However, the dissolution rate changes as the reaction progresses. Indeed, the specific surface area gradually

increased during the process of dissolution [115], which also increases the dissolution rate as stated by the Noyes-Whitney equation. Usually, smaller particle size, as well as high porosity, increase the surface area. A mineral with an increased specific surface area will increase its dissolution rate [139–141]. Specific surface being an important parameter, here, to allow comparable quantitative analysis between goethite and lepidocrocite, maximal concentrations of dissolved iron after 24 hours were normalized to mineral surface area contacted by the solution during the immersion as it was assumed that BET surface area is a suitable indicator of ligand accessibility. However, some have argued that iron oxides' surface area is not as impacting as for other ions as it has been reported that no direct correlation could be inferred between surface area and solubility or that, because particles are small, they form agglomerates that reduce the effective specific surface [87,141].

For that reason, figure 2.30 displays both BET-normalized and raw data of iron ions in solution after 24 hours. Further discussion, addressing selectivity and affinity, will rely on data from non-pH-adjusted experiments to exclude the pH factor and only consider the "raw solution".

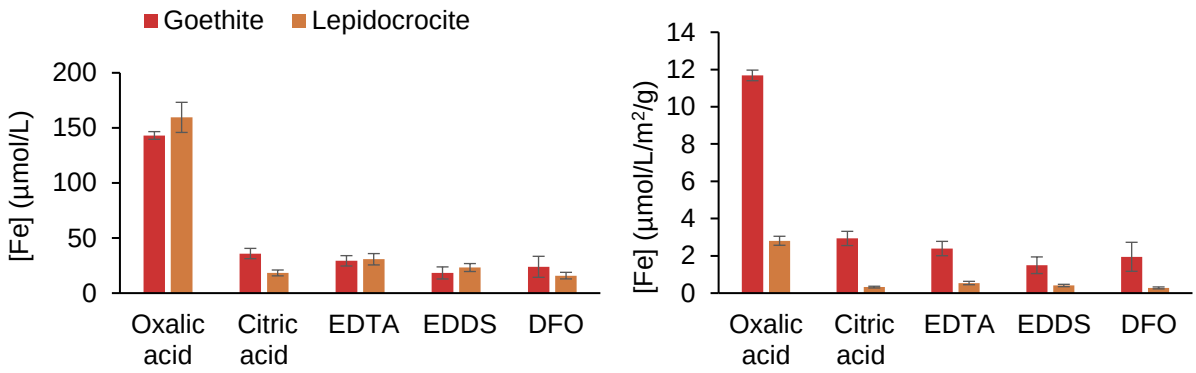

Figure 2.30 Dissolved iron after 1440 minutes (24 hours) of reaction for goethite or lepidocrocite with non pH-adjusted $5 \cdot 10^{-4}$ M ligand solutions. Raw (left) and normalized data over BET surface (right) are displayed.

The results processed from raw data are in accordance with the expected results, with rather similar dissolution of both iron compounds, whereas for normalized results, there seems to be a very low solubilization of lepidocrocite comparatively to goethite. This indicated the formation of agglomerates from the corrosion products. Agglomerates behave as large particles with internal porosity hence rendering the surface area an irrelevant normalization factor [141]. Indeed, looking at particle dimension, for both goethite and lepidocrocite the use of ultrasonic bath reduced the mean size. This is due to deagglomeration of the particles [142]. Indeed, if one takes a deeper look at the particle size distribution (Figure S2.7), the multimodal distribution shifts to lower particle size values for goethite, meaning deagglomeration of some of the particles. To ascertain this hypothesis, the zeta potential of the particle could be measured in order to confirm their inclination to form agglomerates [143].

Overall, solubilization rate is affected by solution conditions in which pH is an important variable. Again, whether proton- and organic ligand-driven reactions happen subsequently, in parallel, combined or compete is dependent on several phenomena in competition, where one or the other parameter can favor one or the other surface-driven reaction (i.e., pH, accessibility of the solid's surface (e.g., surface area, crystallinity). Actually, in nature, low molecular weight organic acids (LMWOA) are secreted to promote iron mineral dissolution [112,144], more precisely to promote the formation of labile iron on the minerals' surface [145], allowing a synergetic phenomenon with siderophores and therefore accelerating iron oxides' dissolution rate [146]. Indeed, siderophores form more stable complexes with Fe^{3+} ions than organic acids with log K_f ranging between 30 to 50 for siderophores, while LMWOA have lower log K_f (e.g., oxalic acid log K_f = 7.5; citric acid log K_f = 17). In addition, diffusion phenomena cannot be ignored, and can also be influenced by a plethora of metrics, including temperature, agitation, concentration of ligands or solids in solution. In order to acknowledge the actual influence of each of the contributing parameters, more work should be foreseen for iron oxides, resorting to a statistical approach such as principal component analysis or ANOVA to ascertain the dominant metrics in the dissolution of the iron oxides studied.

Conclusions drawn for one metal's solid phases, here iron, may not follow similar dissolution behavior for other metals, being function of time, pH, ligand's nature (and concentration). Further tests were thus carried out with copper oxides and sulfides.

2.3.2.2 Copper

Dissolution of cuprite (Cu_2O), chalcocite (Cu_2S), covellite (CuS) and brochantite ($Cu_4SO_4(OH)_6$) was studied over a period of 24 hours, at room temperature, in the presence of different complexing agents. Concentration of solubilized copper ions was determined via ICP-OES and is displayed in figure 2.31. Due to possible experimental errors, results obtained for covellite are addressed in supplementary materials.

Overall, the kinetics of solubilization are very fast for brochantite, reaching its maximum within 10 minutes after contact with ligands. Reaction kinetics for cuprite and chalcocite are more progressive, but still, one can note that the reaction reaches a plateau after 4 hours for cuprite for almost all ligands whereas the equilibrium state does not seem reached for chalcocite. This is in line with literature, stating that sulfides are less soluble than oxides [147].

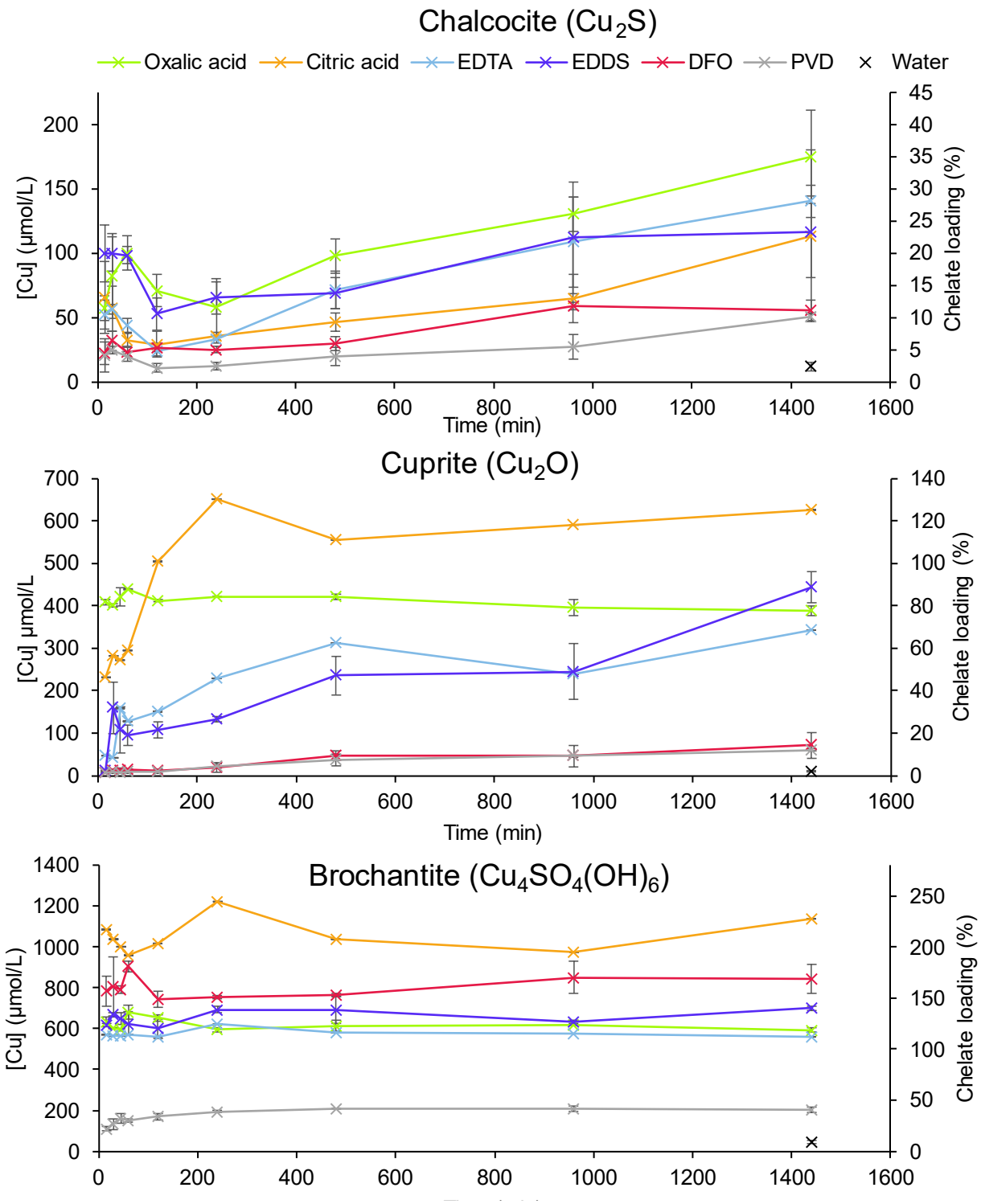

Figure 2.31 Copper detected by ICP-OES after copper solid phase dissolution in presence of several $5 \cdot 10^{-4}$ M ligand solutions (oxalic acid (green), citric acid (orange), EDTA (blue), EDDS (purple), DFO (red), PVD (grey) and water (black)), plotted versus time.

Looking at chalcocite, ANOVA showed a significant better dissolution performance of oxalic acid, EDTA and EDDS, followed by citric acid and then siderophores DFO and PVD respectively. For EDDS and DFO a threshold seems to be reached from 16 hours whereas the other ligand solutions seem to not have reached their equilibrium state. It has been theorized that chalcocite dissolution occurs in two steps

[148], by first transforming into covellite and then covellite dissolving and that the second step is much slower than the first [149]. Indeed, Cu^{+} salts are more insoluble than Cu^{2+} salts [150].

Looking at cuprite solubilization, citric and oxalic acid perform significantly better, with no difference between the two groups (*p*-value = 0.76), followed by EDTA and EDDS, performing equally (*p*-value = 0.99) and then by siderophores. This is not surprising as siderophores are iron-specific and therefore display stability constants with copper that are lower than other ligands. This is also the case for chalcocite.

Regarding brochantite, again, citric acid performs better than any other tested ligand, followed by DFO. Oxalic acid is positioned in-between EDTA and EDDS, with no significant difference, and pyoverdine being far behind.

Interestingly for both brochantite and cuprite, citric acid reaches its maximum after 4 hours, suggesting a high leaching rate [151]. Apart from chalcocite, the dissolution rates of other copper minerals in ligand solutions seem to decrease quite rapidly, showing low variations after 4 hours.

For all copper corrosion products, the trend does not seem to follow a diffusion-driven solubilization or even a linear solubilization contrary to what had been observed in previous studies on different copper chlorides, sulfates or carbonates where it was stated that the dissolution process was driven by the process of diffusion [152]. Other studies have shown that the kinetic model followed by the solubilization of copper is from the pseudo-second order [153]. Here, plotting the reciprocal of the reaction concentration versus time does not give a linear plot, therefore, the second order reaction was not verified, this might be because of the difference in the nature of copper species studied.

In this experiment, there seem to be a systematic error, as seen by the early maximum reached within minutes after solid-ligand solution contact, accounted for by several errors. In addition, there seems to be an excess release of copper, reaching over 100% of chelate loading for cuprite and brochantite (Figure 2.31), preventing to state whether the equilibrium state really has been reached or whether the 100% metal to ligand ratio is due to experimental errors. Here, the experiments were done simultaneously to avoid block effects, but these errors could be corrected with further works, in particular prewashing of minerals to remove any mobile copper on the surface, constant or no stirring, filtering of the solution before analysis. In addition, it would be advisable to continue data point collection until reaching the equilibrium state of the system. This would allow characterization of further slight increase observed for oxalic acid with Cu_2S, and for EDDS with Cu_2O.

On the copper Pourbaix diagram (Figure 2.32), theoretical thermodynamic stability is proportional to the area of the stability region of each species, depicting a stability over large range of conditions: sulfates are less stable than oxides, which have a lower stability than sulfides.

Interestingly, brochantite has the lowest stability range, only matching the initial pH of the 5.10^{-4} M

EDTA solution (5.9), which performs the least in figure 2.31, PVD excluded. For chalcocite, there is no plateau, meaning the equilibrium state is not reached. This is not surprising as, for whichever tested ligand solutions initial pH, Cu_2S can be a predominant species, in addition to a high pK_{sp} (table 2.6), its solubilization is slow, even in presence of ligands. Cuprite is also stable over a large area but has a much lower pK_{sp} (3.2).

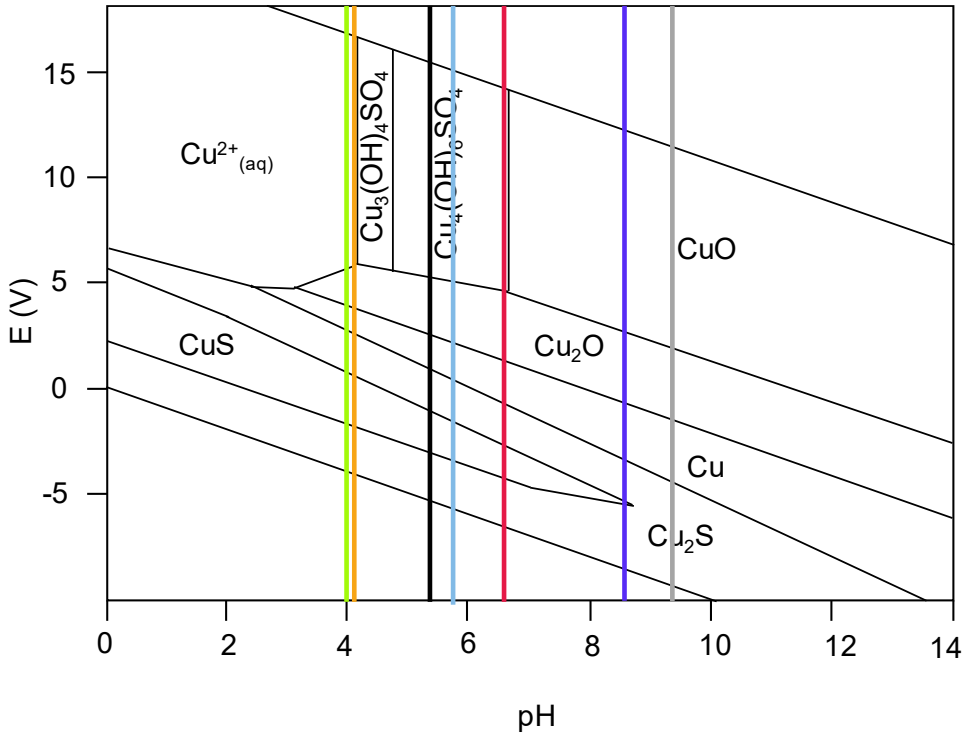

Figure 2.32 Pourbaix diagram for a copper-water-sulfur system at 1 atm and 25 °C, extracted from [100], with the initial pH of $5 \cdot 10^{-4}$ M ligand solutions (oxalic acid (green), citric acid (orange), EDTA (blue), EDDS (purple), DFO (red), PVD (grey) and water (black)).

Acids have lower K_f than other ligands with copper but nevertheless achieve great Cu ions solubilization. This is due to their ability to act as Lewis base (electron donor). To investigate this phenomenon, corrosion products-ligand interaction was done at different pH (4, 7 and 10). The amount of copper detected after 24 hours by ICP-OES in the ligand-solutions adjusted at different pH is plotted on figure 2.33.

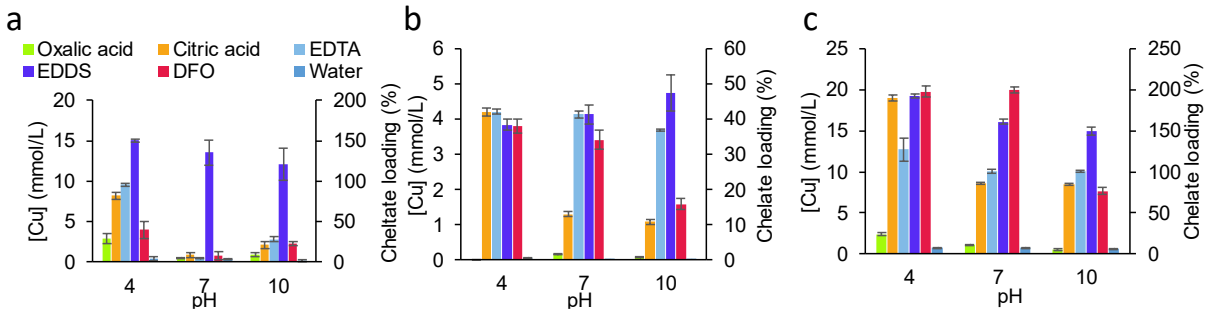

Figure 2.33 Dissolved copper from, chalcocite (a), cuprite (b) and brochantite (c) detected via ICP-OES in 10^{-2} M ligand solutions at pH 4, 7 or 10.

For cuprite, at acidic pH there is a good efficiency of, from best to low performing, EDDS, EDTA, citric acid, DFO and oxalic acid. Out of these, only EDDS also has an effect on cuprite at neutral and alkaline pH. Similar observations were made by Ko *et al.* for citric acid action on cuprite [154], with a decrease of solubilization efficiency with increasing pH. In addition, in the Pourbaix diagram, the stability area of cuprite starts after pH values of close to 4 (Figure 2.32).

Globally, EDTA performs equally well at all three pH values with Cu_2S and brochantite. Other studies have already concluded that copper extraction by EDTA is pH-independent [155,156]. However, in figure 2.33, EDTA seems to be affected by pH for the dissolution of cuprite. The action of EDDS for copper solubilization is not pH-dependent for chalcocite and brochantite either but for cuprite as well [157]. Therefore, overall, EDDS performs better on copper than EDTA. In a paper studying extraction of heavy metals from soils, this trend occurred as well and was interpreted as a lower competition with calcium ions for EDDS ($\log K_f$ for Ca-EDDS=4.6 vs $\log K_f$ for Ca-EDTA=9.09) [158]. However, here, it is also the case although there is no presence of calcium ions in solution, showing that there is an intrinsic practical better complexation of copper by EDDS than EDTA despite their close $\log K_f$ with Cu (Table 2.4). Indeed, according to various authors, EDDS has an acute affinity for copper ions compared to other chelating agents [130,159,160].

DFO performed equally well at acidic and neutral pH for chalcocite and brochantite and only slightly better at acidic pH for cuprite. It does have some effect at alkaline pH for chalcocite and brochantite. Citric acid has some effect for chalcocite and brochantite at even neutral to alkaline pH. Indeed, studies have shown that copper complexes of citric acid are highly stable over the full pH range thanks to the carboxyl groups [161], explaining the extensive use of triammonium citrate in the conservation field for the removal of copper corrosion [162].

Oxalic acid does not perform well at pH 4, even less at neutral to alkaline pH. One can hypothesize that, because its natural pH at 10^{-2} M was measured at 1.9 (Table 2.4), all pH-adjusted solutions were too alkaline to allow oxalic acid action. Indeed, with the neutralization, the actual concentration of oxalic acid was of $1.8 \cdot 10^{-5}$ M.

Overall, on cuprite and chalcocite, exception made for EDDS, copper solubilization occurs accordingly to the stability regions of the Pourbaix diagram. This suggests that solubilization of these copper ores is driven by the amount of copper cations in solution rather than a surface-driven phenomenon as for iron. Notably, the results obtained in Figure 2.33 are contradicting those in Figure 2.31, which might be caused by a systematic error or due to block effects.

Additionally, the experiments were carried out under aerobic conditions, meaning the absence of control over atmospheric oxygen levels. This was selected to mimic conditions during practical treatment. For such, it is important to keep in mind that results obtained and displayed in figures 2.31

and 2.33 probably include side redox reactions, leading to the oxidation of solubilized Cu^{+} into Cu^{2+}. In order to perform a strict evaluation of cuprite or chalcocite solubilization in solution, anoxic conditions would be required.

Similarly to iron, the amount of solubilized copper after 24 h in non-pH-adjusted solutions is displayed in figure 2.34, comparing both raw and specific surface normalized data. The addition of the normalization factor does not seem to affect the results for cuprite and chalcocite, however brochantite's values drop because of its high surface area. It seems that the impact of the presence of agglomerates and particle size is lesser than for iron oxyhydroxides as the phenomenon of solubilization seems to be less of a surface-driven phenomenon but happen mainly on the cations already in solution. In a way, this is in accordance with literature data stating brochantite is very stable, with the highest solubility product constant of all tested corrosion products (Table 2.5). Regarding cuprite and chalcocite, all chelators seem to have a better ability to dissolve cuprite, apart from DFO which yields similar values for all copper corrosion products. Hence, deferoxamine has poor selectivity of cuprite compared to other complexing agents.

Excluding DFO because of its lower affinity for copper compounds, it seems that copper oxide is more easily solubilized than copper sulfide. This is in accordance with common lower solubility of sulfides versus oxides due to lower solubility constants [147]. Indeed, copper sulfides bonds are somewhat covalent whereas copper oxide bonds tend to have more ionic nature [163], thus resulting in a higher bond-dissociation energy for Cu-S bonds.

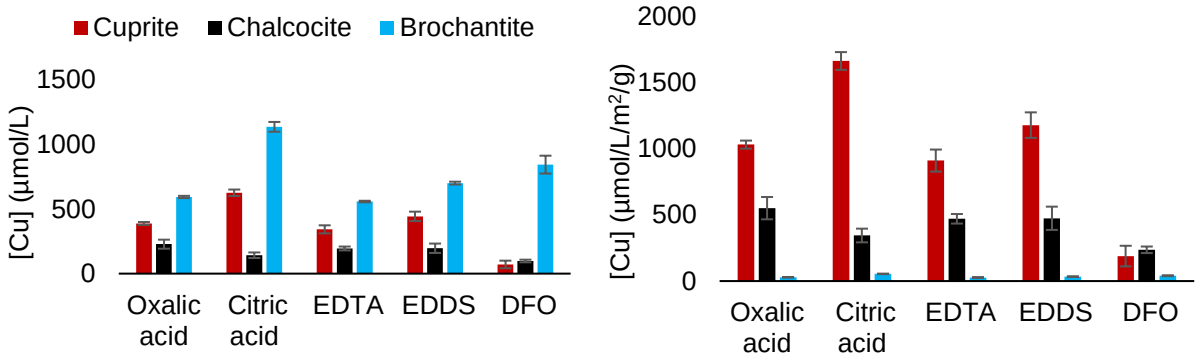

Figure 2.34 Dissolved copper after 1440 minutes (24 hours) of reaction for cuprite, chalcocite and brochantite with non pH-adjusted ligand solutions. Data both raw (left) and normalized over BET surface (right) are displayed.

2.3.2.3 Silver

Quantification of solubilized acanthite in the presence of different organics ligands via ICP-OES gave null results. This can be accounted for by the extremely low solubility of Ag_2S ($logK_{sp} = 51$). Nevertheless, it was deemed interesting to assess the potential action of chelators with soluble silver using UV-Vis spectroscopy. Full spectra were acquired and compared with soluble silver solution of $AgNO_3$. Solely EDDS gave promising results, hence only the corresponding absorbance spectra are shown in Figure

2.35, at relevant range (240-800 nm).

The absorbance spectrum of EDDS alone does not present any particular peak (Figure 2.35, dotted spectrum). On the other hand, silver nitrate alone has a peak at 304 nm. At pH 9 in the $AgNO_3$-EDDS solution a discrete bump at 410 nm can be observed, indicating the transformation of Ag^+ ions with a further conversion into silver nanoparticles (AgNPs) [164]. Silver nanoparticles synthesis using aminoacids as a green reducing agents has been explored in previous research[165], but the use of EDDS is not reported as it is not a reducing agent. Maximal obtention of AgNPs was achieved at pH 9 as the signals are more pronounced, similarly to what has been seen elsewhere [166,167]. Given the wavelength and the shape of the peak (weak and broad), it can be hypothesized that the formed AgNPs have a size between 10-50 nm and are rather aggregated [168–173]. The presence of the peak at 273 nm could be explained by the presence of silver nanoclusters (AgNCs), as it has been reported elsewhere [174] but further investigation would be necessary.

In all cases, the reaction of EDDS with soluble silver rendered the solution more cloudy, as a high baseline is symptomatic of turbidity, which is common with the formation of aggregates [167].

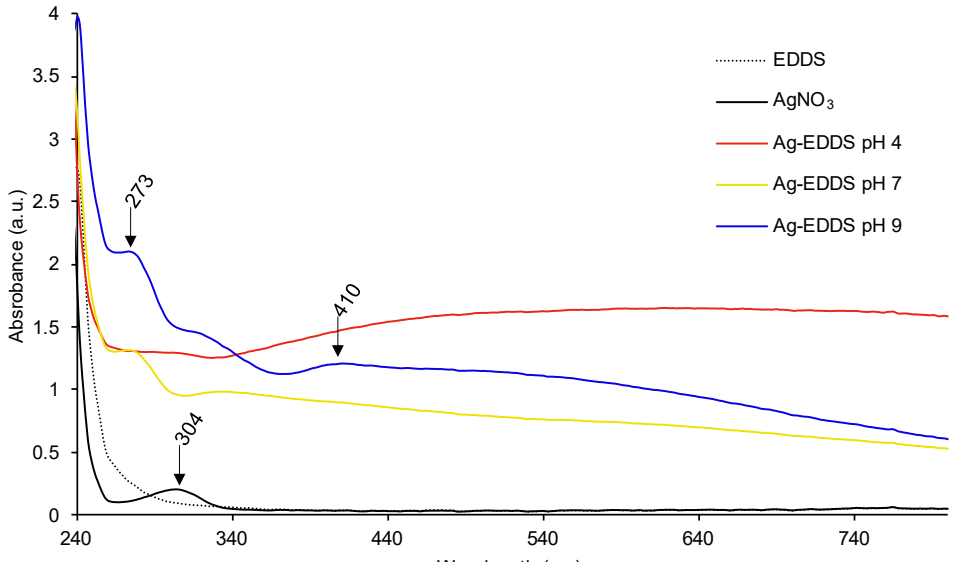

Figure 2.35 Absorbance spectra of EDDS, silver nitrate and mixtures of both solutions at pH 4, 7 and 9.

Additionally, Raman spectroscopy performed on the Ag-EDDS solution (Figure 2.36) detected bands at 98 cm^{-1} and 156 cm^{-1} that can be attributed to Ag crystal lattice [175]. Peaks were also seen at 230 cm^{-1} [176,177], 933 cm^{-1} [176], 1284 cm^{-1} [177,178], 1372 cm^{-1} [177,179,180], which is consistent with the vibrations found for AgNPs but are also detected in bare EDDS or $AgNO_3$ spectra. So far, the signal at 819 cm^{-1} is the only one that is present exclusively in the Ag-EDDS spectrum, meaning a new vibration is detected after mixing of the two components. However, based on literature, it could not be assigned to any particular peak. Although appealing, the results should be pushed by Transmission Electron Microscopy (TEM) to verify the formation of silver nanoparticles or other silver transformation.

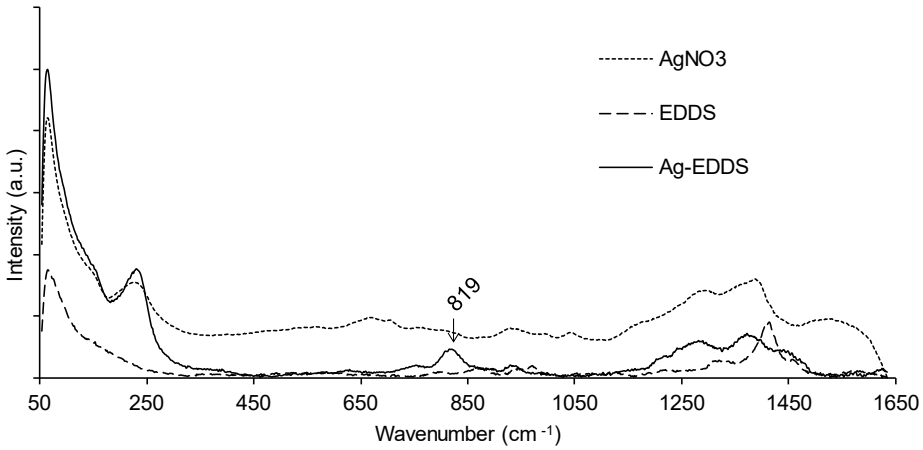

Figure 2.36 Raman spectra (532 nm, 30 × 1 s) of $AgNO_3$, EDDS and a mixture of both in solution.

Unfortunately, silver nanoparticles have a color ranging from yellow to reddish-brown [19], according to the size and shape, which does not seem relevant to study further in the conservation field for removal of silver tarnishing as it does not comply with the aesthetic expectations for silver objects, i.e., shiny grey.

2.3.3 Main findings

Iron

- Several diffusion- or surface driven-reactions coexisting (i.e., complexation, protonation etc) therefore difficult to predict any kinetical model
- Acidic sequestering agents seem to promote a diffusion-controlled model whereas for the others it is more surface-controlled, although both phenomena apparently coexist
- DFO is the chelating agent least affected by pH change and effective over most of the pH range.

Copper

- DFO has a low affinity for cuprite
- EDTA and EDDS show no selectivity
- EDDS is effective over the full pH range for the corrosion products studied here
- Copper solubilization seems to be related to solubility of corrosion products rather than a surface-driven reaction

Silver

- Ag_2S cannot be solubilized by any of the studied ligands
- EDDS can react with soluble silver at neutral to alkaline pH to form AgNPs

2.4 Conclusion

Metal uptake using living organism was tested on soluble and insoluble iron and copper sources. The fungus *Aspergillus niger* was found to yield interesting results on iron plates whereas *Beauveria bassiana* was found to yield worthy results on copper plates. Both mechanisms seem to be related to the formation of iron or copper oxalates respectively. Silver resistance tests carried out on *A. ferrooxidans* and *P. yamanorum* showed interesting results for *A. ferrooxidans*, with bacterial growth at concentrations of up to 1 mM Ag^+. Research should be carried further with biosurfactants, dead or living fungal biomass or aminoacids.

To limit the use of living organisms, attempts at producing metabolites of interests for metal complexation/remediation were performed. The yields were not satisfactory and the purification not optimal. Attempts at enhancing the siderophore production could be foreseen.

Finally, the affinity between different corrosion products found on historical objects and ligands was tested to evaluate the different interactions between the two types of compounds. The siderophore deferoxamine is the only complexing agent that shows effectiveness over the full pH range for iron. However, it has a low affinity for copper compounds, particularly for cuprite compared to EDTA and EDDS. Regarding the kinetics of reaction, different corrosion products do not dissolve at the same rate most of the time. However, it would be hasty to conclude on this as so many parameters come into account. For silver, the biodegradable complexing agent EDDS is the only one that seem to have an effect on the element, in soluble form only but not as solid phase, with the formation of silver nanoparticles.

2.5 Bibliography

1. *Classification of Organisms*; Federal Office of Public Health FOPH, Federal Office for the Environment FOEN, 2013 https://www.bafu.admin.ch/bafu/en/home/topics/biotechnology/publications-studies/publications/classification-of-organisms.html
2. Baakza, A.; Vala, A.K.; Dave, B.P.; Dube, H.C. A Comparative Study of Siderophore Production by Fungi from Marine and Terrestrial Habitats. *J. Exp. Mar. Bio. Ecol.* **2004**, *311*, 1–9, doi:10.1016/j.jembe.2003.12.028.
3. Holinsworth, B.; Martin, J.D. Siderophore Production by Marine-Derived Fungi. *BioMetals* **2009**, *22*, 625–632, doi:10.1007/s10534-009-9239-y.
4. Franco, L. de O.; Maia, R. de C.C.; Porto, A.L.F.; Messias, A.S.; Fukushima, K.; Campos-Takaki, G.M. de Heavy Metal Biosorption by Chitin and Chitosan Isolated from Cunninghamella Elegans (IFM 46109). *Brazilian J. Microbiol.* **2004**, *35*, 243–247, doi:10.1590/S1517-83822004000200013.
5. Albini, M. Fungal Biogenic Patina: Optimization of an Innovative Conservation Treatment for Copper-Based Artefacts, PhD thesis, University of Neuchâtel, 2018.
6. Oh, J.-J.; Kim, J.Y.; Kim, Y.J.; Kim, S.; Kim, G.-H. Utilization of Extracellular Fungal Melanin as an Eco-Friendly Biosorbent for Treatment of Metal-Contaminated Effluents. *Chemosphere* **2021**, *272*, 129884, doi:10.1016/j.chemosphere.2021.129884.
7. Gadd, G.M.; de Rome, L. Biosorption of Copper by Fungal Melanin. *Appl. Microbiol. Biotechnol.* **1988**, *29*, 610–617, doi:10.1007/BF00260993.
8. Comensoli, L.; Kooli, W.; Monachon, M.; Albini, M.; Junier, P.; Joseph, E. The Potential of Microorganisms for the Conservation-Restoration of Iron Artworks. In Proceedings of the Metal 2019, 9th interim meeting of the ICOM-CC metals working group; Neuchâtel, Switzerland, 2019; pp. 242–249.
9. Gadd, G.M. Interactions of Fungi with Toxic Metals. In *The Genus Aspergillus*; Springer US: Boston, MA, 1994; pp. 361–374.
10. Sauer, M.; Porro, D.; Mattanovich, D.; Branduardi, P. Microbial Production of Organic Acids: Expanding the Markets. *Trends Biotechnol.* **2008**, *26*, 100–108, doi:10.1016/j.tibtech.2007.11.006.
11. Albelda-Berenguer, M.; Monachon, M.; Joseph, E. Siderophores: From Natural Roles to Potential Applications. In *Advances in Applied Microbiology*; 2019; pp. 193–225.
12. Weber, K.A.; Achenbach, L.A.; Coates, J.D. Microorganisms Pumping Iron: Anaerobic Microbial Iron Oxidation and Reduction. *Nat. Rev. Microbiol.* **2006**, *4*, 752–764, doi:10.1038/nrmicro1490.
13. Scheepers, G.; Koster, M.; Bennekom, J. Van Exploring the Use of Acidithiobacillus Ferrooxidans for the Removal of Sulphides from Tarnished Silver. *Estud. Conserv. e Restauro* **2019**, *2*, 19–30.
14. Pooley, F.D. Bacteria Accumulate Silver during Leaching of Sulphide Ore Minerals. *Nature* **1982**, *296*, 642–643, doi:10.1038/296642a0.
15. Brandel, J.; Humbert, N.; Elhabiri, M.; Schalk, I.J.; Mislin, G.L.A.; Albrecht-Gary, A.M. Pyochelin, a Siderophore of Pseudomonas Aeruginosa: Physicochemical Characterization of the Iron(Iii), Copper(Ii) and Zinc(Ii) Complexes. *Dalt. Trans.* **2012**, *41*, 2820–2834, doi:10.1039/c1dt11804h.
16. Cornelis, P.; Hohnadel, D.; Meyer, J.M. Evidence for Different Pyoverdine-Mediated Iron Uptake Systems among Pseudomonas Aeruginosa Strains. *Infect. Immun.* **1989**, *57*, 3491–3497, doi:10.1128/iai.57.11.3491-3497.1989.
17. Braud, A.; Hoegy, F.; Jezequel, K.; Lebeau, T.; Schalk, I.J. New Insights into the Metal Specificity of the Pseudomonas Aeruginosa Pyoverdine-Iron Uptake Pathway. *Environ. Microbiol.* **2009**, *11*, 1079–1091, doi:10.1111/j.1462-2920.2008.01838.x.
18. Haefeli, C.; Franklin, C.; Hardy, K. Plasmid-Determined Silver Resistance in Pseudomonas Stutzeri Isolated from a Silver Mine. *J. Bacteriol.* **1984**, *158*, 389–392, doi:10.1128/jb.158.1.389-392.1984.

19. González, A.L.; Noguez, C.; Beránek, J.; Barnard, A.S. Size, Shape, Stability, and Color of Plasmonic Silver Nanoparticles. *J. Phys. Chem. C* **2014**, *118*, 9128–9136, doi:10.1021/jp5018168.
20. Guilger-Casagrande, M.; Lima, R. de Synthesis of Silver Nanoparticles Mediated by Fungi: A Review. *Front. Bioeng. Biotechnol.* **2019**, *7*, 1–16, doi:10.3389/fbioe.2019.00287.
21. Palmieri, F. Bacterial Oxalotrophy as an Alternative Biocontrol Approach for the Fight against Pulmonary Aspergillosis, Université de Neuchâtel, 2021. https://libra.unine.ch/entities/publication/a19301cf-46fb-46bd-ae3d-09e17bffea98/details
22. Comensoli, L.; Maillard, J.; Kooli, W.; Junier, P.; Joseph, E. Soluble and Solid Iron Reduction Assays with Desulfitobacterium Hafniense. *Bio-Protocol* **2018**, *8*, doi:10.21769/bioprotoc.3002.
23. Stookey, L.L. Ferrozine---a New Spectrophotometric Reagent for Iron. *Anal. Chem.* **1970**, *42*, 779–781, doi:10.1021/ac60289a016.
24. Gangakhedkar, N.S. Colour Measurement Methods for Textiles. In *Colour Measurement*; Elsevier, 2010; pp. 221–252.
25. Aisen, P. Chemistry and Biology of Eukaryotic Iron Metabolism. *Int. J. Biochem. Cell Biol.* **2001**, *33*, 940–959, doi:10.1016/S1357-2725(01)00063-2.
26. Winterbourn, C.C. Toxicity of Iron and Hydrogen Peroxide: The Fenton Reaction. *Toxicol. Lett.* **1995**, *82–83*, 969–974, doi:10.1016/0378-4274(95)03532-X.
27. Eid, R.; Arab, N.T.T.; Greenwood, M.T. Iron Mediated Toxicity and Programmed Cell Death: A Review and a Re-Examination of Existing Paradigms. *Biochim. Biophys. Acta - Mol. Cell Res.* **2017**, *1864*, 399–430, doi:10.1016/j.bbamcr.2016.12.002.
28. Comensoli, L. Interaction between Microbes, Iron and Chlorine for the Development of Biotechnological Approaches to Stabilize Corroded Iron, PhD thesis, University of Neuchâtel, 2017.
29. Voß, B.; Kirschhöfer, F.; Brenner-Weiß, G.; Fischer, R. Alternaria Alternata Uses Two Siderophore Systems for Iron Acquisition. *Sci. Rep.* **2020**, *10*, 3587, doi:10.1038/s41598-020-60468-7.
30. Odoni, D.I.; van Gaal, M.P.; Schonewille, T.; Tamayo-Ramos, J.A.; Martins dos Santos, V.A.P.; Suarez-Diez, M.; Schaap, P.J. Aspergillus Niger Secretes Citrate to Increase Iron Bioavailability. *Front. Microbiol.* **2017**, *8*, doi:10.3389/fmicb.2017.01424.
31. Li, S.; Hihara, L.H. A Micro-Raman Spectroscopic Study of Marine Atmospheric Corrosion of Carbon Steel: The Effect of Akaganeite. *J. Electrochem. Soc.* **2015**, *162*, C495–C502, doi:10.1149/2.0881509jes.
32. Galeas, S.; Valdivieso-Ramírez, C.S.; Pontón, P.I.; Goetz, V.; Guerrero, V.H. Photocatalytic Activity of Fe/Ti-Based Compounds Obtained from Ferro-Titaniferous Mineral Sands via a Simple Soft Chemistry Route. *J. Phys. Conf. Ser.* **2022**, *2238*, 012006, doi:10.1088/1742-6596/2238/1/012006.
33. Edwards, H.G.M.; Russell, N.C. Vibrational Spectroscopic Study of Iron(II) and Iron(III) Oxalates. *J. Mol. Struct.* **1998**, *443*, 223–231, doi:10.1016/S0022-2860(97)00390-6.
34. Comensoli, L.; Bindschedler, S.; Junier, P.; Joseph, E. Iron and Fungal Physiology: A Review of Biotechnological Opportunities. *Adv. Appl. Microbiol.* **2017**, *98*, 31–60, doi:10.1016/bs.aambs.2016.11.001.
35. Lee, S.O.; Tran, T.; Jung, B.H.; Kim, S.J.; Kim, M.J. Dissolution of Iron Oxide Using Oxalic Acid. *Hydrometallurgy* **2007**, *87*, 91–99, doi:10.1016/j.hydromet.2007.02.005.
36. Zelenskaya, M.S.; Izatulina, A.R.; Frank-Kamenetskaya, O. V.; Vlasov, D.Y. Iron Oxalate Humboldtine Crystallization by Fungus Aspergillus Niger. *Crystals* **2021**, *11*, 1591, doi:10.3390/cryst11121591.
37. Selwyn, L. *Metals and Corrosion: A Handbook for the Conservation Professional*; Canadian Conservation Institute, 2004; ISBN 9780662379843.
38. Liaud, N.; Giniés, C.; Navarro, D.; Fabre, N.; Crapart, S.; Gimbert, I.H.-; Levasseur, A.; Raouche, S.; Sigoillot, J.-C. Exploring Fungal Biodiversity: Organic Acid Production by 66 Strains of

Filamentous Fungi. *Fungal Biol. Biotechnol.* **2014**, *1*, 1–10, doi:10.1186/s40694-014-0001-z.
39. Gadd, G.M.; Griffiths, A.J. Effect of Copper on Morphology of Aureobasidium Pullulans. *Trans. Br. Mycol. Soc.* **1980**, *74*, 387–392, doi:10.1016/s0007-1536(80)80168-9.
40. Joseph, E.; Cario, S.; Simon, A.; Wörle, M.; Mazzeo, R.; Junier, P.; Job, D. Protection of Metal Artifacts with the Formation of Metal-Oxalates Complexes by Beauveria Bassiana. *Front. Microbiol.* **2012**, *2*, doi:10.3389/fmicb.2011.00270.
41. Fomina, M.; Hillier, S.; Charnock, J.M.; Melville, K.; Alexander, I.J.; Gadd, G.M. Role of Oxalic Acid Overexcretion in Transformations of Toxic Metal Minerals by Beauveria Caledonica. *Appl. Environ. Microbiol.* **2005**, *71*, 371–381, doi:10.1128/AEM.71.1.371-381.2005.
42. Gutknecht, N.; Joseph, E. Stabilisation of Archaeological Copper-Alloy Objects from Chloride-Induced Active Corrosion with Beauveria Bassiana. In *Metal 2019 Proceedings of the Interim Meeting of the ICOM-CC Metals Working Group*; Chemello, C., Brambilla, L., Joseph, E., Eds.; Neuchâtel, Switzerland, 2019; pp. 12–15 ISBN 978-92-9012-458-0.
43. Nevin, A.; Melia, J.L.; Osticioli, I.; Gautier, G.; Colombini, M.P. The Identification of Copper Oxalates in a 16th Century Cypriot Exterior Wall Painting Using Micro FTIR, Micro Raman Spectroscopy and Gas Chromatography-Mass Spectrometry. *J. Cult. Herit.* **2008**, *9*, 154–161, doi:10.1016/j.culher.2007.10.002.
44. Joseph, E.; James, S.; Albelda-Berenguer, M.; Albini, M.; Comensoli, L.; Cornet, E.; Domon Beuret, E.; Kooli, W.; Brambilla, L.; Mathys, L.; et al. Ground-Breaking Approaches for a Green and Sustainable Metal Conservation. In Proceedings of the Proceedings of 19th ICOM-CC Triennial Conference Transcending Boundaries: Integrated Approaches to Conservation; ICOM-CC: Beijing, 2021.
45. WU, X. ling; QIU, G. zhou; GAO, J.; DING, J. nan; KANG, J.; LIU, X. xing Mutagenic Breeding of Silver-Resistant Acidithiobacillus Ferrooxidans and Exploration of Resistant Mechanism. *Trans. Nonferrous Met. Soc. China (English Ed.* **2007**, *17*, 412–417, doi:10.1016/S1003-6326(07)60107-1.
46. Schalk, I.J.; Hannauer, M.; Braud, A. New Roles for Bacterial Siderophores in Metal Transport and Tolerance. *Environ. Microbiol.* **2011**, *13*, 2844–2854, doi:10.1111/j.1462-2920.2011.02556.x.
47. Cecchi, G.; Marescotti, P.; Di Piazza, S.; Zotti, M. Native Fungi as Metal Remediators: Silver Myco-Accumulation from Metal Contaminated Waste-Rock Dumps (Libiola Mine, Italy). *J. Environ. Sci. Heal. - Part B Pestic. Food Contam. Agric. Wastes* **2017**, *52*, 191–195, doi:10.1080/03601234.2017.1261549.
48. Zareh, M.M.; El-Sayed, A.S.; El-Hady, D.M. Biosorption Removal of Iron from Water by Aspergillus Niger. *npj Clean Water* **2022**, *5*, 58, doi:10.1038/s41545-022-00201-1.
49. Ayele, A.; Haile, S.; Alemu, D.; Kamaraj, M. Comparative Utilization of Dead and Live Fungal Biomass for the Removal of Heavy Metal: A Concise Review. *Sci. World J.* **2021**, *2021*, 1–10, doi:10.1155/2021/5588111.
50. Hawkes, W. A Preliminary Investigation into the Etching Effect of Saponin and Acidified Thiourea in the Cleaning of Sterling Silver, Master thesis, West Dean College, 2016. https://www.researchgate.net/publication/340948905_A_preliminary_investigation_into_the_etching_effect_of_saponin_and_acidified_thiourea_in_the_cleaning_of_sterling_silver
51. Marchant, R.; Banat, I.M. Biosurfactants: A Sustainable Replacement for Chemical Surfactants? *Biotechnol. Lett.* **2012**, *34*, 1597–1605, doi:10.1007/s10529-012-0956-x.
52. Müller, M.M.; Kügler, J.H.; Henkel, M.; Gerlitzki, M.; Hörmann, B.; Pöhnlein, M.; Syldatk, C.; Hausmann, R. Rhamnolipids-Next Generation Surfactants? *J. Biotechnol.* **2012**, *162*, 366–380, doi:10.1016/j.jbiotec.2012.05.022.
53. Henkel, M.; Geissler, M.; Weggenmann, F.; Hausmann, R. Production of Microbial Biosurfactants: Status Quo of Rhamnolipid and Surfactin towards Large-Scale Production. *Biotechnol. J.* **2017**, *12*, 1–10, doi:10.1002/biot.201600561.
54. de Figueiredo Junior, J.C.D.; Asevedo, S.S.; de Souza e Silva, M.L.S.; Araújo, A.C.; Quites, M.R.E.

The Cleaning of Silver Objects With a Basic Solution of Sodium Glycinate: A Study on Artificially and Naturally Tarnished Silver. *Stud. Conserv.* **2021**, *66*, 375–383, doi:10.1080/00393630.2020.1859876.

55. Albelda-Berenguer, M.; Monachon, M.; Joseph, E. *Siderophores: From Natural Roles to Potential Applications*; 1st ed.; Elsevier Inc., 2019; Vol. 106; ISBN 9780128169759.
56. Max, B.; Salgado, J.M.; Rodríguez, N.; Cortés, S.; Converti, A.; Domínguez, J.M. Biotechnological Production of Citric Acid. *Brazilian J. Microbiol.* **2010**, *41*, 862–875, doi:10.1590/S1517-83822010000400005.
57. Louden, B.C.; Haarmann, D.; Lynne, A.M. Use of Blue Agar CAS Assay for Siderophore Detection. *J. Microbiol. Biol. Educ.* **2011**, *12*, 51–53, doi:10.1128/jmbe.v12i1.249.
58. Duckworth, O.W.; Markarian, D.S.; Parker, D.L.; Harrington, J.M. A Two-Column Flash Chromatography Approach to Pyoverdin Production from Pseudomonas Putida GB1. *J. Microbiol. Methods* **2017**, *135*, 11–13, doi:10.1016/j.mimet.2017.01.019.
59. Schwyn, B.; Neilands, J.B. Universal Chemical Assay for the Detection and Determination of Siderophores. *Anal. Biochem.* **1987**, *160*, 47–56, doi:10.1016/0003-2697(87)90612-9.
60. Krasnoff, S.B.; Howe, K.J.; Heck, M.L.; Donzelli, B.G.G. Siderophores from the Entomopathogenic Fungus Beauveria Bassiana. *J. Nat. Prod.* **2020**, *83*, 296–304, doi:10.1021/acs.jnatprod.9b00698.
61. Osman, Y.; Gebreil, A.; Mowafy, A.M.; Anan, T.I.; Hamed, S.M. Characterization of Aspergillus Niger Siderophore That Mediates Bioleaching of Rare Earth Elements from Phosphorites. *World J. Microbiol. Biotechnol.* **2019**, *35*, 93, doi:10.1007/s11274-019-2666-1.
62. Shin, S.H.; Lim, Y.; Lee, S.E.; Yang, N.W.; Rhee, J.H. CAS Agar Diffusion Assay for the Measurement of Siderophores in Biological Fluids. *J. Microbiol. Methods* **2001**, *44*, 89–95, doi:10.1016/S0167-7012(00)00229-3.
63. Milagres, A.M.F.; Machuca, A.; Napoleão, D. Detection of Siderophore Production from Several Fungi and Bacteria by a Modification of Chrome Azurol S (CAS) Agar Plate Assay. *J. Microbiol. Methods* **1999**, *37*, 1–6, doi:10.1016/S0167-7012(99)00028-7.
64. Rapti, S.; Boyatzis, S.C.; Rivers, S.; Pournou, A. Siderophores and Their Applications in Wood, Textile, and Paper Conservation. In *Microorganisms in the Deterioration and Preservation of Cultural Heritage*; Springer International Publishing: Cham, 2021; pp. 301–339 ISBN 9783030694111.
65. Rapti, S.; Boyatis, S.; Rivers, S.; Velios, A.; Pournou, A. Removing Iron Stains from Wood and Textile Objects: Assessing Gelled Siderophores as Novel Green Chelators. In Proceedings of the Gels in the Conservation of Artconservation; Angelova, L., Ormsby, Bronwyn Townsend, Joyce Wolbers, R., Eds.; Archetype Publications: London, 2017; pp. 343–348.
66. Monachon, M.; Albelda-berenguer, M.; Lombardo, T.; Cornet, E.; Moll-dau, F.; Schramm, J.; Schmidt-ott, K.; Joseph, E. Evaluation of Bio-based Extraction Methods by Spectroscopic Methods. *Minerals* **2020**, *10*, 1–17, doi:10.3390/min10020203.
67. Bosch-Roig, P.; Ranalli, G. The Safety of Biocleaning Technologies for Cultural Heritage. *Front. Microbiol.* **2014**, *5*, doi:10.3389/fmicb.2014.00155.
68. Comensoli, L.; Maillard, J.; Albini, M.; Sandoz, F.; Junier, P.; Joseph, E. Use of Bacteria To Stabilize Archaeological Iron. *Appl. Environ. Microbiol.* **2017**, *83*, 1–14, doi:10.1128/AEM.03478-16.
69. Visca, P.; Imperi, F.; Lamont, I.L. Pyoverdine Siderophores: From Biogenesis to Biosignificance. *Trends Microbiol.* **2007**, *15*, 22–30, doi:10.1016/j.tim.2006.11.004.
70. Rehm, K.; Vollenweider, V.; Kümmerli, R.; Bigler, L. A Comprehensive Method to Elucidate Pyoverdines Produced by Fluorescent Pseudomonas Spp. by UHPLC-HR-MS/MS. *Anal. Bioanal. Chem.* **2022**, *414*, 2671–2685, doi:10.1007/s00216-022-03907-w.
71. Ghssein, G.; Ezzeddine, Z. A Review of Pseudomonas Aeruginosa Metallophores: Pyoverdine, Pyochelin and Pseudopaline. *Biology (Basel).* **2022**, *11*, 1711, doi:10.3390/biology11121711.
72. H. Budzikiewicz; M. Schafer; J.-M. Meyer Siderotyping of Fluorescent Pseudomonads - Problems in the Determination of Molecular Masses by Mass Spectrometry. *Mini. Rev. Org. Chem.*

2007, *4*, 246–253, doi:10.2174/157019307781369968.
73. Chiadò, A.; Varani, L.; Bosco, F.; Marmo, L. Opening Study on the Development of a New Biosensor for Metal Toxicity Based on Pseudomonas Fluorescens Pyoverdine. *Biosensors* **2013**, *3*, 385–399, doi:10.3390/bios3040385.
74. Albesa, I.; Barberis, L.I.; Pajaro, M.C.; Eraso, A.J. Pyoverdine Production by Pseudomonas Fluorescens in Synthetic Media with Various Sources of Nitrogen. *Microbiology* **1985**, *131*, 3251–3254, doi:10.1099/00221287-131-12-3251.
75. Xiao, R.; Kisaalita, W.S. Purification of Pyoverdines of Pseudomonas Fluorescens 2-79 by Copper-Chelate Chromatography. *Appl. Environ. Microbiol.* **1995**, *61*, 3769–3774, doi:10.1128/aem.61.11.3769-3774.1995.
76. Fuchs, R.; Schafer, M.; Geoffroy, V.; Meyer, J.-M. Siderotyping A Powerful Tool for the Characterization of Pyoverdines. *Curr. Top. Med. Chem.* **2001**, *1*, 31–57, doi:10.2174/1568026013395542.
77. Wei, H.; Aristilde, L. Structural Characterization of Multiple Pyoverdines Secreted by Two Pseudomonas Strains Using Liquid Chromatography-High Resolution Tandem Mass Spectrometry with Varying Dissociation Energies. *Anal. Bioanal. Chem.* **2015**, *407*, 4629–4638, doi:10.1007/s00216-015-8659-5.
78. Meyer, J.M.; Gruffaz, C.; Raharinosy, V.; Bezverbnaya, I.; Schäfer, M.; Budzikiewicz, H. Siderotyping of Fluorescent Pseudomonas: Molecular Mass Determination by Mass Spectrometry as a Powerful Pyoverdine Siderotyping Method. *BioMetals* **2008**, *21*, 259–271, doi:10.1007/s10534-007-9115-6.
79. Albelda-Berenguer, M. Biological Strategies for the Preservation of Waterlogged Archaeological Wood, PhD thesis, University of Neuchâtel, 2020.
80. Joseph, E. Biopassivation Method for the Preservation of Copper and Bronze Artefacts. *Front. Mater.* **2021**, *7*, doi:10.3389/fmats.2020.613169.
81. Albini, M.; Comensoli, L.; Brambilla, L.; Domon Beuret, E.; Kooli, W.; Mathys, L.; Letardi, P.; Joseph, E. Innovative Biological Approaches for Metal Conservation. *Mater. Corros.* **2016**, *67*, 200–206, doi:10.1002/maco.201408168.
82. Joseph, E. Groundbreaking Approaches to Green and Sustainable Metals Conservation. In Proceeding of the ICOM-CC triennial conference (Beijing, China). **2021**.
83. Oddy, A.; Scott, D.A. *Copper and Bronze in Art: Corrosion, Colorants, Conservation*; 2002; Vol. 47; ISBN 0892366389.
84. Amaro, J.K.C.; Xavier, L.V.; Ribeiro, M.M.A. de C.; Vieira, B.S.; Mendes, G. de O. Optimization of Oxalic Acid Production by Fungi for Biotechnological Solubilization of Rock Phosphate. *Sci. Agric.* **2023**, *80*, doi:10.1590/1678-992x-2021-0076.
85. Tandy, S.; Ammann, A.; Schulin, R.; Nowack, B. Biodegradation and Speciation of Residual SS-Ethylenediaminedisuccinic Acid (EDDS) in Soil Solution Left after Soil Washing. *Environ. Pollut.* **2006**, *142*, 191–199, doi:10.1016/j.envpol.2005.10.013.
86. Vandevivere, P.C.; Saveyn, H.; Verstraete, W.; Feijtel, T.C.J.; Schowanek, D.R. Biodegradation of Metal−[S,S]-EDDS Complexes. *Environ. Sci. Technol.* **2001**, *35*, 1765–1770, doi:10.1021/es0001153.
87. Cornell, R.M.; Schwertmann, U. Solubility. In *The Iron Oxides*; Wiley, 2003; pp. 201–220.
88. Peters, R.W. Chelant Extraction of Heavy Metals from Contaminated Soils. *J. Hazard. Mater.* **1999**, *66*, 151–210, doi:10.1016/S0304-3894(99)00010-2.
89. Knepper, T. Synthetic Chelating Agents and Compounds Exhibiting Complexing Properties in the Aquatic Environment. *TrAC Trends Anal. Chem.* **2003**, *22*, 708–724, doi:10.1016/S0165-9936(03)01008-2.
90. Kim, J.-O.; Lee, Y.-W.; Chung, J. The Role of Organic Acids in the Mobilization of Heavy Metals from Soil. *KSCE J. Civ. Eng.* **2013**, *17*, 1596–1602, doi:10.1007/s12205-013-0323-z.
91. Goli, M.B.; Pande, M.; Bellaloui, N. Effects of Chelating Agents on Protein , Oil , Fatty Acids , and Minerals in Soybean Seed #. **2014**, doi:10.4236/as.2012.34061.

92. Zhang, Y.; Zhou, M. A Critical Review of the Application of Chelating Agents to Enable Fenton and Fenton-like Reactions at High PH Values. *J. Hazard. Mater.* **2018**, doi:10.1016/j.jhazmat.2018.09.035.
93. Orama, M.; Hyvönen, H.; Saarinen, H.; Aksela, R. Complexation of [S,S] and Mixed Stereoisomers of N,N′-Ethylenediaminedisuccinic Acid (EDDS) with Fe(III), Cu(II), Zn(II) and Mn(II) Ions in Aqueous Solution. *J. Chem. Soc. Dalt. Trans.* **2002**, 4644–4648, doi:10.1039/B207777A.
94. Palchoudhury, S.; Baalousha, M.; Lead, J.R. Methods for Measuring Concentration (Mass, Surface Area and Number) of Nanomaterials. In; 2015; pp. 153–181.
95. Tanaka, H.; Kawano, M.; Koga, N. Thermogravimetry of Basic Copper(II) Sulphates Obtained by Titrating NaOH Solution with CuSO4 Solution. *Thermochim. Acta* **1991**, *182*, 281–292, doi:10.1016/0040-6031(91)80012-8.
96. Vlek, P.L.G.; Blom, T.J.M.; Beek, J.; Lindsay, W.L. Determination of the Solubility Product of Various Iron Hydroxides and Jarosite by the Chelation Method. *Soil Sci. Soc. Am. J.* **1974**, *38*, 429–432, doi:10.2136/sssaj1974.03615995003800030018x.
97. Rizo, J.; Díaz, D.; Reyes-Trejo, B.; Arellano-Jiménez, M.J. Cu 2 O Nanoparticles for the Degradation of Methyl Parathion. *Beilstein J. Nanotechnol.* **2020**, *11*, 1546–1555, doi:10.3762/bjnano.11.137.
98. Myers, R.J. The New Low Value for the Second Dissociation Constant for H2s: Its History, Its Best Value, and Its Impact on the Teaching of Sulfide Equilibria. *J. Chem. Educ.* **1986**, *63*, 687–690, doi:10.1021/ed063p687.
99. Ion Exchange and Ion Exchangers: An Introduction. In *Ion Exchange in Environmental Processes*; John Wiley & Sons, Inc.: Hoboken, New Jersey, 2017; pp. 1–49.
100. Zittlau, A.H.; Shi, Q.; Boerio-Goates, J.; Woodfield, B.F.; Majzlan, J. Thermodynamics of the Basic Copper Sulfates Antlerite, Posnjakite, and Brochantite. *Geochemistry* **2013**, *73*, 39–50, doi:10.1016/j.chemer.2012.12.002.
101. Monnier, J.; Guillot, I.; Legrand, L.; Dillmann, P. Reactivity Studies of Atmospheric Corrosion of Heritage Iron Artefacts. *Corros. Conserv. Cult. Herit. Met. Artefacts* **2013**, 285–310, doi:10.1533/9781782421573.3.285.
102. Kraemer, S.M. Iron Oxide Dissolution and Solubility in the Presence of Siderophores. *Aquat. Sci. - Res. Across Boundaries* **2004**, *66*, 3–18, doi:10.1007/s00027-003-0690-5.
103. Ambikadevi, V..; Lalithambika, M. Effect of Organic Acids on Ferric Iron Removal from Iron-Stained Kaolinite. *Appl. Clay Sci.* **2000**, *16*, 133–145, doi:10.1016/S0169-1317(99)00038-1.
104. Zhang, Y.; Kallay, N.; Matijevic, E. Interaction of Metal Hydrous Oxides with Chelating Agents. 7. Hematite-Oxalic Acid and -Citric Acid Systems. *Langmuir* **1985**, *1*, 201–206, doi:10.1021/la00062a004.
105. Zaier, I.; Billiotte, J.; Charmoille, A.; Laouafa, F. The Dissolution Kinetics of Natural Gypsum: A Case Study of Eocene Facies in the North-Eastern Suburbs of Paris. *Environ. Earth Sci.* **2021**, *80*, 8, doi:10.1007/s12665-020-09275-x.
106. Dokoumetzidis, A.; Macheras, P. A Century of Dissolution Research: From Noyes and Whitney to the Biopharmaceutics Classification System. *Int. J. Pharm.* **2006**, *321*, 1–11, doi:10.1016/j.ijpharm.2006.07.011.
107. Thibault de Chanvalon, A.; Metzger, E.; Mouret, A.; Knoery, J.; Geslin, E.; Meysman, F.J.R. Two Dimensional Mapping of Iron Release in Marine Sediments at Submillimetre Scale. *Mar. Chem.* **2017**, *191*, 34–49, doi:10.1016/j.marchem.2016.04.003.
108. Isaacs, H.S. The Behavior of Resistive Layers in the Localized Corrosion of Stainless Steel. *J. Electrochem. Soc.* **1973**, *120*, 1456, doi:10.1149/1.2403283.
109. Gao, Y.; Glennon, B.; He, Y.; Donnellan, P. Dissolution Kinetics of a BCS Class II Active Pharmaceutical Ingredient: Diffusion-Based Model Validation and Prediction. *ACS Omega* **2021**, *6*, 8056–8067, doi:10.1021/acsomega.0c05558.

110. Dash, S.; Murthy, P.N.; Nath, L.; Chowdhury, P. Kinetic Modeling on Drug Release from Controlled Drug Delivery Systems. *Acta Pol. Pharm. - Drug Res.* **2010**, *67*, 217–223.
111. Murphy, W.M.; Oelkers, E.H.; Lichtner, P.C. Surface Reaction versus Diffusion Control of Mineral Dissolution and Growth Rates in Geochemical Processes. *Chem. Geol.* **1989**, *78*, 357–380, doi:10.1016/0009-2541(89)90069-7.
112. Reichard, P.U.; Kretzschmar, R.; Kraemer, S.M. Dissolution Mechanisms of Goethite in the Presence of Siderophores and Organic Acids. *Geochim. Cosmochim. Acta* **2007**, *71*, 5635–5650, doi:10.1016/j.gca.2006.12.022.
113. Schwertmann, U. Solubility and Dissolution of Iron Oxides. *Iron Nutr. Interact. Plants* **1991**, 3–27, doi:10.1007/978-94-011-3294-7_1.
114. Hassan, A.; Mahmoud, M.; Bageri, B.S.; Aljawad, M.S.; Kamal, M.S.; Barri, A.A.; Hussein, I.A. Applications of Chelating Agents in the Upstream Oil and Gas Industry: A Review. *Energy & Fuels* **2020**, *34*, 15593–15613, doi:10.1021/acs.energyfuels.0c03279.
115. Tamura, H.; Ito, N.; Kitano, M.; Takasaki, S. A Kinetic Model of the Dissolution of Copper(II) Oxide in EDTA Solutions Considering the Coupling of Metal and Oxide Ion Transfer. *Corros. Sci.* **2001**, *43*, 1675–1691, doi:10.1016/S0010-938X(00)00171-2.
116. Bellotti, D.; Remelli, M. Deferoxamine B: A Natural, Excellent and Versatile Metal Chelator. *Molecules* **2021**, *26*, 3255, doi:10.3390/molecules26113255.
117. Verma, A.; Kore, R.; Corbin, D.R.; Shiflett, M.B. Metal Recovery Using Oxalate Chemistry: A Technical Review. *Ind. Eng. Chem. Res.* **2019**, *58*, 15381–15393, doi:10.1021/acs.iecr.9b02598.
118. Silwamba, M.; Ito, M.; Tabelin, C.B.; Park, I.; Jeon, S.; Takada, M.; Kubo, Y.; Hokari, N.; Tsunekawa, M.; Hiroyoshi, N. Simultaneous Extraction and Recovery of Lead Using Citrate and Micro-Scale Zero-Valent Iron for Decontamination of Polluted Shooting Range Soils. *Environ. Adv.* **2021**, *5*, 100115, doi:10.1016/j.envadv.2021.100115.
119. Shi, Z.; Hu, S.; Li, R.; Lu, Y. Dissolution and Precipitation Processes. In *Reference Module in Earth Systems and Environmental Sciences*; Elsevier, 2022.
120. Kang, K.; Schenkeveld, W.D.C.; Biswakarma, J.; Borowski, S.C.; Hug, S.J.; Hering, J.G.; Kraemer, S.M. Low Fe(II) Concentrations Catalyze the Dissolution of Various Fe(III) (Hydr)Oxide Minerals in the Presence of Diverse Ligands and over a Broad PH Range. *Environ. Sci. Technol.* **2019**, *53*, 98–107, doi:10.1021/acs.est.8b03909.
121. Wells, M.L.; Mayer, L.M.; Donard, O.F.X.; de Souza Sierra, M.M.; Ackelson, S.G. The Photolysis of Colloidal Iron in the Oceans. *Nature* **1991**, *353*, 248–250, doi:10.1038/353248a0.
122. Borer, P.; Sulzberger, B.; Hug, S.J.; Kraemer, S.M.; Kretzschmar, R. Wavelength-Dependence of Photoreductive Dissolution of Lepidocrocite (γ-FeOOH) in the Absence and Presence of the Siderophore DFOB. *Environ. Sci. Technol.* **2009**, *43*, 1871–1876, doi:10.1021/es801353t.
123. Siffert, C.; Sulzberger, B. Light-Induced Dissolution of Hematite in the Presence of Oxalate: A Case Study. *Langmuir* **1991**, *7*, 1627–1634, doi:10.1021/la00056a014.
124. Borer, P.; Hug, S.J.; Sulzberger, B.; Kraemer, S.M.; Kretzschmar, R. Photolysis of Citrate on the Surface of Lepidocrocite: An in Situ Attenuated Total Reflection Infrared Spectroscopy Study. *J. Phys. Chem. C* **2007**, *111*, 10560–10569, doi:10.1021/jp0685941.
125. Borer, P.; Sulzberger, B.; Hug, S.J.; Kraemer, S.M.; Kretzschmar, R. Photoreductive Dissolution of Iron(III) (Hydr)Oxides in the Absence and Presence of Organic Ligands: Experimental Studies and Kinetic Modeling. *Environ. Sci. Technol.* **2009**, *43*, 1864–1870, doi:10.1021/es801352k.
126. Walte, T.D.; Morel, F.M.M. Photoreductive Dissolution of Colloidal Iron Oxides in Natural Waters. *Environ. Sci. Technol.* **1984**, *18*, 860–868, doi:10.1021/es00129a010.
127. Boukhalfa, H.; Reilly, S.D.; Michalczyk, R.; Iyer, S.; Neu, M.P. Iron(III) Coordination Properties of a Pyoverdin Siderophore Produced by Pseudomonas Putida ATCC 33015. *Inorg. Chem.* **2006**, *45*, 5607–5616, doi:10.1021/ic060196p.
128. Rueda, E.H.; Grassi, R.L.; Blesa, M.A. Adsorption and Dissolution in the System Goethite/Aqueous EDTA. *J. Colloid Interface Sci.* **1985**, *106*, 243–246, doi:10.1016/0021-

9797(85)90401-1.
129. Fioravante, I.; Nunes, R.; Acciari, H.; Codaro, E. Films Formed on Carbon Steel in Sweet Environments - A Review. *J. Braz. Chem. Soc.* **2019**, doi:10.21577/0103-5053.20190055.
130. Orama, M.; Hyvönen, H.; Saarinen, H.; Aksela, R. Complexation of [S,S] and Mixed Stereoisomers of N,N′-Ethylenediaminedisuccinic Acid (EDDS) with Fe(III), Cu(II), Zn(II) and Mn(II) Ions in Aqueous Solution. *J. Chem. Soc., Dalt. Trans.* **2002**, 4644–4648, doi:10.1039/B207777A.
131. Xiao, Z.; Wedd, A.G. The Challenges of Determining Metal–Protein Affinities. *Nat. Prod. Rep.* **2010**, *27*, 768, doi:10.1039/b906690j.
132. Toporivska, Y.; Gumienna-kontecka, E. The Solution Thermodynamic Stability of Desferrioxamine B (DFO) with Zr. *J. Inorg. Biochem.* **2020**, *198*, 110753, doi:10.1016/j.jinorgbio.2019.110753.
133. Alberti, G.; Zanoni, C.; Magnaghi, L.R.; Biesuz, R. Deferoxamine-Based Materials and Sensors for Fe(III) Detection. *Chemosensors* **2022**, *10*, 468, doi:10.3390/chemosensors10110468.
134. Dhungana, S.; White, S.; Crumbliss, A.L. Crystal Structure of Ferrioxamine B : A Comparative Analysis and Implications for Molecular Recognition. **2001**, 810–818, doi:10.1007/s007750100259.
135. Sebulsky, M.T.; Shilton, B.H.; Speziali, C.D.; Heinrichs, D.E. The Role of FhuD2 in Iron (III) - Hydroxamate Transport in Staphylococcus Aureus. *J. Biol. Chem.* **2003**, *278*, 49890–49900, doi:10.1074/jbc.M305073200.
136. Macchia, A.; Ruffolo, S.A.; Rivaroli, L.; La Russa, M.F. The Treatment of Iron-Stained Marble: Toward a "Green" Solution. *Int. J. Conserv. Sci.* **2016**, *7*, 323–332.
137. White, G.F.; Edwards, M.J.; Gomez-Perez, L.; Richardson, D.J.; Butt, J.N.; Clarke, T.A. Mechanisms of Bacterial Extracellular Electron Exchange. In; 2016; pp. 87–138.
138. Borggaard, O.K. Kinetics and Mechanisms of Soil Iron Oxide Dissolution in EDTA, Oxalate and Dithionate. In Proceedings of the Proceedings of the 9th international Clay conference; Strasbourg, 1990; Vol. 85, pp. 139–148.
139. Hans, M.; Erbe, A.; Mathews, S.; Chen, Y.; Solioz, M.; Mücklich, F. Role of Copper Oxides in Contact Killing of Bacteria. *Langmuir* **2013**, *29*, 16160–16166, doi:10.1021/la404091z.
140. Cardoso, D.; Narcy, A.; Durosoy, S.; Chevalier, Y. The PH Dependence of Dissolution Kinetics of Zinc Oxide. *Colloids Surfaces A Physicochem. Eng. Asp.* **2022**, *650*, 129653, doi:10.1016/j.colsurfa.2022.129653.
141. Cardoso, D.; Narcy, A.; Durosoy, S.; Bordes, C.; Chevalier, Y. Dissolution Kinetics of Zinc Oxide and Its Relationship with Physicochemical Characteristics. *Powder Technol.* **2021**, *378*, 746–759, doi:10.1016/j.powtec.2020.10.049.
142. Sompech, S.; Srion, A.; Nuntiya, A. The Effect of Ultrasonic Treatment on the Particle Size and Specific Surface Area of LaCoO3. *Procedia Eng.* **2012**, *32*, 1012–1018, doi:10.1016/j.proeng.2012.02.047.
143. Vergouw, J.M.; Difeo, A.; Xu, Z.; Finch, J.A. An Agglomeration Study of Sulphide Minerals Using Zeta Potential and Settling Rate. Part II: Sphalerite/Pyrite and Sphalerite/Galena. *Miner. Eng.* **1998**, *11*, 605–614, doi:10.1016/S0892-6875(98)00045-4.
144. Wang, Z.; Schenkeveld, W.D.C.; Kraemer, S.M.; Giammar, D.E. Synergistic Effect of Reductive and Ligand-Promoted Dissolution of Goethite. *Environ. Sci. Technol.* **2015**, *49*, 7236–7244, doi:10.1021/acs.est.5b01191.
145. Lin, Q.; Wang, Y.; Yang, X.; Ruan, D.; Wang, S.; Wei, X.; Qiu, R. Effect of Low-Molecular-Weight Organic Acids on Hematite Dissolution Promoted by Desferrioxamine B. *Environ. Sci. Pollut. Res.* **2018**, *25*, 163–173, doi:10.1007/s11356-017-9045-y.
146. Biswakarma, J.; Kang, K.; Schenkeveld, W.D.C.; Kraemer, S.M.; Hering, J.G.; Hug, S.J. Linking Isotope Exchange with Fe(II)-Catalyzed Dissolution of Iron(Hydr)Oxides in the Presence of the Bacterial Siderophore Desferrioxamine-B. *Environ. Sci. Technol.* **2020**, *54*, 768–777, doi:10.1021/acs.est.9b04235.

147. Harrison, M.R.; Francesconi, M.G. Mixed-Metal One-Dimensional Sulfides—A Class of Materials with Differences and Similarities to Oxides. *Coord. Chem. Rev.* **2011**, *255*, 451–458, doi:10.1016/j.ccr.2010.10.008.
148. Fisher, W.W.; Roman, R.J. *The Dissolution of Chalcocite in Oxygenated Sulfuric Acid Solution*; Socorro, New Mexico, 1971; https://geoinfo.nmt.edu/publications/monographs/circulars/downloads/112/Circular-112.pdf
149. Toro, N.; Moraga, C.; Torres, D.; Saldaña, M.; Pérez, K.; Gálvez, E. Leaching Chalcocite in Chloride Media—A Review. *Minerals* **2021**, *11*, 1197, doi:10.3390/min11111197.
150. Fiaud, C.; Safavi, M.; Vedel, J. Identification of the Corrosion Products Formed on Copper in Sulfur Containing Environments. *Mater. Corros. und Korrosion* **1984**, *35*, 361–366, doi:10.1002/maco.19840350802.
151. Shabani, M.A.; Irannajad, M.; Azadmehr, A.R. Investigation on Leaching of Malachite by Citric Acid. *Int. J. Miner. Metall. Mater.* **2012**, *19*, 782–786, doi:10.1007/s12613-012-0628-9.
152. Huda, K. A Note on the Efficacy of Ethylenediaminetetra-Acetic Acid Disodium Salt as a Stripping Agent for Corrosion Products of Copper. *Stud. Conserv.* **2002**, *47*, 211–216, doi:10.1179/sic.2002.47.3.211.
153. Kołodyńska, D. Application of a New Generation of Complexing Agents in Removal of Heavy Metal Ions from Different Wastes. *Environ. Sci. Pollut. Res.* **2013**, *20*, 5939–5949, doi:10.1007/s11356-013-1576-2.
154. Ko, C.K.; Lee, W.G. Effects of PH Variation in Aqueous Solutions on Dissolution of Copper Oxide. *Surf. Interface Anal.* **2010**, *42*, 1128–1130, doi:10.1002/sia.3238.
155. Di Palma, L.; Mecozzi, R. Heavy Metals Mobilization from Harbour Sediments Using EDTA and Citric Acid as Chelating Agents. *J. Hazard. Mater.* **2007**, *147*, 768–775, doi:10.1016/j.jhazmat.2007.01.072.
156. Barona, A.; Aranguiz, I.; Elías, A. Metal Associations in Soils before and after EDTA Extractive Decontamination: Implications for the Effectiveness of Further Clean-up Procedures. *Environ. Pollut.* **2001**, *113*, 79–85, doi:10.1016/S0269-7491(00)00158-5.
157. Tandy, S.; Bossart, K.; Mueller, R.; Ritschel, J.; Hauser, L.; Schulin, R.; Nowack, B. Extraction of Heavy Metals from Soils Using Biodegradable Chelating Agents. *Environ. Sci. Technol.* **2004**, *38*, 937–944, doi:10.1021/es0348750.
158. Hauser, L.; Tandy, S.; Schulin, R.; Nowack, B. Column Extraction of Heavy Metals from Soils Using the Biodegradable Chelating Agent EDDS. *Environ. Sci. Technol.* **2005**, *39*, 6819–6824, doi:10.1021/es050143r.
159. Song, Y.; Ammami, M.-T.; Benamar, A.; Mezazigh, S.; Wang, H. Effect of EDTA, EDDS, NTA and Citric Acid on Electrokinetic Remediation of As, Cd, Cr, Cu, Ni, Pb and Zn Contaminated Dredged Marine Sediment. *Environ. Sci. Pollut. Res.* **2016**, *23*, 10577–10586, doi:10.1007/s11356-015-5966-5.
160. Evangelou, M.W.H.; Ebel, M.; Schaeffer, A. Chelate Assisted Phytoextraction of Heavy Metals from Soil. Effect, Mechanism, Toxicity, and Fate of Chelating Agents. *Chemosphere* **2007**, *68*, 989–1003, doi:10.1016/j.chemosphere.2007.01.062.
161. Zabiszak, M.; Nowak, M.; Taras-Goslinska, K.; Kaczmarek, M.T.; Hnatejko, Z.; Jastrzab, R. Carboxyl Groups of Citric Acid in the Process of Complex Formation with Bivalent and Trivalent Metal Ions in Biological Systems. *J. Inorg. Biochem.* **2018**, *182*, 37–47, doi:10.1016/j.jinorgbio.2018.01.017.
162. Sansonetti, A.; Bertasa, M.; Corti, C.; Rampazzi, L.; Monticelli, D.; Scalarone, D.; Sassella, A.; Canevali, C. Optimization of Copper Stain Removal from Marble through the Formation of Cu(II) Complexes in Agar Gels. *Gels* **2021**, *7*, 111, doi:10.3390/gels7030111.
163. Cui, W.; Zhang, Y.; Chen, J.; Zhao, C.; Li, Y.; Chen, Y.; Lee, M.-H. Comparative Study on Surface Structure, Electronic Properties of Sulfide and Oxide Minerals: A First-Principles Perspective. *Minerals* **2019**, *9*, 329, doi:10.3390/min9060329.

164. Al-Jahani, G.M.A.M. Thymus Vulgaris (Thyme) as a Natural Organic Matter to Biosynthesis Silver Nanoparticles and Their Antibacterial Efficiency. *Int. J. Pharm. Res. Allied Sci.* **2021**, *10*, 118–121, doi:10.51847/oBv07gPJ5C.
165. Shankar, S.; Rhim, J.W. Amino Acid Mediated Synthesis of Silver Nanoparticles and Preparation of Antimicrobial Agar/Silver Nanoparticles Composite Films. *Carbohydr. Polym.* **2015**, *130*, 353–363, doi:10.1016/j.carbpol.2015.05.018.
166. Sivasubramanian, K.; Sabarinathan, S.; Muruganandham, M.; Velmurugan, P.; Arumugam, N.; Almansour, A.I.; Kumar, R.S.; Sivakumar, S. Antioxidant, Antibacterial, and Cytotoxicity Potential of Synthesized Silver Nanoparticles from the Cassia Alata Leaf Aqueous Extract. *Green Process. Synth.* **2023**, *12*, doi:10.1515/gps-2023-0018.
167. Fu, L.-M.; Hsu, J.-H.; Shih, M.-K.; Hsieh, C.-W.; Ju, W.-J.; Chen, Y.-W.; Lee, B.-H.; Hou, C.-Y. Process Optimization of Silver Nanoparticle Synthesis and Its Application in Mercury Detection. *Micromachines* **2021**, *12*, 1123, doi:10.3390/mi12091123.
168. Saion, E.; Gharibshahi, E.; Naghavi, K. Size-Controlled and Optical Properties of Monodispersed Silver Nanoparticles Synthesized by the Radiolytic Reduction Method. *Int. J. Mol. Sci.* **2013**, *14*, 7880–7896, doi:10.3390/ijms14047880.
169. Mohammed Fayaz, A.; Balaji, K.; Kalaichelvan, P.T.; Venkatesan, R. Fungal Based Synthesis of Silver Nanoparticles—An Effect of Temperature on the Size of Particles. *Colloids Surfaces B Biointerfaces* **2009**, *74*, 123–126, doi:10.1016/j.colsurfb.2009.07.002.
170. Alim-Al-Razy, M.; Asik Bayazid, G.M.; Rahman, R.U.; Bosu, R.; Shamma, S.S. Silver Nanoparticle Synthesis, UV-Vis Spectroscopy to Find Particle Size and Measure Resistance of Colloidal Solution. *J. Phys. Conf. Ser.* **2020**, *1706*, 012020, doi:10.1088/1742-6596/1706/1/012020.
171. De Leersnyder, I.; Rijckaert, H.; De Gelder, L.; Van Driessche, I.; Vermeir, P. High Variability in Silver Particle Characteristics, Silver Concentrations, and Production Batches of Commercially Available Products Indicates the Need for a More Rigorous Approach. *Nanomaterials* **2020**, *10*, 1394, doi:10.3390/nano10071394.
172. Njoki, P.N. Transformation of Silver Nanoparticles in Phosphate Anions: An Experiment for High School Students. *J. Chem. Educ.* **2019**, *96*, 546–552, doi:10.1021/acs.jchemed.8b00602.
173. Harra, J.; Mäkitalo, J.; Siikanen, R.; Virkki, M.; Genty, G.; Kobayashi, T.; Kauranen, M.; Mäkelä, J.M. Size-Controlled Aerosol Synthesis of Silver Nanoparticles for Plasmonic Materials. *J. Nanoparticle Res.* **2012**, *14*, 870, doi:10.1007/s11051-012-0870-0.
174. Ergashovich, Y.K.; Abdukhalilovich, arymsakov A.; Sharaphovna, R.S. Bactericidal Hydrogel Based on Sodium-Carboxymethylcellulose Contained Silver Nanoparticles: Obtaining and Properties. *Open J. Polym. Chem.* **2018**, *08*, 57–69, doi:10.4236/ojpchem.2018.84006.
175. Martina, I.; Wiesinger, R.; Schreiner, M. Micro-Raman Characterisation of Silver Corrosion Products : Instrumental Set Up and Reference. *e-Preservation Sci.* **2012**, *9*, 1–8.
176. Mabrouk, M.M.; Mansour, A.T.; Abdelhamid, A.F.; Abualnaja, K.M.; Mamoon, A.; Gado, W.S.; Matter, A.F.; Ayoub, H.F. Impact of Aqueous Exposure to Silver Nanoparticles on Growth Performance, Redox Status, Non-Specific Immunity, and Histopathological Changes of Nile Tilapia, Oreochromis Niloticus, Challenged with Aeromonas Hydrophila. *Aquac. Reports* **2021**, *21*, 100816, doi:10.1016/j.aqrep.2021.100816.
177. Joshi, N.; Jain, N.; Pathak, A.; Singh, J.; Prasad, R.; Upadhyaya, C.P. Biosynthesis of Silver Nanoparticles Using Carissa Carandas Berries and Its Potential Antibacterial Activities. *J. Sol-Gel Sci. Technol.* **2018**, *86*, 682–689, doi:10.1007/s10971-018-4666-2.
178. Zannotti, M.; Rossi, A.; Giovannetti, R. SERS Activity of Silver Nanosphere, Triangular Nanoplates, Hexagonal Nanoplates and Quasi-Spherical Nanoparticles: Effect of Shape and Morphology. *Coatings* **2020**, *10*, 288, doi:10.3390/coatings10030288.
179. Stamplecoskie, K.G.; Scaiano, J.C.; Tiwari, V.S.; Anis, H. Optimal Size of Silver Nanoparticles for Surface-Enhanced Raman Spectroscopy. *J. Phys. Chem. C* **2011**, *115*, 1403–1409, doi:10.1021/jp106666t.

180. Naja, G.; Bouvrette, P.; Hrapovic, S.; Luong, J.H.T. Raman-Based Detection of Bacteria Using Silver Nanoparticles Conjugated with Antibodies. *Analyst* **2007**, *132*, 679, doi:10.1039/b701160a.

2.6 Supplementary materials

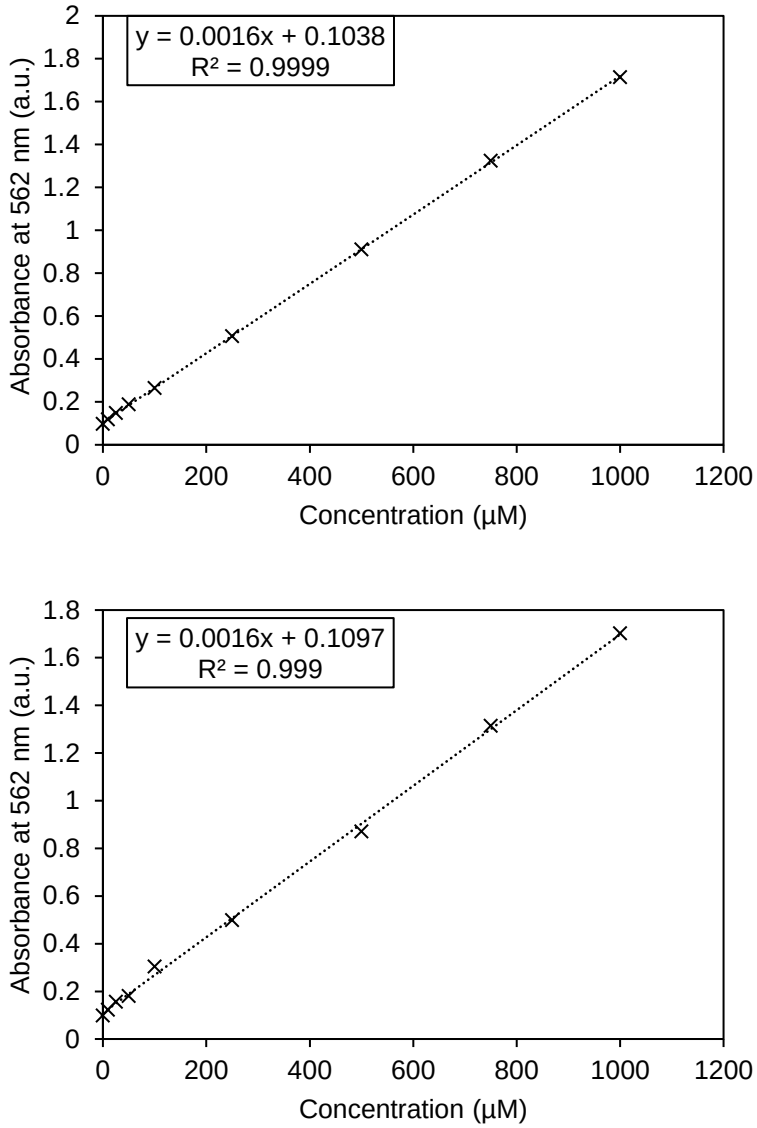

Figure S2.1 Calibration curve for calculating (a) Fe^{2+} concentrations via Ferrozine assay prepared with known concentrations of Fe^{2+}. (b) total iron concentrations via Ferrozine assay prepared with known concentrations of Fe^{3+} supplemented with hydroxylamine-HCl.

Table S2.1 ICP-OES instrumentation details Quantification is based on comparison with calibration curves using standards.

Gas flow	Plasma (Argon)	15 L/min
	Auxiliary (compressed air)	0.2 L/min
	Nebulizer (nitrogen)	0.6 mL/min
Plasma	Plasma view	axial
	Power	1300 W
Peristaltic pump	Sample flow rate	1.3 mL/min
Limits of Detection	Fe	0.1 µg/L
	Cu	0.4 µg/L
	Ag	0.6 µg/L

Table S2.2 Composition of SM medium used for pyoverdine production from *Pseudomonas yamanorum* DSM 2005

KH_2PO_4	3 g
K_2HPO_4	6 g
$(NH_4)_2SO_4$	1 g
$MgSO_4 \cdot 7H_2O$	0.2 g
Succinic acid	4 g
Milli-Q	1 L
NaOH solution	To adjust to 6.8/7

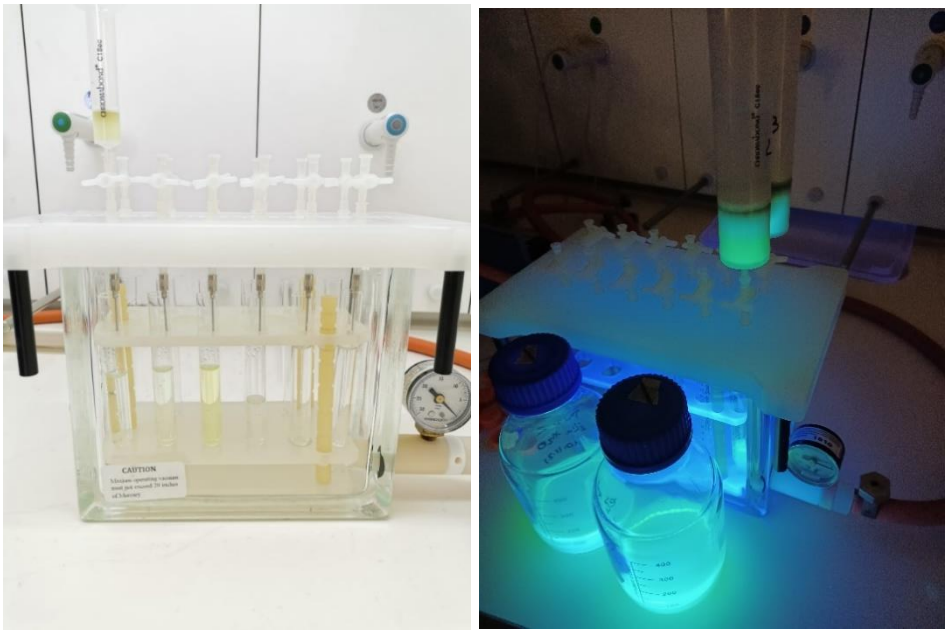

Figure S2.2 Pyoverdine SPE under day light (left) and under UV light (right).

Table S2. 3 Quantity of MeOH or H_2O SPE-eluted, salt-free pyoverdine using LC-UV.

	MeOH	Milli-Q water
Concentration (mg/L)	298 ± 63	608 ± 189

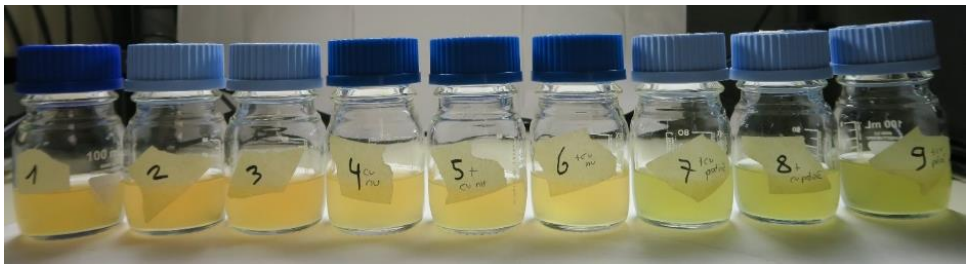

Figure S2.37 Liquid cultures of *B. bassiana*, in plain malt solution (1, 2, 3), in cuprite amended medium (4, 5, 6) or in atacamite-brochantite-amended medium (7, 8, 9).

Table S2.4 Detected oxalate (mg/mL) in *Beauveria bassiana* cultures after 5 days.

Plain culture	Culture with corroded plate	Culture with patinated plate
0.30 ± 0.03	0.245 ± 0.007	0.87 ± 0.02

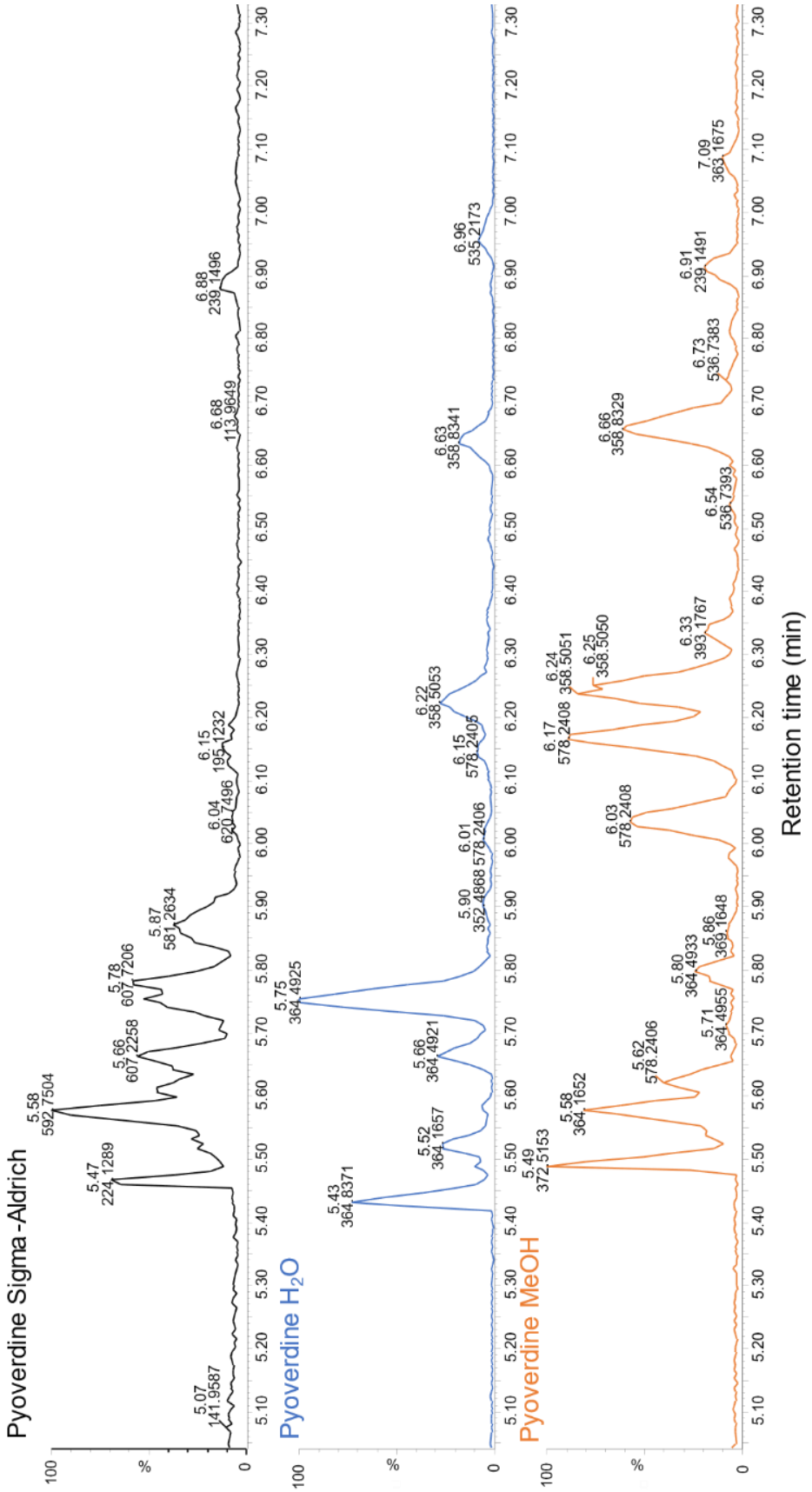

Figure S2.4 TOF-MS chromatograms of pyoverdine standard (black), and pyoverdine enriched fractions from *Pseudomonas yamanorum* DSM 2005 supernatant obtained by RP-C18 solid phase extraction upon elution with H_2O (blue), or methanol (orange).

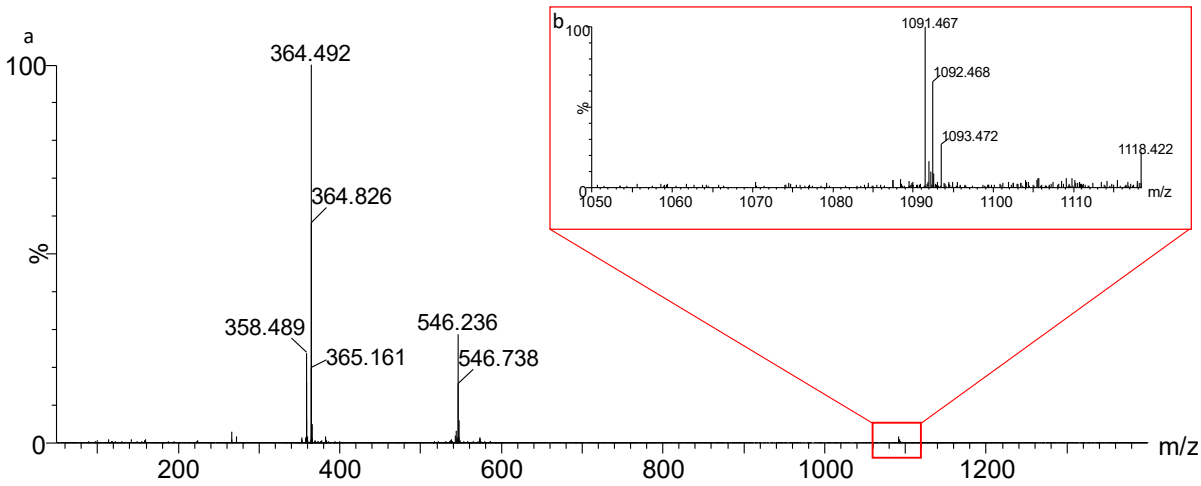

Figure S2.5 TOF-MS spectrum of pyoverdine eluted with H_2O at a retention time of 5.75 min.

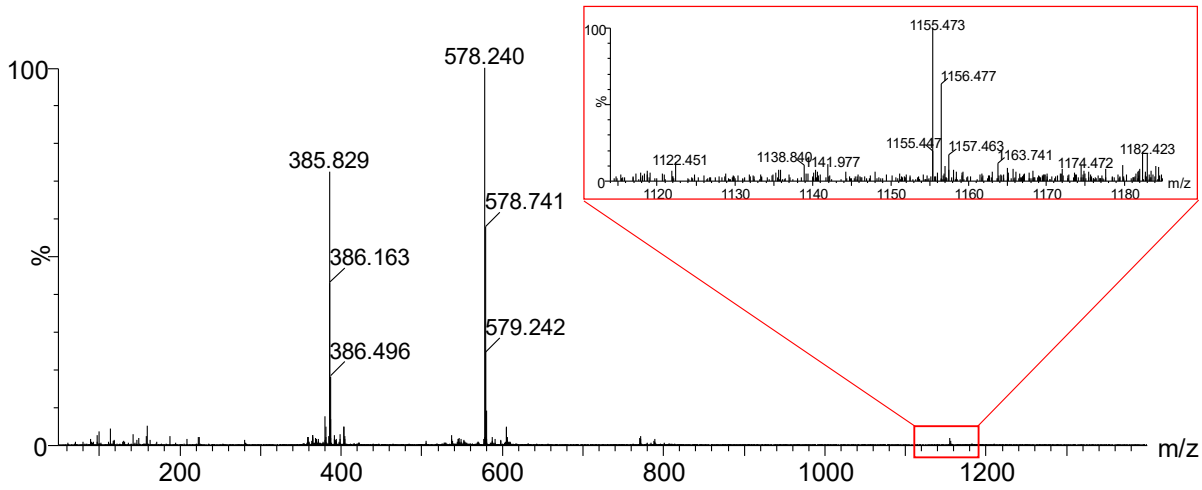

Figure S2.6 TOF-MS spectrum of pyoverdine eluted with MeOH at a retention time of 6.03 min.

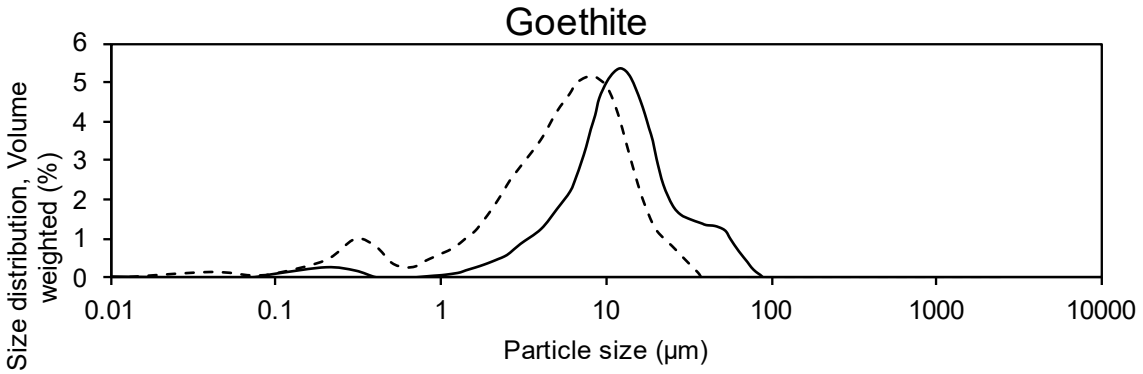
Goethite
Size distribution, Volume weighted (%)
0
1
2
3
4
5
6
0.01
0.1
1
10
100
1000
10000
Particle size (µm)

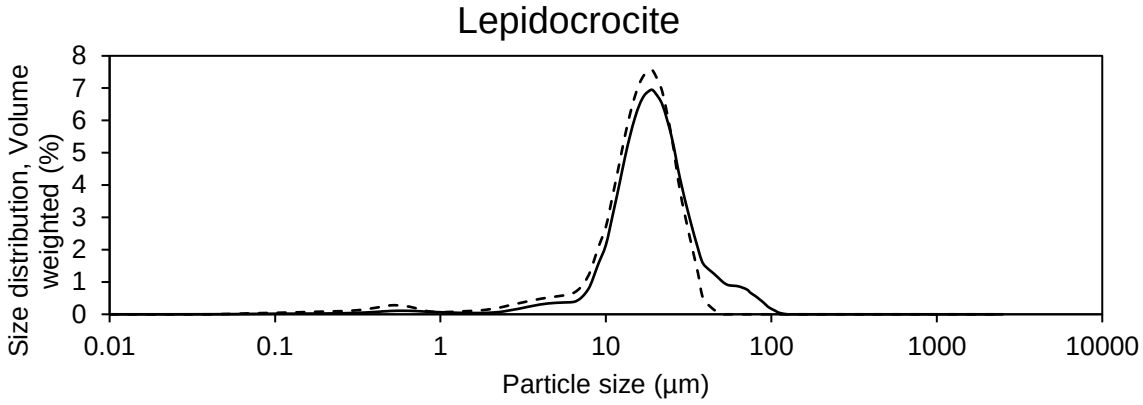
Lepidocrocite
Size distribution, Volume weighted (%)
0
1
2
3
4
5
6
7
8
0.01
0.1
1
10
100
1000
10000
Particle size (µm)

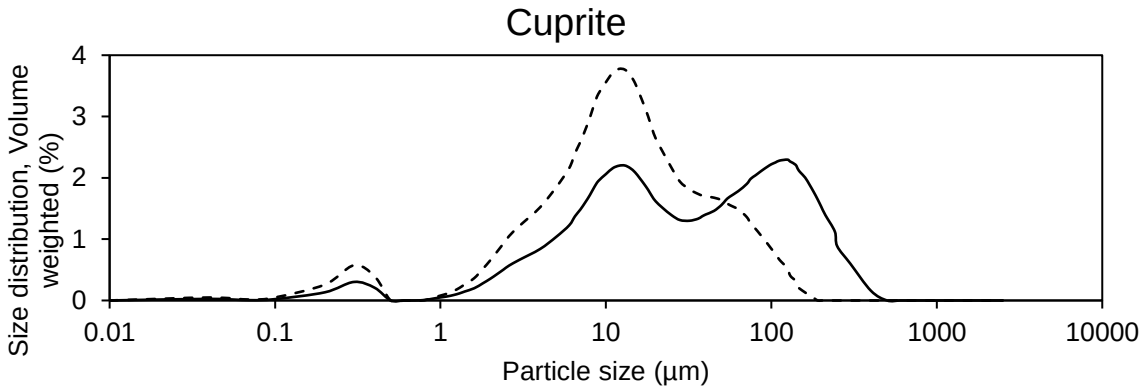
Cuprite
Size distribution, Volume weighted (%)
0
1
2
3
4
0.01
0.1
1
10
100
1000
10000
Particle size (µm)

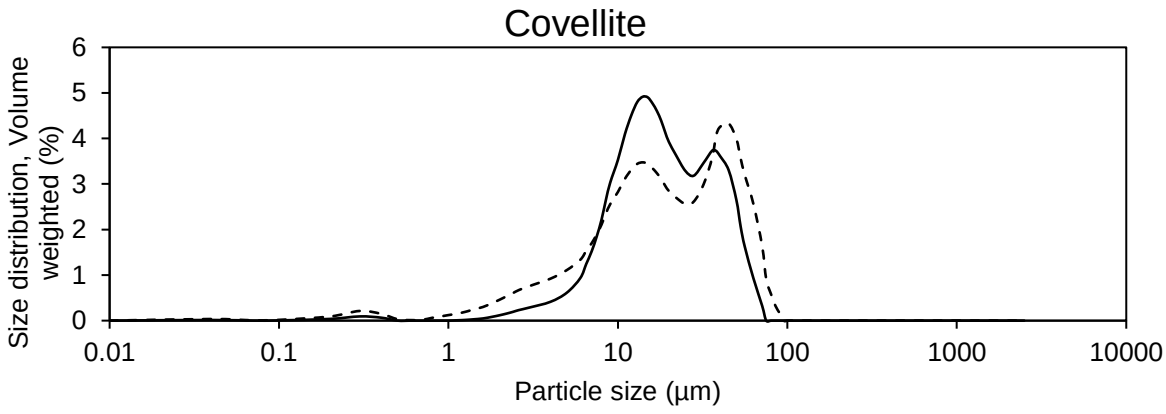
Covellite
Size distribution, Volume weighted (%)
0
1
2
3
4
5
6
0.01
0.1
1
10
100
1000
10000
Particle size (µm)

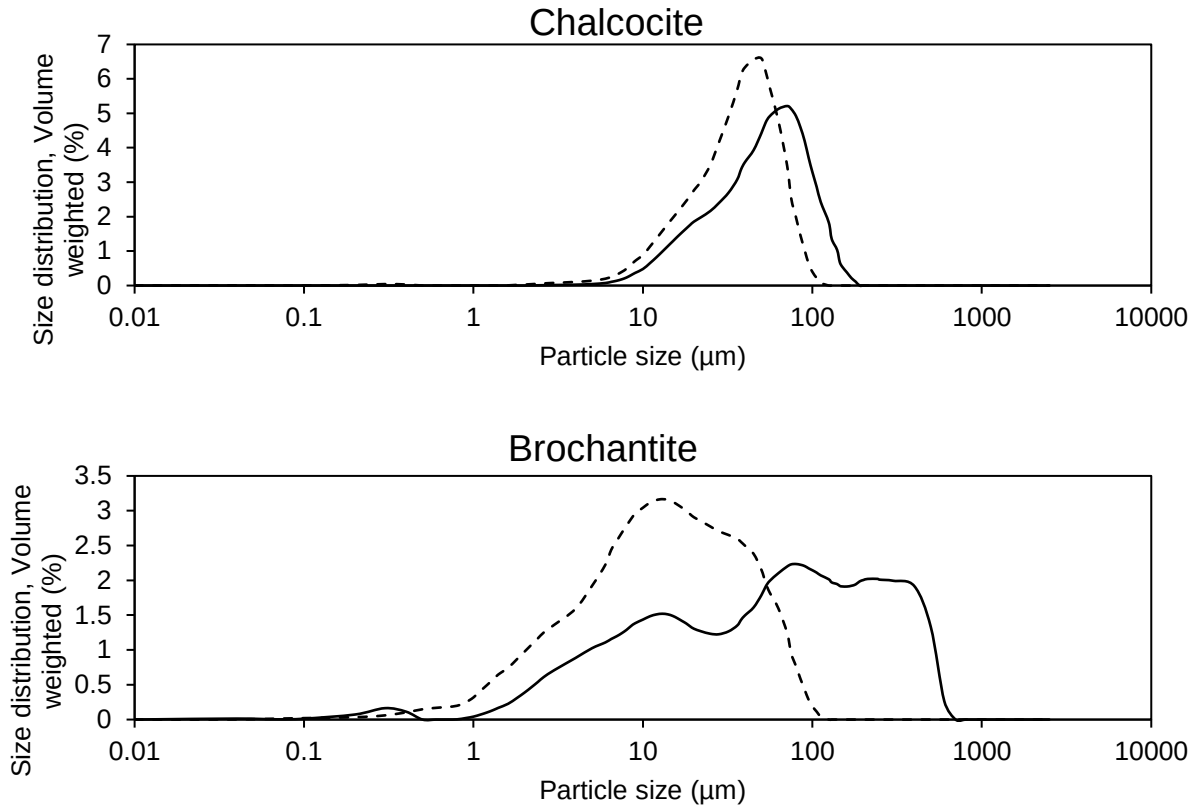

Figure S2.7 Particle size distribution of powdered corrosion products studied, before (full line) and after (dotted line) sonication.

Interaction of covellite with different complexing agents

For covellite, the presence of ligands does not statistically significantly enhance the solubilization, apart from EDDS (Figure S2.8). The amount of copper ions detected in solution after 24 hours is extremely high for water alone (155 µmol/L) in figure S2.8 or even close to 5 mM in water at pH 7 (Figure S2.9), the value are close to 10^{16} times higher than the theoretical solubility of CuS, which is the square root of the $K_{sp,}$ hence close to $8 \cdot 10^{-19}$ mol/L. In addition, the absence of increase of the concentration in solution overtime could suggests a lack of significance and that some corrosion powder was mistakenly pipetted and analyzed, even after the two centrifugations, due to the powder static forces. For such, to overcome these systematic errors, it would be interesting to reiterate the study, prewashing the minerals to remove any mobile copper and filter the solutions. Nevertheless, covellite is reported to be a very stable copper sulfide [148].

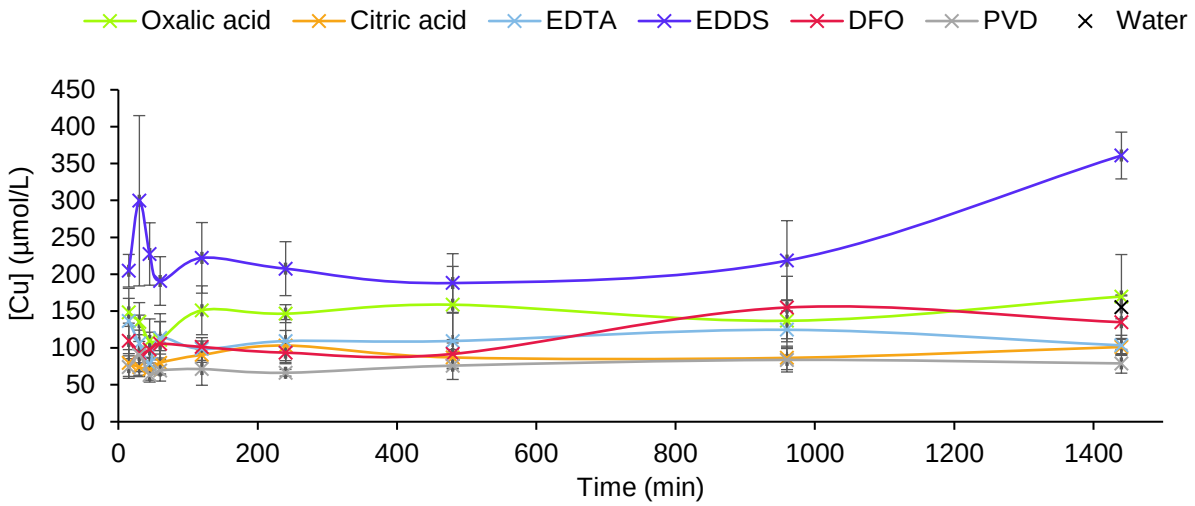

Figure S2.8 Copper ions detected by ICP-OES after covellite dissolution in presence of several $5 \cdot 10^{-4}$ M ligand solutions (oxalic acid (green), citric acid (orange), EDTA (blue), EDDS (purple), DFO (red), PVD (grey) and water (black)), plotted versus time.

When studying the influence of pH, similarly to the solubilization versus time, no significant result stands out for covellite (Figure S2.7). It has been stated before that covellite is insensitive to acidic environment [181]. Indeed, looking at the E-pH diagram (figure 2.32), its range of existence is in the acidic to neutral range.

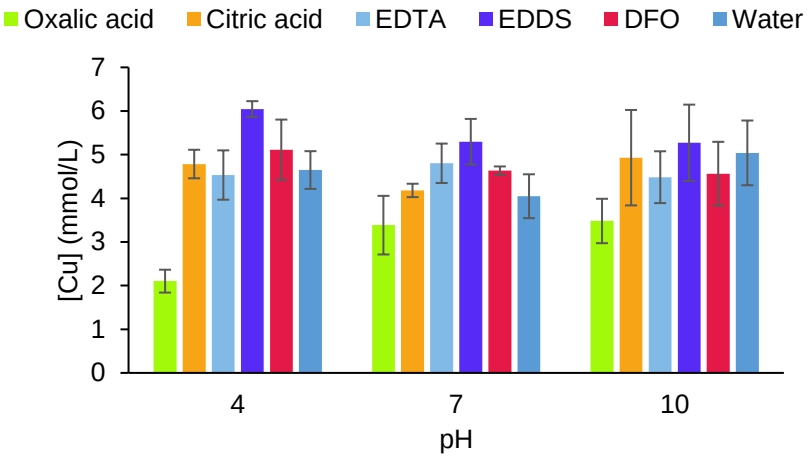

Figure S2.9 Dissolved copper from covellite detected via ICP-OES in 10^{-2} M ligand solutions at pH 4, 7 or 10.

3. Hydrogel formulations as reliable cleaning systems

This chapter is based on the following articles:

Cuvillier, L .; Passaretti, A.; Guilminot, E.; Joseph, E., Agar and chitosan hydrogels' design for metal uptaking treatments. Gels. 10(1). 2024, doi: 10.3390/gels10010055

Following the previous chapter in which active agents were investigated, a deeper look is taken into delivery systems. There exist several possibilities (e.g., micelles, emulsions) but gels are the most resorted to due to their ease of implementation. In the widest sense, a hydrogel is a water-based formulation thickened with a polymer forming a three-dimensional network in the liquid medium. Their interesting properties allow a precise and selective cleaning process, including on vertical or other complex surfaces [1]. Gels materials can be selected or modified according to the desired working properties.

These devices need to be studied to ascertain their innocuous use and evaluate further applications for the safeguarding of heritage. In particular, assessment of gel preparation protocols, compatibility between polymers and active agents (i.e., chelators) or introduction into new branches of metal conservation (e.g., archaeological findings) are relevant.

Compatibility between the chosen active agents and the used hydrogel is a key question to be raised before studying the application of any three-pronged formulations (water - active agents - polymer). Indeed, sometimes, it is not possible to combine them. For instance, the presence of microorganisms would prevent the use of gels requiring a heating step as it would kill most of microorganisms, but it can also be due to the lack of suitable pH ranges. Apart from xanthan gum, few gelling agents allow the thickening of acidic solutions. It is indeed crucial to ensure that incorporation of the polymer to form the hydrogel will not damage the added agents, in particular the high temperature needed to prepare agar or gellan could damage the chelating properties of the complexing agents [2]. Similarly, it is better if the added active agents do not modify the physico-chemical properties of the selected gel. These compatibility factors should be taken into account by the operator and pondered, depending on possible compromises and the desired outcome.

In this chapter, several concerns about the use of gels are tackled.

First, the design of hydrogels is scrutinized, comparing the properties of agar, a well-established gel in the conservation field, and another hydrogel formulation based on chitosan, an emerging polymer for cultural heritage conservation purposes [3–5]. Chitosan is a natural, non-toxic polymer, and shows interesting prospects for corrosion removal applications as it is reported to take up some metals [6–8]. For such, it is a promising gelling agent to study. Comparing their mechanical and structural properties, a multi-analytical approach is utilized, including Attenuated Total Reflectance-Fourier Transformed Infrared (ATR-FTIR), rheological measurements, swelling evaluation and cryo-Scanning Electron Microscopy (cryo-SEM).

Using similar techniques, the influence of the addition of a selected chelating agent from the previous chapter, a microbial siderophore called deferoxamine, on agar and chitosan's properties is examined. Finally, the formulations are tested for their silver ions chelating ability on silver ions using FT-Raman

spectroscopy. Agar and/or chitosan's copper and iron ions inherent uptake has already been demonstrated [9–11].

In addition to adequate compatibility, a reliable delivery system should be easy to both apply and remove on metal artefacts, leaving no marks or residues on the treated surfaces. This means observing several criteria, in particular the correct adherence of the hydrogel on vertical surfaces and three-dimension aspect of real objects, for the full duration of the treatment.

For such, as a second approach towards the use of gels as delivery system for cultural heritage substrates, the question of residues is addressed in this chapter. Starting by assessing the capacity of several polymers to leave residues and evaluating their actual harmfulness on metals, followed by studying their possible detection using various techniques, in particular UV- and XRF-detection.

3.1 Overview of gels selected in the span of the HELIX project

Agar is one of the most used delivery system in cultural heritage conservation [12–17]. It is bioderived as it is extracted from red seaweed membranes [18]. It is appreciated by conservators thanks to good mechanical and retention properties [13,19]. Moreover, it is easily accessible, rather affordable and the fact that it is peelable and therefore easy to remove is valued. In addition to agar, both gellan and xanthan gums are rather common bacterial-based gels resorted to in cultural heritages practices and studies. Cellulose-derived compounds (i.e. Carboxymethylcellulose, Tylose ®, Klucel ®) although bioderived were not considered in this chapter as their production requires extensive synthesis steps [20], which would not comply with the principles of green chemistry (see Chapter 5) [21]. An overview of the main characteristics of the three studied common gels is proposed in Table 3.1.

Table 3.1 Classical bioderived hydrogels studied in the span of this work.

Substrate	Origin	Structure	Used concentration	pH range	Preparation	Texture
Agar	Algae	Double helix	30 g·L^{-1}	4.5-9	Hot	Peelable
Xanthan	Bacteria	Random coil	50 g·L^{-1}	2-12 [22]	Cold	Viscous
Gellan	Bacteria	Double helix	30 g·L^{-1}	2.5-11 [23]	1. Hot 2. Cold	1. Peelable 2. Soft

An additional compound, chitosan, is also evaluated. It is a naturally derived material from chitin that has been praised in the past decades, especially in the medical field or for environmental heavy metal remediation [8,24]. Recently, chitosan is more and more used in cultural heritage studies, for instance for its protective assets as coating or anti-microbial activity as nanoparticles [3,5,25]. In addition, chitosan is a known compound for the complexation of some metals and in particular copper ions [7,9]. The abundant amino and hydroxyl groups are responsible for this ability [26,27]. More recently, it was also found to be able to chelate iron [10]. Regarding its properties as a gelling agent for cleaning, it is to be noted that it can be prepared in a peelable way using alkaline solutions [24], thus reducing the chance of residues when removing the gel after treatment, which is of concern for heritage conservation professionals [28]. Here, a chitosan-based gel is evaluated and its physico-chemical properties compared to those of agar. Furthermore, and interestingly for this metal remediation project, this chitosan gel formulation has been reported to have silver complexing abilities [29].

3.2 Hydrogels design

3.2.1 Materials and methods

3.2.1.1 Gels preparation

3.2.1.1.1 Agar

3% w/v agar gels (1.5 g agar in 50 mL solution) were prepared in either milli-Q water or a $3 \cdot 10^{-2}$ M Deferoxamine (DFO)(Desferal®, Novartis) solution. $3 \cdot 10^{-2}$ M concentration was used as it was reported in other works using DFO [30]. For DFO a stock solution was used (0.5 g DFO in 25 mL water). The mixtures were boiled, cooled down twice and then molded carefully to obtain a 3 mm thick gel. The double heating technique has been shown to improve the mechanical properties [31]. Obtained gel can be observed on Figure S3.1a.

3.2.1.1.2 Chitosan-based gel (CS-ItA-Lcys)

95% deacetylated chitosan (Chitoscience Chitosan 95/200 from Heppe Medical Chitosan GmbH), itaconic anhydride and L-Cysteine (Merck) were ground in mass proportion 1:1:1 in a mortar [29]. The last two compounds are added as they are reported to react and produce poly(thioether amide), connected to the formation of thioether and carboxyl groups known to have complexing abilities towards silver ions. In addition, their presence allows a straightforward gelification of chitosan [29].

In a beaker, 30 mL milli-Q water or $3 \cdot 10^{-2}$ M DFO solution was added under stirring to the mixture composed of 1 g of each reagents (chitosan, itaconic anhydrid and L-cysteine), resulting in a 10% w/v proportion hence leading to a 3.3% w/v of chitosan in the final gel, referred to as CS-ItA-LCys. This allows to obtain a viscous gel, chitosan solubilizing and gelling under the action of the weak itaconic acid formed by reaction of itaconic anhydride with water [32,33]. The viscous gel was centrifuged at 5000 rpm for 5 min to remove air bubbles and then poured slowly and carefully into a mold to obtain a 3 mm thick gel. NaOH 3 M was poured in the mold onto the gel and left for 2 hours in order to obtain a rigid gel, flipping the gel to obtain a homogeneous gel. The gel was then thoroughly rinsed with milliQ water to neutralize [24]. More precisely, the gel was immersed into milliQ water which was changed twice per day for 5 days. Obtained gel can be observed on Figure S3.1b.

3.2.1.2 Gels characterization for polymer comparison and/or active agents addition evaluation

3.2.1.2.1 Cryo-SEM imaging

SEM imaging was performed in order to observe the supramolecular structure of the gels. Samples of agar and CS-ItA-LCys gels were prepared following a procedure that allows the conservation of the microstructure of the matrix, as described by Rabhani *et al.* [34]. Cryo-SEM experiments were performed

using a Quorum PP3010 cryo-transfer system using a Quanta FEG250. Small samples (10 × 5 mm) of agar or CS-ItA-LCys gels were placed on an aluminum stub using carbon conductive glue and the stub was secured on the specimen holder. The sample was then rapidly immersed into liquid nitrogen and transferred into the preparation chamber under vacuum. A fractured surface of gel was obtained by hitting the top part of the sample with a knife inside the chamber. The sample was then sublimed inside the SEM chamber allowing water removal without distortions and potential subsequent artifacts during imaging. To avoid charging problems, the sample was sputter-coated with platinum. In all cases, the imaging was performed using an accelerated voltage of 6-10 kV and a working distance of 7.9-13.6 mm. Image analysis was performed using ImageJ software.

3.2.1.2.2 Swelling properties

The swelling ratio gives the ratio between the mass of the final hydrogel and the mass of the two components in the initial mixture, which can be calculated using the equation:

$$G = \frac{Ws - Wd}{Wd} \times 100 \quad (1)$$

where Wd is the weight of the dried hydrogel and Ws is the weight of the swollen gel after preparation [35]. Gels were weighted immediately after preparation and put in an oven at 70 °C for 8 hours, then weighted. The measurements were performed on six replicates.

3.2.1.2.3 Rheological measurements

To investigate the mechanical properties of hydrogels formulations, rheology was performed, in particular using the amplitude sweep technique. This technique evaluates viscoelastic systems (e.g., pastes, gels). The amplitude of the oscillatory shear strain (i.e., deformation) is gradually increased at a constant frequency. The resulting stress (storage (G') and loss (G'') moduli) is plotted as a function of the shear strain. G' and G'' provide information about the behavior of the studied system according to its elastic and viscous fractions respectively [36]. Amplitude sweep was assessed using an Anton Paar MCR 302e rheometer with a 25 mm profiled plate-plate measuring system, thus avoiding the slipping effect, at a temperature set at 25 °C. A normal force of 1 N and frequency of 10 Hz were applied to the analyzed gel samples. Two measurements were performed on each gel sample.

3.2.1.2.4 Fourier Transformed Infrared Spectroscopy

Spectra (4000-650 cm^{-1}) of dried gels were acquired using an iS5 Thermo Scientific spectrometer with a diamond attenuated total reflectance (ATR) crystal plate (iD5 ATR accessory), collecting 16 scans at a resolution of 4 cm^{-1}. Collection and data processing were conducted with Omnic software. Baseline and atmospheric corrections were performed on the resulting spectra to remove residual signatures of atmospheric CO_2 and H_2O.

3.2.1.3 Compatibility between active agents and gel preparation protocol

Compatibility of added agents with heat-requiring protocols for gels preparation was evaluated using an Ultra-Violet-Visible (UV-Vis) spectrophotometer VICTOR Nivo Multimode Microplate Reader from Perkin Elmer. In particular, the heating resistance of the siderophore, deferoxamine (DFO) (Desferal®, Novartis), was examined. For such, equimolar (10^{-2} M) solutions (100 µL) of ferric nitrate ($Fe(NO_3)_3 \cdot 9H_2O$) and DFO were mixed, both before and after boiling of the siderophore solution. UV-Visible spectra of the mixture, diluted if necessary, were acquired in the visible range 400-850 nm.

3.2.1.4 FT-Raman spectroscopy for gels complexing abilities

This technique is the coupling of a Raman accessory with a FTIR instrument. Raman measurements were performed with a emission wavelength of 1064 nm, allowing a reduction of the fluorescence effect and a more direct correlation between observed vibrational band and molecular bonds [37]. The application of FT-Raman spectroscopy is particularly employed in medicine and biology [37], but also in energy storage, especially with the development of ionogels [38].

Here, it was used to assess the complexing abilities of the CS-ItA-LCys gel towards silver ions and therefore evaluate the bonds forming between CS-ItA-LCys and silver ions. Prepared chitosan-based gel samples were immersed in 20 mM $AgNO_3$ solution for 24 hours and then stocked in milli-Q water. Chelation abilities of the gel after immersion were analyzed using an FT-Raman (Bruker RFS100 with a continuous YAG laser at 1064 nm as the source). Swollen gel samples were analyzed with a laser power of 500 mW in the range 50-4000 cm^{-1} and with between 100 and 300 accumulations to get a signal to noise ratio sufficient to ascertain peaks detection.

3.2.2 Results and discussion

3.2.2.1 Comparison of classical agar versus novel chitosan gel formulations

3.2.2.1.1 Structural properties of the polymers' networks

Based on obtained cryo-SEM images, agar and chitosan polymers show a different general structural appearance. Agar microstructure is overall denser (Figure 3.1), with pores of 0.4 ± 0.1 µm, that are quite regular and connections between the polymer chains resemble thick threads (Figure 3.1d). Agar gelification is known to be achieved by the transformation from a fluctuating disordered coil conformation in solution to a rigid ordered, co-axial structure, forming connections between the double helices in the gel network [39,40], resulting in precise junction points between threads, as observed on Figure 3.1b and d.

CS-ItA-LCys structure is less neat, less homogeneous, with pores larger and less defined, hindering from measuring the average pore diameter (Figure 3.1a). The separation between pores for Cs-ItA-LCys can be described as walls rather than threads (Figure 3.1c).

For chitosan, it becomes a polyelectrolyte because of the protonation of $–NH_2$ groups, and the chitosan acidic solution can be then transformed into hydrogel when it comes in contact with alkali and progressively gelifies [26]. At acidic pH, the chitosan is soluble, and the subsequent adjunction of sodium hydroxide creates an instable system. The porous structure is generated during phase separation which is induced by the brutal pH modification when immersed into NaOH and gives a less refined structure. The polymer phase prevents the holes to gather when the system is perturbed due to the pH change, therefore having a structure resembling a sponge. When the solvent is removed by rinsing for neutralization, the formed polymeric walls surrounding the solvent regions must be strong enough to preventing pores collapsing and, hence, thick enough to maintain the porous microstructure [41].

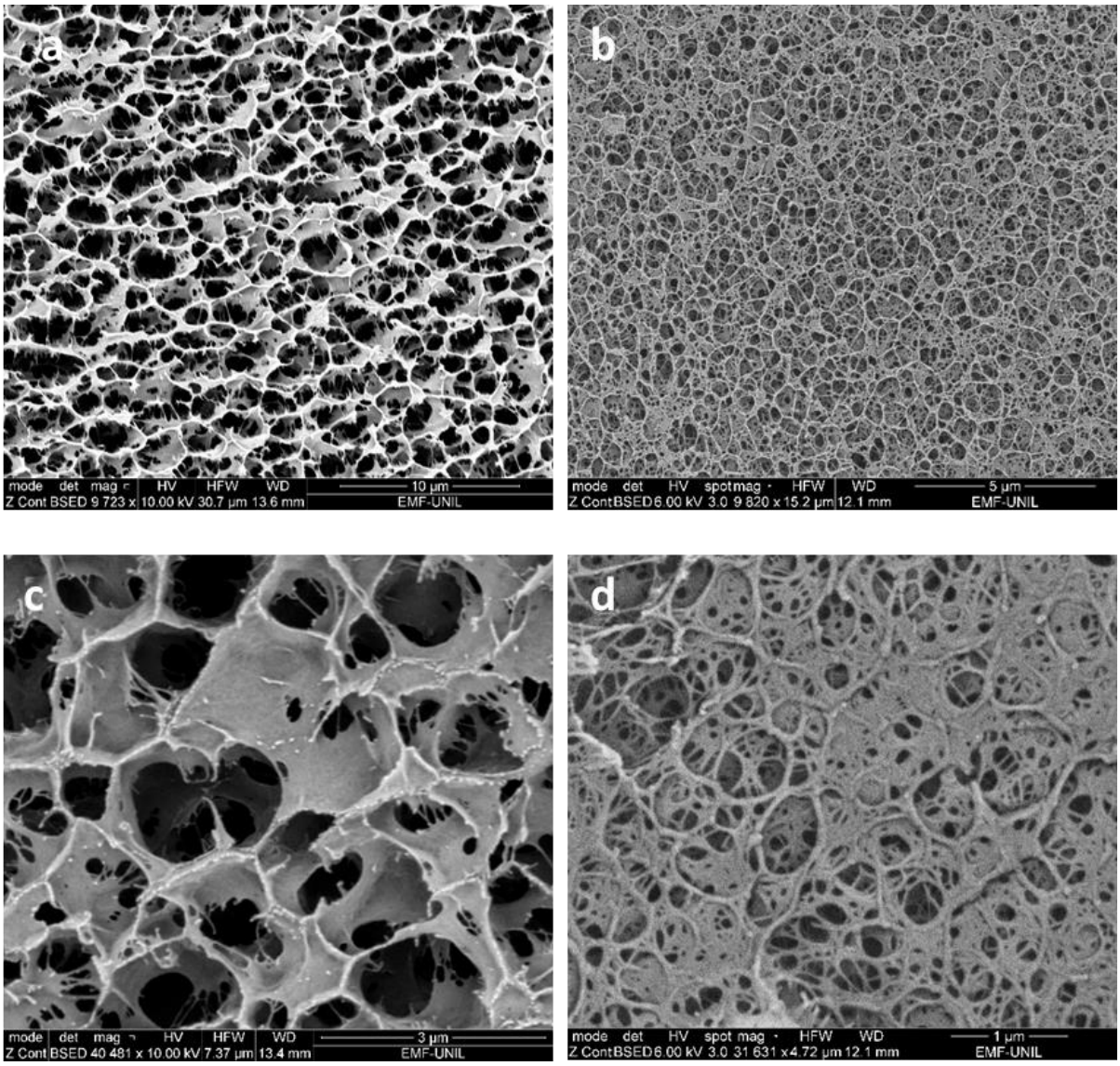

Figure 3.1 Cryo-SEM observations of (a) 3.3% w/v chitosan-based gel (b) 3% w/v agar gel and at higher magnification for (c) chitosan-based gel and (d) agar gel.

Furthermore, on cryo-SEM observations of the prepared chitosan-formulation structure, it seems that the outer layer of the gel is compact and acts as a thick membrane. The average thickness of the CS-ItA-LCys gel outer layer is 1.20 ± 0.09 µm (Figure 3.2a) versus 0.50 ± 0.24 µm for the plain agar gel (Figure 3.2b and c). The presence of this thicker membrane for the CS-ItA-LCys formulation can thus hinder aqueous permeability during immersion.

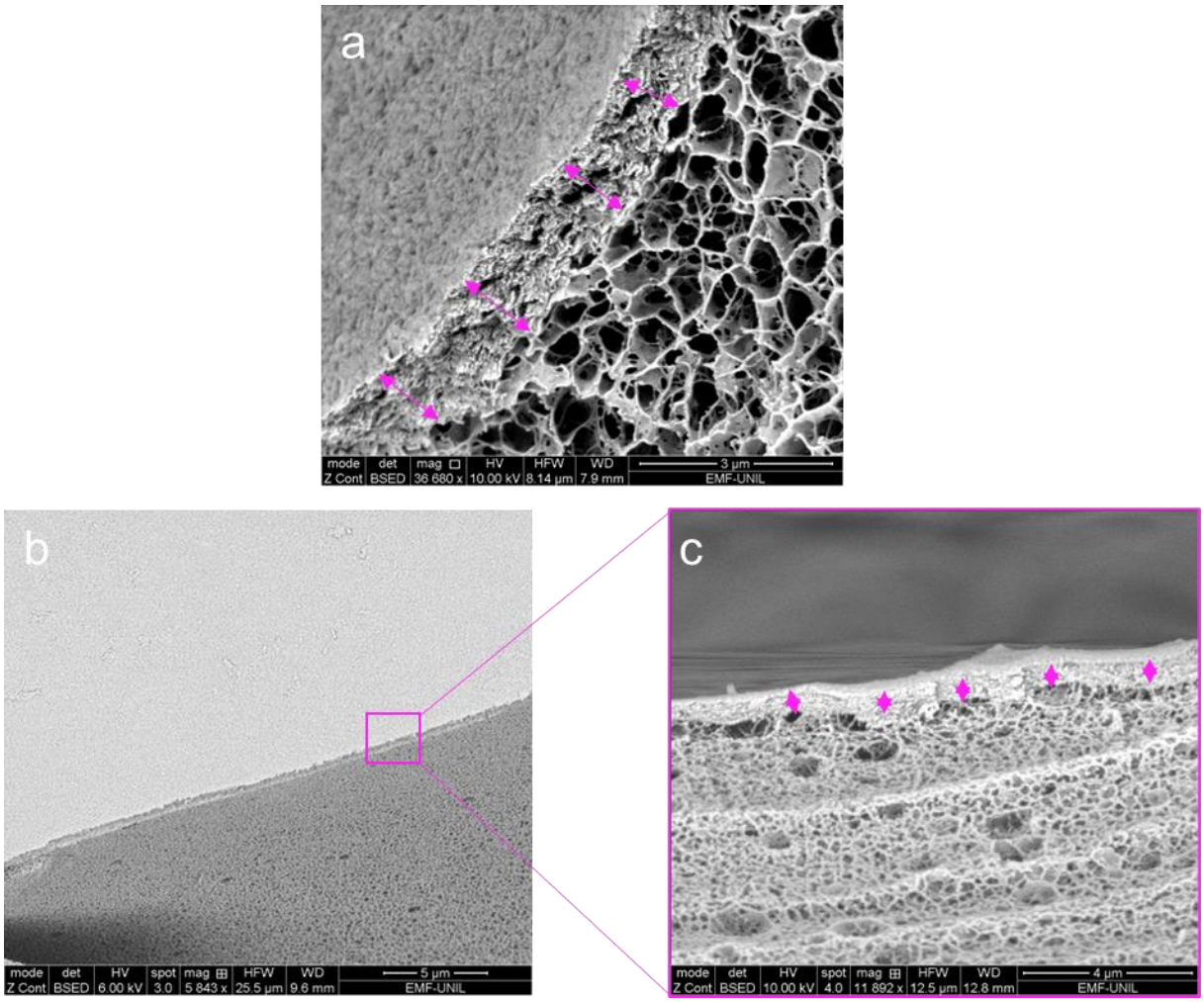

Figure 3.2 Cryo-SEM membrane observations of (a) 3.3% w/v plain chitosan-based gel (b) 3% w/v plain agar gel. Membrane thickness is indicated with purple double arrows. A close-up of the agar membrane is observed in the purple square (c).

The presence of this membrane is explained by the quick diffusion of the non-solvent (NaOH, used to rigidify the dissolved CS-ItA-LCys mixture) at the surface and then slower diffusion of NaOH in the core of the gel [24,42]. To achieve a more homogenous layer in comparison to the inner structure, ammonium hydroxide (NH_4OH) vapors could be used as a way to rigidify the gel while obtaining a thinner membrane, although being more hazardous [24]. Other studies suggest that to limit this membrane formation, increasing the concentration of the basic solution used for rigidification would weaken the hydrogen bonds of the gel and allow better exchanges with external surfaces or solutions [43]. This should be studied further in the case of application of chitosan-based gels for the cleaning of metal artefacts. Indeed, this thick outer layer could inhibit the diffusion of ions taken up inside the gels and therefore limit the efficiency of the gel as cleaning method. On agar, the thin membrane is rather accountable on the surface tension phenomenon, where cohesive forces between the gel polymeric chains will be stronger and denser at the edges of the gel structure to overcome the lack of surrounding similar molecules.

3.2.2.1.2 Swelling properties

Chitosan-based gel has a lower swelling ratio than agar gels, meaning it is able to hold-in lower fractions of aqueous solutions (Figure 3.3). According to literature, the swelling ratio increases with the increasing mesh size (i.e., pore diameter) [44]. Comparing two different polymers here, it is not possible to make that statement. As exposed when discussing cryo-SEM observations of the polymers, agar network is denser, meaning a lower average pore diameter, however, its swelling ratio is higher (2160 ± 42 vs. 1200 ± 289 for CS-ItA-LCys). Therefore, other explanations could be possible such as pores connections or the presence of the membrane on CS-ItA-LCys's outer layer which slows down the exchanges between the gel matrix and the solvent.

From the obtained swelling results, it appears that the CS-ItA-LCys gel shrinks. This was visually observed during NaOH treatments where the gel shrank in the petri dish. The final concentration of chitosan is then approximately the double of agar gel.

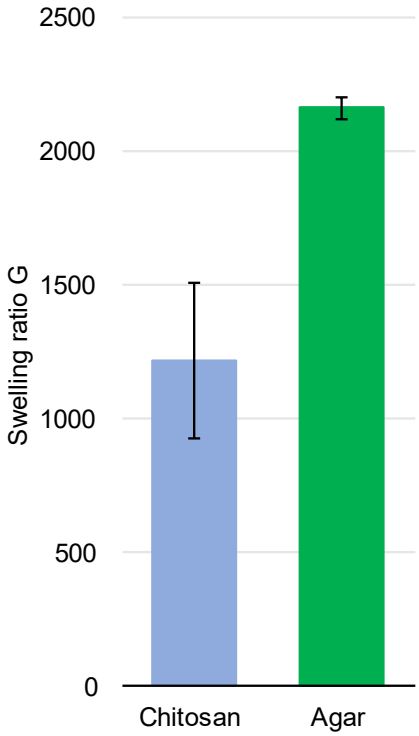

Figure 3.3 Swelling ratio of CS-ItA-LCys and agar gels in water.

3.2.2.1.3 Mechanical properties

Rheological measurements of CS-ItA-LCys are compared with those of agar (Figure 3.4).

The linear viscoelastic (LVE) range is the interval where storage modulus G' and loss modulus G'' remain constant with the increasing applied deformation. This occurs in both agar and CS-ItA-LCys amplitude sweep measurements (Figure 3.4), demonstrating an undisturbed structure from the sample at lower deformations. The plateau of G' describes the rigidity of the sample at rest and the plateau of

G'' is a measure of the viscosity of the gel. Here, the storage modulus G' is higher than the loss modulus G'' for both agar and CS-ItA-LCys, indicating that the gels have a solid-like behavior [36]. Indeed, in case of G'>G", the analyte behaves like a viscoelastic solid, and therefore can be considered to have a gel-like structure. Agar's storage and loss modulus at the LVE range (about 44 000 and 2000 Pa respectively) are higher than the ones of CS-ItA-LCys (about 7000 and 800 Pa respectively)which signifies that the agar gel is more firm [36]. In addition, the greater the G'/G'' ratio between the moduli, the more the sample shows the properties of a pure solid. With a G'/G'' ratio of 22 and 8.75 for agar and CS-ItA-LCys respectively, the CS-ItA-LCys gel has a more fluid behavior than agar. This can be related to the structural aspect of CS-ItA-LCys. Although having a thick outer membrane and walls, it displays a less dense inner network, hence a more flowing, less stiff behavior, similarly to breasts implants or reverse spherification in molecular gastronomy for instance.

In the amplitude sweep test, there are two remarkable points:

- The yield point, at the end of the LVE-region and flow point, at the intersection of the curves for G' and G''. The yield point or yield stress γ_L is the value of the shear stress at the limit of the LVE region. It is the moment when the applied strain starts to damage the samples irreversibly and the moduli are no longer constant.
- The flow point or flow stress, which is the value of the shear stress at the crossover point between storage and loss modulus for materials with a gel character. It is the point further which G'' becomes greater than G', and beyond which the material will behave as a liquid and therefore "flow".

The yield stress (Figure 3.4 dashed lines) of agar is close to 41000 Pa, happening at 1.6% of shear strain, and the one of CS-ItA-LCys 6700 Pa occurring at 2.5 % of shear strain.
Interestingly, at the end of the LVE, agar gel's loss modulus G'' rises sharply at higher deformations. This phenomenon suggests an initial consistent and interconnected three-dimensional network formed by cross-linked polymers [45]. When reaching the loss modulus's maximum, the gel breaks down starting with some microcracks. The microcracks formation results in an energy exchange, transferred to the surrounding area as friction [45]. The rapid decrease afterwards indicates the final rupture of the gel, hence the passage to the flow area.
In reverse, the loss modulus of CS-ItA-LCys barely exhibits a bump to reach its maximum at higher shear strain values. Contrary to agar, there are no microcracks because no increase after the yield point. Both gels have a yield stress happening at close shear strains but agar's decrease of storage modulus G' is more brutal, whereas the CS-ItA-LCys's decrease of the storage modulus is more progressive,

meaning that agar gel is more likely to break into larger pieces than CS-ItA-LCys when reaching its flow point (Figure 3.4, dotted line).

CS-ItA-LCys's flow point is therefore reached at high shear strains, beyond 100%, which shows it is more resistant to deformation than agar, reaching its flow point (3400 Pa) at 14.9% of shear deformation. Agar is more brittle than CS-ItA-LCys, this is shown by the ratio of flow point over yield point's shear strains (9.3). A smaller ratio indicates a more brittle material as it means the material is destroyed as soon as it starts deforming. CS-ItA-LCys on the other hand is more malleable (over 40).

Both gels, although peelable, show very different mechanical behavior. CS-ItA-LCys being more flexible it is easier to reach contact with the surface as it is less stiff. CS-ItA-LCys's resistance to deformation could make it fit to manipulation by conservators to apply on metal surfaces.

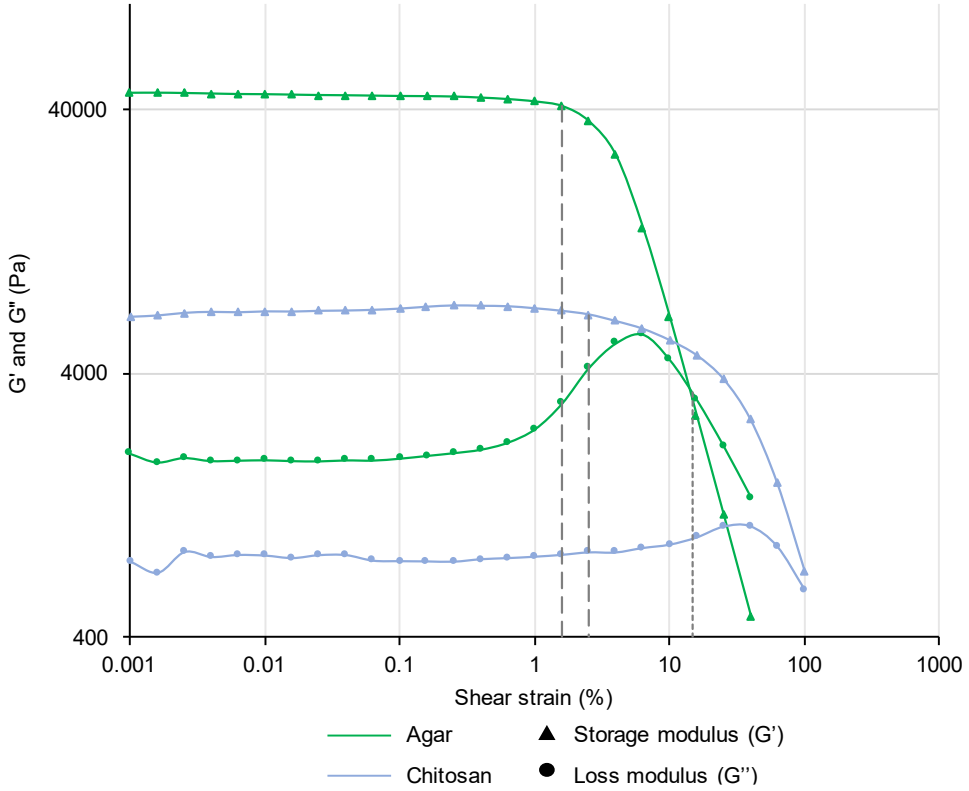

Figure 3.4 Storage (G') and loss (G'') modulus measurements of 3% w/v agar gel (green) or chitosan-based formulation (blue).

3.2.2.2 Amendment of hydrogels with the metal complexing agent deferoxamine

3.2.2.2.1 Compatibility between active agents and gel preparation protocol

The compatibility of the chelating agent deferoxamine with gel formulations that would require a heating step, (e.g., agar) is demonstrated. The iron-deferoxamine complex is known to absorb at 448 nm [46]. From the obtained absorbance spectra (Figure 3.5, spectrum Fe-DFOh), it is clear that the siderophore deferoxamine still possesses chelating properties after reaching temperatures over 100 °C,

confirming literature data [47]. Indeed, the characteristic absorbance peak of the Fe-DFO complex at 448 nm is still present.

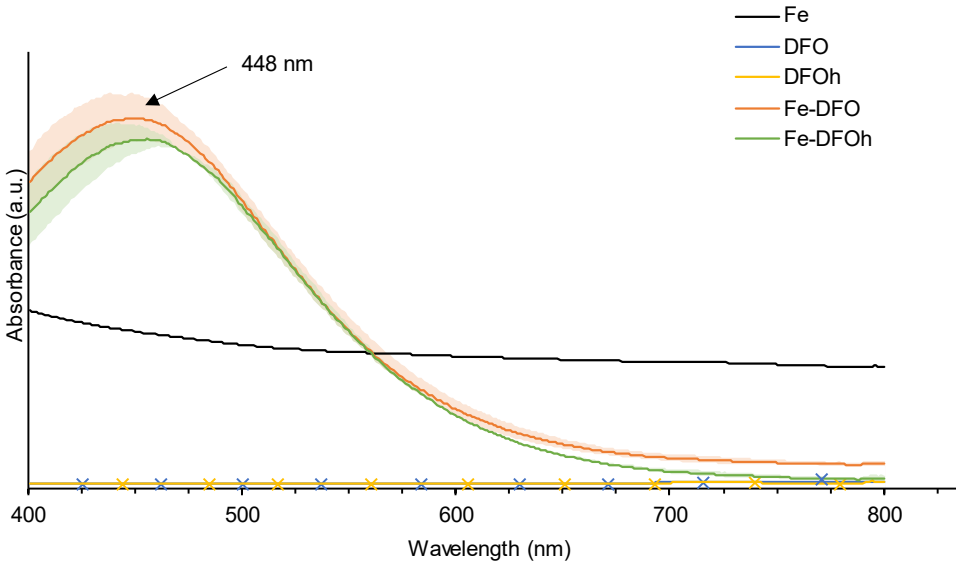

Figure 3.5 Mean UV-Visible spectrum and standard deviation (acquired in the range 400-850 nm) of solubilized iron(III) (Fe), deferoxamine (DFO), deferoxamine after heating (DFOh), iron-deferoxamine complex (Fe-DFO) and Fe-DFO complex after heating of deferoxamine (Fe-DFOh).

3.2.2.2.2 Cryo-SEM Imaging

Both agar and agar-DFO gel formulations show a rather uniform network of interconnected polysaccharides chains (Figure 3.6). The density of the network is similar, as well as the measured average pore diameter for plain agar and DFO-agar gel (0.4 ± 0.1 µm vs 0.4 ± 0.1 µm respectively), which means similar amount of junction zones between double helices of agar gel structure. For CS-ItA-LCys (plain and DFO-amended), analogous observations are made (data not shown).

Cryo-SEM observations of the matrix microstructure suggest that the metabolites do not interact with the polymer but rather stay confined in the liquid phase. The addition of siderophores does not affect the overall facies.

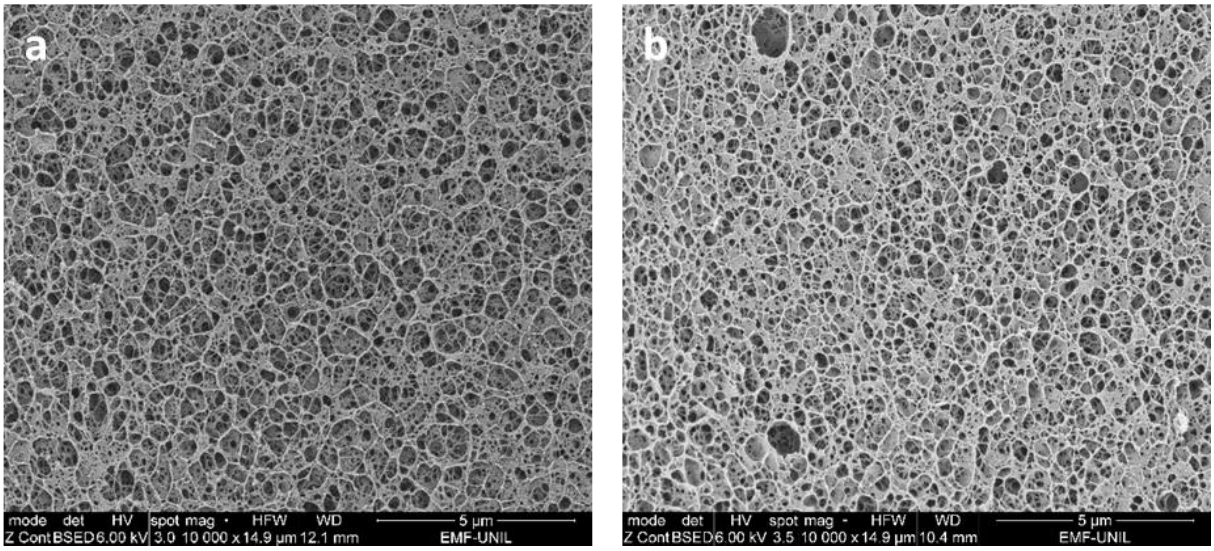

Figure 3.6 Cryo-SEM observations of (a) 3% w/v plain agar gel (b) 3% w/v agar gel amended with DFO solution.

3.2.2.2.3 Rheological measurements

Amplitude sweep tests are plotted on figure 3.7 a and b for agar and CS-ItA-LCys formulations respectively. For each gel (agar and CS-ItA-LCys), both formulations (i.e., with or without amendment of bio-based complexants) displayed a similar linear viscoelastic range. The amplitude sweep measurements showed the storage (G') and loss (G'') moduli exhibit a plateau prior to the yield point, with G'>G'' therefore all samples can be defined as gel-like materials.

The yield stress of agar is close to 37000 Pa, happening at 0.65% of shear strain, whereas values obtained for agar-DFO are about 46000 Pa and 0.6% (Figure 3.7a, dashed lines).
For CS-ItA-LCys, the yield stress is close to 6700 Pa, happening at 2.5% of shear strain, values close to the ones obtained for CS-ItA-LCys-DFO, about 5300 Pa and 2.5 % (Figure 3.7b, dashed lines). According to replicates, differences in values were connected to manipulation errors, namely anecdotic differences in thickness of the gels added to minimal polymer concentration changes.

Loss modulus G'' of both formulations of agar and agar-DFO gels rise sharply at higher deformations, reaching a maximum between 4% and 6% shear strain. This means that microcracks start to develop before the complete breakdown of the sample.

Prior to decrease, no augmentation of CS-ItA-LCys-DFO loss modulus occurs, contrarily to CS-ItA-LCys's one where there is a small increase.

Agar-DFO possesses a flow point, where storage and loss modulus curve intercept (G'=G'') at a shear strain of 17.1% and shear stress of 2960 Pa, quasi-identical to those of the agar gel (20.6%, 2394 Pa) (Figure 3.7a, dotted line). Regarding CS-ItA-LCys, the flow point is reached beyond 100% of shear strain in both formulations.

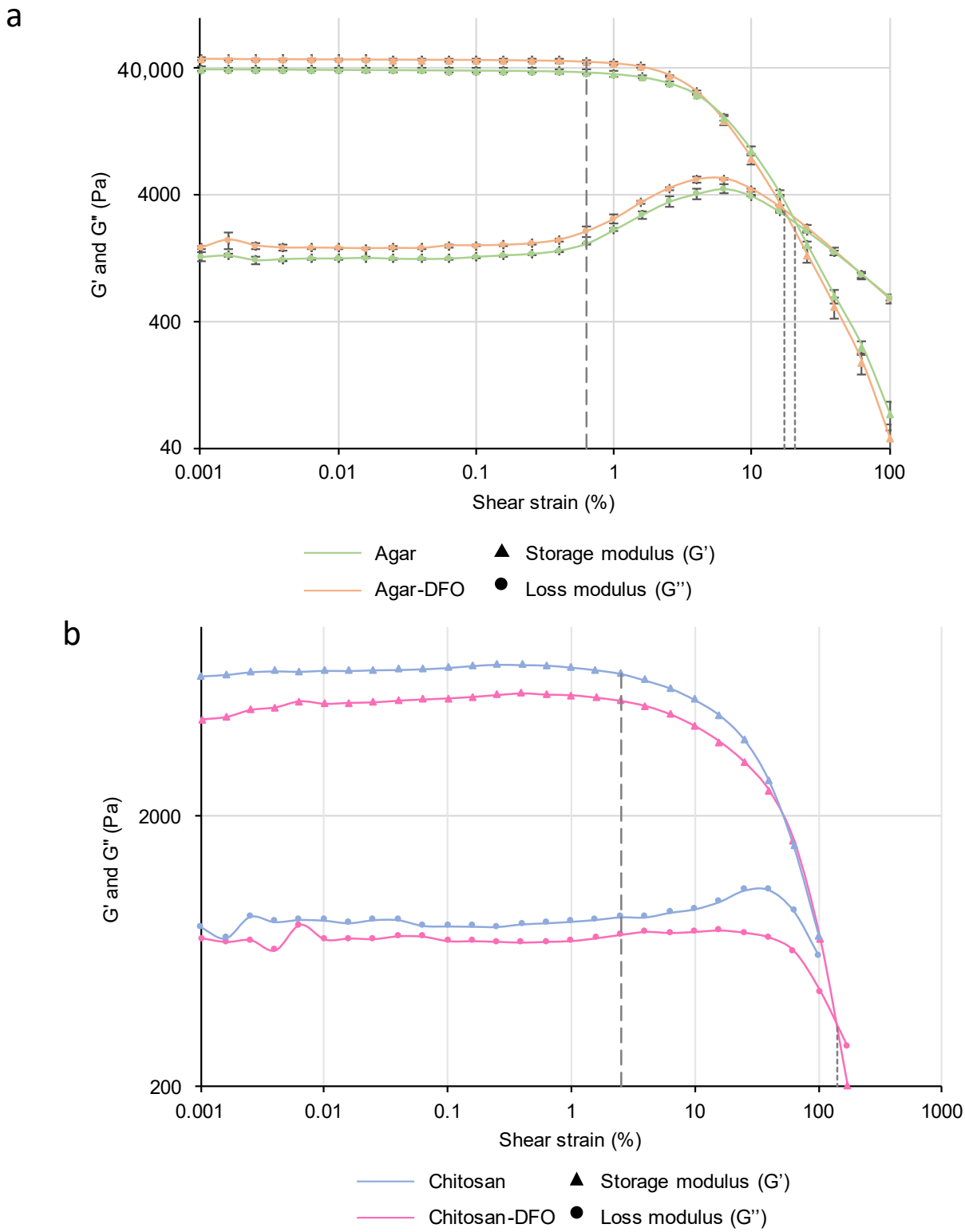

Figure 3.7 Storage (G′) and loss (G′′) modulus measurements of (a) 3% w/v agar gel prepared without (orange) or with DFO amendment (green) and (b) 3.3% w/v chitosan-based gel prepared without (blue) or with DFO amendment (pink).

As inferred with electron microscopy observations, agar and CS-ItA-LCys gels would act as carriers for the metabolites' solution. The fact that the added molecules do not interact with the polymeric structure could be spread to other metal-sequestering agents. Still, the absence of modification of the mechanical behavior should also be considered in regard to the pH of the added solution. For instance, in the case of agar, the DFO solution has a similar pH than agar, rather neutral, but studies have proven that gel properties change slightly with pH, gel rigidity decreasing with an important pH variation [48,49]. This was explained by the difference in length of flexible chains from the helical network of agar gel. Gels at pH values closer to neutral have been shown to have longer and more flexible polymer chains than those with more extreme pH values. Below 5.5 and above 8, hydrolysis of the polymer reduces its molecular weight [39,49]. Consequently, gel network's elasticity, rigidity and connectivity also decreases [49,50]. Short chains are stiff, correlating to the more fragile behavior of agar gel. Molecular weight reduction of agar subsequently reduces the probability to form junction zones in addition to the flexibility of the molecular chains, that would withhold the network structure of gel through interhelical association [49]. Low molecular weights chains (short chains) impede the formation of interchain bonds: i.e., the amount of hydrogen bonds formed within a junction zone would then be comparatively low [51,52]. Hence, at neutral pH, long chains, being more flexible, can be extended further before destruction of the helical network and therefore conserve the mechanical properties of agar gels. More extreme pH values of other chelating solutions implemented in agar gels would therefore decrease the strain at fracture [49].

Regarding CS-ItA-LCys, it has been found that it was related to the organization of the polymer chains [53], the increase of solution pH leading to a preference for a parallel crosslinking, and consequently increases the mechanical strength of the hydrogel [54].

3.2.2.2.4 ATR-FTIR spectroscopy

3.2.2.2.4.1 Agar

The obtained agar spectra displayed the typical vibrational bands of polysaccharides originated form red seaweed (Figure 3.8, orange spectrum). Bands at 3289 cm^{-1} and 2923 cm^{-1} are assigned to the stretching modes of OH and CH respectively [55–57]. The band at 1634 cm^{-1} is attributed to the OH bending mode of water remaining in the gel although it was dried [55]. The peak at 1373 cm^{-1} is assigned to ester sulfate, which presence could be interpreted as the agar species and method of extraction [56]. The band at 1250 cm^{-1} stands for S==O stretching mode [58]. The bands observed at 1063 and 931 cm^{-1} are characteristic vibrational bands of 3,6-anhydro-galactose, corresponding to the glycosidic bond and the C-O-C bridge respectively [55–57]. Bands between 800 and 900 cm^{-1} are characteristics of 3,6-anhydro-galactose network [55,58].

Regarding the deferoxamine mesylate salt spectra (Figure 3.8, green spectrum), the medium sharp vibrational band at 3306 cm^{-1} is attributed to N—H bond (amine II) [59,60]. Bands at 2855 and 2928 cm^{-1} are asymmetric and symmetric stretching modes of CH_2, respectively [59,60]. Bands at 1622 ,1565, 1396, 1268 cm^{-1} are attributed to C==O stretching from the hydroxamate (amine I), C—N stretching and N—H bending (amine II), and the O—H deformation bands respectively [59–61]. 1041, 989 and 963 cm^{-1} bands result from the stretching mode of N—O of the hydroxamate groups [59–61].

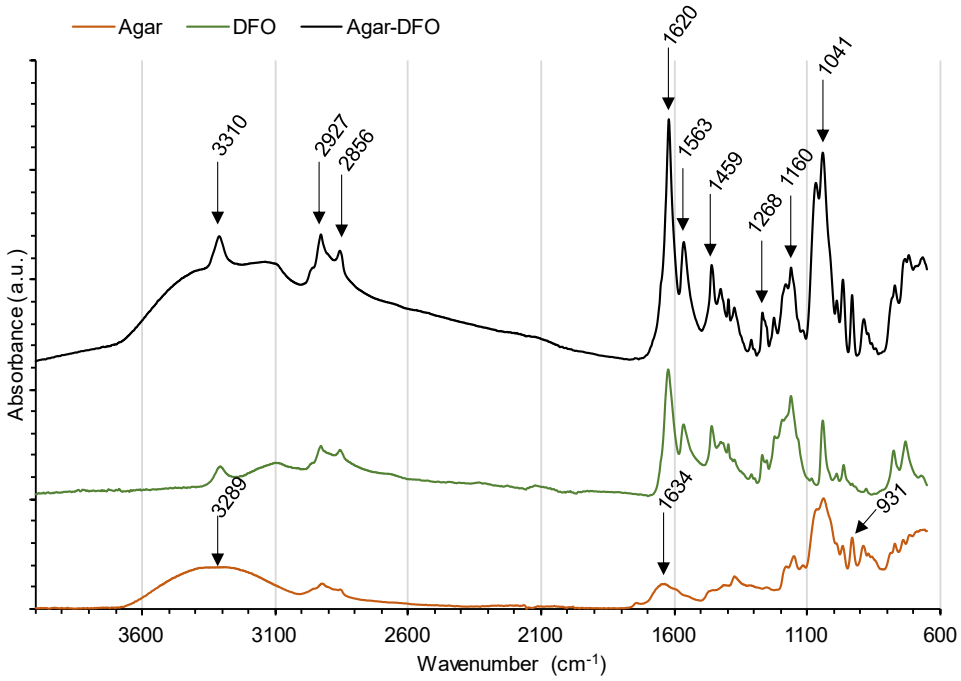

Figure 3.8 ATR-FTIR spectra of plain agar gel (orange), DFO (green) and an agar-DFO gel (black). Bands indicated on the agar-DFO spectra are the main ones related to the presence of deferoxamine.

As can be observed on Figure 3.8, newly formed Agar-DFO hydrogels ATR-FTIR spectra are composed of a combination of bands from the initial spectrum of DFO and respective gels, which suggests no new main bonds were created, hence suggesting siderophores sit in the pores of the gels. The presence of all bands attributed to amine, amide or hydroxyl groups confirms the absence of new molecular bonds or functionalization through those chemical groups. Following the upload of DFO, no change could be observed neither regarding bands frequencies nor band width, strengthening the conclusion of an absence of any interaction between the gel and the chelator. Recapitulative attribution of bands is available in table 3.2. All bands from the newly formed gels could be attributed to the initial components of the gel, including the fingerprint region (1000-600 cm^{-1}) (not detailed), thus confirming that the metabolites do not interact with the polymer but rather stay confined in the liquid phase. For such, this suggests that the treatment's reaction rate is ruled by the movement of the liquid phase inside the network and therefore the diffusion of DFO solution inside the gel.

Table 3.2 Assigned ATR-FTIR bands for Agar gel, DFO and Agar-DFO gel. Relative band height is indicated by the first letter w=weak, m=medium, s=strong, v=very. Shape is indicated by sharp, br=broad or shoulder.

Band assignment	Wavenumber (cm^{-1})		
	Agar	Deferoxamine	Agar-DFO
N—H stretch.		m, sharp	3310m, sharp
—OH	3289, br		3137, br
C—N—H		3099w, br	
CH_2 as. stretch.		2928vw, sharp	2927w, sharp
-CH	2923w, sharp		
CH_2 s. stretch.		2855w, sharp	2856vw, sharp
C==O stretch.		1622vs, sharp (hydroxamate)	1620vs, sharp
O—H bend.	1634m		
C—N—H		1565m, sharp	1563m, sharp
CH_3		1459m, sharp	1459m, sharp
C—H		1425w	1426w
O—H deform.		1396m	1396w, sharp
-C—N stretch.	1314vw		1310vw
C—N stretch N—H bend.		1268vw	1268vw
S==O	1252vw		1254, shoulder
C—N stretch.		1161m	1160m
N—O stretch.		1041vs, sharp 989w, sharp 963m, sharp	1041vs 989w, sharp 966m, sharp
C==O (3,6-anhydro-a-L-galactose)	931m, sharp		931m, sharp

3.2.2.2.4.2 Chitosan

FTIR spectra of the CS-ItA-LCys formulation prepared with DFO solution (Figure 3.9) showed no clear peak apparition.

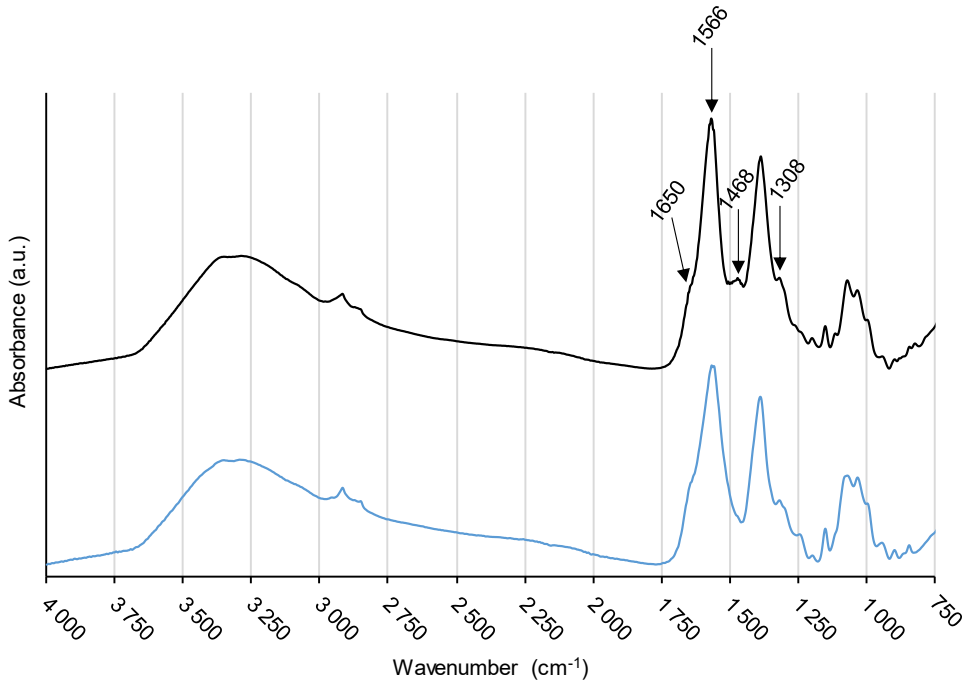

Figure 3.9 FTIR spectra of chitosan-based formulation containing itaconic anhydride and L-cysteine, prepared with either DFO solution (black) and water (blue).

Indeed, most bands from DFO are overlapping the ones from chitosan in particular the N—H and O—H in the 3000-3500 cm^{-1} region, along with bands corresponding to primary and secondary amides (1650 and 1566 cm^{-1}) and C—N stretching (1308 cm^{-1}). A detailed investigation of the CS-ItA-LCys formulation FTIR spectra is proposed in the following section (2.2.3).

It is worth noting that papers have loaded chitosan nanoparticles with deferoxamine for medicinal iron-uptake purposes [62]. Here, this was not reproduced as a peelable delivery-system was wanted. In that context, a shift in the –OH bands in FTIR spectra allowed to conclude the formation of hydrogen bonds between OH or amino groups of chitosan and DFO [62]. In the case here-presented, no shift was observed, the peak for hydroxyl bond stretching being at 3351 or 3293 cm^{-1} for both plain and DFO-amended CS-ItA-LCys. This might be explained by chitosan being already functionalized with the itaconic acid/L-cysteine mixture, hence bonds were not free to react. Interestingly, the shoulder at 1468 cm^{-1} in the chitosan-based formulation (Figure 3.9, blue spectrum) becomes a weak sharp peak in the chitosan-based formulation amended with DFO, which could stand for further functionalization. This would therefore allow the use of the CS-ItA-LCys formulation without or with the addition of secondary metabolites which could boost the formation of chelated complex inside the gel and therefore the cleaning action, in particular for iron, as more metal ions could be taken up.

3.2.2.3 Inherent capacity of chitosan-formulation to take up silver ions

Chitosan is a compound praised for the complexation of metals and in particular copper ions [7,9]. Its potent iron and copper complexation has already been solidly demonstrated in literature [10,63]. For copper, adsorption via the abundant amino and hydroxyl groups present is responsible for this ability [26,27,64,65].

In this chapter, the chitosan-based formulation assessed was produced through a simple one pot protocol, grinding together highly deacetylated chitosan, itaconic anhydride and L-cysteine [29]. As mentioned in section 2.1.1.2, the last two compounds are added as they are reported to react and produce poly(thioether amide) and gelify in a straightforward way with chitosan. The presence of resulting thioether and carboxyl groups is believed to endow the hydrogel potent complexing ability to silver ions [29].

However, the method used to demonstrate silver complexation, ICP-AES measurement of silver in the gel after immersion, is questionable as it could be solely due to the absorption of the silver ions inside the gel. Spectroscopic investigations are proposed to evaluate the molecular structure of the gel formulation and the supposedly formed bonds with silver.

3.2.2.3.1 Chitosan-based gel molecular structure

ATR-FTIR spectroscopy was used to ascertain the molecular structure of the newly formed chitosan-based formulation, composed of itaconic anhydride and L-cysteine (Figure 3.10).

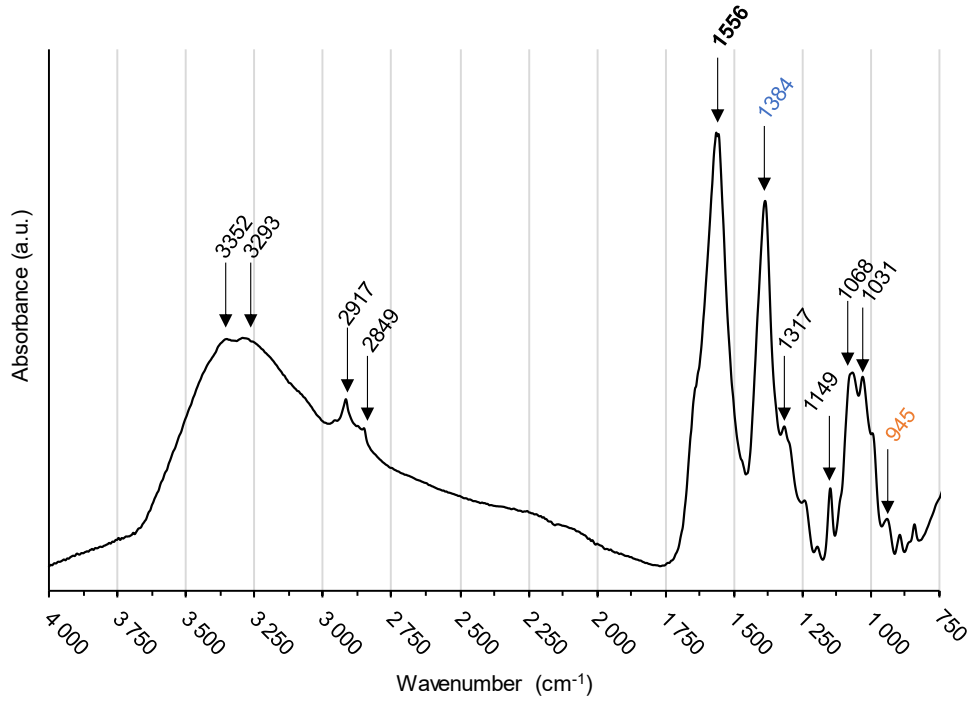

Figure 3.10 ATR-FTIR spectra of chitosan-based gel prepared with itaconic anhydride and L-cysteine and water. Bands in blue are related to the presence of itaconic anhydride, in orange to the presence of L-cysteine and in bold to the modification of chitosan structure.

Most bands are assignable to chitosan's molecule (Table 3.3). The broad band at 3000-3500 cm^{-1} is attributed to stretching vibrations of N—H and O—H , with small signals at 3294 and 3351 cm^{-1} respectively [32,66]. Bands at 2917 and 2849 cm^{-1} are assigned to —CH_3 and —CH_2 stretching vibrations respectively [66]. Amide I and amide II bands from chitosan neckbone structure are responsible for the shoulder at 1633 cm^{-1} and intense peak at 1556 cm^{-1} respectively, with the latter slightly shifted to lower wavenumbers from what is observed in pure chitosan [32,66–68], this could be related to the addition of a new group after the amide bond formation [66,67,69]. Potentially, it could be the addition of the thioether groups mentioned priorly but so far, the nature of this new group cannot be determined. Contributions from chitosan's C—N groups stretching vibrations are observable at 1317 cm^{-1} [6,68], The bands at 892, 1031, 1068 and 1149 cm^{-1} are the ones typically reported for chitosan gels' and are ascribed to polysaccharides [6,66,68–70], along with weak bands at 1194 and 992 cm^{-1} [71].

The peak noticeable at 1384 cm^{-1} is typical of carboxyl groups present in itaconic acid structure [32]. However, the shoulder at 1468 cm^{-1} supports the fact that the functionalization of chitosan did occur as it could be related to the thiolation of chitosan, due to the addition of L-cysteine [66,67], along with the small peak at 1243 cm^{-1} that could also be representative of thiol groups [72]. In addition, the peak at 945 cm^{-1} can be attributed to the presence of S-H in the gel, due to the addition of L-cysteine in the formulation [25].

Table 3.3 Assigned absorption bands of one-pot chitosan-itaconic acid -L-cysteine formulation. Relative band height is indicated by the first letter w=weak, m=medium, s=strong, v=very. Shape is indicated by sharp, br=broad or shoulder. In blue are the bands related to the presence of itaconic acid and in orange related to the presence of L-cysteine. In bold are the bands suggesting modification of chitosan's structure.

Band assignment	Wavenumber (cm^{1})
O-H stretching	3351m, br
N-H stretching	3293w, br
CH_3 stretching	2917s, sharp
CH_2 stretching	2849w, sharp
C=O amide I	1633w, shoulder
-NH_2 amide II	1556vs, sharp
-CH_2 bending	1468vw, shoulder
C=O carboxylate group	1384vs, sharp
C-N stretching	1317w, br
C-SH	1243w
C-O-C	1149m, sharp
C-O stretching	1068m, sharp
C-O stretching	1031m, sharp
S-H	945vw, sharp
C-H bending	895w shoulder

Although direct thiolation of chitosan has been reported in papers [67], there are more electronic displacements existing for the itaconic compounds, making them more likely to react. Either as proposed by Lai *et al.*, through an intermediary compound formed from L-cysteine and itaconic anhydride (IAn). IAn and L-cysteine would react together after IAn ring opening, caused by the presence of L-cysteine. Further polymerization into poly(thioether amide) would occur (Figure 3.11a), allowing this poly(thioether amide) to be grafted onto chitosan chains, linking two chitosan chains together as proposed in Figure 3.12a [29].

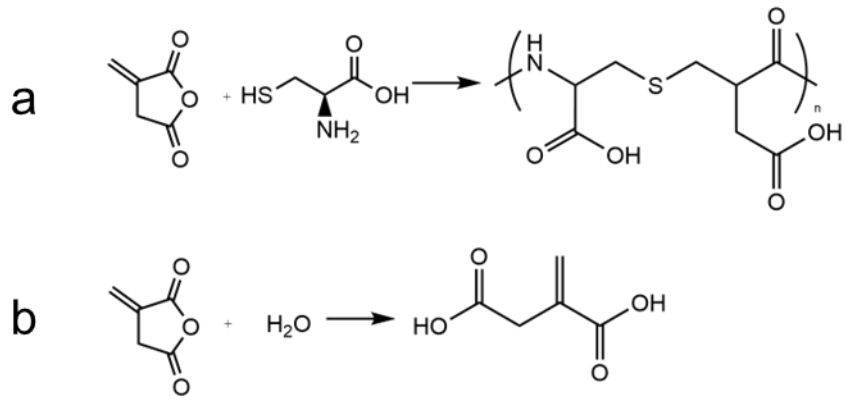

Figure 3.11 (a) poly(thioether amide) formation from itaconic anhydride and L-cysteine, (b) ring opening of Itaconic anhydride into itaconic acid.

The second option could be the ring opening of IAn using the presence of water, obtaining itaconic acid (IA) (Figure 3.11b) [33]. IA could react with chitosan, followed by subsequent grafting of L-cysteine to the IA side. In order to graft two chitosan chains together as proposed in literature, there would be the need to have a molar ratio of IAn:L-cysteine of 2:1 to allow for the subsequent grafting of another IA to priorly linked L-cysteine, IA that would attach itself to another chitosan chain (Figure 3.12b).

It could also be the case that most of the L-cys/IA blocks reacted on one side mainly and only few of them are linking two chitosan chains together, therefore allowing for a close to 1:1 needed molar ratio as used in here-tested formulation, or part of the L-cysteine could just be present floating in the gel but not necessarily attached to the rest of the structure. To get a more comprehensive analysis and try to understand the structure of the obtained hydrogels other techniques might be complementary, in particular nuclear magnetic resonance [69].Detailed investigation of the proposed mechanisms is beyond the scope of this research., but an insight of the reaction pathway of the second option discussed is given in Figure S3.2.

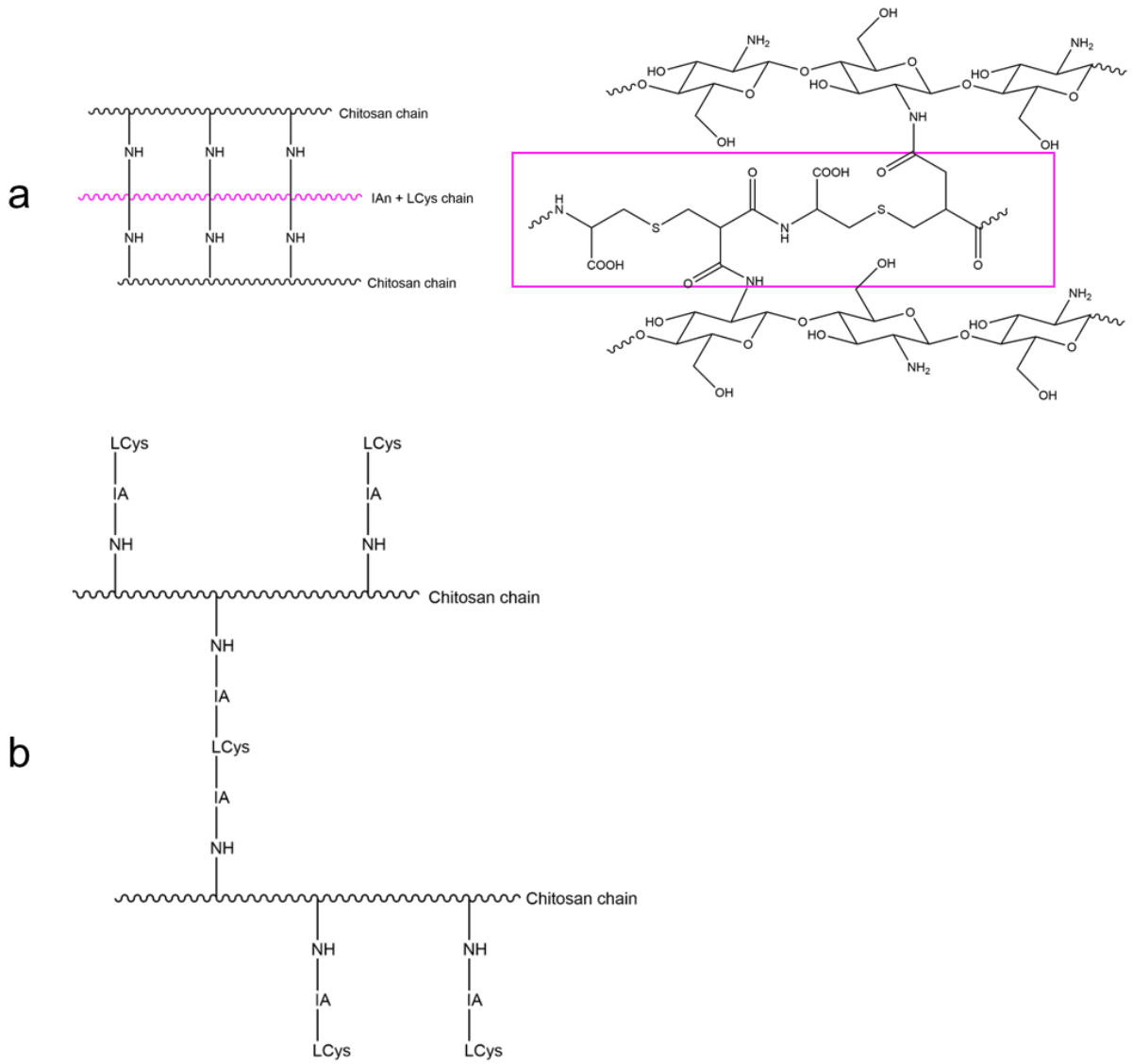

Figure 3.12 Schematic representation of chitosan functionalization through (a) poly(thioether amide), (b) successive Itaconic acid and L-Cysteine grafting.

Spectral analyses allow to validate the presence of IA or L-c0ysteine functional groups in the chitosan matrix, however, the complete structure cannot be confirmed based on solely FTIR spectroscopy. In any case, the presence of thiol groups and carboxyl groups in the polymer still might confer further complexing ability to the chitosan polysaccharide structure.

3.2.2.3.2 Complexing abilities

The complexation capacity of the CS-ItA-LCys gel with silver is assessed by Raman spectroscopy. Most bands from the Raman spectra of CS-ItA-LCys immersed into $AgNO_3$ solution can be attributed to silver nitrate or plain CS-ItA-LCys (Figure 3.13), in particular, the band at 1048 cm^{-1} is typical of silver nitrate [73]. The band at 1641 cm^{-1} is believed to be a combination of the bands at 1636 cm^{-1} and 1645 cm^{-1} ascribed to silver nitrate's NO^{3-}, and chitosan's N-C=O respectively [74–76]. The band at 2890 cm^{-1} are interpreted as stretching vibrations of CH_2 groups from chitosan [74,77].

On bare CS-ItA-LCys's spectrum, bands at 897, 1092 and 1375 cm^{-1} are typical Raman shifts for chitosan [74,77].

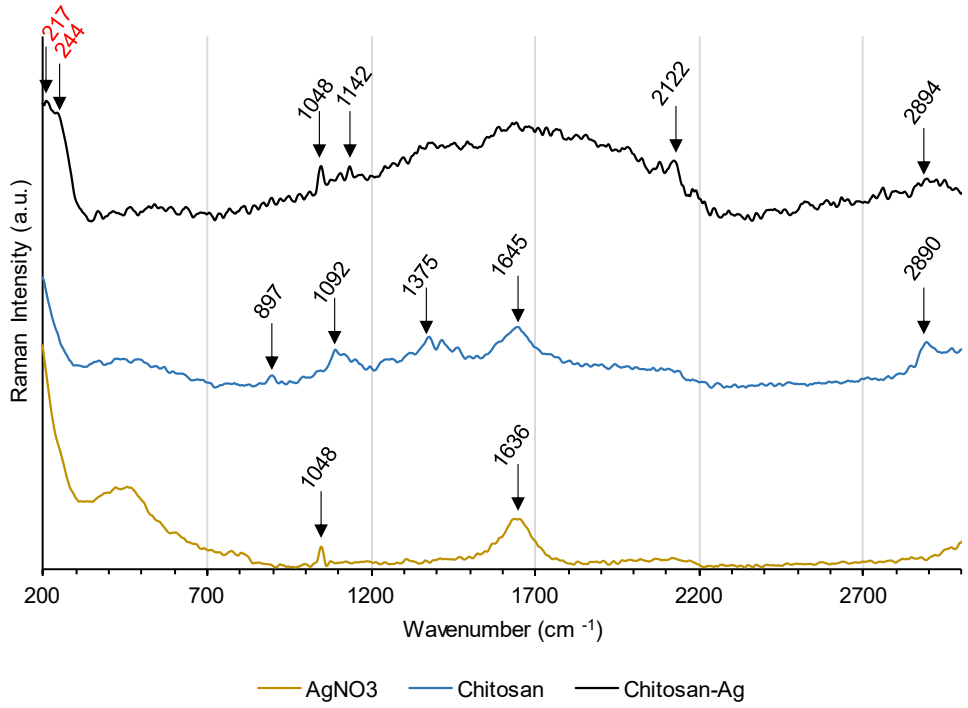

Figure 3.13 Raman spectra of $AgNO_{3(aq)}$, chitosan-based gel and chitosan-based gel after immersion into $AgNO_3$ solution. Peaks related to formed bonds with Ag are in red.

Two remarkable new signals were observed, a small peak at 217 cm^{-1}, representative of the vibration mode of the Ag-O [78], and a shoulder at 244 cm^{-1} which is ascribed to the vibration mode of Ag-S bonds [79]. Therefore, FT-Raman analysis confirmed the existence of new bonds involving both silver and atoms from the CS-ItA-LCys formulation, thus proving the complexing potential of the CS-ItA-LCys formulation tested and comes as a support for the proposed molecular structure of CS-ItA-LCys chelating silver (Figure 3.14).

As a perspective, similar characterization was attempted to test agar-silver molecular interactions and should be continued (data not shown).

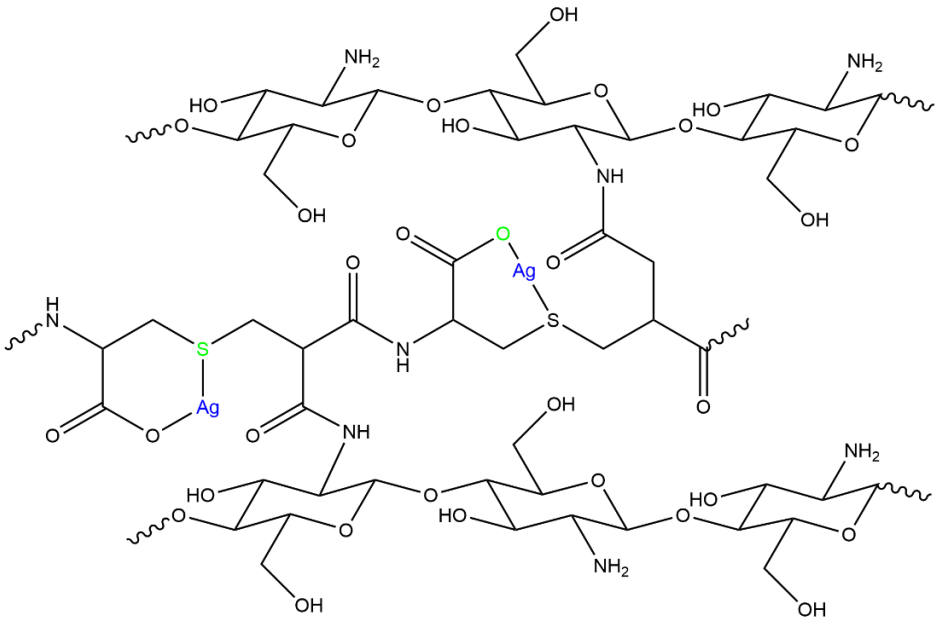

Figure 3.14 CS-ItA-LCys complexation of silver ions as proposed in literature [29].

3.2.3 Conclusion

The objectives of this study were to assess biobased gels as carriers for treatments for tarnish removal on historical metals.

Cryo-SEM and rheological evaluations showed mechanical and structural differences between agar and chitosan-based gels. Although both are rigid gels, agar can be poured directly hot on the surface to perfectly match the shape of the treated surface whereas CS-ItA-LCys has to be applied once solidified. Interestingly, CS-ItA-LCys being more flexible than rigidified agar, it should be able to fit to the objects' features.

Data also showed the compatibility of both agar and CS-ItA-LCys formulations with the natural chelating agent deferoxamine, allowing for enhanced iron, or even copper, chelation. Additionally, the potential assets of a chitosan-based formulation to take up silver ions were demonstrated. Tangible proof by Fourier-transform Raman spectroscopy of created bonds over the complexation of silver ions by CS-ItA-LCys is relevant for cultural heritage professionals. This is a first step into the formulation of gels with inherent complexing abilities, therefore avoiding the use of additional chemicals or agents. Indeed, minimalism is a concept appraised for it environmental pertinence, limiting the impact of anthropological activities [80]. In addition, chitosan's properties are already exploited mainly protective coatings on metal artefacts [4,81,82]. Those demonstrated complexing abilities are of interest in particular for stained composite metal artefacts (i.e., paper, fabrics) where the use of additional compounds in the gel is uncertain due to potential undesired interactions.

These findings must be pushed forward for a potential application in cultural heritage conservation and on actual insoluble corrosion products encountered on objects, in particular silver sulfides. Although further research is necessary to evaluate the effect of the complexing property on almost insoluble tarnish corrosion products (Ag_2S), applications could be foreseen on brocades for instance, to remove copper or silver tarnish from the sterling silver threads. It would also be interesting to assess the chelating ability of a chitosan gel formulated without the adjunction of L-cysteine and itaconic anhydride.

Chitosan's antimicrobial [70], protective and chelating properties make it a particularly great candidate for composite metal/organic materials where biodeterioration is a concern. Indeed, organic materials are often subject to damages related to microbial growth [83]. Chitosan's potential remains outweighed by the different aspects to improve, in particular the compatibility with eventual complexing agents loaded in the chitosan formulation.

The outcomes of such study could be of interest to other fields of application, for instance environmental concern for, wastewater treatment and bioremediation of copper or silver contaminated sites as the peelable nature of both gels would allow an easy removal of the gel film, whether on an object surface or in a polluted environment.

3.3 The residue question

While the use of gels and their development for heritage conservation is thriving, several concerns about the use of gels arose as the systems are being widely incorporated by conservators as a cleaning tool: Will these substances have long-term effects on the surface and substrates after treatment? Which gels are more prone to leaving residues and which are the parameters influencing the phenomenon? These interrogations are even more relevant when it comes to metal artefacts as by definition, contact with water is the one of the core catalysts of the corrosion process [84]. There are two aspects to consider. First, the treating solution contained in the matrix can be deleterious to the object if not cleared properly. Indeed, water-based solution are not very volatile hence the time of exposure to the metal can be of concern, especially because the constrained cleaning solutions are, on purpose, active on metal. Right after the treatment, if not cleared properly, a gel is a stockpile of active agent that could create a prolonged contact point between the cleaning agent and the surface and therefore induce a permanent overcleaned spot. Second, the polymer itself can also be of concern if not removed properly for numerous reasons. Indeed, numerous hydrogels used in cultural heritage conservation are bio-based materials [85], which generally implies the presence of polysaccharides. Polysaccharides are nutrients for microorganisms [86], somehow offering a good environment for their development, potentially causing microbial induced corrosion (MIC) or other biodeterioration [87]. Hydrogel residues, although dry, are risky as they can swell due to ambient moisture if stored in a place with a high relative humidity (RH) [88], there again encouraging localized corrosion.

The Getty foundation, under its publication "Solvent Gels" addressed the concern on paintings, concluding that there are systematic remains of treating gels on surfaces, and even greater if the surface is porous or rough [28]. In addition, the amount varies up to a factor of 10 depending on the clearance strategy of the conservator [28]. It is therefore safe to say several aspects can be accounted for the presence of residues.

First, the texture of the surface to which the gel is applied is crucial. The nature of the treated metal should be considered, such as the porosity of the surface in parallel with the presence of embossed decorations, scratches or carvings. Porosity facilitates any swelling solution to infiltrate the artefact and the presence of decorations render the removal tricky by increasing the adhesiveness between the gel and the surface or making tricky for gels to reach in the angles. In addition, the roughness of a surface directly affects the area of contact between the gel and the metal. Indeed, more numerous asperities will increase the total surface of contact. In addition, studies have shown that the adhesion between a solid surface and a visco-elastic material, like gels, is dependent on the pressure of contact between the two materials in addition with the time of contact [89,90]. The time of contact indeed influences the

"flowing" of the materials into the asperities but also the further drying of the gel which increases the adhesion to the surface. The flowing of the gel could also be influenced by the temperature of gels when applied hot, like gellan gum or agar. A fluid gel will indeed reach small pores, angles or asperities more easily. Moreover, drying of the gel is also governed by the thickness of the gel deposited. This thickness can also have an influence in the removal of peelable gel, as it will influence the angle of removal and therefore the adhesion [91].

To sum up, there is a great number of factors affecting the remnant of residues left onto the surface:

- Surface texture (e.g., porosity, decorations)
- Adhesion (i.e., tack, viscosity)
- Pressure of contact
- Time of contact
- Thickness of applied gel
- Method of clearance

Moreover, these factors are intricated as they have concomitant effects. It is a real knot to unweave that would require an extensive rheological study resorting to tools like chemometrics or ANOVA of the data. This approach was not performed in the span of this work as this is first insight that is proposed here.

Among all parameters cited here before, the tack and viscosity of the gel might be the most decisive. It is basically the "stickiness" of the gel. In the following section, a general idea of the tackiness of gels mentioned in Table 3.1 is proposed, along with an evaluation of the impact of gel residues on metal surfaces.

3.3.1 Residues: a preliminary evaluation of risks

3.3.1.1 Materials and methods

3.3.1.1.1 Capacity to produce residues

Stickiness and adhesive properties were evaluated using the so called "tack tests", usually used to evaluate adhesiveness of polymeric materials [92]. It is a quantitative and objective version of the "thumb test", evaluating whether one feels the material sticking between their fingers. A probe will come into contact with the studied system, collecting data of the normal force applied onto the probe while pulling-out.

There are two main types of rupture mode occurring when performing this test. The cohesive rupture occurs at the material, either as long stringiness or sudden brittle fracture (Figure 3.15 b and c respectively). The adhesive rupture occurs at the interface between the adhesive and the substrate (Figure 3.15 a).

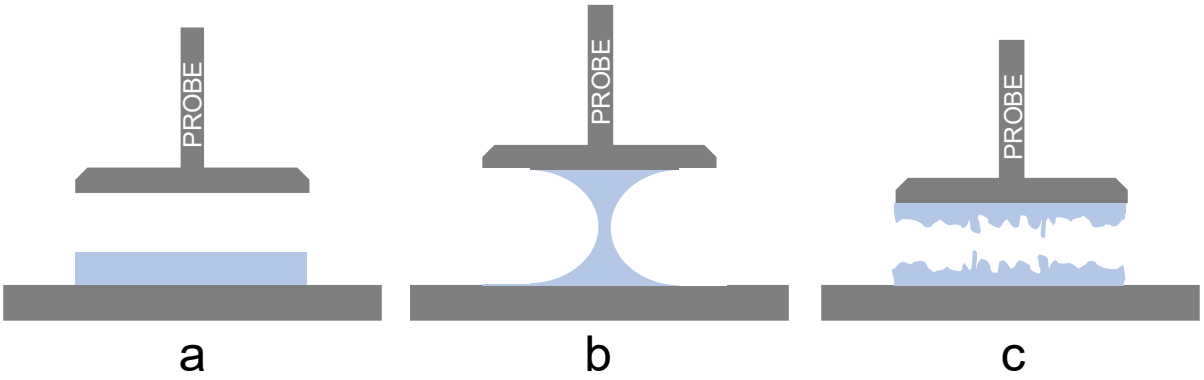

Figure 3.15 Failure modes on tack test: (a) adhesive rupture, (b) cohesive rupture with long stringiness and (c) cohesive rupture with brittle fracture.

These failure modes will influence the tackiness, measured by the normal force generated during a tack test. A material is considered sticky when the rupture occurs at the material, therefore obtaining a cohesive rupture. In this work, since the test was done at a constant velocity, the normal force variation was evaluated.

Tack measurements are performed with the Anton Paar MCR 302e rheometer. The probe tack test device, made of steel, is profiled to avoid slipping of samples and measures 25 mm in diameter. Tests were carried out at a temperature of 25 °C, controlled thanks to Peltier effect in the lower plate. Thickness of the sample was disregarded as only a qualitative evaluation was desired here. Gel samples, as prepared according to table 3.4, are placed on the bottom plate, then the top plate is lowered to reach full contact with the gel. As the samples were not perfectly flat, the force at the detection of the surface was increased to ensure the geometry of the plate covers the sample completely and to obtain full contact. Depending on the sample, the detection force has been set on 0.25 N and 5 N. During the test, the top plate moves up vertically at a constant speed, subjecting the sample to stretching (Figure S3.3), and the normal force underwent by the top plate is recorded as a function of time. The tack test was programmed for the probe to decrease at 10 μm/s for 5 s. Direction is then reversed twice at the same speed for a similar duration. Final step is the increase of the probe at a velocity of 50 μm/s for 100 s.

Table 3.4 Gels preparation for tack test measurements.

Gel	Concentration	Preparation
Agar	4.3% w/v	Heating of polymer-H_2O solution to 90°C twice and left to solidify at RT in a petri dish
Gellan gum, hot	3% w/v	
Gellan gum, RT	3% w/v	Stirring of polymer and H_2O at RT and left for swelling for 1 hour
Xanthan gum	5% w/v	

3.3.1.1.2 Evaluation of the impact of gel residues on iron alloys

To appraise the actual impact of residues on metal and their effect in further corrosion, oximetry measurements were performed on iron alloy samples. Out of the studied alloys, iron-based alloys are the ones with a first corrosion step having a clear oxygen consumption following the reaction, allowing to link oxygen consumption and further degradation of the metal. Copper and silver alloys tarnish being more ascribable to sulfur consumption.

This technique was first introduced in 2010 by the Matthiesen research group from the National Museum of Denmark to estimate the corrosion rate of metal objects [93], evaluating the oxygen consumption occurring in a small volume of air containing the object. This method relies on optical measurements, making it possible to measure oxygen content through transparent materials [94].

2 × 2 cm low-carbon steel samples from Tartaix (France) were artificially corroded adapting ASTM G48-11 procedure by immersing the samples into 0.4 M $FeCl_3$ and then 9.8 M H_2O_2 to accelerate corrosion formation and obtain a thin layer of iron oxyhydroxides. Their surface was then prepared to remove pulverulent products with sandblasting, rinsing with 70% (v/v) ethanol and air drying. Experiments were replicated three times.

On each sample, 200 µL of gel or solution were deposited onto the surface to mimic potential residues, following Table 3.5. Xanthan gum (Vanzan NF-C, CTS) was chosen as it empirically appears to leave more residues. Controls were performed using gel alone or corroded sample without any deposit to ascertain that the eventual oxygen consumption can be related to the interaction between the substrate and the gel and is not intrinsic to the studied components of the system. Samples were immediately sealed into hermetic 5×5×0.3 cm ESCAL-aluminum pouches (Long Life for Art, Germany), with a volume of approximately 8.4 cm^3. Containing an oxygen sensor spot stuck onto the transparent film and 1 mL of a 30% (v/v) glycerol solution in a 2 × 2 cm receptacle to have high relative humidity over 90%

[95]. A schematic representation of the set-up is provided in Figure S3.4. An RH sensor was placed in one of the pouches to confirm these values. Oxygen saturation was read twice per day for 5 days and then once per day for 15 days or until the system became anoxic, with an optical oxygen meter from PreSens (Fibox3) along with their sensor foil SF-PSt3-NAU-YOP.

Table 3.5 Summary of different residues deposited onto corroded steel samples.

Sample name	Deposited residue or sample
Fe	Corroded steel sample
Xan	Xanthan 5% w/v
Fe-Xan	Xanthan 5% w/v spread on sample surface
Fe-Xan-d	Xanthan 5% w/v spread on sample surface and dried by leaving unprotected overnight
Fe-Xan-DFO	Xanthan 5% w/v + $3 \cdot 10^{-2}$ M DFO spread on sample surface
Fe-Xan-EDTA	Xanthan 5% w/v + $3 \cdot 10^{-2}$ M EDTA spread on sample surface
Fe-DFO	$3 \cdot 10^{-2}$ M DFO solution
Fe-EDTA	$3 \cdot 10^{-2}$ M EDTA solution

3.3.1.2 Results and discussion

3.3.1.2.1 Capacity to produce residues

Normal force measured through tack tests can be consulted in Figure 3.16 and associated data in Table 3.6. The time needed to go back to zero (i.e., the elongation time), which means for the gel to detach from the probe, is also representative of the adhesive effect. Indeed, in the first place, the force will increase with the probe displacement because of a nucleation phenomenon, which means there are voids appearing at the interface between the material and the probe. Nucleation stops when the force reaches its maximum and then cavities start to grow at the interface, resulting in a decrease of the force. The longer the time to reach zero, the longer a sample elongates and is prone to stick onto a surface.

For xanthan and RT-prepared gellan gels, typical cohesive ruptures patterns are obtained (Figure 3.16) [92]. Xanthan has the maximum tack value as defined by a long elongation time and the largest area under the tack curve. RT-prepared gellan has lower elongation time and under-curve area. Additionally, it exhibits a different curve shape than xanthan, with higher normal force maximum and faster decrease after reaching this maximum. This is because the type of cohesive rupture is different. For xanthan the rupture is long and smooth whereas for gellan the rupture is more brittle, corresponding to Figure 3.15b and 3.15c respectively.

Gellan gum prepared by boiling the solution shows a short elongation time upon separation, thus exhibiting an adhesive rupture, which occurs at the interface between the gellan and the substrate. Agar gel displays a rather brief elongation time and rather small area under the curve. From the obtained data, it can be said that both RT-prepared gellan and xanthan are tacky gels, with high adhesion to the surface, which is coherent with what is observed in practice. On the other hand, the hot preparation of both gellan and agar gives a peelable gel with a low adhesion to the surface. It can then be hypothesized that double helix networks give a good cohesion to the gel itself but a weak adhesion with the surface.

This explains why pre-formed agar gels do not have a great adhesion to the surface [1], because the network is already set and does not conform to the texture of the surface's micro-roughness. The stickiness of the gel to the surface will therefore rather depend on the surface roughness when the gel is poured hot on the surface.

Table 3.6 Tack tests measurements data summarizing up the area under the curve and the elongation time.

Gel	Area under the curve	Elongation time (s)
Agar	0.8	11
Gellan gum, hot	4.26	5.3
Gellan gum, RT	3.79	31.9
Xanthan gum	10.10	> 98.5

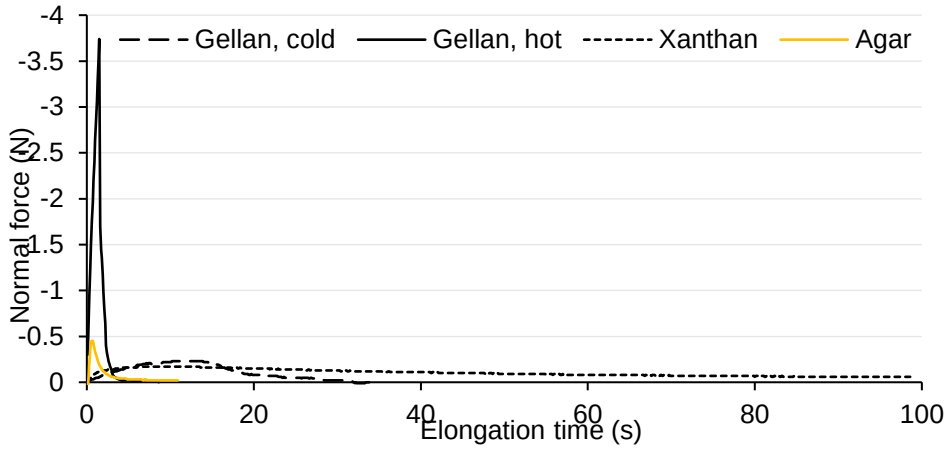

Figure 3.16 Tack tests measurements of agar, xanthan and gellan gels.

3.3.1.2.2 Evaluation of the impact of gel residues on iron alloys

The evolution of oxygen saturation of the different samples is shown in Figure 3.17. Most samples with wet residues (Fe-Xan, Fe-Xan-EDTA, Fe-EDTA, Fe-Xan-DFO), whether gel solution, have a high oxygen

consumption rate compared to control samples, confirming the noxious impact of residues. Differentiation can be made regarding the plain gel deposited on metal (Fe-Xan) that had a slightly lower oxygen consumption rate, about 7.7 O_2% per day versus 13.3 O_2 % for other residues. Exception is made for residual DFO solution (Fe-DFO) which displays an average O_2 consumption rate of 2 O_2% per day. One hypothesis for this behavior is the corrosion inhibition properties of siderophores [96], most precisely in this case deferoxamine [97]. The corroded sample used as control (Fe) does not show any sign of oxygen consumption. Interestingly, the gel control (Xan) starts to have a noticeable increase in oxygen consumption rate after 5 days, which is imputed to the growth of aerobic microorganisms. Indeed, there was a clear visual growth of microorganisms (Figure S3.5). This growth was not observed on the gel deposited on the metal sample (Fe-Xan) but cannot be completely excluded. One could think that metals can be toxic for microorganisms and therefore reduce the risk of contamination but the fact that MIC exists, along with the results obtained in Chapter 2, section 1.2 does not support this global toxicity of metals over microbes.

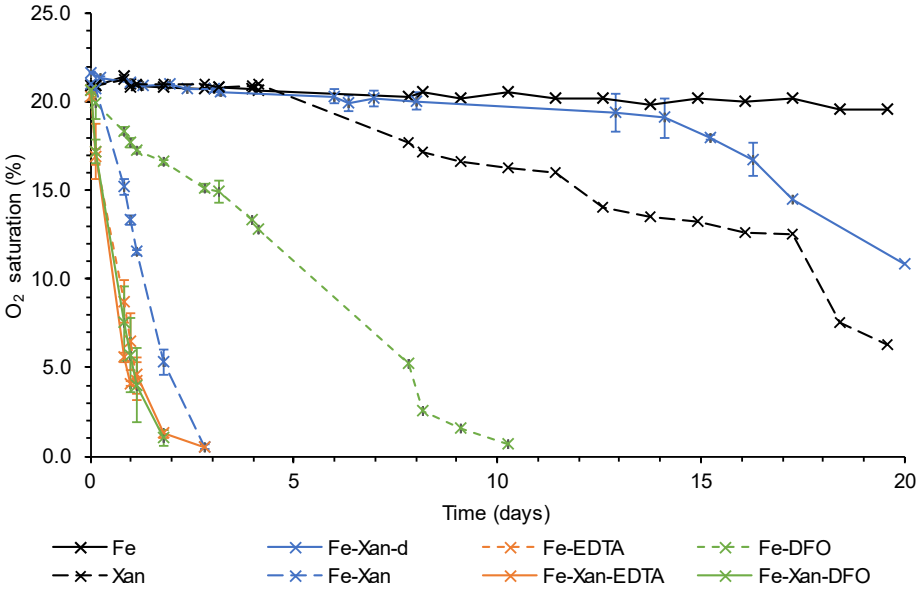

Figure 3.17 Oxygen saturation versus time of studied samples. Errors bars are related to independent replicas.

These oximetric results confirm the deleterious effect that gel residues can have on iron. Corrosion rate is slightly emphasized by the presence of active agents. However, gels usually do not stay swollen for such a long time, even in a high RH storage and usually start to dry after 30 minutes when exposed to ambient air [98]. For the dried gel (Fe-Xan-d), oxygen consumption starts to be noticeable after approximately two weeks. This is accounted for the time it takes for the gel to swell back due to surrounding moisture and start to corrode with electrolytes.

Gels have inadequate long-term effects on iron-based substrates related to the fact that they act as

reservoirs for moisture or potentially corrosive substances, more than the presence of polysaccharides in itself.

3.3.2 Detection of residues after gel removal

As discussed in the previous session, the presence of gel residues can be deleterious for metal substrates. Hence, it is of interest to detect these residues. Here, it is wished to evaluate the implementation of easy-to-use detection techniques as a routine step used by conservators after clearance while performing treatments via gels.

The detection and potential quantitative determination of small amounts of gel residues require a very sensitive analytical technique. In principle, there are several possible analytical approaches for measuring gel residues such as scanning electron microscopy (SEM), which did not provide satisfactory results as it was difficult to differentiate the residues from varnish or other organic materials on the images [99]. Moreover, the size and shape of a real object to be treated make SEM difficult to use for this purpose in a non-destructive way. In addition, SEM is a very localized technique and cannot really take notice of the global gel residues present on the full surface.

Direct chemical analyses of the material using gas chromatography coupled with mass spectroscopy (GC-MS) were performed on paintings and paper [100], but are not applicable to metal surfaces as it requires sampling of the surface.

Direct weight difference is too small (i.e., 10-100 $\mu g/cm^2$ [28]) to be measured and quantified accurately using even a very sensitive analytical balance and the cleaning procedure removing some of the material makes it even more difficult to evaluate the actual weight difference ascribed to gel residues presence.

Imaging via FTIR spectroscopy is theoretically an adequate tool to detect organic molecules such as polysaccharides. However, these instruments do not allow much eccentricity in terms of object morphology, limiting the possible specimen to analyze to rather flat surfaces. In addition, when it comes to spread of the technique, this would be very difficult to apply on archeological samples due to some overlapping bands between polysaccharides and functional groups unrelated to the treatment (i.e. sediments, undesired organic compounds, dirt) rendering the definitive identification of gel residues delicate [101], unless perhaps resorting to a "correlation" tool on the software.

Last but not least, using chemical tracers is of interest as it is largely tunable, for instance by using fluorochromes or radioactive markers, as tested by the Getty Institute [28,102].

Alternatively, the cleaning gel can be doped with a recognizable heavy element, which would permit the use of an elemental analysis method (i.e., energy dispersive spectroscopy or X-ray Fluorescence) to make a semiquantitative estimate of gel residues and even to map the presence of gel residue across the cleaned surface. The use of radioactively labeled materials as tracers, although offering certain

advantages such as less interference and more precision considering the background radioactivity of an object is low, has to be performed with care, in a laboratory approved for work with radioactive material and by trained and certified personnel [28]. In addition, the cost is rather high. The option of markers could help trace cleaning system but does not allow to differentiate whether the residues are the polymer or the fluid [28]. To palliate, grafting of fluorescent markers directly on the polymers can be envisaged [103], however, it is not a straightforward procedure. In addition, as discussed with oximetric measurements, both the polysaccharides and/or the contained solution can initiate the corrosion process.

Here, detection methods are assessed to evaluate the residue potential of agar and xanthan gels as they are both biobased and display very different properties as observed in section 3.1.2.1, agar being a widely used, rigid peelable gel, applicable on large surfaces and xanthan, also well used in the field, is sticky and viscous but easy to prepare in any situation as it does not require heating. Based on practice and/or conservators' feedback, agar is perceived to leave less residues, but that could not be the case at microscale after clearance. Although the original idea was to detect residues thanks to a technique that would allow conservators to check for gel remains after treatment, it turns out that because of the sensitive techniques needed, all techniques require rather peculiar equipment. However, in the case of conservators having access to this equipment, protocols were designed, as much as possible, to be simple, cost-effective and not detrimental to the objects.

Hereunder, two main approaches for the detection of residues on historical metals are proposed and studied, relying on the use of fluorescent or elemental markers via UV-induced visible fluorescence imaging or X-ray fluorescence detection.

An imaging approach allows a global overview of the artefacts, offering the possibility to understand the influence of the object's features on the presence of residues. For such, an insight is also provided using XRF mapping in order to check the influence of the overall morphology (e.g., decoration features, scratches) on the presence and position of residues.

3.3.2.1 Materials and methods

3.3.2.1.1 Samples

Brass ($Cu_{63}Zn_{37}$) samples obtained from Tartaix (France) were used.

For UV-fluorescence, samples were prepared in different ways to assess the effect of the surface roughness on the amount of residues detected. In particular, in addition to bare brass surface, scratches were produced thanks to a scalpel, and surface sandblasting was performed using corundum abrasive. Such zones were delimited by tape to an area of 2 cm^2.

To assess the UV-imaging technique further on real objects, more representative of existing features and

decorations, a cardholder made of silver-alloy and a steel calix were used as sacrificial test objects (Figure 3.18). The objects were selected because they exhibited carvings and/or embossments on the surface, which is believed to influence the adhesion of residues. In addition, they were flat enough to be compatible with the depth of field of the camera (see section 3.2.1.2). Both agar and xanthan were tested on the card holder, with fluoresceine as marker and xanthan gum was assessed on the calix with rhodamine as marker.

Figure 3.18 Calix (left) and card-holder (right) used as sacrificial objects for the detection of gel residues amended with fluorescent markers.

For XRF, in addition to a brass plate, a lead plate was used. Both metal plates were carved using a metal toothpick and scratches depth was measured using a P7 profilometer from KLA on a 2246 μm line with a velocity of 20 μm/s and an applied force of 1 mg for lead and 2 mg for brass. Lead was chosen to replace iron-based alloys as it is easier to carve. Overall, scratches engraved on lead were much deeper (110 ± 60 μm) than those on brass (13.6 ± 4.6 μm) due to the different hardness of the two metals. Gels were deposited on the plates and removed following a specific pattern with curve, right angles and crossing lines (Figure S3.6). Plates were then analyzed using XRF mapping.

3.3.2.1.2 Techniques

Detection via fluorescent markers

Out of the potential markers, fluorescent ones are suitable if the metal doesn't display important natural fluorescence quenching [104]. This would cause interference in the received signals, rendering the differentiation between natural fluorescence and marked residues complex. In the case of historical metal artefacts, contrary to archeological objects, the existing quenching is rather low, but not absent (e.g., corrosion products, cleaning products used during past conservation interventions, coatings, minerals…).

As mentioned, the natural quenching of compounds at the surface of the metal object could interfere. As such, three fluorescent markers (Grosseron, France) were selected in order to cover the visible spectrum and palliate any natural fluorescence of the assessed sample: quinine, fluoresceine, and rhodamine B, emitting respectively in the blue ($\lambda_{em\text{-}max}$= 460 nm), green ($\lambda_{em\text{-}max}$= 517 nm) and red-orange ($\lambda_{em\text{-}max}$= 565 nm) part of the spectrum (Figure S3.7).

Pictures of the samples were taken before and after gel application, to check for natural fluorescence, adapting a protocol from Truffa--Giachet *et al*. [105]: in a blackroom, imaging under UV illumination was performed on all samples with an unfiltered Nikon D810 (Nikon Corp., Tokyo Japan) equipped with a 60 mm AF-S Micro NIKKOR 1:2.8 ED objective. It is a macro-objective, not allowing high depths of field which was suitable for the studied samples as they were flat. The camera was placed onto a fixed support which ensures similar shot conditions hence reproducibility. Samples were placed on a black non-emitting cardboard and illuminated by 2 UV-A lamps (PHILIPS TLD 36W/08) with an emission peak at 365 nm and mounted at 45 °. A schematic representation of the set up can be observed in Figure S3.8. A standard UV chart from UV-innovation (United States)[6] was used as reference for further calibration and white balance correction of the obtained images. Pictures were taken in manual mode ISO 64, f/4 aperture, 4 s exposure allowing good detection of visible fluorescence and noise reduction. Pictures were post-processed using Lightroom Classic software (Adobe). Residues detection was performed on Adobe Photoshop software. Images were cropped to remove edge effects due to the presence of masking tape. The Eyedropper tool was used to select the range of shades corresponding to each used marker. Pixels fitting in that range were counted and the percentage of residues on the sample's surface calculated as follow $\frac{Residues\ pixels}{Total\ image\ pixels} \times 100$.

As this selection step was dependent on the human eye, it was performed by two different operators that are not colorblind. Indeed, although pixels can be identified by a specific value, the range of pixels fitting into the category of residues could be overestimated by the software in particular for the shades with a low luminosity, therefore this pixel selection step was required.

[6] https://www.uvinnovations.com/

A Zeiss Axio Imager M2 optical microscope equipped with a KSL 70 device with a UV lamp emitting at 365 nm was used for a more acute residues observation on samples, using the ×20 objective.

Detection via XRF

Detection of residues thanks to X-ray Fluorescence (XRF) spectroscopy is only possible with the implementation of markers in the gels' network. Indeed, elements composing polysaccharides (C, H, O, N) are too light to be detected by this method. Prerequisites for a marker to be eligible are water solubility or good dispersion in water, unlikely presence on heritage pieces, non-toxic and ideally affordable. Initially, it was thought to use potassium (KNO_3) as a marker. However, because of its relative lightness, in addition to its Kα peak (3.608 keV) overlapping with the Lβ of palladium (3.604 keV), it was discarded from the study. Indeed, these elements are inherent of the XRF device hence always detected. Because the aim is to detect very low amounts, probably the same order of magnitude as the Palladium signal threshold from the portable instrument the obtained spectra were not adequate to achieve any detection related to gel residues deposition. In this section, two salts with heavy elements, Hf (Hafnium) and W (Tungsten), HfO_2 and Na_2WO_4 were selected based on the criteria mentioned previously and assessed as potential markers for gel residues detection using point analysis XRF to ascertain the correct detection of the signal.

A M6 Jetstream micro-XRF scanner from Bruker was utilized for XRF mapping with 50 kV tension, 600 μA current with a step of 260 μm and acquisition time of 100 ms per point depending on the sample.

A Tracer III-V$^+$ portable XRF from Bruker was used for point analysis on agar gels. Settings were 40 kV, 13 μA and 60 s of acquisition time. Point analyses were performed on agar gels of thickness of 0.45 or 0.1 cm and on 0.6 mL of xanthan gum spread as homogeneously as possible in a 2 × 2 cm box to get a thickness of approximately 0.1 cm, as precise thickness was not achievable due to high viscosity. The window size was 3 × 4 mm.

To assess the good repartition of markers inside the gels, SEM-EDS maps of the marked agar gels were obtained using a field emission JEOL JSM 7600F scanning electron microscope with a 20 kV accelerating voltage, 1.6 nA current and 8mm working distance coupled with a SDD energy dispersive spectrometer (BRUKER, Quantax).

Measurements for residue quantification assays were performed with the portable XRF, using a collimator to reduce the window size (0.3 × 0.3 mm) and measure precisely in the scratches, avoiding flat surface around.

For both UV and XRF detection, two-way ANOVA was performed on datasets using Rstudio to verify the significance of obtained results.

3.3.2.1.3 Gel preparation and application

Xanthan (Vanzan NF-C, CTS) was prepared by stirring 5% w/v of gelling powder into the solution constituted of water and adequate markers. The mixture was then left to cool down before application. For agar gels (AgarArt, CTS), 3% w/v of gelling powder was added to the marked solutions, heated, left to cool and heated a second time before applying.

Application of agar gel was done when still hot (around 45 °C) onto the metal surface and deposition of xanthan gel as achieved at room temperature, in both case using a Pasteur pipette to reach a thickness of about 3 mm. Each gel application was performed in triplicate. A control reference where no gel was applied was also considered along with the application of gels with no markers. Gels were left on for 20 minutes. Agar was removed via peeling and xanthan using a spatula. Clearance was performed using a cotton swab dipped in 70%$_v$ ethanol until residues are no longer visible with naked eye.

For UV detection, concentration of the markers was chosen so it was visible under UV illumination at very low applied gel thickness (0.1 mm): 1.5 mM for quinine, 0.1 mM for fluoresceine and 1.67×10^{-2} mM for rhodamine B

For XRF, gels were prepared with solutions of both HfO_2 and Na_2WO_4 at concentrations of 3800 mg/L. HfO_2 being insoluble in water, it was necessary to use an ultrasonic bath to obtain a correct dispersion of the salt in the solution and in the gel.

For residue quantification assays using XRF, gels were prepared with 1000 mg/L Na_2WO_4 solution, to lower the concentration and assess the detection limit. Gels were then deposited onto carved lead metal plates. It was removed in two different ways:

- Classical clearance a conservator would do, removing as much gel as possible according to naked eye visibility with a cotton swab
- Cutting the gel right at the surface with a scalpel, voluntarily leaving residues into the scratches.

3.3.2.2 Results and discussion

3.3.2.2.1 UV-fluorescence imaging

Figure 3.19 shows the percentage of residues on the tested metal surfaces.

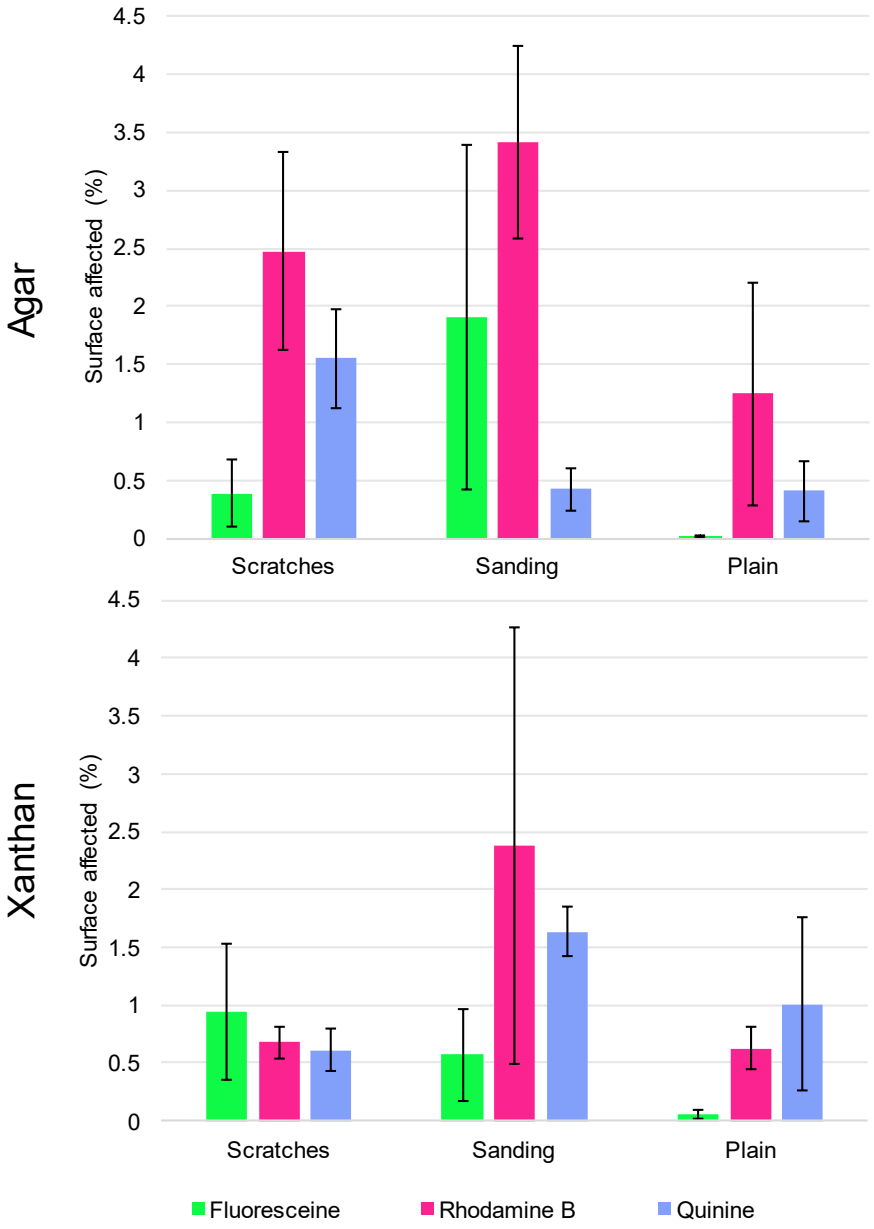

Figure 3.19 Percentage of surface covered with detected marked gels on different brass surface roughness.

Both for agar and xanthan gels, the percentage of surface affected by residues does not exceed 4%, taking into account standard deviation. Although results are slightly lower for xanthan gel, there is a more noticeable variation (high standard deviation values).

Taking a closer look at the different markers, they all display different surface covering percentages, although in the same interval (as deduced from the high standard deviation).

For agar, a statistically significant difference was observed as average surface covered with residues according to the type of markers, in particular between rhodamine and the two other markers quinine and fluoresceine (p=0.0408 and 0.0455 respectively), but not according to the surface type (i.e., plain, scratched, sanded) with p-values well above 0.05.

Few residues could be detected on the untouched surface. For both gels, the surface treated by sandblasting displayed more residues than the one with scratches. This is due to the higher specific surface available thanks to the numerous tiny holes created by sand-blasting [89].

In particular for xanthan, interestingly, it is rather the surface type that comes as statistically significant ($F = 4.43$, $p = 0.0271$) rather than the type of markers used ($F = 2.320$, $p = 0.1269$). Between the different surface texture, a statistically significant difference is observed between sanding and plain surfaces ($p = 0.03$).

Rhodamine is the most detected marker, most likely because the solution stained the surface pink after application with a red-pinkish hue. Regarding quinine, while processing images it was noticed that dust or impurities (e.g., cotton fibers) show a similar blueish hue than the marker. Therefore, it was not possible to distinguish pixels accounting for the presence of exogenous compounds or quinine-marked gel residues. As a consequence, fluoresceine seems to be the most reliable marker if the natural fluorescence of the objects allows for its use.

The major difference between the two gels was the aspect of detected residues. Indeed, agar residues were present in the form of tiny and/or thin parts of the gel that broke from the main applied piece whereas for xanthan it was more diffuse and spread over the surface. In addition, it is worth mentioning that the clearance of the gels was much different, it requires greater number of cotton swab movement to achieve visible reduction of agar (1 or 2 passages) and xanthan (closer to 5 passages) presence on the surface to obtain visually comparable surfaces, until the gel was no longer visible. These observations are in opposition with the results above where mean surface with detected residues barely exceeded 2% for xanthan of the surface where it reached 4% for agar. It is believed that because of the diffuse aspect of xanthan residues, the intensity of pixels was not high enough to be detected via the UV-imaging technique.

To understand better this aspect of xanthan residues, UV-light microscopy was used (Figure 3.20). The veil for xanthan was much more visible using the microscope while agar residues were localized, also at the microscale. This raises the question of the limit of detection of the UV-induced imaging technique. Although giving a comprehensive overview of the residues' distribution over the surface, it fails detecting thin residual pieces of gel.

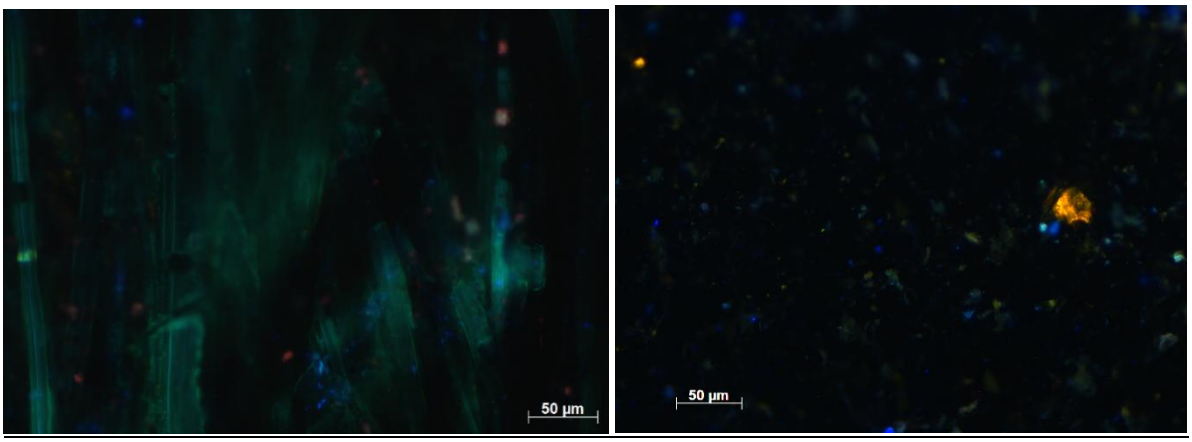

Figure 3.20 UV-light microscope observations of xanthan-fluoresceine veil (left) and agar-rhodamine on metal (right).

The selection of the shades related to the marker used in the post-processing steps involves a subjective choice based on one's perspective. To evaluate the importance of the influence of the human factor, two operators performed the post-treatment on similar images (Table 3.7), using fluoresceine markers to avoid staining (visible with rhodamine) or dust influence (for quinine) as explained in the previously. Results obtained on plain brass samples were particularly adverse. This is most likely due to the perception of the limit of detection, until which pixel hue is it really a residue? Excluding plain samples, evaluating xanthan results, the difference between the two operators on sand-blasted or scratched surface was rather high (60 and 84% of surface covering respectively) with substantial standard deviation difference for the sand-blasted surface (133%). Looking at agar deposited residues, results were rather coherent with a difference not greater than 26% and similar standard deviation. In addition, post-hoc two-way ANOVA tests gave p-values > 0.9 for all groups. For such, it can be stated that the human factor does not have a statistically significant strong influence on the global qualitative residue detection and does not allow any quantitative and even semi-quantitative approach. To achieve more standardized procedures and eliminate the human factor, it would be interesting to create a script allowing an automatic colorimetric range of shades detection for each marker based on a color space.

Table 3.7 Surface covering percentage affected by fluoresceine-marked gels; post-processing performed by different operators

Surface type	Operator	Agar		Xanthan	
		Mean	Standard deviation	Mean	Standard deviation
Scratches	A	0.489	0.318	1.747	0.744
	B	0.388	0.287	0.948	0.589
	Difference (%)	26	10	84	26
Sandblasting	A	1.646	1.389	0.356	0.170
	B	1.907	1.490	0.570	0.397
	Difference (%)	16	7	60	133
Plain	A	0.055	0.023	0.151	0.088
	B	0.019	0.007	0.056	0.033
	Difference (%)	190	228	169	166

Evaluation of the technique on objects

Based on results on flat samples, it was originally thought to use fluoresceine on objects as it does not suffer from the presence of dust and does not stain the surface. For such, it was considered the most appropriate marker. It was possible to pursue with this idea on the card holder but not for the calix. On the steel calix, the control picture before application displays yellowish and blue reminiscing fluorescence (Figure 3.22), most likely deposits from previous cleaning interventions (e.g., abrasive paste remains), and the presence of dust respectively. For such, rhodamine was preferred although it might stain the object. Because it was a sacrificial object for study purposes, it was acceptable to do so.

As can be seen on Figure 3.21, the presence of agar seems well lower than the one of xanthan on the card holder. Image processing shows 0.82% of surface covering where agar was applied versus 5.74% on the zones where xanthan was applied. Visual aspect of the residues confirms what was observed on flat samples: pieces of gel remaining for agar versus spread of the gel all over the surface in thin layer for xanthan.

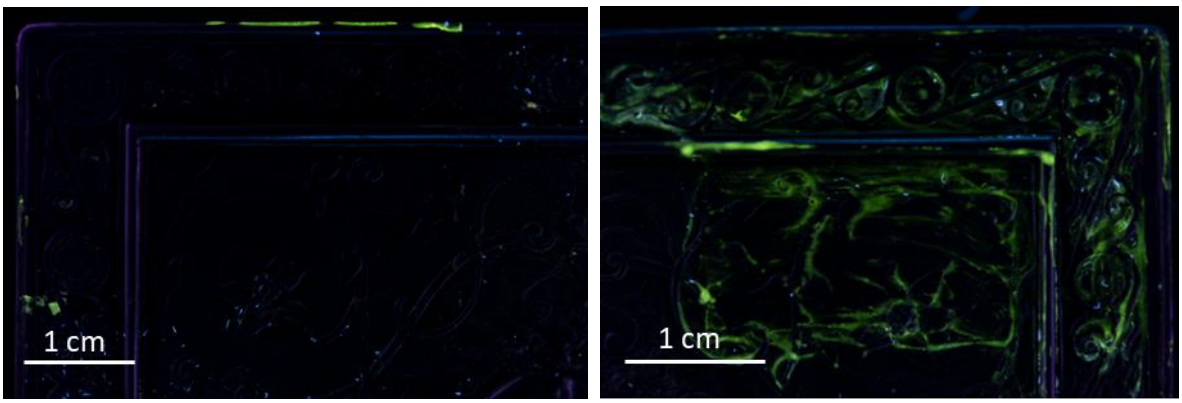

Figure 3.21 Cardholder after application of agar (left) and xanthan (right) gels amended with fluoresceine solution.

On the calix (figure 3.22), after removal and clearance of the xanthan gel, over 7% of the surface was affected by residues, with a clear accumulation in carvings. Results are to be interpreted with caution as it could be due to the staining of surface by the rhodamine-marked gel. However, the distribution of affected pixels fits with the carvings present on the surface, thus reinforcing the idea that the clearance of xanthan gum can hardly be complete in these features.

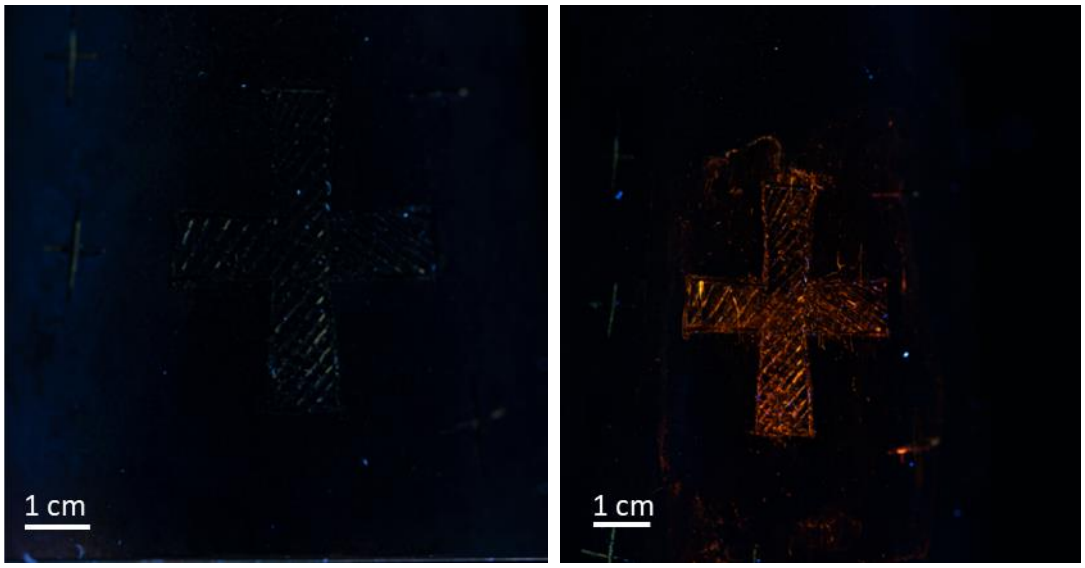

Figure 3.22 Close-up picture of a cross carving on the calix object before (left) and after (right) application of Xanthan gel amended with rhodamine solution.

Overall, the UV-imaging technique may not be reliable depending on the used fluorochrome. Moreover, the limit of detection is relatively low. There is a high lack of coherence and therefore reliability in the results, as can be deducted from the high standard deviation values calculated. In addition, results figure 3.19 were differing from what is being observed in practice, *id est* xanthan gum being complicated to remove and agar leaving few residues (as seen using UV-light microscopy, Figure 3.20). Moreover, the application of UV-light imaging to objects with more protuberant features would require several images and extensive post-processing of the pictures collected.

Residue quantification would therefore require additional studies, refining the concentration of markers and post-processing of acquired images. However, it is a good technique to have a global and qualitative overview of the presence of residue and the features associated with higher probability of gel residues.

3.3.2.2.2 XRF detection

Because the hafnium-based salt is insoluble, it required the use of ultrasonic bath to obtain a correct dispersion during gel preparation and the equal distribution repartition of the markers inside the agar gels was therefore assessed. In order to do so, both XRF mapping and SEM-EDS mapping were performed (Figure 3.23). Both techniques show the homogeneous repartition of sodium tungstate. On the other hand, the hafnium oxide maps show the presence of clumps on both techniques, as expected since it is insoluble.

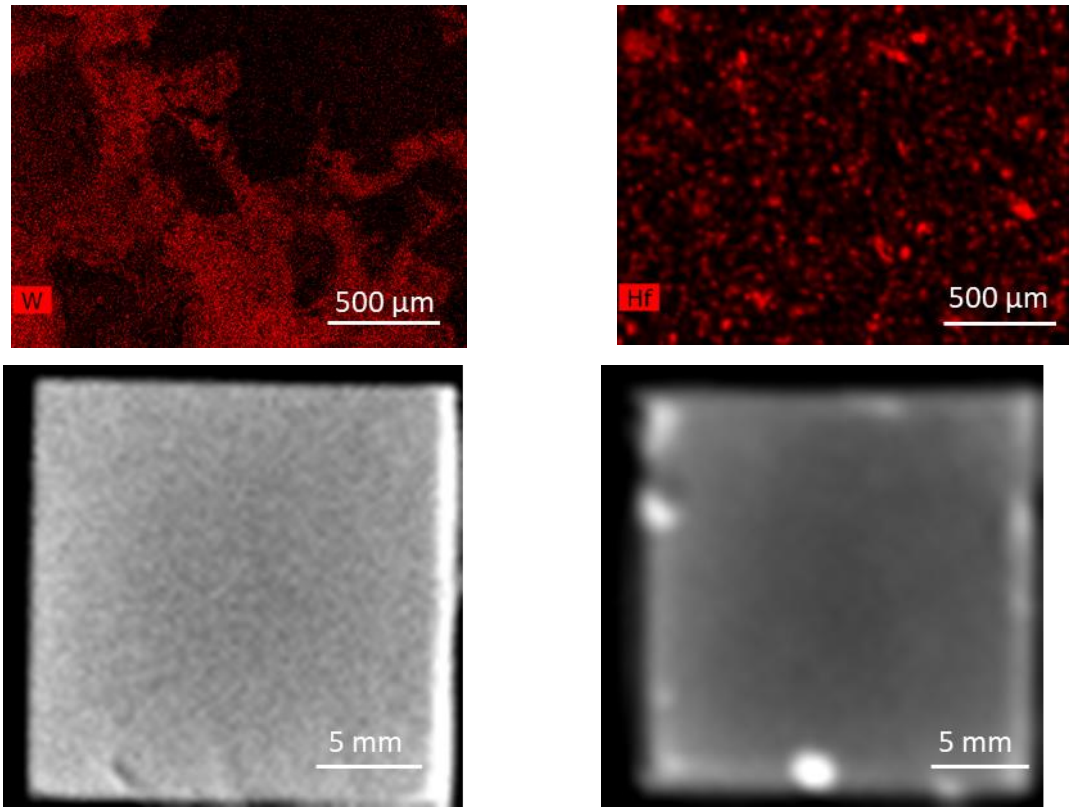

Figure 3.23 SEM-EDS (top) and XRF (bottom) maps of agar gel marked with Na_2WO_4 (left) and HfO_2 (right).

The area of the Kα peak from the collected XRF spectra on marked agar gels after point analysis are reported in table 3.8. Kα peak surface area was found to be significant by both markers or gel thickness with *p*-values<0.05. Interestingly, the Kα peak area was different depending on the thickness of the sample for both HfO_2 or Na_2WO_4 marked agar: the thinner is the gel, the greater is the peak area. This is due to the matrix effect. Indeed, the thicker the matrix the lower will be the detected signal. This can seem counter intuitive but, roughly, the atoms present in the matrix shield the signals from the heavy elements present in low amount [106]. This is due to mainly two absorption phenomena: attenuation of the incident X-ray source and absorption of the heavier elements fluorescent emission [107]. Interestingly, for the purpose of residue detection, this physical phenomenon is rather beneficial. Thinner residues will not necessarily mean weaker signals, hence increasing the limits of detection.

Table 3.8 Kα peak surface area in 0.1, 0.45 and 1 cm thick agar gels containing HfO_2 or Na_2WO_4 (3800 mg/L).

Gel thickness (cm)	HfO_2	Na_2WO_4
0.1	1 940 000 ± 26 000	1 300 000 ± 6 100
0.45	1 680 000 ± 39 000	1 270 000 ± 13 000
1	1 530 000 ± 20 500	n/a

Kα peaks from both markers have interferences with other x-ray peaks from elements present in the brass alloy. In particular, hafnium Kα1 (7.8990 keV) can interfere with copper Kα1 (8.0267 keV) and Kα2 (8.0463keV) peaks whereas tungsten Kα1 peak (8.3989 keV) can interfere with zinc Kα1 (8.0463 keV) and Kα2 (8.0267 keV). The interference is more problematic in the case of Hf and Cu as the rays are close and Cu's Kα1 is strong in intensity.

XRF map on brass is unreadable for both markers (Figure S3.8). Indeed, peak interferences are too strong. Peak deconvolution was performed but did not help to obtain more exploitable maps. To counteract that, it would be theoretically possible increase the concentration of the markers in the gel to allow for an easier deconvolution vs peaks ascribed to copper or zinc. Still, using Hf as a marker is more ideal on non-copper-based alloys and W on alloys not containing zinc.

On lead (Figure 3.24), markers could be detected, especially in the carved decorations. Hafnium is more visible than tungsten. Supposedly, this is due to the insoluble nature of the hafnium oxide, deposited at the bottom of the scratches, even after removal. One hypothesis is that the hydrogel was adsorbed by the cotton swab, leaving the marker down. When comparing agar and xanthan application, the Hf-amended xanthan gel shows more residues than the Hf-amended agar one. In addition, there are traces of wiped xanthan gel the half bottom of the plate (Figure 3.24, arrow), confirming that xanthan spreads over the metal surface because of its viscous texture. On the other hand, agar gel residues seemed to be detected after clearance, both for W and Hf, at the bottom of the scratches. Regardless of the marker, there is a trend for agar to leave residues in the embossing.

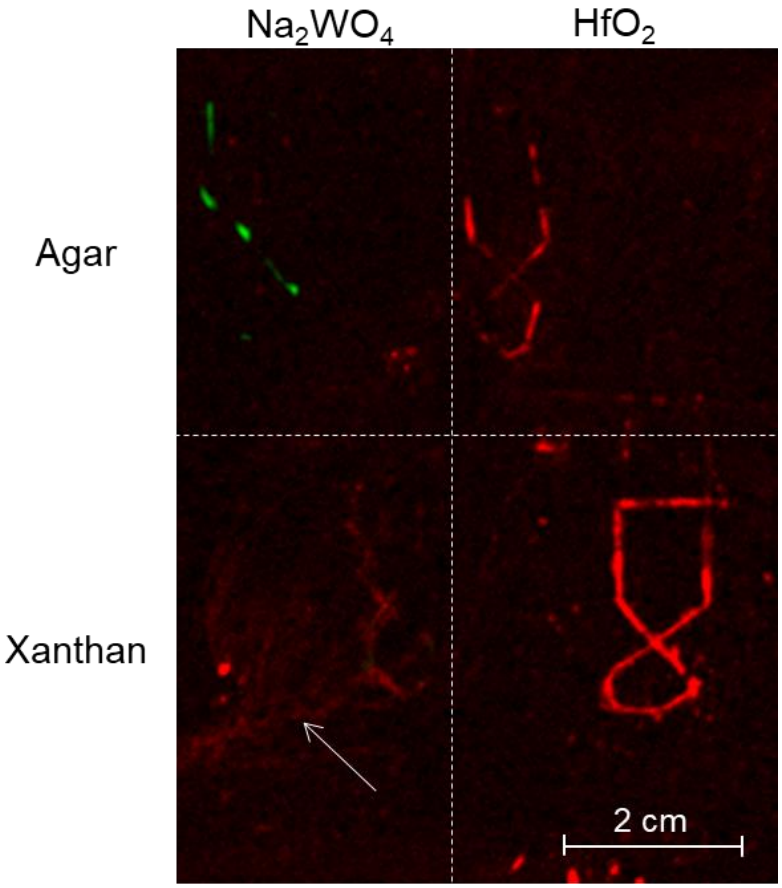

Figure 3.24 XRF mapping of lead after deposition of W (green) or Hf- (red) marked agar and xanthan gels on the left and right side of the plate respectively. Arrow indicates traces of wiped Hf-amended xanthan gel.

It is difficult to make assertive conclusions based on this study, however, trends can be observed. In particular, the selected markers, Hf and W are not relevant to use on copper alloys for the residue study. Indeed, to be able to detect them despite the overlapping peaks with Cu and Zn respectively, a large quantity of gel is necessary, which conflicts with the residue's detection.

Comparing both markers, Na_2WO_4 achieved a more homogeneous repartition inside the gel and HfO_2's repartition was still acceptable but found itself problematic when removing the gel because there was a deposit. Overall, sodium tungstate is easier to put in place and more affordable although care must be taken towards the presence of zinc in the studied surface.

XRF mapping on lead allowed to confirm the results previously observed with fluorescent markers: agar residues being more punctual, mainly located in embossments and xanthan residues more getting spread, as expected.

To evaluate semi-quantitatively the amount of gel left on the surface after clearance, Na_2WO_4-amended agar and xanthan loaded with sodium tungstate were deposited on a carved lead plate. Area of the obtained peaks after point XRF analysis using a collimator can be seen in Table 3.9.

Table 3.9 Area of W Kα peak from XRF signals after measurements on lead plate with Na_2WO_4-amended deposited gels.

	Agar	**Xanthan**
Cotton-swab clearance until obtention of no visible residues	2000 ± 500	4000 ± 500
Voluntary residues	5000 ± 500	5000 ± 500

The amount of gel residues detectable in the scratches after a clearance a conservator would perform is lower than voluntary residues for both agar and xanthan. There is a significant difference between the two types of clearance for agar, whereas the detected amount of xanthan is similar regardless of the method used to remove the gel. This shows it is more difficult to remove this type of gel even with a careful thorough clearance.

Further works might develop the technique for residue detection to evaluate the minimal volume that can be detected by portable XRF, in particular thanks to the use of standard curves. However, particular attention should be given to the matrix effect.

This could allow the quantification of residues left and would help evaluating their actual impact on surfaces. Indeed, in section 3.1.2.2, the impact of an arbitrary quantity of 50 µL/cm² of residues was evaluated, but depending on the actual amount of left residues, effects on the metal surface could be significantly different.

3.3.2.2.3 Other possibilities for residues detection

The tremendous number of factors contributing to the possible presence of residues renders preventive actions to avoid them complex. The main lever of action therefore stands with the clearance of the gel [101], for instance working under a microscope or binocular when removing the gel, addressing a particular attention to carvings or areas with features. The use of Japanese paper underneath the applied gel can also be foreseen, keeping in mind that this alternative reduces the contact between the surface and the gel and therefore the efficacy of the treatment [13].

The advantage of working with biobased formulations is that it allows to diminish the quantity of harmful compounds likely to be deposited on the surface and therefore to damage the objects as time goes by, in particular with porous or uneven surfaces. Moreover, for health concerns, it is better to avoid the presence of noxious residues on artefacts, as shown by the presence of pesticides on natural history collections for instance [108].

Other techniques are yet to be assessed regarding their use for residues detection. First, the use of staining markers. The idea behind the use of staining markers is, similarly to what is done in biology, to label specific chemical groups that would allow the detection of the targeted compounds. Indeed,

some compounds will react with specific organic materials (e.g., proteins) and create colored compounds that allows their easy detection. Some articles report the existence of markers to stain polysaccharides, namely “Stains-all” and “Lugol” [109]. The former is a carbocyanine dye that is used for the staining of proteins. It also stains polysaccharides turning from red-purple to blue-purple in their presence. The main drawback rendering its use tricky is the fading occurring under light in a matter of minutes [110], that would imply working in the absence of light. In addition, because it can stain several types of functional groups, it is not the most selective marker. The latter, Lugol is an iodine solution used as an antiseptic or a reagent to detect starches. Iodine’s interaction with polysaccharides makes it a potential marker for gel detection. Additionally, the use of a iodine-based compound on silver- or copper-alloys is complex as it would result in the tarnishing of surfaces [111]. Indeed, iodine reacts with silver and copper to form AgI or CuI respectively [112,113].

Although interesting as it would only require the staining marker as a ready-to-use solution, safety and removal from objects remain to be tested prior to any implementation in workshop and adoption by conservators as an easy routine step after gel treatment. In addition, as discussed priorly, not only the gel matrix is relevant in the case of residues but also the amended active agent.

Other spectroscopic techniques can also be foreseen, for instance Hyper Spectral Imaging (HSI) that gives the full spectral emission of each analyzed pixel in a particular spectral range (visible, near infra-red etc). It is to be determined whether a marker would be needed with this technique or whether gels have a unique spectral fingerprint. In addition, apparatus now allow the coupling of this technique with XRF [114], which seems to be an interesting perspective for residues detection.

3.4 Conclusion and perspectives

The agar gel was demonstrated to be a reliable carrier for the deferoxamine siderophore, allowing to achieve a fully bioderived formulation for corrosion removal. Novel chitosan-based formulation have shown actual complexation of silver ions without the need of chelating agents in the formulation. These novel gels should be studied further to achieve better formulation and to be tested on actual metal corrosion. Formulation improvement or further tests could be examination of chitosan without the addition of L-Cysteine for instance. The formulation of a combined chitosan/agar gel could also be of interest for further study as it has been reported that this mix forms rigid hydrogel films with enhanced swelling properties compared to pure chitosan [56].

Double helix network gels (i.e., gellan gum and agar) tend to have less adhesive features, due to the interhelical network that displays forces higher than the ones between the gel and the surface. This is a factor why agar seems to be a more reliable option than xanthan with respect to the amount of residues left on surfaces after treatment although it is not easy to detect residues and therefore to be assertive in that regard. Indeed, oximetric measurements showed that residues are a potential danger to iron-based objects. To evaluate the noxiousness of residues on copper and silver objects, a similar experimental design could be performed, using an H_2S detector instead as Cu and Ag tarnishing posing visual concerns is due to a reaction with reduced sulfur compounds rather than with oxygen.

Techniques assessed here for residue detection serve as qualitative for research insights rather than routine solutions conservators can apply in their practice in order to ascertain performing a comprehensive removal of their gel treatments. Indeed, there would be the subsequent need to remove markers with solvents, and then potentially have solvent residues, which is also an issue as it is always preferred to limit interventions [28].

Overall, the XRF technique seems to be relevant for detection of residues provided that an appropriate marker is used. XRF mapping confirmed the results obtained with Ultraviolet visible fluorescence imaging, showing the repartition of the gel residues rather in the carvings of the object's surface, as expected. In addition, a first attempt at quantifying residues was proposed, with a need for fine-tuning. Regarding the actual quantification of residues, other techniques might as well be promising with the emergence of more complex analytical devices, for instance coupled HSI-XRF imaging that would allow localization and potential quantification of gels.

To ascertain the reliability of the proposed formulations, the combined action of selected active agents and gels must be assessed on actual corroded samples and studied using a standardized, quantifiable procedure.

3.5 Bibliography

1. Guilminot, E.; Gomez, A.; Raimon, A.; Leroux, M. Use of Gels for the Treatment of Metals. In Proceedings of the Metal 2019 Proceedings of the Interim Meeting of the ICOM-CC Metals Working Group; Chemello, C., Brambilla, L., Joseph, E., Eds.; International Councils of Museums - Committee for Conservation, 2019; p. 473.
2. Sokhanvarian, K.; Nasr-El-Din, H.A.; De Wolf, C.A. Thermal Decomposition of Chelating Agents and a New Mechanism of Formation Damage. In Proceedings of the SPE European Formation Damage Conference & Exhibition; SPE: Noordwijk, the Netherlands, 2013.
3. Wang, X.; Hu, Y.; Zhang, Z.; Zhang, B. The Application of Thymol-Loaded Chitosan Nanoparticles to Control the Biodeterioration of Cultural Heritage Sites. *J. Cult. Herit.* **2022**, *53*, 206–211, doi:10.1016/j.culher.2021.12.002.
4. Boccaccini, F.; Giuliani, C.; Pascucci, M.; Riccucci, C.; Messina, E.; Staccioli, M.P.; Ingo, G.M.; Di Carlo, G. Toward a Green and Sustainable Silver Conservation: Development and Validation of Chitosan-Based Protective Coatings. *Int. J. Mol. Sci.* **2022**, *23*, doi:10.3390/ijms232214454.
5. Giuliani, C.; Pascucci, M.; Riccucci, C.; Messina, E.; Salzano de Luna, M.; Lavorgna, M.; Ingo, G.M.; Di Carlo, G. Chitosan-Based Coatings for Corrosion Protection of Copper-Based Alloys: A Promising More Sustainable Approach for Cultural Heritage Applications. *Prog. Org. Coatings* **2018**, *122*, 138–146, doi:10.1016/j.porgcoat.2018.05.002.
6. dos Santos, L.N.; Santos, A.S.; das Graças Fernandes Dantas, K.; Ferreira, N.R. Adsorption of Cu (II) Ions Present in the Distilled Beverage (Sugar Cane Spirit) Using Chitosan Derived from the Shrimp Shell. *Polymers (Basel).* **2022**, *14*, 573, doi:10.3390/polym14030573.
7. Trimukhe, K.; Varma, A. A Morphological Study of Heavy Metal Complexes of Chitosan and Crosslinked Chitosans by SEM and WAXRD. *Carbohydr. Polym.* **2008**, *71*, 698–702, doi:10.1016/j.carbpol.2007.07.010.
8. Chan, K.; Morikawa, K.; Shibata, N.; Zinchenko, A. Adsorptive Removal of Heavy Metal Ions, Organic Dyes, and Pharmaceuticals by Dna–Chitosan Hydrogels. *Gels* **2021**, *7*, 1–10, doi:10.3390/gels7030112.
9. Mekahlia, S.; Bouzid, B. Chitosan-Copper (II) Complex as Antibacterial Agent: Synthesis, Characterization and Coordinating Bond- Activity Correlation Study. *Phys. Procedia* **2009**, *2*, 1045–1053, doi:10.1016/j.phpro.2009.11.061.
10. Grange, C.; Aigle, A.; Ehrlich, V.; Salazar Ariza, J.F.; Brichart, T.; Da Cruz-Boisson, F.; David, L.; Lux, F.; Tillement, O. Design of a Water-Soluble Chitosan-Based Polymer with Antioxidant and Chelating Properties for Labile Iron Extraction. *Sci. Rep.* **2023**, *13*, 7920, doi:10.1038/s41598-023-34251-3.
11. Sansonetti, A.; Bertasa, M.; Corti, C.; Rampazzi, L.; Monticelli, D.; Scalarone, D.; Sassella, A.; Canevali, C. Optimization of Copper Stain Removal from Marble through the Formation of Cu(II) Complexes in Agar Gels. *Gels* **2021**, *7*, 111, doi:10.3390/gels7030111.
12. Bertasa, M.; Chiantore, O.; Poli, T.; Riedo, C.; Di Tullio, V.; Canevali, C.; Sansonetti, A.; Scalarone, D. A Study of Commercial Agar Gels as Cleaning Materials. In Proceedings of the Gels in the Conservation of Art; Angelova, L. V., Ormsby, B., Townsend, J.H., Wolbers, R., Eds.; Archetype Publications: London, 2017; pp. 11–18.
13. Sansonetti, A.; Bertasa, M.; Canevali, C.; Rabbolini, A.; Anzani, M.; Scalarone, D. A Review in Using Agar Gels for Cleaning Art Surfaces. *J. Cult. Herit.* **2020**, *44*, 285–296, doi:10.1016/j.culher.2020.01.008.
14. Cremonesi, P. Rigid Gels and Enzyme Cleaning. *Smithson. Contrib. to Museum Conserv.* **2012**, *3*, 179–183.
15. Canevali, C.; Fasoli, M.; Bertasa, M.; Botteon, A.; Colombo, A.; Di Tullio, V.; Capitani, D.; Proietti, N.; Scalarone, D.; Sansonetti, A. A Multi-Analytical Approach for the Study of Copper Stain Removal by Agar Gels. *Microchem. J.* **2016**, *129*, 249–258, doi:10.1016/j.microc.2016.07.007.

16. Bosch-Roig, P.; Lustrato, G.; Zanardini, E.; Ranalli, G. Biocleaning of Cultural Heritage Stone Surfaces and Frescoes: Which Delivery System Can Be the Most Appropriate? *Ann. Microbiol.* **2015**, *65*, 1227–1241, doi:10.1007/s13213-014-0938-4.
17. Giordano, A.; Cremonesi, P. New Methods of Applying Rigid Agar Gels: From Tiny to Large-Scale Surface Areas. *Stud. Conserv.* **2021**, *66*, 437–448, doi:10.1080/00393630.2020.1848272.
18. Tamura, M.; Takagi, K. Towards the Sustainable Use of Agar / Agarose in Conservation: A Case Study of the Izu Peninsula, Japan. In *Gels in the Conservation of Art*; Angelova, L. V., Ormsby, B., Townsend, J.H., Wolbers, R., Eds.; Archetype Publications: London, UK, 2017; pp. 152–154 ISBN 9781909492509.
19. Cuvillier, L.; Passaretti, A.; Guilminot, E.; Joseph, E. Testing of the Siderophore Deferoxamine Amended in Hydrogels for the Cleaning of Iron Corrosion. *Eur. Phys. J. Plus* **2023**, *138*, 569, doi:10.1140/epjp/s13360-023-04159-y.
20. Zainal, S.H.; Mohd, N.H.; Suhaili, N.; Anuar, F.H.; Lazim, A.M.; Othaman, R. Preparation of Cellulose-Based Hydrogel: A Review. *J. Mater. Res. Technol.* **2021**, *10*, 935–952, doi:10.1016/j.jmrt.2020.12.012.
21. Anastas, P.; Eghbali, N. Green Chemistry: Principles and Practice. *Chem. Soc. Rev.* **2010**, *39*, 301–312, doi:10.1039/B918763B.
22. Kuppuswami, G.M. Fermentation (Industrial) and Production of Xanthan Gum. In *Encyclopedia of Food Microbiology*; Elsevier, 2014; pp. 816–821.
23. Tako, M.; Sakae, A.; Nakamura, S. Rheological Properties of Gellan Gum in Aqueous Media. *Agric. Biol. Chem.* **1989**, *53*, 771–776, doi:10.1080/00021369.1989.10869354.
24. Fiamingo, A.; Montembault, A.; Boitard, S.E.; Naemetalla, H.; Agbulut, O.; Delair, T.; Campana-Filho, S.P.; Menasché, P.; David, L. Chitosan Hydrogels for the Regeneration of Infarcted Myocardium: Preparation, Physicochemical Characterization, and Biological Evaluation. *Biomacromolecules* **2016**, *17*, 1662–1672, doi:10.1021/acs.biomac.6b00075.
25. Messina, E.; Giuliani, C.; Pascucci, M.; Riccucci, C.; Staccioli, M.P.; Albini, M.; Di Carlo, G. Synergistic Inhibition Effect of Chitosan and L-Cysteine for the Protection of Copper-Based Alloys against Atmospheric Chloride-Induced Indoor Corrosion. *Int. J. Mol. Sci.* **2021**, *22*, 10321, doi:10.3390/ijms221910321.
26. Nie, J.; Wang, Z.; Hu, Q. Chitosan Hydrogel Structure Modulated by Metal Ions. *Sci. Rep.* **2016**, *6*, 36005, doi:10.1038/srep36005.
27. Verma, C.; Quraishi, M.A. Chelation Capability of Chitosan and Chitosan Derivatives: Recent Developments in Sustainable Corrosion Inhibition and Metal Decontamination Applications. *Curr. Res. Green Sustain. Chem.* **2021**, *4*, 100184, doi:10.1016/j.crgsc.2021.100184.
28. Stulik, D.; Miller, D.; Khanjian, H.; Khandekar, N.; Wolbers, R.; Carlson, J.; Petersen, C. Solvent Gels for the Cleaning of Works of Art: The Residue Question. In *Solvent Gels for the Cleaning of Works of Art: The Residue Question*; Wolbers, R., Ed.; Getty Institute of Conservation, 2004; Vol. 1, p. 180 ISBN 0-89236-759-8.
29. Lai, H.; Liu, S.; Yan, J.; Xing, F.; Xiao, P. Facile Fabrication of Biobased Hydrogel from Natural Resources: L-Cysteine, Itaconic Anhydride, and Chitosan. *ACS Sustain. Chem. Eng.* **2020**, doi:10.1021/acssuschemeng.0c00774.
30. Rapti, S.; Boyatis, S.; Rivers, S.; Velios, A.; Pournou, A. Removing Iron Stains from Wood and Textile Objects: Assessing Gelled Siderophores as Novel Green Chelators. In Proceedings of the Gels in the Conservation of Artconservation; Angelova, L., Ormsby, Bronwyn Townsend, Joyce Wolbers, R., Eds.; Archetype Publications: London, 2017; pp. 343–348.
31. Guilminot, E. The Use of Hydrogels in the Treatment of Metal Cultural Heritage Objects. *Gels* **2023**, *9*, 191, doi:10.3390/gels9030191.
32. Sirviö, J.A.; Kantola, A.M.; Komulainen, S.; Filonenko, S. Aqueous Modification of Chitosan with Itaconic Acid to Produce Strong Oxygen Barrier Film. *Biomacromolecules* **2021**, *22*, 2119–2128, doi:10.1021/acs.biomac.1c00216.

33. Teleky, B.-E.; Vodnar, D. Biomass-Derived Production of Itaconic Acid as a Building Block in Specialty Polymers. *Polymers (Basel).* **2019**, *11*, 1035, doi:10.3390/polym11061035.
34. Rahbani, J.; Behzad, A.R.; Khashab, N.M.; Al-Ghoul, M. Characterization of Internal Structure of Hydrated Agar and Gelatin Matrices by Cryo-SEM. *Electrophoresis* **2013**, *34*, 405–408, doi:10.1002/elps.201200434.
35. Chaudhary, J.; Thakur, S.; Sharma, M.; Gupta, V.K.; Thakur, V.K. Development of Biodegradable Agar-Agar/Gelatin-Based Superabsorbent Hydrogel as an Efficient Moisture-Retaining Agent. *Biomolecules* **2020**, *10*, 939, doi:10.3390/biom10060939.
36. Mezger, T.G. *Applied Rheology: With Joe Flow on Rheology Road*; Paar, A., Ed.; GmbH, 2018; ISBN 9783950401608.
37. Kavukcuoglu, N.B.; Pleshko, N. Infrared and Raman Microscopy and Imaging of Biomaterials. In *Comprehensive Biomaterials*; Elsevier, 2011; pp. 365–378.
38. Marie, A.; Said, B.; Galarneau, A.; Stettner, T.; Balducci, A.; Bayle, M.; Humbert, B.; Le Bideau, J. Silica Based Ionogels: Interface Effects with Aprotic and Protic Ionic Liquids with Lithium. *Phys. Chem. Chem. Phys.* **2020**, *22*, 24051–24058, doi:10.1039/D0CP03599H.
39. Armisén, R.; Gaiatas, F. Agar. In *Handbook of Hydrocolloids*; Elsevier, 2009; pp. 82–107.
40. Lahrech, K.; Safouane, A.; Peyrellasse, J. Sol State Formation and Melting of Agar Gels Rheological Study. *Phys. A Stat. Mech. its Appl.* **2005**, *358*, 205–211, doi:10.1016/j.physa.2005.06.022.
41. Ivankova, E.M.; Dobrovolskaya, I.P.; Popryadukhin, P. V.; Kryukov, A.; Yudin, V.E.; Morganti, P. In-Situ Cryo-SEM Investigation of Porous Structure Formation of Chitosan Sponges. *Polym. Test.* **2016**, *52*, 41–45, doi:10.1016/j.polymertesting.2016.03.018.
42. Takara, E.A.; Marchese, J.; Ochoa, N.A. NaOH Treatment of Chitosan Films: Impact on Macromolecular Structure and Film Properties. *Carbohydr. Polym.* **2015**, *132*, 25–30, doi:10.1016/j.carbpol.2015.05.077.
43. Nakayama, R.; Katsumata, K.; Niwa, Y.; Namiki, N. Dependence of Water-Permeable Chitosan Membranes on Chitosan Molecular Weight and Alkali Treatment. *Membranes (Basel).* **2020**, *10*, 351, doi:10.3390/membranes10110351.
44. Canal, T.; Peppas, N.A. Correlation between Mesh Size and Equilibrium Degree of Swelling of Polymeric Networks. *J. Biomed. Mater. Res.* **1989**, *23*, 1183–1193, doi:10.1002/jbm.820231007.
45. Ghebremedhin, M.; Seiffert, S.; Vilgis, T.A. Physics of Agarose Fluid Gels: Rheological Properties and Microstructure. *Curr. Res. Food Sci.* **2021**, *4*, 436–448, doi:10.1016/j.crfs.2021.06.003.
46. Cheung, W.; Patel, M.; Ma, Y.; Chen, Y.; Xie, Q.; Lockard, J. V.; Gao, Y.; He, H. π-Plasmon Absorption of Carbon Nanotubes for the Selective and Sensitive Detection of Fe 3+ Ions. *Chem. Sci.* **2016**, *7*, 5192–5199, doi:10.1039/C6SC00006A.
47. Pawlaczyk, M.; Schroeder, G. Deferoxamine-Modified Hybrid Materials for Direct Chelation of Fe(III) Ions from Aqueous Solutions and Indication of the Competitiveness of In Vitro Complexing toward a Biological System . *ACS Omega* **2021**, *6*, 15168–15181, doi:10.1021/acsomega.1c01411.
48. Yu, Z.; Zhan, J.; Wang, H.; Zheng, H.; Xie, J.; Wang, X. Analysis of Influencing Factors on Viscosity of Agar Solution for Capsules. *J. Phys. Conf. Ser.* **2020**, *1653*, 012059, doi:10.1088/1742-6596/1653/1/012059.
49. Norziah, M.H.; Foo, S.L.; Karim, A.A. Rheological Studies on Mixtures of Agar (Gracilaria Changii) and κ-Carrageenan. *Food Hydrocoll.* **2006**, *20*, 204–217, doi:10.1016/j.foodhyd.2005.03.020.
50. Mitchell, J.R. The Rheology of Gels. *J. Texture Stud.* **1980**, *11*, 315–337, doi:10.1111/j.1745-4603.1980.tb01312.x.
51. Yoshimura, M.; Nishinari, K. Dynamic Viscoelastic Study on the Gelation of Konjac Glucomannan with Different Molecular Weights. *Food Hydrocoll.* **1999**, *13*, 227–233, doi:10.1016/S0268-005X(99)00003-X.

52. Tao, H.; Guo, L.; Qin, Z.; Yu, B.; Wang, Y.; Li, J.; Wang, Z.; Shao, X.; Dou, G.; Cui, B. Textural Characteristics of Mixed Gels Improved by Structural Recombination and the Formation of Hydrogen Bonds between Curdlan and Carrageenan. *Food Hydrocoll.* **2022**, *129*, 107678, doi:10.1016/j.foodhyd.2022.107678.
53. Nie, J.; Wang, Z.; Hu, Q. Difference between Chitosan Hydrogels via Alkaline and Acidic Solvent Systems. *Sci. Rep.* **2016**, *6*, 36053, doi:10.1038/srep36053.
54. Xu, H.; Matysiak, S. Effect of PH on Chitosan Hydrogel Polymer Network Structure. *Chem. Commun.* **2017**, *53*, 7373–7376, doi:10.1039/C7CC01826F.
55. Huang, J.; Voigt, M.; Wackenrohr, S.; Ebbert, C.; Keller, A.; Maier, H.J.; Grundmeier, G. Influence of Hydrogel Coatings on Corrosion and Fatigue of Iron in Simulated Body Fluid. *Mater. Corros.* **2022**, *73*, 1034–1044, doi:10.1002/maco.202112841.
56. Elhefian, E.; Nasef, M.M.; Abdul, H.Y. Preparation and Characterization of Chitosan/Agar Blended Films: Part 1. Chemical Structure and Morphology. *E-Journal Chem.* **2012**, *9*, 1431–1439.
57. Samiey, B.; Ashoori, F. Adsorptive Removal of Methylene Blue by Agar: Effects of NaCl and Ethanol. *Chem. Cent. J.* **2012**, *6*, 14, doi:10.1186/1752-153X-6-14.
58. Andriamanantoanina, H.; Chambat, G.; Rinaudo, M. Fractionation of Extracted Madagascan Gracilaria Corticata Polysaccharides: Structure and Properties. *Carbohydr. Polym.* **2007**, *68*, 77–88, doi:10.1016/j.carbpol.2006.07.023.
59. Umemura, M.; Kim, J.-H.; Aoyama, H.; Hoshino, Y.; Fukumura, H.; Nakakaji, R.; Sato, I.; Ohtake, M.; Akimoto, T.; Narikawa, M.; et al. The Iron Chelating Agent, Deferoxamine Detoxifies Fe(Salen)-Induced Cytotoxicity. *J. Pharmacol. Sci.* **2017**, *134*, 203–210, doi:10.1016/j.jphs.2017.07.002.
60. Siebner-Freibach, H.; Yariv, S.; Lapides, Y.; Hadar, Y.; Chen, Y. Thermo-FTIR Spectroscopic Study of the Siderophore Ferrioxamine B: Spectral Analysis and Stereochemical Implications of Iron Chelation, PH, and Temperature. *J. Agric. Food Chem.* **2005**, *53*, 3434–3443, doi:10.1021/jf048359k.
61. Murugappan, R.; Karthikeyan, M.; Aravinth, A.; Alamelu, M. Siderophore-Mediated Iron Uptake Promotes Yeast–Bacterial Symbiosis. *Appl. Biochem. Biotechnol.* **2012**, *168*, 2170–2183, doi:10.1007/s12010-012-9926-y.
62. Lazaridou, M.; Christodoulou, E.; Nerantzaki, M.; Kostoglou, M.; Lambropoulou, D.; Katsarou, A.; Pantopoulos, K.; Bikiaris, D. Formulation and In-Vitro Characterization of Chitosan-Nanoparticles Loaded with the Iron Chelator Deferoxamine Mesylate (DFO). *Pharmaceutics* **2020**, *12*, 238, doi:10.3390/pharmaceutics12030238.
63. Zia, Q.; Tabassum, M.; Gong, H.; Li, J. A Review on Chitosan for the Removal of Heavy Metals Ions. *J. Fiber Bioeng. Informatics* **2019**, *12*, 103–128, doi:10.3993/jfbim00301.
64. Mallik, A.K.; Kabir, S.F.; Bin Abdur Rahman, F.; Sakib, M.N.; Efty, S.S.; Rahman, M.M. Cu(II) Removal from Wastewater Using Chitosan-Based Adsorbents: A Review. *J. Environ. Chem. Eng.* **2022**, *10*, 108048, doi:10.1016/j.jece.2022.108048.
65. Yang; Chai; Zeng; Gao; Zhang; Ji Efficient Removal of Copper Ion from Wastewater Using a Stable Chitosan Gel Material. *Molecules* **2019**, *24*, 4205, doi:10.3390/molecules24234205.
66. Guaresti, O.; Basasoro, S.; González, K.; Eceiza, A.; Gabilondo, N. In Situ Cross–Linked Chitosan Hydrogels via Michael Addition Reaction Based on Water–Soluble Thiol–Maleimide Precursors. *Eur. Polym. J.* **2019**, *119*, 376–384, doi:10.1016/j.eurpolymj.2019.08.009.
67. Radhakumary, C.; Antonty, M.; Sreenivasan, K. Drug Loaded Thermoresponsive and Cytocompatible Chitosan Based Hydrogel as a Potential Wound Dressing. *Carbohydr. Polym.* **2011**, *83*, 705–713, doi:10.1016/j.carbpol.2010.08.042.
68. Dan, S.; Kalantari, M.; Kamyabi, A.; Soltani, M. Synthesis of Chitosan-g-Itaconic Acid Hydrogel as an Antibacterial Drug Carrier: Optimization through RSM-CCD. *Polym. Bull.* **2022**, *79*, 8575–8598, doi:10.1007/s00289-021-03903-7.
69. Medeiros Borsagli, F.G.L.; Carvalho, I.C.; Mansur, H.S. Amino Acid-Grafted and N-Acylated

Chitosan Thiomers: Construction of 3D Bio-Scaffolds for Potential Cartilage Repair Applications. *Int. J. Biol. Macromol.* **2018**, *114*, 270–282, doi:10.1016/j.ijbiomac.2018.03.133.
70. Mohamed, N.A.; Fahmy, M.M. Synthesis and Antimicrobial Activity of Some Novel Cross-Linked Chitosan Hydrogels. *Int. J. Mol. Sci.* **2012**, *13*, 11194–11209, doi:10.3390/ijms130911194.
71. Gieroba, B.; Sroka-Bartnicka, A.; Kazimierczak, P.; Kalisz, G.; Lewalska-Graczyk, A.; Vivcharenko, V.; Nowakowski, R.; Pieta, I.S.; Przekora, A. Spectroscopic Studies on the Temperature-Dependent Molecular Arrangements in Hybrid Chitosan/1,3-β-D-Glucan Polymeric Matrices. *Int. J. Biol. Macromol.* **2020**, *159*, 911–921, doi:10.1016/j.ijbiomac.2020.05.155.
72. Esquivel, R.; Juárez, J.; Almada, M.; Ibarra, J.; Valdez, M.A. Synthesis and Characterization of New Thiolated Chitosan Nanoparticles Obtained by Ionic Gelation Method. *Int. J. Polym. Sci.* **2015**, *2015*, 1–18, doi:10.1155/2015/502058.
73. Valmalette, J.-C.; Tan, Z.; Abe, H.; Ohara, S. Raman Scattering of Linear Chains of Strongly Coupled Ag Nanoparticles on SWCNTs. *Sci. Rep.* **2014**, *4*, 5238, doi:10.1038/srep05238.
74. Zając, A.; Hanuza, J.; Wandas, M.; Dymińska, L. Determination of N-Acetylation Degree in Chitosan Using Raman Spectroscopy. *Spectrochim. Acta Part A Mol. Biomol. Spectrosc.* **2015**, *134*, 114–120, doi:10.1016/j.saa.2014.06.071.
75. Song, Y.; Hemley, R.J.; Liu, Z.; Somayazulu, M.; Mao, H.; Herschbach, D.R. High-Pressure Stability, Transformations, and Vibrational Dynamics of Nitrosonium Nitrate from Synchrotron Infrared and Raman Spectroscopy. *J. Chem. Phys.* **2003**, *119*, 2232–2240, doi:10.1063/1.1586695.
76. Yu, Y.; Ramachandran, P. V.; Wang, M.C. Shedding New Light on Lipid Functions with CARS and SRS Microscopy. *Biochim. Biophys. Acta - Mol. Cell Biol. Lipids* **2014**, *1841*, 1120–1129, doi:10.1016/j.bbalip.2014.02.003.
77. Zhang, K.; Helm, J.; Peschel, D.; Gruner, M.; Groth, T.; Fischer, S. NMR and FT Raman Characterisation of Regioselectively Sulfated Chitosan Regarding the Distribution of Sulfate Groups and the Degree of Substitution. *Polymer (Guildf).* **2010**, *51*, 4698–4705, doi:10.1016/j.polymer.2010.08.034.
78. Waterhouse, G.I.N.; Bowmaker, G.A.; Metson, J.B. The Thermal Decomposition of Silver (I, III) Oxide: A Combined XRD, FT-IR and Raman Spectroscopic Study. *Phys. Chem. Chem. Phys.* **2001**, *3*, 3838–3845, doi:10.1039/b103226g.
79. Martina, I.; Wiesinger, R.; Schreiner, M. Micro-Raman Characterisation of Silver Corrosion Products : Instrumental Set Up and Reference. *e-Preservation Sci.* **2012**, *9*, 1–8.
80. Palafox, C.L. When Less Is More: Minimalism and the Environment. *Environ. Earth Law J.* **2020**, *10*.
81. Giuliani, C.; Pascucci, M.; Riccucci, C.; Messina, E.; Salzano de Luna, M.; Lavorgna, M.; Ingo, G.M.; Di Carlo, G. Chitosan-Based Coatings for Corrosion Protection of Copper-Based Alloys: A Promising More Sustainable Approach for Cultural Heritage Applications. *Prog. Org. Coatings* **2018**, *122*, 138–146, doi:10.1016/j.porgcoat.2018.05.002.
82. Carneiro, J.; Tedim, J.; Fernandes, S.C.M.; Freire, C.S.R.; Gandini, A.; Ferreira, M.G.S.; Zheludkevich, M.L. Chitosan as a Smart Coating for Controlled Release of Corrosion Inhibitor 2-Mercaptobenzothiazole. *ECS Electrochem. Lett.* **2013**, *2*, doi:10.1149/2.002306eel.
83. Kakakhel, M.A.; Wu, F.; Gu, J.-D.; Feng, H.; Shah, K.; Wang, W. Controlling Biodeterioration of Cultural Heritage Objects with Biocides: A Review. *Int. Biodeterior. Biodegradation* **2019**, *143*, 104721, doi:10.1016/j.ibiod.2019.104721.
84. *Corrosion*; Shreir, L.L., Jarman, R.A., Burstein, G.T., Eds.; Elsevier, 1994; ISBN 9780080523514.
85. Passaretti, A.; Cuvillier, L.; Sciutto, G.; Guilminot, E.; Joseph, E. Biologically Derived Gels for the Cleaning of Historical and Artistic Metal Heritage. *Appl. Sci.* **2021**, *11*, 3405, doi:10.3390/app11083405.
86. Madigan; Martinko; Dunlap; Clark *Brock Biology of Microoganisms, 12th International Edition*; Pearson Education, 2009; ISBN 978-0321536150.
87. Junier, P.; Joseph, E. Microbial Biotechnology Approaches to Mitigating the Deterioration of

Construction and Heritage Materials. *Microb. Biotechnol.* **2017**, *10*, 1145–1148, doi:10.1111/1751-7915.12795.
88. Gao, Y.; Chai, N.K.K.; Garakani, N.; Datta, S.S.; Cho, H.J. Scaling Laws to Predict Humidity-Induced Swelling and Stiffness in Hydrogels. *Soft Matter* **2021**, *17*, 9893–9900, doi:10.1039/D1SM01186C.
89. Hui, C.Y.; Lin, Y.Y.; Baney, J.M. The Mechanics of Tack: Viscoelastic Contact on a Rough Surface. *J. Polym. Sci. Part B Polym. Phys.* **2000**, *38*, 1485–1495, doi:10.1002/(SICI)1099-0488(20000601)38:11<1485::AID-POLB80>3.0.CO;2-1.
90. Creton, C.; Leibler, L. How Does Tack Depend on Time of Contact and Contact Pressure? *J. Polym. Sci. Part B Polym. Phys.* **1996**, *34*, 545–554, doi:10.1002/(SICI)1099-0488(199602)34:3<545::AID-POLB13>3.0.CO;2-I.
91. Williams, J.A.; Kauzlarich, J.J. The Influence of Peel Angle on the Mechanics of Peeling Flexible Adherends with Arbitrary Load–Extension Characteristics. *Tribol. Int.* **2005**, *38*, 951–958, doi:10.1016/j.triboint.2005.07.024.
92. Fujii Yamagata, A.L. Les Propriétés Adhésives et Rhéologie Interfaciale de Mortiers Colles, Paris Saclay, 2018. https://theses.hal.science/tel-01990594
93. Matthiesen, H.; Wonsyld, K. In Situ Measurement of Oxygen Consumption to Estimate Corrosion Rates. *Corros. Eng. Sci. Technol.* **2010**, *45*, 350–356, doi:10.1179/147842210X12710800383602.
94. H Matthiesen Henning; Stemann-Petersen, K. A Fast and Non-Destructive Method to Document and Quantify the Efficiency of Metals Conservation. *ICOM-CC Met. Conf.* **2013**.
95. Forney, C.F.; Brandl, D.G. Control of Humidity in Small Controlled-Environment Chambers Using Glycerol-Water Solutions. *Horttechnology* **1992**, *2*, 52–54, doi:10.21273/HORTTECH.2.1.52.
96. McCafferty, E.; McArdle, J. V. Corrosion Inhibition of Iron in Acid Solutions by Biological Siderophores. *J. Electrochem. Soc.* **1995**, *142*, 1447–1453, doi:10.1149/1.2048595.
97. Pérez-Miranda, S.; Zamudio-Rivera, L.S.; Cisneros-Dévora, R.; George-Téllez, R.; Fernández, F.J. Theoretical Insight and Experimental Elucidation of Desferrioxamine B from Bacillus Sp. AS7 as a Green Corrosion Inhibitor. *Corros. Eng. Sci. Technol.* **2021**, *56*, 93–101, doi:10.1080/1478422X.2020.1824441.
98. Fontaine, C.; Lemoine, S.; Pelé-Meziani, C.; Guilminot, E. The Use of Gels in Localized Dechlorination Treatments of Metallic Cultural Heritage Objects. *Herit. Sci.* **2022**, *10*, 117, doi:10.1186/s40494-022-00752-z.
99. Burnstock, A.; White, R. THE EFFECTS OF SELECTED SOLVENTS AND SOAPS ON A SIMULATED CANVAS PAINTING. *Stud. Conserv.* **1990**, *35*, 111–118, doi:10.1179/sic.1990.35.s1.024.
100. Riedo, C.; Rollo, G.; Chiantore, O.; Scalarone, D. Detection and Identification of Possible Gel Residues on the Surface of Paintings after Cleaning Treatments. *Heritage* **2021**, *4*, 304–315, doi:10.3390/heritage4010019.
101. Scott, C.L. The Use of Agar as a Solvent Gel in Objects Conservation. *AIC Objects Spec. Gr. Postprints* **2012**, *19*, 71–83.
102. Stulik, D.; Dorge, V.; Khanjian, H.; Khandekar, N.; Tagle, A. de; Miller, D.; Wolbers, R.; Carlson, J. Surface Cleaning: Quantitative Study of Gel Residue on Cleaned Paint Surfaces. *Stud. Conserv.* **2000**, *45*, 188–194, doi:10.1179/sic.2000.45.Supplement-1.188.
103. Sullivan, M.; Duncan, T.; Berrie, B.H.; Weiss, R.G. Rigid Polysaccharides Gels for Paper Conservation-a Residue Study. In Proceedings of the Gels in the Conservation of Art; Angelova, L., Ormsby, B., Townsend, J., Wolbers, R., Eds.; Archetype Publications: London, UK, 2017; pp. 42–50.
104. Allusse, G.; Jebali, S. Détection Des Résidus de Gels Dans Le Cadre Du Projet 'Gels Métaux,' Polytech' Nantes, 2020.
105. Giachet, M.T.; Schröter, J.; Brambilla, L. Characterization and Identification of Varnishes on

Copper Alloys by Means of UV Imaging and FTIR. *Coatings* **2021**, *11*, doi:10.3390/coatings11030298.
106. Thirion-Merle, V. Spectrométrie de Fluorescence X. In *Circulation et provenance des matériaux dans les sociétés anciennes*; Dillmann, P., Bellot-Gurlet, L., Eds.; Archives contemporaines, 2014; p. 360 ISBN 9782813001634.
107. Bowers, C. Matrix Effect Corrections in X-Ray Fluorescence Spectrometry. *J. Chem. Educ.* **2019**, *96*, 2597–2599, doi:10.1021/acs.jchemed.9b00630.
108. Deering, K.; Spiegel, E.; Quaisser, C.; Nowak, D.; Rakete, S.; Garí, M.; Bose-O'Reilly, S. Exposure Assessment of Toxic Metals and Organochlorine Pesticides among Employees of a Natural History Museum. *Environ. Res.* **2020**, *184*, 109271, doi:10.1016/j.envres.2020.109271.
109. Sandu, I.C.A.; Schäfer, S.; Magrini, D.; Bracci, S.; Roque, C.A. Cross-Section and Staining-Based Techniques for Investigating Organic Materials in Painted and Polychrome Works of Art: A Review. *Microsc. Microanal.* **2012**, *18*, 860–875, doi:10.1017/S1431927612000554.
110. Goldberg, H.A.; Warner, K.J. The Staining of Acidic Proteins on Polyacrylamide Gels: Enhanced Sensitivity and Stability of "Stains-All" Staining in Combination with Silver Nitrate. *Anal. Biochem.* **1997**, *251*, 227–233, doi:10.1006/abio.1997.2252.
111. Patnaik, R.N.; Bose, S.K.; Sircar, S.C. Influence of an Applied Field on the Tarnishing of Silver and Copper in Iodine Vapour. *Br. Corros. J.* **1977**, *12*, 57–63, doi:10.1179/000705977798319594.
112. Smyth, D.M.; Cutler, M. Tarnishing Reactions of Silver in Iodine Atmospheres. *J. Electrochem. Soc.* **1959**, *106*, 107, doi:10.1149/1.2427277.
113. Dutta, K.P.; Roy, S.K.; Bose, S.K.; Sircar, S.C. Estimation of Ionic Conductivity of CuI through Tarnishing Studies of Copper in Iodine Atmosphere. *Mater. Res. Bull.* **1973**, *8*, 301–308, doi:10.1016/0025-5408(73)90008-1.
114. Catelli, E.; Li, Z.; Sciutto, G.; Oliveri, P.; Prati, S.; Occhipinti, M.; Tocchio, A.; Alberti, R.; Frizzi, T.; Malegori, C.; et al. Towards the Non-Destructive Analysis of Multilayered Samples: A Novel XRF-VNIR-SWIR Hyperspectral Imaging System Combined with Multiblock Data Processing. *Anal. Chim. Acta* **2023**, *1239*, 340710, doi:10.1016/j.aca.2022.340710.

3.6 Supplementary materials

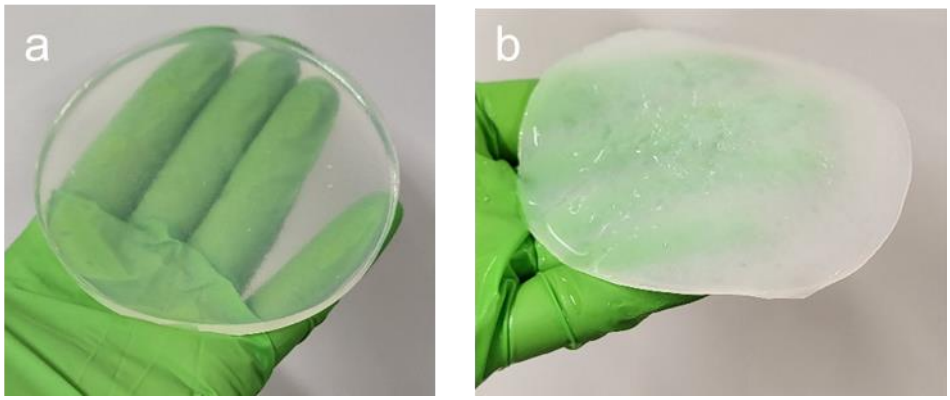

Figure S3.1 (a) 3% w/v agar gel and (b) 3.3% w/v CS-ItA-LCys gel obtained.

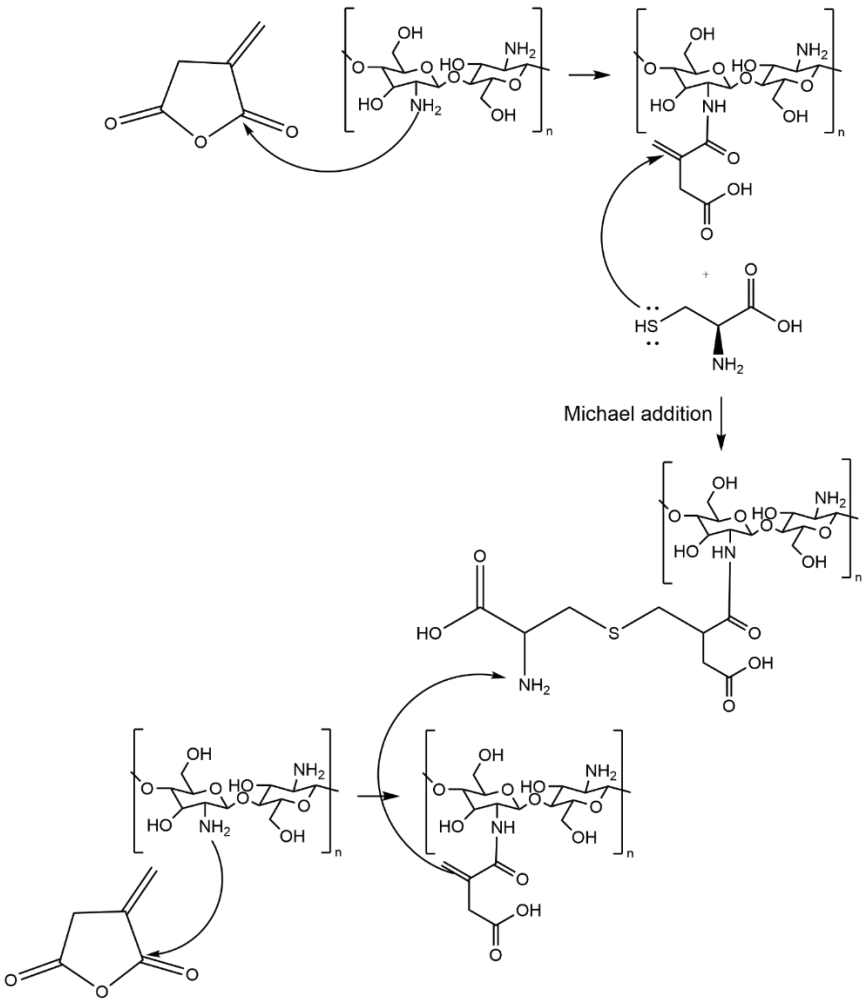

Figure S3.2 Possible reaction of chitosan with IAn and L-Cysteine.

Figure S3.3 Set-up for the tack test measurements on xanthan gum, probe increasing and stretching the material, showing a cohesive rupture.

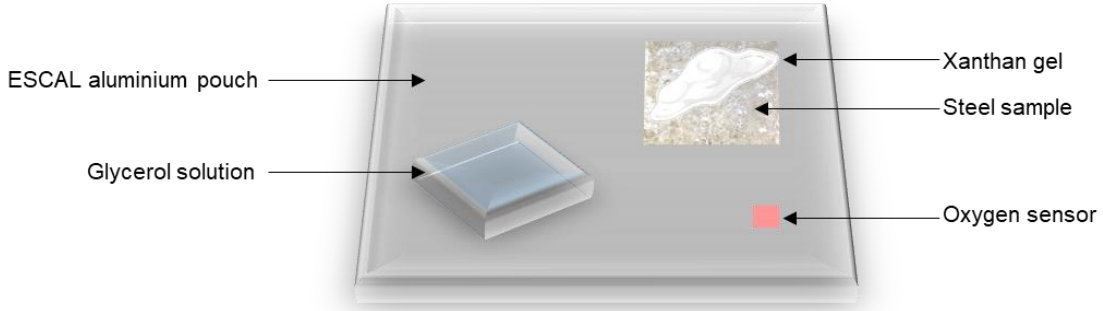

Figure S3.4 Set-up for oxygen consumption measurements.

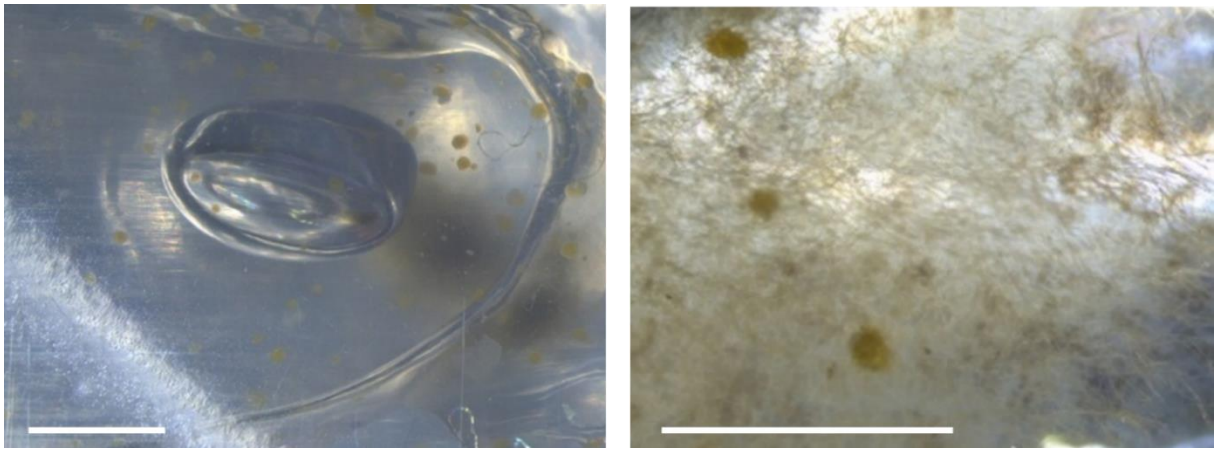

Figure S3.5 Optical microscope observations of the pouch with gel only (Xan) after 20 days and the apparition of biomass. Scale bars account for 2 mm.

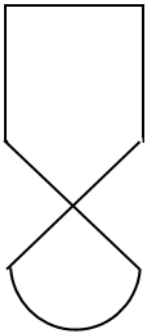

Figure S3.6 Carved pattern used for the disposition of marked gels on metal plates.

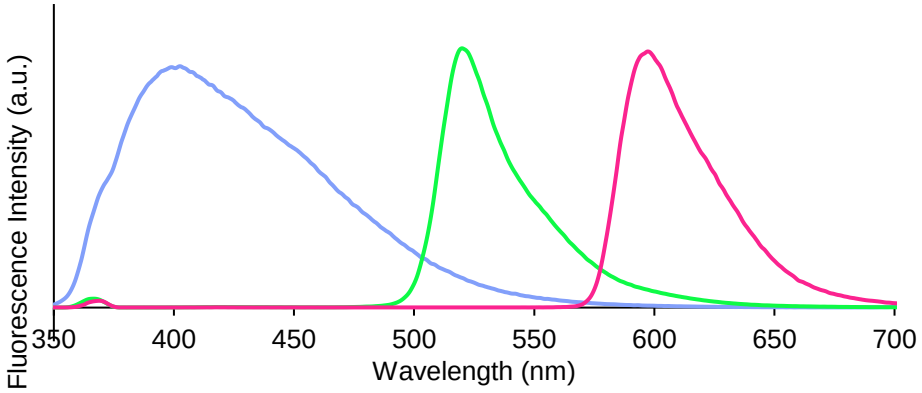

Figure S3.7 Emission spectra of quinine (blue), fluoresceine (green) and rhodamine (pink) at λ_{ex}= 365 nm.

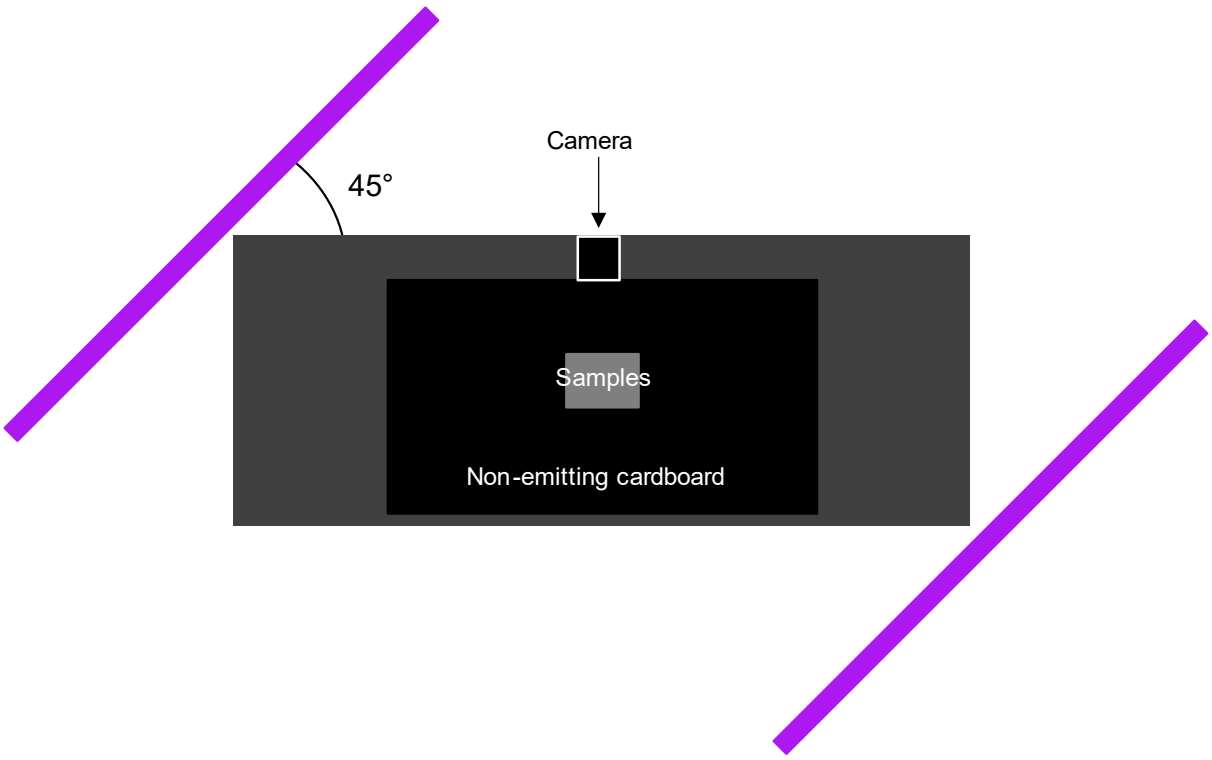

Figure S3.8 UV photography set-up.

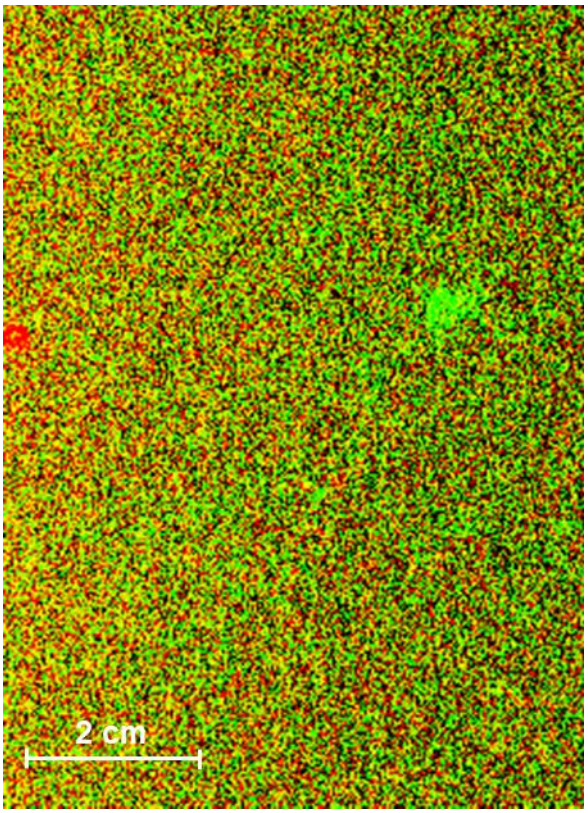

Figure S3.9 XRF mapping of brass after deposition of Hf (red) or W (green) marked agar and xanthan gels.

4. Evaluation of biobased hydrogels amended with sustainable chelators for metal cleaning

This chapter is based on the following articles and proceedings:

Cuvillier, L.; Passaretti, A.; Guilminot, E.; Joseph, E. Testing of the Siderophore Deferoxamine Amended in Hydrogels for the Cleaning of Iron Corrosion. *Eur. Phys. J. Plus* **2023**, 138, 569, doi:10.1140/epjp/s13360-023-04159-y

Cuvillier, L.; Passaretti, A.; Dupuy, V.; Raimon, A.; Guilminot, E.; Joseph, E. Exploiting Biologically Synthetized Chelators in Conservation: Gel-Based Bio-Cleaning of Corroded Iron Heritage Objects. In Proceedings of the Metal 2022, 10th interim meeting of the ICOM-CC metals working group; Mardikian, P., Näsänen, L., Arponen, A., Eds.; Helsinki, Finland, 2022.

The aim of this chapter is to evaluate the combined performance of selected bio-based delivery systems (i.e., hydrogels) and chelating agents for their ability to clean actual bulk corrosion. Evaluation of the designed formulations' performance, in addition with the study of the applications, was performed on model samples from each studied metal (iron, copper, and silver alloys), as they are frequently used in historical and decorative arts.

To allow a more thorough study, only two of the priorly tested chelating agents were assessed. Specifically, the efficacy of the siderophore deferoxamine (DFO) and ethylenediamine-*N*,*N*'-disuccinic acid (EDDS) was examined.

DFO has already been tested on iron-contaminated wood, paper and textile artworks, due to its high affinity for iron, as evidenced by its stability constant (log β), a measure of the interaction strength between two components forming a complex: 30.4 for DFO versus 25 for EDTA [1,2]. DFO chelates iron at a 1:1 molar ratio and turns bright orange-red upon complexation, allowing to easily ascertain its activity. EDDS has not yet been tested for cultural heritage conservation purposes, nevertheless it performed extremely well on corrosion powder, especially for copper, as shown in Chapter 2. Its affinity for copper is similar to EDTA (log $\beta_{Cu\text{-}EDDS}$ = 18.7 and log $\beta_{Cu\text{-}EDTA}$ = 18.8) [3]. Although a high reported log $\beta_{Fe\text{-}EDDS}$ (20.6) [3], EDDS was not assessed on iron due to its lower performances on powdered goethite and lepidocrocite (Chapter 2). Acids supplements are excluded as their extreme acidic pH is a drawback to find compatible gelling agents. Although they showed great performances in Chapter 2, their low pH is also of concern for conservation purposes, when treating composite objects for instance.

The second component of the formulation is the hydrogel matrix to be implemented with the previously mentioned active agents. Several polymers, especially polysaccharides, can be employed in the design of DFO or EDDS-based hydrogels when it comes to their pH compatibility and conservation of gel properties (Chapter 3). Only naturally derived gelling agents were considered here, namely gellan and xanthan gums which are obtained from bacteria, and agar, which is extracted from red seaweed (Chapter 3). A small insight in the use of a chitosan formulation is also provided for copper samples.

Bare metal samples of the selected alloys were artificially corroded using standard accelerated ageing procedures. Artificial ageing often results in model samples that are not representative of actual corrosion [4]. It was therefore interesting to carry the study on both artificially and naturally altered samples to verify any differences.

Particular attention was dedicated to ascertaining the optimal treatment duration by applying the cleaning agents during different time periods. This allowed a better understanding of the kinetics of action of the formulation on corroded surfaces. For conservation purposes, modifications of application parameters (i.e., reiteration, concentration of active agents) were performed in order to advise

professionals on how to practically use these compounds. In addition, to understand the long-term behavior of cleaned surfaces, in particular eventual corrosion regrowth, monitoring of the cleaned surface over time was performed. For comparison, some samples were treated with cleaning methods traditionally used in metal conservation.

The cleaning agents most commonly used by conservators are sodium salts of ethylenediamine-tetraacetic acid (EDTA). It complexes iron at a molar ratio of 1:1, according to pH, and turns light yellow after iron complexation [5]. As shown in Chapter 2, EDTA shows great complexing abilities, especially at acidic pH for iron but also in the alkaline range for copper. Indeed, EDTA is largely used for this versatility in addition to its high formation constant with a wide range of metals and heavy metals [6]. However, despite its easy availability and low cost, EDTA is classified as an irritant and it must be used with appropriate caution [7]. Although the quantities used in cultural heritage conservation are much smaller than in other industrial applications, EDTA is not biodegradable and its environmental impact is a worldwide concern [8].

Mock-up samples appearance, morphology and composition was assessed and documented via complementary non-invasive analytical techniques on the samples' surface. To ensure a correct characterization, analyses were performed at macro- and micrometric scales, relying on optical microscopy, colorimetry, and Raman microscopy. The used formulations were also analyzed using atomic absorption spectroscopy to assess the metal taken up inside the gel matrix. Model samples were then characterized with the same analytical techniques carried out before cleaning. Finally, after evaluation on model samples, a corpus of liturgical objects was then submitted to specific cleaning formulations. This validation step was of utmost importance as it permitted to confirm the efficiency of HELIX hydrogels on real artefacts and therefore gave an overview of cleaning possibilities to end-users.

4.1 Iron

4.1.1 Evaluation on model samples

4.1.1.1 Materials and methods

For reproducibility purpose, each experiment was performed in triplicate, exception made where mentioned differently. Details regarding analytical techniques can be found in the supplementary materials of this chapter.

4.1.1.1.1 Samples

Two types of samples were employed, artificially corroded or naturally corroded steel samples, referred as AS and NS respectively in the text. Steel samples (30 × 30 × 1 mm) were obtained from Tartaix (France) and artificially corroded adapting ASTM G48-11 procedure by immersing the samples into 0.4 M $FeCl_3$ for 30 minutes, followed by a quick immersion in 9.79 M H_2O_2 to accelerate corrosion formation and then left to dry for at least 24 hours. The bare steel samples were used as non-corroded reference samples as well. Naturally corroded mild steel samples (20 × 30 × 1 mm) were obtained from a conservation workshop (Arc'Antique, Nantes, France), where over a period of more than 10 years they underwent corrosion due to uncontrolled indoor conditions. The corrosion layer is believed to be mainly composed of goethite and lepidocrocite, common compounds that develop during indoor iron corrosion [9,10].

4.1.1.1.2 Cleaning evaluation and risk assessments on artificially corroded samples

Tests on artificially corroded steel samples (AS) were performed to assess the uptake of insoluble iron phases and the innocuity of deferoxamine on steel. A 3% w/v agar gel amended with a $3{\cdot}10^{-2}$ M DFO (Desferal®, Novartis) aqueous solution (pH = 6.8) was applied for 20 minutes on AS. This gel was also applied on a non-corroded steel sample to evaluate the aggressiveness of DFO solution on metallic iron. Similar process was performed using an EDTA (PanReac AppliChem) aqueous solution (pH = 4.2), at the same concentration. A sample with plain 3% w/v agar gel (not amended with siderophores) was used as control. Experiments were carried out in triplicates. Samples were characterized by means of optical microscopy, Eddy-current measurements for thickness evaluation of the corrosion layer, colorimetry, and Fourier Transformed Infrared (FTIR) spectroscopy before and after gel application.

4.1.1.1.3 Study of application parameters

Application parameters and kinetics were studied on naturally corroded steel samples (NS) as the corrosion layer was more homogeneously spread than what was obtained for AS and therefore allowed to obtain more comparable results.

A 3% w/v agar gel was amended with different DFO water solutions at concentration of 0, $3{\cdot}10^{-4}$, $3{\cdot}10^{-3}$, $3{\cdot}10^{-2}$ and $6{\cdot}10^{-2}$ M (respective pH = 7.51, 7.68, 7.16, 6.79 and 6.65) and applied to naturally corroded steel

samples for 10 minutes. A $6 \cdot 10^{-2}$ M stock solution of Desferal® (2 g Desferal® in 50 mL milli-Q water) was prepared and diluted 2, 20 and 200 times to reach concentrations of $3 \cdot 10^{-2}$, $3 \cdot 10^{-3}$, $3 \cdot 10^{-4}$ M. The application was repeated six times for a total application time of 60 minutes. For comparison, a 3% w/v agar gel amended with a $6 \cdot 10^{-2}$ M water solution of Na_2EDTA was tested using the same reiterative protocol. Samples were characterized by means of colorimetry and optical microscopy before and after gel application. Atomic Absorption Spectroscopy (AAS) of the gels was performed to ascertain the iron contained in the gel after application.

It is known that a polymer matrix will have an influence on the diffusion of the solute, which could influence the kinetics of the cleaning intervention, but to what extent? For such, iron chelation was assessed after immersion of naturally corroded steel samples for 10 and 30 minutes, 1 h, 5 h and 24 h in a $6 \cdot 10^{-2}$ M solution of DFO or after application of a 3% w/v agar DFO-gel with the same parameters (i.e., concentration and application duration). For the gel application, the gels were covered to minimize the drying phenomenon. The experiments were carried out at room temperature, approximately 20 °C. Immersion solution and gels were analyzed using AAS comparing their iron content before and after contact with iron samples.

4.1.1.1.4 Selection of best performing gel formulation

Three naturally derived polymers amended with a $3 \cdot 10^{-2}$ M solution of DFO were assessed on the NS. Several application methods were evaluated as detailed in Table 4.1. Each gel formulation was applied for 10 minutes and removed using a cotton swab dipped in 70% v/v ethanol.

Table 4.1 Polysaccharides selected for the study.

Gelling agent	**Xanthan gum**	**Agar-agar**		**Gellan gum**	
Brand, supplier	Vanzan©, CTS	AgarArt©, CTS		Phytagel™, Sigma Aldrich	
Source	*Xanthomonas campestris*	*Gelidium* and *Gracilaria* red seaweeds		*Sphingomonas elodea*	
Preparation	5% w/v in H_2O and stirring	3% w/v in H_2O, heated to 90 °C twice		3% w/v in H_2O, stirring	3% w/v in H_2O, heated to 90 °C
Application	With a spatula at room temperature	Dripped when still hot	Cooled preformed rigid foil	With a spatula at room temperature	Dripped when still hot
Texture	Viscous	Rigid, peelable	Rigid	Gooey	Rigid, peelable

4.1.1.1.5 Behavior of cleaned surfaces over time

Cleaned naturally corroded samples (triplicates) were stored for a year under uncontrolled indoor conditions in Nantes, France. Temperature (T) and relative humidity (RH) variation in the storage place over the year are respectively 17 °C < T < 21 °C and 45% < HR < 60 %. Colorimetric and visual evaluations were performed after one year to ascertain long-term efficacy of the cleaning intervention.

4.1.1.2 Results and discussion

4.1.1.2.1 Cleaning evaluation and risk assessments on artificially corroded samples

The application of a 3% w/v agar gel amended with DFO on non-corroded steel showed no visual modification as can be deduced by the similar aspect observed via optical microscopy before and after application (Table 4.2). In addition, the colorimetric values of the sample prior to the application of the gel were left unchanged for all coordinates (L*, a*, b*). Lack of changes following application of the DFO-amended gel suggests the absence of interaction of the siderophores with uncorroded steel (Table 4.2). This is explained by the fact that siderophores target iron in its ferric, or sometimes ferrous, rather than elemental form [11]. It is therefore effective on FeOOH compounds but will not affect the Fe of the steel. This property makes it safe to use this compound on iron-based surfaces, without risking of affecting the original iron metal surface. This conclusion is based on visual results solely, which is the

main tool used by conservators, however, to ascertain an objective absence of activity of DFO on steel, elemental analysis of the gel samples would be necessary.

Table 4.2 Optical microscopy observation and colorimetric values of bare iron samples before and after 3% w/v Agar-DFO gel application. Scale bar accounts for 2 mm.

	Before cleaning			**After cleaning**		
Optical microscopy						
Colorimetric values	L*	a*	b*	L*	a*	b*
	65.7 ± 0.3	0.7± 0.4	3.0 ± 1.0	66.7 ± 0.9	0.8 ± 0.1	3.9 ± 0.6

Cleaning gels application on artificially corroded steel samples allowed to remove the corrosion layer, as shown by digital microscope observations (Table 4.3). A clear decrease of the corrosion layer thickness was confirmed by Eddy current measurements, dropping from 4 ± 1.1 μm to 1.2 ± 0.25 μm for DFO and 2.1 ± 0.9 μm to 1.1 ± 0.55 μm for EDTA. When no active agents were implemented in the gel, the corrosion layer thickness remained similar, around 2.2 μm. The inhomogeneity of the artificially created corrosion layer is to be noted, whether from visual or thickness point of view, thus leading to the preferred use of naturally corroded samples in the following sections of the study. Still, these samples allow a qualitative comparison.

Table 4.3 Artificially corroded steel samples (AS) before and after 3% w/v Agar-DFO or Agar-EDTA gel application. Scale bar indicates 2 mm. Corrosion layer thickness before and after application of a 3% w/v Agar gel amended with $3 \cdot 10^{-2}$ M solution of DFO or $3 \cdot 10^{-2}$ M solution of EDTA. 3% w/v plain gel without complexing agent serves as control.

	Before cleaning	**After cleaning**
DFO	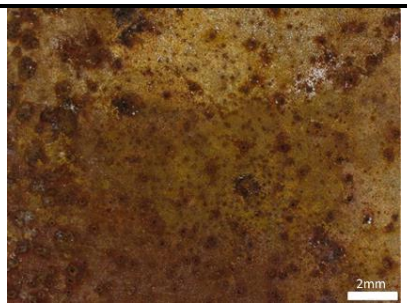	
Corrosion thickness	4.0 ± 1.1 μm	1.2 ± 0.3 μm
EDTA	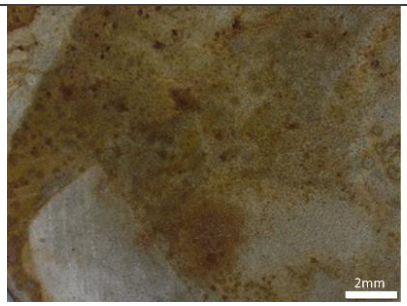	
Corrosion thickness	2.1 ± 0.9 μm	1.1 ± 0.6 μm
Control	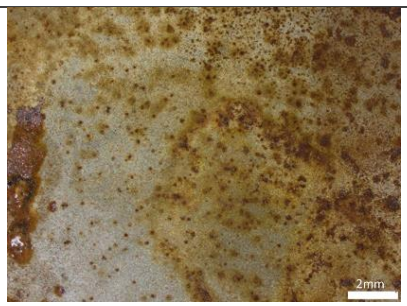	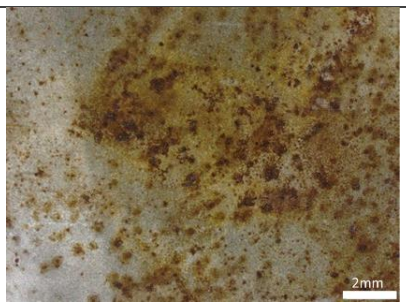
Corrosion thickness	2.2 ± 0.6 μm	2.1 ± 0.6 μm

According to ICOM-CC English terminology, cleaning can be considered a "remedial conservation" or "restoration" act [12]. In the case of indoor metal objects, often the corrosion layer is not detrimental and therefore, the aim of the cleaning intervention is either to retrieve, as much as possible, the aesthetical appearance of the metal before corrosion or to improve the readability of the objects. Regarding the results obtained on AS through the three-color coordinates, for the b coordinate, color shifts between DFO and control or EDTA and control were found to be statistically significant (p-value

= 0.004 and 0.019, respectively), but not between EDTA and DFO (p= 0.83). The a coordinate did not show any statistically significant difference, regardless of the treatment, oppositely to the L coordinate where the shift was confirmed by ANOVA. It appears that lightness L* increased in samples cleaned with deferoxamine-based gel formulation (Figure 4.1) to reach a value of L*= 58.0 ± 1.9 after treatment. Samples treated with EDTA-amended agar gel on the contrary turned darker as shown with a negative ΔL* value, reaching a value of L*= 48.0 ± 1.2 further from the bare steel (L*= 65.7 ± 0.3). This is possibly due to its acidic pH of 4.2 of $3 \cdot 10^{-2}$ M EDTA solution (vs a pH of 6.8 for DFO), which can alter metallic iron. In both cases (DFO or EDTA-amended gels), a* and b* coordinates were both shifted towards lower values, indicating that the cleaned surfaces turned less yellow and less red, as expected with the removal of iron corrosion products. This color change to less red and yellow is adequate as it bears witness of the removal of rust. The final appearance is up to the curator, the client, or the conservator according to the look desired but a lessening of the orangish layer is often desired. Color variations on the control corroded samples where a plain gel was applied are not observed (Δb) or very low (1.6 ± 0.1 and -1 ± 0.7 for ΔL and Δa respectively). Though low, the variation for the control samples might be explained by some rust being stripped off when peeling off the agar gel from the surface.

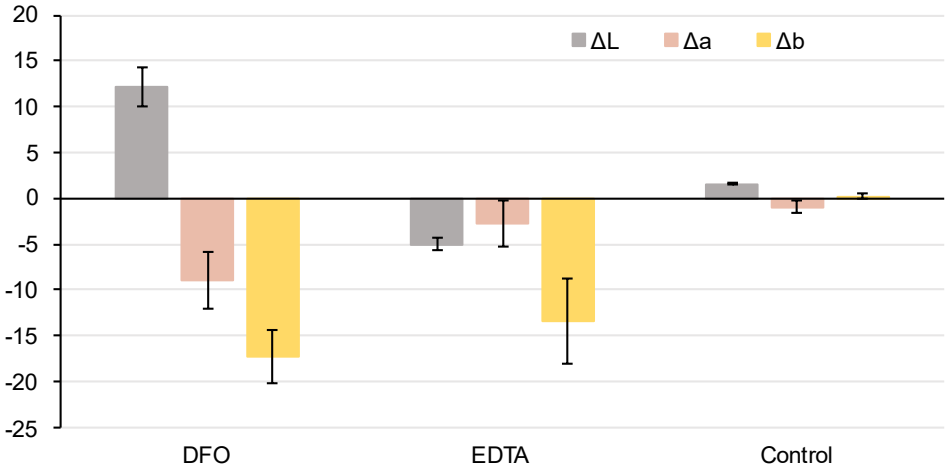

Figure 4.1 Variations of CIELab colorimetric coordinates of the artificially corroded steel samples before and after application of a 3% w/v Agar gel amended with $3 \cdot 10^{-2}$ M solution of DFO or $3 \cdot 10^{-2}$ M solution of EDTA. 3% w/v plain gel without complexing agent serves as control. Surface before treatment: L* = 38.3 ± 0.9, b* = 9.9 ± 0.8, a* = 15.0 ± 2.3

In addition, FTIR spectra of the artificially corroded steel samples after cleaning (Figure 4.2b) did not display the characteristic bands of iron corrosion products identified before treatment (Figure 4.2a). Similar spectra as non-corroded bare steel samples were obtained (Figure 4.2c). The observed spectrum has O-H bending bands at 746 cm^{-1} and 1021 cm^{-1} that are assigned to lepidocrocite. Similarly, the presence of goethite is determined thanks to the presence of bands at 793 cm^{-1}, 887 cm^{-1} and 1126 cm^{-1} [13,14]. The 1658 cm^{-1} peak and a broad band at 3000-3500 cm^{-1} are characteristic of adsorbed water

within the iron corrosion layer [13–15]. These results confirmed the removal of iron oxyhydroxides that were present on the surface.

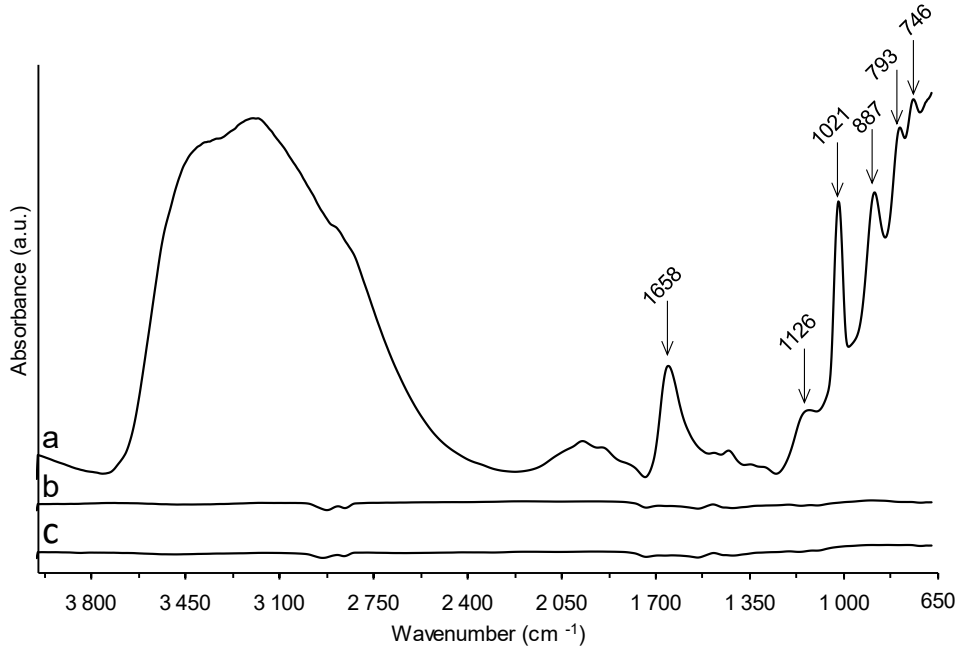

Figure 4.2 Representative FTIR spectra (4 cm^{-1} resolution, 16 scans) of artificially corroded steel samples before treatment (a), after treatment (b) and non-corroded bare steel sample (c).

4.1.1.2.2 Selection of best-performing hydrogel formulation

After preliminary evaluation of DFO on AS, the cleaning performances of different polysaccharide gels amended with $3{\cdot}10^{-2}$ M DFO solution were evaluated.

Based on visual observations and total color difference (Table 4.4), DFO-agar hot gel and DFO-gellan gel prepared at room temperature showed the highest color change ΔE, close to 14, and the best visual observations with a bright metal visible on most of the sample's surface. They achieved the best performances in terms of corrosion removal with no statistical difference between the two groups (*p*-value = 0.99). The DFO-gellan hot gel achieved mild cleaning following the same protocol with a color change of 9.3 ± 0.6 and with a showing underlying metal, but less bright than for the forementioned formulations. However, this lower performance was not found to be statistically significant compared to hot agar or room temperature gellan (p = 0.07 and 0.08 respectively, above the 0.05 threshold). Performances of the rigid DFO-agar gel and the DFO-xanthan gel prepared and applied at room temperature were poor, with a barely noticeable color change (3.6 ± 0.7 and 2.5 ± 2 respectively), under the ΔE = 5 limit for perceptible change by human eye [16]. Differences between DFO-xanthan and DFO-rigid agar were also not significant (p = 0.96).

Table 4.4 Optical microscopy and color difference of iron samples treated for 10 min with $3{\cdot}10^{-2}$ M DFO-amended gels. Scale bar is 5mm.

	Optical microscopy	ΔE
Agar applied hot	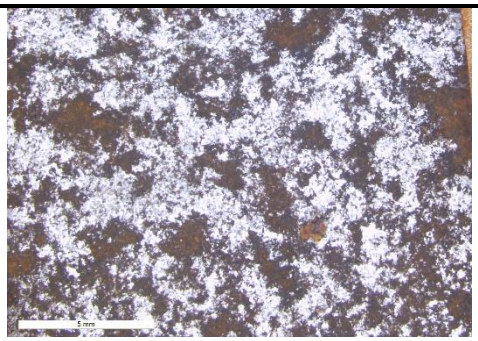	14.0 ± 1.9
Gellan gum prepared and applied at room temperature	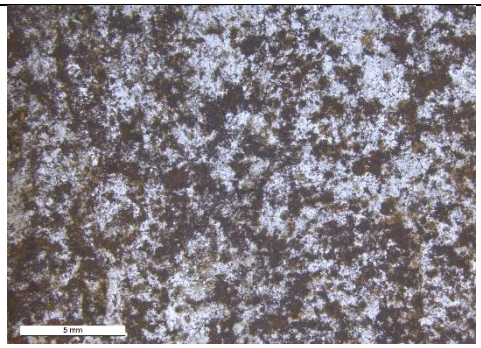	14.0 ± 3.0
Gellan gum applied hot	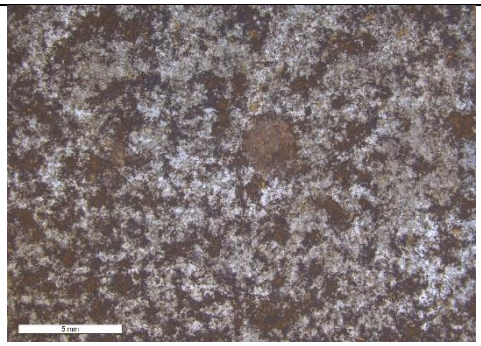	9.3 ± 0.6
Rigid, cold applied agar	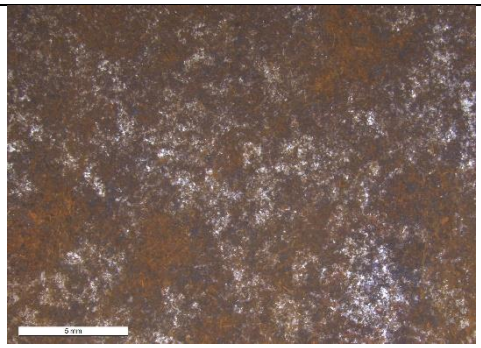	3.6 ± 0.7

Xanthan, applied at room temperature	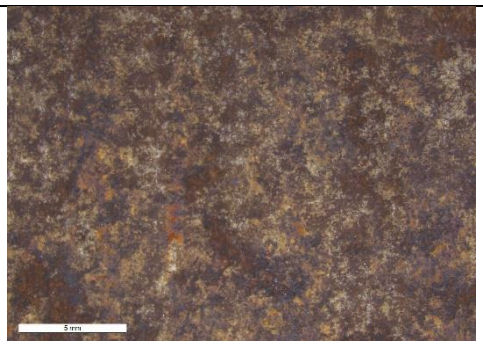	2.5 ± 2.0

On Figure 4.3, a more precise interpretation of L*a*b* coordinates of naturally corroded steel samples before and after cleaning is shown. After cleaning with DFO-loaded hot applied agar gel, room-temperature gellan gel and to a lesser extent hot gellan gel, the surface color was brighter (higher values of L*) and the hue turned to blue-green (lower values of a* and b*). This can be attributed to the removal of the red-orange iron corrosion products. By contrast, low surface color changes were observed on the samples treated with DFO-amended gels based on xanthan gum or rigid cold agar. After xanthan gum application, a thin layer of gel remained that could not be removed by cotton swab clearing. As seen in Chapter 3, a thin veil of xanthan remains present even after removal and clearing of the surface. In addition, in the case of Xanthan-DFO gel, the gel gets tinted, through complex formation, with an orangish hue that causes a low color change. For the applied rigid DFO-amended agar gel, no clear visual modifications were observed, probably due to the failure of the cold and rigid agar matrix to adhere to the surface and achieve close contact with the corroded iron-alloy surface [17]. Despite its great cleaning performances and potential, DFO-amended gellan gum gel at room temperature needs extra attention at the removal step because its texture implies the need for a careful clearing after removal, especially when applied to eventual carvings present on iron-based objects. This more detailed data processing enhanced that outcomes in terms of corrosion removal were obtained with, from best to least performing: 3% w/v DFO-agar gel applied hot, DFO-gellan gel prepared and applied cold (at room temperature) followed by hot-applied DFO-gellan gel to finish with the rigid DFO-agar gel applied cold as well as DFO-xanthan gel. Still, it is interesting to mention the presence of carboxylic groups in the gellan gum molecular structure which could be an advantage for the purpose of metal corrosion removal.

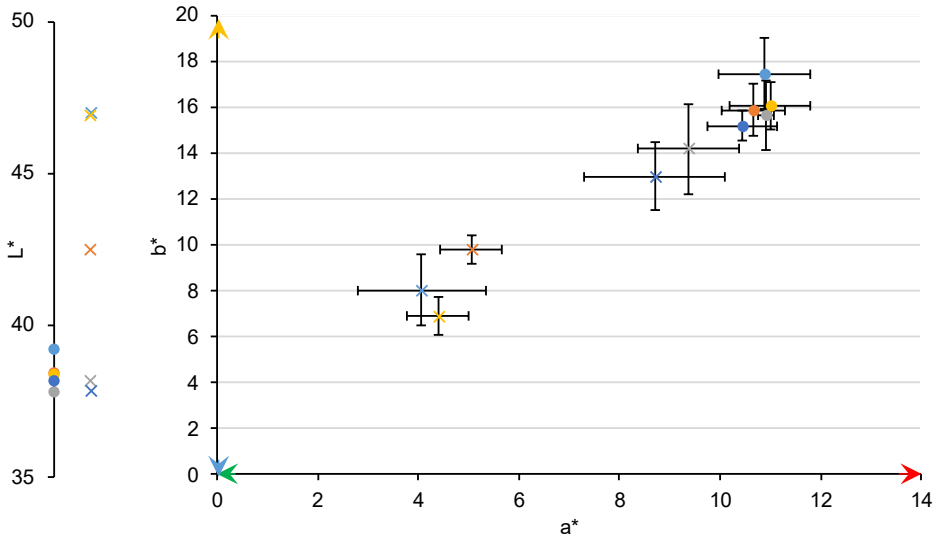

Figure 4.3 L*a*b* color coordinates measured on naturally corroded steel samples before (circles) and after (crosses) cleaning using different gel matrixes: Cold prepared and applied gellan gum (light blue), hot applied gellan (orange), cold (grey) and hot (yellow) applied agar and xanthan gum (dark blue), loaded with $3 \cdot 10^{-2}$ M DFO solution.

4.1.1.2.3 Study of application parameters

In this section, parameters influencing the outcome of the cleaning intervention were assessed, in particular parameters related to the formulation (i.e., concentration of siderophore in the gel) as well as related to the application (i.e., time of application and reiteration). In regard to the results obtained in the previous section, only agar-DFO gels were studied.The influence of the agar gel matrix onto the kinetics of uptake was also looked at.

Color difference of NS before and after cleaning showed a similar variation than the amount of iron taken up by the agar gels (Figure 4.4). After 3% w/v agar gel application of DFO at different concentrations on naturally corroded steel samples, colorimetric results show an important hue change at concentration starting from $3 \cdot 10^{-2}$ M (Figure 4.4). This value for efficacy limit was confirmed by AAS analyses of the used gels, where iron concentration in gel increases rapidly from the same concentration of $3 \cdot 10^{-2}$ M and in a linear trend with the increasing DFO concentration. Thus, a $6 \cdot 10^{-2}$ M concentration was selected for the further experiments described below, as it allows a greater performance. Both iron taken up and samples' color change follow a proportional increase with increasing DFO concentration. The chelate loading of each gel is on average 6.9, 1.1, 0.6 and 0.6% for $3 \cdot 10^{-4}$, $3 \cdot 10^{-3}$, $3 \cdot 10^{-2}$ or $6 \cdot 10^{-2}$ M DFO respectively.

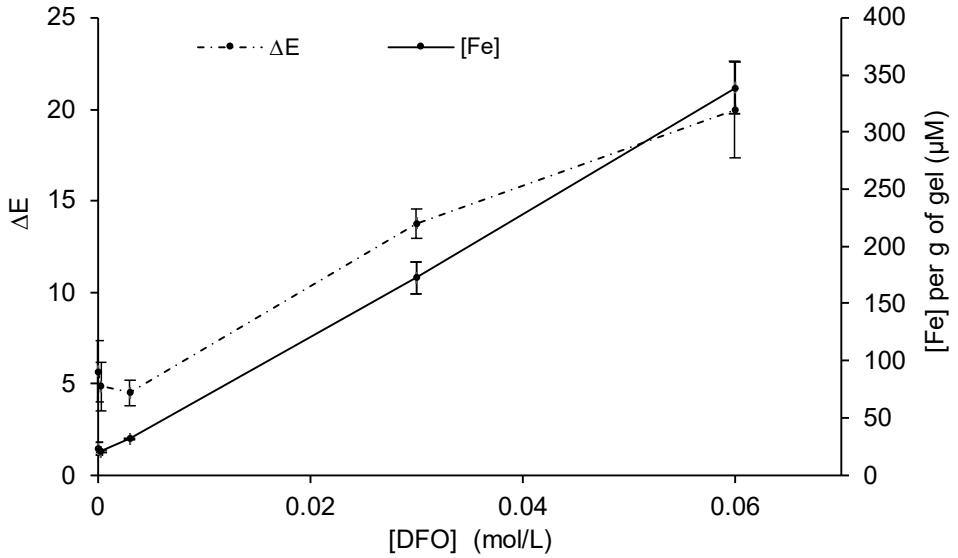

Figure 4.4 Iron content of 3% w/v agar gels amended with 0, $3 \cdot 10^{-4}$, $3 \cdot 10^{-3}$, $3 \cdot 10^{-2}$ or $6 \cdot 10^{-2}$ M of DFO solution, after treatment. Sample color difference measured before and after application of gel formulations.

The complexation reaction caused the uncolored gel to turn vivid red-orange (Figure 4.5a). Color change of the gels before and after a 10-minute application is visible starting at the minimal tested DFO-concentration ($3 \cdot 10^{-4}$ M), but iron uptake is not yet visible using AAS (Figure 4.5b). Color change seems more sensitive to ascertain low quantities of iron present in the agar gel than the used spectroscopic technique AAS. However, no direct correlation could be drawn between the amount of extracted iron and the visual appearance of the gel during treatment as the variation were not following a similar pattern (Figure 4.5, black curves). Iron taken up is following a linear regression ($R^2 = 0.99$) over the span of the tested DFO concentrations whereas gel color change ΔE is rapidly increasing until $3 \cdot 10^{-2}$ M and is then followed by a limited color change. Indeed, the hues of the agar gel amended with $3 \cdot 10^{-2}$ M and $6 \cdot 10^{-2}$ M DFO solutions were close ($\Delta E = 80 \pm 7$ and 81 ± 1 respectively) despite the greater complexation action of the higher concentration, as determined by AAS ([Fe] = 8.1 ± 0.4 and 20 ± 3 mg/L respectively). When considering the three CIELab color coordinates, ΔL and Δa follow a logarithmical regression, similarly to ΔE ($R^2 = 0.97$, 0.96 and 0.98 respectively). However, Δb does not show the same pattern, decreasing after $3 \cdot 10^{-3}$ M, therefore going towards less yellow values. This explains why, although the global ΔE of the $3 \cdot 10^{-2}$ M and $6 \cdot 10^{-2}$ M DFO-amended gels after complexation were similar ($\Delta E = 80 \pm 7$ and 81 ± 2 respectively), although a slight difference can be observed visually with a less orange and more red color at the maximal concentration. Still, although not proportional to the amount of iron taken up, this feature of deferoxamine is an interesting metrics to assess the iron uptake, and thus the cleaning action, as it can be easily monitor by the operator.

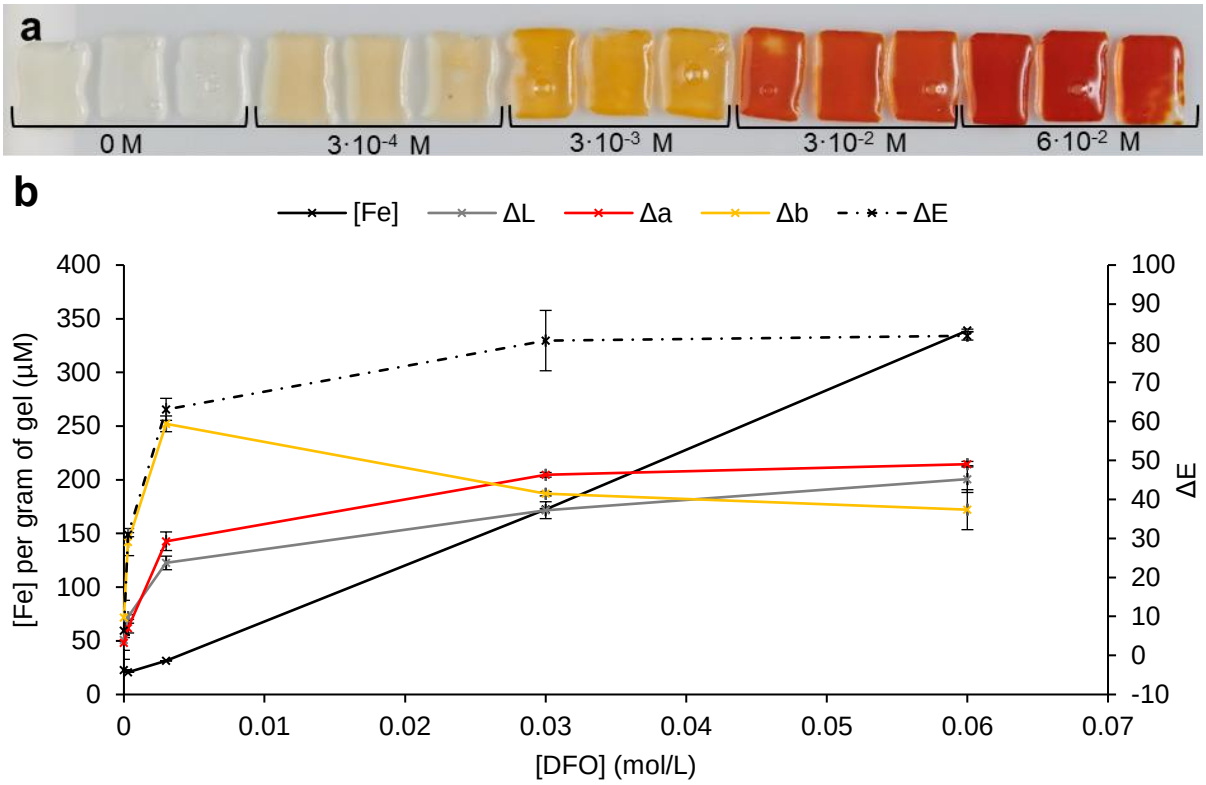

Figure 4.5 (a) Different concentrations of DFO-amended 3% w/v agar gels applied to the naturally corroded steel samples (NS) for 10 min and (b) graphical representation of ΔE, ΔL, Δa and Δb on the gel and the extracted iron concentration before and after treatment with DFO-amended 3% w/v agar gels.

Deferoxamine binds with iron in a 1:1 molar ratio, meaning that a $6 \cdot 10^{-2}$ M DFO solution can take up up to 3.3 g/L of iron, as confirmed by the plateau reached at 5 hours ([Fe] = 3.3 ± 0.1 g/L) for iron concentration in Figure 4.6.

Figure 4.6 shows a threshold in the iron uptake after 5-hours contact of naturally corroded iron sample with a $6 \cdot 10^{-2}$ M DFO water solution that is not present when using a gel matrix. This can be explained by the modification of the diffusion coefficient within the agar gel which follows the Higuchi model, usually used for drug release from a matrix. It states that drug release from a matrix is a square root of time-dependent process and is based on Fick's law of diffusion [18]. It is indeed the case for the diffusion of iron ions within the agar-DFO gel which follows a linear regression when plotted versus the square-root of time. The diffusion coefficient D of Fe^{2+} and Fe^{3+} in water at room temperature has been determined to be of $7.19 \cdot 10^{-10}$ and $6.04 \cdot 10^{-10}$ $m^2 \cdot s^{-1}$ respectively [19]. In gel, there are several phenomena to be accounted for that will obstruct the diffusion and therefore decrease the related diffusion coefficient. First, there could be the binding of the solute by the gel, which is often disregarded [20]. Second, obstruction could be observed related to the fineness of the gel network. Indeed, if pores are smaller than the solute molecules, the gel would act as a filter. In the case of agar gels, this phenomenon is not relevant. Indeed, as seen in Chapter 3, the pores of the 3% w/v agar network are of 0.4 ± 0.1 µm,

well above Fe^{3+} ionic radius (0.069 nm) [21]. Third, and the most important here, the solute molecule must go around the gel threads from the network, increasing the path length for the diffusion of solute and therefore the gel coefficient of diffusion is lower.

The concentration of the gel is therefore a crucial parameter in the determination of any diffusion coefficient as a high polymer concentration implies dense network/small pores and consequently long pathlength and low water-filled spaces for the solute to be transported [22,23]. The diffusion coefficient of Fe^{3+} in 3%w/v agar gel was determined to be $3.19 \cdot 10^{-10}$ $m^2 \cdot s^{-1}$ [24]. The presence of a ligand (complexing agent) is known to also decrease the diffusion of the solute (here, iron) inside a gel [24,25]. Indeed, the resulting molecule's size is larger, with a higher molecular weight. The increase of molecular weight is known to decrease the diffusion coefficient [23].

In gel, the metal to ligand ratio hardly reaches 3% after 24 hours of application. This could be interpreted as an inefficiency of the gel in terms of chelate loading, showing the equilibrium state is never reached in gel. Nevertheless, the use of gel still permits a better control and overall a lower volume of treating solution to be used for corrosion removal as it is very localized and restrained. In addition, the use of gel enhances the level of control, which is appreciated by conservators, in spite of the lower efficiency.

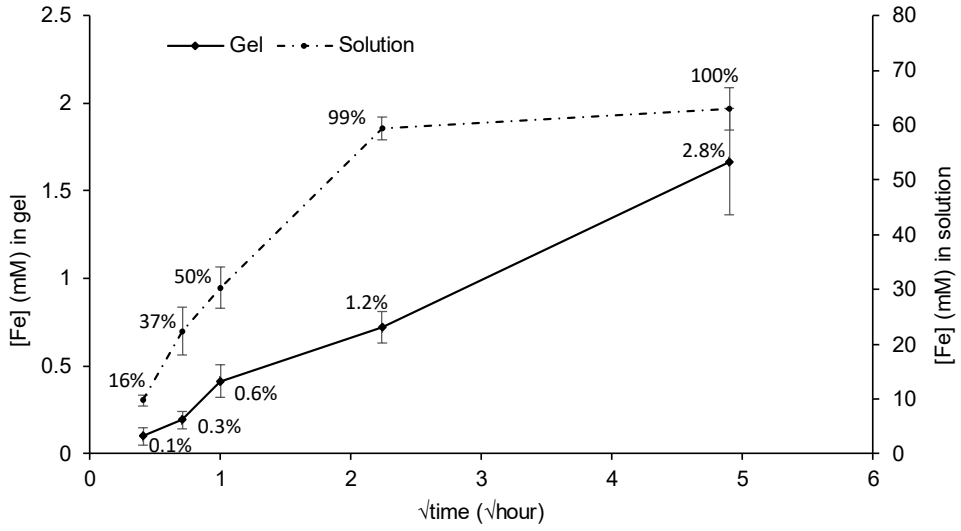

Figure 4.6 Iron uptake by a 3% w/v agar gel amended with $6 \cdot 10^{-2}$ M solution of-DFO in contact with NS (plain line) and by a $6 \cdot 10^{-2}$ M DFO water solution after immersion of NS (dotted line) for 10 min, 30 min, 1 h, 5 h and 24 h at 20°C. Percentages represent the metal to ligand ratio.

In table 4.5, the differences according to the number of reiterations of the gel application on naturally corroded steel samples can be observed, where six gel applications of 10 minutes are visually performing better than a unique application of 60 minutes. Indeed, after a single 60 min application of 3% w/v agar gel amended with $6 \cdot 10^{-2}$ M DFO water solution, pits were still visible whereas a more homogeneous surface aspect was obtained when the same gel was applied for 6 × 10 min. These results are confirmed by colorimetry values in which multiple reiterations resulted in a higher color variation

than achieved with the same formulation applied as a continuous application (ΔE = 21.2 ± 0.7 and 18.0 ± 3.5 respectively). As supported by ANOVA, the color difference between the two types of application is not statistically significant. Nevertheless, the relative standard deviation, higher for the single 60 minutes application, supports the better performance of the 6 × 10 min applications, as supported by the less homogeneous visual observation. This suggests that, for a better cleaning performance of the gel formulation, successive short application times provide a more effective cleaning than a long one. In addition, reiterated applications allow for a greater control on the intervention as progress of the cleaning is evaluated at shorter intervals.

AAS measurements showed that the total taken up iron concentration was similar when the gel formulation was applied 6 × 10 min or as a single 60 min application ([Fe] = 0.68 ± 0.12 and 0.69 ± 0.03 mM respectively). This is in accordance with the fact that the iron uptake rate seems to be linear up until 1 hour (0.38 mmol/L/h), and then drops to 0.01 mmol/L/h (Figure 4.6). This can be explained by the drying of the gel rendering it less effective although precautions were taken to limit the phenomenon. DFO and EDTA showed close performances when regarding the color difference before and after application (ΔE = 21.2 ± 0.7 and 16.0 ± 3.0 respectively), with the EDTA-amended gel color variation before and after cleaning being slightly lower. The results obtained with 3% w/v agar gel amended with $6 \cdot 10^{-2}$ M Na_2EDTA water solution, also applied to the naturally corroded steel samples for 6 × 10 min, were similar to those obtained with DFO-amended 3% w/v agar gel in terms of the visual appearance of the samples after cleaning and iron uptake ([Fe] = 0.73 ± 0.04 and 0.68 ± 0.12 mmol/L respectively) . On model samples, the siderophore performed equally as the well-established active agent EDTA, which is of good prospect for the implementation of such biologically-produced compound in praxis.

Table 4.5 Summary of the color variation of the naturally corroded samples before and after cleaning (ΔE), the amount of iron extracted using 3% w/v hot applied agar gels amended with DFO or EDTA solution at $6 \cdot 10^{-2}$ M, and micrographs of the samples' surfaces after the intervention. Scale bar indicates 5 mm.

	ΔE	**Total [Fe] extracted from use gels (mM)**	**Optical microscopy observation**
Untreated sample	n/a	n/a	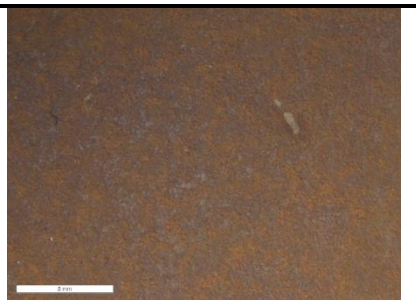
$6 \cdot 10^{-2}$ M DFO-amended agar gel 1 × 60 minutes	18.0 ± 3.5	0.69 ± 0.03	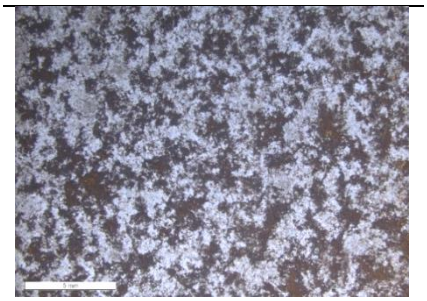
$6 \cdot 10^{-2}$ M DFO-amended agar gel 6 × 10 minutes	21.2 ± 0.7	0.68 ± 0.06	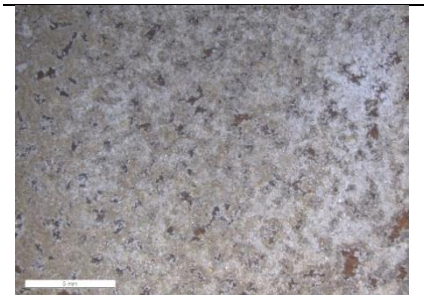
$6 \cdot 10^{-2}$ M EDTA-amended agar gel 6 × 10 minutes	16.0 ± 3.0	0.74 ± 0.04	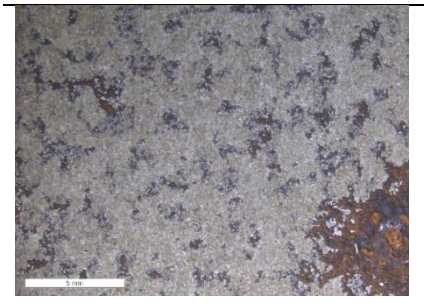

4.1.1.2.4 Long-term behavior of the treated pieces

The average color difference ΔE of the naturally corroded steel samples after cleaning and after one year stored in uncontrolled indoor conditions was of 3 (± 1.7) on areas treated with DFO-amended agar gel and 4 (± 1.7) for EDTA-amended agar gel. ΔE values obtained for both DFO and EDTA cleaning method are inferior to 5, such color differences are thus not perceptible to the human eye [16]. In addition, digital microscope observations showed a similar surface appearance after 1-year storage (Figure 4.7). Although the clearing protocol should ensure the absence of residues from the used gel and solution (see Chapter 3, section 3), recent studies present deferoxamine as a reliable corrosion inhibitor, thanks to its hydroxamate group [26]. This is to be underlined as this property could be of interest for cultural heritage application, as this compound could have a "2-in-1" action, offering both cleaning and corrosion-inhibiting activity.

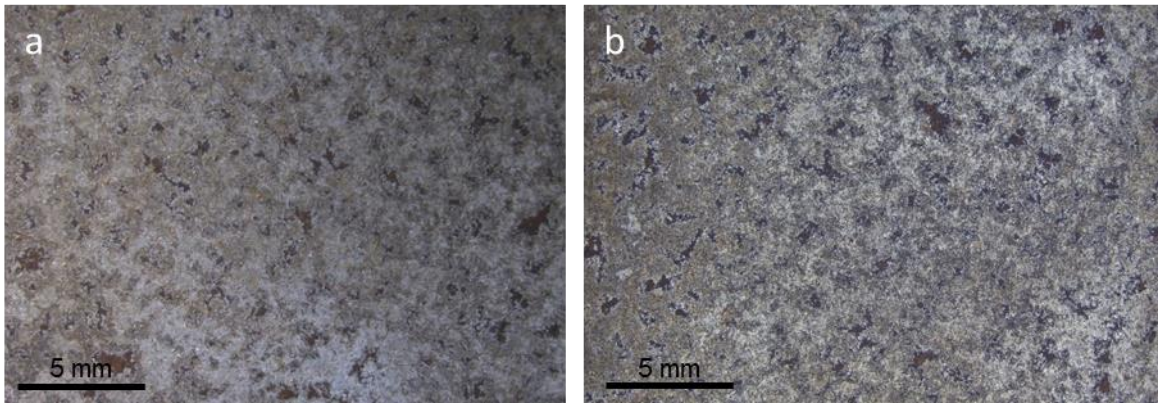

Figure 4.7 Naturally corroded steel sample immediately after Agar-DFO cleaning (a) and one year after intervention (b).

4.1.2 Evaluation on case studies

4.1.2.1 Materials and methods

Following the advice of Aymeric Raimon, conservator at the Arc'Antique laboratory in Nantes (France), two iron-based artefacts were selected: (i) a candle holder from the Diocese of Nantes (France), as historical object; (ii) a helmet belonging to the personal collection of Raoul de Rochebrune (1849–1924) and bequeathed to the Dobrée Museum of Nantes (France) in 1930, as archaeological objects (Table 4.6). Although the focus of this work is directed towards historical relics, it was deemed interesting to also assess the formulations on archaeological objects for research purposes and subsequent work perspectives, to broaden the field of application of the developed formulations. The objects were marked by diverse corrosion phases and conservation conditions.

Consequently, the treatment aims for the two objects differed and had to be specifically defined for each type (historical or archaeological object).

For the diocesan candle holder, a continuous and homogeneous thin red layer, typical of surface oxida-

tion was observed. The metallic surface was well preserved, and a black patina was sporadically present. The goal was to reduce the reddish corrosion layer until the metallic surface by means of gentle chemical cleaning, in order to limit metal brightness and preserve the black patina present. Based on mock-up results, the religious artworks received, on three distinct areas, 3% w/v agar gels amended either with DFO or EDTA solutions (both at a concentration of $6 \cdot 10^{-2}$ M) in two applications of 15 minutes; the application of agar gel without any chelator served as a control.

For the helmet, the lack of conservation of the original surface can be explained by the fact that, like most of the collection, these archaeological objects were probably discovered in a fluvial environment, which would explain its stripped aspect. Heterogeneous crevices or pit corrosion were seen and the strong areas of abrasion on its outer parts indicated that it had been cleaned in the past using chemical and/or mechanical means. A black patina, considered as the original surface, was present only sporadically, its loss probably being the result of uncontrolled cleaning. Further loss would lead to the undesired exposure of the metallic surface. As the dense red corrosion layer visible on the crevices served as evidence of the historical journey of the object, its conservation was desirable. The aim is therefore to clean in a controlled manner to remove some of the corrosion products to reach the original surface while keeping the dense red corrosion in the pits. Three different areas on the interior surface of the helmet were treated. Due to the thick corrosion present on both objects, the overall cleaning consisted of the application of 3% w/v agar gels amended either with DFO or EDTA solutions (both at a concentration of $6 \cdot 10^{-2}$ M) for 3 × 20 min. The control consisted of plain agar gel applied (without chelator) following the same protocol.

Table 4.6 Recapitulative table of iron-based objects selected as case studies.

	Objects	
		
	Candleholder	**Helmet**
Description	Historical piece. Thin corrosion layer.	Archeological object. Sediments and corrosion compounds displayed in its stratigraphy.
Provenance	Diocese of Nantes (France)	Dobrée Museum (Nantes, France)
Application	2 × 15 minutes	3 × 20 minutes

Before and after cleaning, optical microscopy images were acquired. Raman spectroscopy was used to examine the helmet after cleaning on both treated and untreated areas. Due to the geometry of the objects and the desire to avoid as much as possible the contact with the surface, colorimetric measurements were not performed. Analytical measurements parameters are detailed in the supplementary materials at the end of this chapter.

4.1.2.2 Results and discussion

Visual observations of the candleholder indicated an efficient cleaning with DFO-amended 3% w/v agar gel. The removal of the iron corrosion products revealed the underlying metal and the objects' details (Figure 4.8).

Figure 4.8 Digital microscope images of details from the candleholder before (a, b) and after (c, d) cleaning with $6 \cdot 10^{-2}$ M DFO-amended agar gels. Scale bar indicates 5 mm.

On the helmet, the presence of corrosion products was observed in each zone, even after EDTA-amended gel application, which appeared more aggressive. The achievement of the desired resulting degree of cleaning was difficult, as the metallic surface became apparent after the intervention (Figure 4.9).

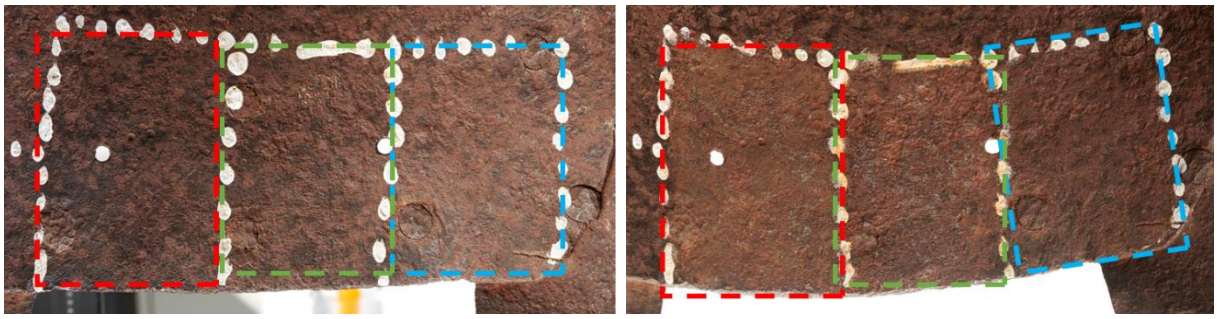

Figure 4.9 Visual observation of the helmet before (left) and after (right) cleaning with EDTA- (red), DFO- (green) or plain agar (blue) gels.

AAS of the gels used on the helmet was performed to evaluate the amount of iron extracted using the different formulations which yielded to 0.18 mmol/L for EDTA- vs. 0.097 mmol/L for DFO- gels of iron detected in gels after a 20-minute application. Detection of iron in the control gel yielded 3 μmol/L. Raman analyses performed on the helmet after cleaning identified the presence of calcium-based compounds (e.g., $CaSO_4$, $CaCO_3$) along with iron oxy-hydroxides on the areas treated with DFO-amended 3% w/v agar gel but not with EDTA-amended 3% w/v agar gel (Figure 4.10) [27,28].

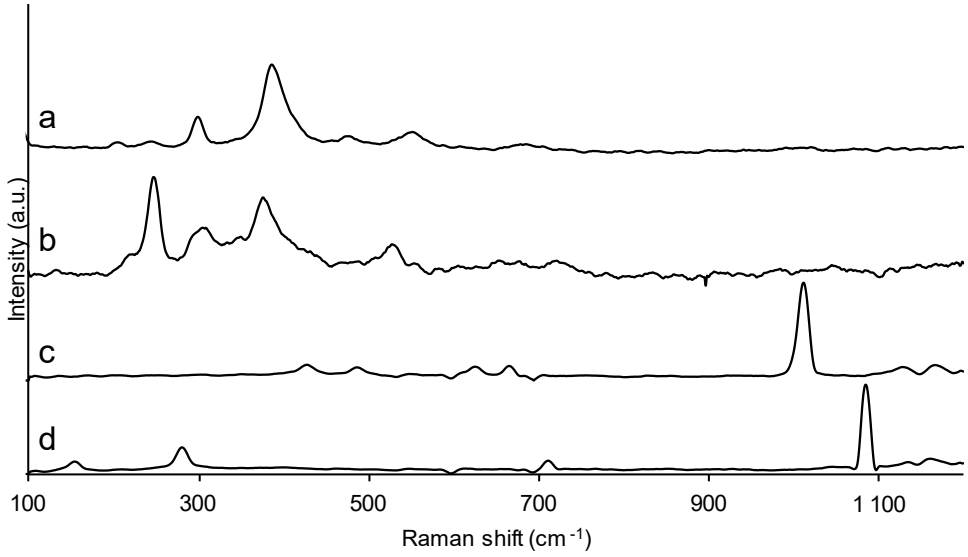

Figure 4.10 Raman spectra (633 nm, 0.1 mW, 4 × 30 s accumulations, 50×) of goethite α-FeOOH (a), lepidocrocite γ-FeOOH (b), anhydrite $CaSO_4$ (c) and calcite $CaCO_3$ (d) obtained on the helmet.

The presence of calcium-based compounds, coming from sediments, resulted in the DFO-amended 3% w/v agar gel being less effective. Unlike EDTA, that can bind iron and calcium (log $\beta_{Fe3+\text{-}EDTA}$ = 25 and log $\beta_{Ca2+\text{-}EDTA}$ = 10.9), DFO is specific for iron and its affinity for calcium ions is poor (log $\beta_{Fe3+\text{-}DFO}$ = 30.6 and log $\beta_{Ca2+\text{-}DFO} \leq 3.03$) [1,2,29]. Although less sustainable [7,8], EDTA offers the benefit of tackling sediments as well as corrosion products in one step thanks to its relatively high formation constant with a large variety of metal cations [6]. Unfortunately, it was not possible to quantify calcium uptake by the

gels by AAS due to interferences from the presence of other elements in the solutions, giving incoherent results.

DFO's specific affinity for iron supports the use of this compound as a suitable and reliable agent for the cleaning of historical iron-based indoor objects presenting simple corrosion stratigraphy. When the stratigraphy is more complex, such as when it includes sediments, a preliminary mechanical cleaning may be necessary to allow further DFO-cleaning to reach the iron corrosion phases more easily.

Recapitulated main findings

Performed experiments allowed to emit assumptions on the functioning of microbial-extracted metabolites on iron-based substrates:

- Agar applied hot is the polysaccharide gel that performed best.
- Deferoxamine does not act on plain metal, hence being safe for the object.
- Cleaning efficacy is achieved for DFO concentration of $6 \cdot 10^{-2}$ M or more.
- DFO-Fe complex is vividly colorful which helps monitoring the treatment.
- Sorption of iron through the agar matrix follows the Higuchi model, lower than in solution.
- Short applications perform better than extended ones and allow for a better control.
- DFO achieves similar results than EDTA on corroded steel surfaces presenting iron oxyhydroxides compounds.
- Although affinity is possible with other ions, deferoxamine is made to be iron-specific. It performs less on some ion such as Ca^{2+} which implies a low efficiency on sedimental layer from archeological objects.
- The treatment seems stable over time, in addition to potential corrosion inhibitive properties of DFO that is an additional asset.

4.2 Copper

4.2.1 Evaluation on model samples

4.2.1.1 Materials and methods

4.2.1.1.1 Samples

Copper and brass ($Cu_{63}Zn_{37}$) obtained from Tartaix (France) were tarnished adapting patination recipes using "liver of sulfur" with potassium sulfide [30]. Briefly describing the procedure, a 20% w/v solution of Na_2S was applied on the metal to be tarnished using a cotton swab, immediately rinsed with water and dried. This allows the formation of cuprite (Cu_2O) and chalcocite (Cu_2S) [31,32]. The obtained tarnish was defined as a dark tarnish according to ASTM copper strip corrosion standard (Figure S4.1). Treated zones dimensions were 30 × 20 mm. In the text, artificially aged samples are referred to as AAC or AAB for copper and brass respectively.

Naturally aged copper samples (NAC) were obtained from the reverse side of a 20-years exposed rooftop sheet metal from La-Chaux-de-Fonds (Switzerland) and cut in dimension of 30 × 30 mm. The corrosion layer of AAC, AAB and NAC sample types, characterized beforehand by Raman spectroscopy, was mainly identified as cuprite thanks to the peak at 147 cm^{-1}.

4.2.1.1.2 Treatment evaluation

A 3% w/v agar gel with DFO water solutions at concentrations of 0, $3{\cdot}10^{-4}$, $3{\cdot}10^{-3}$, $3{\cdot}10^{-2}$ and $6{\cdot}10^{-2}$ M was applied to the artificially aged samples for 15 minutes in order to evaluate which minimal concentration of DFO is needed for effective copper uptake as it may differ from the concentration used for iron in the previous section.

In a second step, a 3% w/v agar gel amended with either DFO, EDDS or EDTA at 3.10^{-2} M along with a plain agar gel as control was applied for 15, 30, 60, 120 minutes. Experiments were carried out at room temperature, approximately 20 °C. Samples were characterized by means of colorimetry and optical microscopy before and after gel application. Atomic Absorption Spectroscopy (AAS) of the used gels was performed to ascertain the amount of copper contained in the gel after application. Details are to be found in the supplementary materials of this chapter but AAS sample preparation involved dissolving the gel with 10 mL nitric acid and gauged to 100 mL using milli-Q water.

On NAC, the latter process was reiterated with additional periods of 240, 480 and 1440 minutes.

In addition, as an insight, NAC were treated with the chitosan formulation described in Chapter 3 as chitosan is known for its copper complexing abilities. The chitosan formulation (CS-ItA-Lcys) was not loaded with chelating agents and was simply deposited onto the samples for the allocated times.

In all cases, after removal of the gel, a cotton swab dipped in ethanol 70% v/v was used to clear the surface.

4.2.1.2 Results and discussion

Focusing on AAS results (Figure 4.11), there is an increase in metal uptake from the Agar-DFO gel at $3 \cdot 10^{-2}$ M on the AAC substrate ([Cu] = 0.73 ± 0.07 mg/L), the same active agent concentration to what is being observed for iron, whereas the increase starts at $3 \cdot 10^{-3}$ M for brass.

For AAC there is a strong decrease of copper concentration at $6 \cdot 10^{-2}$ M, however, this should be interpreted carefully given the rather important value calculated as standard deviation (SD). Given this high SD, it is suggested that this decrease is rather due to the lack of homogeneity of the tarnish layer between treated AAC samples. This lack of homogeneity is also the reason behind a systematic error, showing $3 \cdot 10^{-2}$ M more performing than $6 \cdot 10^{-2}$ M and for which the experiment would need to be repeated more times. Regarding brass, after an obvious rise of the amount of copper taken up within the gel from $3 \cdot 10^{-3}$ M, the growth rate is lowered, reaching a threshold of copper taken up (average of 0.29 ± 0.05 mg/L).

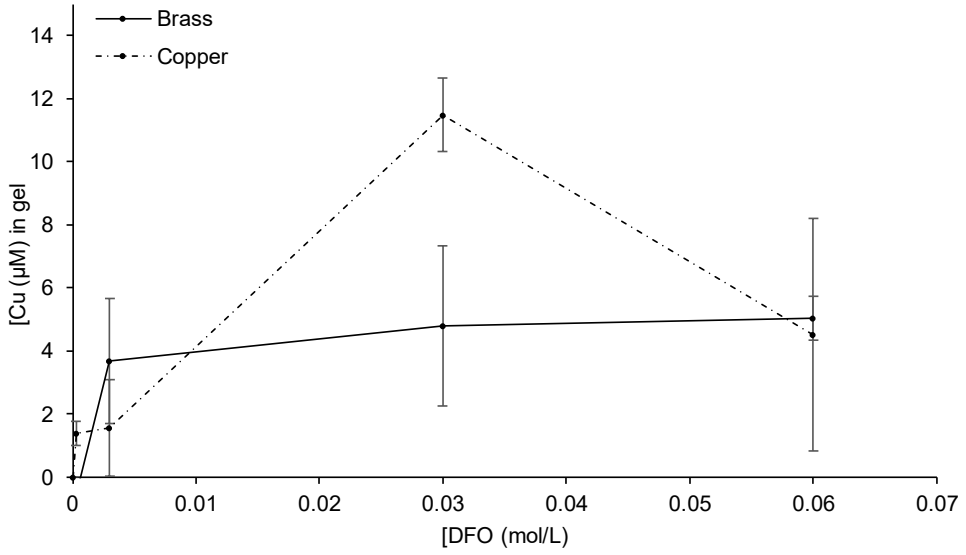

Figure 4.11 Copper detected by AAS in 3% w/v agar gels loaded with different concentrations of DFO after a 10-minute application on AAC or AAB samples.

Interestingly, previous conclusions drawn from AAS are contradicted when looking at the colorimetric data (Figure 4.12): a clear color difference before and after cleaning for brass starting from DFO concentration of $3 \cdot 10^{-2}$ M ($\Delta E = 40 \pm 2$) whereas a clear shift for copper taken upis seen starting at $3 \cdot 10^{-3}$ M when looking at AAS results. For copper plates, almost no changes are detected by colorimetry, with all ΔE values standing below 5, the limit of perceptible change [16].

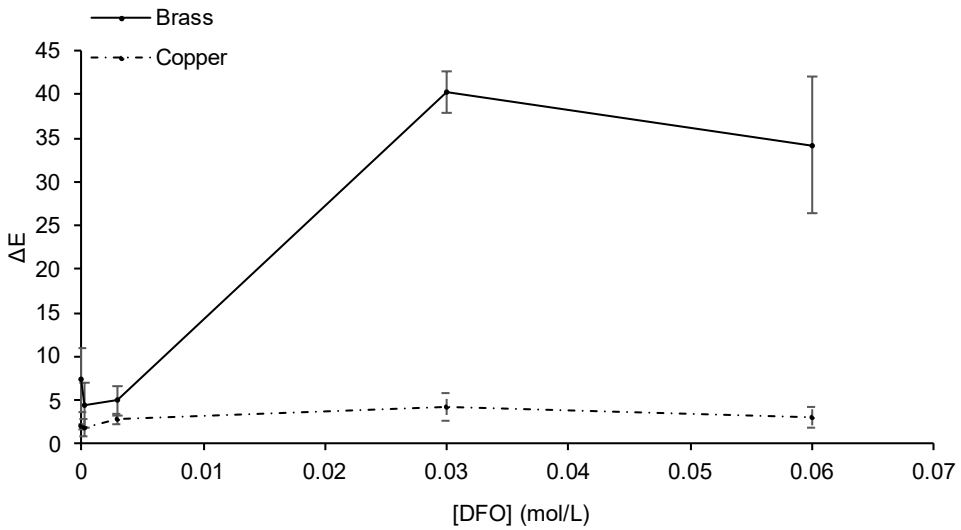

Figure 4.12 Color difference ΔE on copper AAC and brass AAB samples after application of 3% w/v agar gels loaded with different concentrations of DFO for 15 minutes.

One way to explain the difference of results between the two analytical method is the clearing step. After clearance of the gel using this method, the visual appearance of AAB is modified (Table 4.7). Indeed, the use of the cotton swab allowed, thanks to its mechanical action, to remove the tarnish layer present on brass. Basically, the treating gel weakens the structure of the tarnish layer allowing it to be mechanically removed using very light force [33]. On the other hand, for copper, this phenomenon was less prominent (Table 4.7), rendering a non-homogenous visual aspect of the surface. This was connected to the adherence of the tarnish layer onto the different alloys. Indeed, jewelers, who often resort to artificial patination techniques, have reported that a "liver of sulfur" ageing does not take well on brass [34]. For that reason, further experiments were carried out on copper samples only. Noticeable performance was therefore achieved from $3 \cdot 10^{-2}$ M of deferoxamine, which was used for further tests.

Table 4.7 Optical microscope observations of copper and brass samples before and after application of a $3 \cdot 10^{-2}$ M DFO-containing 3% w/v agar gel.

	Before cleaning	After cleaning
Copper	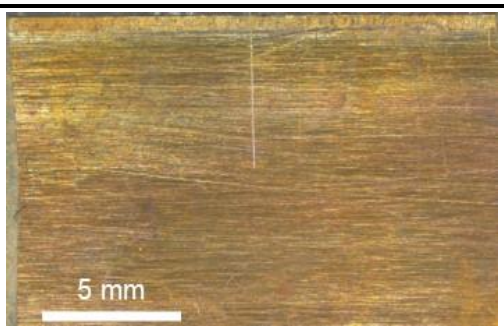	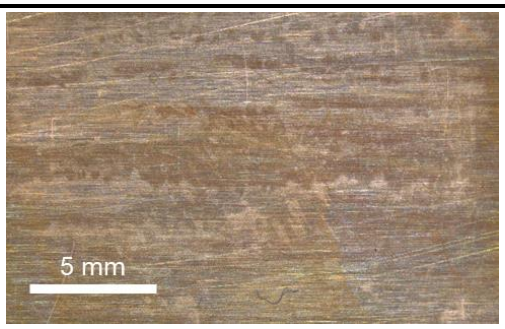
Brass	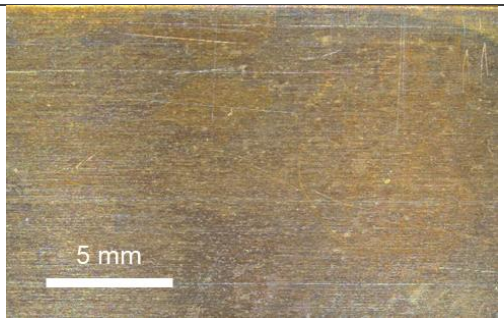	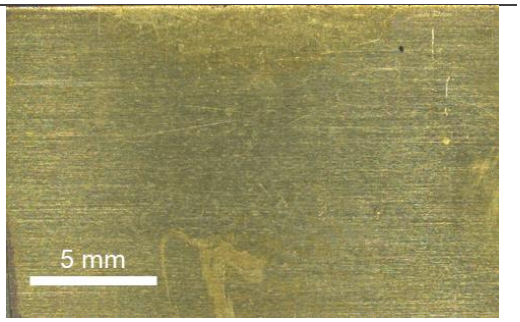

Globally, a similar trend is seen between artificially and naturally aged samples in copper uptake (Figure 4.13 a and c), with EDTA being the most performant followed by EDDS. Slight differences can be noticed regarding the latter, its performance is closer to DFO on NAC whereas it is in-between EDTA and DFO in terms of copper uptake for AAC. For NAC, a statistical analysis showed there was no significant difference ($p > 0.05$) between the performance of DFO and EDDS, but an existing shift between the amount of copper taken up or the color difference with EDTA or plain agar. It can therefore be stated that on naturally aged coupons, EDTA performs best, followed by EDDS and DFO with equal results and way better than the plain agar gel control.

However, the amount of copper uptake between the two types of samples (AAC and NAC) differs by circa an order of magnitude (0.1% of EDTA loaded with Cu in AAC and up to 1% in NAC, figure 4.13). Of course, a rapid tarnishing achieved on AAC cannot reach the thickness and adherence of a patina/tarnish layer created progressively over a period of years.

When it comes to color difference (Figure 4.13 b and d), the tendency is a bit different between AAC and NAC where EDDS is most performant in the case of AAC ($\Delta E = 15 \pm 2$ at maximum). On NAC, EDTA is performing best with a maximum ΔE of 27 ± 4.

There is a lack of consistency obtained for AAS and colorimetry or AAS in the case of artificial tarnish, i.e., high standard deviation, preventing from making hypothesis with strong grounds. Indeed, Tuckey post-hoc tests showed there were not significant difference in both ΔE and amount of copper taken up

according to the type of solution amended inside the gel, the plain gel not performing any better than chelator-loaded ones. This phenomenon is not new in heritage sciences and albeit the existence of "artificial" corrosion standards (e.g., ASTM, ISO) [35], the plethora of existing natural patina makes these standards almost irrelevant and therefore only scarcely used. The difficulty to obtain accurate artificial tarnishes that are representative and give way to reliable results have therefore been studied in other papers, with the emergence and input of updated and optimized synthesis, unfortunately not universal [36]. So far, as much as possible, although more difficult to obtain, the use of naturally aged samples is preferred to avoid a discrepancies between in-lab studies and future applications. Therefore, for the sake of accuracy, the kinetics of the cleaning of copper by studied formulations was assessed on NAC (Figure 4.3c).

Although at different values, the three complexing agents EDTA, EDDS and DFO display an identical curve for AAS measurements (Figure 4.13c). There is a first small plateau after 120 minutes (2 hours) of cleaning. This decrease of reaction rate is most likely due to the drying of the gel, with therefore a low amount of complexing molecules present in the matrix [37]. This drying can be observed on Figure 4.14.

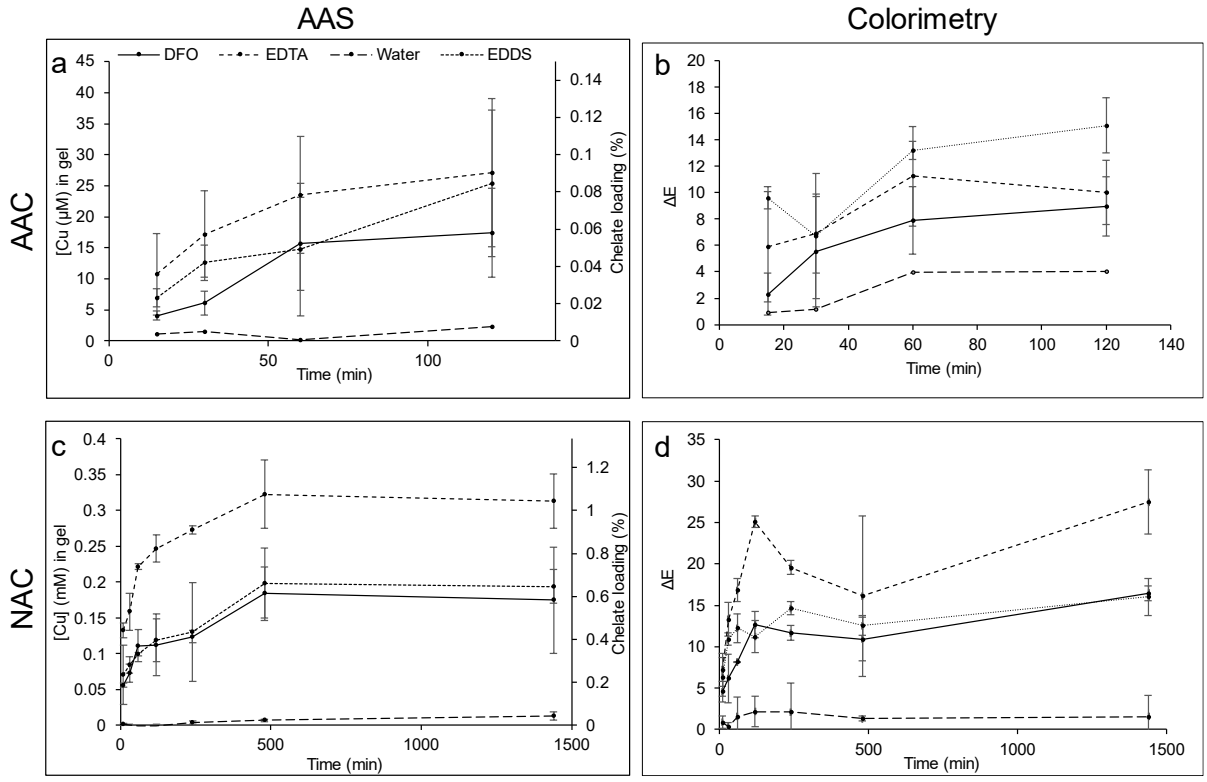

Figure 4.13 AAS measurements on gels after application on AAC (a) and NAC (b) and color difference before and after application on AAC (c) and NAC (d).

After 240 minutes (4 hours), there is a slight increase in the uptake rate before reaching a threshold starting at 8 hours. Again after 4 hours of application, the gels dried completely and physically adhered

to the surface. Their removal was therefore resulting in a strong stripping mechanical action which removed part of the remaining tarnish (Figure 4.14).

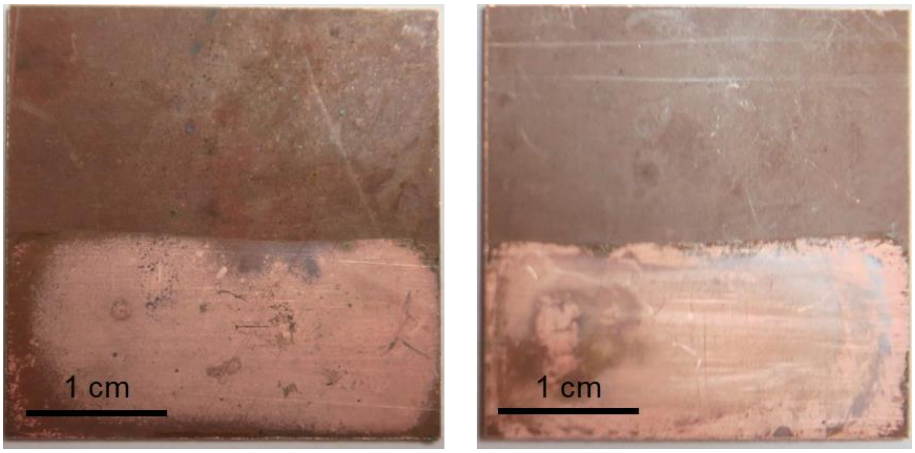

Figure 4.14 NAC samples (3 × 3 cm) after removal of complexing agar gel with EDDS, applied for 2 hours (left) and 8 hours (right).

In addition, the gel being completely dried, no reaction can occur and that explains the threshold observed after 8 hours.

Drying in the context of gel-based method is an already reported phenomenon, where in the case of desalination treatment of archeological objects it is the loss of contact between the gel and the object that is reported [38]. Gel drying can be explained with several parameters including relative humidity of the environment or thickness of the applied gel. This adds up to better reaction rates and better control into why shorter applications are preferred. If longer reaction is needed, placing the gel into a confined space is therefore advised, covering with watch glass on a flat surface or even plastic film.

As DFO chelates copper at a 1:1 molar ratio [39], it was possible to calculate the theoretical uptake of copper in a $3 \cdot 10^{-2}$ M DFO solution which is of 1900 mg/L. In the study, the threshold reached after 8 hours attained 0.17 mmol/L (0.5 % of chelate loaded). The diffusion coefficient of Cu^{2+} in water at room temperature is $7.14 \cdot 10^{-10}$ $m^2 \cdot s^{-1}$. Similarly to what has been discussed previously for iron, the diffusion coefficient is much lower in gel. In addition to those phenomena (presence of the polymer network and of the complexing agents), the drying of the gels prevents to study the Higuchi model diffusion as there was a change in the volume of the matrix system (the gel). Nevertheless, the loss of metal to ligand efficiency using gels is counterbalanced by the assets their use displays in terms of safety of cleaning conservation treatments.

Regarding color differences for NAC, (Figure 4.13d), the three active agents (i.e., DFO, EDDS and EDTA) follow a similar color difference variation, in particular with a strong rise until 120 minutes of application. Afterwards, as concluded with AAS results, variations are caused by drying of the gels. This drying implies further edge effects or scratches on the samples that impact the global visual appearance of the samples, being less homogeneous (Figure 4.14).

The use of DFO-, EDDS- or EDTA-amended agar gels for cleaning copper surfaces gave the gels a blue or green very light hue after use, but not as important as for iron-DFO complexation hence not as relevant to monitor the cleaning process.

On another note, corrosion regrowth on cleaned copper samples is unavoidable overtime as cuprite can form spontaneously when exposed to oxygen in a matter of days [40]. For such, it is common to leave a layer of cuprite when cleaning copper-based artefacts, as it is considered protective [41]. There would therefore be the need of a cleaning agent that is selective enough to remove tarnish (mainly chalcocite) but not affect cuprite, as it has been mentioned in other works studying copper cleaning [42]. Unfortunately, as seen in Chapter 2, of EDTA and EDDS seem to solubilize Cu_2O better than Cu_2S (Table 4.8). On the contrary, DFO showed no enhanced solubilization for Cu_2S over Cu_2O but still, there is no selectivity to avoid removing cuprite.

Evaluation of long-term behavior of cleaned surface overtime is therefore not as relevant as for iron as cuprite will form spontaneously and rapidly overtime as soon as it is cleaned and exposed to oxygen [43].

Table 4.8 Copper solubilized (normalized to BET surface area) (μmol/L/m²/g) after 24 h immersion of Cu_2O or Cu_2S powder in solutions of EDTA, DFO or EDDS - see methods in Chapter II, section 3.1.

	EDTA	**DFO**	**EDDS**
Cu_2O	911 ± 83	189 ± 78	1178 ± 97
Cu_2S	470 ±36	236 ± 98	475 ± 88

4.2.1.2.1 Preliminary tests for the application of the chitosan formulation for copper cleaning purposes

Regarding the direct application of CS-ItA-LCys on corroded copper samples (Figure 4.15), its metal removing performances are not statistically significant until 240 minutes (4 hours) of application. After 8 hours of application a statistically significant color modification (p-value = 0.003) can be observed between samples treated by agar or CS-ItA-LCys, as it is just above the limit of $\Delta E = 5$. The application of the plain CS-ItA-LCys formulation compared to plain agar showed better results ($\Delta E = 7 \pm 3$ vs. 3 ± 3, respectively, after 24 hours) but that are not significant when controlled via ANOVA. Contrary to agar gels, no drying of the gels is occurring thanks to the neutralization step that soaks the gel and the existence of a thicker membrane that prevents evaporation. Because the gel is molded beforehand, the contact is not as close and therefore the interaction between the gel and the surface is not as immediate and strong as for agar gel dripped hot onto the surface.

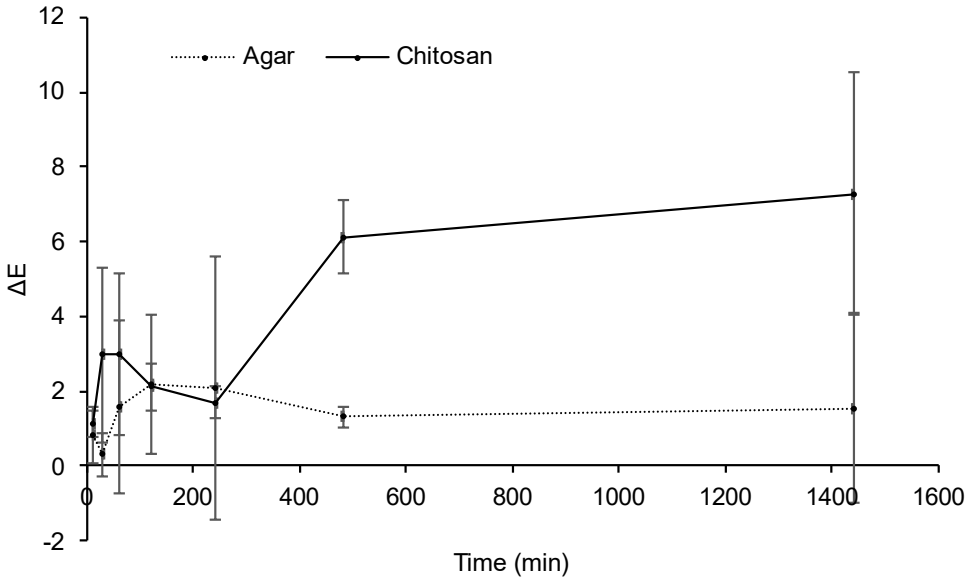

Figure 4.15 Color difference after application of CS-ItA-LCys on NAC samples.

Interestingly, a blueish coloration, typical of Cu^{2+} ions, of the CS-ItA-LCys gel after application was seen on the outer part of the gel surface, as soon as 4 hours after application (Figure 4.16). Unfortunately, quantification of copper inside CS-ItA-LCys was not possible due to the difficulty to dissolve samples for AAS measurements [44]. Nevertheless, it is an interesting perspective. Another foreseeable work would be to assess whether the phenomenon is due to adsorption, absorption, or complexation.

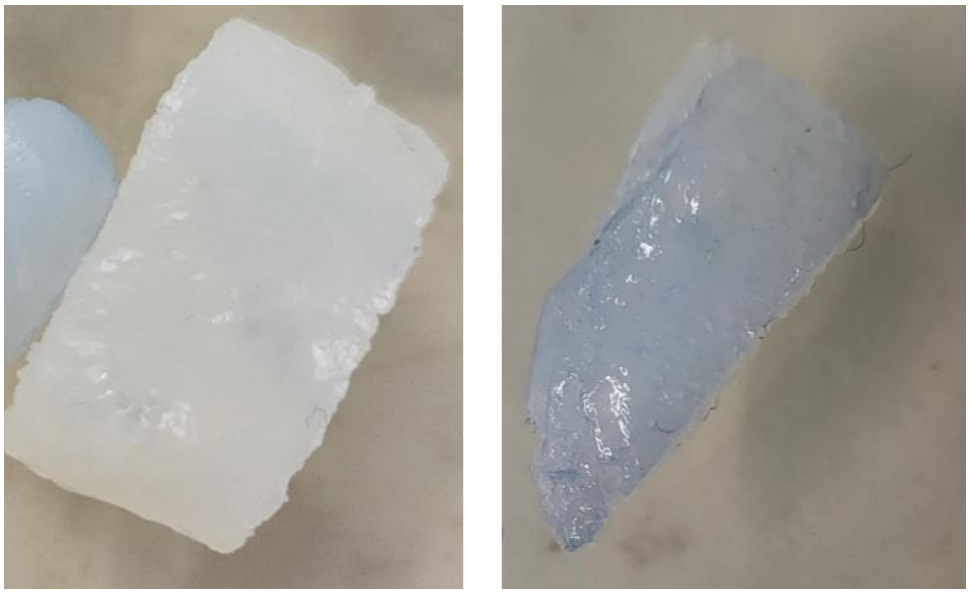

Figure 4.16 CS-ItA-LCys gels after before (left) and after (right) application on NAC samples.

4.2.2 Evaluation on case studies

Different historical copper-based objects were used for case studies.

4.2.2.1 Materials and methods

4.2.2.1.1 Brass orthodox polyptych

First, an orthodox polyptych made of brass (Figure 4.17) and provided by the Musée Dobrée in Nantes was used to compare different formulations.

Figure 4.17 Brass orthodox polyptych obtained lent by the Musée Dobrée (Nantes, France).

The following text is a translation, from French, of the condition report established by the conservator Aymeric Raimon regarding the artefact. "*This object was in an intermediate state of conservation, with the presence of many scratches but surprisingly no residues from abrasive cleaning pastes usually used on that type of object. It is composed of four brass panels showing a molded religious scene on the front whereas the back is flat.*

The corrosion displayed on this object's surface seems to be sulfur compounds, according to the homogenous iridescence, going from blue to purple. There is also a global patination of the metal is the brownish hue. Finally, some red corrosion pits/dots can be observed on the edges of the plate. Those might be copper oxides. The diagnostic is therefore atmospheric corrosion, repeated handling of the object without gloves and most likely repeated over-cleaning explaining the scratches".

The aim of the treatment was to retrieve the original brightness of the brass.

On this object, several tests were performed on the back of one of the panels using, similarly as on model samples, DFO, EDTA and EDDS solution at concentration of $3 \cdot 10^{-2}$ M in 3% w/v agar gel. They were

applied for 10 minutes and repeated if necessary. A zone was treated using a 60-minutes application of DFO-agar gel. The surface was further cleared with 70% v/v ethanol using a cotton swab.

Pre- and post-intervention evaluation was performed by optical microscopy, colorimetry and Raman spectroscopy employed as described in supplementary materials. Copper uptake by the applied gels was quantified using Atomic Absorption flame spectroscopy in a similar way as explained previously.

4.2.2.1.2 Brass lamp

The second object treated was a lamp, lent from the Historical Museum of Lausanne (MHL) (Figure 2.8). It displayed a slight tarnish, as defined by the ASTM copper strip corrosion standard (Figure S4.1) [45] . The aim of the treatment was to lower the tarnish layer of the external part without reaching an extremely bright appearance of the metal. The internal part was not treated due to the fragile condition of the glass.

To achieve this light cleaning and from previous tests, it was chosen to work with a $3 \cdot 10^{-2}$ M DFO-agar gel in order to be able to perform a progressive removal. Due to the fragility of the object, only pictures and visual observations could be performed on the lamp to assess the cleaning performances.

Figure 4.18 Brass lamp lent by the MHL, before intervention. Scale represents 3 cm.

4.2.2.1.3 Silvered pocket-watch

A silver-based pocket-watch lent by the Historical Museum of Lausanne (MHL) was studied to remove spots of blueish corrosion compounds (Figure 4.19). The elemental composition of the alloy was assessed using an X-ray Fluorescence (XRF), parameters details in supplementary materials.

Compounds were characterized using optical microscopy, FTIR and Raman spectroscopy as detailed in supplementary materials. The full external part of the pocket-watch was treated by the application of $3 \cdot 10^{-2}$ M DFO agar gel for 20 minutes and rinsed with ethanol as described previously for other objects.

Figure 4.19 Pocket-watch lent by the Historical Museum of Lausanne (MHL). Scale is 2 cm.

4.2.2.2 Results and discussion

4.2.2.2.1 Brass orthodox polyptych

Raman spectra performed on the surface (Figure 4.20) revealed the presence of cuprite, represented by the bands at 148 and 217 cm^{-1} [46]. Most likely, copper sulfide compounds could not be detected due to high fluorescence from the sample or non-interpretable signal to noise ratio.

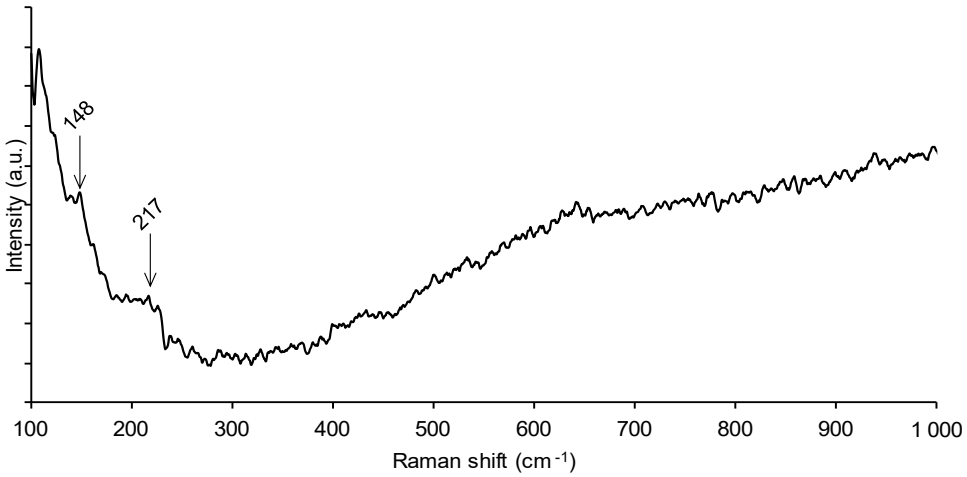

Figure 4.20 Raman spectrum (514.5 nm laser, 2.5 mW power, 6 × 30 s accumulations, 50× objective) of the brass polyptych before cleaning.

EDTA and EDDS reached a similar performance when considering color difference before and after one application of 10 minutes, with $\Delta E = 16.9$ and 15.5 respectively. As expected, the zone treated with DFO is cleaned in a more progressive way, reaching a close color difference (14.9) as for EDTA and EDDS after a total of 6 applications of 10 minutes (Figure 4.21).

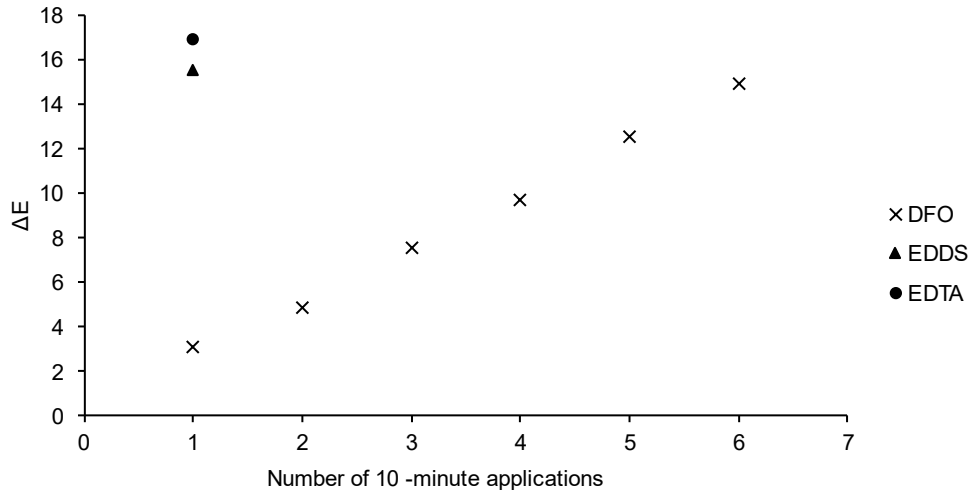

Figure 4.21 Color difference ΔE after 10-minute applications of 3.10^{-2} M DFO-, EDDS- or EDTA-amended agar gels on the brass polyptych.

Interestingly, the cleaning progression seems linear with an average ΔE between each gel removal of ΔE = 2.4 ± 0.4. Taking a closer look at colorimetric data after completion of the intervention (Figure 4.22), all zones become lighter by a ΔL ≈ 15. Regarding a* and b* coordinates, EDTA and EDDS have a similar shift with almost colinear directional vectors (Figure 4.22, arrows), going towards lesser yellow values, although a slight difference in the norm. On the other hand, for DFO, there is close to no change in the b* axis (Δb = 0.52), but rather an increase of the reddish appearance of the evaluated zone, as can been observed on Figure 4.22 with a* coordinate shifting towards values corresponding to red and on Figure 4.23 with visual observation of the treated zone. The much lower affinity between DFO and Cu_2O than EDTA and EDDS and Cu_2O (table 4.8), makes it less likely for the siderophore to remove cuprite, which is a reddish corrosion compound, and therefore influence the appearance in that direction.

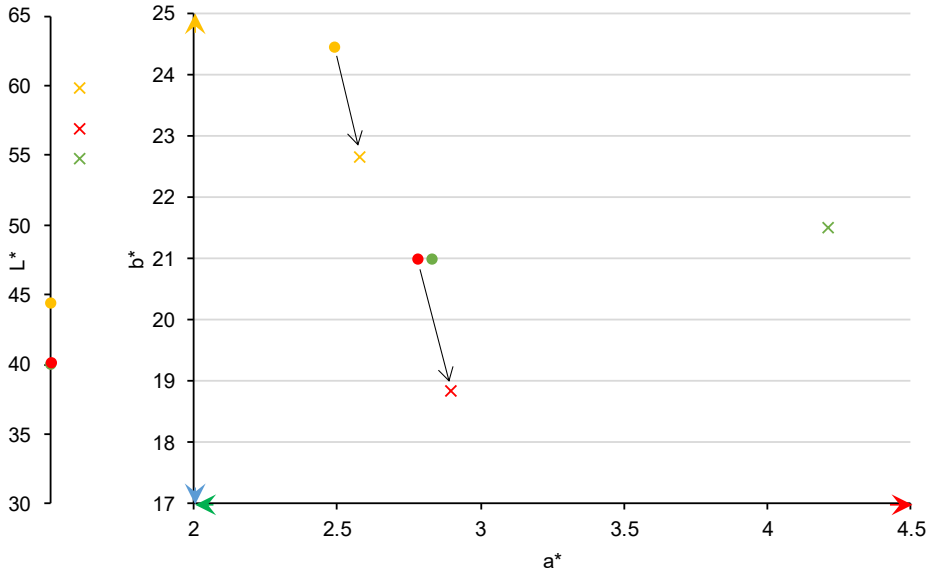

Figure 4.22 CIELab color coordinates measured on the brass polyptych before (circle) and after (crosses) application of DFO- (green), EDDS- (yellow), or EDTA-(red) agar gels.

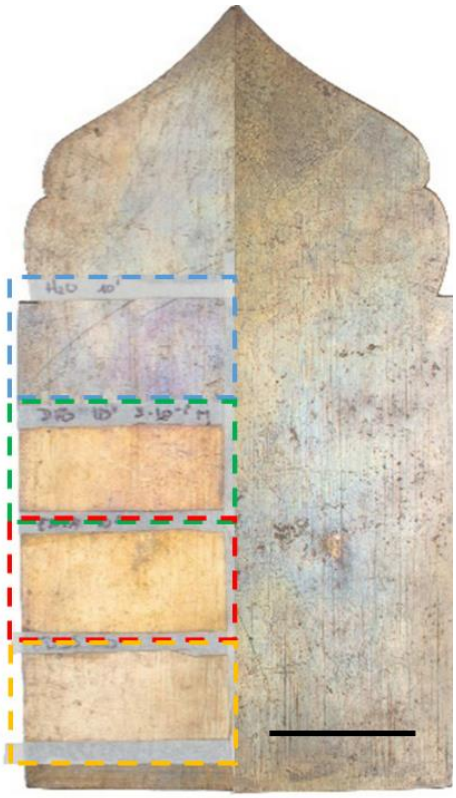

Figure 4.23 Brass polyptych after applications of plain (blue), DFO (green), EDTA (red) or EDDS (yellow) implemented agar gels. Scale is for 3 cm.

When it comes to AAS results, it shows that the EDTA gels took up almost twice copper than the other gels (Table 4.9). This is in good accordance with the results obtained on NAC (Figure 4.13c). The sum of the total of copper taken up by repeated application of DFO-amended gels is still lower than one application of EDTA or EDDS.

Table 4.9 Color difference of the brass polyptych ΔE after treatment and total amount of copper taken up by treating gels.

	ΔE	**[Cu] (μM)**
EDTA	17	35
EDDS	15	16
DFO	14.9	15

Overall, based on visual observations, which prevail for conservators, EDDS-amended gel achieved a comparable performance in comparison to EDTA-amended gel. Its biodegradability and lower toxicity make it an interesting alternative to implement in the field. On the other hand, siderophores (DFO) have a smooth action and allow to perform a more progressive and controlled cleaning. Indeed, DFO affinity for copper (logβ Cu-DFO = 13.7) is lower than EDTA or EDDS (respectively logβ = 18.8 and 18.7) [47,48]. Therefore, both DFO and EDDS could be used, according to the desired results and the expectations of cleaning.

4.2.2.2.2 Brass lamp

A 10-minutes application of the DFO-agar gel on the lamp external surface allowed to reach a visually brighter appearance that is quite subtle (Figure 4.24 a and b). Indeed, on Figure 4.24c where only half of the surface is treated, it is obvious that there is lowering of the iridescent aspect of the object.

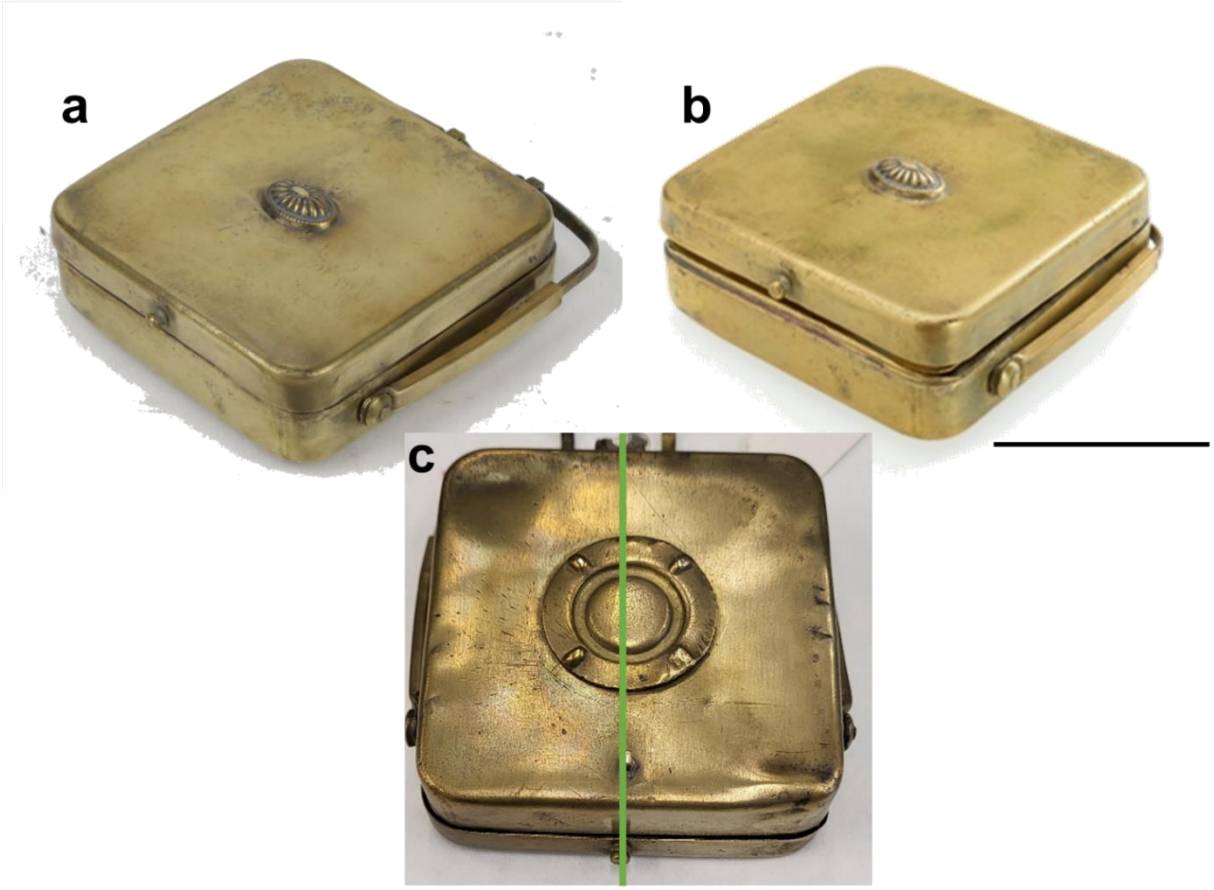

Figure 4.24 Brass lamp before (a) and after (b) cleaning and during intervention (c) with right side cleaned. Scale is 3 cm.

4.2.2.2.3 Silvered pocket-watch

The watch elemental composition, determined by means of XRF, is a silver alloy containing 85.2% of silver and 12.1% of copper, the remaining 2.7% being split between trace elements. Therefore, the presence of copper in the alloy composition backs up the idea of copper corrosion compounds that were initially suspected, given the blue-green color of the spots. Raman analyses detected the presence of silver sulfide on the unaffected areas (Figure 4.25), identifiable by the shoulders at 90 and140 cm^{-1}, standing for Ag crystal lattice, and the peak at 243 cm^{-1} representative of Ag-S bonds [49].

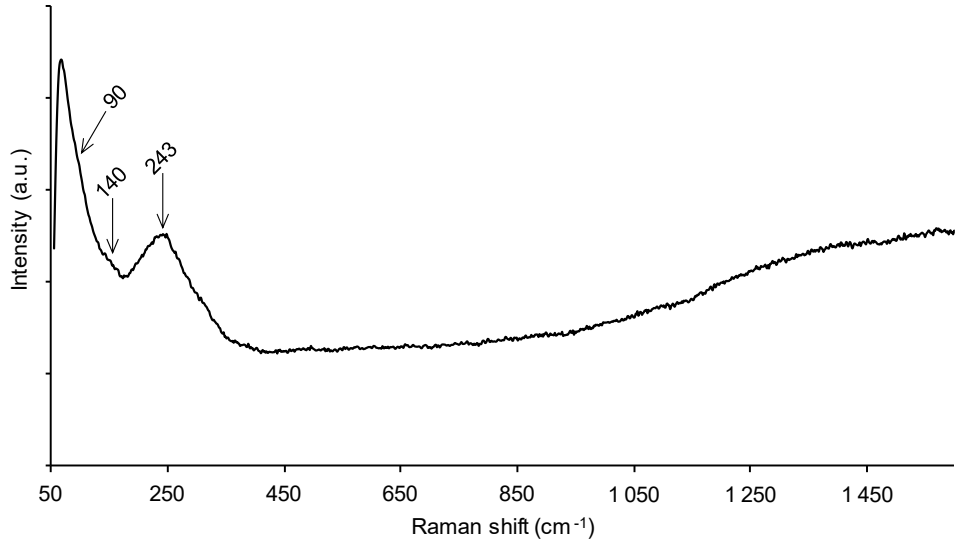

Figure 4.25 Raman spectrum (532 nm, 1 mW, 30 × 1 s accumulations, 50×) of the silver pocket-watch before treatment on zones not displaying blueish stains.

Copper carboxylates and oxalates could be identified on the object's surface thanks to FTIR spectroscopy (Figure 4.26). Bands at 651, 833, 1056, 1416, 1447, 1585, 1625, 2854, 2919, 2957 and 3358 cm^{-1} are characteristic of copper carboxylates. The bands at 1364 and 1663 cm^{-1} are characteristic for copper oxalates [50–53].

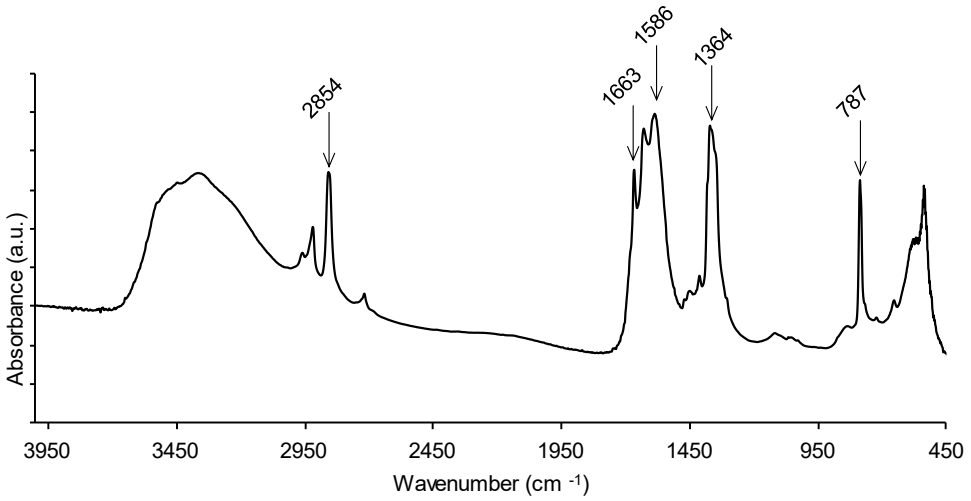

Figure 4.26 FTIR spectrum of the silver pocket-watch on the blue stains (reflectance mode, 4 cm^{-1} resolution, 16 scans).

It is possible that because of friction wearing, the watch's coating got thinned, making it no longer protective. Poor storage conditions overtime might have put the watch in contact with other metallic objects and giving way to a galvanic corrosion phenomenon forming these copper spots between the copper content of the watch and the other metals [54] or the simple fact of being in a poorly controlled indoor environment can result in the copper from the alloy reacting with the protective organic coatings and transforming into copper carboxylates, here a mix containing copper oxalates [55,56].

Visual observations after application of the DFO-amended agar gel (Figure 4.27) show an efficient removal of the greenish spots.

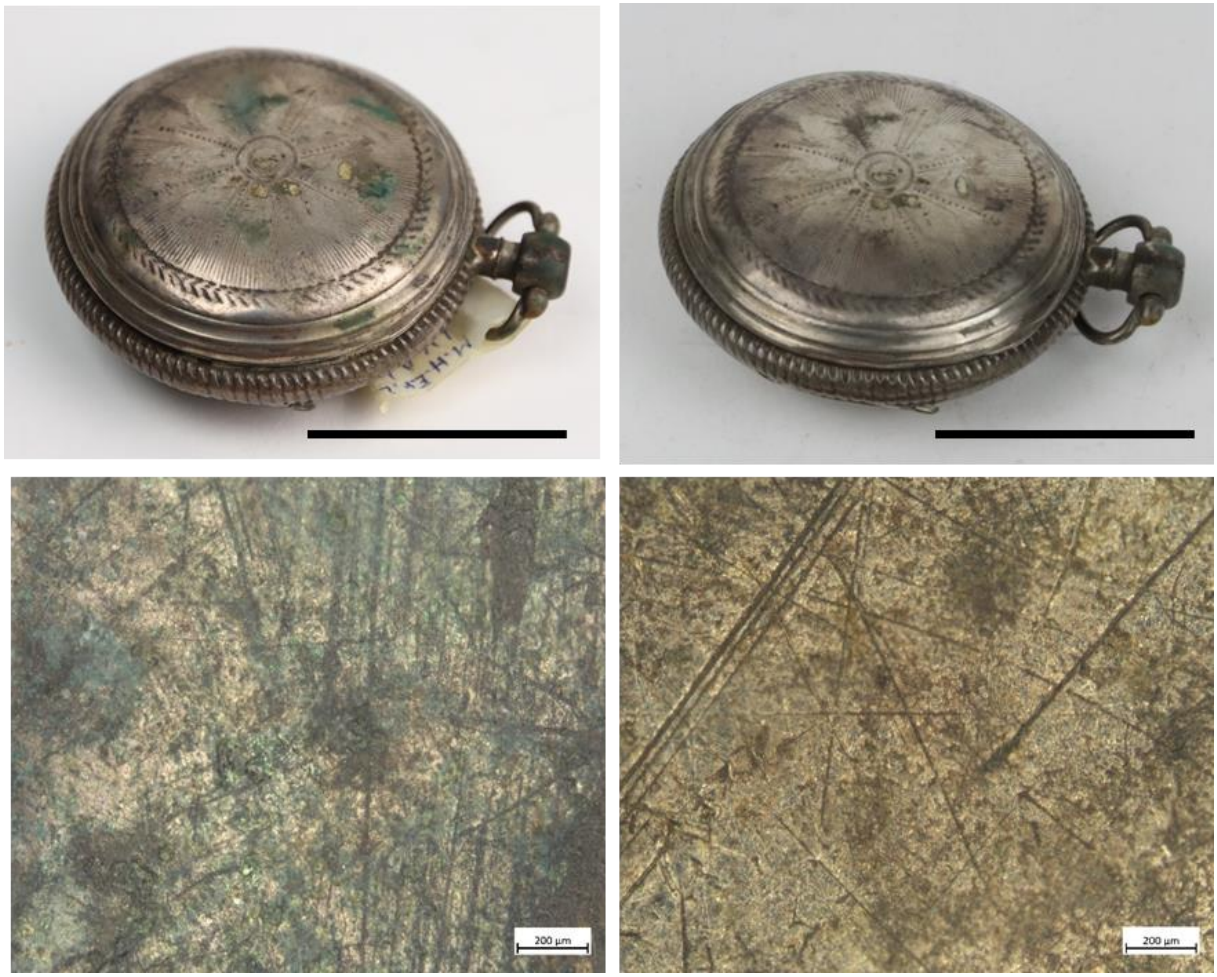

Figure 4.27 Pictures (scale is 2 cm) (top) and optical microscopy (5× objective) observation (bottom) of the silvered pocket-watch.

Recapitulated main findings

- Representative samples of tarnished copper, and to a greater extent brass, are challenging to achieve through artificial ageing.
- EDTA is the best performing complexing agent for the cleaning of copper regarding color and copper uptake criteria. EDDS performance is nearly as good.
- Deferoxamine lower affinity for copper-based corrosion compounds makes it a treatment alternative with a more progressive action.
- Drying of the gel starting after 2 hours diminishes the rate to take up metals and gives way to unesthetic surface damages.
- Preliminary tests into direct application of CS-ItA-LCys formulation studied in Chapter 3 on tarnished copper give encouraging results.

4.3 Silver

Although no hint of actual silver uptake by tested green chelators (i.e., DFO, EDDS, PVD) have been observed in Chapter II, other works have shown some efficiency, in particular of EDDS on tarnished silver objects [57]. For that reason, tests were also carried out on silver samples.

4.3.1 Evaluation on model samples

4.3.1.1 Materials and methods

Sterling silver Ag925 samples (30 × 30 × 1 mm) were obtained from GYR (Switzerland). Artificial tarnishing was adapted from a protocol reported by Siatou *et al* [58]. Briefly a 20% w/v solution of commercially available albumin (egg white powder from PROZIS) was used in a closed container with the samples suspended over the surface. The box was placed in an oven at 80 °C until reaching the desired tarnishing level. This protocol allows the deposition of homogeneous H_2S vapor on the samples' surface and therefore a gradual creation of silver sulfide (Ag_2S).

A 3% w/v agar gel amended with either DFO, EDDS or EDTA at $6 \cdot 10^{-2}$ M along with a plain agar gel as control was applied for 10, 30, 60, 120 minutes. Experiments were carried out at room temperature, approximately 20 °C. In all cases, after removal of the gel, a cotton swab dipped in ethanol 70% v/v was used on the surface. A comparison control was done by cleaning samples with an abrasive paste ($CaCO_3$).

Samples were characterized before and after intervention using colorimetric measurements along with optical microscopy observations. Chelating gels were analyzed for their total silver content using AAS. Parameters used are detailed in supplementary materials.

4.3.1.2 Results and discussion

AAS results do not permit to state that chelators-amended gels take up silver (Figure 4.28). Indeed, the amount of silver detected is extremely low (below 10 μmol/L), if not inexistent when accounting for standard deviation which is in the same range as obtained mean values. Few noticeable values obtained for DFO- and water-gels after 15 minutes of application ([Ag] = 10 and 50 μmol/L respectively) are rendered unreliable as the standard deviation is greater than the mean value (30 and 80 respectively).

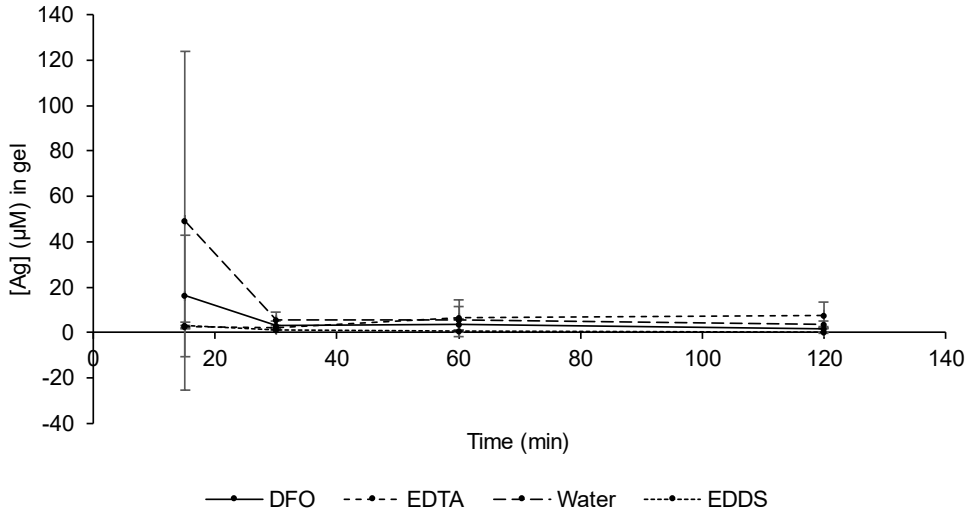

Figure 4.28 Silver concentration in gels after application on tarnished silver samples.

Similarly, colorimetric data do not allow to prove any silver tarnish removal for DFO- or EDTA-amended agar gels (Figure 4.29). However, EDDS yields a clearly perceptible color difference with a maximal ΔE value of 13 ± 5 after 60 minutes of application, close to the mechanical cleaning method (ΔE = 11 ± 4). Although the considerable standard deviation shows a lack of reproducibility for the EDDS-based gel, the good performance of EDDS compared to other chelators (DFO, EDTA and water) was confirmed to be statistically significant with p-values < 0.05 for each over the timespan studied.

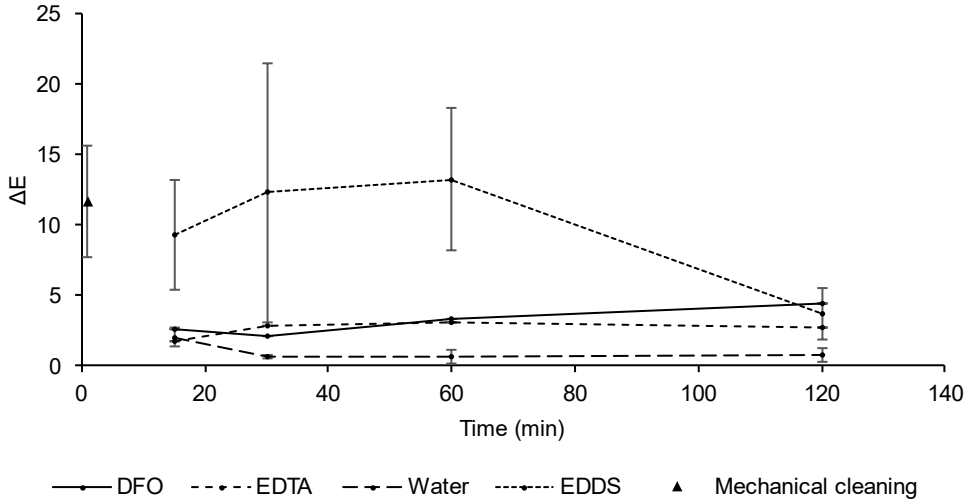

Figure 4.29 Color difference ΔE of silver sample before and after cleaning by DFO-, EDDS-, EDTA- or plain 3% w/v agar gels or by mechanical cleaning (abrasive paste).

These results are in opposition to what has been said elsewhere, where EDDS and DFO achieved results that were judged acceptable for cleaning [57]. The difference of results might be related to the tarnishing protocol used or, most likely, to the action of the cotton swab that acts a mechanical tool as well, as small scratches in the tarnish can be seen in the microscopical observations (Figure 4.30) in addition to the absence of silver detection within the used gels. This is consistent with the previously encountered

results in Chapter 2 and the lack of solubilization of silver by any of the tested complexing agents (i.e., DFO, EDDS, EDTA, PVD or LMOWA)). However, this mechanical rubbing only occurred when an EDDS-containing gel was applied. This, added to the results observed in Chapter 2 with the synthesis of silver nanoparticles when $AgNO_3$ was put in contact with EDDS, pushes to open a perspective on the effect of EDDS on soluble and insoluble forms of silver.

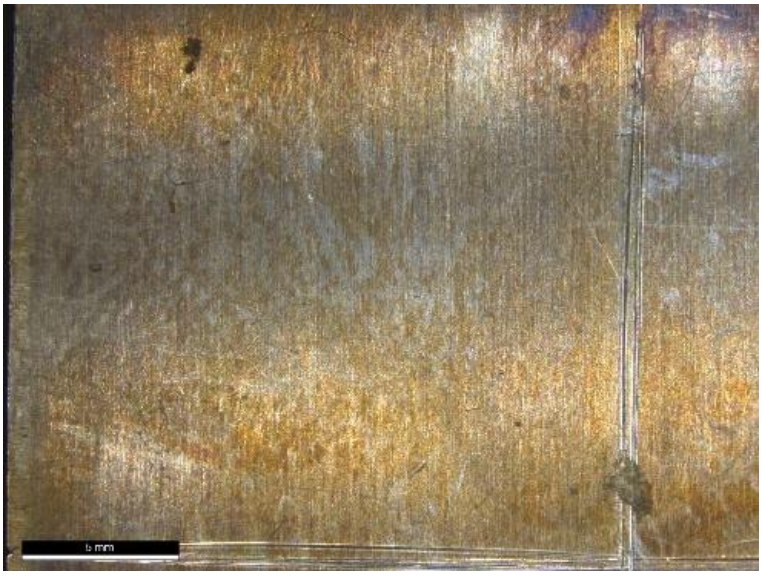

Figure 4.30 Optical microscope observation of silver sample after application of an EDDS-agar gel and rinsing with a cotton swab. Scale bar indicates 5 mm.

4.3.2 Evaluation on case studies

4.3.2.1 Materials and methods

Although there was a lack of convincing results on model samples, tests were performed on a silver cup, obtained from the collection of the Musée Dobrée, Nantes, France (Figure 4.31).

Figure 4.31 Silver cup lent by the Musée Dobrée.

The conditions report performed by conservator Aymeric Raimon states as follows : « *Medium conservation state. The external surface is carved with vegetal or feather-like decorations. From the color, the object is obviously made of silver but the grade of the metal is unknown. Non-homogeneous sulphuration of the external surface can be observed. The upper part is slightly homogeneously yellow with some fingerprint traces that led to higher degrees of tarnishing. The decorated part, which corresponds to the place where the cup is grabbed is highly tarnished, due to sweat and organic compounds present on fingers, with iridescences going from blue to purple, sometimes even hiding the decorations. The bottom is not tarnished. Interestingly, no residues of ancient cleaning could be observed. Ideally, the aim of the treatment would be to retrieve the shiny aspect of the metal.* "

4.3.2.2 Results and discussion

In the case of the cup, the presence of silver inside the gels was null. On the other hand, visual observations showed slight changes, especially for the EDDS-treated part (Figure 4.32). This gives credit to the hypothesis giving EDDS some efficiency in helping removing silver tarnish in combination with soft mechanical tool such as cotton swabs. Further studies using green solutions for silver cleaning should be investigated, for instance outputs exposed in Chapter 2: the use of dead or living fungal biomass for the uptake of silver [59,60], of amino acids to form silver nanoparticles [61], of sodium glycinate to complex silver [62], or of biosurfactants [63].

Figure 4.32 Silver cup lent by the Musée Dobrée after treatment, centered on the EDDS-treated part (white trapezoid).

Recapitulative main findings

- No silver uptake could be observed using AAS.
- EDDS enhances mechanical removal of Ag_2S using cotton swab.

4.4 Conclusion

This chapter demonstrated the promising use of the siderophore deferoxamine (DFO) and the aminopolycarboxylic acid (EDDS), to remove corrosion from corroded iron and copper samples. Tests on silver-tarnished samples were not conclusive, as expected, given the lack of solubilization of silver sulfide observed in Chapter 2.

Cleaning gels amended with the siderophore DFO allowed the removal of iron corrosion from naturally altered samples with a performance similar to that of Na_2EDTA, which is traditionally employed for cultural heritage interventions. Moreover, the use of DFO at neutral pH allows a mild clearing step, in contrast to EDTA solutions, which has an acidic pH. On naturally aged copper samples, EDDS showed outcomes similar to the traditionally used petrochemical EDTA and positions itself as an appropriate bio-based alternative. On the other hand, siderophores have a lower affinity for copper, their use on that substrate is therefore smooth and progressive with the need for repetitions to reach a similar cleaning effect as EDTA, which appears as a good complementary method to the existing possibilities. Hence, the use of DFO on copper is adapted to a reduction of the tarnish where EDDS is suited for a thorough removal of sulfides and oxides to retrieve a bright metal surface. It therefore demonstrates the possibilities to go towards a practice with less health and environmental concerns and no compromise related to the cleaning efficiency. However, a further look into siderophore types and their different stability constants with iron and other metals, could help sharpening the cleaning performances, by eventually targeting other compounds, such as sediments, present on the objects.

Use of siderophores in naturally originated hydrogels was possible. In general, finest cleaning with the metabolites-amended agar gel was achieved when applied hot, at a concentration of DFO not lower than $3 \cdot 10^{-2}$ M and with frequent reiteration, which also allows better control of the intervention by the operator. It is worth mentioning that a preliminary fine-tuning of the application parameters may be performed according to the intended intervention and the application parameters and the final protocol will depend on the nature of the objects to be cleaned. Therefore, our results should be interpreted as preliminary guidelines. DFO-amended agar gel may be more effective when applied to objects with a thin corrosion layer, such as indoor historical artefacts, rather than archaeological items heavily corroded and with common presence of exogenous sediments.

The successful use of metabolite-amended agar gels on various copper objects obtained from museums is great proof for the versatility of the formulations, encouraging the use in real-praxis of those novel and biologically-based solutions.

On another note, this work highlights the importance of artificial ageing. Indeed, inaccurate

reproduction of the natural deteriorative phenomenon may imply unreliable results which can be misleading regarding possible outcomes after application on real cases. Therefore, as much as possible, it is suggested to work on naturally aged samples corresponding to the targeted corrosion pattern.

In the span of the HELIX project, the aim is to attain sustainable formulations that do not compromise on the efficiency, as demonstrated in this chapter, but are also safe for the object, the operator, and the environment. Therefore, assessment of developed formulations can only be complete after evaluation of different sustainability criteria in addition to their performances, comparatively to commonly used substances.

4.5 Bibliography

1. Farkas, E.; Enyedy, É.A.; Csóka, H. A Comparison between the Chelating Properties of Some Dihydroxamic Acids, Desferrioxamine B and Acetohydroxamic Acid. Polyhedron 1999, 18, 2391–2398, doi:10.1016/S0277-5387(99)00144-8.
2. Rapti, S.; Boyatzis, S.C.; Rivers, S.; Pournou, A. Siderophores and Their Applications in Wood, Textile, and Paper Conservation. In Microorganisms in the Deterioration and Preservation of Cultural Heritage; Springer International Publishing: Cham, 2021; pp. 301–339 ISBN 9783030694111.
3. Orama, M.; Hyvönen, H.; Saarinen, H.; Aksela, R. Complexation of [S,S] and Mixed Stereoisomers of N,N′-Ethylenediaminedisuccinic Acid (EDDS) with Fe(III), Cu(II), Zn(II) and Mn(II) Ions in Aqueous Solution. J. Chem. Soc. Dalt. Trans. 2002, 4644–4648, doi:10.1039/B207777A.
4. Woloszyk, K.; Garbatov, Y.; Kowalski, J. Indoor Accelerated Controlled Corrosion Degradation Test of Small- and Large-Scale Specimens. Ocean Eng. 2021, 241, 110039, doi:10.1016/j.oceaneng.2021.110039.
5. Filipsky, T.; Říha, M.; Hrdina, R.; Vávrová, K.; Mladěnka, P. Mathematical Calculations of Iron Complex Stoichiometry by Direct UV-Vis Spectrophotometry. Bioorg. Chem. 2013, 49, 1–8, doi:10.1016/j.bioorg.2013.06.002.
6. Harris, D.C. Quantitative Chemical Analysis, 9th Ed.; W.H. Freeman and Company: New York, NY, USA, 2015; ISBN 978-1-4641-3538-5.
7. Kaurin, A.; Gluhar, S.; Maček, I.; Kastelec, D.; Lestan, D. Demonstrational Gardens with EDTA-Washed Soil. Part II: Soil Quality Assessment Using Biological Indicators. Sci. Total Environ. 2021, 792, 148522, doi:10.1016/j.scitotenv.2021.148522.
8. Gluhar, S.; Kaurin, A.; Lestan, D. Soil Washing with Biodegradable Chelating Agents and EDTA: Technological Feasibility, Remediation Efficiency and Environmental Sustainability. Chemosphere 2020, 257, 127226, doi:10.1016/j.chemosphere.2020.127226.
9. Monnier, J.; Guillot, I.; Legrand, L.; Dillmann, P. Reactivity Studies of Atmospheric Corrosion of Heritage Iron Artefacts. Corros. Conserv. Cult. Herit. Met. Artefacts 2013, 285–310, doi:10.1533/9781782421573.3.285.
10. Bellot-Gurlet, L.; Neff, D.; Réguer, S.; Monnier, J.; Saheb, M.; Dillmann, P. Raman Studies of Corrosion Layers Formed on Archaeological Irons in Various Media. J. Nano Res. 2009, 8, 147–156, doi:10.4028/www.scientific.net/JNanoR.8.147.
11. Albelda-Berenguer, M.; Monachon, M.; Joseph, E. Siderophores: From Natural Roles to Potential Applications; 1st ed.; Elsevier Inc., 2019; Vol. 106; ISBN 9780128169759.
12. ICOM-CC Terminology to Characterize the Conservation of Tangible Cultural Heritage. In Proceedings of the ICOM-CC 15th Triennial Conference; New Delhi, 2008; pp. 64–67.
13. Cui, H.; Ren, W.; Lin, P.; Liu, Y. Structure Control Synthesis of Iron Oxide Polymorph Nanoparticles through an Epoxide Precipitation Route. J. Exp. Nanosci. 2013, 8, 869–875, doi:10.1080/17458080.2011.616541.
14. Borth, K.W.; Galdino, C.W.; Teixeira, V. de C.; Anaissi, F.J. Iron Oxide Nanoparticles Obtained from Steel Waste Recycling as a Green Alternative for Congo Red Dye Fast Adsorption. Appl. Surf. Sci. 2021, 546, 149126, doi:10.1016/j.apsusc.2021.149126.
15. Feng, Y.; Ge, S.; Li, J.; Li, S.; Zhang, H.; Chen, Y.; Guo, Z. Synthesis of 3,4,5-Trihydroxy-2-[(Hydroxyimino) Methyl] Benzoic Acid as a Novel Rust Converter. Green Chem. Lett. Rev. 2017, 10, 455–461, doi:10.1080/17518253.2017.1400590.
16. Kim, A.-R.; Kim, H.-S.; Park, S.-O. Measuring of the Perceptibility and Acceptability in Various Color Quality Measures. J. Opt. Soc. Korea 2011, 15, 310–317, doi:10.3807/JOSK.2011.15.3.310.
17. Guilminot, E.; Gomez, A.; Raimon, A.; Leroux, M. Use of Gels for the Treatment of Metals. In Proceedings of the Metal 2019 Proceedings of the Interim Meeting of the ICOM-CC Metals Working Group; Chemello, C., Brambilla, L., Joseph, E., Eds.; International Councils of Museums - Committee for Conservation, 2019; p. 473.

18. Paraakh, M. Release Kinetics– Concepts and Applications. Int. J. Pharm. Res. Technol. 2019, 8, doi:10.31838/ijprt/08.01.02.
19. Buffle, J.; Zhang, Z.; Startchev, K. Metal Flux and Dynamic Speciation at (Bio)Interfaces. Part I: Critical Evaluation and Compilation of Physicochemical Parameters for Complexes with Simple Ligands and Fulvic/Humic Substances. Environ. Sci. Technol. 2007, 41, 7609–7620, doi:10.1021/es070702p.
20. Lauffer, M.A. Theory of Diffusion in Gels. Biophys. J. 1961, 1, 205–213, doi:10.1016/S0006-3495(61)86884-7.
21. Callister Jr, W.D.; Rethwisch, D.G. Characteristics, Application, and Processing of Polymers; 2018; ISBN 9781119321590.
22. Sebti, I.; Blanc, D.; Carnet-Ripoche, A.; Saurel, R.; Coma, V. Experimental Study and Modeling of Nisin Diffusion in Agarose Gels. J. Food Eng. 2004, 63, 185–190, doi:10.1016/S0260-8774(03)00299-1.
23. Samprovalaki, K.; Robbins, P.T.; Fryer, P.J. Investigation of the Diffusion of Dyes in Agar Gels. J. Food Eng. 2012, 111, 537–545, doi:10.1016/j.jfoodeng.2012.03.024.
24. Coulaud, J.; Stien, C.; Gonneau, E.; Fiallo, M.; Brumas, V.; Sharrock, P. A New Spectroscopic Method for Measuring Ferric Diffusion Coefficient in Gelatin-Based Dosimeter Gels. Biomed. Phys. Eng. Express 2019, 5, 065028, doi:10.1088/2057-1976/ab50ce.
25. Leaist, D.G.; Hao, L. Tracer Diffusion of Some Metal Ions and Metal–EDTA Complexes in Aqueous Sodium Chloride Solutions. J. Chem. Soc., Faraday Trans. 1994, 90, 133–136, doi:10.1039/FT9949000133.
26. Pérez-Miranda, S.; Zamudio-Rivera, L.S.; Cisneros-Dévora, R.; George-Téllez, R.; Fernández, F.J. Theoretical Insight and Experimental Elucidation of Desferrioxamine B from Bacillus Sp. AS7 as a Green Corrosion Inhibitor. Corros. Eng. Sci. Technol. 2021, 56, 93–101, doi:10.1080/1478422X.2020.1824441.
27. Antunes, V.; Candeias, A.; Oliveira, M.J.; Longelin, S.; Serrão, V.; Seruya, A.I.; Coroado, J.; Dias, L.; Mirão, J.; Carvalho, M.L. Characterization of Gypsum and Anhydrite Ground Layers in 15th and 16th Centuries Portuguese Paintings by Raman Spectroscopy and Other Techniques. J. Raman Spectrosc. 2014, 45, 1026–1033, doi:10.1002/jrs.4488.
28. Criado, M.; Martínez-Ramirez, S.; Bastidas, J.M. A Raman Spectroscopy Study of Steel Corrosion Products in Activated Fly Ash Mortar Containing Chlorides. Constr. Build. Mater. 2015, 96, 383–390, doi:10.1016/j.conbuildmat.2015.08.034.
29. Campanella, L.; Cardellicchio, F.; Dell'Aglio, E.; Reale, R.; Salvi, A.M. A Green Approach to Clean Iron Stains from Marble Surfaces. Herit. Sci. 2022, 10, 79, doi:10.1186/s40494-022-00715-4.
30. Hughes, R.; Rowe, M. The Colouring, Bronzing, and Patination of Metals : A Manual for the Fine Metalworker and Sculptor : Cast Bronze, Cast Brass, Copper and Copper-Plate, Gilding Metal, Sheet Yellow Brass, Silver and Silver-Plate; Thames, Hudson, Eds.; Watson-Guptill Publications: New York, N.Y., 1991; ISBN 0823007626.
31. Ropret, P.; Kosec, T. Raman Investigation of Artificial Patinas on Recent Bronze – Part I: Climatic Chamber Exposure. J. Raman Spectrosc. 2012, 43, 1578–1586, doi:10.1002/jrs.4068.
32. Bongiorno, V.; Campodonico, S.; Caffara, R.; Piccardo, P.; Carnasciali, M.M. Micro-Raman Spectroscopy for the Characterization of Artistic Patinas Produced on Copper-based Alloys. J. Raman Spectrosc. 2012, 43, 1617–1622, doi:10.1002/jrs.4167.
33. Tsurumaki, A.; Chiarucci, C.; Khaire, S.; Dal Bosco, C.; Gentili, A.; Navarra, M.A. Removal of Copper Corrosion Products by Using Green Deep Eutectic Solvent and Bio-Derivative Cellulose Membrane. Polymers (Basel). 2022, 14, 2284, doi:10.3390/polym14112284.
34. Lewton-Brain, C. Using Liver of Sulfur Available online: https://www.ganoksin.com/article/using-liver-of-sulfur/ (accessed on 16 May 2023).
35. Masi, G.; Esvan, J.; Josse, C.; Chiavari, C.; Bernardi, E.; Martini, C.; Bignozzi, M.C.; Gartner, N.; Kosec, T.; Robbiola, L. Characterization of Typical Patinas Simulating Bronze Corrosion in Outdoor Conditions. Mater. Chem. Phys. 2017, 200, 308–321, doi:10.1016/j.matchemphys.2017.07.091.

36. Timoncini, A.; Brattich, E.; Bernardi, E.; Chiavari, C.; Tositti, L. Safeguarding Outdoor Cultural Heritage Materials in an Ever-Changing Troposphere: Challenges and New Guidelines for Artificial Ageing Test. J. Cult. Herit. 2023, 59, 190–201, doi:10.1016/j.culher.2022.12.003.
37. Zaitoun, M.A.; Lin, C.T. Chelating Behavior between Metal Ions and EDTA in Sol - Gel Matrix. J. Phys. Chem. B 1997, 101, 1857–1860, doi:10.1021/jp963102d.
38. Fontaine, C.; Lemoine, S.; Pelé-Meziani, C.; Guilminot, E. The Use of Gels in Localized Dechlorination Treatments of Metallic Cultural Heritage Objects. Herit. Sci. 2022, 10, 117, doi:10.1186/s40494-022-00752-z.
39. Bellotti, D.; Remelli, M. Deferoxamine B: A Natural, Excellent and Versatile Metal Chelator. Molecules 2021, 26, 3255, doi:10.3390/molecules26113255.
40. Krätschmer, A.; Odnevall Wallinder, I.; Leygraf, C. The Evolution of Outdoor Copper Patina. Corros. Sci. 2002, 44, 425–450, doi:10.1016/S0010-938X(01)00081-6.
41. Scott, D.. Copper and Bronze in Art: Corrosion, Colorants, Conservation; Scott, D.A., Ed.; Getty Institute of Conservation: Los Angeles, 2002; ISBN 978-0-89236-638-5.
42. Werneck, B.; Tsurumaki, A.; Navarra, M.A. Removal of Copper Corrosion Using In-Situ and Ex-Situ Film Formed from Hydrogels. J. Archaeol. Sci. Reports 2023, 47, 103801, doi:10.1016/j.jasrep.2022.103801.
43. Otero, E.; Bastidas, J.M.; López, W.; Fierro, J.L.G. Characterization of Corrosion Products on Chalcographic Copper Plates after 200 Years' Exposure to Indoor Atmospheres. Mater. Corros. 1994, 45, 387–391, doi:10.1002/maco.19940450704.
44. Choudhuri, K.; Blevins, G.M.; Kober, U.A.; Lapitsky, Y. Bicarbonate-Mediated Dissolution of Chitosan-Based Polyelectrolyte Complex Gels. Polymer (Guildf). 2023, 283, 126242, doi:10.1016/j.polymer.2023.126242.
45. Eldebss, T.M.A.; Farag, A.M.; Shamy, A.Y.M. Synthesis of Some Benzimidazole-Based Heterocycles and Their Application as Copper Corrosion Inhibitors. J. Heterocycl. Chem. 2019, 56, 371–390, doi:10.1002/jhet.3407.
46. Ciupiński, Ł.; Fortuna-Zaleśna, E.; Garbacz, H.; Koss, A.; Kurzydłowski, K.; Marczak, J.; Mróz, J.; Onyszczuk, T.; Rycyk, A.; Sarzyński, A.; et al. Comparative Laser Spectroscopy Diagnostics for Ancient Metallic Artefacts Exposed to Environmental Pollution. Sensors 2010, 10, 4926–4949, doi:10.3390/s100504926.
47. Nurchi, V.M.; Cappai, R.; Spano, N.; Sanna, G. A Friendly Complexing Agent for Spectrophotometric Determination of Total Iron. Molecules 2021, 26, 3071, doi:10.3390/molecules26113071.
48. Orama, M.; Hyvönen, H.; Saarinen, H.; Aksela, R. Complexation of [S,S] and Mixed Stereoisomers of N,N′-Ethylenediaminedisuccinic Acid (EDDS) with Fe(III), Cu(II), Zn(II) and Mn(II) Ions in Aqueous Solution. J. Chem. Soc., Dalt. Trans. 2002, 4644–4648, doi:10.1039/B207777A.
49. Martina, I.; Wiesinger, R.; Schreiner, M. Micro-Raman Characterisation of Silver Corrosion Products : Instrumental Set Up and Reference. e-Preservation Sci. 2012, 9, 1–8.
50. Salvadó, N.; Butí, S.; Cotte, M.; Cinque, G.; Pradell, T. Shades of Green in 15th Century Paintings: Combined Microanalysis of the Materials Using Synchrotron Radiation XRD, FTIR and XRF. Appl. Phys. A 2013, 111, 47–57, doi:10.1007/s00339-012-7483-4.
51. Otero, V.; Sanches, D.; Montagner, C.; Vilarigues, M.; Carlyle, L.; Lopes, J.A.; Melo, M.J. Characterisation of Metal Carboxylates by Raman and Infrared Spectroscopy in Works of Art. J. Raman Spectrosc. 2014, 45, 1197–1206, doi:10.1002/jrs.4520.
52. Moita, M.F.R.; Duarte, M.L.T.S.; Fausto, R. Investigation of the Structure of the Columnar Liquid-Crystalline Phase of Copper(II) Carboxylates. An FTIR Spectroscopic Study. J. Chem. Soc. Faraday Trans. 1994, 90, 2953, doi:10.1039/ft9949002953.
53. Peres, R.S.; Baldissera, A.F.; Armelin, E.; Alemán, C.; Ferreira, C.A. Marine-Friendly Antifouling Coating Based on the Use of a Fatty Acid Derivative as a Pigment. Mater. Res. 2014, 17, 720–727, doi:10.1590/S1516-14392014005000032.

54. Fink, C.G. The Electrochemical Restoration of Badly Corroded Silver-Copper Alloy Objects. Science. 1949, 109, 597–597, doi:10.1126/science.109.2841.597.a.
55. Elia, A.; De Wael, K.; Dowsett, M.; Adriaens, A. Electrochemical Deposition of a Copper Carboxylate Layer on Copper as Potential Corrosion Inhibitor. J. Solid State Electrochem. 2012, 16, 143–148, doi:10.1007/s10008-010-1283-6.
56. Rosi, F.; Cartechini, L.; Monico, L.; Gabrieli, F.; Vagnini, M.; Buti, D.; Doherty, B.; Anselmi, C.; Brunetti, B.G.; Miliani, C. Tracking Metal Oxalates and Carboxylates on Painting Surfaces by Non-Invasive Reflection Mid-FTIR Spectroscopy. In; 2019; pp. 173–193.
57. Biscarel, I. Mise Au Point d'un Protocole de Nettoyage et de Revêtement de Protection Pour Des Objects Ethnographiques En Argent, Master thesis, Haute Ecole Spécialisée de Suisse Occidentale, 2022. https://www.he-arc.ch/wp-content/uploads/2023/03/2022_BISCAREL_PosterMA-1.pdf
58. Siatou, A.; Castro, Y.; Nurit, M.; Chatoux, H.; le Goïc, G.; Degrigny, C.; Brambilla, L.; Mansouri, A. A Methodological Approach for Multi-Temporal Tracking of Silver Tarnishing. In Proceedings of the Proceedings of the 4th ACM International workshop on Structuring and Understanding of Multimedia heritAge Contents; ACM: New York, NY, USA, October 10 2022; pp. 5–13.
59. Mazzoni, M.; Alisi, C.; Tasso, F.; Cecchini, A.; Marconi, P.; Sprocati, A.R. Laponite Micro-Packs for the Selective Cleaning of Multiple Coherent Deposits on Wall Paintings: The Case Study of Casina Farnese on the Palatine Hill (Rome-Italy). Int. Biodeterior. Biodegrad. 2014, 94, 1–11, doi:10.1016/j.ibiod.2014.06.004.
60. Ayele, A.; Haile, S.; Alemu, D.; Kamaraj, M. Comparative Utilization of Dead and Live Fungal Biomass for the Removal of Heavy Metal: A Concise Review. Sci. World J. 2021, 2021, 1–10, doi:10.1155/2021/5588111.
61. Shankar, S.; Rhim, J.W. Amino Acid Mediated Synthesis of Silver Nanoparticles and Preparation of Antimicrobial Agar/Silver Nanoparticles Composite Films. Carbohydr. Polym. 2015, 130, 353–363, doi:10.1016/j.carbpol.2015.05.018.
62. de Figueiredo Junior, J.C.D.; Asevedo, S.S.; de Souza e Silva, M.L.S.; Araújo, A.C.; Quites, M.R.E. The Cleaning of Silver Objects With a Basic Solution of Sodium Glycinate: A Study on Artificially and Naturally Tarnished Silver. Stud. Conserv. 2021, 66, 375–383, doi:10.1080/00393630.2020.1859876.
63. Marchant, R.; Banat, I.M. Biosurfactants: A Sustainable Replacement for Chemical Surfactants? Biotechnol. Lett. 2012, 34, 1597–1605, doi:10.1007/s10529-012-0956-x.

4.6 Supplementary materials

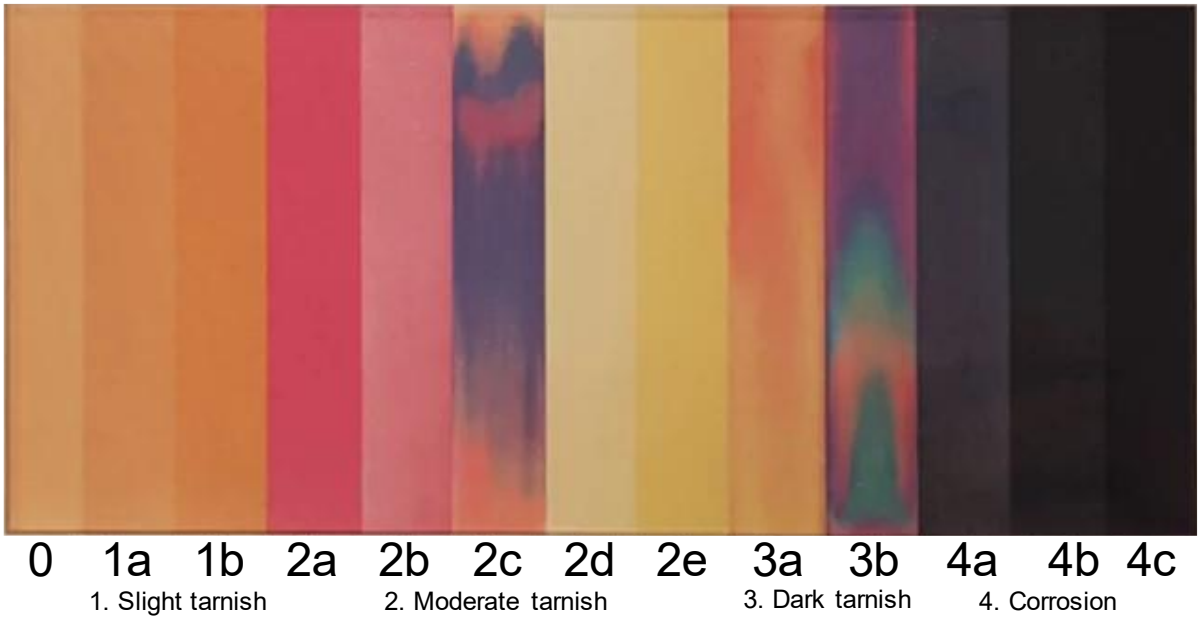

Figure S4.1 ASTM copper strip corrosion standard, obtained from [490]. 0 corresponds to a freshly polished metal.

Analytical techniques

Colorimetry

A Minolta CM-508D spectrophotometer was used for colorimetry measurements. The setup was as follows: illuminant D65, d/8° geometry, 10° observer, window size 8 mm, CIELab color space. For iron samples specular component was excluded (SCE) whereas for copper and silver samples the setup was specular component included (SCI) to account for the gloss of samples. Measurements were performed as triplicates per chosen area.

ΔE* was calculated using the standard color variation formula in CIELab where L^*_1, a^*_1 and b*1 are the coordinates in the colorimetric space of the first measurement, and L^*_2, a^*_2, b^*_2 those of the second measurement. Triplicated measurements.

$$\Delta E^* = \sqrt{(L_2^* - L_1^*)^2 + (a_2^* - a_1^*)^2 + (b_2^* - b_1^*)^2}$$

ΔE*, the total color difference index provides an overall estimation of the color difference but is not representative of the qualitative difference (L*, a*, b*) of the color changes. For that reason, sometimes graphs showing the three-color coordinates were preferred. ΔL, Δa and Δb were calculated using the following formula: $\Delta\alpha=\alpha_{after}-\alpha_{before,}$ where α_{after} is L*, a* or b* after cleaning and α_{before} is L*, a* or b* before cleaning or before artificial corrosion.

Optical microscopy

Optical microscopy images were acquired using a Leica DMS1000 Digital microscope system with Leica Application Suite software for iron and copper samples as well as for iron-based objects. For copper-based objects, optical microscopy observations were carried out using an Axiolab microscope (Zeiss) in Dark field mode.

Atomic Absorption Spectroscopy

A Thermo Fisher iCE 3300 double-beam atomic absorption spectrometer equipped with an acetylene-air flame was used to determine the amount of iron, copper or silver present in gel formulations or DFO solutions after application. Detection limits were of 0.1, 0.01 , 0.002 μg/L for Fe, Cu and Ag respectively. The gels were first dissolved in 10 mL of 70% v/v HNO_3 and gauged to 100 mL with deionized water. The solutions were not filtered, in order to allow a determination of the total amount of chemical elements present including both the ones complexed but also the ones that were stripped from the surface by the mechanical peeling action of the gel. Measurements were performed as triplicates. Obtained results were normalized by the weight of each gel to have comparable results.

Fourier Transformed Infrared spectroscopy

For both iron samples and copper-based objects a Thermo Fisher Nicolet iN10MX was used in reflectance mode. FTIR Spectra were recorded with the following parameters: 650-4000 cm^{-1} spectral range, 4 cm^{-1} resolution, 16 scans. Post-processing of the spectra was achieved with Omnic software. Baseline correction and atmospheric correction were performed to remove residual signatures of atmospheric CO_2 and water in the spectra.

Eddy current measurements

The corrosion thickness was measured with a Phynix Surfix Pro S gauge and FN 0.2 probe (PHYNIX GmbH & Co. KG, Neuss, Germany) using the F-mode (magnetic induction principle for ferrous alloys) with a measurement range of 0–200 μm. Before measurement, zero-calibration with an accuracy of +/– (0.7 μm + 1.5 %) was carried out on a steel sample obtain for Tartaix, not corroded. Measurements were carried out in triplicates on each replicate and the average value calculated.

Raman spectroscopy

A Renishaw Virsa™ Raman analyzer micro spectrometer equipped with 50× magnification objective was employed using a 785 nm laser. To examine naturally tarnished copper, spectra were recorded with a laser power of 3 mW in the spectral range of 50–1250 cm^{-1} with fifty accumulations of 1 s each. The silver-watch was examined using the same device, with a 532 nm laser and a laser power of 1 mW. Spectra were recorded in the spectral range of 60-1600 cm^{-1} with thirty accumulations of 1 s each. The data were post-processed using GRAMS software.

A Jobin Yvon Horiba T640000 Raman micro spectrometer equipped with 50× magnification objective was employed to examine the iron-based helmet using a 633 nm laser with a laser power of 0.1 mW. Spectra were recorded in the spectral range of 100–1500 cm^{-1} with four accumulations of 30 s each. For the brass polyptych, the same equipment was used but using a 514.5 nm laser with a laser power of 2.5 mW. Spectra were recorded in the spectral range of 100–1200 cm^{-1} with six accumulations of 30 s each. The data were post-processed using Omnic software.

X-Ray Fluorescence

A Niton™ XL3t handheld analyzer from Thermo Scientific (50 kV, Ag anode) mode was used using the mode "general metals".

Statistical analysis of datasets were performed using one way or two way ANOVA, in the R software.

5. Assessment of sustainability and real praxis transfer of the proposed alternatives

« Science sans conscience n'est que ruine de l'âme »

François Rabelais

The HELIX project is designed to seek sustainable alternatives to conservators' common practices, in particular through bioderived and microbial solutions. However, some questions should be raised when working on such break-through projects. How can sustainability be evaluated? Are targeted end-users actually going to use the innovation? What would be the reasons for the proposed alternatives to remain at lab-scale?

In this chapter, an afterthought is carried out about greenness and especially an attempt to quantify this concept in a standardized way. The proposed alternatives are assessed and compared to current solutions, using Life Cycle Assessment and relying on European standards for environmental evaluation of products. Finally, a discussion is proposed towards the implementation into praxis by end-users including the use of microbial extract themselves and the use of hydrogel formulations on corroded metals.

5.1 Greenness

In the HELIX project, there is the will to go towards greener approaches. But really, what is greenness? Some articles have tried understanding the meaning given by conservation scientists, noticing a lack of clear definition of the term [1].

Because chemistry is seen as a dangerous science, it is common for people to associate the word chemical with toxic, as opposed to the natural-green association. Nevertheless, green chemistry has been defined almost 30 years ago as the ''design of chemical products and processes to reduce or eliminate the use and generation of hazardous substances.'' [2]. This definition is rather broad and adds up to the current large use of the term by marketing companies, making it a meaningless phrase. The greatest example of the lack of precise meaning is the emergence of green-washing [3]. Briefly, it is the use of a form of marketing or advertising propaganda to influence the public into thinking that an entity's products, intentions or policies are environmentally friendly [3]. The existence of such practice raised some concerns in the span of this work. What are the requirements for something to be called green and does this research project actually fit to the definition? As a first approach, it is interesting to look at what has been theorized as the twelve principles of green chemistry.

Green chemistry's key aspect is the concept of design, as it is something that can, so far, only be achieved by human intention. The twelve principles of Green Chemistry, listed in Table 5.1, are rules to help chemists achieve a design in accordance with the intended goal of sustainability, throughout all stages of the chemical life-cycle of the developed product [2].

Table 5.1 Twelve principles of Green Chemistry, in bold are the ones most applicable in the HELIX project.

Pollution prevention	Prioritize the prevention of waste rather than cleaning up and treating waste after it has been created. Plan ahead to minimize waste at every step
Atom economy	Reduce waste at the atomic scale by optimizing the number of atoms from all reagents incorporated into the final product. Use atom economy to evaluate reaction efficiency
Less hazardous chemical synthesis	Design chemical reactions and synthetic routes to be as safe as possible. Consider the hazards of all substances handled during the reaction, including waste
Design safer chemicals	Minimize toxicity directly by molecular design. Predict and evaluate aspects such as physical properties, toxicity, and the environmental fate throughout the design process

Safer solvents and auxiliaries	Choose the safest solvent available for any given step. Minimize the total amount of solvents and auxiliary substances used, as these make up a large percentage of the total waste created
Design for energy efficiency	Choose the least energy-intensive chemical route. Avoid heating and cooling as well as pressurized and vacuum conditions (i.e., ambient temperature and pressure are optimal)
Use renewable feedstocks	Use chemicals which are made from renewable (i.e., plant-based) sources rather than other chemicals originating from petrochemical sources.
Reduce derivatives	Minimize the use of temporary derivatives such as protecting groups. Avoid derivatives to reduce reaction steps, resources required, and waste created.
Catalysis	Use catalytic instead of stoichiometric reagents in reactions. Choose catalysts to help increase selectivity, minimize waste, and reduce reaction times and energy demands.
Design for degradation	Design chemicals that degrade and can be discarded easily. Ensure that both chemicals and their degradation products are not toxic, bio accumulative, or environmentally persistent.
Real-time analysis for pollution prevention	Monitor chemical reactions in real-time as they occur to prevent the formation and release of any potentially hazardous and polluting substances.
Inherently safer chemistry for accident prevention	Choose and develop chemical procedures that are safer and inherently minimize the risk of accidents. Know the possible risks and assess them beforehand.

In the HELIX project, as discussed in chapter 4, atom efficiency is rarely attained. Indeed, the chelate loading hardly reaches values above 3% for iron and 1% for copper in gels, never reaching the equilibrium state. Consequently, it can be said that the use of gels hinders the atom efficiency of the overall treating system. However, considering the application, conservators value this delivery system as being easier to control. For such, one should consider both approaches (greenness and atom efficiency versus practicity for objects treatment), and balance according to their subjective needs and sensibility.Overall, a cautious design helps eliminating intrinsic hazards within chemicals and processes, whether it is eco-toxicity, physical hazards, carbon emissions or less trivial ones like ozone

depletion. A hazard is defined as the capacity to cause harmful consequences whether to humans or the environment. Inherent hazards of a chemical substances can be minimized. They may come from the raw materials that are used, the production phase as well as the final products obtained. In addition, the idea of reducing hazards across all the life-cycle stages has been shown to be economically profitable [2]. Consequently, to ascertain the green and sustainable design of the HELIX hydrogels formulations, a Life Cycle Assessment (LCA) of selected compounds and formulations was performed.

5.2 Life cycle assessment (LCA)

A Life Cycle Assessment (LCA) is a reference method used to evaluate the environmental impact of a product, process, or activity throughout its entire life cycle, from raw material extraction to end-of-life disposal, including fabrication, transportation and use [4]. It is a useful tool for decision-making and product development, as it allows for the identification of areas where improvements can be made to reduce environmental impact and increase sustainability. It therefore allows to act on the design of the product (e.g., choice of materials). It also helps understanding better the issues and making informed decisions. It permits a comparison of products or services with equal function and allows to identify pollution displacements and prioritize eco-design actions.

LCA analyses can be conducted on different levels of the product life cycle, such as cradle-to-gate (from raw material extraction to the factory gate), cradle-to-grave (from raw material extraction to end-of-life disposal), or even cradle-to-cradle (from raw material extraction to end-of-life disposal and subsequent recycling). The choice of the boundary and scope of the LCA study depends on the goal and purpose of the analysis.

The European norms ISO 14040 and 14044 define and frame the requirements and guidelines for conducting LCA studies. They outline a set of sixteen impact categories to be considered in an LCA (Table 5.2) [5]. Using a multicriteria approach and adhering to them helps ensur the validity and comparability of LCA studies.

During the Life Cycle Assessment, emissions are being united behind actionable numbers meaning that different emissions causing the same impact are converted into one unit and therefore one impact category. As an example, the impact category "Climate change" is expressed in kg CO_2 equivalents (kg CO_2 eq). However, other greenhouse gases than carbon dioxide emissions can have an impact on climate change as well (e.g., CH_4, N_2O, etc.). By converting the other greenhouse gases emissions in CO_2 equivalents, it becomes possible to give a unique metric for climate change under one impact category. Other categories also have their reference compound (e.g., P, N, Sb, U^{235}).

In order to make sense of the data generated by an LCA, a single score is often calculated to represent the overall environmental impact. The lower the single score, the less the evaluated system is impactful. This single score takes into account all of the different impact categories evaluated in the assessment. To do so, scores obtained in each impact categories are normalized and weighted. For the normalization step, results obtained for the studied system are compared to reference values. This is done to understand the relative impact, giving a sense of the proportions of emissions compared to reference values. Here, the normalization reference is the impact of an average European citizen. The resulting score is then multiplied by a weighting factor. This step assigns weighting factors to the categories based

on societal preferences. It reflects the relative importance of the different impact categories. The values used for normalization and weighting factors can therefore vary depending on context, geographical parameters etc. It is still important to keep in mind that while normalization and weighting factors help simplifying and communicating LCA results, they also involve subjectivity and potential debate for determined values, arguing what is "normal" or how much weight should be assigned to one or the other impact categories depending on perspectives [6].

The presence of these different impact categories helps avoiding a false good idea, for instance to act on one of the criteria without realizing it worsens the "weight" of another category. It is often the case that a solution that seems greener in theory in fact turns out to be less sustainable than expected, as only one criterion is taken into account.

The main categories (highest contributions) that can be related to the HELIX project are in bold in Table 5.2 and an explanation for each of these is given thereafter:

- Climate change: Takes into account greenhouse gas emission such as CO_2, CH_4, N_2O
- Particulate matter: Takes into account all direct emissions of fine particles or precursors like NO_x and SO_2
- Eutrophication, freshwater: Takes into account all the emissions (PO_4^{3-}, H_3PO_4, N containing compounds) responsible for the proliferation of algae in freshwater environments
- Ecotoxicity, freshwater: Takes into account the emissions of bio-accumulable substances that have harmful consequences on living organisms such as heavy metals, persistent organic pollutants (POPs), etc.
- Resource use, fossils: Takes into account non-renewable energy sources such as fuel, oil, coal, uranium, natural gases
- Resource use, minerals and metals: Takes into account mineral resources consumption

Table 5.2 Impact categories considered with their normalization and weighting factors [7]. Bold categories as the most relevant ones to the HELIX project.

Main concerns	Impact categories	Unit	Global normalization factor	Weighting factors (%)
Biodiversity and human health	**Climate change**	**kg CO_2 eq**	**8.10×10^3**	**21.60**
	Photochemical-ozone formation, human health	kg NMVOC[7] eq	4.06×10^1	4.78
	Water use	m^3 water eq	1.15×10^{-4}	8.51
Human health	Ozone depletion	kg CFC[8]eq	5.36×10^{-2}	6.31
	Human toxicity, cancer effects	CTUh[9]	1.69×10^{-5}	2.13
	Human toxicity, non-cancer effects	CTUh	2.3×10^{-4}	1.84
	Particulate matter	**Disease incidence**	**5.95×10^{-4}**	**8.96**
	Ionizing-radiation, human health	kBq U^{235} eq	4.22×10^3	5.01
Biodiversity	Acidification	mol H^+ eq	5.56×10	6.20
	Eutrophication, terrestrial	mol N eq	1.77×10^2	3.71
	Eutrophication, freshwater	**kg P eq**	**1.61**	**2.80**
	Eutrophication, marine	kg N eq	1.95×10	2.96
	Land use	Pt[10]	8.2×10^5	7.94
	Ecotoxicity freshwater	**CTUe[11]**	**4.27×10^4**	**1.92**
Resources	**Resource use, fossils**	**MJ**	**6.50×10^4**	**7.55**
	Resource use, minerals and metals	**kg Sb eq**	**6.37×10^2**	**8.32**

A good example of this bias in the cultural heritage field is the STiCH platform [8]. It is an online tool to help conservators with the choice of their working materials with an environmental focus. It is a

[7] Non-Methane Volatile Organic Compounds
[8] Trichlorofluoromethane
[9] Comparative Toxicity Unit for human health
[10] The Pt unit used is a dimensionless value. A value of 1 Pt means one thousandth of the one-year environmental burden of the average European population [4].
[11] Comparative toxicity unit for the environment

carbon calculator and therefore cannot be regarded as an extensive LCA overview. Nevertheless, it is a good start to introduce those concepts in the field and to raise awareness to end-users.

While both LCA and carbon calculators can be used to assess the environmental impact of a product, process, or activity, there are some key differences that make LCA more relevant in certain situations. A carbon calculator typically focuses on calculating the carbon footprint of a product, process, or activity. This means that it primarily considers greenhouse gas emissions, corresponding to the impact category "Climate change", and may not take into account other environmental impacts, such as resource depletion or toxic wastes. Carbon calculators are typically less comprehensive than LCA and may not provide a full picture of the environmental impact. On the other hand, LCA is a more complete methodology that considers a wide range of environmental impacts, including greenhouse gas emissions, resources depletion, energy use, and emissions to air, water, and land. It also takes into account the entire life cycle from raw material extraction to end-of-life disposal and can identify opportunities for improvement at each stage of the life cycle. LCA is therefore more relevant than a carbon calculator in situations where a comprehensive evaluation of the environmental impact is needed. LCA can provide a more complete understanding of the environmental impacts and trade-offs associated with different options, and can help inform decision-making for sustainable development. However, it is important to note that LCA has its limits [9]. It requires a significant amount of data and resources, not always under open-access, and results may vary depending on the assumptions and data used in the analysis. There is also a risk a misinterpretation from unadvised users. LCA should be used as one tool among others to inform decision-making and should be complemented with other sustainability metrics which can be used in combination with LCA to provide a more comprehensive view of sustainability. By considering multiple indicators, decision-makers can gain a more complete understanding of the sustainability and make more informed decisions. Additionally, social and economic impact metrics are not typically included in LCA but can provide important information about the social and ethical implications of a product or process.

5.2.1 Materials and Methods

A LCA was carried out based on the ISO 14040:1997 and ISO 14044:2006 standards [10,11]. The methodology for this LCA analysis relies on the competence of the EVEA consultancy company[12], specialized in LCA evaluations.

[12] https://evea-conseil.com/en, s.issartial@evea-conseil.com

5.2.1.1 Goal definition

The first aim is to obtain the environmental footprint of raw materials used for HELIX formulations in comparison to petrochemically sourced alternatives (Table 5.3).

Table 5.3 Raw materials studied in the LCA.

	Raw material	CAS number	Origin
Polymers	Agar-agar	9002-18-0	Biosourced
	Gellan gum	71010-52-1	Biosourced, fermented
	Xanthan gum	11138-66-2	Biosourced, fermented
	Carboxymethyl cellulose (CMC)	9000-11-7	Biosourced[13]
	Polyvinyl alcohol (PVA)	9002-89-5	Petrosourced
Complexing agents	EDDS	20846-91-7	Petrosourced
	Na_2EDTA	6381-92-6	Petrosourced
	Deferoxamine	70-51-9	Biosourced, fermented
	Borax	1303-96-4	Mineral
	D.I. water	7732-18-5	

Second, it is sought for to evaluate the environmental footprint of some cleaning hydrogel formulations (Table 5.4) based on priorly studied raw materials and considering the impact of the preparation method, the use phase and the end-of-life (cradle to grave system). Carboxymethyl cellulose (CMC) and Polyvinyl alcohol (PVA-borax) were added to studied hydrogels as they are often resorted to in heritage conservation but not considered bio-based to be studied further in the thesis (Chapter 1 section 4).

Finally, a look is taken at the health hazards of all the raw materials based on bibliographic study using bibliographic references and collaborative databases.

The main objective is to compare the hydrogels developed in the span of this project versus those that are currently used by end-users in metal heritage conservation, both in terms of environmental and health impact. The functional unit, used to normalize things in order to have a comparable overview, was defined as cleaning 1 dm^2 of tarnished copper. As can be seen on Table 5.4, formulations containing DFO need bigger quantity to fulfill the functional unit due to the lower affinity of DFO than other studied complexing agents with copper.

[13] Although bio-derived from cellulose, carboxymethyl cellulose production may require reagents hazardous for the aquatic environment (e.g., chloroacetic acid used for the synthesis of carboxymethyl cellulose) [65].

Table 5.4 Formulations evaluated. Completely bio-sourced ones are in italic.

Formulations	Quantity for the functional unit
PVA/Borax/Na_2EDTA/Water	30
Agar-agar/DFO/Water	*120 (4×30 mL applications)*
Xanthan/DFO/Water	*120 (4×30 mL applications)*
Agar/EDDS/Water	*30*
Agar/Na_2EDTA/Water	30

5.2.1.2 Scope definition

A cradle to grave system boundary was proposed, which considers steps from raw materials extraction to the end-of-life (figure 5.1). A European geographical scope was considered for raw materials production and formulations and a Swiss scope for the end-of-life treatment as the use was considered in Switzerland in the span of this project. Transport of the formulations and raw materials as well as packaging of raw materials or end products were excluded from the analysis.

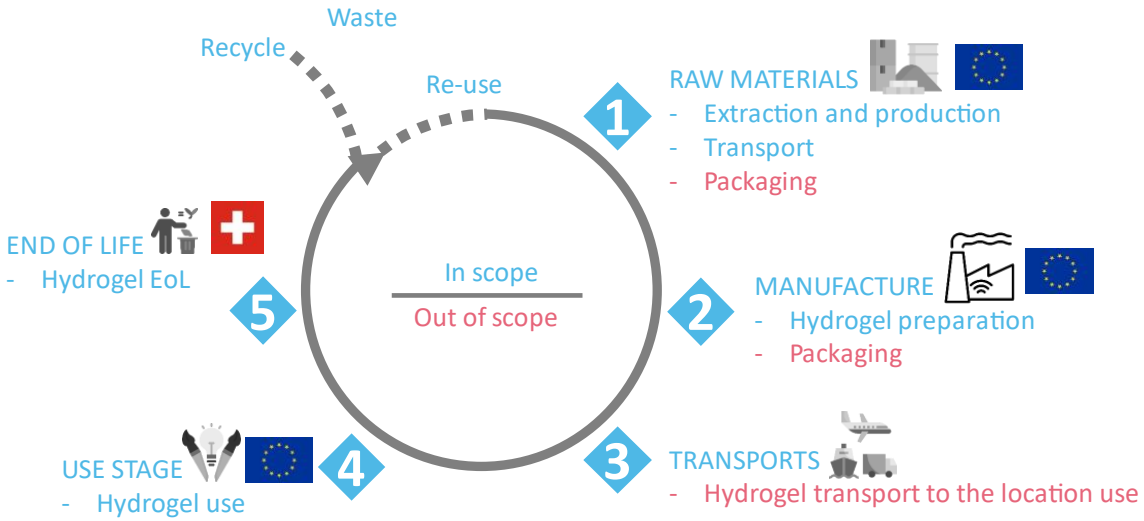

Figure 5.1 Recapitulative scope of the LCA study carried out in this chapter.

5.2.1.3 Impact categories

Out of the sixteen impact categories based on the recommendation of the European commission, six were found suitable to be used for this evaluation of cleaning hydrogels (Table 5.2, bold characters). These six categories are the ones that contribute the most to the final single scores of studied raw materials or formulations (i.e., characterized, normalized, and weighted).

5.2.1.4 Data collection

The software used for the LCA is SimaPro, which is the reference software in the field. Modeled data available (i.e., CMC, Na_2EDTA, PVA and borax) were extracted from the database EcoInvent 3.8 or World Food LCA. The methodological reference were the ISO norms 14044 and 14040 and the calculation method Environmental Footprint (EF) 3.0. Contributors considered for those data were the raw material input (i.e., the initial reagents necessary to their synthesis, including water), the chemical factory needed to perform the synthesis (i.e., building, laboratories, equipment, etc.), the energy necessary to the synthesis, the wastewater needing treatment after synthesis and finally the emissions released during synthesis.

Some of the raw materials studied were not available in the EcoInvent database, therefore required a bibliographic study to determine the production process and model these compounds. A semi specific approach was performed for some of the compounds, meaning evaluating the desired molecule based on the reactive molecules needed for its synthesis, if they were readily available in the database. Hypotheses for the related compounds are detailed below.

5.2.1.4.1 EDDS

The modeling hypothesis for EDDS production (35% solution) was based on [12] and EVEA generic chemical substance synthesis sheet. It should be pointed out that the referred paper is relative to a lab-scale production. A semi specific approach was conducted to model EDDS with the reagents used for its synthesis.

Although EDDS has been cited as possibly bio-sourced [13], this way of producing it is not yet adapted to industrial production and therefore the chemical reaction between ethylene bromide and L-aspartic acid is the main industrial production route for EDDS, with an estimated yield of 25% [12]. L-aspartic acid (LAA) was evaluated further as there are two alternatives to its production: the direct fermentation from sugar-containing substrate (Data for L-aspartic acid were extracted from World Food LCA database) or production using fumaric acid in the presence of high concentration of ammonia as carbon source (Table S5.1) [14,15]. The latter displays very high yields (over 95%). In the final model, production of LAA by fumaric acid is used.

Identified contributors were main reagents for EDDS synthesis and production (i.e., water, sodium hydroxide, ethylene bromide, sodium carbonate and L-aspartic acid), the energy used for the synthesis (e.g., heaters, stirrer), chemical factory (i.e., process emissions from the chemical plant) and emissions from the synthesis.

5.2.1.4.2 Agar

Two species of algae can be used for agar production, *Gracilaria*, mainly cultivated or *Gelidium*, harvested from wild bushes. Depending on the bibliographic source, the percentage of industrially used species is significantly different, ranging from 53% to 99% for *Gracilaria* versus 44% to 1% for *Gelidium* [16,17]. Here, the agar extraction protocol modelled is considered to yield a production of 26% for *Gelidium* and 33% for *Gracilaria* [16,18–20], considering low-scale production based on available data. The final model considers using the *Gelidium* species as it is claimed to be the species used by CTS restauro®, the main brand used by conservators for agar supplies. The harvest is considered made by hand, although mechanical ways are probably more relevant nowadays, but there is a lack of information on these techniques to allow proper model.

For agar, contributors include the necessary factory (i.e., the building itself) for the transformation process of red algae into gelling powder, the energy necessary for the transformation process, the transport (e.g., of the algae from the cultivation or harvesting places to the factory), the contribution of the cultivation process, the production of the gelling powder (i.e., chemicals and water used) and the wastewater from the production that needs to be treated afterwards.

5.2.1.4.3 Fermented compounds

For the compounds obtained by fermentation (i.e., xanthan gum, gellan gum and deferoxamine (DFO), see Table 5.3), the upstream process, meaning steps related to the inoculum development, is not taken into account. Regarding the downstream process, only generic steps, i.e. centrifugation, filtration and extraction are considered. Because high purity is not highly necessary for heritage conservation purposes, further purification steps using organic solvents like ethanol or isopropanol for xanthan and gellan gums are not taken into account. For DFO, there are seven purification steps, using multiple hazardous organic solvents (e.g., methanol, methyl isobutyl ketone (MIBK), chloroform), followed by preparation of DFO methane sulfonate salt form which are also discarded.

For all fermented compounds, contributors were the added carbon source (e.g., sugar from beets or glucose, soybean etc.), the production medium (i.e., water and chemicals), wastewater from the production of the gelling powder, production factory and biological wastes.

For confidentiality reasons, common suppliers were not compliant with sharing the details of their fermentation processes. Data is therefore based on EVEA generic fermentation sheet using Brew report hypothesis and bibliographic study to input carbon source, production medium, fermentation

conditions, productivity, yield and process energy [21]. All models are based on low scale processes as most industrial ones are not detailed in open access.

Xanthan gum

Hypothesis for the model of xanthan gum is based on articles from García-Ochoa *et al.* and Kuppiswami *et al.* with a production yield of 56% and a concentration in the final broth of 22.5 g/L [22,23]. Carbon source considered for the final model is sucrose (40 g/L). For instructive purposes, alternatives were also modeled, for instance the input of a glucose carbon source or the use of lower electricity power (1 kW^3 instead of 5 kW^3). The production medium considered is detailed in Table S5.2.

Gellan gum

Hypothesis for modelling is based on a publication presenting the optimization of cultural medium for gellan gum production with a verification experiment in a 5 L bioreactor with a production yield of 50% and a concentration in the final broth of 19.9 g/L [24,25]. The carbon source was considered to be sucrose (40 g/L), and the production medium detailed in Table S5.3.

Deferoxamine

The production yield considered is 24% with a concentration of product in the final broth of 4.8 g/L. The production medium is detailed in Table S5.4 and the carbon source input was hypothesized as mannitol (20 g/L). Publications related to the production of deferoxamine are few and not very detailed [26–28].

5.2.1.4.4 Borax

For borax, several hypotheses were considered. First, the use of Borax decahydrate versus anhydrous borax. In addition, boron is a rare element which is not found in nature alone in free form. It is generally found in combination with other elements in salts or ores and has been classified among the eight critical materials since 2017 [29]. For such, resource scarcity of tincal, the main boron ore, was then evaluated using different sources and using a characterization factor. The characterization factor for borax (8.41×10^{-3} kg Sb eq/kg) was created using the average on the abiotic depletion values for tincal and boron (4.27×10^{-5} and 1.68×10^{-2} kg Sb eq/kg) [29]. Indeed, for tincal a new value for the abiotic depletion was recently published but is not implemented yet in the new Environmental Footprint EF method (3.1) because potentially underestimated [29]. The other value for boron is rather old and potentially overestimated and therefore obsolete but considered because updated with the ratio boron to tincal.

5.2.1.5 Gels preparation

The formulation and preparation for PVA-borax gels was based on publication from the CSGI group [30]. It considered 3% w/v PVA, 0.6%$_{w/v}$ borax and $3 \cdot 10^{-2}$ M Na_2EDTA.

For agar formulation, the protocol described previously was implemented [31], using 3% w/v agar and complexing agents concentration of $3 \cdot 10^{-2}$ M for Na_2EDTA, EDDS and DFO.

For xanthan formulation, simple mixing of 5% w/v xanthan gum with $3 \cdot 10^{-2}$M DFO, as explained in [31]. The loss percentage, meaning the gel remaining in the beaker or container, was estimated at 5 wt.%. The energy input was considered using an agitating heating plate (heating power 630 W, absorbed engine agitation power 30 W, restituted engine agitation power 23 W).

5.2.1.6 Use phase considerations

Consumables as beakers, syringe, spatula and wooden sticks (cotton holder) have not been modelled as they are reusable. Pipettes, latex gloves, ethanol solution for rinsing, cotton and cleaning paper have been considered according to Table 5.5. The weight of these consumables is considered for the simulation. For latex gloves, models accounting for gloves of 11.88 g and 6.86 g were considered, according to the thickness of the gloves.

Table 5.5 Consumable considered in the modelling of the Use Phase of hydrogels.

Consumables	**PVA-Borax-Na_2EDTA Agar-EDDS Agar-Na_2EDTA**	**Agar-DFO**	**Xanthan-DFO**
Pipette	1 pipette – 2 g		
Latex gloves	1 glove pair – 11.88 g (max weight)		
Ethanol solution	10 mL		
Cotton	0.4 g	1 g	2 g
Cleaning paper	5 g		

5.2.1.7 End of life of the formulations

The application of the UseTox model, recommended by the European Commission [32], to characterize ecotoxic impacts of wastes in freshwaters and on human health is relevant when it comes to chemical substances that are rinsed down a sink, in addition to being identifiable by a CAS number. In the case of hydrogels for cultural heritage conservation, it appears, after discussion with conservators that most gels are not rinsed but discarded with a cotton swab and water and put with solid waste. The end of life considered is therefore incineration.

In addition, after use, the compounds are not present under their initial form as the complexing agents become metal-ligand complexes that need to be identified with a new CAS number, which is not the case for all the M-L complexes studies. Indeed, it is important to note that the biodegradability of a M-L complex is different than the biodegradability of the involved complexing agent alone [33]. In addition

to the scarcity of available relevant data in UseTox model, there is no model that allows to estimate and compare the ecotoxicity of incinerated substances. Incineration decomposes matter in several types of emission including water, gas, heavy metals and organic compounds. Metals cannot be eliminated by combustion and therefore can be found in incineration residues.

The stakes are therefore rather on the presence of metal ions than the complexing agent used. However, there are no possible levers of action as the cleaning of metal will always involve the presence of metal ions.

All things considered, an estimation of biogenic carbon of studied formulations is proposed. Indeed, adapting the data with the actual proportion of biogenic carbon in the formulations allows to compare the impact of the end of life via incineration depending on the nature of the raw materials used in the formulations. Basically, it considers that the CO_2 released after combustion is a "neutral" or "no net" emission as the carbon embodied in biomass was taken up during photosynthesis for instance and therefore can be seen as a constant CO_2 amount overtime, almost as a circular carbon cycle and therefore having no impact on the global LCA.

It is relevant to note that this end-of-life evaluation is country-specific as in Switzerland 99% of municipal solid wastes are considered incinerated whereas if a French scope had been considered, the percentage would have dropped to 61% according to EcoInvent values.

5.2.1.8 Raw materials hazards evaluation

To complete the LCA, another approach has been considered to evaluate the ecotoxicity of studied formulations. Bibliographic assessments using REACH (Registration, Evaluation, Authorization and Restriction of Chemicals Regulation) database has been carried out, which allowed to evaluate the environmental and health impacts of the raw materials and make better choices upstream. REACH database is a database where users report hazards related to materials based on their own experience [34].

Furthermore, substances that may have serious and often irreversible effects on human health and the environment can be identified as substances of very high concern (SVHC). If a substance is identified as an SVHC, it will be added to the Candidate List for eventual inclusion in the Authorization List. Companies may have immediate legal obligations following the inclusion of a substance in the Candidate List.

5.2.2 Results and discussion

First, each compound will be assessed individually and then the different formulations combining singular raw materials and preparation will be evaluated. Afterwards, the use phase and the end of life of each cleaning gel will be considered. Finally, an overview of the impact of each formulation from

cradle to grave will be proposed. In complement, an overview of the hazards brought by each raw material is given.

5.2.2.1 Raw materials

5.2.2.1.1 EDDS

For the raw material EDDS, contributors' repartition into the input of the main impact categories is proposed in figure 5.2. The main reagents, L.-aspartic acid and ethylene bromide are the most impactful contributors in the production of EDDS, regardless of the impact category evaluated, whereas contributors related to the process itself (energy, chemical factory, EDDS emission) are rather low.

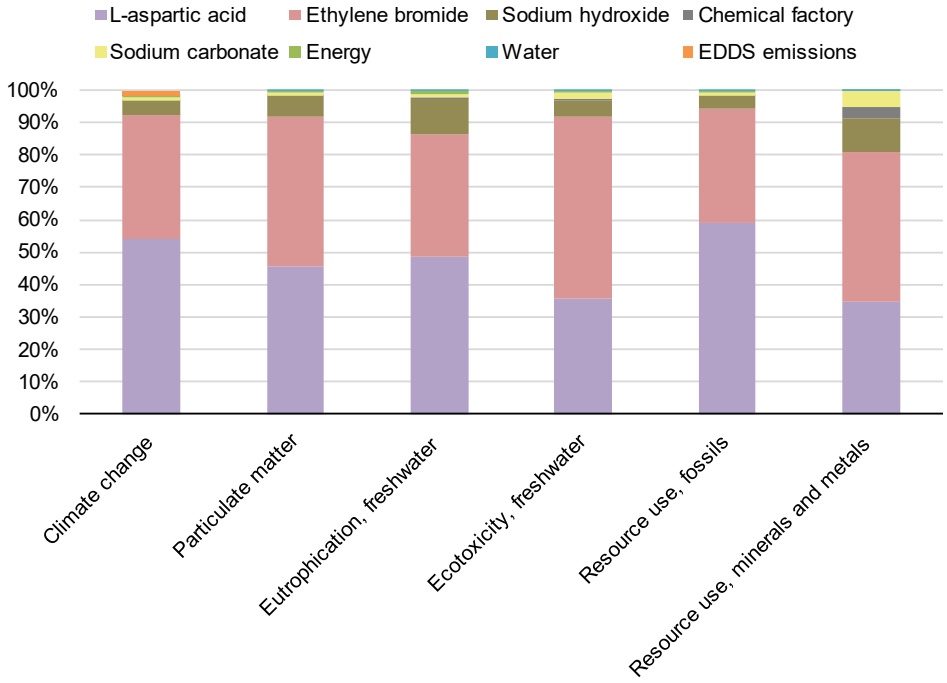

Figure 5.2 EDDS solution potential main impact contributors according to the different impact categories relevant for the purpose of this research project.

Ethylene bromide, one of the two main contributors to EDDS environmental impact is usually prepared using ethene and dibromide, for such, no lever of action could be performed on the production route.As L-aspartic acid is the other main contributor to EDDS environmental footprint, a deeper look was taken at its different production routes. It turns out that L-aspartic acid produced from fumaric acid is clearly less impactful than when prepared from sugar-containing substrate, with a "Climate change" impact contribution of respectively 0.53 and 2.88 mPt for 1 kg of solution (Figure 5.3), along with being more representative of the industrial production route. In the case of the EDDS used in the HELIX project (purchased from Sigma Aldrich), no information was given by the provider regarding the origin of L-aspartic acid used for the synthesis.

Although fumaric acid and ammonia are not considered safe nor green compounds, this lower score is accounted for by the significantly higher yield for the fermentation medium with fumaric acid (above

95% vs. 29% for the direct sugar fermentation route) [14], which has a direct impact on the environmental footprint of EDDS itself, through the semi specific approach, with a single score evaluation decreased by a factor of over 7 with production using fumaric acid (Figure 5.3).

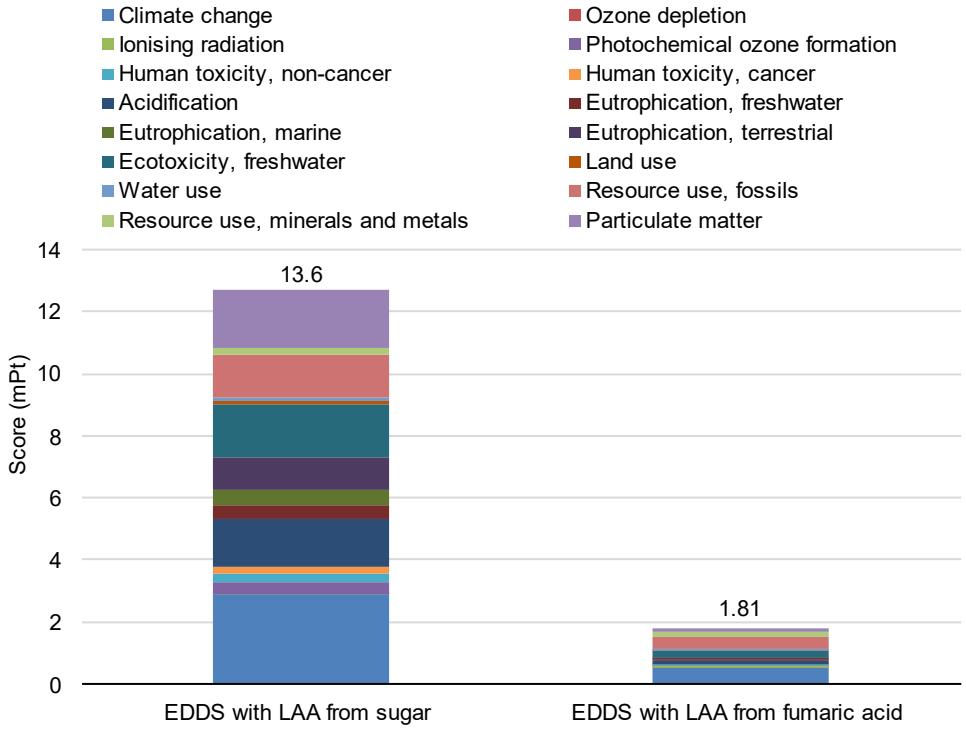

Figure 5.3 Single score of 1 kg EDDS solution comparing production using L-aspartic acid made by fermentation from fumaric acid as carbon source rather than sugar-containing substrate.

5.2.2.1.2 Agar

The weight of different contributors (e.g., energy, wastewater, production including water and reagents) into the different impact categories for different agar seaweeds is displayed in Figure 5.4.

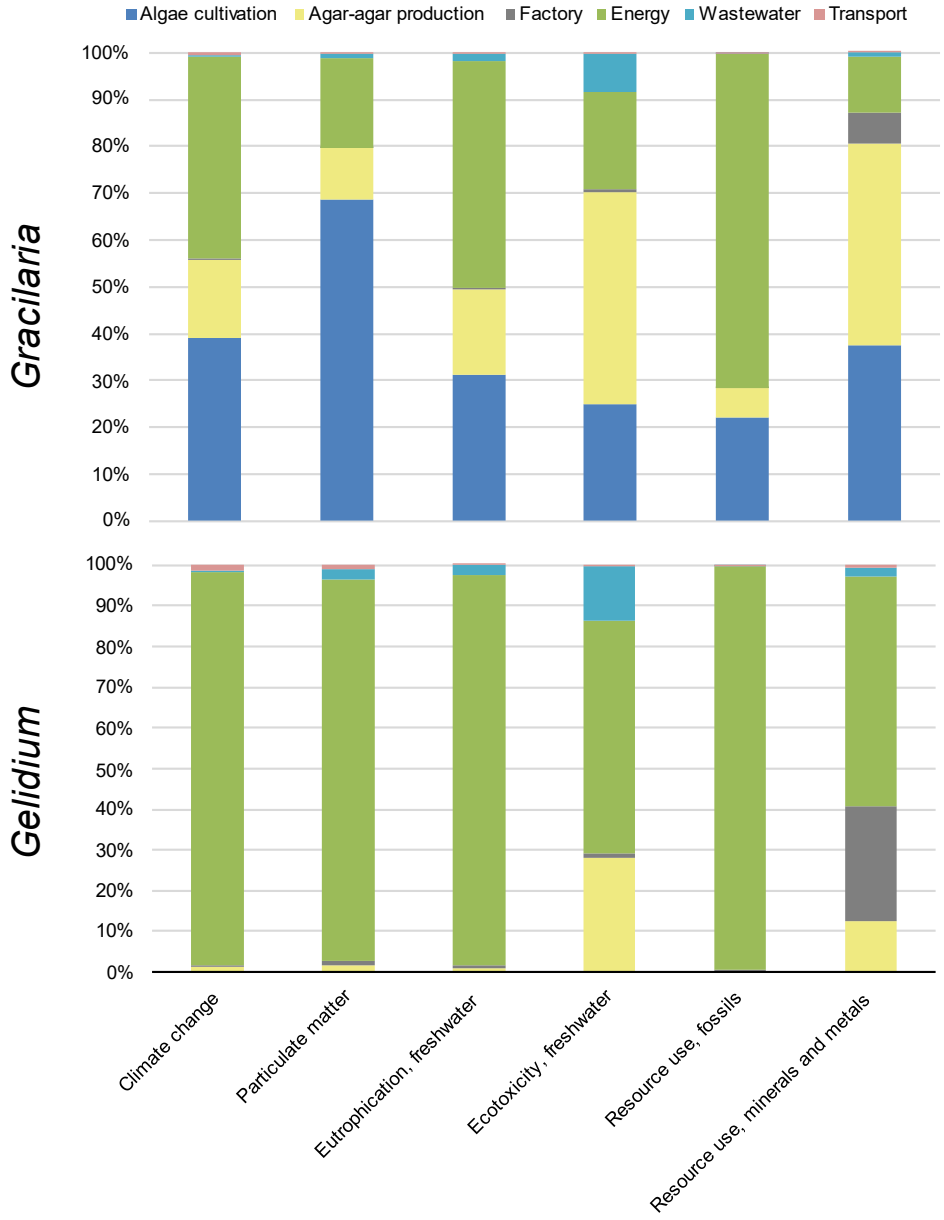

Figure 5.4 Agar-agar main potential impact contributors according to the different impact categories relevant for the purpose of this research project.

Single score of agar from cultivated plants (*Gracilaria* spp.) is impacted by algae cultivation and production whereas for agar from harvested species (*Gelidium* spp.) the impact is mainly due to the energy used for production. It is important to note that according to the species of algae used the results appear to be significantly different. Indeed, the two main species used are *Gracilaria*, cultivated and *Gelidium*, which is wild. *Gracilaria* algae are the most used for food-grade agar whereas *Gelidium* species are mainly used for bacteriological and pharmaceutical purposes, because they render a higher-quality

agar with better gelifying properties [35,36]. The latter usually has a lower impact as harvesting does not require most of the equipment necessary for cultivation, in particular land artificialization for the cultivating site, the factory premises and energy to run, pesticides etc. [17]. This is shown by the single score of both agar types, combining the values of each impact category (Figure 5.5).

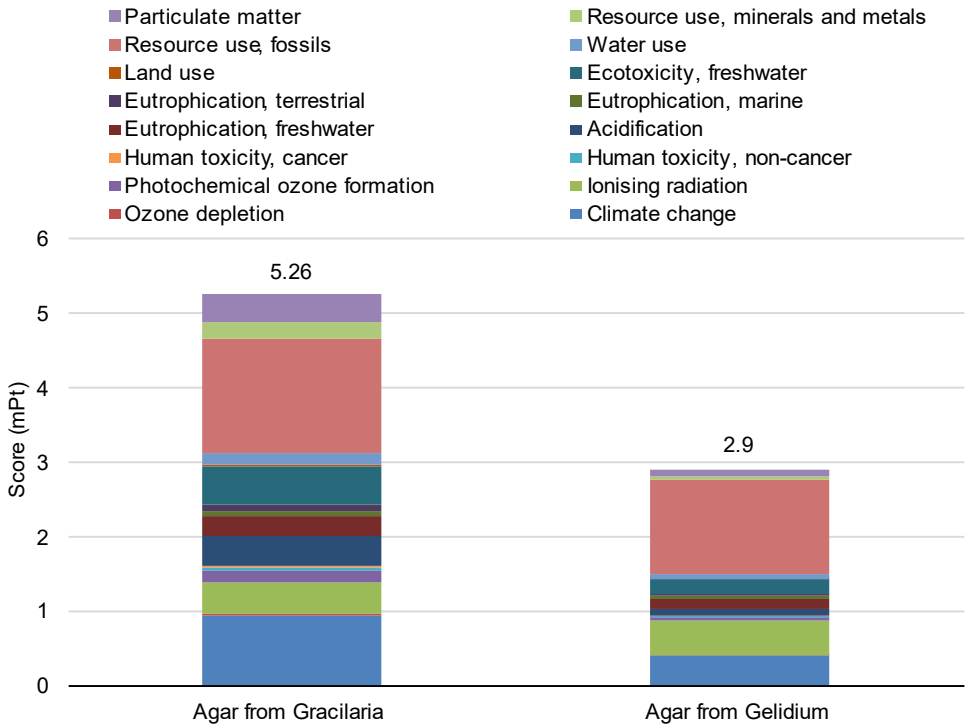

Figure 5.5 Single score of 1 kg agar comparing production form *Gracilaria* algae versus *Gelidium* algae.

Unfortunately, LCA does not address bio-sourced resources scarcity, which is a concern to be raised for agar plants [37]. Indeed, *Gelidium* agar market shattered from >90% to <1% from 1960s to 2020. A global shortage of *Gelidium* was reported in 2018 [17]. Harvesting, although less impactful, has a direct influence on the structure of seaweed beds and marine biodiversity [17], especially if performed mechanically, which on the long run directly affects availability of the resource.

5.2.2.1.3 Fermented compounds

The main contributors to substances produced by fermentation are usually energy, production medium and carbon source used during fermentation. It is therefore crucial to know these parameters accurately. Generally, in industrial processes, the carbon source tends to be the main source of impact whereas production medium tends to be the lowest one amongst the three cited. Hence, the modelling is highly limited by the lack of information or variations in the production medium, carbon sources and yields available in literature.

Xanthan gum

According to the hypothesis based on a yield of 56% (22.5 g/L of xanthan gum in the final broth), sucrose (40 g/L) as the input carbon source and using production medium detailed in Table S5.2 [22,23], the main

contributor for “Climate change”, “Particulate matter”, “Eutrophication, freshwater” and ”Resource use, fossils” categories is the energy use. On the other hand, production medium is the main contributor for the categories related to “Resource use, minerals and metals” and “Ecotoxicity, freshwater” (Figure 5.6).

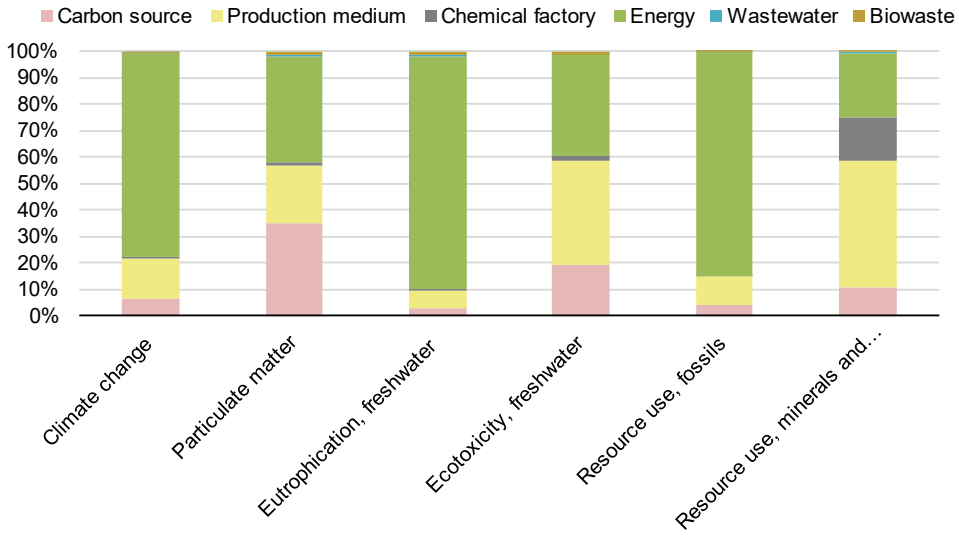

Figure 5.6 Xanthan gum main potential impact contributors according to the different impact categories relevant for the purpose of this research project.

On Figure 5.7, in order to appreciate the impact of the different hypotheses, different situations were modeled and displayed as single score. The first variation concerned the nature of the carbon source. For a similar final production of 22.5 g/L, the use of sucrose and glucose at the same concentration (40 g/L) achieved similar results (1.55 and 1.57 mPt respectively) whereas the use of sugar from sugarcane reached a slightly higher score of 1.82 mPt. Regarding the production medium, if its composition reported in Table S5.2 was modified to an agar-containing Yeast-Peptone-Glycerol (YPG) medium, the single score would rise by over 300%. If the electricity used for the fermentation was lowered to 1 kW/m^3, instead of the 5 kW^3 normally considered, the single score would drop by 30%. Finally, the obtention of a higher yield of 65 g/L instead of 22.5 g/L in the final broth would also result in the decrease of the final single score of xanthan gum. This proves the importance of accurate data for a reliable modelling as results can vary substantially.

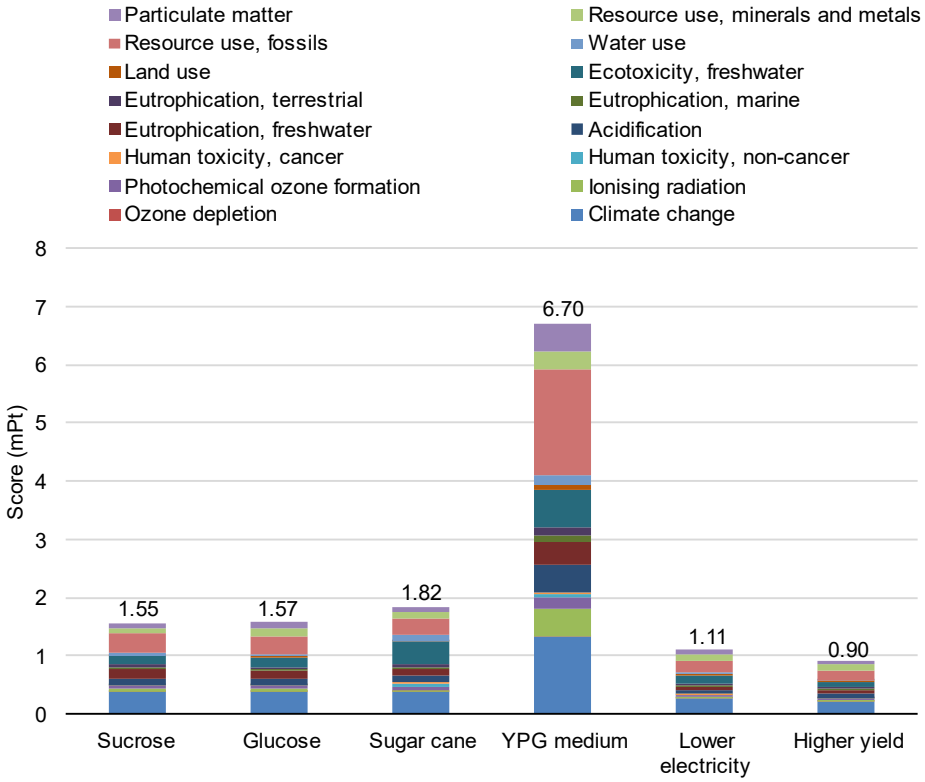

Figure 5.7 Potential input variation impact on xanthan gum.

Gellan gum

For gellan gum, energy is the main contributor impacting on "Climate change", "Eutrophication, freshwater" and "Resource use, fossils" categories whereas production leads the impact of "Particulate matter", "Ecotoxicity, freshwater" and "Resource use, minerals and metals» categories (Figure 5.8).

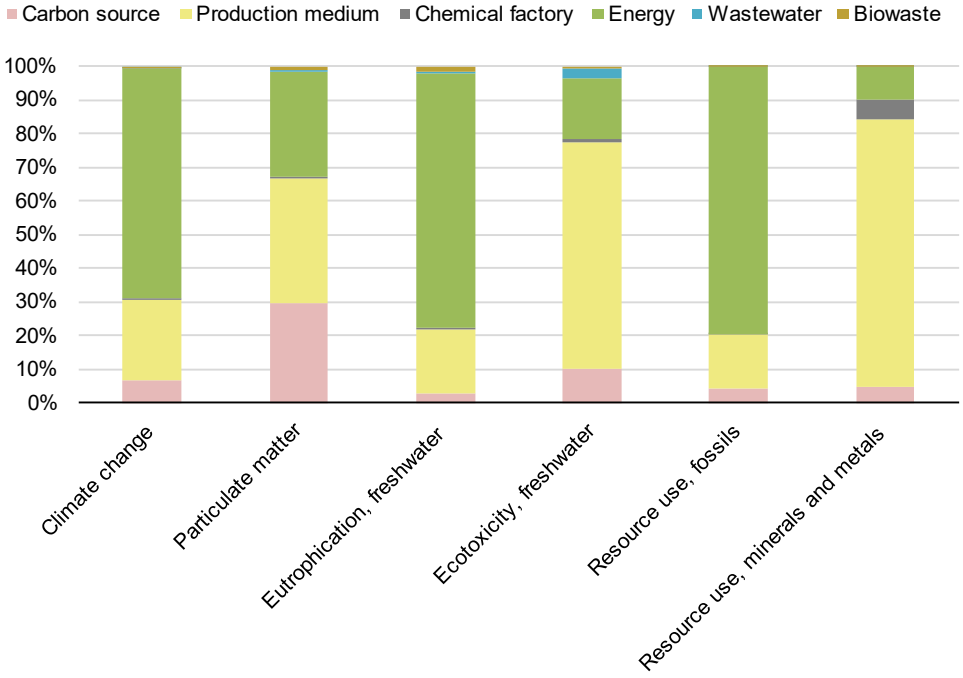

Figure 5.8 Gellan gum main potential impact contributors according to the different impact categories relevant for the purpose of this research project.

Also here, a modification in the fermentation process can influence the overall result. Hence, depending on the culture medium, the environmental impact of gellan gum is lowered by a factor of 4 (Figure 5.9), reaching a score close to the one of xanthan gum. Indeed, the presence of agar in the medium negatively influences by a factor of 3 [24,38]. Unfortunately, available references do not precise which is the most used pathway in industrial production of gellan gum and after contacting the providers (CTS®), no data was available for sharing due to industrial secret. Literature also shows a huge variation in gellan gum yields, which could be related to strain phenotype or quantification medium [38].

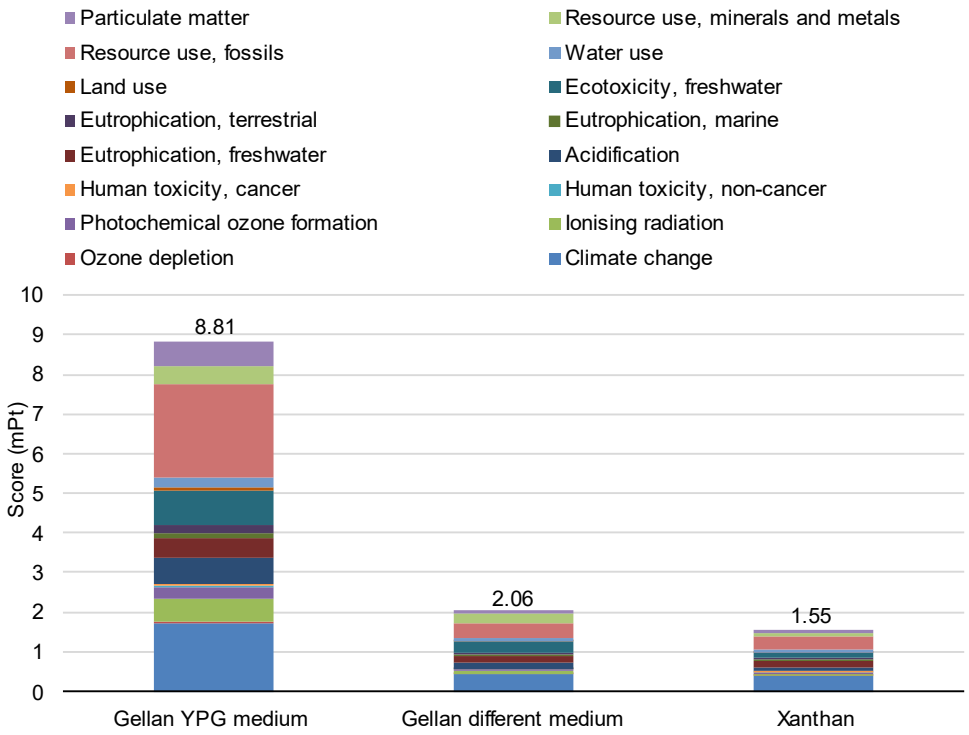

Figure 5.9 Single score of 1 kg gellan gum comparing production media (YPG or medium reported in Table S5.3) and single score of modeled xanthan.

Deferoxamine

For the siderophore deferoxamine, the main contributors are production medium and energy for the six main impact categories as can be seen on Figure 5.10. Deferoxamine is the fermented compound with the highest environmental impact based on hypothesis from the bibliographic study with a single score of 10.83 mPt for 1 kg of DFO, which is expected to be even higher as the used compound in HELIX formulation is the pharmaceutical grade one from Novartis and therefore requiring all the purification steps not taken into account here.

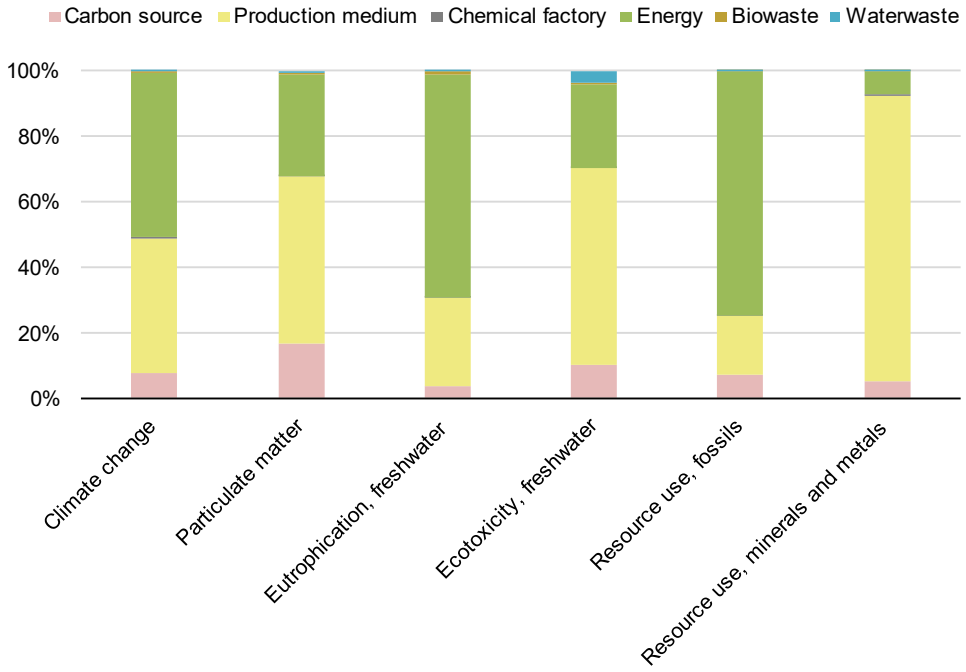

Figure 5.10 Deferoxamine main potential impact contributors according to the different impact categories relevant for the purpose of this research project.

5.2.2.1.4 Carboxymethyl cellulose

Based on the data from the EcoInvent 3.8 database, the main contributor for the production of Carboxmethyl cellulose (CMC) is the energy input (Figure S5.1.) for the process and the single score is 0.35 mPt for 1 kg of CMC.

5.2.2.1.5 Na_2EDTA

For Na_2EDTA, the main contributor is raw material input (Figure S5.2), especially sodium cyanide for all impact categories. The single score is 0.51 mPt for 1 kg based on EcoInvent values.

5.2.2.1.6 PVA

PVA's main contributor is also raw material input (Figure S5.3), in particular vinyl acetate and the polymerization process. 1 kg of PVA reaches a single score of 1.13 mPt based on EcoInvent values.

5.2.2.1.7 Borax

For borax, the main contributor is the energy related to the refinement process, apart for the "Resource use, minerals and metals" category for which it is the raw material input. (Figure S5.4)

If the borax form considered is not anhydrous but decahydrate form, as reported in PVA-borax formulations [30], the consumption of energy is reduced, as taking out water from the mineral requires energy [39].

The borax modeled for the final model is disodium tetraborate decahydrate which is originally refined from the original borax ore, tincal. This compound is not so prevalent and therefore it was deemed relevant to implement a rarefaction factor for the abiotic depletion of this compounds. In that case, borax

is regarded as very impactful due to the escalation of the weight of the category "Resource use, minerals and metals" (Figure 5.11).

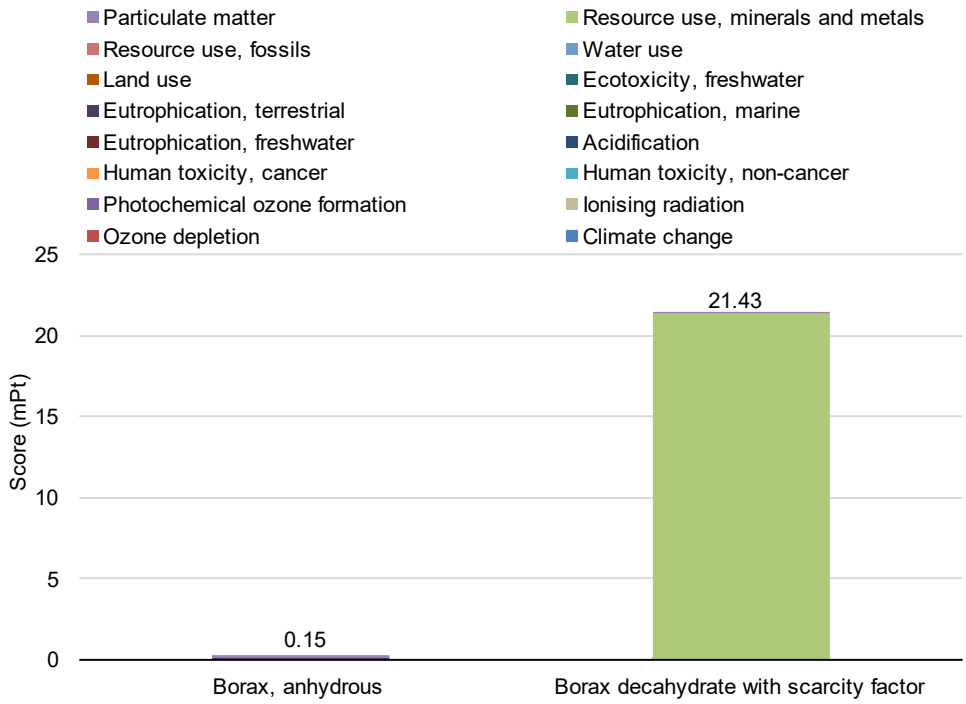

Figure 5.11 Single score of 1 kg borax comparing the implementation of a factor rendering the scarcity of the tincal resource.

It is to be noted that the robustness of the category "Resource use, minerals and metals" is classified by experts as "recommended but to use with caution" based on uncertainty of the actual reserve and different methodologies.

5.2.2.2 Raw materials comparison by single score

Overall, energy is the most impactful contributor on the evaluation criteria as seen for *Gelidium* agar, xanthan and gellan gum, DFO, CMC and borax. For fermented compounds (i.e., xanthan, gellan, DFO), production medium is also a major actor in the weight of the impact categories whereas for others (i.e., CMC, EDTA, PVA and borax) it's the raw materials input. In this section, single scores from each raw material are compared (Figure 5.12). As already mentioned, results are very dependent on data and hypotheses made on the numerous parameters. Nothing is unchangeable, especially compounds that required modeling. For such, made hypotheses are important in order to have a reliable, transparent comparison [40].

Comparing single scores, modeled compounds (i.e., DFO, EDDS, borax, agar, gellan and xanthan gum) are the ones with the highest scores (Figure 5.12).

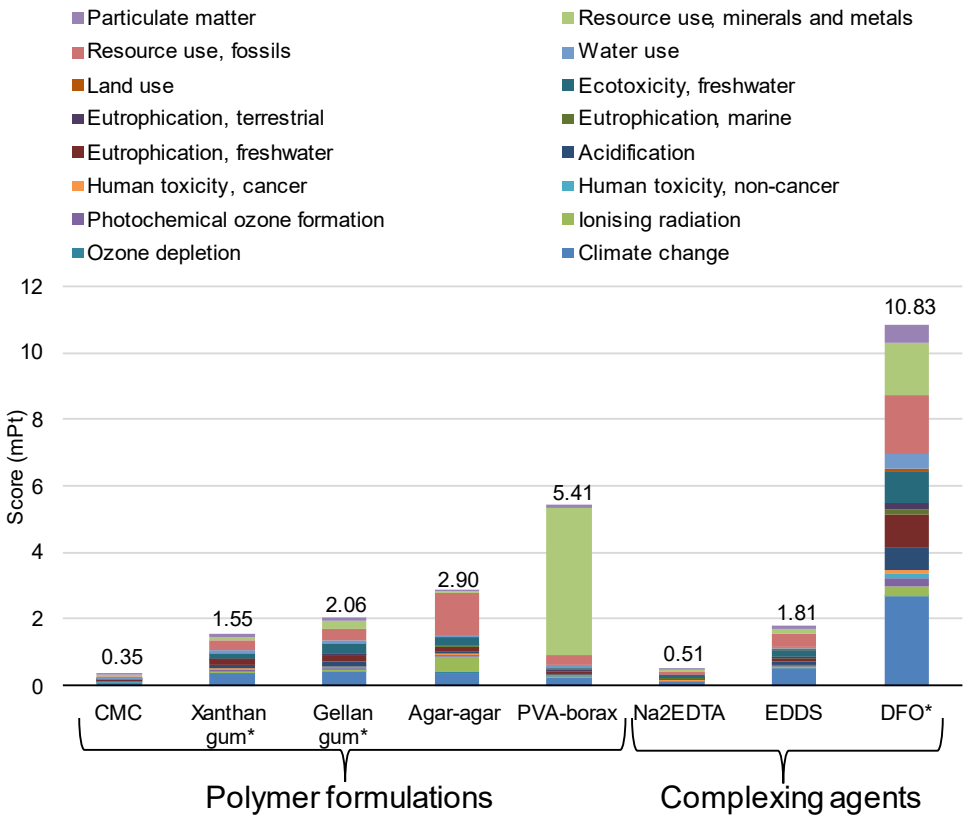

Figure 5.12 Raw materials comparison by single score, for 1 kg. Asterisks stand for fermented materials.

The relatively high score of modeled materials, in particular DFO, compared to RM already existing in the database (i.e., CMC, Na_2EDTA and borax), can be put on the lab-scale bibliography that was used, meaning a low-scale process were the yield is often not optimized. Indeed, the yield is usually lower than for industrial processes. For instance, in the case of DFO, the single score is probably overestimated compared to what is produced industrially as assumptions were made on publications producing DFO in a low-scale process.

Modeling hypotheses put aside, bio-sourced compounds often give a positive a priori whereas their impact can be rather dissatisfactory. There are several reasons that can be accounted for this such as the production route not being competitive yet or fermentation eventually "costing" a lot due to the use of a carbon source. Even following the green principle of atom economy and improving the efficiency of the reaction with the minimal amount of sugar (i.e., carbon source) needed, the addition of such compounds in the culture broth is environmentally costly. Finally, biotic-resource depletion, although not yet taken into account into calculations [41], can also render the bio-based compounds impertinent in a similar way the consideration of abiotic depletion did for borax. Other LCA also report the "false good idea" of using bio-based compounds as long as the industrial production route is not adapted [42,43]. Critical aspects to be considered for biotic-resource depletion would be the regeneration rate the studied resource along with the capacity of the ecosystem to secure its provision. Both aspects are

essential to determine the renewability of the resource. Indeed, if the extraction rate outweighs the regeneration rate, the resource will tend to exhaustion [44].

We can however highlight that CMC and Na_2EDTA appear to have the lowest impact of all materials. DFO has the highest impact of the materials produced from fermentation and it is expected to be even higher considering the downstream processes required to obtain DFO (i.e., extraction and purification steps). PVA-Borax appears to have the highest impact of hydrogel matrixes, this is due to the tincal rarefaction factor that was implemented for the impact category "Resource use, minerals and metals". In Table 5.6, the total single score from Figure 5.12 is relatively compared to the "Climate change" category score. CMC and Na2EDTA remain the most performing raw materials respectively and DFO the least performing one. Nevertheless, the other compounds ranking (in orange in the table) differs if considering the total score or only the carbon emissions (i.e., "Climate change" category). In particular, the PVA-borax polymer rises in the ranking as it is mainly the category "Resources, minerals and metals" giving its low global single score. This shows that the use of different impact categories is useful and as it can completely modify the perceived impact of a compound compared to taking into account only one aspect of the impact. For that reason, carbon calculator, solely considering "Climate change" and therefore CO2 emissions can find themselves irrelevant.

Table 5.6 Impact of raw materials taking into account uniquely "Climate change" impact category or global single score of impact categories. In orange are the rankings that are modified comparatively to single score.

Raw materials	Single score (mPt)	Ranking via single score	Climate change score (mPt)	Ranking via carbon emissions
CMC	0.35	1	0.084	1
Na_2EDTA	0.51	2	0.111	2
Xanthan gum	1.55	3	0.386	4
EDDS	1.81	4	0.526	7
Gellan gum	2.06	5	0.441	6
Agar-agar	2.9	6	0.398	5
PVA-borax	5.41	7	0.245	3
DFO	10.83	8	2.67	8

It remains difficult to compare the environmental impact of the nine raw materials between each other as a lot of hypotheses have been used to model raw materials. Overall, the materials present in the database are the least impactful, with CMC being the lowest one. This is due to the modelling limits:

- There is a lack of information from suppliers on their process (inputs, outputs, and energy) especially for agar-agar and the ingredients produced by fermentation, that were modelled based on publications mainly reporting lab-scale experiments.
- The inability to take into account biotic resource scarcity and the impact of *Gelidium* algae harvest on biodiversity of agar.
- The existence of different rarefaction factor for the abiotic depletion of Boron/Tincal and the low robustness of the impact category "Resources, minerals and metals".

5.2.2.3 Environmental impact evaluation of hydrogels formulations and their application

In this section, the environmental impact of each raw material on the cleaning formulation is presented and discussed. Afterwards, the different formulations are compared relatively to their performance on the functional unit (1 dm^2 of copper).

Regarding the contribution from each of the raw materials in the formulations, although DFO is the RM used in smallest amount, it is the most impactful one on most of the impact categories (Figure 5.13). The weight percentage parameter represents the quantity, in weight, of each compound in the formulation.

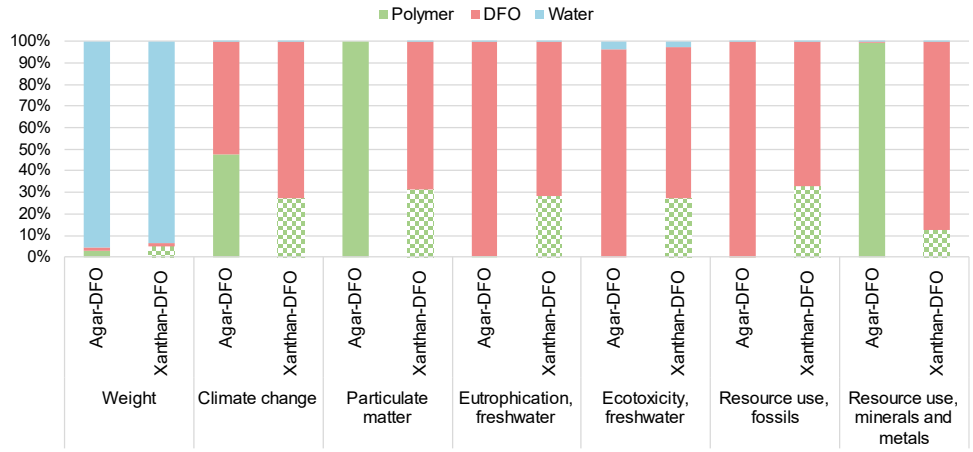

Figure 5.13 Raw materials contributions to impact categories for DFO-containing formulations taking into considering an application with 4 reiterations.

Notably, Na_2EDTA potential impacts are negligible in the formulations where it is used. It is relatively similar for borax, with an exception for the "Resource use, minerals and metals" category (Figure 5.14).

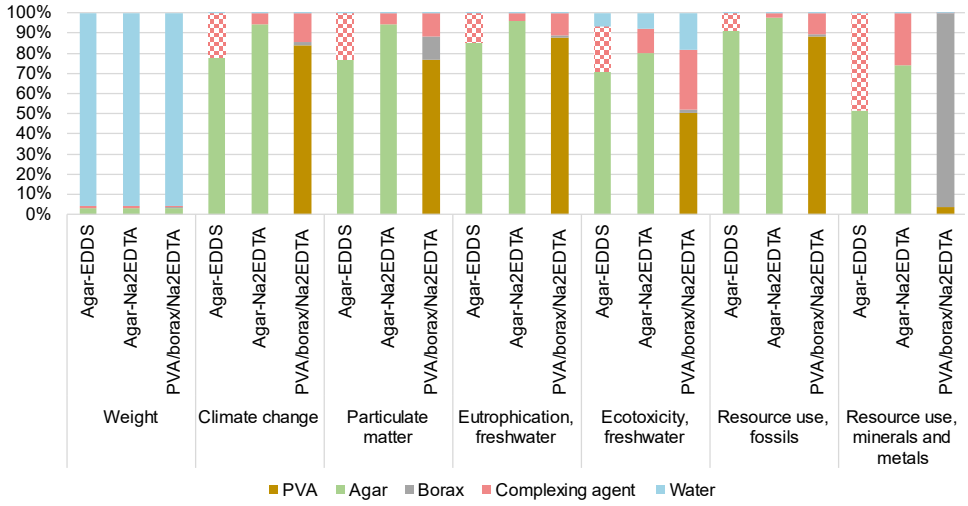

Figure 5.14 Raw materials contributions to impact categories for PVA-borax-EDTA, Agar-EDDS and Agar-EDTA formulations.

The single score comparison of the five studied formulations (Figure 5.15), based on the functional unit shows that those that require reiterations (application of 4 × 30 mL) are the most impactful and also the ones containing DFO.

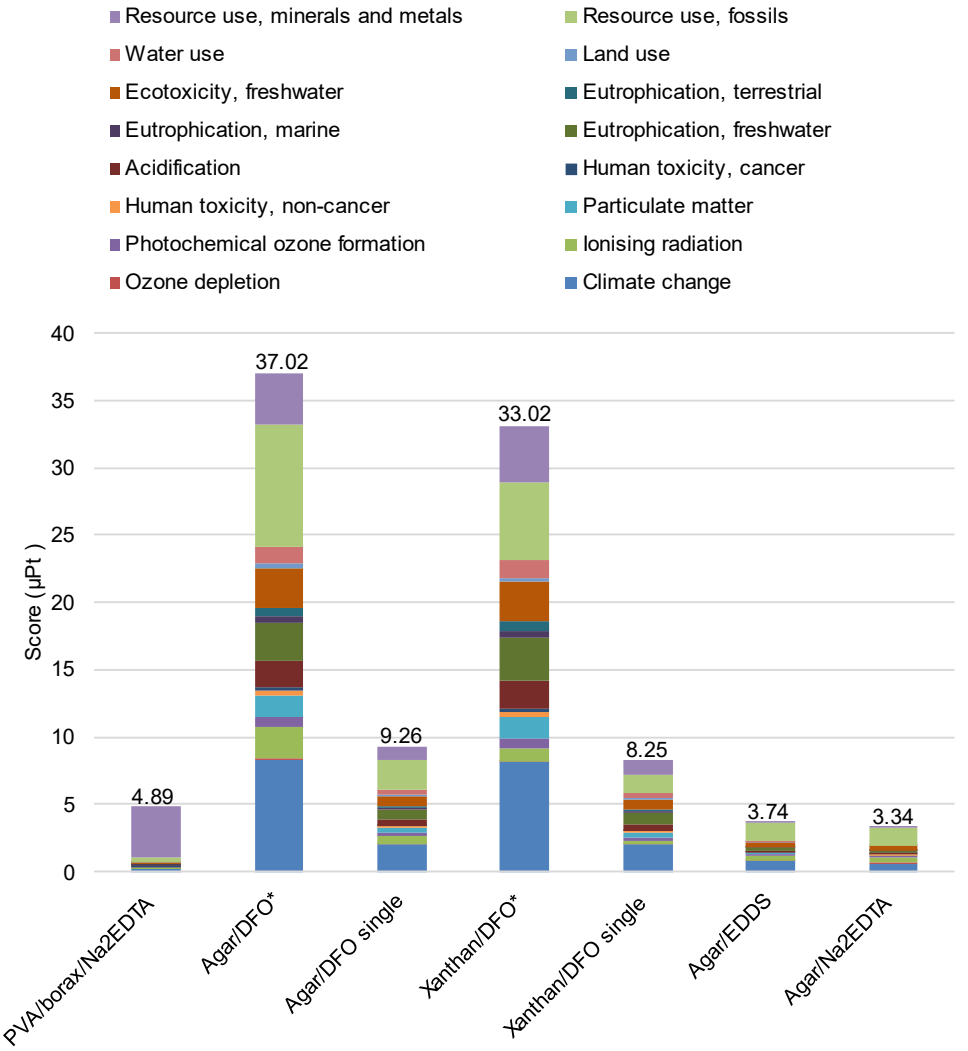

Figure 5.15 Single score comparison of hydrogels formulations, to clean 1 dm² of copper (functional unit). Formulations with an asterisk are the ones requiring 4 applications.

However, if we were considering that all hydrogels only required a single application, the most impactful formulation would remain Agar/DFO and Xanthan/DFO. Hence, their high score is related to the presence of the most impactful raw material (DFO) rather than the number of applications. The three other formulations are quite close in terms of potential environmental impact, around 4 µPt, whereas a single application with a DFO-containing formulation already reaches over 8 µPt.

It is worth to note that hydrogels are composed of over 90% of water and therefore the overall impact of formulation is relatively low considering the scarce quantity of polymer and chelating agents present in the final volume, explaining why the order of magnitude is µPt. Indeed, for one application of 30 mL, the quantity of active ingredients is lower than 2 g.

5.2.2.4 Use phase

The use phase considers all the consumables that are needed to apply the treating gels. On Figure 5.16, the weight of the different consumables of the application of single application formulations (i.e.,

PVA/Borax/Na_2EDTA, Agar/Na_2EDTA, Agar/EDDS) on the six main impact categories used can be seen. Regarding the use phase, latex gloves are by far the most impactful contributor as they account for 65.5 to 88% of the impact (Figure 5.16). This statement is valid regardless of their grade (weight).

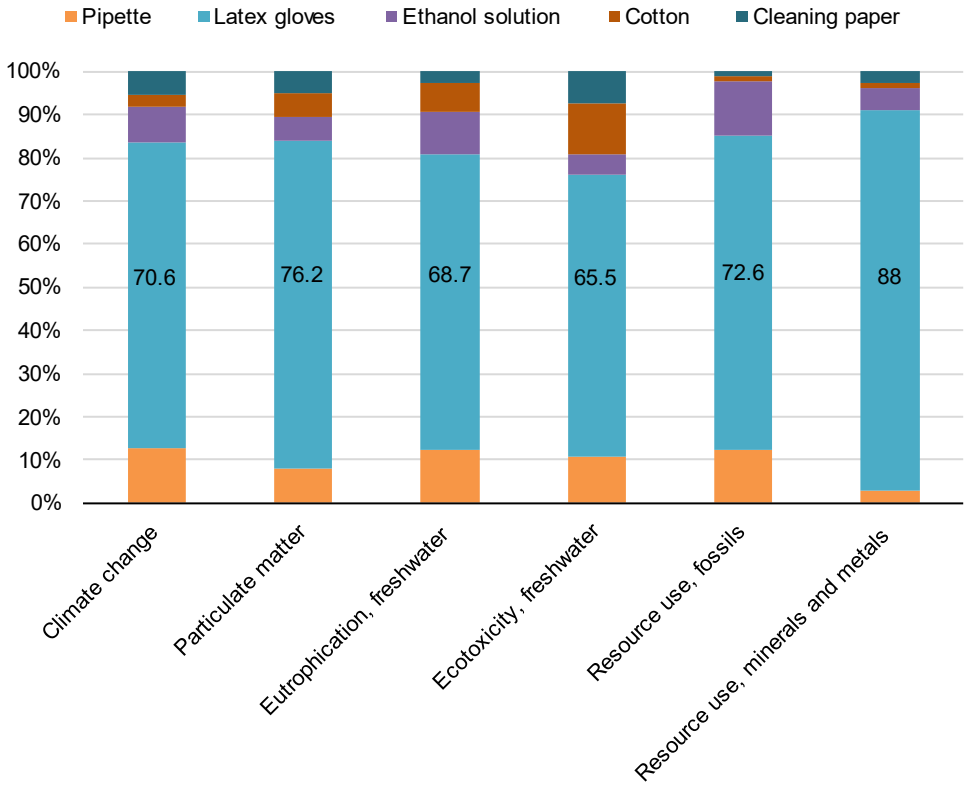

Figure 5.16 Use phase lifecycle main potential impact contributor comparison of single application formulations (i.e., PVA-borax/Na_2EDTA, Agar/Na_2EDTA, Agar/EDDS).

5.2.2.5 End of Life

The end of life (EoL) of formulations was considered as being thrown to solid waste and further incinerated. For such, it is relevant to account for the biogenic carbon present in the formulations as some of the gels are partially or totally bio-based materials. Despite the fact DFO-containing formulations are used in more important quantities due to reiterations, their EoL do not have the highest potential impact in terms of "Climate change» as the formulations contain 100% biogenic carbon (Table 5.7). Their performance is followed by the Agar/EDDS gel, that contains 92% of biogenic carbon. Indeed, the fumaric acid used for the production of LAA is accounted fossil. The Agar/Na_2EDTA formulation achieves contrasted results, thanks to the presence of agar is the formulation. Finally, EoL of PVA/Borax/Na_2EDTA formulation has the greatest potential impact on "Climate change" as it contains 0% biogenic carbon (Table 5.7).

Table 5.7 Percentage of biogenic carbon contained by studied formulations and impact of "Climate change" score of the End-of-Life phase.

Formulations	Percentage of biogenic carbon	Climate change score (× 10^{-3} kg CO_2 eq)
PVA/Borax/Na_2EDTA/Water	0	38.41
Agar/DFO/Water	100	6.68
Xanthan/DFO/Water	100	6.68
Agar/EDDS/Water	92	4.76
Agar/Na_2EDTA/Water	58	17.21

5.2.2.6 Global life cycle

On Figure 5.12 were discussed the single score of the raw materials and on figure 5.15 the single scores of the formulations. Here, to evaluate the different steps of the life cycle of the hydrogels, Figure 5.17, shows the total single score, detailing the impact of each step.

Raw materials are the main contributor to the global impact in Agar/DFO (74.6%) and Xanthan-DFO (72.1%), due to the presence of DFO in the formulation.

The use phase is the main contributor regarding PVA/borax/Na_2EDTA (56.4%), Agar/EDDS (65%) and Agar/Na_2EDTA (65.6%) formulations, mainly because of the use of gloves.

Product end of life represents 1.7 to 7.5% of the hydrogels impact on the single score, but, if only regarding the "Climate change" impact category, rises up to 31% of contribution for PVA/borax/Na_2EDTA. This is because the formulation is not bio-based and therefore contains no biogenic carbon. This is an example of why looking at only one of the impact categories, like carbon calculator, can be misleading, or not as accurate.

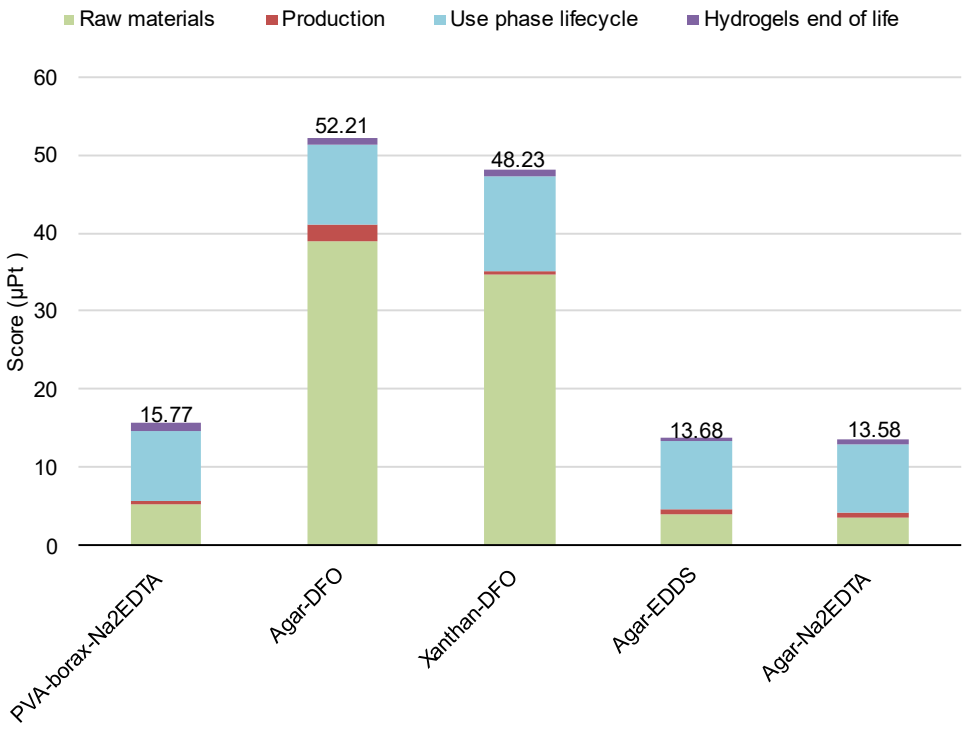

Figure 5.17 Hydrogels comparison by phase contribution using single score.

A recapitulative table of the ranking of the different formulations is proposed in Table 5.8. Ranking goes from 1 to 5 with the first rank being the best environmental performing (lowest single score). DFO-containing formulations are overall the two with the worst rankings compared to other formulations, looking at either climate change or total single score. However, they perform best when looking only at the EoL aspect thanks to their high biogenic carbon content. The PVA-based gel's performance is mediocre. The formulation composition is ranked first if only looking at "Climate change" but last when taking into account the other impact categories, in particular "Resource use, minerals and metals" due to the presence of borax in the formulation. Agar/EDDS and agar/Na_2EDTA's ranks are in the top two most of the time.

The change of rank again shows the importance of considering all categories and not only looking at carbon emissions ("Climate change"), which can be misleading.

Table 5.8 Ranking of formulations according to the "climate change" category or the global single score for the composition, the end of life or the full life cycle. Raking goes from 1 to 5 corresponding to best to least performing.

	Formulation composition		**End of life (biogenic carbon incineration)**	**Global life cycle**	
	Climate change	Single score	Climate change	Climate change	Single score
Agar/EDDS	3	2	1	1	2
Agar/Na_2EDTA	2	1	4	2	1
Agar/DFO	5	5	2	5	5
Xanthan/DFO	4	4	2	4	4
PVA/borax/Na_2EDTA	1	3	5	3	3

5.2.2.7 Raw materials hazard assessments

For polymers, only xanthan gum and PVA are reported as hazardous. On the REACH database, the first one is reported to cause serious eye and skin irritation and is assigned pictograms GHS07  whereas the second one is reported to cause damage to organs therefore being annotated with pictogram GHS08  . Overall, most polymers are not considered hazardous except for PVA.

Focusing on complexing agents, Na_2EDTA is reported, by a significant number of notifiers, to be associated with a range of hazards including damage to organs, eye/skin/respiratory irritation, harmful to aquatic life with long lasting effects and labelled with GHS07 or GHS08 pictograms by 66% and 24% of 453 notifiers respectively. DFO is reported to cause skin, eye and respiratory irritation as well as being allergenic and is also labelled with GHS07 and GHS08 pictograms for 56% and 44% of the registered users (9) respectively. The only complexing agent considered to have a low hazard level is EDDS. Borax is reported by most notifiers as potentially damaging fertility or unborn child and is labeled GHS08 by 99% of total notifiers (2843). In addition, $Na_2B_4O_7{\cdot}10H_2O$ is on the candidate list of SVHC for Authorization, for its toxicity for reproduction. Raw materials considered the most hazardous for human health are PVA, borax, deferoxamine and Na_2EDTA, therefore classified with a high hazard. EDDS not being reported as hazardous, although registered on REACH, makes it a compound with a low hazard level. Xanthan gum only having one pictogram for irritation is classified medium hazard level in further discussion. As a result, the hydrogel formulation considered the less hazardous for human health is Agar-EDDS.

However, similarly to what is done for LCA, if one performs a semi specific approach regarding health hazards, i.e. assessing reagents, EDDS is more concerning than it seems. Indeed, ethylene bromide is one of the two main impact contributors. From EDDS's two main contributors, LAA was the relevant compound for environmental hazards, driving the LCA results depending on its production route. Nevertheless, for health hazards, ethylene bromide is the one on which there is a concern to have for health. Indeed, it is classified as a serious health hazard (GSH08), having acute toxicity (GSH06) and being hazardous to the environment (GSH07) by the European Chemical Agency. Of course, conservators are not in contact with this substance so its health impact may seem irrelevant but the healthy safety of chemical factory workers out of Europe shall not be disregarded. As stated, although the reaction of ethylene bromide with L-aspartic acid is currently the main route for industrial production of EDDS. Other methods resorting to maleic acid and ethylene diamine, less toxic than its bromide counterpart, exist, but produce racemic EDDS. Only the (S,S) stereoisomer is of interest due to its biodegradable properties and commercial availablity [45]. As mentioned in section 2.1.4.1, production routes using microorganisms, ethylenediamine and fumaric acid exist [13], but are not relevant in terms of LCA and environmental impact due to their low yield, making them unsuitable so far for industrial production., If using the same approach for EDTA, it is produced using formaldehyde, ethylene diamine and sodium cyanide , all of which are assigned with two or more safety pictograms, including GSH06 and GSH08. Formaldehyde is also of very high concern (SVHC) since it is carcinogenic.

Concerning environmental hazards, only EDDS and EDTA are reported on the REACH database. EDTA is not readily biodegradable but (S,S)-EDDS is [13,33,46]. It is reported that iron-EDTA complexes are to a certain degree photolyzable in water and soil [47], and that iron-EDDS complexes are photodegradable [48]. No data could be found concerning complexes formed with copper or deferoxamine.

5.2.2.7.1 Environmental impact vs Raw Materials hazard assessment

Both environmental impact and health hazards make part of global sustainability, therefore, it is interesting to confront both obtained results. A visual representation considering both aspects is proposed on Figure 5.18 according to ratings attributed on Table 5.9. Ratings and classification in Table 5.9 were based on the REACH outputs. For the environmental impact, the rating was made considering the LCA hypothesis for each treatment (Figure 5.15). The one with the highest single score (Agar-DFO) was given a mark of 10/10 and other formulations were rated in proportion to this using a simple cross-multiplication. For the health hazard level, a subjective rating was used, giving a mark of 10/10 for a formulation using only "High" risk RM (i.e., PVA/borax/Na_2EDTA) and a 2/10 for one using only "Low" risk RM (i.e., Agar/EDDS) and positioning the others in-between regarding the rating of their RM.

Table 5.9 Rating of environmental impact and hazard level of evaluated hydrogel formulations.

Formulations	Environmental impact (based on Figure 5.15)	Environmental impact rating /10	Hazard level of RM	RM hazard subjective rating /10
PVA/Borax/Na_2EDTA	4.89	1.32	High/High/High	10
Agar-agar/DFO	37.02	10	Low/High	5
Xanthan/DFO	33.02	8.91	Medium/High	7
Agar/EDDS	3.74	1.01	Low/Low	2
Agar/Na_2EDTA	3.36	0.91	Low/High	5

PVA/borax/Na_2EDTA has a low potential environmental impact but uses the most hazardous raw materials (RM). DFO-containing formulations have the highest environmental impact and use an ingredient with a respiratory health hazard. Agar/EDDS formulation does not contain any hazardous materials and has a low potential environmental impact; hence it appears to be the best option considering both criteria.

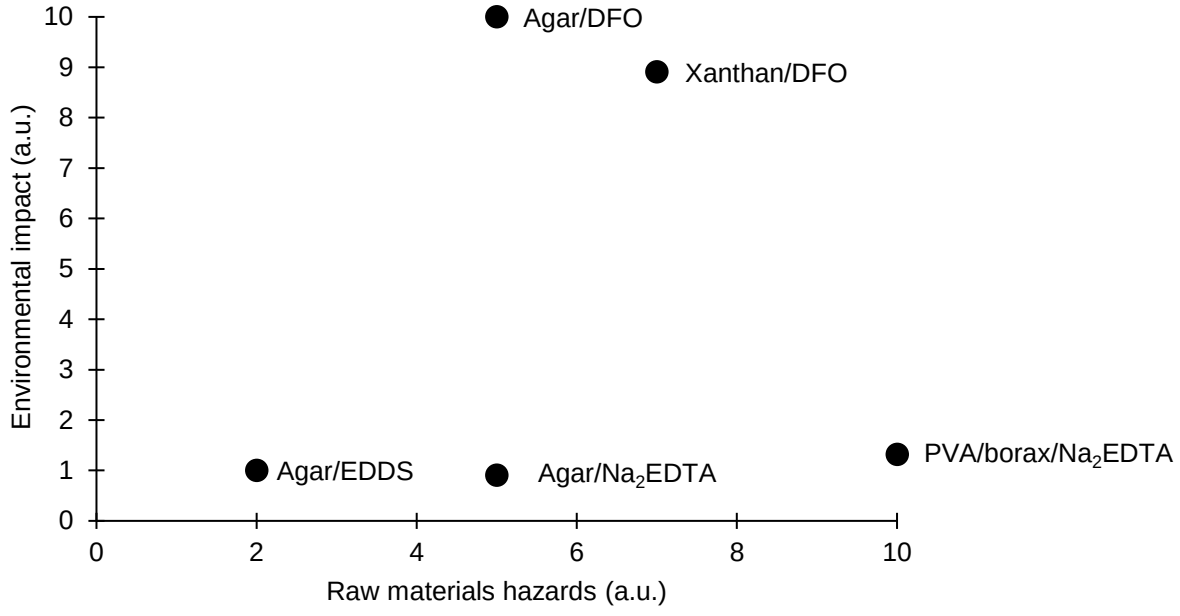

Figure 5.18 Environmental impact vs. Raw material hazards of studied hydrogel formulations.

5.2.3 Discussion

The current availability and transparency of data hampered the exhaustive comparison between petrochemical and HELIX alternatives for cleaning hydrogels. It would be desirable to have more transparent data in the public domain from suppliers and producers. Only by this way it is possible to make unbiased comparison with full insight over all impact categories and have a full interpretation of the results.

The cradle to grave environmental performances of bio-based cleaning hydrogels were compared to petrochemical alternatives. A comprehensive assessment was performed using 16 impact categories following the ISO14044 and 14040 norms. Globally, this analysis shows that for bio-based hydrogels from the HELIX project to be preferable to fossil or petrochemical-based alternatives, further improvements in regard to environmental performance are needed. The highest contributors for raw materials were most of the time production medium and energy, mostly affecting the "Climate change" impact category. Only for Borax, the impact category with more weight becomes "Resource use, minerals and metals". The considered end-of-life has relatively low relevance, whether accounting for biogenic carbon or not. For DFO-containing formulations, the major impact was the raw materials input whereas for the others it is accountable on the use phase, in particular to the presence of latex gloves. Although used materials might have a low health hazard, end-users will undeniably use gloves for the protections of the objects to avoid fingerprint marks. A lever of action is to use cotton gloves, reusable gloves, or even biodegradable ones [14].

Overall, the results show that to make bio-based hydrogels preferential in terms of environmental impact, more accurate data or changes in production are needed. This is in line with findings from previous LCA studies comparing bio- and petrochemical alternatives [42,49,50]. Fermentation is, unfortunately, often not the best compromise yet. In addition, as the production medium is the main contributor to the environmental impact for most data modelled, the use of a waste as carbon source could be an idea to lower the impact of that category similarly to what can be done to produce gelifying agents Poly hydroxy butyrate (PHB) [51], trying to reach a circular production [52]. The trend of using waste biomass instead of harvested biomass is becoming more relevant [53]. Furthermore, other bio-based options for cleaning that are not relaying on fermentation could be thought for, such as plants (e.g. soap nuts) [54].

When it comes to the overall sustainability, apart from DFO, the studied bio-based compounds turned out more relevant because less hazardous for the environment and human health regarding the use by conservators.

[14] https://www.showagroup.com/eu-en/shop/6110pf

It is also interesting to note that the low-scale production non-solely affects the yields and therefore the environmental performances of bio-based compounds but also the cost of such products, in particular EDDS and DFO, which consequently become less competitive.

To conclude, better industrial production should be sought.

5.3 Potential obstacles to the spread of microbial technologies

Often, the use of microorganisms is valued for a greener impact, however the LCA proposed above showed that it is important not to use shortcuts and risk falling into the greenwashing category. Indeed, it is interesting to identify the different limits that can come with the use of microorganisms.

The use of bacteria, fungi, yeast, or their metabolites (e.g., biosurfactants, enzymes, low molecular weight organic acid, siderophores etc.) as an alternative for the safeguard of heritage materials in the future is promising. Nevertheless, it requires as much caution as common practices currently in use given the duality of microorganisms. Indeed, despite their potential benefits to the cultural heritage field, biodegradation is also a crucial variable in the alteration of metals as stated previously with microbially induced corrosion. A thorough publication from Junier *et al.* tackles the issue of microbial approaches for cultural heritage conservation [55]: some aspects are reported here. A metabolic pathway can display both positive or negative effects according to the target involved, which enhances the necessity of a controlled handling of the organisms and a perfect knowledge of the substrate. An in-depth monitoring of any residues after the use of biological systems on metal is mandatory as any presence of remaining cells, dead or alive, could have dramatic consequences, most likely inducing further corrosion. Research has shown that certain bacteria on outdoor bronze were of influence to the nature of the patina, where some compounds appear because of the biological processes involved by the present microorganisms [56]. Therefore, surfaces treated using bio-based agents must be carefully examined before and after cleaning in order to validate these alternative approaches.

It is well-known that '*time is money*', therefore time-consuming bio-based treatments, as green and safe as they would be, would not compete to less sustainable but rapid-to-implement traditional methods. The cost could be even high because of the arrangement needed to maintain a viable atmosphere for the used microorganisms. In addition, these specific conditions would also need to be reached for the storage of the microorganisms, which is not realistic for conservation departments on a regular basis.

On top of that, safety and regulation are not to be forgotten. Indeed, they can impair the spread or transfer of a given technology between countries that classify pathogenicity differently.

To overcome the handling of living microorganisms and the issues mentioned above, it is necessary to fully understand the metabolic processes and pathways involved behind. In cases where the living organisms is not mandatory, it would allow the sole use of the active metabolites, requiring conditions that are not as strict. This would allow to decrease costs as there would no longer be the need of maintaining certain parameters such as temperature, anaerobic pressure, or pH, either during treatment or for storage. In addition, the direct use of pure extracts is favored when applied to cultural heritage conservation. Certainly, the medium compounds could have drawbacks on the preservation of the

objects. The addition of any extract, with a carbon source and other nutrients, can favor the development of negative autochthonous organisms present on the objects. In addition, the use of purified metabolites could allow the use of constant and higher concentrations of the active molecules and a longer shelf-life. Nevertheless, the isolation of pure compounds to exclude toxic compounds would increase costs and environmental impact.

Last but not least, the scaling up of such technologies is of concern. The delivery of microorganisms, even more of the specific metabolites, requires time and ad-hoc scientific devices for the production, characterization, and purification of the compounds. As discussed above, the low scale production of the compounds has an influence on both the environmental impact and the retailing price, which are both drawbacks when weighing the pros and cons of the method. As the use of these methods will increase in future, there will be the need of an automatization of the protocols and resorting to dedicated biotech companies. Such suppliers already exist but are not promoted within the conservation community, which is a small market area compared to waste treatment. This enhances the cost issue of resorting to such bio-based methods.

Green methods implementation in daily life of conservation professionals will, once potential obstacles are overcome, be beneficial, not only for the environment but also with respect to health concerns as well. As an example, other conservation specialties are paving the way for the extensive use of enzymes on paper and paintings [57,58]. The greatest challenge along with the technical aspect, is the implementation into the praxis. This requires great interdisciplinary coordination and divulgation for these green advances to be accepted by the whole conservation community. The negative perception of microorganisms naturally raises concerns and apprehension and reluctances towards their application on heritage artefacts. In order to allow professionals to adapt to these novel alternatives, their involvement in the research and development process in necessary, organizing workshops and events allowing them to handle the newly developed technologies. In addition, these moments of exchange can allow open discussions, which are crucial in this interdisciplinary research field [59]. Many research projects are in the end not implemented by end-users for various reasons, mostly because the research work was not performed in close collaborations with conservators to stick to their needs. In particular, high cost of novelties often makes them stay in the lab and never cross the frontier to go to conservation departments. In order to achieve a tool that will be used and implemented in the practice, a decision-making model was presented to conservators during workshops presentation of the gel formulations derived from the HELIX project.

5.4 Implementation in real praxis

In certain conservation fields or countries, it is common for conservators to use flowcharts, also known as "decision-making models" (DMM), similarly to medical professionals for diagnostics. The premise is that, to treat things appropriately, a systemic approach to make diagnostic decisions is key. Some conservation specialties, in particular modern and contemporary art, although not pioneers, are advanced when it comes to the use and study of these models [60,61].

There are several difficulties to overcome when putting in place such tools. First of all, the question of terminologies, as different people have different definitions of the same word. In addition, according to the background of the conservator, one problem can be tackled using different approaches. For the same metal object, there may be as many proposed treatments as the number of conservators that were asked, of which none prevails or is considered the correct one.

Finally, this kind of tool can never be exhaustive, and it is up to the professional to be aware of this and integrate the particular case they face. These tools are not intended to do the work of diagnosis and decision making in place of conservators, but rather to set markers, list questions and steps that are important in the decision-making process and only guide the professional in its pondering. It is only suggesting the parameters that are needed to be considered for the conservators to make their own decisions. Decision will always be in the hand of the end-user, but DMM help structure and systemize the thought and allow to check for possible solution to the faced diagnostic. These models are not intended to give a strict description of which decisions should be made. They rather act as a framework for how the decision should be made, as an aid to explicating and controlling the considerations which in practice are often implicit, and finally as an instrument to check and provide an insight into the decisions ultimately taken. Consequently, it helps justifying decisions that may later be consulted and a fortiori questioned by others.

The transmissible conceptualization of the decision-making process is possible, as some examples can be found in literature [62–64]. Indeed, DMM can also be used as communication tools, if it is simple and vulgarized, to explain to external collaborators the choice of one intervention over another for instance. To help conservators figure out the different possibilities regarding hydrogels formulations, a bêta version of a DDM was presented, which allowed them to tune the formulations according to their specific need. Feedbacks from conservators following the workshop allowed the design of a participative flow-chart, linking lab-research and real praxis (Figure 5.19).

Figure 5.19 Decision-making model for the cleaning of historical metals targeted in the HELIX project. Biobased compounds are in green. Yellow frames are related to the nature of the object and blue frames are related to the type of treatment desired.

In the case of the cleaning of metal with gelled active agents, it was first necessary to mention characteristics rather than specific types of gel. Indeed, this allows conservators to adapt their treatment to means and materials available in the workshop. The model is thought in two parts for the gel cleaning strategies of historical metals (Fe, Cu, Ag).

First, addressing the question "Which gel should I use on my object?". The model starts with the following question "Is it possible to rinse the object by immersion?" The answer to this question can be yes or no. If the object can be rinsed, any type of gel can be used, as it would not matter having to rinse it thoroughly with water in case of presence of gel residues. Independent conservators may therefore prefer to use viscous/sticky gels as they can be more affordable (CMC that can be purchased easily from furniture stores under the name Tylose®). Sometimes the object cannot be rinsed. This can be for various reason including the presence of water-sensitive compounds in composite objects (e.g., wood, textile…). In the case of a non-rinseable object, further steps proceed on the right side of the decision tree. If the object is fragile, meaning some of its components are not very adherent and must be handle with very low pressure or action (e.g., presence of flakes (corrosion, paint, metal gild…)) then the use of gels is not recommended but rather a very cautious addressing of the problem. If there is no fragility, the use of a rigid gel is recommended. Their ability to be peeled-off allows to leave low residues, allowing to be more lenient on the clearance step. Their retention is also often higher than viscous gels, which is an asset for the water-sensitive part of the object.

The second question to be addressed is "Which active agent to choose?" according to the problematic the object exposes. To answer this question, the first step is to wonder "Which kind of metal am I facing?".

If it is a silver alloys, one should check whether it is pure or alloyed with another element (most of the time copper i.e., sterling silver). In the first case, cleaning with chelating agent is not ideal and electrochemical or mechanical cleaning should be preferred. In the second case, to avoid staining by the reduction of copper corrosion compounds, a first step of chemical cleaning should be observed to remove all the copper degradation compounds, using strong complexing agents for instance EDDS or EDTA. Once all the copper compounds are removed, a second step using electrochemical cleaning can be foreseen.

If the object is made of a copper-based alloy, often on historical metals there are two main results desired. Either the homogenization of the object surface (e.g., when the tarnish layer is part of the object's history), or the complete removal of the tarnish to reach a clingy, precious surface (e.g., to show off the luxury of the object). In the first case, the use of siderophore is of help as the medium stability constant between DFO and copper allows to perform a controlled and smooth cleaning. In the second

case, EDTA and EDDS perform very well for the total and quick removal of the undesired tarnishing layer, or any other light corrosion compound present.

Last, in this work, iron-based alloys. If one is looking for a fast, broad action, meaning a strong action and broad removal of compounds present giving back a shiny metallic aspect, the use of EDTA is recommended. Indeed, it does not display high selectivity for iron and therefore can remove any other type of undesired compounds such as eventual exogenous deposits in conjunction with iron removal. If there is the wish to focus on iron, siderophores or acids (citric, oxalic) are best suited. DFO is preferred if the pH must be neutral, for instance acid sensitive compounds (i.e., organic materials also present), or the cleaning progressive. Otherwise, acids can be used if pH can be way below 7.

To give all information to end-users, tables with pH range parameters (which is the most important compatibility constraints for gelification) were implemented in the DDM. The information should be considered for each case. For instance, depending on their concentration, the pH of certain active agents might be or not suitable for certain gelling agents.

Decision-making models represent a compromise between different considerations that can sometimes conflict (e.g., ideal gel and ideal active agent are not compatible). These considerations therefore must be pondered by the conservators, depending on the outcome that is expected for each individual case. Again, the questions formulated in the instructions only indicate a direction. The pros and cons of each individual case must be weighed by the professional, considering their experience and knowledge, the expected results, to guide the final decision in various paths. The final decision, thus, is both a compromise and a reflection of the relevant factors.

In the span of the HELIX project, exchange moments were organized in the laboratory Arc'Antique in Nantes (France) in June 2023, involving 10 conservators specialized in metal objects and in November 2023 in Haute Ecole Arc in Neuchâtel (Switzerland) with 12 participants. The aim was to present the developed formulations and allow stakeholders to explore them, test them on objects and case-studies and give feedback regarding the use of the gels formulated in the project, in comparison to the ones already existing. In addition, these workshops allowed to explain the science behind the developed products along with the assets and drawbacks for professionals to be able to make decisions with all tools in their hands.

Globally, conservators preferred to use peelable gels, in particular agar as it is affordable, non-toxic or polluting, can easily be adapted to all surfaces and leaves few residues. Contrary to what is found in literature, they are not bothered by the heating step of the preparation. The only drawback mentioned towards the use of gel was the time required for the preparation, which in the end levels up the cost. Indeed, although less solution is used and would ideally reduce the final cost, it does not outweight the longer preparation time. Some of them reported up to 30% of supplementary costs compared to the

same active agents applied in solution and related to labor costs, which may be displeasing to most clients.

Bioderived chelators were praised for their soft and progressive cleaning action. First, the use of rather pH neutral compounds was appreciated as it allowed to avoid unvoluntary stripping. Then, the gradual action raised interests especially for jewelry as it allows to modulate the cleaning action. In particular, DFO formulations were approved as they seemed more progressive than EDTA, for example when tested on Islamic art and gilded metals. Indeed, iron oxides underneath the gold plating usually go through the gildings. As they are harder than gold, it is not possible to use mechanical cleaning and current cleaning solutions are too aggressive, chelating the corrosion products underneath the gilding layer, which ends up being stripped away. Nevertheless, the prices and access difficulty, in particular for deferoxamine, renders its actual use hardly possible. Indeed, for a $6 \cdot 10^{-2}$ M solution of DFO, EDDS or EDTA the cost of the corresponding amount of active substances for DFO, EDDS or EDTA would be of 315.66 CHF, 16.48 CHF and 0.166 CHF respectively[15].

Regarding the DDM, most of them knew about the tool and found it relevant as a "cheat sheet" or to first introduce a concept to students for instance.

[15] https://ctsconservation.com/fr/, https://www.sigmaaldrich.com/CH/de/product/aldrich/92698, https://compendium.ch/fr/product/18367-desferal-subst-seche-500-mg

5.5 Conclusion

It is difficult to define greenness, however current European guidelines helped figure out pros and cons of proposed alternatives [5,6,10,11]. It is difficult to have a clear answer to whether formulations studies in the span of this project are actually "green" given the different parameters and hypothesis. The attempt to model bio-based compounds selected for the cleaning of historical metal artefacts led to the poor score of DFO-containing formulations. For these formulations, the main contributor of the global single score was the raw materials input, in particular energy and production medium necessary. For other formulations, the use phase was the step accounting for most of the global single score, especially because of the use of gloves. In addition to the lack of specific data for the modeling of fermented compounds, one drawback of the LCA is the lack of accounting biotic depletion, for agar seaweeds, whereas it could be implemented for abiotic depletion of borax. When opposing environmental and toxicity of the different formulations studied, Agar-EDDS gels appear to perform better than any other formulation because of low hazard and environmental impact of raw materials. Nevertheless, the consideration of ethylene bromide in the production route renders it hazardous in the upstream process, especially for health hazards for chemical production workers.

In praxis, conservators showed enthusiasm regarding new alternatives. Indeed, those alternatives bring new possibilities, in particular a more gradual cleaning and therefore can be of use to particular situations for which there are no suitable solutions so far. Nevertheless, current cost and availability are prohibitive and would reduce the use to very particular cases.

5.6 Bibliography

1. Del Curto, D.; Turrina, A. Towards a Reasoned Glossary of Green Conservation: A Semantic Review of Green-Oriented Terms in the Field of Cultural Heritage. *Sustainability* **2023**, *15*, 12104, doi:10.3390/su151612104.
2. Anastas, P.; Eghbali, N. Green Chemistry: Principles and Practice. *Chem. Soc. Rev.* **2010**, *39*, 301–312, doi:10.1039/B918763B.
3. Pizzetti, M.; Gatti, L.; Seele, P. Firms Talk, Suppliers Walk: Analyzing the Locus of Greenwashing in the Blame Game and Introducing 'Vicarious Greenwashing.' *J. Bus. Ethics* **2021**, *170*, 21–38, doi:10.1007/s10551-019-04406-2.
4. Astuti, R.; Kurniawan, B.C.; Setiyawan, D.T. Implementation of Life Cycle Assessment (LCA) in Environmental Impact Evaluation on Production of Ground Coffee. *E3S Web Conf.* **2021**, *306*, 04019, doi:10.1051/e3sconf/202130604019.
5. European Commission Environmental Footprint Methods Available online: https://green-business.ec.europa.eu/environmental-footprint-methods_en.
6. European Commission European Platform on LCA (EPLCA) Available online: https://eplca.jrc.ec.europa.eu/lifecycleassessment.html.
7. European Commission *Understanding Product Environmental Footprint and Organisation Environmental Footprint Methods*; 2021; ISBN 978-92-76-57214-5.
8. STiCH Carbon Calculator Available online: https://stich.culturalheritage.org/carbon-calculator/#browse.
9. Egas, D.; Azarkamand, S.; Casals, C.; Ponsá, S.; Llenas, L.; Colón, J. Life Cycle Assessment of Bio-Based Fertilizers Production Systems: Where Are We and Where Should We Be Heading? *Int. J. Life Cycle Assess.* **2023**, *28*, 626–650, doi:10.1007/s11367-023-02168-8.
10. ISO Environmental Management—Life Cycle Assessment, Principles and Framework, ISO 14040: 1997. *Eur. Comm. Stand. CEN, Brussels, Belgium* **1997**.
11. ISO Environmental Management, Life Cycle Assessment, Requirements and Guidelines, ISO 14044:2006. *Eur. Comm. Stand. CEN, Brussels, Belgium* **2006**.
12. Neal, J.A.; Rose, N.J. Stereospecific Ligands and Their Complexes. I. A Cobalt(III) Complex of Ethylenediaminedisuccinic Acid. *Inorg. Chem.* **1968**, *7*, 2405–2412, doi:10.1021/ic50069a043.
13. Takahashi, R.; Yamayoshi, K.; Fujimoto, N.; Suzuki, M. Production of (s, s)-Ethylenediamine-n, N'-Disuccinic Acid from Ethylenediamine and Fumaric Acid by Bacteria. *Biosci. Biotechnol. Biochem.* **1999**, *63*, 1269–1273, doi:10.1271/bbb.63.1269.
14. Appleton, H.; Rosentrater, K.A. Sweet Dreams (Are Made of This): A Review and Perspectives on Aspartic Acid Production. *Fermentation* **2021**, *7*, 49, doi:10.3390/fermentation7020049.
15. Kisumi, M.; Ashikaga, Y.; Chibata, I. Studies on the Fermentative Preparation of <scp>l</Scp> -Aspartic Acid from Fumaric Acid. *Bull. Agric. Chem. Soc. Japan* **1960**, *24*, 296–305, doi:10.1080/03758397.1960.10857668.
16. Martínez-Sanz, M.; Gomez-Barrio, L.P.; Zhao, M.; Tiwari, B.; Knutsen, S.H.; Ballance, S.; Zobel, H.K.; Nilsson, A.E.; Krewer, C.; Östergren, K.; et al. Alternative Protocols for the Production of More Sustainable Agar-Based Extracts from Gelidium Sesquipedale. *Algal Res.* **2021**, *55*, 102254, doi:10.1016/j.algal.2021.102254.
17. Mouga, T.; Fernandes, I.B. The Red Seaweed Giant Gelidium (Gelidium Corneum) for New Bio-Based Materials in a Circular Economy Framework. *Earth* **2022**, *3*, 788–813, doi:10.3390/earth3030045.
18. Zuhria S, A.; Siswi Indrasti, N.; Yani, M. Study of the Environmental Impact of Agar Flour Using the Life Cycle Assessment (LCA) Method. *J. Teknol. Ind. Pertan.* **2021**, 343–355, doi:10.24961/j.tek.ind.pert.2021.31.3.343.
19. Gioele, C.; Marilena, S.; Valbona, A.; Nunziacarla, S.; Andrea, S.; Antonio, M. Gracilaria Gracilis, Source of Agar: A Short Review. *Curr. Org. Chem.* **2017**, *21*, 380–386,

doi:10.2174/138527282066161017164605.
20. Nil, S.; Ali Mehidi, S.; Zellal, A.; Abi Ayad, S. Effects of Season on the Yield and Quality of Agar from Gelidium Sesquipedale (Rhodophyta) from Mostaganem, Algeria. *African J. Biotechnol.* **2016**, *15*, 350–355, doi:10.5897/AJB2015.15004.
21. Patel, M.; Crank, M.; Dornburg, V.; Hermann, B.; Roes, L.; Hüsing, B.; Overbeek, L.; Terragni, F.; Recchia, E. *Medium and Long Term Opportunities and Risks of the Biotechnological Production of Bulk Chemicals from Renewable Resources*; Utrecht, 2006;
22. García-Ochoa, F.; Santos, V..; Casas, J..; Gómez, E. Xanthan Gum: Production, Recovery, and Properties. *Biotechnol. Adv.* **2000**, *18*, 549–579, doi:10.1016/S0734-9750(00)00050-1.
23. Kuppuswami, G.M. Fermentation (Industrial) and Production of Xanthan Gum. In *Encyclopedia of Food Microbiology*; Elsevier, 2014; pp. 816–821.
24. Zhang, J.; Dong, Y.; Fan, L.; Jiao, Z.; Chen, Q. Optimization of Culture Medium Compositions for Gellan Gum Production by a Halobacterium Sphingomonas Paucimobilis. *Carbohydr. Polym.* **2015**, *115*, 694–700, doi:10.1016/j.carbpol.2014.09.029.
25. Soumiya, S.; Santhiagu, A.; Manjusha Chemmattu, M. Optimization of Cultural Conditions of Gellan Gum Production from Recombinant Sphingomonas Paucimobilis ATCC 31461 and Its Characterization. *J. Appl. Biol. Biotechnol.* **2021**, doi:10.7324/JABB.2021.9108.
26. Chiani, M.; Akbarzadeh, A.; Farhangi, A.; Mehrabi, M.R. Production of Desferrioxamine B (Desferal) Using Corn Steep Liquor in Streptomyces Pilosus. *Pakistan J. Biol. Sci.* **2010**, *13*, 1151–1155, doi:10.3923/pjbs.2010.1151.1155.
27. Chiani, M.; Akbarzadeh, A.; Farhangi, A.; Mazinani, M.; Saffari, Z.; Emadzadeh, K.; Mehrabi, M.R. Optimization of Culture Medium to Increase the Production of Desferrioxamine B (Desferal) in Streptomyces Pilosus. *Pakistan J. Biol. Sci.* **2010**, *13*, 546–550, doi:10.3923/pjbs.2010.546.550.
28. Mortazavi, M.; Akbarzadeh, A. Improvement of Desferrioxamine B Production of Streptomyces Pilosus ATCC 19797 With Use of Protease Inhibitor and Minerals Related to Its Activity. *Indian J. Clin. Biochem.* **2012**, *27*, 274–277, doi:10.1007/s12291-012-0197-8.
29. Çolak, A.; Laratte, B.; Elevli, B.; Çoruh, S. Abiotic Depletion of Boron: An Update Characterization Factors for CML 2002 and ReCiPe. *Minerals* **2022**, *12*, 435, doi:10.3390/min12040435.
30. Riedo, C.; Caldera, F.; Poli, T.; Chiantore, O. Poly(Vinylalcohol)-Borate Hydrogels with Improved Features for the Cleaning of Cultural Heritage Surfaces. *Herit. Sci.* **2015**, *3*, 23, doi:10.1186/s40494-015-0053-2.
31. Cuvillier, L.; Passaretti, A.; Dupuy, V.; Raimon, A.; Guilminot, E.; Joseph, E. Exploiting Biologically Synthetized Chelators in Conservation : Gel-Based Bio-Cleaning of Corroded Iron Heritage Objects. In Proceedings of the Metal 2022, 10th interim meeting of the ICOM-CC metals working group; Mardikian, P., Näsänen, L., Arponen, A., Eds.; Helsinki, Finland, 2022.
32. Saouter, E.; Aschberger, K.; Fantke, P.; Hauschild, M.Z.; Bopp, S.K.; Kienzler, A.; Paini, A.; Pant, R.; Secchi, M.; Sala, S. Improving Substance Information in USEtox ®, Part 1: Discussion on Data and Approaches for Estimating Freshwater Ecotoxicity Effect Factors. *Environ. Toxicol. Chem.* **2017**, *36*, 3450–3462, doi:10.1002/etc.3889.
33. Vandevivere, P.C.; Saveyn, H.; Verstraete, W.; Feijtel, T.C.J.; Schowanek, D.R. Biodegradation of Metal−[S,S]-EDDS Complexes. *Environ. Sci. Technol.* **2001**, *35*, 1765–1770, doi:10.1021/es0001153.
34. European Union European Chemical Agency Available online: https://echa.europa.eu/fr/information-on-chemicals/registered-substances?p_p_id=dissregisteredsubstances_WAR_dissregsubsportlet&p_p_lifecycle=1&p_p_state=normal&p_p_mode=view&_dissregisteredsubstances_WAR_dissregsubsportlet_javax.portlet.action=dissRegist.
35. Bixler, H.J.; Porse, H. A Decade of Change in the Seaweed Hydrocolloids Industry. *J. Appl. Phycol.* **2011**, *23*, 321–335, doi:10.1007/s10811-010-9529-3.

36. Belattmania, Z.; Bhaby, S.; Nadri, A.; Khaya, K.; Bentiss, F.; Jama, C.; Reani, A.; Vasconcelos, V.; Sabour, B. Gracilaria Gracilis (Gracilariales, Rhodophyta) from Dakhla (Southern Moroccan Atlantic Coast) as Source of Agar: Content, Chemical Characteristics, and Gelling Properties. *Mar. Drugs* **2021**, *19*, 672, doi:10.3390/md19120672.
37. Tamura, M.; Takagi, K. Towards the Sustainable Use of Agar / Agarose in Conservation: A Case Study of the Izu Peninsula, Japan. In *Gels in the Conservation of Art*; Angelova, L. V., Ormsby, B., Townsend, J.H., Wolbers, R., Eds.; Archetype Publications: London, UK, 2017; pp. 152–154 ISBN 9781909492509.
38. Dev, M.J.; Warke, R.G.; Warke, G.M.; Mahajan, G.B.; Patil, T.A.; Singhal, R.S. Advances in Fermentative Production, Purification, Characterization and Applications of Gellan Gum. *Bioresour. Technol.* **2022**, *359*, 127498, doi:10.1016/j.biortech.2022.127498.
39. Türkbay, T.; Laratte, B.; Çolak, A.; Çoruh, S.; Elevli, B. Life Cycle Assessment of Boron Industry from Mining to Refined Products. *Sustainability* **2022**, *14*, 1787, doi:10.3390/su14031787.
40. Walker, S.; Rothman, R. Life Cycle Assessment of Bio-Based and Fossil-Based Plastic: A Review. *J. Clean. Prod.* **2020**, *261*, 121158, doi:10.1016/j.jclepro.2020.121158.
41. Langlois, J.; Fréon, P.; Delgenes, J.-P.; Steyer, J.-P.; Hélias, A. New Methods for Impact Assessment of Biotic-Resource Depletion in Life Cycle Assessment of Fisheries: Theory and Application. *J. Clean. Prod.* **2014**, *73*, 63–71, doi:10.1016/j.jclepro.2014.01.087.
42. Vural Gursel, I.; Moretti, C.; Hamelin, L.; Jakobsen, L.G.; Steingrimsdottir, M.M.; Junginger, M.; Høibye, L.; Shen, L. Comparative Cradle-to-Grave Life Cycle Assessment of Bio-Based and Petrochemical PET Bottles. *Sci. Total Environ.* **2021**, *793*, 148642, doi:10.1016/j.scitotenv.2021.148642.
43. Belboom, S.; Léonard, A. Does Biobased Polymer Achieve Better Environmental Impacts than Fossil Polymer? Comparison of Fossil HDPE and Biobased HDPE Produced from Sugar Beet and Wheat. *Biomass and Bioenergy* **2016**, *85*, 159–167, doi:10.1016/j.biombioe.2015.12.014.
44. European Commission Abiotic and Biotic Resources Impact Categories in LCA. *JRC Tech. Rep.* **2020**, doi:10.2760/232839.
45. Takahashi, R.; Fujimoto, N.; Suzuki, M.; Endo, T. Biodegradabilities of Ethylenediamine- N , N ′-Disuccinic Acid (EDDS) and Other Chelating Agents. *Biosci. Biotechnol. Biochem.* **1997**, *61*, 1957–1959, doi:10.1271/bbb.61.1957.
46. Tandy, S.; Ammann, A.; Schulin, R.; Nowack, B. Biodegradation and Speciation of Residual SS-Ethylenediaminedisuccinic Acid (EDDS) in Soil Solution Left after Soil Washing. *Environ. Pollut.* **2006**, *142*, 191–199, doi:10.1016/j.envpol.2005.10.013.
47. Sýkora, V.; Pitter, P.; Bittnerová, I.; Lederer, T. Biodegradability of Ethylenediamine-Based Complexing Agents. *Water Res.* **2001**, *35*, 2010–2016, doi:10.1016/S0043-1354(00)00455-3.
48. Jaber, S.; Leremboure, M.; Thery, V.; Delort, A.-M.; Mailhot, G. Mechanism of Photochemical Degradation of Fe(III)-EDDS Complex. *J. Photochem. Photobiol. A Chem.* **2020**, *399*, 112646, doi:10.1016/j.jphotochem.2020.112646.
49. Winter, B.; Meys, R.; Bardow, A. Towards Aromatics from Biomass: Prospective Life Cycle Assessment of Bio-Based Aniline. *J. Clean. Prod.* **2021**, *290*, 125818, doi:10.1016/j.jclepro.2021.125818.
50. Becker, M.; Ziemińska-Stolarska, A.; Markowska, D.; Lütz, S.; Rosenthal, K. Comparative Life Cycle Assessment of Chemical and Biocatalytic 2′3′-Cyclic GMP-AMP Synthesis. *ChemSusChem* **2023**, *16*, doi:10.1002/cssc.202201629.
51. Getachew, A.; Woldesenbet, F. Production of Biodegradable Plastic by Polyhydroxybutyrate (PHB) Accumulating Bacteria Using Low Cost Agricultural Waste Material. *BMC Res. Notes* **2016**, *9*, 509, doi:10.1186/s13104-016-2321-y.
52. European Parliament Circular Economy: Definition, Importance and Benefits Available online: https://www.europarl.europa.eu/news/en/headlines/economy/20151201STO05603/circular-economy-definition-importance-and-benefits.

53. Thakur, N.; Salama, E.-S.; Sharma, M.; Sharma, P.; Sharma, D.; Li, X. Efficient Utilization and Management of Seaweed Biomass for Biogas Production. *Mater. Today Sustain.* **2022**, *18*, 100120, doi:10.1016/j.mtsust.2022.100120.
54. Hawkes, W. A Preliminary Investigation into the Etching Effect of Saponin and Acidified Thiourea in the Cleaning of Sterling Silver, West Dean College, 2016. https://www.researchgate.net/publication/340948905_A_preliminary_investigation_into_the_etching_effect_of_saponin_and_acidified_thiourea_in_the_cleaning_of_sterling_silver
55. Junier, P.; Joseph, E. Microbial Biotechnology Approaches to Mitigating the Deterioration of Construction and Heritage Materials. *Microb. Biotechnol.* **2017**, *10*, 1145–1148, doi:10.1111/1751-7915.12795.
56. Timoncini, A.; Costantini, F.; Bernardi, E.; Martini, C.; Mugnai, F.; Mancuso, F.P.; Sassoni, E.; Ospitali, F.; Chiavari, C. Insight on Bacteria Communities in Outdoor Bronze and Marble Artefacts in a Changing Environment. *Sci. Total Environ.* **2022**, *850*, 157804, doi:10.1016/j.scitotenv.2022.157804.
57. Cremonesi, P. Rigid Gels and Enzyme Cleaning. *Smithson. Contrib. to Museum Conserv.* **2012**, *3*, 179–183.
58. Barbabietola, N.; Tasso, F.; Alisi, C.; Marconi, P.; Perito, B.; Pasquariello, G.; Sprocati, A.R. A Safe Microbe-Based Procedure for a Gentle Removal of Aged Animal Glues from Ancient Paper. *Int. Biodeterior. Biodegrad.* **2016**, *109*, 53–60, doi:10.1016/j.ibiod.2015.12.019.
59. Joseph, E. *Microorganisms in the Deterioration and Preservation of Cultural Heritage*; Joseph, E., Ed.; Springer International Publishing: Cham, 2021; ISBN 978-3-030-69410-4.
60. CICS *The Decision-Making Model for Contemporary Art and Presentation*; Köln, 2021; https://www.th-koeln.de/mam/downloads/deutsch/hochschule/fakultaeten/kulturwissenschaften/f02_cics_gsm_fp__dmmcacp_190613-1.pdf
61. Marçal, H.; Macedo, R.; Nogueira, A.; Duarte, A. Whose Decision Is It? Reflections about a Decision Making Model Based on Qualitative Methodologies. *CeROArt* **2013**, 0–15, doi:10.4000/ceroart.3597.
62. Florescu, M. "Voyage En Carrosse". Etude et Conservation-Restauration d'un Prototype de Micro-Car En Aluminium de Paul Arzens (Musée Du Conservatoire Des Arts et Métiers, Paris; En Dépôt à La Cité de l'Automobile, Mulhouse). Evaluation de Différents Traitements Des Su, Institut National du Patrimoine, Paris, 2015.
63. Heremans, Rebecca Blanchaert, K. Stabbing Our Own House: A Biography of Joseph Beuys's Wirtschaftswerte. In Proceedings of the Living Matter: The Preservation of Biological Materials in Contemporary Art; Rivenc, R., Roth, K., Eds.; Getty Institute of Conservation: Mexico City, 2019.
64. Phillips, S.; van der Laan, S. Flora and Fauna as Art: A Contemporary Art Conservation Approach to Living Systems. In Proceedings of the Living Matter: The Preservation of Biological Materials in Contemporary Art; Rivenc, R., Roth, K., Eds.; Getty Institute of Conservation: Mexico City, 2019.
65. Duplat, V.; Rouchon, V.; Desloges, I.; Papillon, M.C. Steel versus Paper : The Conservation of a Piece of Modern Art Consisting of a Rust Print on Paper. *J. Pap. Conserv.* **2009**, *10*, 26–34.

5.7 Supplementary materials

Table S5.10 Production medium considered in the hypothesis model for EDDS with L-aspartic acid from fermentation using fumaric acid as carbon source

Peptone	5%
Yeast extract	3%
Ammonia	14.3 %

Table S5.2 Production medium considered in the hypothesis model for xanthan gum

Citric acid	2.1 g/L
NH_4NO_3	1.144 g/L
KH_2PO_4	2.866 g/L
$MgCl_2$	0.507 g/L
Na_2SO4	0.089 g/L
H_3BO_3	0.006 g/L
ZnO	0.006 g/L
$FeCl_3$, 6 H_2O	0.020 g/L
$CaCO_3$	0.020 g/L
Concentrated HCl	0.13 ml/L

Table S5.3 Production medium considered in the hypothesis model for gellan gum

KH_2PO_4	9.2 g/L
Na_2HPO_4	7.5 g/L
K_2SO_4	4.3 g/L
$MgSO_4$	3.2 g/L

Table S5.4 Production medium considered in the hypothesis model for deferoxamine

Soybean flour	20 g/L
KH_2PO_4	32 g/L

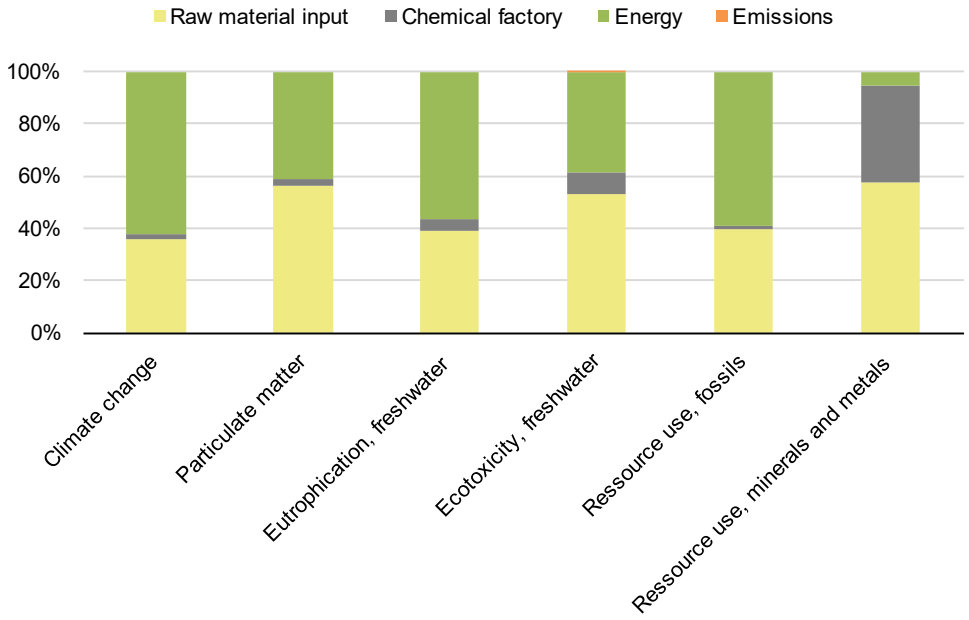

Figure S5.1 Carboxymethyl cellulose main potential impact contributors according to the different impact categories relevant for the purpose of this project

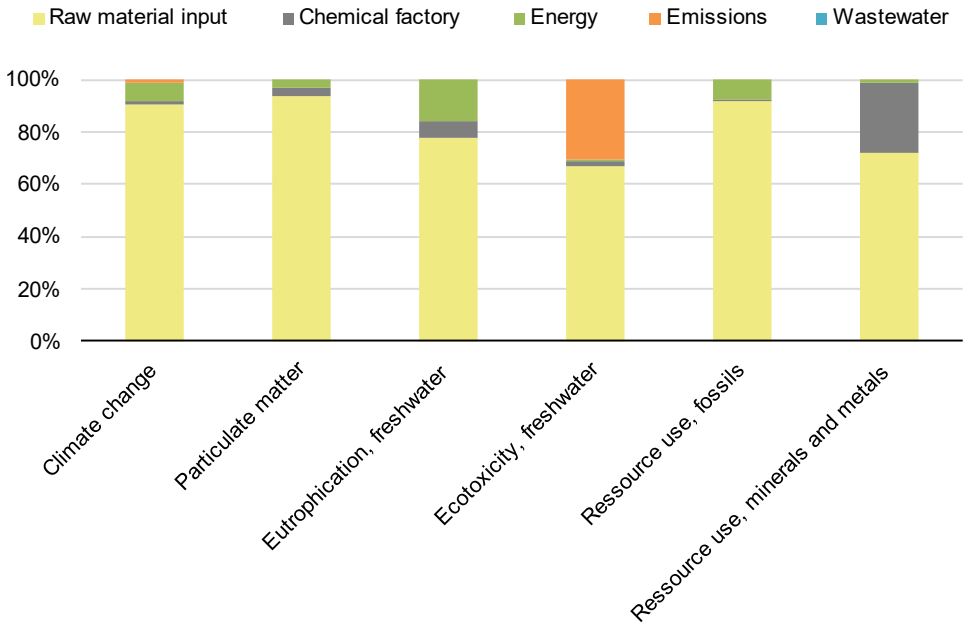

Figure S5.2 Na_2EDTA main potential impact contributors according to the different impact categories relevant for the purpose of this project

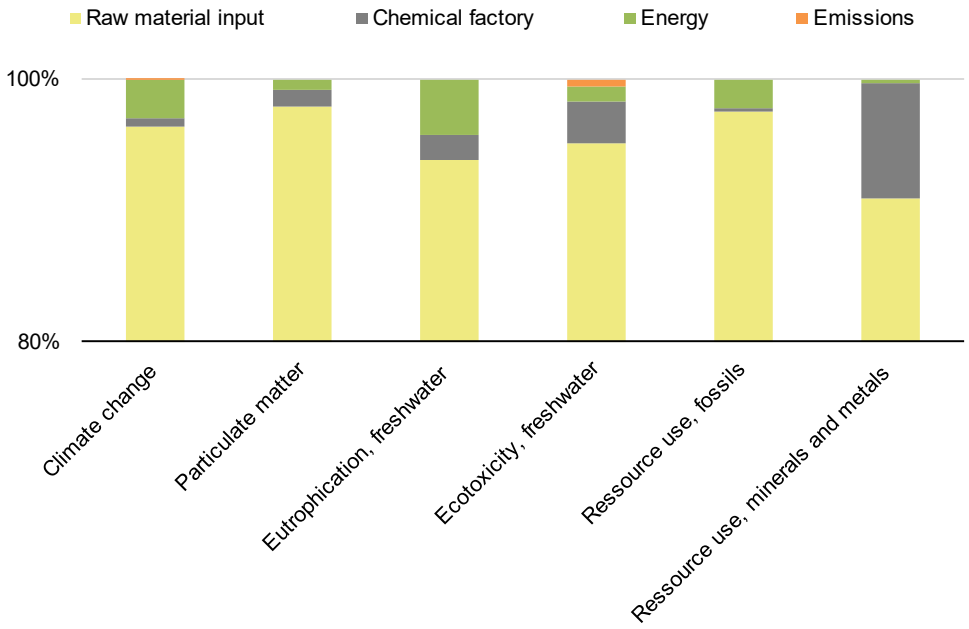

Figure S5.3 PVA main potential impact contributors according to the different impact categories relevant for the purpose of this research project

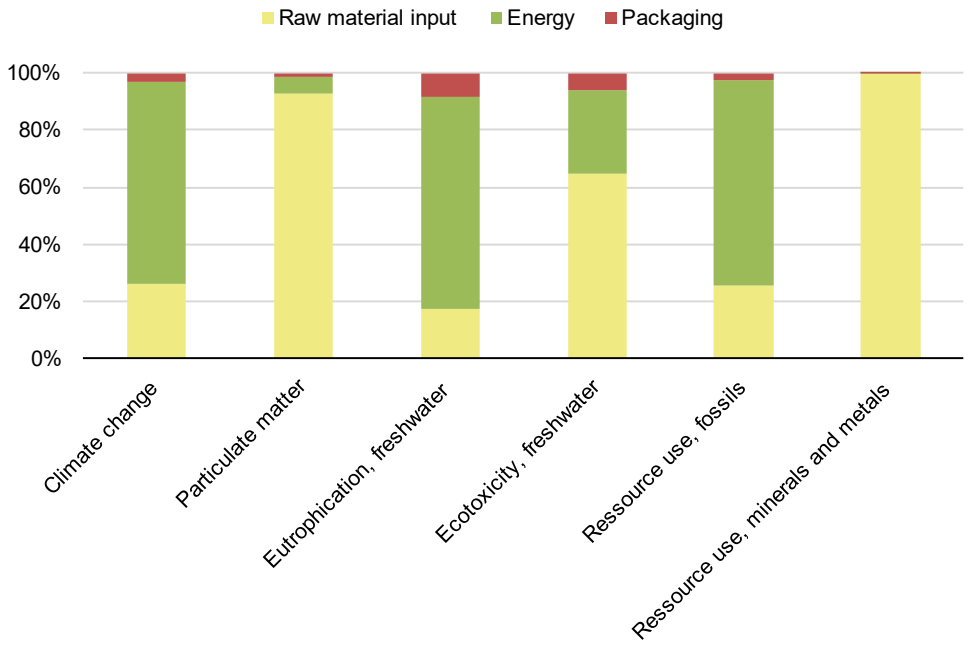

Figure S5.4 Borax main potential impact contributors according to the different impact categories relevant for the purpose of this research project

6. General conclusion

6.1 Complete text

In Chapter 2, the research focused on biocleaning and metal dissolution in aerobic conditions. The findings unveiled several important insights. The validation of fungal biocleaning highlighted the effectiveness of *Aspergillus niger* for iron removal and *Beauveria bassiana* for copper removal. These fungi exhibited promising capabilities for sustainable bioremediation. However, to deepen the understanding of the biocleaning process, further investigation into the metabolic pathways responsible for oxalates formation is needed. Additionally, the study revealed the remarkable resistance of *Acidithiobacillus ferrooxidans* to silver concentrations of up to 1 mM. To harness this resistance for practical applications, future research could involve strain silver resistance training. Furthermore, the potential of fungal biosorption of silver and the use of dead biomass for silver uptake deserve closer examination.

Regarding metal dissolution processes, it was observed that they appear to be governed by both diffusion and surface-controlled mechanisms, especially for iron oxides. The behavior of different acids and deferoxamine siderophore in metal dissolution was discussed. Acids performed optimally at low pH, while deferoxamine siderophore exhibited effectiveness across a broad pH range. These conclusions open the door for comprehensive statistical analysis, considering various factors such as particle size, agglomeration, metal-to-ligand ratios, and the entire pH range.

Copper corrosion examination demonstrated a lower affinity of deferoxamine (DFO) towards Cu_2O in comparison to EDTA and EDDS. Notably, the research demonstrated that while complexing solutions did not dissolve silver sulfide, the use of EDDS might yield the production of silver nanoparticles. In addition to these findings, potential avenues must be explored in silver remediation, in particular the utilization of other natural compounds, such as biosurfactants.

Chapter 3 explored hydrogel formulations' design and the gel residue question. One key finding was the different rheological properties of chitosan-based formulations compared to agar's. CS-ItA-LCys's mechanical behavior is less rigid. Chitosan formulations displayed a thick outer layer membrane and less dense inner structure. In addition, it exhibited silver complexing properties, making them promising for practical applications. To expand the range of applications, it is recommended to explore alternative natural polymers, such as curdlan or combinations of several polymers.

Another insight from this chapter was related to non-rigid polymers, such as gellan prepared at room temperature and xanthan gum, which were found to be more likely to leave residues. Oximetry showed the potential deleterious effects of gel residues on steel-based substrates. Further research should assess their noxiousness, particularly on copper-based substrates.

Methods for residues detection were also examined, indicating that qualitative detection of residues can be achieved using UV markers and photography. Furthermore, X-ray fluorescence (XRF) analysis

confirmed expected residue patterns for agar and xanthan (i.e., xanthan leaving thin spread residues over the surface) and opened possibilities for quantitative residue detection using the XRF technique.

Chapter 4 delved into corrosion cleaning with siderophores, shedding light on effective strategies for artefacts restoration. Notably, obtaining representative artificially corroded samples proved to be a challenging task.

The research uncovered the effectiveness of shorter repeated gel applications over longer ones, optimizing the cleaning process.

The choice of chelating agents, plays a critical role in the cleaning process. While EDTA exhibited a more aggressive cleaning approach with broad actions on compounds present, DFO demonstrated a more iron-selective and progressive approach, allowing for better control of treatment. The neutral pH of the studied siderophore was found to provide a smoother cleaning action.

Gel treatments were found to be less efficient than wet treatment in terms of chelator loading, but gels' advantages, in particular higher control and precision, counteract for this observation.

Significantly, the research marked a successful treatment of iron and copper artifacts using these strategies. To further extend the applicability of these methods, it is recommended to study the long-term behavior of treated surfaces and would be interesting to test other siderophores with different affinity constants.

Chapter 5 scrutinized the assessment of environmental impacts associated with the corrosion cleaning process. While conducting the research, several crucial findings and perspectives emerged. One significant finding was the challenge of obtaining comprehensive and assertive environmental overviews due to a lack of available data. Moreover, the study demonstrated that bio-based compounds, such as deferoxamine (DFO), may not necessarily be less environmentally impactful, primarily due to considerations related to the production medium. To mitigate these environmental impacts, future research avenues should explore the use of non-fermented natural products and leverage biowaste as a carbon source to achieve a circular economy.

The study also underscored the significance of the usage phase, which often contributes the most to the global lifecycle of corrosion cleaning formulations.

Among the formulations studied, Agar-EDDS stood out as the most environmentally and health-friendly option, offering a balance between efficacy and environmental responsibility

To facilitate the implementation of these formulations from labs to workshops, decision-making models were found to be a valuable tool. Professional opinions emphasized the importance of the compounds studied in filling critical gaps in corrosion removal tools, particularly for progressive corrosion removal.

The research has laid a strong foundation for further exploration of environmentally responsible strategies in the field of corrosion cleaning.

6.2 Bullet list

In normal font are the main findings, in italic characters are the associated research perspectives.

CHAPTER 2

- Validation of the use of fungi for biocleaning. *Aspergillus niger* for iron and *Beauveria bassiana* for copper removal
    - *Deeper investigation of metabolic pathways of oxalates formation to understand biocleaning process and the actual role of the fungi*
- Resistance of *Acidithiobacillus ferrooxidans* to silver concentrations up to 1 mM
    - *Perform strain silver resistance training*
    - *Study fungal biosorption of silver*
    - *Study the use of dead biomass for silver uptake*
- Iron dissolution processes appear to be both diffusion and surface-controlled processed
- Acids perform best at low pH whereas deferoxamine siderophore perform almost equally over the full pH range
- DFO shows lower affinity towards Cu_2O compared to EDTA and EDDS
    - *Perform statistical analysis with multiple variables including particle size and agglomeration, metal to ligand various ratios, full pH range, etc.*
- No silver sulfide dissolution was witnessed using complexing solutions but silver nanoparticles were produced using EDDS on silver nitrate.
    - *Use of other natural compounds for silver remediation such as biosurfactants*

CHAPTER 3

- Chitosan-based formulation is more malleable than agar, with a thick outer layer membrane
- No interaction between agar or chitosan polymer chains and deferoxamine
- Chitosan-based formulation shows silver complexing properties
    - *Explore other natural polymers such as curdlan or mix of several polymers to obtain different properties*
    - *Investigate further the chitosan-based formulation*
- Non-rigid polymer (i.e., gellan prepared at room temperature and xanthan gum) are tackier hence more likely to leave residues
- Gel residues can be deleterious for iron-based substrates in particular due to the contained solutions
    - *Assess residues noxiousness on copper-based substrates*
- Qualitative detection of residues can be performed using UV-markers and photography, with a very low detection limit
- XRF confirmed expected results, using adequate marker Na_2WO_4, that agar leaves punctual residues and xanthan spread ones
    - *Attempt quantitative residues detection using XRF*

CHAPTER 4

- Difficult to obtain representative artificially corroded samples
- Shorter repeated gel applications perform better than long ones
- EDTA achieves a more aggressive cleaning with a broad action on compounds present
- DFO is more iron-selective
- DFO is progressive, in particular for copper, allowing for better control of treatment
- Neutral pH of siderophores gives a smoother cleaning action
- Successful treatment of iron and copper artefacts
    - *Study of long-term behavior of treated surface*
    - *Testing of other siderophores with different affinity constants*

CHAPTER 5

- Lack of available data prevents from making an assertive overview
- Bio-based compounds, in particular DFO, are not necessarily less environmentally impactful due to production medium
    - *Use non-fermented natural products*
    - *Use biowaste as carbon source to achieve circular economy*
- Use phase if often the highest contribution in the global lifecycle
- Agar-EDDS is the best formulation among those studied considering environmental and health hazards
- Decision-making model is useful to boost the implementation of formulations from labs to workshops
- Some of the studied compounds praised by professional for filling a gap in the tools currently available, in particular for progressive corrosion removal

7. List of related publications and dissemination

7.1 Peer-reviewed publications

1. **Cuvillier, L** .; Passaretti, A.; Guilminot, E.; Joseph, E., Agar and chitosan hydrogels' design for metal uptaking treatments. *Gels*. 10(1). **2024**, doi: 10.3390/gels10010055
2. Passaretti, A.; **Cuvillier, L**.; Sciutto, G.; Joseph, E. Innovative perspective for the cleaning of historical iron: novel bio-organogel for the combined removal of undesired organic coatings and corrosion. Under publication
3. Passaretti, A*.; **Cuvillier, L**.*; Guilminot, E.; Sciutto, G.; Joseph, E. Biocleaning of historical iron artworks: innovative green gels amended with microbial derivatives. *Front. Mater.* **2023,** 10 doi: 10.3389/fmats.2023.1277972 **Both first authors have the same contribution*.
4. **Cuvillier, L**.; Ganesan, S.; James, S.; Monachon, M.; Passaretti, A.; Albelda-Berenguer, M.; Mathys, L.; Joseph, E. Green corrosion mitigation and conservation strategies for metal heritage in *EFC series (Greenbook), Bridging the gap: corrosion science for heritage context*, Edition, D. Neff, Eds. Academic Press, **2023**, ISBN 9780443186905 Under publication
5. **Cuvillier, L**.; Passaretti, A.; Guilminot, E.; Joseph, E. Testing of the Siderophore Deferoxamine Amended in Hydrogels for the Cleaning of Iron Corrosion. *Eur. Phys. J. Plus* **2023**, 138, 569, doi:10.1140/epjp/s13360-023-04159-y
6. Passaretti, A.; **Cuvillier, L**.; Sciutto, G.; Guilminot, E.; Joseph, E. Biologically Derived Gels for the Cleaning of Historical and Artistic Metal Heritage. *Appl. Sci*. **2021**, *11*, 3405. 11 citations
7. Joseph, E.; Albelda-Berenguer, M.; Cornet, E.; **Cuvillier, L**.; James, S.; Mathys, L.; Monachon, M.; Passaretti, A.; Russo, S. Innovative Approaches towards a Green and Sustainable Metal Conservation. *Chimia (Aarau).* **2020**, *74*, 611, doi:10.2533/chimia.2020.611.

7.2 Oral communications

1. Passaretti, A.; **Cuvillier, L.**; Künzi C-A.; Brambilla, L.; Joseph, E. Multi-analytical characterisation of Art Déco dinanderie: single-point and map analysis of Jean Dunand's metal artworks. RAA 2023, 11th International Conference on the Application of Raman Spectroscopy in Art and Archaeology. Athens, Greece. September 6-9 2023
2. Passaretti, A.*; **Cuvillier, L.***; Guilminot, E.; Sciutto, G.; Joseph, E. Biopulitura di artefatti metallici in collezioni storiche. Bioscienze nei beni culturali convegno. Rome, Italy. April 5th 2023. **Both first authors contributed equally*
3. Passaretti, A.; Cuvillier, L.; Künzi C-A.; Brambilla, L.; Joseph, E. Multi-analytical characterisation of Art Déco dinanderie: single-point and map analysis of Jean Dunand's metal artworks. RAA 2023, 11th International Conference on the Application of Raman Spectroscopy in Art and Archaeology. Athens, Greece. September 6-9 2023
4. **Cuvillier, L.;** Joseph, E.; Approches vertes alternatives dans la conservation des métaux et matériaux composites. Conférence Internationale MATERIAUX 2022. Lille, France. October 24-28 2022. *Replacement of supervisor as invited speaker for a keynote*
5. **Cuvillier, L**.; Passaretti, A.; Dupuy, V.; Raimon, A.; Guilminot, E.; Joseph, E. Exploiting Biologically Synthetized Chelators in Conservation: Gel-Based Bio-Cleaning of Corroded Iron Heritage Objects. 10th interim meeting of the ICOM-CC metals working group Conference proceedings. Helsinki, Finland. September 5-9 2022.
6. Passaretti, A.; **Cuvillier, L.**; Guilminot, E.; Sciutto, G.; von Reuss, S.; Joseph, E. Innovative green gels for the biocleaning of historical metal heritage**.** CHEMCH – 6th International Congress Chemistry for Cultural Heritage**.** Ravenna, Italy. July 4-8 2022
7. **Cuvillier, L**.; Guilminot, E.; Joseph, E. Développement de traitement de nettoyage du patrimoine métallique historique (Fe, Ag, Cu) à l'aide de métabolites intégrés dans des hydrogels Journée d'échanges Gels métaux, Paris, France. May 23rd 2022
8. Passaretti, A*.; **Cuvillier, L**.*; Guilminot, E.; Sciutto, G.; Joseph, E. Sustainable cleaning of metal artworks using innovative biologically derived water- and solvent-gels 4th Green conservation of Cultural Heritage conference. Rome, Italy. February 3-4 2022. **Both first authors contributed to the oral presentation*

7.3 Other communications

1. Passaretti, A.*; Cuvillier, L.*; Guilminot, E.; Sciutto, G.; Joseph, E. Biocleaning of historical iron artworks: innovative green gels amended with microbial derivatives. Short communication in proceedings. Heritage for the Future, Science for Heritage, A European Adventure for Research and Innovation. Paris, France. March 15-16 2022. **Both first authors have the same contribution.*

7.4 Posters

1. Passaretti, A.; **Cuvillier, L.**; Guilminot, E.; Sciutto, G.; Joseph, E. Sustainable cleaning in metal conservation: bio-derived hydrogels applied on altered iron-based heritage. InArt2022, Paris, France. June 28 – July 1st 2022

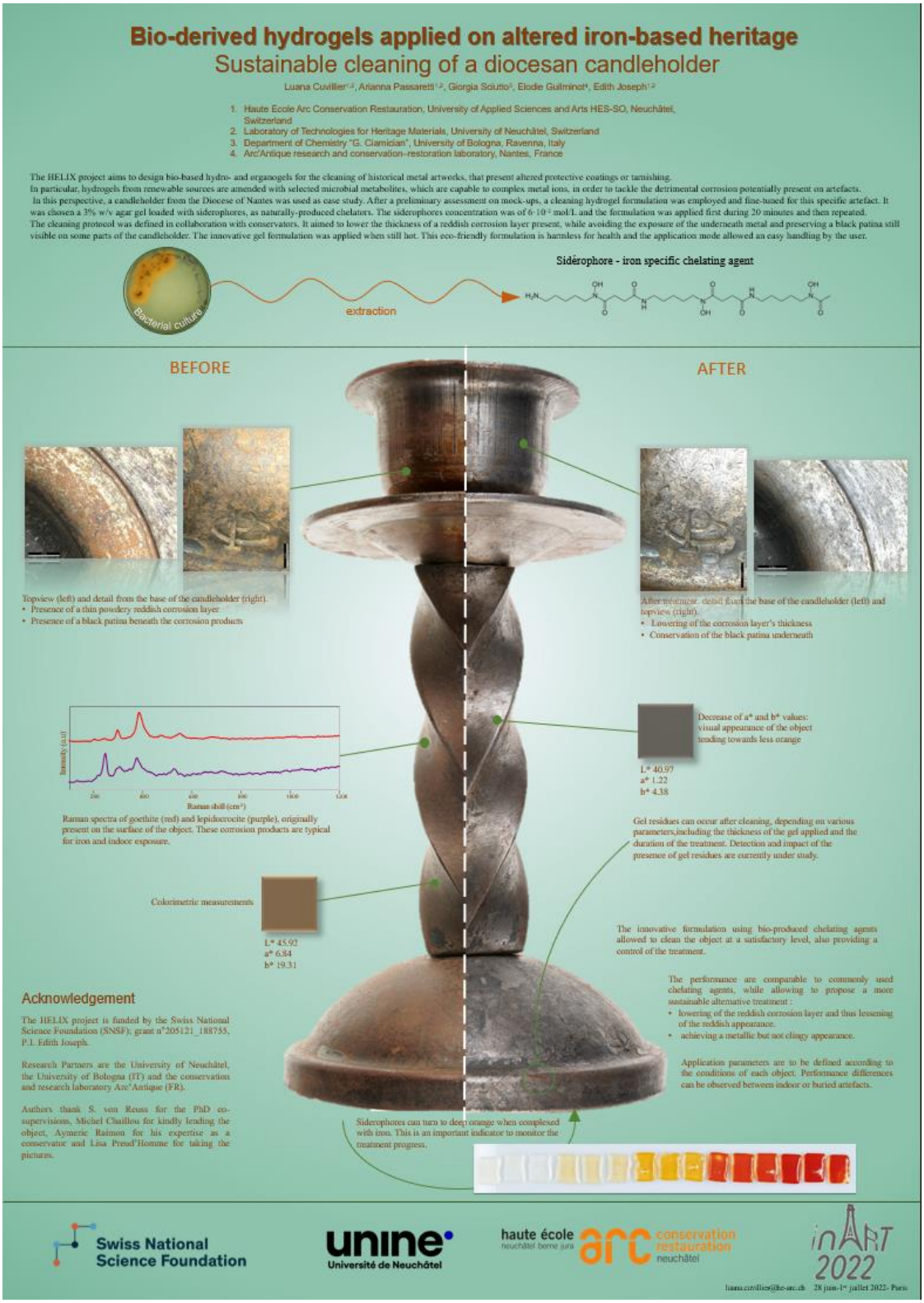

2. Passaretti, A.*; **Cuvillier, L.***; Joseph, E. Biocleaning of historical metal artworks using innovative green gels amended with microbial derivatives. Annual pHD students meeting 2022, HES-SO. Lausanne, Switzerland. May 22 2022. **Both first authors have the same contribution.*

Bio-cleaning of historical metal heritage

Passaretti Arianna*, Cuvillier Luana*, Joseph Edith
Haute Ecole Arc Conservation-Restauration, HES-SO
Laboratoire des Technologies pour les Matériaux du Patrimoine, University of Neuchâtel

Context

In metal heritage preservation the core problem is the spontaneous process of corrosion, which alters original features or damages the integrity of artworks. As a result, it is common to remove corrosion when detrimental.
As alternative, The application of organic coatings is a favored method to prevent corrosion. However, these products are also sensitive to ageing factors through time. Therefore, there might arise the necessity of removing - and replacing - them once their protection purpose is compromised.

In the last decades, growing research attention towards safe and sustainable conservation practices has been carried out, in response to traditional cleaning methods potentially harmful for human health and the environment or artworks.

Previous studies have demonstrated the efficiency of particular microorganisms and their metabolites when exploited in conservation approaches. In addition, the employment of gels provides a controlled and adjustable cleaning action as well as a significant reduction of active agents quantity, appearing thus as an attractive delivery system for sustainable conservation treatments.

Methodology

Colour, morphology and chemical composition of gels and metal mock-ups are investigated before and after cleaning with complementary analytical techniques: colorimetry, optical microscopy, X-Ray Fluorescence, Raman and Fourier-transform Infrared spectroscopies, Scanning Electron Microscopy.

Furthermore, gels are also characterized by means of Atomic Absorption spectroscopy and rheology in order to define uptake rate and mechanical properties respectively.

Attention is given to the definition of an ad-hoc protocol, taking in account gel load concentration, duration and application repetition of the treatment.

Conclusion

HELIX green formulations show comparable outcomes with conventional cleaning methods on both corrosion and organic coatings.

Remarkably, it is possible to easily control the cleaning action adjusting the time and number of applications.

For an extensive use of bio-based gels in metal conservation, several points appear crucial:

- Close cooperation between scientists and stakeholders, to formulate reliable alternatives;
- Non-prohibitive cost of the proposed bio-gels;
- Easy set-up in workplaces or purchase by conservators.

Acknowledgments and contact

The HELIX project is funded by the Swiss National Science Foundation (SNSF); grant n°205121_188755, P.I. Edith Joseph.

Research Partners are the University of Neuchâtel, the University of Bologna (IT) and the conservation and research laboratory Arc'Antique (FR).
Authors thank E. Guilminot, G. Sciutto and S. von Reuss for the PhD co-supervisions.

contact@he-arc.ch: luana.cuvillier; arianna.passaretti

Research goal

The HELIX project seeks to develop eco-friendly, bio-based and easy-to-use gels for the cleaning of altered historical metal artworks, in particular on iron- and copper- based alloys. The ability of specific microbes to uptake metallic ions is exploited in parallel with the efficiency of specific bio-based solvents, in order to remove detrimental corrosion as well as altered or undesired organic protective coatings. Concurrently, high attention is addressed to the selection of bio-derived gelling agents to design green water- and solvent-gels.

Analysis and results

Metal corrosion removal

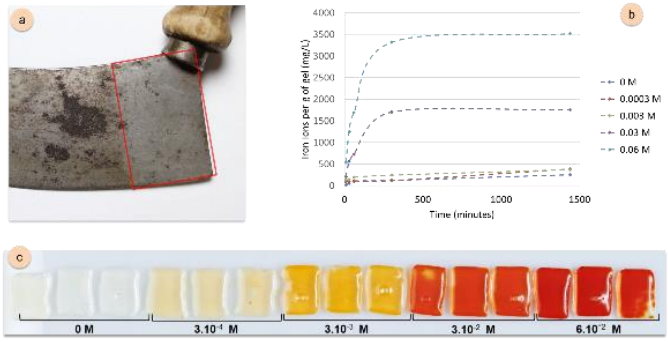

Figure 1. (a) Corroded iron-based mezzaluna knife after the application of a siderophore-amended 3% w/v agar gel during 20 minutes (red rectangle). (b) Quantity of Fe-ions absorbed by 3% w/v agar gels loaded with siderophores ($6 \cdot 10^{-2}$, $3 \cdot 10^{-2}$, $3 \cdot 10^{-3}$ and $3 \cdot 10^{-4}$ M) and applied during 10 and 30 minutes, 1, 5 and 24 hours on corroded iron. (c) Siderophore-amended 3% w/v agar gels (in triplicates) at different concentrations after a 10-minute application on corroded iron.

Organic coatings cleaning

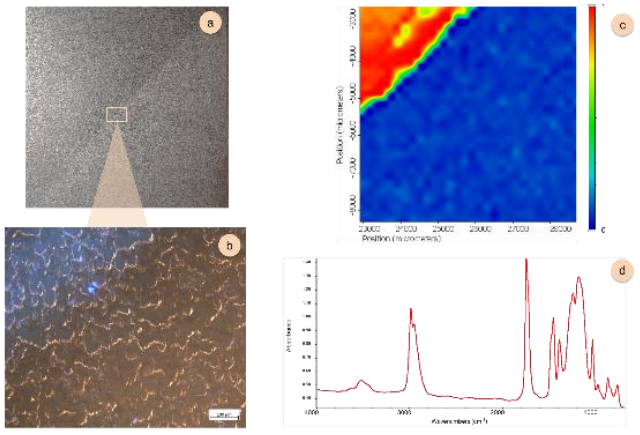

Figure 2. (a) Iron sample coated with an acrylic resin (paraloid B72) that has partly been removed using a Polyhydroxybutyrate-ethyl lactate gel. (b) Detail of the sample under UV illumination: evident difference between coated (left top half) and cleaned (right bottom half) regions. (c) FTIR correlation map collected in reflectance mode on coated (left top half) and cleaned (right bottom half) regions, using (d) a reference spectrum of paraloid B72. Correlation scale from min (blue) to max (red).

References

A. Passaretti, L. Cuvillier, G. Sciutto, E. Guilminot, and E. Joseph, "Biologically Derived Gels for the Cleaning of Historical and Artistic Metal Heritage," Appl. Sci., vol. 11, no. 8, p. 3405, Apr. 2021, doi: 10.3390/app11083405.
L. Cuvillier, A. Passaretti, A. Raimon, V. Dupuy, E. Guilminot, E.Joseph. Exploiting biologically synthetized chelators in art conservation: bio-cleaning gels for altered iron heritage. In Proceedings of the Metal 2022, 10th interim meeting of the ICOM-CC metals working group; Helsinki, Finland, 2022. [in press]
E. Joseph, M. Albelda-Berenguer, E. Cornet, L. Cuvillier, S. James, L. Mathys, M. Monachon, A. Passaretti and S. Russo. (2020). Innovative approaches towards a green and sustainable metal conservation. Chimia, 74, 611. https://doi.org/10.2533/chimia.2020.611
E. Joseph, P. Junier. (2020). Metabolic processes applied to endangered metal and wood heritage objects: Call a microbial plumber! New Biotechnology, 56, 21-26. https://doi.org/10.1016/j.nbt.2019.11.003

8. Curriculum Vitae

Luana CUVILLIER

18.12.1996
Avenue des Portes-Rouges 3, 2000 Neuchâtel, SWITZERLAND
+41 78 200 52 59
luana.cuvillier@gmail.com

EDUCATION

Ph.D., Chemistry,
University of Neuchâtel, Feb 2020 – Nov 2023
Biotechnology applied to the conservation of metal artefacts, in collaboration with Laboratory Arc'antique (Nantes)
SNSF funded research, part of the HELIX project titled '' Investigating metal bioremediation for the preservation of historical metal artworks"
Thesis title: Development and evaluation of sustainable hydrogel formulations for the microbial cleaning of historical metal artefacts.
Supervisors: Professor Edith Joseph, Dr. Elodie Guilminot and Professor Stephan von Reuss
MSc, Material Sciences
Graduate School of Biology, Chemistry and Physics of Bordeaux, Sep 2016 – Sep 2019
General engineering school with modules including chemistry (inorganic, analytical, quantic, polymers, organic), material characterization, thermodynamics, mechanical studies
Sep 2017 – Jun 2018 Erasmus, University of Chemistry and Technology, Prague, Czechia
Preparatory classes,
University of Bordeaux, Sep 2014- Jul 2016
2-year intensive undergraduate studies in Chemistry, Physics and Mathematics

RESEARCH

Ph.D., Chemistry, *Iron, copper and silver bioremediation on cultural heritage artefacts using microogranisms and/or their metabolites implemented in natural hydrogels*

University of Neuchâtel (Switzerland), Feb 2020 – Nov 2023, Supervision by Prof. Edith Joseph, Dr. Elodie Guilminot

- Metabolites (siderophores) production, extraction (SPE) and characterization
- Evaluation of fungal Fe/Cu uptake or bacterial Ag resistance (UV-vis assays, microscope observations).
- Evaluation of the affinity between corrosion products and chelators at different given pH. (ICP-OES, UV-vis)
- Study of metal uptake by conventional and novel natural hydrogels (FT-Raman, Cryo-SEM, Rheology, FTIR).
- Study of residues left by the hydrogels on metal surface, imaging approach (XRF, fluorescence)
- Evaluation of the formulation's performances on metal pieces (colorimetry, AAS, Raman, FTIR)
- Evaluation of the formulation's performances regarding sustainability (LCA)

Side tasks:

- Understanding of the biomineralization pathways of copper unstable compounds into copper oxalates (fungal cultures, colorimetry and FTIR)
- Characterization of valuable objects from the artist Jean Dunand (FTIR and Raman analysis)
- Assistance in practical lessons of bachelor students (BSc in medicine, pharmacy and biology)

Undergraduate research internship, *Tin degradation study in medieval sculptures decorations*

Centre Energie Atomique, Grenoble (France), Mar – Sep 2019, Supervision by Dr. Karine Froment

- Analysis of tin corrosion products (XRD, SEM-EDS, FTIR) and understanding of tin degradation process

Research internship, *Electroporation of OMVs with gold and silver nanoparticles as potential drug carriers.*

The MacDiarmid Institute, Victoria University, Wellington (New Zealand), Jun- Nov 2018, Supervision by Dr. Renee Goreham

- Nanoparticles synthesis (gold)
- Bacterial vesicles extraction (SEC)
- Electroporation
- Characterization (TEM-EDX, zeta potential, DLS, UV-vis, PL)

Research project, *Study of silk degradation*

University of Chemistry and technology, Prague (Czechia), Feb-Jun 2018, Supervision by Dr. Markéta Škrdlantová

Characterization of different silk grades after artificial ageing on various types of storage cardboards (mechanical tests, viscosity, colorimetry)

Research project, *Study of X-chromic pigments*

ICMCB, University of Bordeaux (France), Oct – May 2016, Supervision by Dr. Manuel Gaudon

State of the Art and synthesis of piezo-thermochromic pigments at the ICMCB.

RELEVANT SKILLS

Communication

French *Native speaker* – English *C2* – Spanish *B2*

Thriving an oral presentation *Workshop in 2021*

Poster conception and realization *Course in 2021*

Softwares

Microscoft office *Advanced* – Adobe programs *Intermediate* – LaTeX *Intermediate* – R *Intermediate*

Laboratory skills

First aid certificate *PSE1, France* – Radioprotection certificate *SUVA, Switzerland*

Experimental design - Chemometrics *MOOC in 2023*

Working in sterile conditions

Microbial cultures

Metabolites extraction *Siderophores, OMV*

Mineral synthesis *Gold and silver nanoparticles, corrosion*

Open Science *Workshop in 2022*

Characterization

FTIR

Raman

Atomic absorption spectroscopy

UV-vis spectroscopy

Mineral characterization *XRD*, *Laser diffraction analysis*

Elemental analysis *EDS, XRF*

DLS/Zeta Potential

Spectrocolorimetery

Optical microscopy

Electron microscopy (SEM, TEM) *Workshop in 2021*

Laboratory life

Organization of social events

Working with emotions and Emotional intelligence at work *Course in 2022*

Overcome conflicts and obstacles *Course in 2021*

Transversal skills

Long distance swimmer

SSI Freediver

French National Security and Rescue Certificate *BNSSA*

Artistic Gymnastics Judge for national competitions